DOCTOR OF PHILOSOPHY

Design and application of a recirculating flume for the assessment of geotechnical and geophysical indicators of cohesive sediment erodibility.

Wing, Paul Michael

Award date:
1994

Awarding institution:
Bangor University

DESIGN AND APPLICATION OF A RECIRCULATING FLUME FOR THE ASSESSMENT OF GEOTECHNICAL AND GEOPHYSICAL INDICATORS OF COHESIVE SEDIMENT ERODIBILITY

BY

PAUL MICHAEL WING.

A thesis submitted in accordance with the requirements of the University of Wales for the degree of Doctor of Philosophy.

School of Ocean Science
University College of North Wales
Menai Bridge
Gwynedd

MCMXCIV

SUMMARY.

A laboratory seawater flume was designed and constructed for experimental studies of the erosion characteristics of cohesive sediments. The upright orientation of the flume and the use of an impeller drive system reduced the amount of cross stream flow over the test bed area and allowed the flow to be accurately controlled and replicated on separate flume runs. The flume was designed to use a relatively small volume of seawater so that suspended sediment concentrations could be accurately measured. The flume was used to explore the relationship between threshold shear stress (τ_{ch}) and physical bed properties measured using non-destructive geophysical techniques.

The flume was instrumented to measure flow velocity, bed shear stress, and resuspended sediment concentration. The two flow parameters were measured using hot film probes. Calibration of the bed stress probe was carried out in a purpose built flume which could generate stress values measured by manometer tubes. Suspended sediment concentration was measured using infra red optical backscatter sensors which were calibrated in situ by gravimetric analysis of filtered samples. Three physical bed properties were measured: moisture content using standard soil mechanics techniques; acoustic shear wave velocity (Vs), using pizo-electric bender elements; and electrical formation factor (FF), using resistivity probes. Bed porosity was derived from measured formation factor using calibrations obtained in a modified oedometer cell. Rigidity modulus (μ) was obtained using the measured shear wave velocity and calculated bed density (derived from porosity).

Flume samples were remoulded estuarine muds. Moisture content was varied by adding water to samples prior to installation in the flume; moisture contents of 110-165% were thus obtained. These samples had FF values of 1.05-1.75%, and Vs values of 0.5-4.0 ms^{-1}.

Experiments identified significant relationships between τ_{ch} and the measured bed properties. The most important relationships were with Vs and μ. These relationships can be described by power relationships such that $\tau_{ch} \propto \mu^{0.2}$ and $\tau_{ch} \propto Vs^{0.2}$. These experiments indicate that the erosion potential of a cohesive bed can be predicted by geophysical measurement of bed properties.

ACKNOWLEDGEMENTS.

I would like to thank the numerous members of the school of ocean science for there advice and help when I needed it, especially all the members of the sediment laboratory. In particular I wish to thank, Dr Colin Jago my supervisor for his help and guidance, Dr Kevin Black my co-worker on this project for his assistance, and Drs Jim Bennel and Ian McDermott for their help and advice with the shear wave and resistivity measuring equipment.

I also wish to extend my gratitude to all members of the technical staff for their help with this project, the design and construction of equipment, and without whom none of this project would have been possible. In particular, the members of the workshop for their diligence and patience with Kevin and myself over the construction and commissioning of the flume and other pieces of equipment.

I am grateful for the assistance of Dr J. Best at Leeds University for the use of the Laser Doppler Anometer in the calibration of the hot film anometer probe, and Dr Tim O'Hare who wrote the software programme that controlled the DASH-8 card.

I must also thank my parents and friends especially Deborah for keeping me committed to the work, during the more painful moments of Ph.D research.

CONTENTS.

CHAPTER 4

Resistivity Theory and Measurements

CHAPTER 5

Instrumented Recirculating Flume

CHAPTER 6

Flume Sediment Erosion Experiments

CHAPTER 7

Conclusions

NOTATION.

β	Bulk compressibility
β_s	Solid compressibility
β_w	Fluid compressibility
Δ	Dilation
ε	Erosion rate
ε_f	Floc erosion rate
η	Pore fluid viscosity
θ	Shields entrainment function
θ_c	Threshold Shields value
λ	Lame's constant
μ	Rigidity modulus / Coefficient of molecular viscosity
μ_f	Complex rigidity modulus of the frame
π	Phi
ρ	Bulk density
ρ_o	Bulk resistivity
ρ_m	Surface (double layer) resistivity
ρ_s	Solid density / Solid (grain) resistivity
ρ_w	Fluid density / Fluid resistivity
σ	Poisson's ratio
τ	Shear stress
τ_0	Bed Shear stress
τ_c	Threshold bed shear stress
τ_{ch}	Characteristic bed stress
τ_{cr}	Critical shear stress
υ	Kinematic viscosity
ϕ	Coefficient of permeability expressed in velocity units / Phi grain size units
ω	Angular frequency / Water (moisture) content

A	Area
a	Pore size parameter /
a'	Structure factor
b	Mass-coupling factor
C	Current density / Suspended sediment concentration / Sediment bed concentration
C_{eq}	Equilibrium suspended sediment concentration
C_D	Drag coefficient
C_L	Lift coefficient
C_m	Mechanical compliance
C_0	Initial suspended sediment concentration
D	Grain diameter
E	Young's modulus
e	Void ratio
F	Geometric factor
F_D	Drag force
F_G	Gravity force
F_L	Lift force
F_d	Fluid Drag
F_r	Resonant frequency
FF_{app}	Apparent Formation factor

FF_i	Intrinsic Formation factor
G_s	Specific gravity
g	Acceleration due to gravity
I	Current
K	Bulk modulus
K_f	Frame bulk modulus
K_m	Surface (double layer) conductivity
K_s	Solid bulk modulus / Solid (grain) conductivity
K_w	Fluid bulk modulus / Fluid conductivity
k	Permeability coefficient / von karman constant
L	Length
M	Effective mass
M_s	Mass of solids
N_z	Coefficient of eddy viscosity
n	Porosity
R	Resistance
R_{app}	Apparent resistance
Re	Reynolds number
R_m	Surface (double layer) resistance
R_s	Solid (grain) resistance
R_w	Fluid resistance
r	Radius
S	Fraction of pores containing fluid
S_v	Vane shear strength
t	Time
U	Flow velocity
U_{100}	Velocity 100cm above the bed
U_*	Friction velocity
u	Horizontal velocity component
u'	Turbulent horizontal velocity deviation
$\bar{u}$	Turbulent mean velocity
V	Potential difference (Volts)
V_f	Compressional wave velocity in a fluid
V_p	Compressional wave velocity
V_s	Shear wave velocity
V_T	Total volume
v	Lateral velocity component
v'	Turbulent lateral velocity deviation
$\bar{v}$	Turbulent mean lateral velocity
W_0	Particle settling velocity (also W_s)
w	Vertical velocity component
w'	Turbulent vertical velocity deviation
$\bar{w}$	Turbulent mean vertical velocity
x	Horizontal coordinate direction
y	Lateral coordinate direction
Z	Bed roughness length
Z_0	Roughness length
z	Vertical coordinate direction

LIST OF FIGURES.

LIST OF TABLES.

LIST OF PLATES.

CHAPTER 1.

INTRODUCTION.

1.1 Overview.

In sediment transport threshold of motion and erosion rate are obviously crucial considerations, but the difficulty is in assessing which characteristics of the sediment are important determinants and/or predictors of the threshold of motion and rate of erosion. This project is aimed at assessing the relationship between bed properties, in particular rigidity modulus and the erosion of a cohesive sediment bed.

Erosion of cohesive sediments is a far more complex phenomenon than that of non-cohesive sediments. Consider the definition of conditions at the instant of particle entrainment (threshold of grain movement): excellent progress has been made on the determination of threshold conditions for non-cohesive sediments where the critical boundary shear stress can be related to the gravitational force (via the sediment grain diameter), and extensive use is made of Shields and Yalin type threshold curves derived from laboratory data. Figure 1.1 shows a simplified Shields curve which relates grain diameter to the threshold value of Shields entrainment function ($\oint$2.2.6); the use of such plots enables the threshold of motion of a non-cohesive sediment to be determined from its grain size. However in cohesive sediments, the cohesive forces derived from electrochemical and biological processes often exceed gravitational forces, and these forces are governed by a number of factors including clay mineralogy, pore fluid chemistry, meso-and macro-biological activity, and depositional history. This means that it is not the grain diameter alone that determines the threshold of motion in cohesive sediments, but that it is some function of the cohesive strength of the bed. Due to this complexity existing theoretical models which relate boundary layer fluid flows and associated

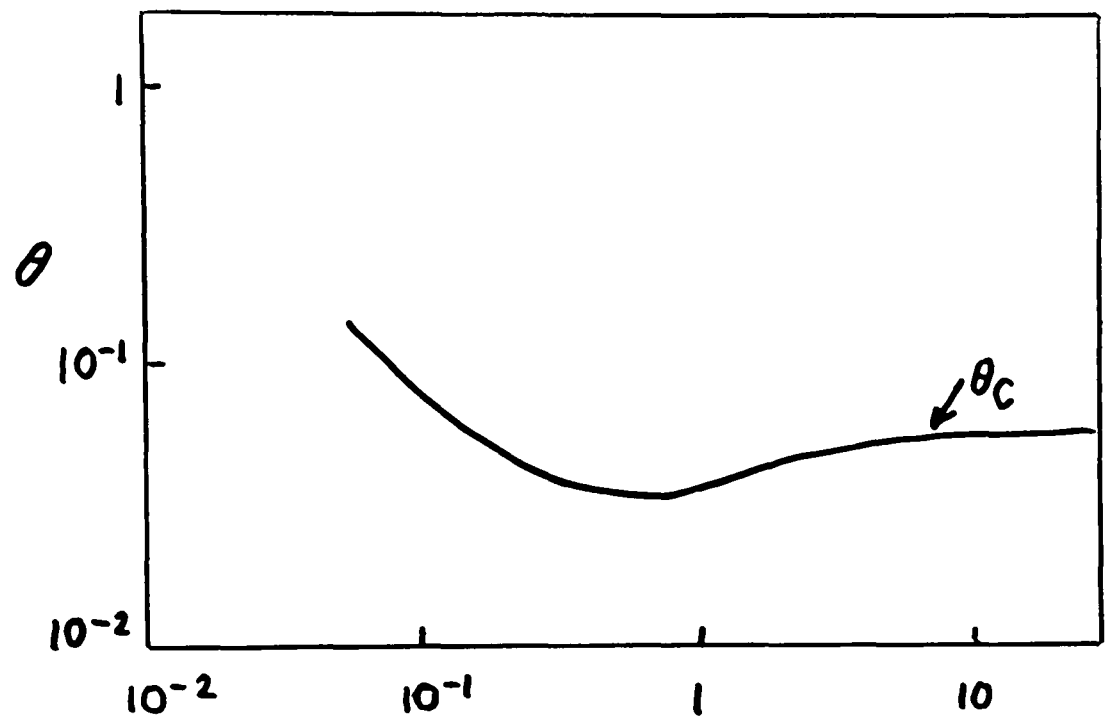

Figure (1.1): Shields threshold curve plotted against grain diameter (from Dyer 1986).

non-cohesive sediment entrainment are not applicable to cohesive sediments.

Cohesive sediments make up the bulk of coastal and shelf deposits in the form of silts, clays, and biogenic detritus. Their part in marine sedimentation, bio-geochemical cycling and pollutant dispersal is an important one; many coastal, estuarine, or water resource engineering projects encounter major problems with cohesive sediments. This makes it all the more necessary that the problems in relating the threshold of grain movement to a physical cohesive sediment property should be overcome. The main problems that need to be over-come can be divided into two categories: (a) how to characterise the threshold (define the threshold so that the same condition is measured in consecutive experiments), (b) how to determine and measure the appropriate physical property or properties (i.e. which property or properties could constitute the x axis on a Shields type threshold curve?).

1.2. **Cohesive Sediment Properties.**

Characterisation of the threshold of erosion of a cohesive sediment bed is not easy, because bed erosion can occur in a variety of forms. Although this variety is a continuous spectrum, it can be broken down into three main groups: (1) Entrainment of single particles or flocs from the bed surface. (2) The entrainment of clumps of the surface layer of the bed, over the complete size range. (3) Mass erosion of the bed where the bed is completely entrained and enters into suspension. This is further complicated by the abrasive action of material already in suspension and the effects of intermittency (sweeps and bursts) in turbulent flows. These turbulent 'sweeps' and 'bursts' are likely to be a major factor in the initiation of erosion. Further complications arise under wave action, which weakens the sediment bed and may form a surface fluidised layer which is then more prone to current transport than an identical bed under the current alone. However this study is concerned only with erosion under unidirectional flows.

Two different parameters have been used to determine an erosion threshold. These are (a) suspended sediment concentration and (b) bed level wastage. Measurement of bed level wastage is only possible in rather ideal conditions where there is a fairly solid bed surface which forms a density step rather then the more usual case where the sediment water interface is a density gradient. This density gradient is especially likely under wave action, as described above. In this investigation the flume design meant that the sediment water interface was always a marked density step and could be monitored by an acoustic instrument. However, spot measurements of an interface are prone to heterogeneous erosion and provide an ambiguous measure of bed wastage, so calculations of erosion rate and threshold were derived from the continuous measurement of suspended sediment concentration by optical backscattering equipment.

Grain diameter is not a very useful property for describing the threshold and rate of erosion of a cohesive sediment. Therefore which physical bed property is best related to erodibility and how can that property be measured? The erodibility of a sediment is determined by the nature of the individual sediment particles and their contacts with each other. In fact the strength of the particle contacts or bonds is what gives the sediment its cohesive characteristic, and there are a large number of physical properties which affect this cohesion. Table 1.1 shows the range of factors which are known, or judged, to affect cohesion and which therefore control erodibility, and Table 1.2 shows a range of characteristics that can be used in erosion studies.

Indeed past research has used all of these characteristics in various combinations, which makes valid comparisons between various studies difficult. However, in the main, it has been shown that bed density and shear strength are the best properties to relate to the critical erosion shear stress, τ_{cr} (Dyer, 1986 for summary). This is a simplification as the bed shear strength is dependent on a wide range of factors. In fact nearly all of the characteristics in Table 1.2 directly or indirectly have an effect on the bed shear strength, except for the rheological properties. These rheological properties are themselves related to bed shear strength and can (and have been) used in erosion studies instead of the bed shear strength. The rheological property used to represent bed shear strength is

Table (1.1); Factors controlling the erosion of cohesive marine sediment beds (Black 1991).

---

1. Fluid Erosive Force

Bed Shear Stress
- oscillatory and unidirectional currents
- fluid turbulence
- boundary roughness
- water column stratification

2. Bed Resistance

Sediment Composition and Texture
- organic content (including microbial exudates)
- epi/infauna; macro- and micro-biological community structure
- clay mineralogy (ion exchange capacity) and clay content
- grain (aggregate) size spectra and sand:silt:clay ratio
- temperature
- gas content
- water content

Pore Fluid Character
- cation/anion composition and species ratio
- salinity and temperature
- pH
- pore fluid pressure
- bubble formation

Eroding Fluid Character
- salinity
- temperature
- pH

Bed Structure
- sediment density profile
- sedimentation and consolidation rate
- hydrodynamic stress history (in situ, placed, flow deposited)
- micro-structure

3. Climatological

Atmospheric Conditions
- irradiance
- temperature
- wind
- rainfall
- [ice]

Table (1.2): Possible characteristics of soft cohesive sediments that can be used in erosion studies (after Black 1991).

Physical Properties

Water Content	Sand: Silt: Clay %
% non-mineral components	Bulk particulate surface area
Spectra	Particle number spectra
Bulk (wet) density	Dry density
Grain Specific density	Floc micro-morphology
Mud micro-fabric	Sediment macrostructure
Flocculated and deflocculated size	

Physio-chemical Properties

Pore water salinity	Pore water pH
Sediment temperature and interface micro-gradients	

Mineralogical Properties

Clay and non-clay mineral types and proportions

Surface area of clay fraction

Cation exchange capacity and sodium absorption ratio of clay fraction

Biological Properties

Floral and faunal composition (macro/meio/micro) to species level

Spatial distribution (patchiness)

Biochemical/Biophysical Properties

Organic content - living carbon (ATP, Chlorophyll a, bacterial biomass and activity
- non-living carbon (particulate and dissolved OM; particulate and dissolved carbohydrate; protein)

Organo-mineral aggregate structure

Rheological Properties

Deformation characteristics; yield strength

Liquid and plastic limits

determined by the constraints of the sediment investigation and different rheological properties give different values for the bed shear strength since they depend on the apparatus and method used and are wholly empirical. They are also related to a representation of a cohesive sediment by a Bingham plastic model (using a yield strength).

In this investigation a more recent visco-elastic model has been used which is parameterised by viscosity, density, and rigidity modulus. The attraction of this method is that the rigidity modulus can be obtained using acoustic shear wave propagation and the value obtained is theoretically rigorous and not technique dependent (though it is frequency dependent). The rigidity modulus is defined as a measure of the bed resistance to shearing strain. It is controlled by exactly the same physical properties as shear strength but it is easier to interpret and by using geophysical techniques can be measured in situ under both field and laboratory conditions.

1.3. **Geophysical Concepts.**

The rigidity modulus is given by the equation,

$$\mu = \left(\rho . V_s^2\right) \tag{1.1}$$

where μ is the rigidity modulus, ρ is the bulk density, and V_s is the acoustic shear wave velocity. The shear wave velocity can be measured in situ, and the bulk density (and other physical properties such as voids ratio and moisture content) can be derived from porosity if the specific density of the sediment is known (on the assumption that the sediment is water saturated since gas in the sediment will affect the shear wave velocity). The sediment porosity can be obtained both in the laboratory and the field by measuring the electrical resistivity (and hence formation factor) of the sediment. It is therefore possible to calculate a rigidity modulus using geophysical measurements of shear wave velocity and formation factor, and both of these can be obtained by non-destructive methods causing only slight disturbance to the sediment structure.

1.3.1. **Acoustic Properties.**

The factors which determine rigidity modulus and shear strength additionally determine affect shear wave velocity. This is simply explained because shear waves can travel only through solids and not fluids. Therefore in a sediment, the main controls of shear wave velocity are the individual sediment particles and the contacts between. Both of these relate to how the sediment will react under shearing strains (hence to erosive flows).

This is shown in a more complex form in the physical model used to describe unconsolidated marine sediments based on the classical theory of the mechanics of porous media developed by Maurice Biot (Stoll, 1991). The theory describes the media as a two component system consisting of a compressible fluid which fills the interstices of a compressible porous frame with shear stiffness and interconnected void spaces. In this system the energy of a propagating acoustic wave is dissipated in three main ways: (a) Intergranular friction - small amounts of 'slip' within the tiny areas of grain to grain contact. (b) Local fluid motion relating to distortion of the void spaces (i.e., squeeze film motion in the annuli near each intergranular contact). (c) Relative motion between the fluid and the solid, controlled by the permeability. This theory and those developed from it show that the shear wave velocity is sensitive to physical properties of the sediment and is affected by many of the same features that affect the sediment shear strength.

1.3.2. **Electrical Properties.**

The electrical resistivity of a sediment is related to its porosity by its formation factor. This dimensionless formation factor is the ratio of the electrical resistance of the sediment to the electrical resistance of the fluid in its interstitial voids. In this way measurements carried out in both the laboratory and in the field with differing equipment configurations can be compared. The connection between formation factor and porosity can be easily seen if it is assumed that the solid fraction of the sediment is a poor conductor and that electrical conductance occurs only in the fluid fraction.

A number of general relationships have been formed so that porosity can be determined from formation factor measurements. However since clay particles have some form of conductance at their surfaces, some method is need to define more exactly (i.e. calibrate) the relationship between porosity and formation factor for the particular sediment under investigation, especially for sediments containing significant amounts of clay.

1.4. **Flume Investigations.**

In order to study the relationship between physical properties and erodibility of a cohesive sediment, an upright re-circulating flume was designed and built for laboratory use. Although this cannot fully replicate field situations, it has the obvious advantage that more control can by exercised on both the flow and sediment characteristics. The flume has been designed specifically to give good, steady, measurable and repeatable flow conditions and the capability of measuring both shear wave velocity and electrical resistivity of the sediment in the flume.

1.5. **Specific Aims.**

The specific aims of this study were therefore:

(1) To design a laboratory flume that permitted measurement of the appropriate geophysical bed properties and erosion characteristics of a cohesive bed.

(2) To investigate the relationship of the bed properties to the threshold of motion.

CHAPTER 2.

COHESIVE SEDIMENT PROCESSES AND PROPERTIES IN THE MARINE ENVIRONMENT.

2.1. Introduction.

Sediment erosion by fluid flow has been studied extensively and a large volume of literature has been produced. Most of this literature relates to studies of the behaviour of granular cohesionless sediments. For these sediments the basic sediment unit is the individual (sand) grain, and the erosion and transport characteristics of these grains are dependent mainly on parameters such as particle size, shape, and density (Dyer, 1986). A number of expressions for the threshold of motion of such grains and their subsequent motion have been developed. The range of expressions covers the range of flow regimes; unidirectional, oscillatory, and combined wave current interactions.

The literature on cohesive sediment behaviour in aqueous flow is also large. However the nature of expressions generated by these studies is far more complicated due to the more complex nature of the bed, and the wide range of parameters and expressions used to define the properties of the bed. This is further complicated by the structure of cohesive beds and the way in which cohesive beds erode. A noncohesive bed erodes normally by the removal of individual grains, but the erosion of a cohesive bed can occur in a number of ways: The removal of individual mineral particles, the removal of flocs of particles, the removal of aggregations of flocs, and the failure of the bed when large clumps of sediment are removed.

For a coherent study of cohesive sediment bed erosion and the properties affecting this to be completed, some basic understanding of the dynamics of the eroding fluid flow and its interaction with the bed, as well as a knowledge of the erosion of non-cohesive sediment beds is needed. The way in which the cohesive bed reacts to an eroding flow is determined by the properties and structure of the bed.

This chapter is aimed at covering these areas and reviewing past research into cohesive sediments. It is divided into two main parts: 1) a general outline of flow properties, their relation to sediment transport, and basic details on the inception of grain entrainment. 2) a review of cohesive sediment behaviour in the marine environment with emphasis on bed erodibility, covering bed structure, formation and properties, past field and laboratory work, and the problems of laboratory flume work.

2.2. Fluid Flow Properties in Relation to Sediment Transport.

2.2.1. Introduction.

The manner of erosion of a sediment bed is dependent on both the properties of the bed and those of the flow. Therefore it is necessary to have some understanding of the properties of the flow that affect erosion and the variation of these properties.

2.2.2. Forces Acting on Particles.

The forces that the flow exerts on the bed are the most important as these will initiate erosion. The forces exerted by a flowing fluid on a particle resting on a submerged boundary are of two types (Middleton and Southard, 1977):

1) forces due to viscous drag acting on the upper exposed surface of the grain,

2) forces due to the unequal distribution of dynamic pressure on the grains surface.

These forces generate vector components of lift and drag.

The drag force (fluid drag) is exerted by the water flowing over the grain surface and is the sum of the form drag and the skin friction. The form drag is the sum of the horizontal components of the pressure (dynamic pressure) set up normal to the surface at every point over a body as the fluid moves around it. The skin friction is a frictional drag due to the shearing of the fluid past the grain surface and is dependent on the fluid viscosity, grain surface roughness and the detailed form of the near surface flow. The form drag reduces the flow's capacity to transport sediment whilst the skin friction is the main cause of sediment movement. If the flow causes turbulence then the energy used to create the turbulence is taken from the flow by additional drag. The total drag can be written as,

$$F_D = \tfrac{1}{2} C_D A U^2 \rho \qquad (2.1)$$

where C_D is the drag coefficient, U is the flow velocity, ρ is the fluid density and A is the projected area of the grain normal to the flow (Dyer, 1986). The total drag is the drag force, F_D, and the term $\frac{1}{2}\rho U^2$ defines the kinetic energy of the fluid.

Sediment grains that protrude into the flow disrupt the streamlines. The compression of streamlines and acceleration of the fluid over the grain causes a reduction in pressure (Bernoulli's theorem). The differences in pressure across the grain give rise to a lift force, F_L, which acts to lift the grain into the flow. It is defined by the same equation as the drag force except the coefficient is termed the lift coefficient.

These equations are given for a perfectly spherical grain which is fully exposed to the flow, for simplicity. For non-cohesive sediments the threshold of grain motion can be defined as the point at which the resultant of the lift and drag forces equals the moment of the gravity force (Allen, 1971). The gravity force F_G, the particles own immersed weight, acts on a grain through its centre of gravity and is related to the cube of its diameter D, and its submerged mass $(\rho_s - \rho)$ where ρ_s is the grain density and ρ the seawater density (Figure 2.1).

$$F_G = \frac{\pi}{6(\rho_s - \rho) g D^3} \qquad (2.2)$$

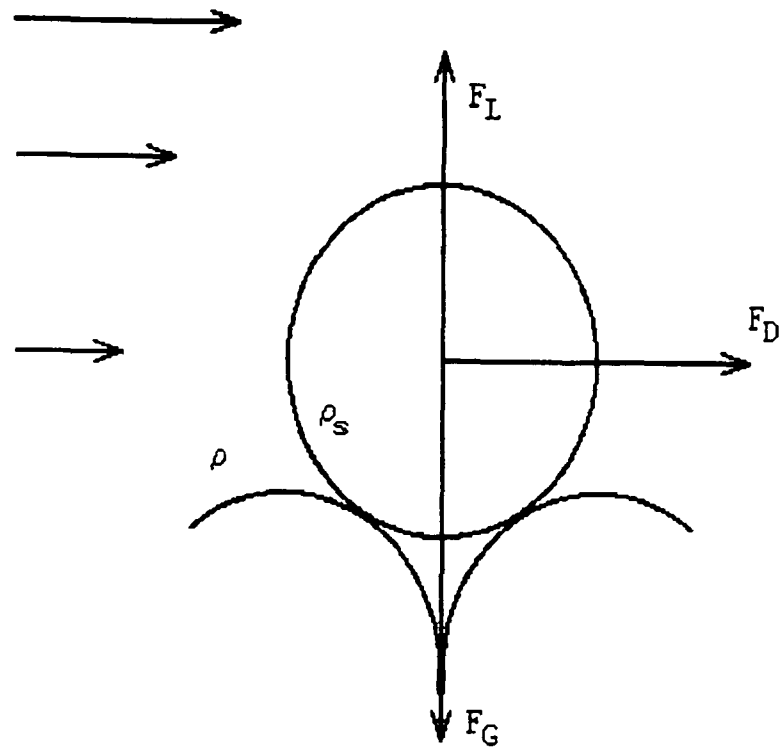

Figure (2.1): Forces acting on a static grain resting on a grain boundary (after Dyer, 1986).

This simple theoretical approach is complicated by a number of factors; including the fact that the grain is likely to be partially shielded by other grains, its forward path blocked by other grains, and it is unlikely to be spherical.

2.2.3. **Flow Regime.**

The nature of the flow will determine the magnitude of the above forces. It will determine the value of the coefficients, this depends on the shape and area of the particles projecting into the flow (the bed roughness) and the Reynolds number. These define the flow conditions in the area of the flow next to the sediment.

The Reynolds number, Re, compares the relative importance of inertial and viscous forces in determining the resistance to flow (Dyer, 1986). It is a dimensionless combination of the flow velocity, fluid kinematic viscosity and some length scale and can be determined for many situations using the appropriate length and velocity scales.

In laminar flow the fluid flows slowly past the boundary and drag is related to the molecular viscosity of the fluid. The velocity gradient near to the wall generates shear stresses on the plane parallel to the wall; the magnitude of these shear stresses depends on the viscosity and the velocity gradient. The shear stress, τ, is caused by the momentum exchange of fluid molecules moving from one layer to another, within the velocity gradient, and defined by,

$$\tau = \mu \frac{du}{dz} \qquad (2.3)$$

where μ is the coefficient of molecular viscosity for the fluid. Fluids where the stress is proportional to the rate of deformation and which agree with the above equation are called Newtonian fluids.

In a turbulent flow the random movement of small eddies generated by the flow produce a complex and quickly changing flow. Any coherence in the flow can only be examined by time averaging and stream lines can be

drawn following average velocity vectors. In this turbulent flow the eddy movements and momentum exchanges are larger then the molecular ones in the laminar flow and the resulting shear stress is larger. Once again the shear stress can be approximately defined,

$$\tau = N_z \frac{d\bar{u}}{dz} \tag{2.4}$$

where N_z is the coefficient of eddy viscosity which has a magnitude several orders larger then the molecular one and $\bar{u}$ is the time averaged velocity. However unlike the molecular viscosity, the eddy viscosity is not a constant, but varies with the mean velocity, and other flow parameters. It is often more useful to define the boundary shear stress in a form with the dimensions of velocity. To do this a friction velocity U_* is defined, such that

$$\tau_0 = \rho U_*^2 \tag{2.5}$$

where τ_0 is the shear stress at the bed.

With time averaging random fluctuations in the flow are averaged and it is possible to distinguish the steady flow which moves the turbulence along and on to which the turbulence is superimposed. The velocity can be separated into three components u, v and w which act in the x stream-wise horizontal direction, the y lateral direction and z vertical direction respectively. At any point and at any instant the velocity u is made up of the time averaged velocity $\bar{u}$ and its turbulent deviation u'. So $u = \bar{u}+u'$ and similarly $v = \bar{v}+v'$ and $w = \bar{w}+w'$.

This turbulent motion generates shear stress in a fluid with a mean velocity gradient. Particles of fluid moving upwards, positive w', will arrive in a layer of faster flow and since they still have most of their original velocity they will in this layer of faster flow have a negative u'. The opposite is also true, particles moving down wards, negative w', will arrive in a layer of slower flow and will therefore have positive u'. This therefore means that on average a positive w' is associated with a negative u' and a positive u' as associated with a negative w'. This results in the time averaged u'w' being negative as well. There are similar interactions for the other planes v'u' and v'w'. As has been explained before these fluid

movements do not result in any net exchange of fluid but they do cause exchanges of momentum. This momentum exchange is the shear stress acting on the plane. Therefore,

$$\tau_{xz} = -\rho u'w' \qquad \tau_{xy} = -\rho v'u' \qquad (2.6)$$

$$\tau_{yz} = -\rho v'w'$$

These turbulent stresses constitute the Reynolds stresses. Of these the most important is the one involving vertical exchanges of momentum, because at the bed this component of stress is involved in the movement of sediment grains.

2.2.4. **The Boundary Layer.**

In studies concerned with the interaction of water flows and sediments, the area of greatest interest is where the flow comes into contact with the sediment. At the sediment surface the generation of friction causes a reduction of the flow velocity. The reduction is highest at the boundary but decreases away from the boundary. This layer, in which these velocity deviations occur, is called the boundary layer. Its thickness d is not easily determined due to the fact that the free stream velocity is approached asymptotically. However in the laboratory the thickness is the height where the velocity is within 1% of the free stream velocity.

So far the flow has been defined in terms of only two flow regimes (laminar and turbulent), but it is possible to expand this to three flow regimes with transition zones between them. Some of the definitions come from work carried out in pipes, and although this is rather specialised there are some similarities to more natural flows.

Nikuradse (1933) used pipes that had been artificially roughened by sticking sand to the insides of the pipes, and defined the regimes in terms of the Reynolds number,

$$Re = \frac{U_* D}{\upsilon} \qquad (2.7)$$

where D is the grain diameter and υ is the kinematic viscosity. The boundaries between the regimes have values of;

$U_*D/\upsilon < 3.5$ - Smooth turbulent flow

$3.5 > U_*D/\upsilon < 68$ - Transitional flow

$U_*D/\upsilon > 68$ - Rough turbulent flow

Sternberg (1968) used a similar classification but for the sea, and produced boundary values of 5.5 and 165.

The structure of the boundary layer and the nature of the flow, whether it is laminar, smooth turbulent or rough turbulent, depend on the roughness of the bed and how the bed elements interact with the flow. Due to its infrequent occurrence in natural flows, laminar flow can be disregarded. The boundary layers of smooth and rough turbulent flows have slight differences.

The boundary layer can described in three parts; the viscous sublayer, the logarithmic layer and the outer layer. The zone close to the wall, thickness 0.1-0.2d, is assumed to have a constant shear stress with height, and the flow in this inner/wall region is not directly affected by external conditions. Due to the importance of viscosity in this zone it is termed the viscous sublayer and flow, although not laminar, has a mean longitudinal velocity profile. Above the viscous sub-layer there is a buffer layer, above which is the logarithmic layer. This is fully turbulent and has a logarithmic velocity profile with height, and eddies generated in this layer can cause disturbances in the viscous sub-layer.

In smooth turbulent flow the viscous sub-layer is of the order of a few millimetres in thickness, and the roughness elements are submerged within this layer and do not affect the flow. However in rough turbulent flow the roughness elements project into the flow and viscosity is no longer important. The viscous sub-layer and the buffer/transitional zone are not present thus allowing the log layer to extend below the tops of the roughness elements. The nature of the flow, as shown by the Reynolds number, is also related to flow velocity. This results in a thining of the

viscous sublayer and a trend towards rough turbulent flow with increasing flow velocity.

The remaining 80-90% of the boundary layer, above the logarithmic layer is termed the outer layer. This layer is highly affected by external conditions, with the flow dependent on wall shear stress but independent of viscosity. The shear stress and turbulence energy diminish towards the top of the boundary layer, where free stream flow occurs. However if the depth is limited then the boundary layer may not be able to develop fully and the free stream velocity will not be reached.

The nature of the turbulent boundary layer means it has a memory. That is, a change in the velocity profile caused by a change in bed roughness will generate a new boundary layer, called the internal boundary layer, which will thicken down stream. The inner layer of this internal boundary layer adjusts rapidly to the new roughness, while above it the new profile merges into the remaining part of the old upstream profile.

With a transition from smooth to rough surfaces the velocity near the bed decreases, the velocity gradient steepens causing increases in U_* and the roughness length. The leading element of this surface (new roughness) will experience a higher shear stress than the elements further down-stream, due to the leading element being the most exposed. A change in roughness of rough to smooth has the opposite affect. The near bed velocity increases, the velocity gradient becomes less severe causing U_* and the bed roughness to decrease. Also the leading element of this new bed regime is sheltered by the rougher up-stream bed elements and will therefore suffer less shear then those elements further down-stream.

The logarithmic layer can be defined by the von Karman-Prandtl equation,

$$\frac{U}{U_*} = \frac{1}{k} \ln \frac{Z}{Z_0} \qquad (2.8)$$

where k is known as the von Karman constant and has a value of 0.4 in the marine environment, and Z_0 is the roughness length. This equation can be

used to determine U_* and the bed shear stress. A plot of U against the lnZ will give a straight line.

However, more likely than not the velocity profile is likely to form a curve, which once extrapolated may give an incorrect bed shear stress. These variations can be caused by a number of disturbing effects which include:

acceleration and deceleration of the flow.
variations in upstream roughness.
bed forms.
stratification in the water due to suspended sediment
inexact determination of the current meter array zero datum
waves.

It is possible to predict the bed shear stress by a number of methods. One is by use of the quadratic stress law,

$$\tau_0=\rho C_D U^2 \qquad (2.9)$$

here C_D is the drag coefficient. In sediment transport the equation is modified to,

$$\tau_0=\rho C_{100} U_{100}^2 \qquad (2.10)$$

where U_{100} is the velocity 1m or 100cm above the bed, C_{100} is usually greater then C_D. Substituting equ (2.5) into equ (2.10) gives,

$$U_*^2=C_{100} U_{100}^2 \qquad (2.11)$$

C_D can be related to Z_0 by using the logarithmic profile. Substituting equ (2.11) into the profiles at Z=100cm, produces,

$$C_{100}=\left[\frac{k}{\ln\left(\frac{100}{Z_0}\right)}\right]^2 \qquad (2.12)$$

Using this it is possible to assign appropriate values of C_{100} and Z_0 to a bed provided its nature is known, see Table 2.1.

For smooth turbulent flow Z_0 can be related to the flow. Chriss and Caldwell (1984) gave the following definitions,

in the lab $Z_0 = \upsilon/9xU_*$

Bottom type	Z_0 (cm)	C_{100}
Mud	0.02	0.0022
Mud/sand	0.07	0.0030
Silt/sand	0.002	0.0014
Sand(unrippled)	0.04	0.0026
Sand(rippled)	0.60	0.0061
Sand/Shell	0.03	0.0024
Sand/gravel	0.03	0.0024
Mud/sand/gravel	0.03	0.0024
Gravel	0.30	0.0047

Table (2.1): Bed roughness lengths and drag coefficients for typical seabed types, (after Soulsby 1983).

in the field $\upsilon/272xU_* < Z_o > \upsilon/4xU_*$

For rough turbulent flow Z_0 can be related to the grain diameter,

for pipe flow $Z_0 = D/30$ Nikuradse (1933).

for channel flow $Z_0 = D/15$ Kamphuis (1974).

2.2.5. Turbulence and Bursting Phenomena.

Observations of the stresses at the boundary, (Nychas et al., 1973; Offen and Kline, 1975) have led to the recognition that the Reynolds stress is produced intermittently and associated with turbulence and a phenomena collectively called bursting, with the major contribution generated by interactions between the positive and negative variations in the x and z directions.

Four types of u'w' events occur, up and down accelerations, and bursts and sweeps. Weak up and down accelerations events occur for 2-5% of the time, sweep and burst phenomena occur for 10-13% of the time, and the flow is quiescent for the remaining 85% of time. Bursts and sweeps make a large contribution to the net stress with bursts making the largest, and their intermittent nature means that 90% of the stress is accounted for in 20% of the time (Soulsby, 1983).

The bursting cycle starts with a transverse vortex rotating with the flow, initiated by a low velocity streak. In rough turbulent flow separation in the lee of an obstacle may create the vortex. In flows with a viscous sub-layer, where low and high velocity streaks occur, the vortex is formed by re-circulation under a streak which has been lifted up by a disturbance. The passage of the leading edge of the cell produces the sweep and the trailing edge the burst. The vortex develops across the streak and moves downstream with the flow, moving upwards and bending forwards as it goes, with the streak below it decelerating and rising up. The vortex is usually inclined at 16 to 20° to the horizontal and travels at 80% of the average flow velocity, developing a hairpin or horse shoe shape and being continually stretched by the velocity gradient as it moves. The final stages are determined by two almost simultaneous but different actions: 1) the occurrence of a sweep, the downward movement of a parcel

of high speed fluid which spreads down stream and sideways; this sweep may go straight between the limits of the vortex or destroy them. 2) the vortex head bursts as its internal motion becomes disordered and fluctuates rapidly (Figure 2.2). Some of these features have been observed: the presence of a sweep at the site of a low speed streak (Grass, 1971) and the coherent remains of the vortex far out into the flow (Head and Bandyopadhyay, 1981)

The bursting phenomena contribute to the Reynolds stress, with the sequence of events in the bursting processes, i.e. ejections, sweeps and interactions, being directly related to the turbulent energy budget in the from of turbulent diffusion, and the sweeps appear to be more important than ejections as the bed roughness increases (Nakagawa and Nezu, 1977). The contribution of bursting phenomena to the Reynolds stress and its affect on sediment erosion under various conditions has been studied by a number of authors (Kline et al., 1967; Corino and Brodkey, 1969; Rao et al., 1971; Grass, 1971; Brodkey et al., 1974; Gordon, 1974; Karcz and Shanmugam, 1974; Heathersaw, 1979; Nakagawa and Nezu, 1981; Allen, 1985b; Shino and West, 1988; Thorne et al., 1989; Clifford, 1990; French and Clifford, 1992).

2.2.6. **Sediment movement.**

Most work has been carried out on the movement of non-cohesive grains larger then 0.0625mm. Using equations(2.1) and (2.2) for the forces acting on a grain, and the Reynolds number it is possible to generate a relationship between flow and the threshold of motion,

$$\frac{\tau_c}{(\rho_s-\rho)gD}=f(Re_*) \qquad Re_*=\frac{DU_*}{\upsilon} \qquad (2.13)$$

The left hand side of this equation is the Shields entrainment function, θ, and its threshold value θ_c; it relates the threshold shear stress with the immersed unit weight of a unit grain layer of the bed. The other side of the equation is the grain or boundary Reynolds number. Shields (1936) used this to generate a threshold curve (Figure 2.3), which has been adapted and modified by further investigations particularly in the low Reynolds

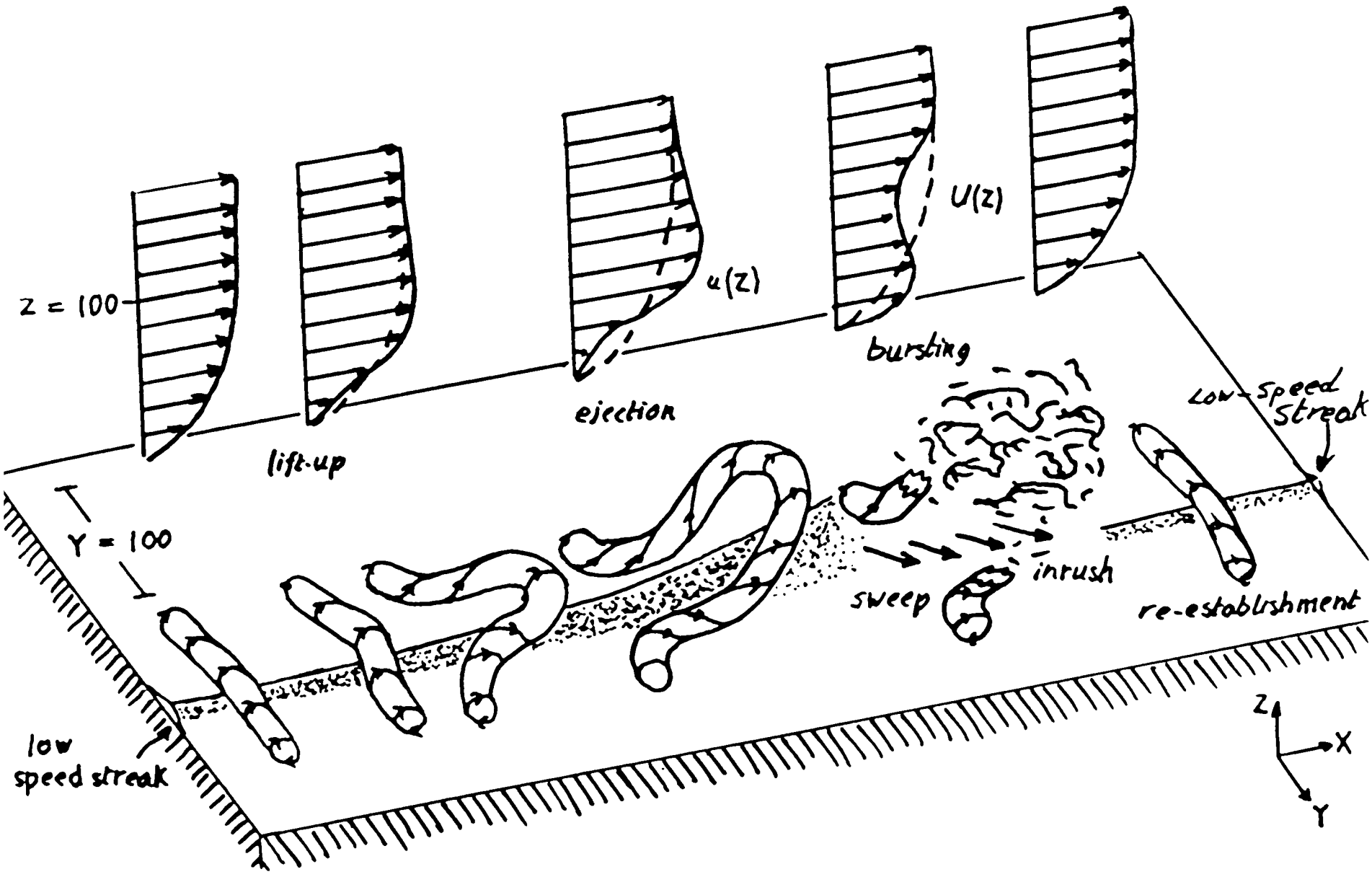

Figure (2.2); Model of the streak bursting cycle. The developing hairpin vortex is shown as it might be seen by an observer travelling with it. The velocity profiles are plotted with respect to the ground (after Allen 1985).

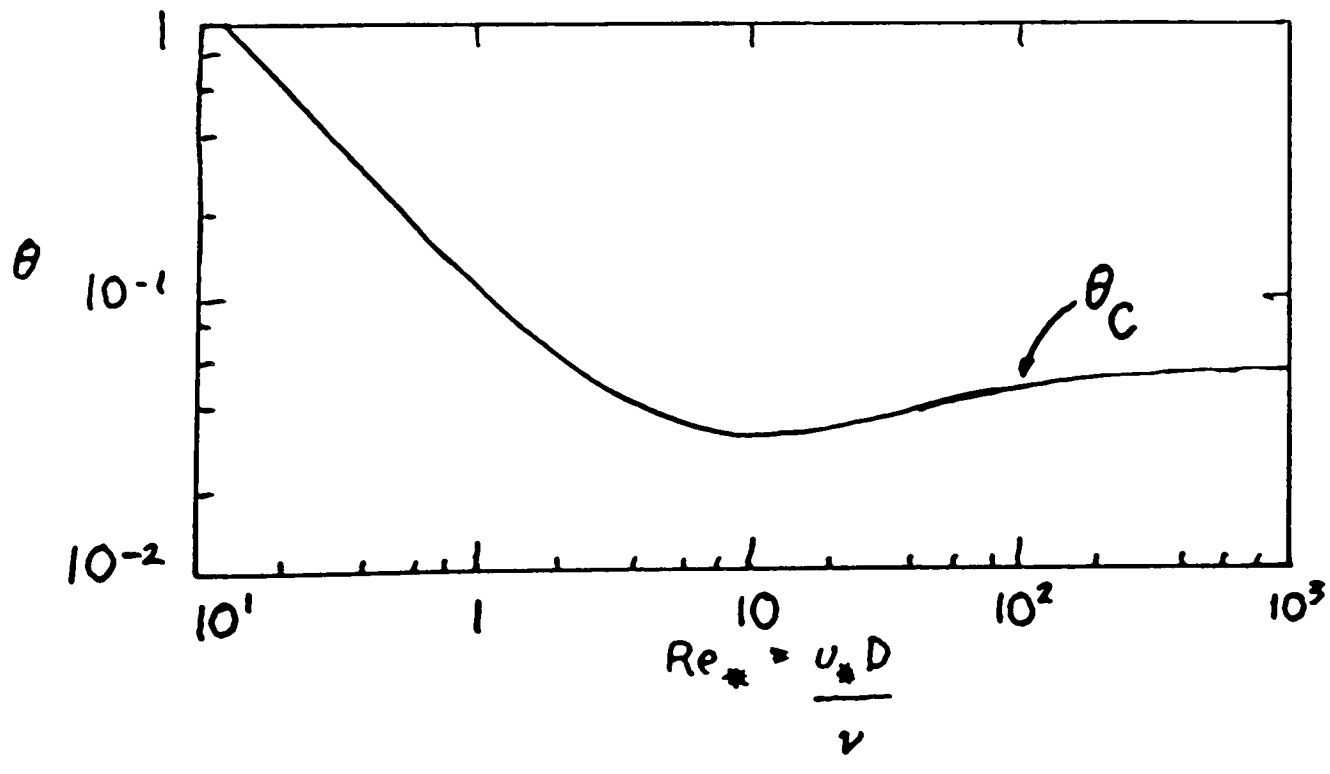

Figure (2.3); Shields threshold curve.

number regime. Miller (1977) expanded the Shields curve to include work on uniform steady flows over flat beds in open flume tanks with parallel side walls. Yalin (1979) combined his own work on the inception of motion under laminar and turbulent flow with results of other previous workers to produce an extended Shields curve (Figure 2.4). The critical axis values are defined by,

$$X_{Cr} = \frac{(\upsilon_*)_{Cr}}{\upsilon} = \frac{U_* D}{\upsilon} = Re_* \qquad (2.14)$$

$$Y_{Cr} = \frac{\rho U_*^2}{(\rho_s - \rho_g)} = \frac{\tau_0}{(\rho_s - \rho) g D} = \theta_c \qquad (2.15)$$

These definitions all use the grain diameter to define the erosion threshold of sediments, but this is inappropriate for fine grained sediments. In estuarine and coastal environments, fine-grained sediments form a continuum of particle sizes with differing erosion thresholds, that vary depending on the sediments complex interaction in the physico-chemical and biochemical characteristics of the environment (Carson et al., 1988; Reynold and Gorsline, 1992). The main disadvantage with using individual grain diameter comes from the bed's increased hold on grains caused by interparticle cohesion, which adds to the gravity force and alters the grain density. Although this results in increased threshold values (so that the left hand end of the Shields curve moves upwards) it is not directly caused by decreasing grain size. Therefore some other formula, using values including grain size, water content and á measure of cohesion, should be used to express sediment properties.

2.2.7. **Turbulent Bursting in Sediment Transport.**

Turbulent bursting phenomena appear to play a part in sediment movement. Sutherland (1967) noted the intermittent bursts of grains from the bed. He connected these bursts with the affects of turbulent eddies disrupting the viscous sub-layer and impinging directly on the bed. Many parts of his model coincide with features of the bursting phenomena. The effect of bursting phenomena on ejecting material upwards has been noted

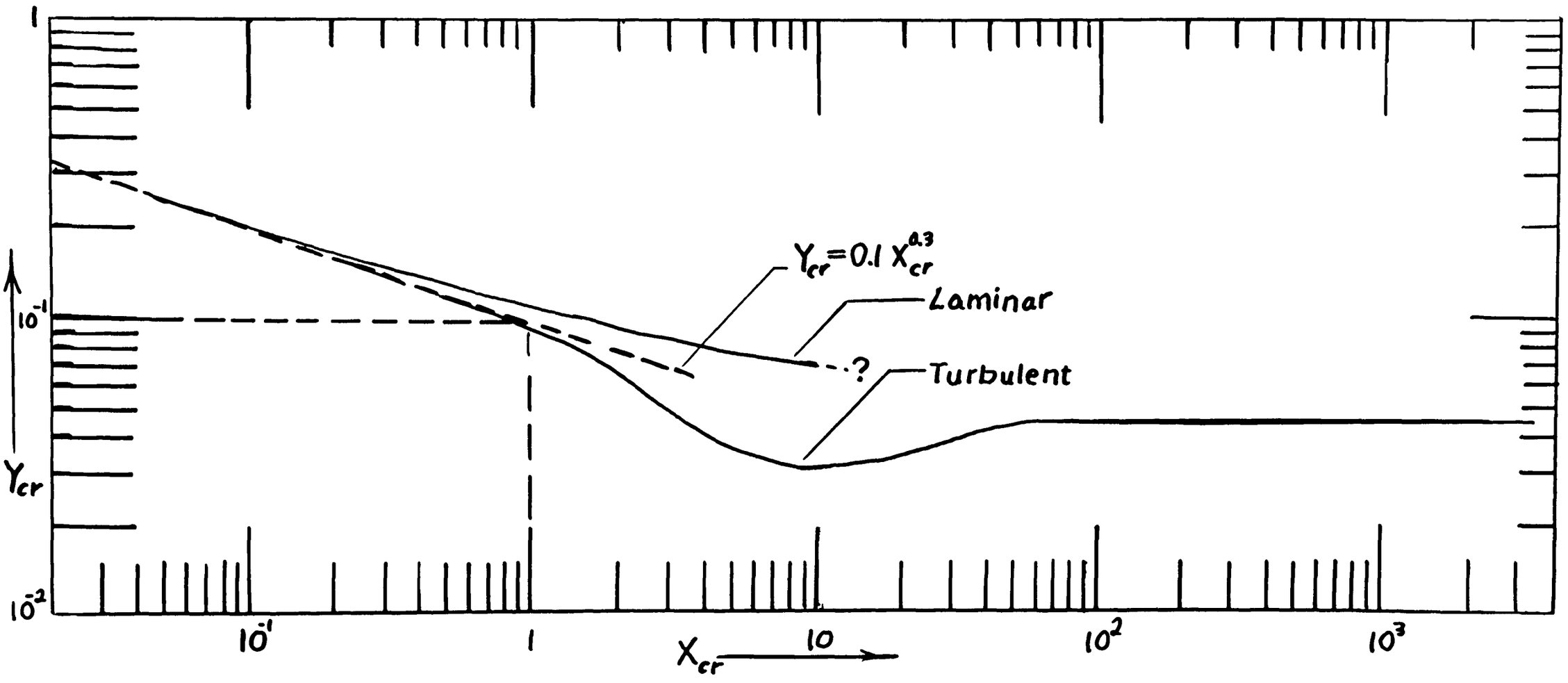

Figure (2.4); Transport inception curves (after Yalin and Karahan 1979).

by a number of workers, Jackson (1976), Sumer and Oguz (1978), Sumer and Deagaard (1981) and Heatherson and Thorne (1985).

Sumer and Oguz (1978) proposed that a burst passing over the bed causes a temporary local adverse pressure gradient which causes the particles to lift off. Bursts adjacent to a smooth boundary can generate pressure fluctuations of up to three times the mean pressure (Willmarth, 1975) and alternatively between three and nine times the horizontal bed shear stress (Bull and Willsi, 1961; Raudkivi and Tan, 1984). The hydrostatic pressure fluctuations associated with a burst can cause localised and instant variations in pore pressure of the sediment. As the burst and its associated pressure peak decay and are advected downstream the peak is replaced by a pressure trough, and the reduced hydrostatic pressure of the trough and the excess pore pressure can increase the ability of the flow to lift particles. The rise of the particle is strongly controlled by the bursting flow structure, which enters the main body of the flow together with the particle. As the burst flow structure deteriorates the particle begins to fall back towards the wall, where it is likely to be entrapped in another burst.

The amount of work relating these bursting phenomenon to cohesive sediment entrainment and suspension is limited, but the rapid pressure fluctuations that occur can result in changes to the sediment surface and may be responsible for the intermittent floc aggregates (Grass, 1970). It has been observed that the network of floc aggregates at the sediment-water interface acts like the 'skin of a drum under static vertical stresses (Paterson, 1989) and that the floc aggregates are deformed before they break up (Parker et al., 1972; Black, 1991; Al Ani et al., 1991). The idea that variation in pore pressure, associated with bursting phenomenon, affects the structural integrity of near-surface floc aggregates (Ross and Mehta, 1990), may imply that tensile forces instead of tangential drag forces are of more importance to the erosion processes (Peirce et al., 1970).

The irregular high energy nature of bursting phenomenon is likely to cause the entrainment of much coarser particles then the average flow velocity alone could accomplish. The observations of large flocs in

suspension against a back ground of finer material at low bed stresses (Black, 1991) and clouds of suspended sediment in shallow tidal environments (Kuo et al, 1978; Vincent et al., 1981; van Leussen, 1988) can be associated to this process.

Heatherson and Thorne (1985) studied bed load motion of sea bed gravel, which they considered was caused principally by sweep type motions and to a lesser extent by outward interactions. If gravel is considered to have a high bed roughness, then these results support those of Nakagawa and Nezu (1977) (previously mentioned), who believed that sweeps become more important then bursts with increasing bed roughness. This observation can be explained if it is assumed that form drag rather then shear stress is the principal cause of gravel movement. This is for motion of the coarser size fractions, but the movement of finer material is affected more by the turbulent bursting processes then by sweeps.

2.2.8. **Non-cohesive Fine Grain Motion.**

Recent investigations into the threshold of movement for fine grain non-cohesive sediments has allowed the Shields curve to be extended. The incorporation of fine grain granular material into the Shields curve has already been defined (Miller 1977). However, fine flaky grains do not conform to this curve; that is the Shields curve cannot be used to determine the threshold of motion for fine flaky grains. Mantz (1977) reported that depending on the length scale used, the data points for flakes either appears above or below the curve for grains. The affect of flow over beds made of fine granular and flaky particles has been investigated by Mantz (1978) and Ress (1964). Ress (1964) used a re-circulating flume and a sediment of washed, well sorted sub-angular 10μm mean diameter (90% in the range 6-18μm, very fine and fine silt range) fragments of quartz and feldspar. At low stress the bed was stable with no movement. At an intermediate stress and with excess sediment in suspension, a primary ripple system was formed whose form was governed by the stress. At high stress values a secondary ripple system formed, but this had a higher and more irregular relief then the primary system. However in both the intermediate and high stress ranges the removal of the

suspended material results in the bed returning to its plane form. He decided that the interaction between the fluid and the sediment was initially viscous. Mantz (1978) looked at the affects of sub critical flows on uniform grains 15-66μm diameter (medium to coarse silt) and micaceous flakes 15.5-76μm (medium silt to very fine sand). He observed that in the granular material, bed-forms, primary ripples, secondary ripples and possibly dunes are formed. For flakes only the single bed form type of parting lineations are observed, generated by streaks in the viscous sub-layer of the smooth turbulent boundary. At higher flow rates the lineations begin to oscillate and eventually enter suspension, possibly caused by low velocity streak bursts.

2.3. **Cohesive Sediments.**

2.3.1. **Introduction.**

As already stated the main kinetic unit of fine-grain marine sediments is the floc, instead of the individual grain. These flocs, of about 40μm diameter (Owen, 1976), form the sediment. Its is the cohesive nature of the flocs and their constituent particles that results in the cohesive behaviour of the sediment. Hamilton (1971) defined cohesion as 'the resistance to shear stress that can be mobilized between adjacent, fine particles that stick, or cohere, to each other. It is considered to be an inherent property of fine grained, clayey sediments that is independent of stress; it is caused by physio-chemical forces of an interparticle, intermolecular, and intergranular nature'. The cohesion of the flocs allows them to bind together to form floc aggregates, which also bind to each other to form floc aggregate networks (Mallik et al., 1988; Partheniades, 1990) which display a 3-dimensional structure with measurable effective stress and displaying plastic and elastic behaviour in concentrations exceeding ~150-200gl^{-1} (Granboulan et al., 1989). It is this cohesion and the complexity of parameters and process affecting the floc properties that creates the complex nature of the bed. This complexity means that it is very difficult to predict the behaviour of the sediment bed and even with a growing body of work, research into the transport processes of cohesive

marine sediment (of which erosion is a part) still lags behind that of its non-cohesive counterpart (Black, 1993; Raudkivi, 1990; Teisson, 1991).

2.3.2. Cohesive Sediments, Size Distribution and Clay Mineralogy.

The main measure used to define the particulate character of a sediment and its division into sub-fractions is the size of the grains. The most commonly used scale is the Udden Wentworth scale (Wentworth, 1922) conventionally expressed on a logarithmic scale proposed be Krumbien (1934),

$$\text{phi} = -\log_2(\text{diameter in mm}).$$

The shape of the grains is also important and is defined by the sphericity and roundness of the grains.

In a very basic way the silt, sand and larger size fractions of a terrigenous sediment are made up of the mechanical erosion products of rocks. These grains are small fragments of rock, that have been formed by the abrasive action of larger particles. However the clay minerals which constitute the clay fraction are the products of the chemical weathering of rock.

Estuarine and marine sediments occur as mixtures of silts, sands and clays and range in texture from fine clays to muddy sands (McCave, 1981). The silt, sand and larger fractions of a sediment are usually chemically inactive and non-cohesive. It is the amount and type of clay material present that determines the cohesive nature of a sediment. It has been suggested that 10% clay fraction by weight is a minimum above which cohesion results in profound changes of sediment properties (Raudkivi, 1990). Generally the greater the clay content the more cohesive the sediment (Pierce et al., 1970; Grissinger et al., 1981; Fukuda and Lick, 1980) and the clay content displays an inverse relationship with the erosion rate (Kuti and Yen, 1976; Fukuda and Lick, 1980; Amos and Mosher, 1985).

The boundary between the clay and silt fractions is a size distinction and not a chemical one. Although most of the clay size fraction is made up of clay minerals, not all particles less then 3.9µm or >8phi are cohesive or clay minerals; they can be very fine grains of other materials. The opposite is also true, clay mineral particles can occur in sizes greater then 3.9µm or coarser than 8phi, and will therefore be termed as silt on the basis of size alone. However most of the clay minerals particles are smaller then 3.9µm and fall into the clay size fraction.

Although clay-sized sediments do not occur on their own, except in caves, very deep seas and lakes (Allen, 1985b), it is necessary to consider them in isolation in order to outline their properties and characteristics because of their major affect on the overall properties of sediments in which they are present.

2.3.2.1. **Clay Mineralogy.**

The clay minerals found in fine sediments are powdered fragments of the detrital clay minerals, predominantly kaolinite, illite, chlorite and montmorillonite (smectite) plus mixed layer clays (Biddle and Miles, 1972). They have specific densities in the range 2600-3000kgm^{-3} according to species, and display large surface areas of the order $10^4 m^2 kg^{-1}$ (Black, 1993). These mineral particles when dispersed in a liquid form colloidal suspensions, where the surface physicochemical forces acting between particles are equivalent to the gravity force acting on individual particles. These colloidal systems of homogeneous dispersions of very small particles, where no appreciable sediment deposition occurs within still water over long periods of time (Nelson, 1959; van Olphen, 1977), are therefore distinct from sediment suspensions in which deposition does occur (Partheniades, 1965).

The clay minerals are hydrated silicates of aluminium and /or iron and magnesium (Grim, 1961) and are made of two basic units, the silica tetrahedral unit and the aluminium octahedral unit. These combine in various ways, incorporating other elements to produce the wide variety of clay minerals. The silica tetrahedron is made up of a silicon ion at the

centre of a tetrahedron of four oxygen ions. These combine to form silica sheets with the oxygen ions at the base of each tetrahedron shared between two tetrahedron (Figure 2.5). The other basic unit is the octahedral unit. This is constructed of an aluminum ion surrounded by six hydroxyl ions in an octahedral configuration, this again forms into sheets by sharing hydroxyl ions (Figure 2.6).

In the simplest clay mineral Kaolinite, a silica sheet combines with one sheet of octahedral units. The tips of the silica tetrahedrons combine with one of the surface layers of the octahedrons units to form a common layer. Two thirds of the atoms in this layer are shared by the silica and aluminum ions and these become oxygen ions instead of hydroxyl ions. Because the structure should be ionically balanced the aluminum ions only fill two thirds of the octahedral sites (Figure 2.7). This two layer kaolinite unit is approximately 7Å thick, and these leaves form regular stacks with each leaf bonded to its neighbour by hydrogen bonds. Hydrogen bonds are made from a hydrogen which is strongly attracted to two other atoms generating a bond that is much stronger then Van der Waals simple attractive forces. Because of its balanced structure, lack of adsorbed cations and lack of inter-layer elements kaolinite is one of the most inert and stable clay minerals. At the other extreme is montmorillonite one of the most unstable and active clay minerals. This mineral is made up of a layer of octahedral units sandwiched between two sheets of silica tetrahedrons (Figure 2.8). These sheets are 9.5Å thick and combine with other sheets although in this case the sheets are bonded together by exchangeable cations and water. The cations are attracted to and neutralize the negative charges on the sheets surface, but they are susceptible to swelling and water desorption, therefore the bonds are not very strong. This type of bonding is also used to join different clay minerals to each other.

The basic formula for kaolinite and montmorillonite without any substitution or other structural disturbances are,

Kaolinite	$Al_4Si_4O_{10}(OH)_8$
Montmorillonite	$Al_4(Si_4O_{10})_2(OH)_4$

The activity of a clay mineral is controlled by a number of features. These include how ionically balanced the structure is; this can vary due

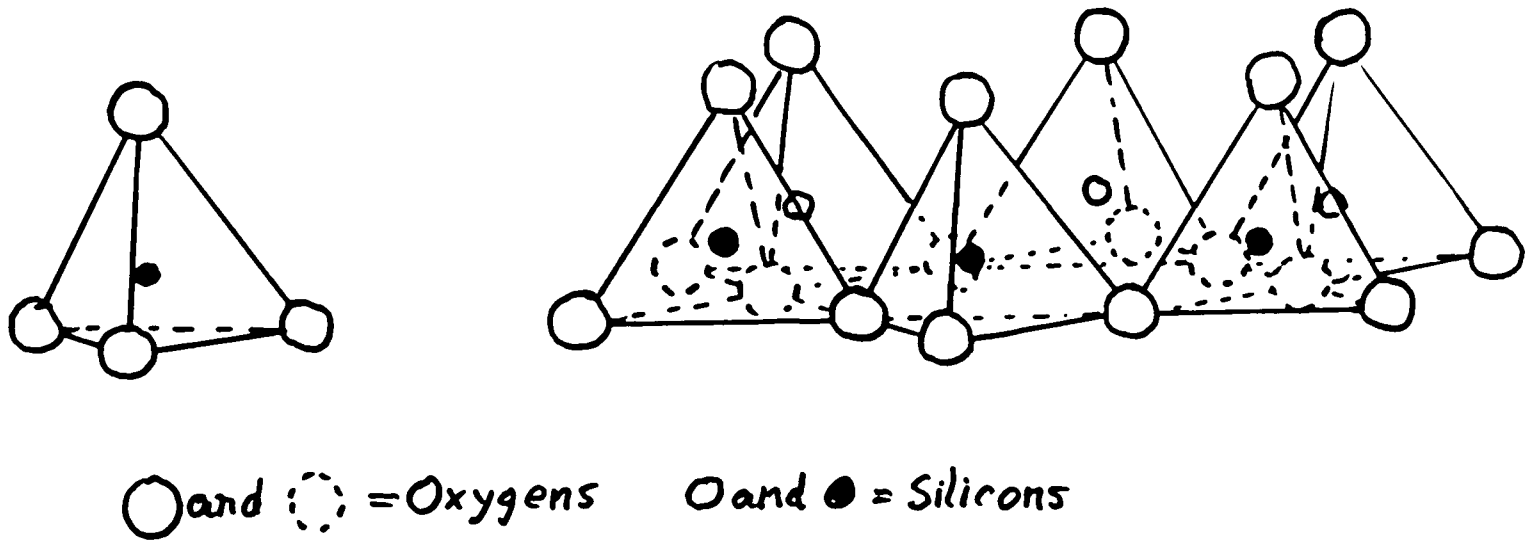

Figure (2.5); Diagrammatic sketch showing the single and sheet structure of the silica tetrahedrons units (Grim, 1953).

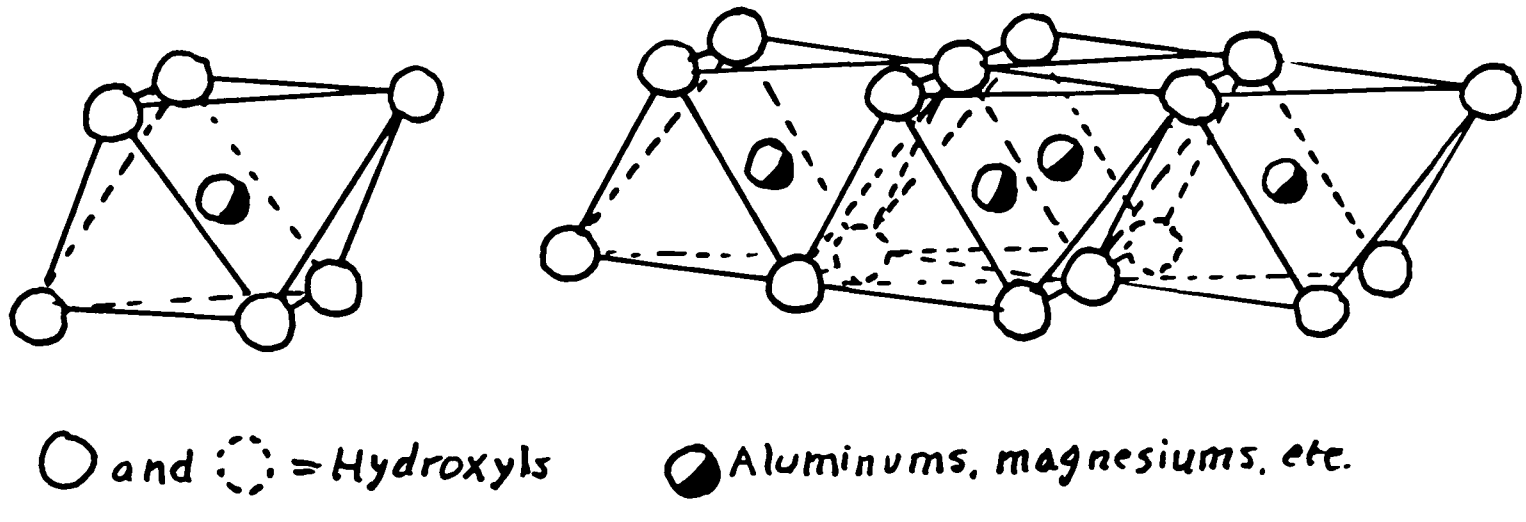

Figure (2.6); Diagrammatic sketch showing the single and sheet structure of the aluminium octahedral units (Grim, 1953).

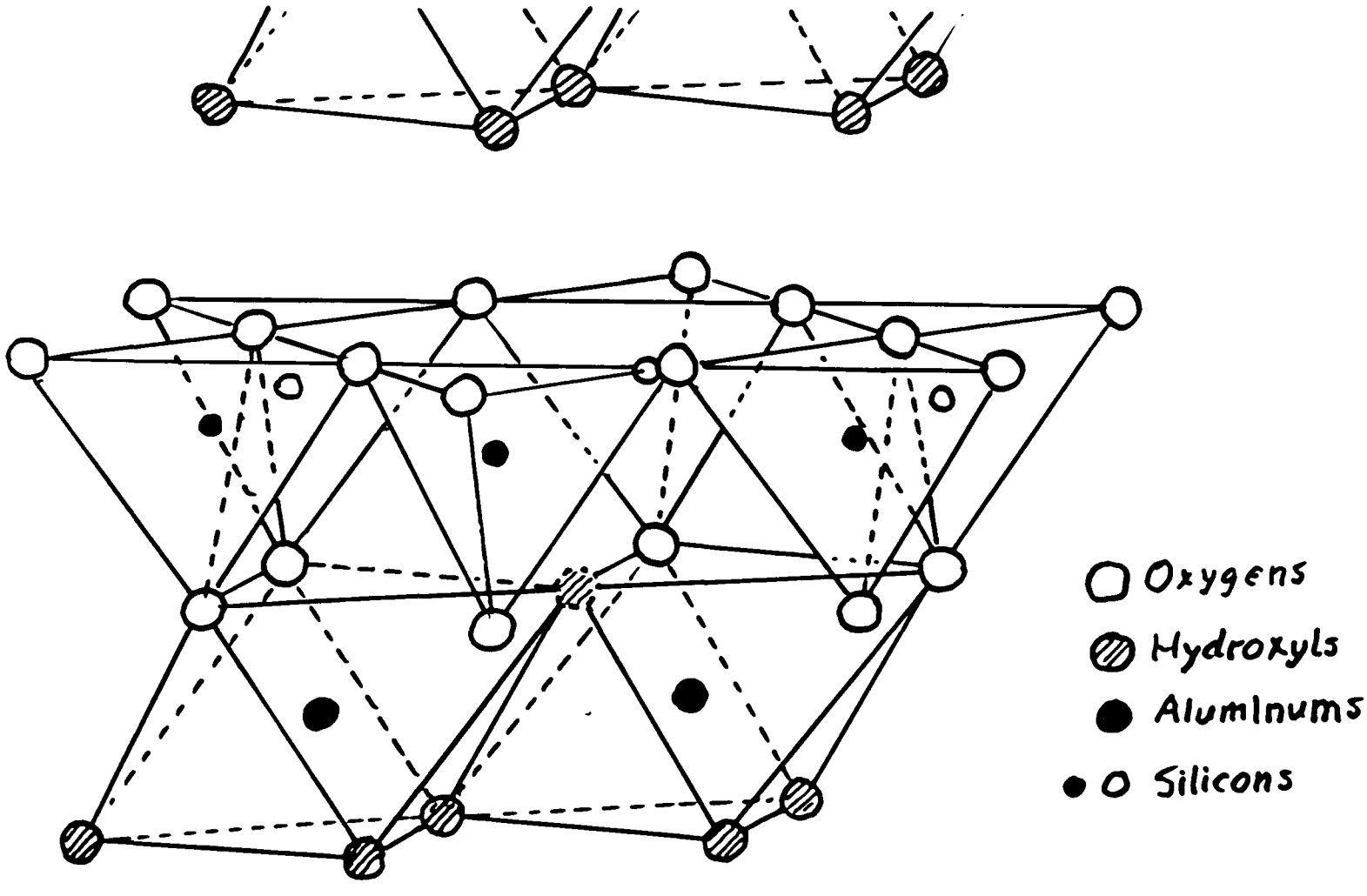

Figure (2.7); Diagrammatic sketch of the structure of the kaolinite layer (Grim, 1953).

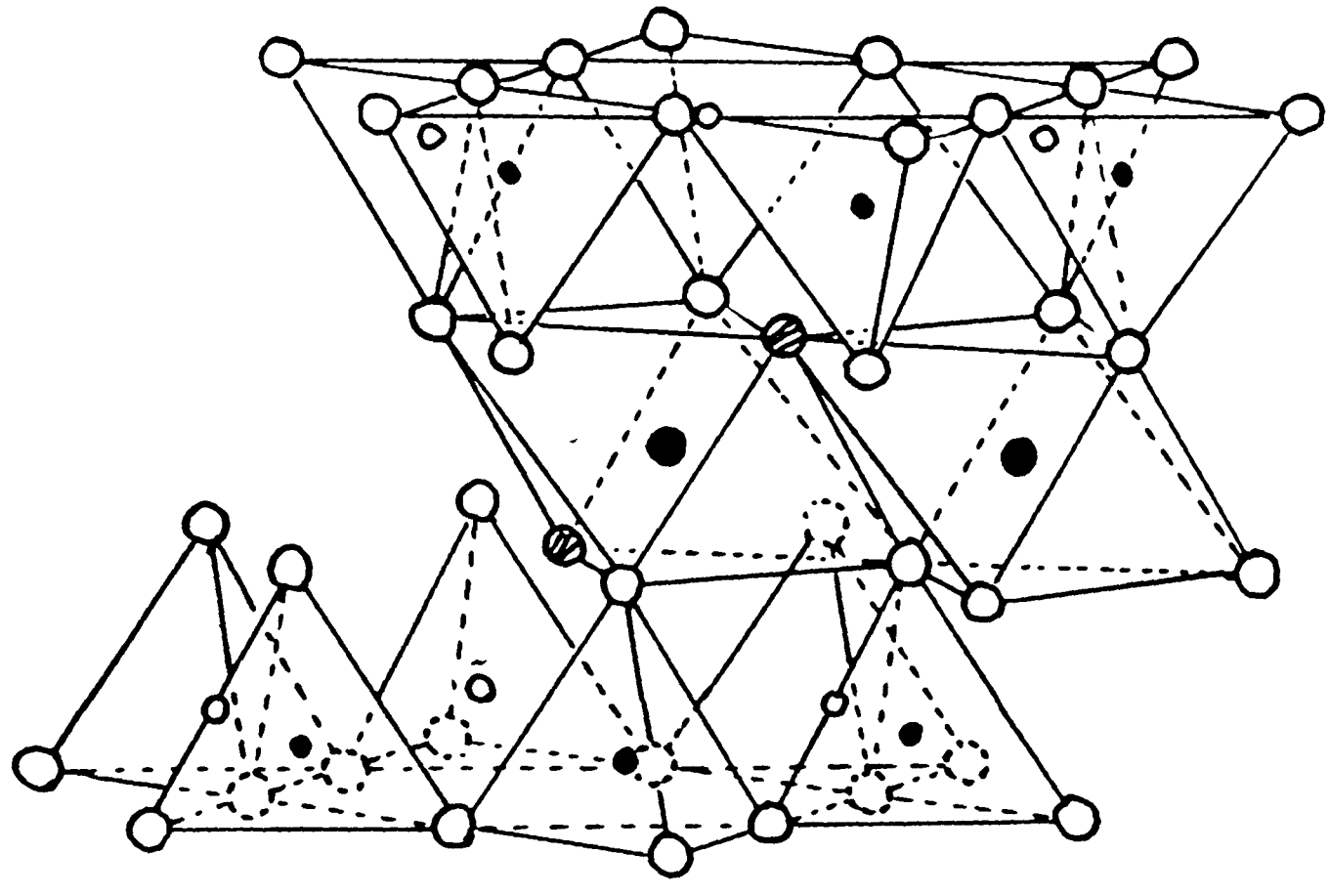

Figure (2.8); Diagrammatic sketch of the structure of montmorillonite (Grim, 1953).

to substitution of other ions into the octahedral site instead of the aluminum, eg. magnesium and iron. It also depends on the type of medium surrounding the clay mineral. The type of material bonding the layers together can be exchanged or hydrated causing the structure to expand or contract. There are other forces between clay minerals the most basic of which are Van der Waals forces (van Olphen, 1977), which are omnidirectional, attractive forces generated between atoms. Although they decay rapidly with distance (as they vary inversely with the square of the distance of separation between particles) and are therefore only affective at short distances, they are the main cause of flocculation in the clay minerals.

The clay particle can generate forces of its own which can be either attractive or repulsive. These forces are caused by a net imbalance of charge in the clay particle. This can be caused either by substitutions of a lower valency ion into the structure in place of a higher valency one resulting in an excess of negative charge, eg. Mg^{2} for Al^{3} in the octahedral sites or by the absorption of so called stabilizing ions, either negative or positive on to the structure. Usually negative ions are adsorbed on the surface and positive ions onto the edges of the clay structure. In kaolinite, hydrogen ions are absorbed onto the edge of the lattice to balance the charge and the point at which the end of the lattice has no overall charge is called the 'point of zero charge', PCZ, also called the 'isoelectric point', IEP. The pH of the surrounding fluid will determine to what extent these counter ions are absorbed onto the lattice.

The strength of the negative charge on the surface of a clay particle is measured by its ability to attract cations to neutralize the negative charge. This is known as the 'cation exchange capacity, CEC', which is defined as the number of cations absorbed per unit weight, measured in meq/100g or eq/kg (meq are milli-equivalents). Typical CEC values, Taylor (1961),

Kaolinite	3-8 meq/100g
Montmorillonite	80 meq/100g.

The affinity of exchangeable cations, called counter ions, depends on a number of properties including concentration and cation nature which is proportional to the electrostatic attraction.

Due to the nature of their charged surfaces, clay particles in water attract a layer of oppositely charged ions, 'counter ions', around them. These counter ions will position themselves around the clay particle to form a layer of counter ions. The thickness and profile of this layer is governed by a number of factors including, the balance between electrostatic repulsive and attractive forces and the diffusion due to thermal motion that would give a uniform chemical potential. The density of positive charge decreases continuously and exponentially outward from the surface of the particle (Southard, 1974), and this electrical arrangement and the charge gradient is the so-called 'diffuse double layer', with the net effect of reducing the magnitude of the negative charge on the particle (Black, 1993) and it plays an important role in the properties of clay suspensions and deposits (Figure 2.9). The electrically neutral system of the clay particle and its double layer are known as the 'clay micelle', and the way in which this double layer interacts with the other forces of the clay minerals will determine how the particles behave towards each other and as a whole.

In suspensions of very small particles, Brownian motion is responsible for keeping the particles suspended. However as flocculation occurs large flocs are likely to settle to the bed. As particles approach each other they exert forces onto each other, and a simple model of this can be created by looking at the interaction of two particles (Figure 2.10a).

Repulsive forces:

(1) interaction of the diffuse double layer.

(2) adsorbed water on the lattice surfaces must be expelled.

(3) inter-penetration of the lattices.

Attractive forces:

(1) mass to mass.

(2) Van der Waals.

If a stable suspension is heated flocculation will occur. The heating contracts the diffuse double layer, due to ions being removed by increased diffusion from thermal motion, which causes a contraction of the repulsion curve that will eventually result in flocculation (Figure 2.10b). The diffuse double layer can be caused to contract in other ways, eg. by increasing

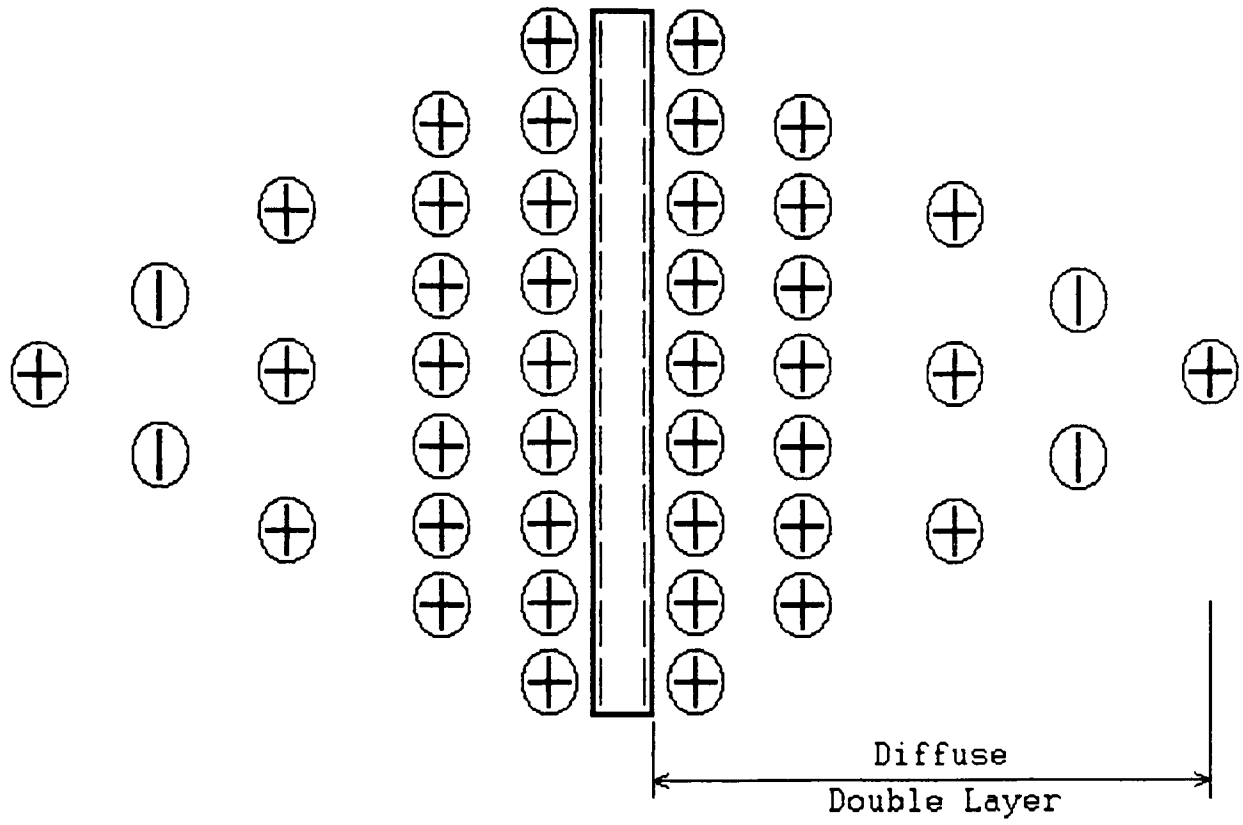

Figure (2.9): The clay micelle (Partheniades, 1971).

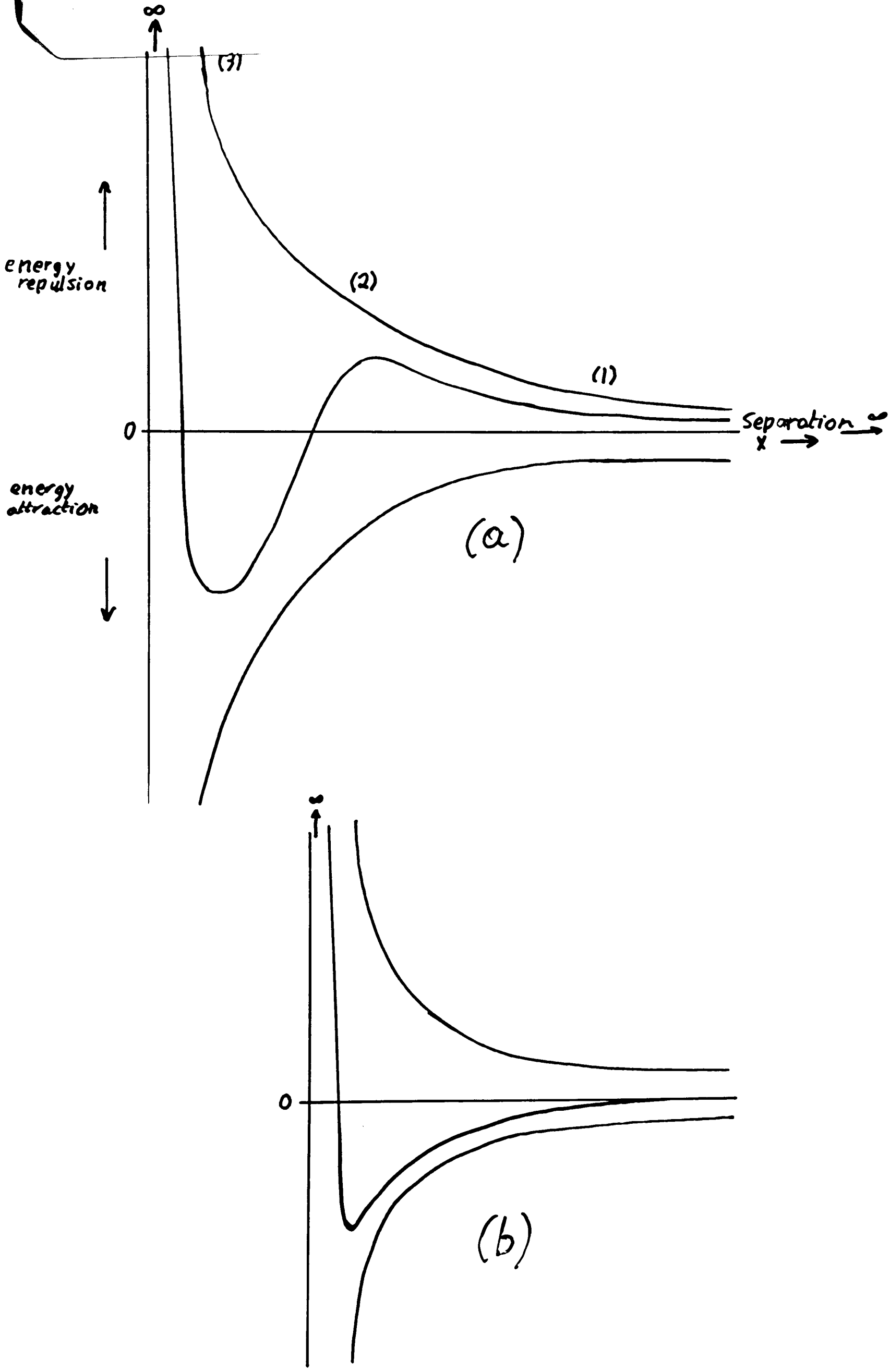

Figure (2.10); Interaction of forces between two clay particles.

either the charge z (electrostatic attraction) or the cation concentration. If no flocculation occurs a disperse deposit is formed.

The various clay minerals range in reactivity and their degree of cohesion (Beutelspacher and van der Marel, 1968; Hamilton, 1971; Biddle and Miles, 1972; Das, 1983). Kaolinite is the most inert of the clay minerals, illitic clays are intermediate and montmorillonite the most cohesive and plastic. Montmorillonite is also most reactive in its ability to attract counter-ions and it can swell considerably on absorbing water which can increase susceptibility to erosion (Postma, 1967; Partheniades, 1971; Allen, 1985b).

2.3.3. **Suspensions and Flocculation.**

Gust and Walger (1976) investigated the influence of suspended cohesive sediment on the boundary layer. They suggested that flows transporting cohesive sediments may have a non- Newtonian flow structure and therefore values of U_{*crit} and rate of erosion would need to be reviewed. Clay minerals entering suspension change the kinematic viscosity of the fluid and thereby alter the tractive force (Martin, 1962). The interaction between turbulent shear forces in the flow and the deformation of aggregates causes a reduction in turbulent drag. Measurements of Gust (1976) indicate that this turbulent drag reduction occurs at eroding and non-eroding velocities and aggregation of suspended clay-mineral particles is suggested as a possible explanation of this phenomena.

In water, clay particles tend to form flocs depending on the conditions (Figure 2.11). In salt water the particles join together randomly and van der Waals forces are the main control on bonding. In non salt water, low cation conditions, the particles join to form a card house structure. This is caused by the electrostatic attraction between negatively charged faces and positively charged edges, this being the main control on bonding. Remoulding or repeated shearing deformation will result in a disperse structure. This disperse structure, lack of flocculation, can also result from the settling of clay particles out of a suspension one by one

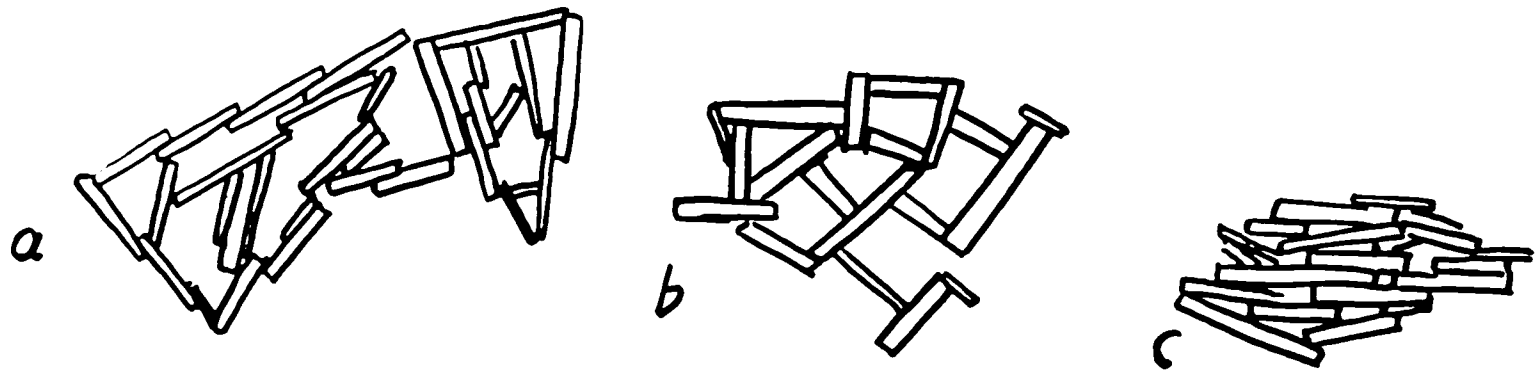

Figure (2.11);Sediment Structures: (a) Salt flocculation. (b) Non-salt flocculation. (c) Dispersion. (Partheniades, 1971)

Figure (2.12); Schematic structure of flocculated bed as it alters with consolidation. (a) Loosest state, flocs grouped into floc aggregates form an aggregate network. (b) Bonds between aggregates are broken and overall clay density increases, but the original aggregate density is still maintained. (c) Aggregates broken up, overall clay density increases while still maintaining the original floc density. Finally with further consolidation the inter-floc voids will disappear and the entire bed density will equal the original average floc density, with more consolidation from then on resulting in a decrease of the interparticle spaces (Partheniades, 1965).

without flocculation occurring. The size of the flocs is determined by the fluid shear stress. If the shear stress is high then only small flocs will form; any large flocs formed will be pulled apart by turbulence and shear stress. In a fluid with low shear stress, large flocs and even aggregates of flocs form. On settling the flocs eventually lose their aggregated structure as the bed consolidates. (Partheniades, 1965 and 1971; Paaswell, 1974; Krone, 1962a). Figure 2.12.

The nature and amount of flocculation depends on the interaction of the diffuse double layer and the van der Waals forces. The size of the diffuse double layer is related to the ion content of the fluid, more generally its salinity. For example, in river water the diffuse double layer and the repulsive electrostatic forces dominate, tending to keep the particles dispersed. Weak, high porosity 'house of cards' type structures where interactions are predominantly edge-face may form (Dyer, 1986), but mild turbulence tends to break these apart. In saline environments, the increase of positive ions (sodium, calcium and magnesium) in the water neutralises the net negative charge on the surface of the particles and results in a strong decrease of the repulsive forces (van Leussen, 1988). This allows attractive forces to dominate leading ultimately to a coagulation of colliding particles. This relation between excess negative charge and salinity is roughly exponential, resulting in flocculation quickly reaching an equilibrium at low salinities. Generally therefore flocculation appears complete above 2-3ppt (Gibbs and Konwar, 1986; Mehta et al., 1989). However the rate of particle flocculation depends on the nature of hydrodynamic processes in the fluid which bring particles close enough together to allow molecular forces to have any effect (Hunt, 1980; McCave, 1984, 1985). At separations of less than 1mm interparticle attractive forces increase in prominence (Dade and Nowell, 1991), but the overall strength of a floc aggregate will depend on the conditions under which it was formed (Wright and Krone, 1989), with aggregates formed under turbulent conditions having greater strength then those formed under quiescent conditions. The strength of the clay structures are determined by interparticle forces and the number of contacts, with the flocculated structure appearing the strongest (Hamilton, 1970). At points of contact or near contact between clay particles, cementation can occur, especially in the presence of iron oxides, calcium, silica and other minerals in solution

in the interstial fluid. When exposed to overburden pressure, pressure-point and re-deposition can occur (Hamilton, 1971).

Only flocs with strong enough internal bonding will reach the bed. Near the bed in the boundary layer the high velocity gradients subject the flocs to highly disruptive forces. Flocs with weak internal bonding will be disrupted and re-entrained into the flow before they are able to bond with the bed, whereas stronger flocs will reach and bond with the bed. Bonds increase in strength and number with time resulting in the property termed 'thixotropy'. This means that the flow velocity threshold at which particles or flocs no-longer remain in suspension and are deposited on the bed, is lower then the flow velocity needed to entrain them (Partheniades, 1968). Biddle and Miles (1972) noted that flocs could contain sand grains. Due to the nature of the flocs, that is a very small weight/volume ratio, they are able to transport and deposit the sand in areas where it would not normally be expected to occur.

2.3.4. **Settling and Deposition.**

The manner in which clay suspensions settle from salt water was looked in to by Einstein and Krone (1962). For flowing water at low velocities they defined three types of deposition depending on the concentration of suspended sediment. At high concentrations flocs form and settle out; as concentrations become less then 10g/l the flocs form and continue to deposit but there is an inter-change of material with the bed. At concentrations below 0.2 to 0.3g/l, the suspension is stable with very few flocs forming and only small amounts of deposition. To begin with very little deposition occurs as initial sediment cover forms on the floor and the initial flocculation progresses. After this initial period the suspension becomes unstable and rapid deposition of flocculation material occurs. At 10g/l the rate of deposition changes and flocs settle independently.

Krone (1962a) carried out a number of laboratory experiments on a 60/40% clay/silt material of illite, montmorillonite and kaolinite. One of these experiments was to look at the affect of suspended sediment concentration on the settling, consolidation and rate of deposition. At low concentrations

the flocs settle out one by one and do not interfere with each other. They form a flocculant sediment that only consolidates slightly with time. Above 10g/l of suspended sediment the flocs hinder the movement of water being displaced by the settling flocs. As settling progresses the pore spaces become smaller, this reduces the permeability of the sediment to escaping water and the rate of consolidation. The flocs settling above the bed are hindered by the up-flowing water and a sharp demarcation of the flocculant sediment appears; it is called 'fluid mud' and is a viscous fluid. The shear of the flow helps in the formation of this fluid mud layer above a more solid (consolidated) layer (Figure 2.13). If left undisturbed the fluid mud will under go structural changes and slowly consolidate onto the bed.

Flume studies of Krone (1962a,b) used San Francisco Bay mud that was added to a 100ft long and 3ft wide re-circulating flume as a slurry, with the return flow velocity being kept high to stop deposition in that part of the flume. The initial results showed that the rate of settling can be described by equations containing factors that are functions of the apparent settling velocity, the depth of the flow, the bed shear stress and the critical shear stress below which no sediment remains in suspension.

In concentrations below 300mg/l, the concentration decreased logarithmically and the rate of deposition decreased with increasing flow velocity.

Velocity	Deposition rate
15cm/s	0.5%/hr
6cm/s	3.0%/hr
0cm/s	3.9%/hr

Above a stress of 0.6 dynes/cm^2 there was no deposition. Concentrations could be related by,

$$\frac{C}{C_0} = e^{(-KT)} \qquad (2.16)$$

where C is the concentration of suspended sediment, C_0 is the initial concentration of suspended sediment, T is the elapsed time and

$$k = \frac{6.6x10^{-4}}{z}(1 - 1.67\tau_w) \qquad [c.g.s.] \qquad (2.17)$$

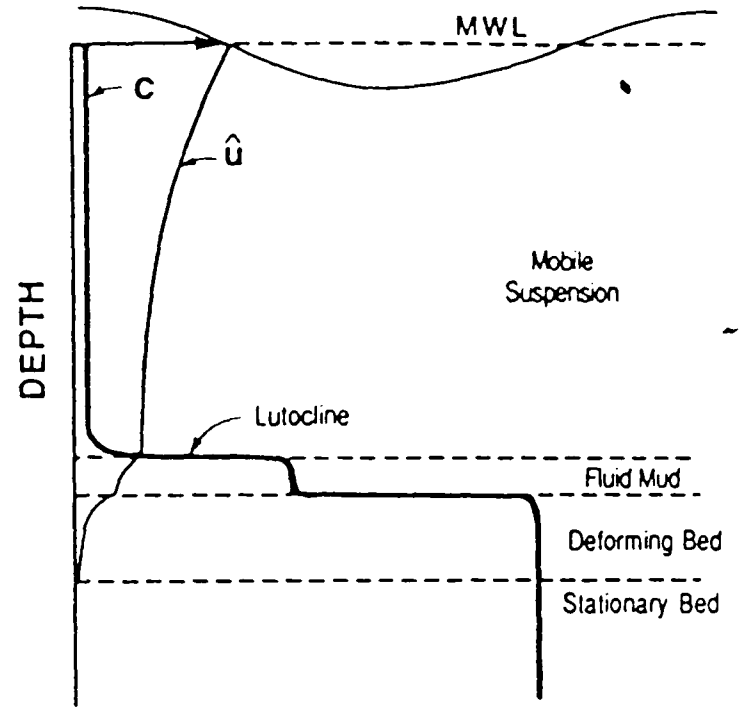

Figure (2.13); Idealized profile of instantaneous vertical concentration and velocity (Mehta 1989).

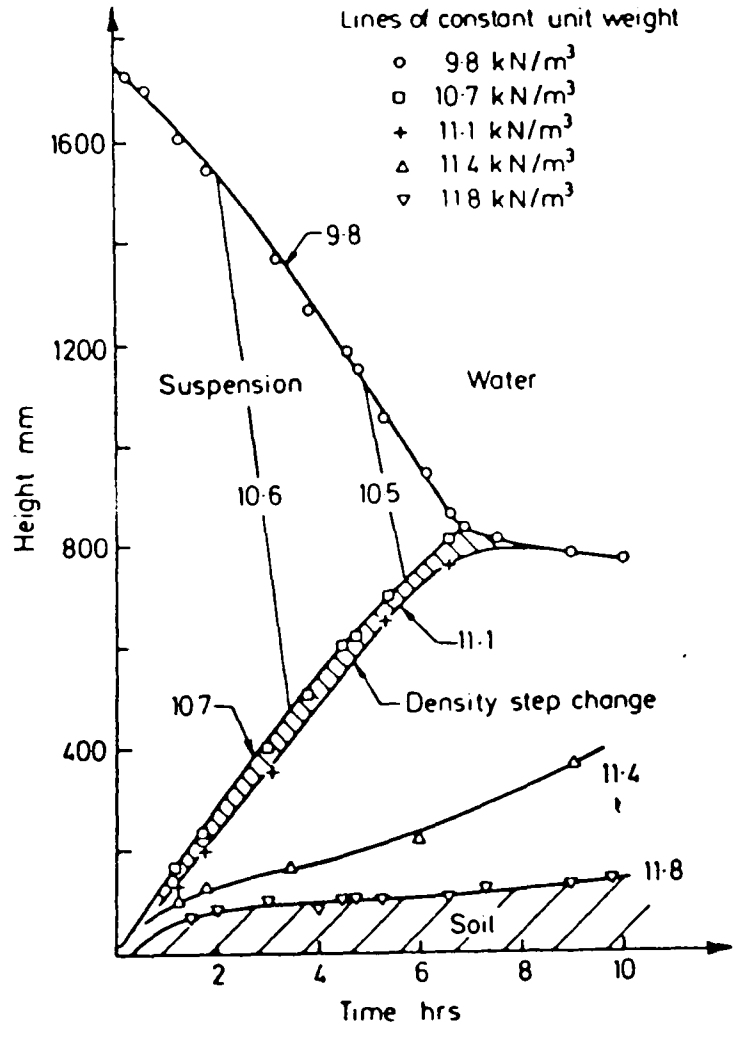

Figure (2.14); Height time plot for suspension interface of a settling suspension with an initial density of 10.7kN/m^3 (Been and Sills, 1981).

For redwood city sediment (mean diameter 25um) in 30cm of water. τ_w is the bottom shear stress. This equation was slightly modified by Einstein and Krone (1962) to,

$$k=\frac{3.3x10^{-4}}{z}(1-1.67\tau_w) \qquad [c.g.s.] \tag{2.18}$$

Below 18cm/s, the frequency of bed particle collisions is independent of velocity. The percentage of colliding particles that join together relates to the shear stress.

$$\frac{dc}{dt}=\frac{-mnW_0P}{z} \tag{2.19}$$

Where m is the particle or floc mass, n is the number of particles per unit volume, W_0 is the settling velocity, P is the probability of sticking, mnW_0 is the flux of particles approaching the bed. If mn is constant and W_0 is nearly independent of C and t then

$$\frac{C}{C_0}=e^{-pt\frac{W_0}{z}} \tag{2.20}$$

assuming that the flow does not affect the floc size and settling velocity, and is nearly independent of concentration and time. The result for concentrations greater then 300mg/l are the same as those discussed by Einstein and Krone (1962).

Partheniades (1964) investigating deposition from suspensions of San Francisco Bay Mud in flowing water achieved similar results to those of Krone (1962). After an initial rapid decrease, the concentration of suspended sediment reached a more or less constant value called the 'equilibrium concentration', this is suggested to be a constant proportion of the total sediment in suspension at the start. He defined a threshold velocity above which a substantial part of the initial suspension is retained in suspension and below which rapid deposition occurs, for a given geometry, roughness and depth.

Partheniades (1966) continued work on cohesive sediment deposition, using a counter rotating annular channel. The speed of the two counter rotating rings, the channel lid and its base, are controlled to generate

uniform conditions across the channel base. The momentum of the downwards moving fluid near the outer wall can be great enough to balance the radial pressure gradient near the channel base and this eliminates the secondary motion there. The sediment used in this initial investigation was a commercial kaolinite clay from South Caralina known as Pearless No.2. It was 65% clay and 35% silt with a mean of 0.9μm, 10.1phi.

He again found that after an initial period of rapid deposition the suspended sediment concentration reached a constant value. The ratio of the equilibrium concentration C_{eq}, to the initial concentration C_0 did not vary by more then 10% for a 16 fold variation in C_0. C_{eq} is nearly a constant function of C_0 and can be approximately defined by

$$\frac{C_{eq}}{C_0}=0.65 \qquad (2.21)$$

C_{eq}/C_0 also correlates well with the average shear stress around the channel boundary. Any secondary currents generated by the rotational motion will affect C_{eq}/C_0 and the rate of deposition. However it is assumed that by controlling the rotational speed, secondary currents have been eliminated and sediment is deposited uniformly and that shear stress across the bed is also uniform. Only a few samples were taken of the material in suspension at equilibrium concentration. These rather sketchy results suggest that most of the deposited material came from the coarse clay particle size fraction, which may mean that flocculation is more important as a settling agent then the initially higher particle weight and settling velocity of the silt fraction.

Partheniades (1968) again using an the annular counter rotating flume defined the rate of deposition dC(t)/dt in terms of the equilibrium concentration C_{eq},

$$\frac{dC(t)}{dt}=-\frac{0.198}{t}C_0\left(1-\frac{C_{eq}}{C_0}\right) \qquad (2.22)$$

t is the time from 10 to 300 minutes.

Assuming that the shear stress τ is uniform across the flume base then the equilibrium concentration can be related to τ. C_{eq}/C_0 is dependent

on τ_{ch} the average shear stress and τ is a power function of τ_{ch} and therefore τ, controls C_{eq}/C_0. C_{eq}/C_0 is related to $\tau-\tau_{min}$ by a logarithmic normal plot law, where τ_{min} is the minimum value of the bed shear stress below which no sediment will stay in suspension. C_{eq}/C_0 also represents the percentage of fine particles that can form flocs strong enough to reach the bed.

Partheniades (1968) described the C_{eq}/C_0 as a function of the bed shear stress (given in psf), related to the shear stress parameter,

$$Pw=\frac{(\Delta w)^2}{1+2\frac{d}{b}} \tag{2.23}$$

and to the bed shear stress by a log-normal relationship, giving the equation below,

$$\frac{C_{eq}}{C_0}=\frac{1}{3.085\sqrt{\pi}}e^{\left(-\frac{1}{2}\left(\frac{\log\Delta Pw-logM}{\sigma_g}\right)^2\right)} \tag{2.24}$$

$$\Delta Pw=Pw-Pw_{\min}$$

where Δw is the relative angular velocity between the channel and the ring (given in rpm), d is the channel depth, b is the channel width, Pw_{min} is the minimum shear stress parameter below which $C_{eq}=0$ and σ_g and M are the geometric standard deviation and mean of ΔPw respectively, which are physio-chemical properties of the water and the sediment.

Been and Sills (1981) looked at the self weight consolidation of a clayey silt suspension. They started with a tube of initially uniform density which showed an initial accumulation of sediment at the bottom and a slowly falling water suspension interface at the top, once sedimentation had been allowed to occur. However there also occurred a region of intermediate density above the bed; this layer had a distinct density step between it and the suspension. This density step rose while the suspension water interface dropped until they met, joined and continued to fall at a reduced rate. This now leaves only one zone above the dense base layer, which gradually consolidates. This intermediate density layer above the bed was most probably equivalent to the fluid mud layer observed by Krone (1962a) (Figure 2.14).

Mehta (1989) deduced an equation for the time rate decrease of sediment mass per unit bed area m, under a steady turbulent flow,

$$\frac{dm}{dt} = -pW_s C \tag{2.25}$$

where p[0,1] is the probability of sediment deposition, W_s is the settling velocity, and C is the depth-averaged suspended sediment concentration. The settling velocity of a diverse suspension can in general be represented by its frequency distribution and its dependence on suspended concentration (indirectly accounting for the aggregation effect) should be considered on a class by class basis. Under these conditions Mehta and Lott (1987) integrated the above equation and obtained an expression for the instantaneous concentration C(t),

$$\frac{C}{C_0} = \sum_{i=1}^{n} \phi(W_{si}) e^{\left(-t\frac{W_{si}}{h}\left(1-\frac{\tau_b}{\tau_{dl}}\frac{W_{sl}}{W_{si}}\left(\frac{\ln(W_{sn}/W_{sl})}{\ln(W_{sn}/W_{sl})}\right)\right)\right)} \tag{2.26}$$

where C_0 is the initial suspension concentration, $\phi(W_{si})$ is the settling velocity frequency distribution with maximum value, $W_{si}=W_{sn}$ and minimum W_{sl}, n is the total number of classes, τ_b is the time-mean bed shear stress, h is the water depth and τ_{dn} and τ_{dl} are the maximum and minimum values, respectively, of the critical shear stress for deposition, τ_d.

2.3.5. **Bed Microstructure.**

Cohesive sediment beds in the marine environment have a complex and heterogenous nature (Hayes, 1964) and display a wide range of properties and appearances. They consist usually of a supported array of fine-grained clay and non-clay mineral particles, integrated with organic material and biological communities (Hughes, 1979; Booth and Dahl, 1985). The sediment/water interface of these deposits is therefore chemically and biologically active (Rhoads and Boyer, 1982; Anderson, 1983) and these processes can have a radical affect on the properties of the deposits.

As with the bed properties there is a range of definitions and models of bed microstructure. This should be expected as the processes and

conditions of bed formation are diverse and likely to lead to varying bed microstructures. Due to the complex nature of the sediments it is difficult to generate anything other then general microstructure models of the deposits (Collins and McGown, 1974; Bennet et al., 1990) but in the future the use of scanning electron microscope (SEM) image analysis and low-temperature SEM work is likely to improve the classification of bed microstructure (Beckett and Read, 1986; Paterson et al., 1986; Wetzel, 1987; Smart, 1991).

Models of bed structure using ideas of colloidal and electrochemical properties of pure clays (Bryant et al., 1990) are inadequate to describe texturally mixed beds, as fine clay particles rarely exist on their own (Eisma, 1986; Carson et al., 1988; Reynolds and Gorsline, 1992). Observations show well-oriented clay particles as 'skins' on the surface of silt particles (Bowles, 1979) and electrochemical interactions between clay flakes are masked by other interactions, with the boundaries between particles being difficult to define (Rhoads et al., 1978).

The sediments usually consist of floc aggregates derived from silt and clay sized particles in suspension (Biddle and Miles, 1972) and the model of Casagrande (1932) is one of the most appropriate for these observed microstructures of combined silt-clay assemblages. The Casagrande model postulates an open 'honeycomb' structure, where sub-adjacent silt particles are embedded within a fine clay matrix. The clays in the areas between silt particles are highly compressed (a bookhouse arrangement) whereas the clays in the more open pore spaces have an open single-plate cardhouse type of structure (Figure, 2.15). Other models in agreement with this have the silt grains rarely touching and supported in a matrix, with multi-plate particles (domains) being the main clay particle component rather then single plate particles (Bowles et al., 1969; Bennet, 1976; Quinn, 1980; Bennet et al., 1981; Bennet and Hulbert, 1986). Both of these models have the coarse particles not in contact with each other but supported by finer particles, the matrix, and can be termed matrix supported (Rezak and Lavoie, 1990).

From these models and other observations (Krone, 1962) it is possible to give order to the structure. The primary particle (zero order)

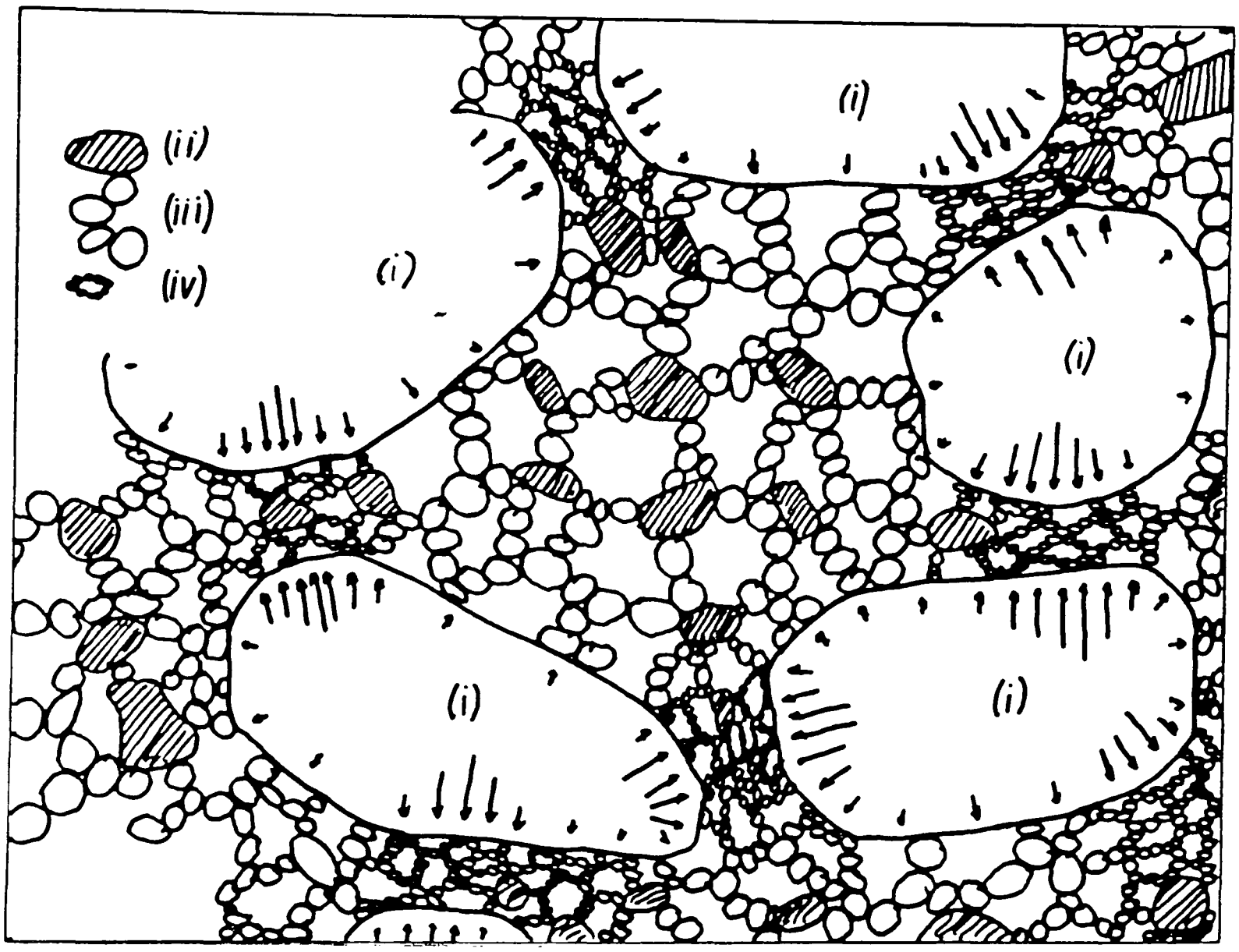

Figure (2.15); The structure of an undisturbed silt-clay sediment as suggested by casagrande. Magnification 10^3. (i) Silt grain. (ii) Clay particles. (iii) Flocculated colloidal particles of a low degree of compaction. (iv) Flocculated colloidal particles of a high degree of consolidation due to local concentration of pressure (Kranck, 1980, modified from Casagrande, 1932).

aggregates are the clay units of the matrix, constructed of a about a dozen platelets in a domain configuration (Raudkivi, 1990) and roughly uniform porosity. These primary, sub-microscopic particles form the basic parts of the higher order clusters or floc aggregates (Umita et al., 1987) and act as the matrix between the coarser particles in the Casagrande model. The floc aggregates join by collision (Partheniades, 1965) and give rise to a bed constructed of a random network of aggregates. Although the exact definition and description of structural hierarchy varies depending on the system used (Figure 2.16a,b). One result of this is that the bed has two types of porosity: primary porosity between chains of floc aggregates and secondary porosity inside individual aggregates (Black, 1993). The presence of biological and organic phases is likely to have some effect on the bed microstructure and the presence and bonding influence of biogenic mucus and organic polyelectrolytes may be responsible for the random fabric (Bennet et al., 1990).

2.3.6. **Erosion.**

A wide range of work has been carried out to determine the properties affecting erosion, these include:

- type and amount of clay material.
- clay mineral orientation.
- sample bulk density.
- pore fluid.
- eroding fluid temperature, salinity, ion content and chemical composition.
- bed structure, environment of deposition.
- time, temperature and rate of formation.
- Stress and flow history.
- Organic material content, type and its state of oxidation.

(Grissinger, 1966; Paaswell, 1974; Ariathurai and Krone, 1976).

Although not every investigation agrees with these ideas, Kamphuis and Hall (1983) decided that erosion is not related to the flow history. Migniot (1968) described bed behaviour in terms of three basic properties,

i) Flocculation of suspension and its settling rate.

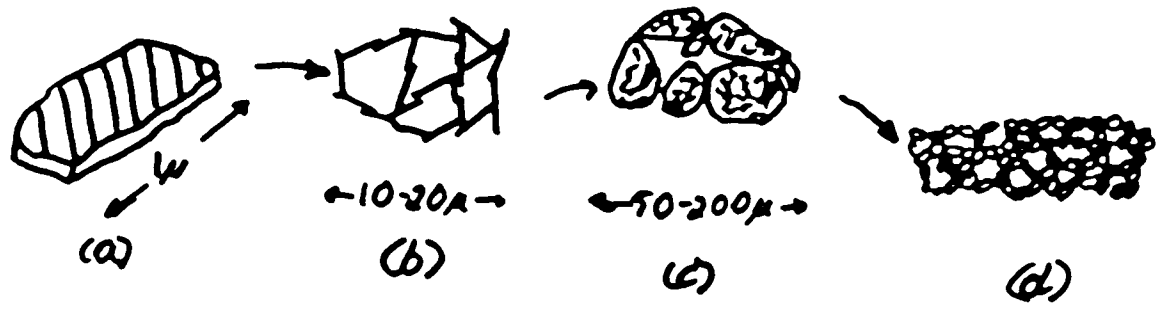

Figure (2.16a); Postulated typical arrangements and sizes of (a) clay particles, (b) flocs and (c) floc groups. (d) Bed deposit (McDowell and O'Connor, 1977).

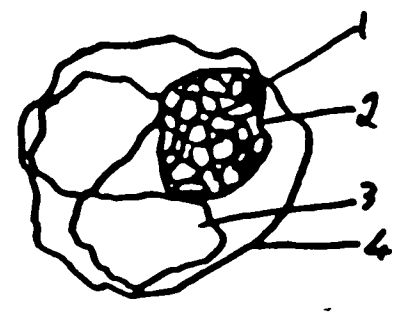

Figure (2.16b); Four level structural hierarchy associated with flocculation of clay particles: (1) primary particles - (2) flocculi - (3) floc - (4) floc aggregate (van Leussen, 1989).

ii) Bedding-down with time (consolidation) and the generation of a density gradient with depth.

iii) Rheological properties during and after consolidation and initial rigidity and viscosity.

2.3.6.1. **Nature of Erosion.**

It possible to identify three methods of cohesive bed erosion; 1) fluid stressing, 2) particle corrasion and 3) cavitation (Allen, 1971). Cavitation is the appearance of vapour bubbles in a non-uniform flow and the collapse of these vapour bubbles near the fluid-sediment interface can cause erosion (Batchelor, 1970). However cavitation occurs in flows at velocities in excess of several meters per second (Allen, 1971), and is therefore rather unusual in estuarine and near-shore tidal environments. This leaves fluid stressing (the direct action of tangential fluid stresses on the bed by the current) and particle corrasion (a form of sand blasting of the bed by suspended particles in the flow) as the important mechanisms or erosion (Kamphuis, 1983).

The nature of the erosion is also related to the strength of the bed. High concentration fluid mud deposits deform as density interfaces and will be re-dispersed under fluid stressing from waves (Migniot, 1966; Maa and Mehta, 1987; Parker, 1987; Otsubo and Muraoka, 1988;). Low strength settled mud deposits show a highly plastic behaviour, but consolidated and partially consolidated beds do not exhibit this bulk plastic behaviour. It is possible to define two forms of primary fluid stressing for these beds (Mehta et al., 1982): 1) surface erosion, in which inter-floc bonds are broken and the sediment is entrained aggregate by aggregate, occurs at low excess bed shear stress in muds of low to moderate strength (Mehta et al., 1989). 2) mass or bulk erosion is observed under very turbulent flows over hard beds and failure occurs in the beds at planes where the bed strength is equivalent to the instantaneous stress (Amos et al., 1992b). This bulk erosion entrains large particles 1-20 mm in diameter, called rip-up clasts or mud pellets, which are then quickly broken down by the flow (Pethick, 1981).

Partheniades (1965) noted the presence of a limiting velocity above which all suspended material will stay in suspension. This limiting velocity is lower than the minimum velocity needed to generate erosion. From Owen (1975),

$\tau_0 > \tau_{cr}$	continuous erosion
$\tau_0 < \tau_d$	continuous deposition
$\tau_d < \tau_0 < \tau_{cr}$	neither deposition or erosion

where τ_0 is the shear stress, τ_{cr} is the critical shear stress for erosion τ_d is the limiting shear stress for deposition (Figure 2.17). Re-suspension occurs when the applied shear stress is equal to or greater than the surface shear strength (Mehta and Parchure, 1982).

Table 1.1 shows parameters postulated by other researchers to have an effect on erosion. Paaswell (1974) discussing other research concluded that erosion is controlled by a complex interaction of a number of factors although, he suggested that erosion begins particle by particle due to relative instability of a particle compared to the rest of the bed. This instability is caused by a number of factors which include normal forces generated by the particles orientation to the flow and the bed surface.

2.3.6.2. Threshold of Particle Motion.

Determination of the threshold of particle motion is a most important object of marine sediment transport work (McClean, 1985; Ünsold and Walger, 1987). The forces acting on cohesive particles in a flow have been described earlier in this chapter.

Both erosion and deposition are related to the bed shear stress (Cole and Miles, 1983). For particles to leave the bed and enter suspension, the critical shear stress, τ_{cr}, must be exceeded (Ariathurai and Arulanandan, 1978; Sheng, 1983). However due to the nature of cohesion, inter-particle bond strength varies through out the bed and can be represented by a Gaussian distribution (Mirtskhoulava, 1990). The turbulent nature of the flow will mean that the instantaneous shear stress at the bed can also be represented by a distribution (Leader, 1983; Kirchener et al., 1988).

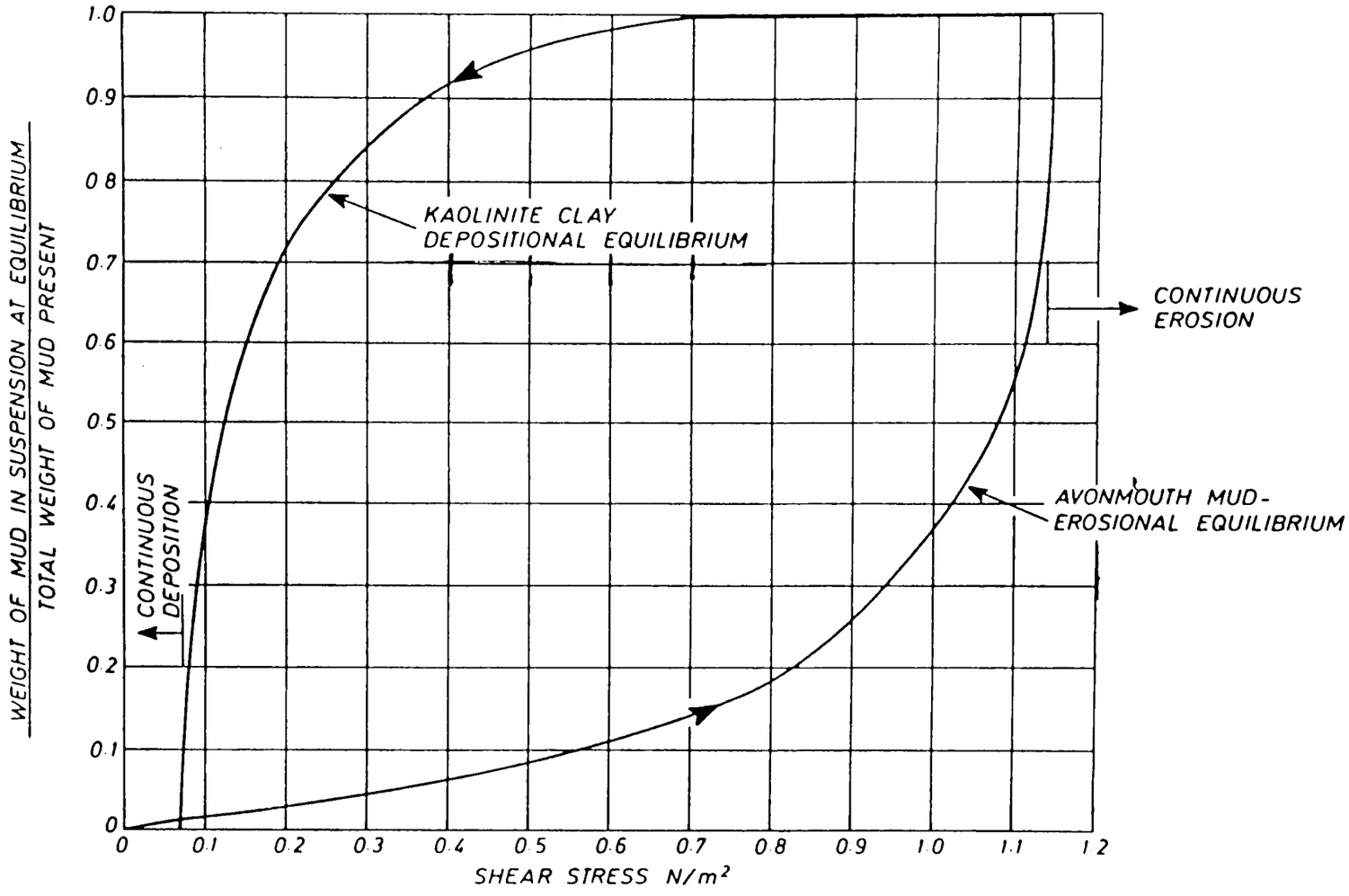

Figure (2.17); Comparison of erosional and depositional equilibrium conditions (after Owen, 1975).

Therefore the overlap of these two distributions will result in erosion and that for any shear stress applied to the bed erosion is likely to occur to a greater or lesser extent, e.g. even at very low shear stress erosion of particles with low bond strengths occurs (Grass, 1970; Partheniades, 1965). This small scale patchy erosion at low stresses has been noted and modelled by a number of authors (Paintel, 1971; Lavelle et al., 1984; Lavelle and Mofjeld, 1987; Raudkivi, 1990) and termed 'sub-critical' erosion (Ünsold and Walger, 1987).

This implies that there is no threshold condition for cohesive sediment beds and that they are behaving as a pseudo-plastic rather than a Bingham plastic material (Dyer, 1986; Maa and Mehta, 1987). A pseudo-plastic exhibits shear thinning behaviour, that is the material's viscosity will decrease with increasing rate of shearing, and in sediments this would relate to a breakdown of the aggregate networks to their floc units (Dyer, 1986). This winnowing, floc disintegration has been recorded by a number of authors (Pierce et al., 1970; Parker et al., 1972; Pierce, 1990; Mirtskhoulava, 1991; Black, 1991; Duck and McManus, 1991). If this floc sub-unit winnowing is common to erosion at low shear stresses, then it is likely that the micro-textural properties of deposited flocs, their silt content and number of primary particles, are going to be fundamental control of sediment fluxes (Black, 1993).

Contrary to this idea however, it is apparent that the bed displays a finite yield strength and that the inter-floc bonds are elastic to some degree. This comes from work by Mirtskhoulava (1966), Croad (1981) and Raudkivi and Tan (1984) in which high frequency turbulent motion in the flow was noted to successively weaken the interparticle bonds of flocs close to their individual threshold, until the bed stress exceeded the cohesive forces and entrained the particle. This 'particle vibration' has been observed for particles in flow where the velocity is above the critical value to entrain detached aggregates and was termed the 'excitation velocity' by Rhoads et al. (1978). Boyer (1980) and Nowell et al. (1981) observed this 'delayed' erosion in biologically active muds and it may be a feature of beds with high levels of productivity. Black (1991) attributed these short term delays of entrainment in flows where the bed stress was greater than the τ_{cr} for natural estuary muds, to 'fatigue' weakening of the floc aggregates.

The number of primary particles, floc sub-units, that a floc aggregate releases to suspension is proportional to its size or degree of aggregation (the number of primary particles it contains), especially as floc aggregate size is inversely proportional to its strength and density (Krone 1976, 1981; Al Ani et al., 1991; Black, 1991). The modified Shields curve implies that fine particles have a greater τ_{cr} then coarse silts and sands due to their interparticle cohesion (Mantz, 1977). All of these features of cohesive sediment erosion need to be considered when looking at the threshold of cohesive sediment erosion.

This means that an exact definition of threshold shear stress is difficult as the bed response varies with varying shear stress. For practicality therefore the threshold τ_{cr} is defined in terms of a time averaged minimum sediment transport rate (Johnston, 1943; Parker and Klingeman, 1982; Mehta and Partheniades, 1982; Parchure and Mehta, 1985; Amos, 1991; Gross and Dade, 1991), for example Drake and Cacchione (1982) defined τ_{cr} in terms of an increase in background suspended sediment concentration by a factor of two.

2.3.6.3. **The Rate of Erosion.**

The erosion threshold defines the shearing force necessary to initiate erosion; the speed, magnitude and pattern at which erosion of the bed continues is the erosion rate. The erosion rate can have a greater influence on the overall water column turbidity than the threshold (Hollick, 1976; Mehta et al., 1989) and therefore erosion is more usefully paramaterised by both its threshold and rate (Lavelle and Mofjeld, 1987; Self et al., 1989; Kraeuter and Wetzel, 1986)

Most research into cohesive sediment erosion has found that for a given shear stress the amount of material in suspension reaches an equilibrium concentration, which has been explained in a number of ways (Partheniades, 1965). Owen (1975) using beds of mud deposited from quiescent suspensions, found erosion occurring at nearly all shear stresses but it was possible to define the erosion into two main groups. At low shear stress the concentration of material in suspension reached an

equilibrium, but above a certain shear stress value erosion continued indefinitely, no equilibrium was reached and the whole bed was eroded. There are two possible explanations;

(1) The bed has a density gradient of increasing density with depth, therefore erosion occurs until a depth is reached at which the density is high enough to resist the erosion and there is neither erosion or deposition (Parchure and Mehta, 1985; Kuijper et al., 1989).

(2) The equilibrium concentration is reached when the rate of deposition equals the rate of erosion, the same explanation as Peirce et al. (1970).

Mehta (1981) defined the erosion rate, ϵ, as: 'the mass of sediment eroded per unit bed surface area per unit time, as a function of the bed shear stress in steady turbulent flows'. In a functional form this is,

$$\epsilon = \frac{dm}{dt} = f\left(\tau_0, \tau_{cr}, \upsilon_1, \upsilon_2, \upsilon_3, \ldots, \upsilon_n\right) \qquad (2.27)$$

where m is the mass of sediment eroded per unit bed area (kgm^{-2}), t is time, τ_0 is the bed shear stress, τ_{cr} is the critical bed shear stress and υ_1-υ_n are parameters representing bed properties that determine the sediments resistance to erosion.

A wide range of equipment has been used to investigate the rate of erosion, but there has been no agreement on the relationship between υ and τ_0. The results suggest that it is either linear, non-linear (a power or exponential relationship) or a combination of two linear trends intersecting at a characteristic bed stress (Allen, 1984; Dyer, 1986).

The erosion rate can be given a bi-linear form,

$$\epsilon = M\left(\tau_0 - \tau_{ch}\right) + \epsilon_{ch} \qquad (2.28)$$

where τ_{ch} is the characteristic bed stress, ε_{ch} is the characteristic erosion rate, τ_0 is the bed shear stress and M is a general erosion rate constant dependent on characteristic bed properties. There are two vales of M: M_1 for $\tau<\tau_{ch}$ and M_2 for $\tau>\tau_{ch}$ with the point (ε_{ch}, τ_{ch}) where $\tau=\tau_{ch}$ marking a change in erosion from a minor to a significant erosional regime (Dade and Nowell, 1991). This bi-linear form has been identified by a number of authors (Epsey, 1963; Christensen and Das, 1973; Gularte, 1978; Fukuda,

1978: Sheng and Lick, 1979) and using a graphical representation it is possible to produce a value of τ_{cr}, although two different methods have been used. The first, using the idea of a minimum flux condition (non-zero rates of erosion), involves extrapolating the M_2 line back to the x-axis to give $\tau_0=\tau_{cr}$ (Johnston, 1943; Krone, 1976; Parchure and Mehta, 1985; Devries, 1992). The other method draws a line directly down from the intersect of the M_1 and M_2 lines to x-axis giving $\tau_{cr}=\tau_{ch}$ (Christensen and Das, 1973; Chapuis and Gatien, 1986) (Figure 2.18), although this is more difficult for cases where intercept of the M_1 and M_2 lines is more of a smooth curve (Hollick, 1976).

Other authors have produced a variation on equ 2.28, (Owen, 1975; Sheng and Lick, 1979; Sheng, 1983; Ariathurai and Arulanandan, 1978; Thorn and Parsons, 1978; Mehta, 1981; Villaret and Paulic, 1986; Ockenden and Delo, 1991),

$$\frac{dm}{dt} = \epsilon = M_a(\tau_0 - \tau_{cr})^n \qquad (2.29)$$

where M_a is the erosion rate 'constant' representing the rate of change in ε and n is an exponent (range 0.8 to 1.3) usually taken as 1 (Puls, 1984). This equation is a special case of equ 2.33 when $M_1=M_2$, however the value of M is related to the method used due to its dependence on the period of time in which the erosion rate is measured (Thorn and Parsons, 1980). M is inversely proportional to τ_{cr} and as would be expected the erosion rate decreases with increasing erosion threshold. This has been developed further, using the relationship $M_1=M.\tau_{cr}$=constant, where M is the slope of the line in $\varepsilon-\tau_0$. M_1 is an empirical constant of the increase in the erosion rate for an increase in the fluid shear at the bed equivalent to the sediment's critical shear stress and can be related to a number of factors used to predict erosion (Ariathurai and Arulanandan, 1978; Sanford et al., 1991).

This equation implies that the rate of erosion will increases linearly with the excess bottom stress, and this has been observed in the laboratory where suspended sediment concentrations continued to increase over many hours for a constant bed shear stress (Krone 1962; Yeh 1979). This 'Type II' surface erosion (Mehta and Partheniades 1982) implies that

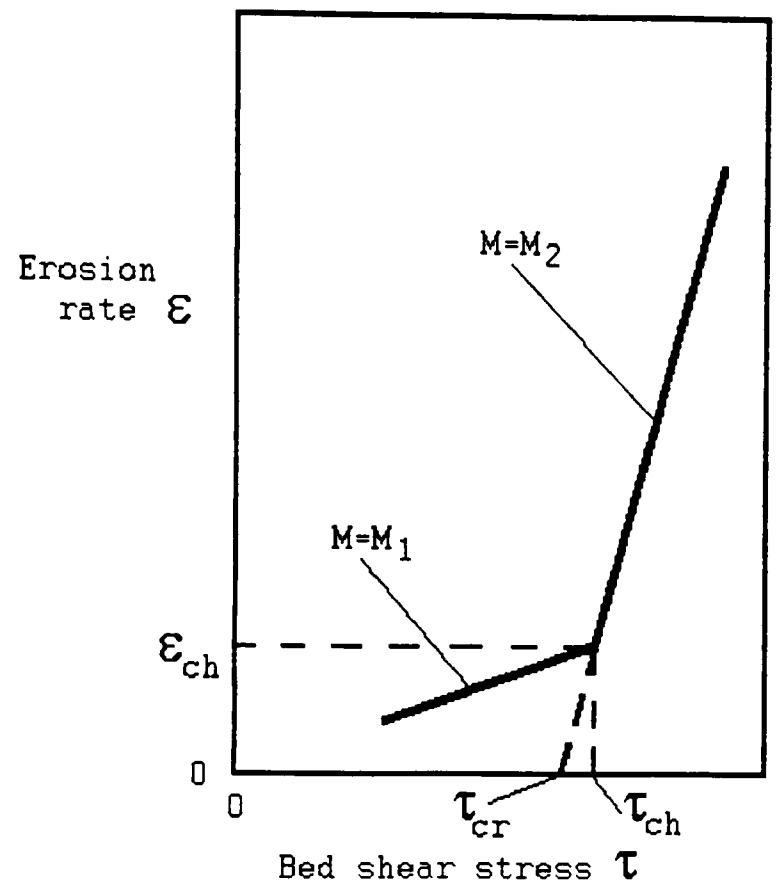

Figure (2.18): Generalised bi-linear form of the relationship between the time-mean bed stress (τ) and the rate of surface erosion (ϵ) from laboratory studies; note τ_{cr}=threshold shear stress, τ_{ch} is a characteristic bed stress, ϵ_{ch} is a characteristic erosion rate (after Mehta, 1981).

no time-dependent deposition occurs, but eventually the erosion will tend to an equilibrium condition due to no more floc entrainment or the concentration of sediment in the flow being high enough to result in deposition.

A slightly different equation can be formed using the normalized excess shear stress (Kandiah 1974; Arulanandan 1975; Bain 1981; Mehta and Partheniades 1982; Kusuda et al 1982; Puls 1984; Sanford et al 1991;),

$$\frac{dm}{dt} = \epsilon = M_b \left(\frac{\tau_0}{\tau_{cr}} - 1 \right)^n \qquad (2.30)$$

where n is once again a constant ranging from 0.43 to 1.16 (Puls, 1984) and M_b has the units ($kgm^{-2}s^{-1}$) of erosion rate and ranges from $0.2x10^{-3}$ to $5x10^{-3}$ (van Leussen and Dronkers, 1988). All of these equations (2.29 and 2.30) give the erosion rate as independent of time, that is unaffected by suspended sediment concentration and the changing properties with depth e.g consolidation. This uniform nature may be true for sediment beds artificially constructed in the laboratory but naturally occurring muds are normally considered to have a vertically stratified surface structure (Black, 1993; Dyer, 1986; Odd, 1988), although it may be possible to use equations 2.29 and 2.30 for modelling erosion in sediments that suffered enough compaction to reduce floc structure to a more homogenous nature (Krone, 1963).

In these vertically stratified beds the erosion rate decays exponentially to zero for a constant fluid stress and can be defined by (Kusuda et al., 1982; Parchure and Mehta, 1982, 1985; Villaret and Paulic, 1986; Sheng and Villaret, 1989),

$$\frac{dm}{dt} = \epsilon = \epsilon_0 . \exp\left[\alpha \left(\tau_0 - \tau_{cr}(z) \right)^n \right] \qquad (2.31)$$

where ε_0 is the floc erosion rate, $\tau_{cr}(z)$ is the sediment shear resistance profile, α is a coefficient and n is 0.5 (Parchure and Mehta, 1985). The floc erosion rate relates to the small amount of erosion that occurs when $\tau_0 = \tau_{cr}(z)$ (Mehta, 1991) and allows this equation to be used on fresh soft deposits, with equations 2.34 and 2.35 of better use for denser deposits with water content well below 100%.

In this type of erosion termed 'Type I' by Mehta and Partheniades (1982) the erosion rate dm/dt decreases with depth as the bed's resistance, represented by τ_{cr}, increases with depth. Erosion stops when the sediment strength is sufficient to resist the fluid shear, e.g. $\tau_0=\tau_{cr}$. Erosion can be restarted by an increase in the bed stress and at high (excess) stresses the erosion rate is quasi-linear (Thorn, 1981; Delo, 1990). This pattern of an exponential trend in erosion has been confirmed by laboratory work (Fukuda and Lick, 1980; Kuijper et al., 1989) and field studies (Peirce et al., 1970: Black, 1991; Amos et al., 1992a,b). Amos et al. (1992a) classified deposits that erode in this way as 'benign' as they are self armouring and do not erode catastrophically (Type II). More generally, as the bed stress is increased in a step wise fashion the nature of erosion is seen to change from Type I erosion of the stratified sediment surface to Type II erosion of the crushed and buried flocs in the more compact and homogeneous sub-layers (Thorn and Parsons, 1980; Mehta and Partheniades, 1982; Amos and Mosher, 1985; Kuijper et al., 1989).

Another explanation of Type I erosion is in terms of a balance between the entrainment of material into suspension by erosion (E), which is a constant, and the settling of material onto the bed (D) that increases with time in proportion to the mass of sediment eroded (Lick, 1982),

$$\frac{dm}{dt} = E - D = \lim_{M \to 0}\left(\frac{\delta M}{\delta t} - W_s C\right) \qquad (2.32)$$

This theory and its proposed equilibrium is dependent on the grain size distribution of the eroding material. Beds which contain large quantities of silt may be able to reach an equilibrium concentration, but in beds of finer sediments with lower settling velocities (W_s) deposition is unlikely as it will only occur at bed stresses very much lower then that needed for erosion τ_{cr}; so this model is unlikely for natural muds (Krone, 1962, 1963; HRS, 1979; Puls, 1984).

Another method of describing the erosion rate without using the critical threshold is by using a power function of the absolute bed stress, $|\tau_0|$, with erosion occurring at all velocities (Abdel-Rahman, 1962; Lavelle et al., 1984),

$$\epsilon = \alpha |\tau_0|^n \tag{2.33}$$

This model is similar to one postulated by Gross and Dade (1991), however it differs from the normal ideas of the sediment acting as a Bingham solid with a yield strength (Amos et al., 1992b) and it may be based on the initial entrainment of the easily re-suspended biogenic 'fluff' at the sediment surface (Black, 1993) rather than actual sediment floc erosion (Burrel, 1983; Güst and Morris, 1989).

As described earlier it is possible to describe erosion in terms of the probability distribution of τ_0 being greater then τ_{cr} and the length of time that this occurs (Otsubo and Muraoka, 1985; Mimura, 1989). The erosion rate is then defined as,

$$\epsilon = \left(P_0 \frac{\hat{t}_0}{t_d} \right) \left(\frac{1}{\hat{t}_0} \right) = \frac{P_0}{t_d} \tag{2.34}$$

where P_0 is the probability of $\tau_0 > \tau_{cr}$, $\hat{t}_0$ is the time scale of the bed stress fluctuations, $P_0\hat{t}_0$ is the length of time when the bed stress can entrain sediment and t_d is the time period required for aggregates to be dislodged. This type of method was used by Partheniades (1965) and more recently with greater success by Ostubo and Muraoka (1985, 1986a,b) and Kirchener et al. (1990) and needs more investigation as it utilises the flow property of turbulent fluctuations.

Dunn (1959), using a submerged jet, developed a linear relationship between the critical shear stress and the vane shear strength. It can be related to the plastic index, the percentage of sediment finer then 0.06mm and various other statistical representations of the particle size distribution. Critical shear stress can be related linearly to unconfined compressional strength, vane shear strength and consolidation, with the greater the consolidation the higher the critical shear stress. In natural deposits the amount of consolidation is related to over burden causing erosion to decrease with depth (Ariathurai and Krone, 1976) and due to the variation of consolidation with time it may be necessary to treat consolidated and partially consolidated beds differently (Mehta and Parchure, 1982).

Arulanandan et al. (1975) observed that erosion occurred at all shear stresses but above a critical shear stress the erosion rate increased linearly; below this critical value, erosion is slow and intermittent. This may be due to bed variations, possibly surface variations; allow pits to form which cause an increase in the surface roughness and increase the rate of erosion (Kamphuis and Hall, 1983); or turbulent bursting phenomena cause a sudden increase in shear above the critical value at random points over the bed. Ariathurai and Krone (1976) suggested that for erosion at shear stresses just above the critical erosion value, the bed erodes particle by particle (surface erosion) and at higher shear stress erosion occurs as a 'mass erosion', with the bed failing and eroding as one. Therefore to model sediment erosion, the erosion rate and critical shear stress of each stratum of the bed must be known.

Mehta and Parchure (1982) looked at a number of properties. The shear strength and bulk density were not constant with depth, with the shear strength increasing rapidly in the soft partially consolidated surface sediment layer, below which the sediment properties are more uniform. In the first hour of deposition, aggregation and thixotropic re-arrangements are controlling the bed properties, but with time over-burden becomes the main property control.

Using Boston Blue Clay, BBC, Berghager and Ladd (1964) looked at erosion and assumed that for water flowing over a smooth cohesive bed it can be assumed that the shearing stress acts down-stream on the bed surface, the effective stress in the sediment at the interface with the water is zero and increasing with depth and the interface is instantaneously drained with the dissipation of excess pore pressure due to shear increases with depth. Erosion started at a higher shear stress then the predicted value and the erosion rate increased with increasing shear stress, with erosion for unconsolidated sediments occurring via a continuous detachment of very fine particles from the bed.

2.3.6.4. Non-Biological Controls of the Threshold and Rate of Erosion.

Even with the problems defined above, it is generally considered that there is a threshold shear stress τ_{cr} which must be exceeded for erosion to occur (Allen, 1970; Ariathurai and Arulanandan, 1978; Dade et al., 1992). The relationship of τ_{cr} to the properties of the bed is very complex and therefore a wide range of relationships using a range of bed properties have been formulated.

The same factors that affect the threshold also affect the erosion rate, but the distribution of properties with depth, sediment loading and the variation of biological activity with depth must also be considered (Lick, 1982; Amos et al., 1992b).

Yield Strength and Density.

A number of authors have noted the possible correlation between the yield strength, τ_y, and erosion threshold τ_{cr}. For cohesive sediments the yield strength is taken to represent the average interparticle bond strength and to be a limiting stress above which irreversible structural deformation of the floc aggregate network occurs (Dade and Nowell, 1991; Dade et al., 1992). If this assumption is made then the critical bed shear stress for grain by grin entrainment can predicted from analysis of the forces acting on component grains of flat mud beds and the erosion resistance can be defined in terms of the cohesive yield stress, particle size, shape, relative density, and packing geometry (Dade et al., 1992).

Allen (1970) gave the relationship between bed shear strength and the critical shear stress as,

$$\tau_{cr} = k\tau_{mud}^{n} \tag{2.35}$$

where τ_{mud} is the bulk shear strength of the bed, k is a variable to account for the bed surface and flow characteristics and n is an exponent. For the erosion rate, the excess shear stress, the differences between the applied shear stress and critical shear stress, is important. Earlier work by Migniot (1968) appears to support this relationship. The erosion threshold increased with τ_y but in two regimes separated by a strength of

approximately $1.5Nm^{-2}$. In the lower regime ($\tau_y<1.5Nm^{-2}$), the relationship was $\tau_{cr}\propto 0.32\tau_y^{1}Nm^{-2}$, whereas in the upper regime, ($\tau_y>1.5Nm^{-2}$) the relationship is more linear with $\tau_{cr}\propto 0.26\tau_yNm^{-2}$. For these experiments, $\tau_y\propto C^4$ where C is the bed concentration or density and therefore $\tau_y\propto C^2$ and $\tau_y\propto C^4$ for the two regimes respectively. The boundary between the two regimes, may mark some fundamental change in either particle packing or bed response (Allen, 1985) and could be a function of the non-linear relationship between C and the effective stress (Ockenden and Delo, 1991).

Similar relationships were defined by Otsubo and Muraoka (1988). They used the yield strength as a rheological parameter to describe the cohesion. They defined two threshold values, τ_{cr1} for the threshold of aggregate motion and τ_{cr2} for significant massive erosion of the bed, with the later yielding the closest correlation between the two variables. These results and that of others suggest that yield strength defined by viscometry may be used as a guide to the critical shear stress of muddy sediments and encouragingly this tool can be used in the field (Hydraulics Research, 1979; Chapuis, 1986; Chapuis and Gatien, 1986). In general the critical shear stress needed for erosion increases with increasing sediment shear strength (Moore and Masch, 1962).

Partheniades (1965) surmised that clay resistance to erosion appears to be independent of microscopic shear strength of the bed, provided that the individual mass shear strength does not exceed the microscopic shear strength of the material. Erosion at shear stresses below the bed shear strength is by single particles or clusters of particles. Once a critical value of shear stress has been exceeded erosion rates increase rapidly and depend strongly on the average shear strength.

As mentioned earlier, yield strength and threshold can be related to bed density. However density is defined in terms of an ideal homogeneous material of uniform grain size (Toorman and Berlamont, 1991) and in natural cohesive sediments the density will vary and be difficult to define precisely due to the variability of sediment properties, e.g grain size, sorting, packing, and biological activity. In sands, the decrease in rigidity with increasing porosity is caused by the reduction in the number of inter-grain contacts with less dense packing (this is only true in sands of a

uniform grain size and angularity) (Hardin and Richart, 1963). As the amount of fine silt and clay increases, the sediment's rigidity is due more to cohesion with the inter-locking and friction of grains becoming less effective. Although numerous factors control cohesion and rigidity, in general cohesion and rigidity decrease with increasing porosity and decreasing grain size for high porosity silt-clays. (Hamilton, 1971).

A number of authors have produced results relating τ_{cr} to C. Thorn and Parsons (1980) and Thorn (1981) summarized work on four muds with concentrations between 75 and 200 kgm^{-3} and τ_{cr} between 0.1 and 1 Nm^{-2} and fitted a single line to the data giving,

$$\tau_{cr}=5.42x10^{-6}C^{2.28} \tag{2.36}$$

A summary of work done at the Hydraulics Research Laboratory (HRL) by Puls (1984) showed that the coefficient varied from 10^{-3} to 10^{-6} and the exponent in the range 0.81 to 2.18 and a re-examination of Mehta and Partheniades data gave an exponent of 1.5 for two flume studies. Dyer (1986) supposed that a deposit generally has a critical erosion shear stress dependent on the square of the exposed density and this is supported by work of Cormault (1971) on muds with a dry density of 200-300kgm^{-3} and where $\tau_{cr} \propto C^2$. Rheological investigations on natural muds by Williams and Williams (1989) support the above results, by suggesting a power law dependence on the yield stress and volumetric concentration.

The relationship of increasing threshold with increasing density, as observed by Thorn (1980) on muds settled from suspension, can be described theoretically. The density reflects the distribution of the mean interparticle spacing, the nature of the sediment fabric (Allen, 1985b). The higher the density the more particles for a given volume, the closer the spacing, and therefore the greater the number and strength of interparticle bonds, resulting in a rise in cohesion and bed strength (Mitchell, 1976). Other results of increasing density, are the disappearance of inter-floc voids (Einstein and Krone, 1962) associated closely with increases in the effective stress (Alexis et al., 1992), and decrease in sediment permeability and water content (Lee and Chough, 1987, Ockenden and Delo, 1991).

The reduction in water content with increasing density can be described by the void ratio, e,

$$e = \frac{volume\ of\ the\ voids}{total\ volume} = \frac{n}{1-n} \qquad (2.37)$$

where n is the sediment porosity. The void ratio is a measure of the degree of compaction (degree of consolidation) and is a fundamental control on erosive strength and shear resistance, since it represents the sum of all interparticle bonds (Paaswell, 1973). The degree of collapse of sediment deposits is thus a limit on the maximum strength (Odd, 1988) and so microstructure development is a control on the sediment's erosion behaviour. Lyle and Smerdon (1965) and Kusuda et al.(1982) showed that τ_{cr} increases with decreasing e or that τ_{cr} is dependent on the degree of compaction. This could mean that sediment deposited during neap conditions may have time to consolidate and therefore not be re-suspended during spring conditions even with higher τ_{cr}. Therefore spring-neap variations in consolidation can have a major affect on sediment erosion and sedimentation (Hawley, 1981; Villaret and Latteux, 1992).

Water Content.

The water content, ω, is related to and is an important control of sediment saturation, porosity, degree of compaction (voids ratio) and bulk density (Hjülström, 1939; Postma, 1967) and has been used in studies of cohesive sediment erosion (Nicholas, 1986; Odd, 1988; Fukuda and Lick, 1980). It is often used instead of an other more difficult to measure variable (Wetzel, 1991), and some workers have found an inverse correlation between wet water content (ratio of weight of water to wet weight of sediment) and critical flow velocity (Southard et al., 1971; Lonsdale and Southard, 1974; Fukuda, 1978; Fukuda and Lick, 1980). The water content has a non-linear relationship with τ_{cr} meaning the it has a greater affect on sediment s that dry out than those that remain saturated (Otsubo and Muraoka, 1988).

Increases in sediment water content should decrease the effective stress, therefore decrease τ_{cr} (Christian, 1991), but cohesive muds may exhibit elastic deformation and can 'take up' seawater changing the bulk

volume without altering the interparticle bond strength (Black, 1991). This behaviour is more likely in muds containing several percent of organic mater and appreciable densities of benthic diatoms which secrete mucus, all of which increase the sediment's ability to hold moisture (Rashid and Brown, 1975; Hamblin and Davies, 1977; Harper and Harper, 1977; Paterson et al., 1989).

Although the water content has been shown to affect the threshold and rate of erosion (Fukuda and Lick, 1980; Lee et al., 1981), it has no measurable change over the surface few millimetres of the deposit (Black, 1991) and therefore cannot account for the time varying pattern of Type I erosion. It may be that water content is not an outstanding primary factor of sediment erodibility and the elastic nature of elastic floc aggregates may explain this (Black, 1993).

Textural and Structural Controls.

Estuarine and coastal muds normally contain a varied mixture of grain sizes, ranging from clay to silts and even sand size fractions, and these cohesive and non-cohesive fractions respond differently to fluid shear, and therefore complicate the sediment's behaviour (Singer and Anderson, 1984; Dade et al., 1992). Observations have shown that the coarser non-cohesive fractions may form bedforms, be winnowed or washed away (Terwindt et al., 1968) or be transported as bedload at the same time as fine cohesive flocs are re-suspended (Grant et al., 1990; Amos et al., 1992b).

The coarser components (sands and silts) influence the bed structure. They themselves are incompressible, unlike the clay matrix, and so during compaction the sand and silt grains tend to squeeze the clay flocs, especially those sandwiched between grains (Reynolds and Gorsline, 1991; Toorman and Berlamont, 1991). The presence of coarser grains influences the nature and patterns of re-suspension of the sediment, and so the nature, micro-texture, structure and integrity of the flocs that form the bed are important controls of bed behaviour (Peirce et al., 1970; Pierce, 1990; Christian, 1991). The shape and surface texture is also

important with the proportion of spherical or platy particles affecting the friction angle and fabric strength. Interlocking of grains has been inferred in coarse (silt size) material to stabilise the bed (Wells, 1988) and observed in the fine fraction (Black, 1991) in muds deposited in high energy areas.

The presence or integration of cohesive and non-cohesive sediments e.g small percentages of sand fractions in muddy sediments and vice versa, can have a profound affect on the threshold value (Smerdon and Beasley, 1959; Evans, 1965; Terwindt and Breusers, 1972; Miller et al., 1977; Reineck and Singh, 1980; Kamphuis and Hall, 1983; Sheng, 1983; Amos and Mosher, 1985; Ockenden and Delo, 1988; Odd, 1988; McTiernan, 1989; Christian, 1991; Faas, 1991; Huh et al., 1991). The threshold value increases with increasing clay content though small amounts of sand in muddy sediments may also increase the threshold.

The obvious inter-relationship of all of these factors means that rather than using one variable the use of a number of variables is likely to give a better explanation of variations in sediment deposits (Thorne, 1985).

The structural control has already been discussed earlier (§ 2.3.6.3.), and it is that stratified muds erode with an exponential decrease in the erosion rate, (Type I), and more uniform muds erode with a constant erosion rate for a constant shear stress. A number of workers have used bed density (or in the laboratory, time elapsed since bed deposition) to try and explain the reason for changes in the erosion rate with depth (Creutzberg and Postma, 1967; Lee et al., 1981; Lick, 1986). In order to explore depth stratification of bed density, dry ice techniques to fine-section the bed have been used, with results that show a relationship between bed strength and density over the surface centimetres and type I erosion of flow-deposited beds (Mehta and Partheniades, 1982; Parchure and Mehta, 1986).

However in natural muds, where these surface gradients do exist (Bassoulett and Le Hir, 1991), it appears that variations within the surface millimetres and between individual flocs are more important, as erosion under tidal flows occurs in these top few millimetres (Rhoads et al.,

1978; Güst and Morris, 1989; Halka et al., 1991; Mehta, 1991). In fact bulk property gradients in the surface millimetres are unlikely (Partheniades, 1984b, 1990) and the change in erosion is more likely to be due to higher individual floc diameters and densities. These larger, more dense flocs with higher settling velocities would have preferentially settled to the base of a depositional slack water deposit (Stow and Bowen, 1978, 1980; Kranck, 1984) and with their inter-bond strength and stronger bonding to the bed are able to withstand fluid stress more then the overlying smaller and weaker flocs (Kline et al., 1967; Krone, 1976; McCave, 1984). Very thin laminations (<0.1-0.2mm) of this type have been observed in the natural, tidally deposited muds (Thompson, 1968; Hesse and Chough, 1980). Storms play an important role in the re-suspension and ensuing differential settling that leads to fine, upward-fining sediment deposits (Wiberg and Butman, 1991; Butman and Wheatcroft, 1991). Kusuda et al.(1982) and Umita et al. (1986, 1987) proposed that the decrease in erosion rate with time was due to the vertical distribution of interstitial voids and the orientation of floc aggregates.

Associated with this is the need to understand the flow history of the bed, due to the fact that sediment aggregates can be re-orientated to the flow at sub-threshold velocities, thus strengthening the bed; a phenomenon termed rheopexy. It has been observed in deep sea deposits under long period, slow tidal currents (Black 1993) but is more difficult to observe in shallow marine environments due to confusion by wave forces (Anderson, 1972; Amos et al., 1992b). Similar observations in turbidite beds (Rees, 1965; Wetzel, 1987) support the idea that this may be the reason for increased stability of beds deposited at very slow flow velocities over statically deposited beds (Mantz, 1977; Kirchener et al., 1990). It is envisaged for erosive flows that whilst the larger more cohesive aggregates reorientate, weaker less strongly bonded flocs are entrained, so resulting in decreased inter-floc porosity from an increased solids fraction and a stronger slightly more resistant bed (Black, 1983). It has been demonstrated, in pure clays, that the individual clay particles may become aligned, although the amount and type of alignment is related to the deposit's water content (Rees, 1965; Push, 1970; Allen, 1971; Moon and Hurst, 1984; Mallik et al 1989; Bennet et al 1990). This orientation may be the reason for the observation of Partheniades (1965) that the surface of

the bed was found to be harder and rougher after an erosion test than at the start.

What is really required is a more detailed, high resolution, investigation of the surface microstructure in relation to erosion.

The affect of clay mineralogy has been looked into by a number of workers including Grissinger (1966), Christensen and Das (1974), Paaswell (1974), Fukuda (1980) and Kamphuis and Hall (1983). In the main, general soil classification indexes are not very useful in the prediction of erosion but structural indexes may be used as a guide to relative erodibility. These include indexes to show void ratio, strength, thixotropy, particle orientation, stress history and swelling potential, of which the last two are important for field laboratory comparisons (Paaswell, 1974).

Paaswell (1974) and Kamphuis and Hall (1983) postulated that under controlled conditions it may be possible to use Plasticity index as a guide to erosion, e.g. high plasticity index, high resistance to erosion and low erosion rate. Plasticity index describes the moisture content of the sediments which depends on the amount of clay present (as it is the clay which absorbs the water). The swelling is related to the amount of water uptake which is in turn related to the clay content; less clay means more sand and silt and so erosion of larger particles. Enger (1964) found that the boundary shear stress needed to produce erosion is dependent on the moisture content, and the higher the water content the lower the critical shear stress (More and Mash, 1962; Gularte et al., 1980). Smerdon and Beasley (1959) utilized the plastic index PI in describing the critical shear stress τ_c.

$$\tau_c = 0.0034(PI)^{0.84} \tag{2.38}$$

and using the dispersion ratio D_r

$$\tau_c = 0.1213(D_r)^{-0.63} \tag{2.39}$$

The plasticity index can also be used to give a measure of activity, defined as

$$\frac{(Change\ in)PI\%}{(Change\ in)Weight\ of\ the\ Clay\ Fraction\%} \tag{2.40}$$

Chemical Controls.

A number of investigations have been carried out on the chemical properties of the pore and eroding fluids of cohesive beds. As mentioned above the stress history and swelling potential are likely to be important factors in erosion. The potential of a clay mineral to swell depends on its chemical structure. As stated previously, two-layer clays eg. Kaolinite are more stable, inert and less likely to swell than three-layer clays eg montmorillonite. The mode of deposition determines the initial structure of the deposit; freshwater deposits have a disperse structure while deposits laid down in sea-water have a flocculated structure. Remoulded deposits tend to have only a few natural bonds and strength relates to their structure. However compaction of a remoulded sediment at a low moisture content will result in swelling at a later date if the sediment becomes saturated.

Because cohesion is very much dependent on the electrochemical behaviour of the clay minerals in the sediment then any changes in the electrochemistry of the environment can have a major affect on the erosive behaviour of the sediment. Degree of dispersion in dispersive clays was considered by Arulanandan and Heinzen (1977), the saturation of an un-consolidated soil causes chemical changes and can allow trapped gas to escape which then disrupts the soil surface making it more vulnerable to erosion. The properties of sodium absorption ratio 'SAR', cation exchange capacity 'CEC' and exchangeable sodium percentage (degree of dispersion) 'ESP' and their affect on erosion are often considered (Sargunam et al., 1974; Kandiah and Arulanandan, 1974; Alizadeh, 1978; Arulanandan et al., 1973, 1975, 1980).

Arulanandan et al. (1975) looked at the influence of pore and eroding fluid on consolidated sediments eroding particle by particle. A number of chemical features were measured, including ESP, SAR and CEC ratios.

$$ESP = \frac{Exchangeable\ Na}{CEC} x100 \qquad (2.41)$$

$$SAR = \frac{Na^{+}}{\frac{1}{2}(Ca^{2+} + Mg^{2+})} \qquad (2.42)$$

A low SAR produces inter particle attraction while a high SAR produces dispersal; this translates to τ_{cr} increasing with increasing CEC for low SAR but decreasing for high SAR. Although the precise relevance of these variables to natural deposits is not certain, they could be used as a guide to erosion susceptibility and re-suspension potential of cohesive beds (in relation to osmotic swelling (Mehta and Parchure, 1982)).

Arulanandan (1975) noted that the strength of cation exchange capacity of multi-valiant cations sets an upper limit on the degree of swelling, thus causing greater resistance to erosion. Work by Raudkivi and Hutchison (1974) appeared to show that zeta potential and ion exchange capacity had no affect on erosion, although the effect of pH variations were not investigated. From knowledge of the clay chemistry it can be seen that cation concentrations affect the bonding between clay particles that determines swelling, and would therefore be expected to have an affect on erosion.

The salinity is a measure of the amount of dissolved salt in the fluid and, along with the ionic concentration of the pore and eroding fluids, it would be expected to affect the clay chemistry. Changes in the pore fluid density give different thresholds for the same sediment and differences between eroding fluid and pore fluid cause changes in the threshold, due to the swelling or contraction of the clay minerals, depending on the ionic concentration and ion type (Sargunam et al., 1973). Increasing salinity causes a decrease in the repulsive inter-grain forces; this results in more dense flocs, higher settling forces (Al Ani et al., 1991) and stronger beds (Moore, 1991). If the salt concentration of the eroding fluid is less than that of the pore fluid, swelling of the clay minerals at the surface will occur and cause a reduction in the critical shear stress (Arulanandan et al., 1975). This may be a result of cementation especially in sediments that are prone to desiccation (Owen, 1975). Some workers (Arulanandan, 1975; Gularte, 1980; Mehta et al., 1982) found an increase in erosion (a reduction in τ_{cr}) with increasing salinity. However it is the difference between the overlying and pore fluid salinities; i.e. the salinity gradient (and its

magnitude) across the sediment water interface, that is of more importance than the salinity of the overlying fluid. Therefore, salinity is a controlling factor in environments where these gradients occur e.g. sediments exposed to rainfall and changes in salinity of the eroding fluid (Ariathurai and Arulanandan, 1978; Allen, 1985b).

Raudkivi and Hutchison (1974) using a commercial kaolinite clay and a low salinity range of distilled water to 0.1 moles of $NaNO_3$ (1.8ppt) (cf. average sea water salinity of 35ppt) found that a salinity rise in this range appeared to cause an increase in erosion with the effect being more pronounced on the finer fractions. Parchure and Mehta (1985) found that salinity variations have little affect above concentrations of 10ppt with the largest effects happening at concentrations of around 2ppt. The affect of low salinity variations on initial rigidity was also noted by Migniot (1968). Salinity variations of this type occur in estuaries. As the salinity of the water increases in the mixing zone of an estuary, different types of clay mineral become cohesive at different salinities. Table 2.2 presents the critical cation and corresponding salinities for potential aggregation of three clay minerals.

Temperature variations can affect both water and clay properties. An increase in temperature reduces the attraction between clay particles by increasing thermal motion, and causes a decreases in the threshold shear stress (Babcock, 1963; Grissinger, 1966; Kandiah, 1974). In the overlying water higher temperatures can cause more frequent turbulent bursting (Taylor and Vanoni, 1972); it will also reduce fluid viscosity and therefore decrease the bed shear stress (Gularte et al 1980). These two properties have opposite affects on the erosion threshold and rate and give a complex picture. This is reflected by seabed data that suggest an erosion increase with falling temperature (Buchan et al., 1967; Newton and Gray, 1972) and work by Ariathurai and Arulanandan (1978) that showed an erosion increase with rising temperature.

Christensen and Das (1973) carried out investigations using pipes lined with a 100% saturated, remoulded, and consolidated sediment of kaolinite, gruclite clay and ottowa sand. They assumed that the clay surface was smooth and evaluated friction factors accordingly from

Clay type	Total cation concentration, in milliequivalents per liter	Salinity in grams per liter
Kaolinite	1.0	0.6
Illite	2.0	1.1
Montmorillonite	43.0	2.4

Table (2.2): Critical cation concentrations and salinities for potential clay mineral aggregation (after Ariathurai and Krone 1976).

diagrams by Moody (1944). At the start of each experiment the erosion rate decreased due to the removal of loose material from the surface. When erosion did commence the rate was at first constant until the increased surface roughness caused rapid increase in the erosion rate. The shear stress at this point, where steady state erosion rate rapidly increases with increasing hydraulic tractive stress, is the critical tractive shear stress. The erosion rate was dependent on a number of factors: flow rate, sediment composition (already mentioned), surface roughness, density, and temperature. Surface roughness appeared to be more important than density and increasing temperature to increasing erosion.

It is postulated that the erosion of a saturated cohesive soil can be interpreted as basically a shearing processes that can be explained in terms of a rate process theory. By use of this approach, the values of the rate parameters (activation energy and number of bonds) are consistent with those obtained for steady state creep. This idea of a rate process has also been looked at by Gularte et al. (1980), using remoulded illite silt in a refrigerated water tunnel of constant pH. It was considered that the erosional response of cohesive sediments can be described with rate process and double layer theories, with solid-to-solid bonding essentially independent of salinity and water content and that the dominant inter-particle forces in surface cohesive erosion are physio-chemical rather than mechanical. Raudkivi and Hutchison (1974) also considered that temperature has an affect along with viscosity and molecular kinetic energy, although the affect of temperature is reduced by increasing salinity and decreasing particle size. However the affect of temperature should be considered of minor importance until the contribution of pH and mineral composition and mixture to erosion has been established.

Rate theory postulated by Christensen and Das (1973), Raudkivi and Hutchison (1974), Gularte et al (1980) and Raudkivi (1990), implies that the erosion rate increases with increasing temperature, as defined by reduced inter-floc cohesion. However it has been suggested that it is not important for poorly sorted sediments (Raudkivi and Hutchison 1967) and that it may in fact influence erosion via its affect on the biological processes in the sediment (Yingst and Rhoads, 1978; McCave, 1984).

In abiotic, pure clay beds the erodibility increases with increasing pH (Montague, 1986). The effect of pH on erosion is complex, as pH will have an effect on biological activity in the sediment and this rather then the pH change could alter the bed's erosive behaviour. Biological processes can also alter the pore fluid pH and these changes can be diurnal due to changing process between night and day. (Bordovsky, 1965; Montague, 1986; Paulic et al., 1986; van Leussen, 1988; Dyer, 1989; Dade and Nowell, 1991).

2.3.6.5. Biological Controls of the Threshold and Rate of Erosion.

Why consider the affects of biological organisms? The activities of biological organisms can have a major affect on the surface sediments by varying their physical and chemical properties and so affect bed stability. These alterations to the bed properties are: (1) changes to the bed roughness; (2) variation of the modal grain size; (3) modification of sediment packing, shear strength and water content. However these factors are interconnected and all three should be considered together when looking at the affects of marine invertebrate benthos on sediment characteristics.

The affects of the marine invertebrate benthos on the benthic boundary layer are mainly limited to a zone stretching from a few centimetres above the bed surface to a few tens of centimetres below the bed surface. The affect of a marine organism on the sediment depends on the behaviour of that organism, and on its interactions with the other organisms. For this reason, marine organism can be defined into two main groups, pioneering and equilibrium assemblages.

The pioneering assemblages colonizes freshly disturbed or new sediment and has to face major physiological problems. The organisms feed from the water column or near the sediment surface. Tube-dwelling polychaetes are the first to colonize, and their tube walls can control the rate of diffusion of ambient pore water solutes into the tube environment, helping to insulate the organism from the sediment (Aller, 1980). The

sedimentary effects of the pioneering species are limited to the near-surface region, less then 2cm, and can be summarized as:

1. Construction of dense tube aggregations, which may affect micro-topography and bottom roughness on a scale dictated by tube diameter, height and spacing.

2. Fluid bioturbation, which pumps water into and out of the near surface sediment through vertically orientated tubes. Particle bioturbation, although present, is of subordinate importance.

3. Surface deposit feeding and suspension feeding, which cover the sediment surface with faecal pellets, especially the fusiform pellets of opportunistic polychaetes (Rhoads and Boyer, 1982).

The equilibrium assemblages cover the high-order successional assemblages that are found in areas of sediment that are rarely disturbed. These are made up of tube-dwelling and free-living organisms that are dominated by infaunal deposit feeders. These stages are associated with a sediment surface that is deeply oxygenated and where the redox potential discontinuity (RPD) reaches depths of over ten centimetres. The redox potential discontinuity (RPD) is the zone in the sediment where anaerobic reactions take over from aerobic reactions due to the low supply of oxygen. In pioneering stages which are inefficient at exchanging the ambient pore water with the overlaying water and oxygenating the sediment the RPD is found closer to the surface. The feeding of the equilibrium stages are concentrated at this depth with the RPD being related to the feeding. This redox region appears also to be a zone of high microorganism productivity (Yingst and Rhoads, 1980). For shallow water environments the sedimentary affects of the equilibrium stages can also be summarized as follows:

1. Transfer of both water and particles over vertical distances of up to 10-20cm takes place.

2. Intensive particle mixing produces homogeneously mixed fabrics and many of the particles at and below the sediment surface may be in the form of faecal pellets.

3. Head-down feeding produces void spaces (feeding pockets) at depth within the sediment.

4. The RPD is located over 2cm into the bottom and commonly to depths of 10-20cm.

5. Surface micro-topography may be featureless and plainer if tidal re-suspension "smooths" over biologically produced features at the sediment surface, or in the absence of smoothing effect, the surface may be covered with numerous feeding pits and faecal or excavation mounds (Rhoads and Boyer, 1982).

Rhoads and Boyer (1982) carried out a laboratory experiment to investigate the affect of pioneering and equilibrium assemblages on the geotechnical properties of two sediments. The equilibrium assemblage organisms decreased the shear strength of the top 2.5cm surface interval by means of particle advection and burrow excavation. They also produced faecal pellets which caused a reduction of the modal grain size reducing particle to particle contacts and increasing porosity.

The pioneering species also produce faecal pellets but due to the lack of effective vertical mixing these pellets are deposited and remain at the surface. The increase in shear strength with this assemblage can also be related to tubes increasing sediment resistance to horizontal shearing forces, and to mucus binding of the particles. The mucus is formed by the near-surface populations of microorganisms and meiofauna that are stimulated by the pumping of water into and out of the surface sediment by the tube organisms.

The experiment also shows a change in sediment properties below the depth of the living macrofauna. This affect is called the "far-field" effect. The depth of the RPD is related to the far feild effect which is believed to be real biological phenomena. Rowe (1974) showed that burrowing anemones can affect sediment shear strength as much as 20cm from their burrows. Yolida limatula can affect microbial ATP (adenosine triphosphate) and, production and consumption of decomposition products well below the sediment that it occupies (Aller, 1978). This is caused by the way in which the clam affects the rate of exchange of pore water constituents. Chemical reaction rates and concentration gradients of dissolved compounds in the pore water are affected by bioturbation especially respiratory pumping. The RPD is maintained by respiratory pumping and is usually below the region of living macrofauna and is a zone of intensive microbial production (Yingst and Rhoads, 1980). The physical properties of the

sediment are influenced by the interstitial meiofauna which are affected by the chemical and physical gradients set up by the macrofauna reworking (Cullen, 1973; Boyer, 1980).

A graded bed is formed at the base of the bioturbation zone, by the reworking and concentration of silt and sand sized particles, with specific densities less then 0.2. This density size stratification is another possible far-field related affect (van Straaten, 1952; Rhoads and Stanley, 1965; Rhoads and Young, 1970; Cadee, 1979).

Bed Roughness: Tubes, Tracks and Burrows.

As organisms burrow, feed, forge, excavate and move about leaving tracks and trails, they alter bed roughness. The features vary in size from sub-millimetre up to meters for ray pits. The effect can increase and decrease bed roughness, and contribute directly to sediment entrainment (Bell and Sherman, 1980; Grant et al., 1990), by changing the micro-topography of the bed surface which increases the roughness, bed friction and therefore probability of sediment erosion (Nowell and Jumars, 1984; Ashely and Grizzle, 1988; Dabron et al., 1991). For small mobile species the homogeneous reworking of the surface results in a smooth flat bottom (Rhoads and Young, 1970). The opposite is true for large sedentary species in which each individual can cause major topographical relief. Another important biological roughness element is tubes that project a few millimetres above the sediment surface. The affect of tubes on the bed is varied and complicated by the association of both sediment stabilizing and destabilizing species with the tube dwelling organisms. Individual tubes can enhance bottom erosion (Eckman et al., 1981) while dense tube fields are related to elevated topography (due to deposition), a decrease in mean grain size, and an increase in the amount of organically rich detritus between the tubes. (Mills, 1967,1969; Myers, 1977a; Lynch and Harrison, 1970; Woodin, 1976; Featherstone and Risk, 1977; Bailey-Brock, 1979).

Flume work carried out with the capitellid polychaete Heteromastus filiformis by Rhoads et al. (1978b), showed that the population increased the critical erosion velocity by 80%. However a simple interpretation is complicated by the fact that the authors also demonstrated in separate

experiments that the entrainment velocities can be increased by as much as 60% by bacterial mucus films.

Nowell and Church (1979) used LEGO@ construction blocks to look at affects of different densities of roughness elements on the marine boundary layer. At low densities (less then 1 unit area of block per 22 unit areas of flume floor) the blocks act as individual isolated elements. Turbulent vortices are shed from individual roughness elements and the turbulent energy is transferred to the bed. Although a complex function of tube height diameter and spacing, they determined that for high densities (1/8-1/12) of tubes the bed stability is enhanced. At these densities maximum turbulent intensity and the rate of turbulent energy dissipation is elevated to near the tops of the roughness elements, which 'protected' the bed within the tube field from high energy turbulence ("skimming flow" sensu Morris, 1955).

The evidence for tube stabilization of the sea floor from changes in sediment elevation, quality and grain size, need to be looked at with care. The tubes may not themselves be totally responsible for stabilizing the bed. The tube dwelling organisms by pumping water across the sediment water interface increase the supply of dissolved nutrients which enhances productivity of bed stabilizing exudates of the chemautotrophic microorganisms or diatoms (Webb, 1969; Aller and Yingst, 1978; Aller, 1980). Bed stabilization can be caused by armouring of the bed by dense amounts of shell material at the sediment interface protecting the bed from erosion (McCall, 1977; Rhoads et al., 1978a). Some of the stabilization affects noted may have been due to the presence of sediment-binding exudates from surface organisms (Eckman et al., ?), fine-grained sediments and faecal pellets around tubes (Mills, 1967; Bailey-Brock, 1979) or mucus secreting bacteria, diatoms and meiofauna (Sanders et al., 1962; Rhoads et al., 1978; Eckman, 1983).

Surface tracks and trails alter bed roughness by changing the exposure and protrusion of grains and the bed micro-topography (Gray, 1974; Eckman et al., 1979; Lee and Swartz, 1980; McCall and Tevesez, 1982; Meadows and Tufail, 1986; Meadows and Tait, 1989). A number of investigations have shown that bed roughness produced by surficial tracks

and trails results in sediment destabilization and lower critical shear velocities. Nowell et al. (1981) have shown that the small clam (4mm) Transenella tantilla reduced the critical shear velocity by 20% in fine sands. Macrofaunal and meiofaunal bioturbation can reduce bed roughness (Cullen, 1973; MacIlvaine and Ross, 1979; Boyer, 1980). Macro and meio-fauna fluff up the interface and decrease critical shear velocities (Boyer, 1980). Ostracods, copepods and foraminifer produce a hummocky relief by their movement just below the surface (Rhoads and Boyer, 1982). The reduction in entrainment in some cases may be due to the lessening of surface particles by meiofauna and microfauna rather then the changes in bed roughness (McCall and Tevesz, 1982). Smaller species can have the affect of reducing the micro-topography of larger organisms thereby creating a smoother bed (Cullen, 1973; Young et al., 1985; Christian, 1991;), which is more able to withstand fluid stressing (Jumars and Nowell, 1984).

Bioturbation, if extensive enough, can result in small-scale vertical stratification of the bed by grain size, giving rise to a bed armoured by a layer of grains too coarse to be eroded (Nowell et al., 1983), although generally bioturbation tends to reduce any gradients in the sediment causing a more homogenous sediment fabric (O'Brien, 1985; Leithold, 1989; Bennet et al., 1990). Burrowing increases the sediment's water content (Harrison and Wass, 1965; Rhoads and Young, 1970; Rhoads, 1970, 1973; Cadee, 1984; Wetzel, 1990), decreases the undrained shear strength (Rhoads and Boyer, 1982) and decreases near surface sediment compaction (Bokuniewicz et al., 1975). However burrows that are lined and strengthened by mucus can locally strengthen the sediment (Meadows et al., 1985; Richardson et al., 1985; Daborn, 1991).

Pelletisation.

Marine benthic invertebrates produce faecal pellets which are usually deposited at the surface. The particles are stripped of most absorbed organic material as they pass through the animal and then bound with mucus into low porosity faecal pellets (Pryor, 1975; Brown, 1982; Gorsline and Reynolds, 1991). Another type of pellet deposited on the surface is pseudofaeces which have been manipulated, but not ingested by an

organism (Rhoads and Boyer, 1982). The fate of these pellets depends on the community present. In equilibrium communities, efficient bioturbation advects the pellets downwards and results in them being evenly distributed throughout the zone (Rhoads, 1967). However with less efficient vertical mixing communities, like the pioneering communities, the pellets remain near the surface. With all stages the result is a change in grain size, eg for muds, a very fine pelletal sand fraction is introduced into the silt-clay matrix (Rhoads and Young, 1970). The sand sized pellets tend to remain until they are broken down by algae and microbes because detrital feeders tend to preferentially select silt and clay sized particles.

The presence of pellets may be expected to lower the threshold shear velocity for entrainment from that for cohesive silt and clay size fractions to that for fine sands. However flume observations have shown that this is not always the case and that the critical shear velocities may increase (Nowell et al., 1981). The possible cause is that in nature it is rare for single particles to move independently of each other and that fine sand sizes are combined with organic-mineral aggregates formed by microbial mucus (Rhoads, 1973; Johnson, 1974).

Mucus.

The formation and occurrences of pellets is controlled largely by microbial, meiofaunal and diatom binding mucus. Mucus binding of sediments by bacteria (Webb, 1966; Reimers, 1982). microalgea (Paterson et al., 1986; Grant et al., 1986; Vos et al., 1988), meiofauna (Riemann and Schrage, 1978) and macrofauna (Grenon and Walker, 1980) may stabilise sediments (Fazio et al., 1982; Webb, 1991). Bacteria bind to objects by using tangled fibres of hydrated, anionic polysaccharides, and these form a felt-like 'glycocalyx' surrounding a cell or colony (Costerton et al., 1981), to the extent that the extracelluar polysacharides can be more abundant then the bacteria themselves (Hobbie and Lee, 1980). These films and mats of exudates will hold mineral grains that come into contact with them (Glogger and Hanselman, 1985), stabilize the sediment, and the films themselves can increase frictional resistance to flow (Gucinski and Baier, 1983; Charaklis, 1984).

Mucus, secreted by epipsammic diatoms, epipelic diatoms and bacteria on the surface of particles, increases the inter-particle cohesion (Black, 1993). Epipelic diatoms that migrate vertically in the surface sediment layers, in response to diurnal and tidal periodicities, can form an extensive network of mucus threads (Round, 1981).

Rhoads et al. (1978b) have demonstrated that microbial binding of medium sand to coarse silt sized spherical glass beads in a flume can occur within three days and increase critical entrainment velocities by up to 60%. The absorption of glycoproteinaceous films onto surfaces enhances bacterial colonization (Baier, 1973; Neihoff and Loeb, 1973), and the negative surface charge of clay minerals promotes rapid absorption of mucopolysaccharide films (Khailov and Finenko, 1970; Neihoff and Loeb, 1972).

The stickiness of mucus binding causes the bed to be eroded by detachment of aggregates from the bed, which then move downstream as tractive or suspended load. The velocities needed for this entrainment are higher then the predicted value for particles of a similar size and as much as 80% higher then the critical excitation velocity (Rhoads and Boyer, 1982). Rhoads et al. (1978b) took this critical excitation velocity to be the velocity at which organic mineral aggregates (including pellets) that project above the bed surface start to vibrate and rock in place. The total amount of mucus present is not of great use in determining the bed response to fluid shear, as the major increase in critical shear velocities are caused by the initial elastic film of mucus bridging the grain to grain contacts; further thickening of this film by more mucus may have relatively little affect. The affect of binding fine material into pellets alters the threshold of erosion, the form of transport (from suspended load to bed load) and increases the settling velocity.

Geotechnical Variations Due to Biological Interactions.

Benthic organisms have a substantial influence on the mass and bulk geotechnical properties of a sediment. Conversely the ease with which a free-living infaunal burrower moves through and feeds upon the sediment is known to be a function of the sediment water content and state of

compaction (Chapman, 1949). The affect on geotechnical properties can be very different for sands and muds. An example of this is the method used by some metazoa and especially bivalves, to facilitate burrowing. They inject water anteriorly into the bottom of their burrow; this causes instantaneous local increase in pore water pressure. The liquid limit of the sediment is exceeded temporarily, and the organism then moves forward into this liquefied region. In sands the excess pore pressure soon dissipates and overburden pressure quickly causes the sediment to collapse on itself. In cohesive silts and clays, the excess pore pressure is not dissipated quickly and the sediment may remain dilated some time after the passage of the organism. In this way the mass properties of the mud reflect the cumulative burrowing history, with the burrowing and pelletisation together causing sediment dilation (pellets decrease packing by increasing inter-pellet voids) (Rhoads and Boyer, 1982).

Water content can be either increased and decreased depending on the benthic community. Equilibrium communities, with their intensive particle bioturbation, can increase water content by 60-70%. Bokouniewicz et al. (1975) showed that burrowing causes a decrease in near-surface sediment compaction and undrained shear strength. With the inefficient vertical mixing of pioneering communities, the bottom can become compacted and the water content decrease by 60%. However the form, frequency, and intensity of physical bottom re-suspension will also affect water content (Tenore et al., 1982).

Exactly how macrofauna tube dwellers increase the sediment shear strength is poorly understood. This may be because the tube structures increase break-away torque of a shear vane or impede the vertical penetration of a penetrometer; for larger tube dwellers tubes may laterally compact the sediment up to several millimetres away from the tube (Aller and Yingst, 1978).

Other stabilisation mechanisms may be less obvious, such as the interaction between macrofauna, meiofauna and microorganisms. For example, pore water irrigation is associated with enhanced production of microbial populations and their mucopolysaccharide exudates. These viscous and elastic binding mucus secretions, generated by bacterial as

well as by macro- and meiofauna, may fill inter-granular pore spaces and many geotechnical properties are related to the water content of the sediment.

2.3.7. **Flume Studies: Advantages and Disadvantages.**

The research into the re-suspension of cohesive sediments has been undertaken using a number of different techniques. The following is a summary of some of these: a circular brass tube (Christensen and Das, 1973), a vertical, rotating annular cylinder (Sargunam, 1973; Ariathurai and Arulanandan, 1978; Chapuis and Gatien, 1986; Chapuis, 1986), a near bed vertically oscillating grid (particle entrainment simulator'; Tsai and Lick, 1986), rotating annular flumes (Creutzberg and Postma, 1979; Fukuda, 1978; Mehta and Partheniades, 1982; Sheng and Lick, 1979; Parchure and Mehta, 1985; Kuijper et al., 1989; Ockenden and Delo, 1991) and straight flumes (Enger and Carison, 1964; Kamphuis and Hall, 1983; Amos and Mosher, 1985; see also van Leussen and Winterwerp, 1990), a number of field flumes (Peirce et al., 1970; Nowell et al., 1985; Güst and Morris, 1990; Black, 1991; Maa et al., 1991; Amos et al., 1992b), submerged water jets (Sutherland 1966, 1967; Moore and Masch, 1962; Paterson, 1989) and miniature bench-top erosion devices (Vos et al., 1988, Schüneman and Kühl, 1991) (after Black, 1993). Although this creates a large volume of data, it is not easy to compare individual experiments to each other, as different researchers have measured different bed properties. In fact, the erosion threshold that is defined may be dependent on the technique used to define it.

Another problem of laboratory based work is that of the bed. Remoulded and artificial (single clays) beds are likely to have properties different form those of natural beds and even blocks of sediment removed from the field and placed in a laboratory tank will undergo some changes particularly at the sediment water interface (Young and Southard, 1978; Sahla et al., 1987; Nowell and Jumars, 1987; Parker, 1991; Ranz-Geurra, 1991; Black, 1993). Changes and/or disturbance of biologically active organisms can drastically alter the response of the sediment to eroding flows (Grant et al., 1982).

Results presented to date demonstrate that near-shore and intertidal muddy sediments display both Type I and Type II erosion, with the former generally more prevalent for the actual interface aggregate networks (Peirce et al., 1970: Black, 1991; Amos et al., 1992a,b). This is consistent with a strength stratified interface and a more uniform variation of shear resistance at depth (van Leussen and Dronkers, 1988) and enables arguments from the many controlled laboratory experiments to be utilised in the interpretation of the field data. These studies have demonstrated that the excess bed stress rather than the absolute value controls the erosion rate. Experimentalists have observed both surface erosion and massive erosion, and combined bed and suspended load transport.

These drawbacks of flume work must be remembered. Laboratory work must also be carried out under reasonably controlled conditions compared to the natural environment. However laboratory work is essential for understanding the processes involved in cohesive sediment behaviour, so as to provide the necessary background data for more complex and less controlled field studies.

2.4. **Summary.**

From the wide range of work done, it appears that the behaviour of a cohesive bed is controlled by a number of properties. For a piece of research to be meaningful, a number of these properties need to be measured. A criteria for the erosion threshold needs to be defined and the nature of the ensuing erosion examined. Although the behaviour of the sediment is complex, both the threshold of erosion and the rate of erosion are related in some way to the shear strength of the sediment. The amount by which the applied shear stress exceeds the bed shear strength (the excess shear stress) is particularly important, especially in relation to the erosion rate. It is therefore important to be able to measure this particular property as well as others, e.g. porosity and density, in situ, without causing any further disturbance to the bed. In the following two chapters a method is outlined by which at least two of these parameters (shear strength (rigidity modulus) and porosity) may be measured using geophysical techniques.

As well as these measurements, others are needed to allow different investigations to be compared, and the usefulness of these new techniques to be compared. This means measuring chemical properties, size distribution, clay mineralogy (content and type), geotechnical parameters, and measurements of the organic content, to name but a few.

CHAPTER 3.

ACOUSTIC THEORY AND MEASUREMENT.

3.1. Acoustic Theory.

3.1.1. Basics.

The way in which acoustic waves propagate through a material is controlled by the properties of the material. In the most basic way the material will behave elastically, as described by elastic theory and Hooke's Law.

Hooke's Law is only applicable for small strains, where the strain and the stress producing it are directly proportional. For large stresses beyond the materials elastic limit, Hooke's Law is no longer applicable and strains resulting from stresses exceeding the elastic limit, do not vanish completely once the stresses are removed.

For an isotropic medium the relationships between stress and strain are relatively simple.

Normal Stress $\sigma_{ii} = \lambda\Delta + 2\mu\varepsilon_{ii}, \quad i = x,y,z;$

Shear Stress $\sigma_{ij} = \mu\varepsilon_{ij}, \quad i,j = x,y,z, \ i \neq j.$

where Δ is the dilatation (change in volume per unit volume), ε_{ii} is the normal strain and ε_{ij} is the shearing strain. λ and μ are called Lame's constants and μ is also known as the modulus of rigidity or the shear modulus (resistance to change in shape). These two constants can be used to describe the elastic behaviour of a material and therefore the way in which an elastic wave will propagate through the medium. Other elastic constants are also used, including Young's modulus (E), Poisson's ratio

(σ) and the bulk modulus (K); all of these can be defined in terms of Lame's Constants.

Young's modulus E is the ratio of uniaxial stress to longitudinal strain under uniaxial loading.

$$E=\frac{\mu(3\lambda+2\mu)}{(\lambda+\mu)} \tag{3.1}$$

Under this uniaxial loading Poisson's σ ratio is the ratio of lateral expansion to longitudinal contraction.

$$\sigma=\frac{\lambda}{2(\lambda+\mu)} \tag{3.2}$$

The bulk modulus K under conditions of isotropic compression is the ratio of hydrostatic pressure to volumetric strain or dilation (resistance to change in volume).

$$K=\frac{3\lambda+2\mu}{3} \tag{3.3}$$

Gassman (1951) defined the system bulk moduli K for saturated sediments in terms of four components: porosity n, the bulk modulus of the pore water K_w, the bulk modulus of the mineral solids K_s and the frame bulk modulus K_f. The porosity determines the relative contributions of the other terms to the overall bulk moduli. Wave speeds in marine sediments are quite sensitive to the elastic properties of the skeletal frame, the frame modulus. These frame modulus may be deduced from empirical relations (Stoll, 1977; and Hamilton, 1971) or alternatively be computed from the self-consistent theory of composites as defined by Berryman (1980, 1981); see Ogushwitz (1985a).

These dynamic properties have an affect on the speed and the attenuation of acoustic waves propagating through a marine sediment. This is evident from the increase of wave speed with depth, caused by the changes in the frame elastic moduli, (due to the rapid near surface decrease in porosity from the compaction and cementation of sediment grains, and improved grain contacts caused by the pressure of the sediment above). Cementation modifies the intergranular elastic behaviour and therefore affects the frame modulus (Ogushwitz, 1985a). The acoustic

properties of a sediment are dependent in a very fundamental way on its frame modulus which, in turn is critically dependent on the nature of grain to grain contacts (Johnson and Plona 1982; Ogushwitz 1985c). The wave equation can be derived in terms of these constants and indicates the propagation of two independent waves, the velocities of which can be defined in terms of elastic constants and the bulk density ρ of the medium. For compressional or P-waves,

$$V_p = \left(\frac{\lambda + 2\mu}{\rho} \right)^{1/2} \tag{3.4}$$

and for shear or S-waves,

$$V_s = \left(\frac{\mu}{\rho} \right)^{1/2} \tag{3.5}$$

Substituting equation (3.3) into (3.4) the P-Wave velocity can be written in terms of the bulk and rigidity moduli.

$$V_p = \left(\frac{K + \frac{4}{3}\mu}{\rho} \right)^{1/2} \tag{3.6}$$

The way in which these two waves travel through a medium is different. In the case of the P-wave the displacement is perpendicular to the wavefront, e.g. the particles of the medium move back and forth parallel to the direction of wave propagation. Particles in the medium are dilated and compressed by the longitudinal displacement of the P-wave, which is also termed the dilatational, longitudinal, irrotational or compressional wave. With the S-wave the displacement is perpendicular to the direction of wave propagation. In fact a rotation is being propagated, but because the angle of rotation is infinitesimal the curvature can be ignored and the particles in the medium are considered to be displaced transversely to the direction of propagation. As the rotation varies from point to point along the path of propagation, the medium is subjected to a varying shearing stress as the wave moves. The S-wave is also termed the shear, transverse or rotational wave and can be resolved into horizontal (SH) and vertical (SV) components.

In a fluid, the shear modulus μ is zero and only a compressional wave can propagate with a velocity V_f, where

$$V_f = \left(\frac{\lambda}{K}\right)^{1/2} = \left(\frac{1}{\beta\rho}\right)^{1/2} \qquad (3.7)$$

and ß is the bulk compressibility of the media, the reciprocal of the bulk modulus.

These equations come from the Hookean model but Hamilton (1971) favoured a 'nearly elastic' or linear visco-elastic model to account for wave attenuation. In this model the rigidity modulus μ and Lame's constant λ in the equations of elasticity are replaced by complex Lame's constants $(\mu+i\mu')$ and $(\lambda+i\lambda')$, which are independent of frequency; μ and λ represent elastic response (as in the Hookean model), and $i\mu'$ and $i\lambda'$ represent damping of wave energy. However, in practice some natural materials, e.g. stiff clays and sands, do behave elastically and V_p, V_s and elastic moduli can be determined for an appropriate strain level (Cratchley, 1982). More recently, a visco-elastic model has been used, which uses parameters of viscosity, density and rigidity modulus. The most important of these is the rigidity modulus μ. The shear velocity can be interpreted as representing the cohesive nature of the bed, which is a function of interactive bonding and attraction, sediment fabric, clay mineralogy, pore fluid chemistry, organic content and depositional history. These are the same properties as those determining shear strength, which means that the rigidity modulus can be used in the same way as the shear strength as a measure of the erodibility. The shear velocity has the advantage that it can be measured more easily in situ and is not technique dependent (although it is related to the frequency used).

From a model suggested by Biot (1962), Hamdi and Taylor Smith (1982) have postulated that it may be possible to calculate the sediment permeability from an equation based on the full frequency range of the model. In Darcy's law the permeability coefficient k in units of area can be transformed into units of velocity ϕ.

$$k = \frac{\phi\eta}{g\rho_w} \qquad (3.8)$$

where η is the fluid viscosity, ρ_w is the fluid density and g is the acceleration due to gravity. The permeability relates to the velocities by the equation,

$$\phi = \frac{ng}{\omega}\left(\frac{\rho}{b\rho - n\rho_w}\right)\frac{V_0^2}{V_\infty^2}\sqrt{\left(\frac{\left[\left(V_p^2/V_0^2\right)-1\right]}{\left[1-\left(V_p^2/V_\infty^2\right)\right]}\right)} \qquad (3.9)$$

where n the fractional porosity, ρ the bulk density, b the mass-coupling factor, ω the angular frequency and V_0 and V_∞ are the zero-frequency and infinite-frequency velocities of the material, respectively.

Using the visco-elastic model, the rigidity modulus can be determined for an appropriate strain level. The variations of the rigidity modulus with strain (Figure 3.1) can be explained if it is considered that the shear wave velocity is related to the interaction of both the solid and fluid parts of the sediment. As a particle moves under the force of the shear waves, any fluid touching it will, due to its viscosity, move as well. The size of the fluid motion will depend on the size of the particle motion, which is determined by the magnitude of strain applied. Therefore the differences between elastic moduli determined by acoustics and those determined by more standard geotechnical techniques are related to differences in strain amplitude used in the different techniques.

In saturated sediments, dynamic rigidity and static shear strength are related to the same factors: sediment structure and the complex factors restricting relative inter-particle movement under stresses (Hamilton, 1971). The resistance to shear stress (shear strength or dynamic rigidity) in sands is related to the grain to grain contacts between mineral particles, the sliding and rolling friction between grains, to the number of inter-grain contacts, and to interlocking between grains. The number of inter-particle contacts depends on grain size and density of packing; for any given particle size, interlocking of grains increases with density of packing and angularity of grains. Porosity is a measure of packing, as shown by the decrease in cohesion and rigidity between fine particles with increasing porosity. In fine silts and clays, shear strength and dynamic rigidity are related to cohesion between fine particles. Intergranular stress is a function of this grain packing (grain size, shape, sorting, and

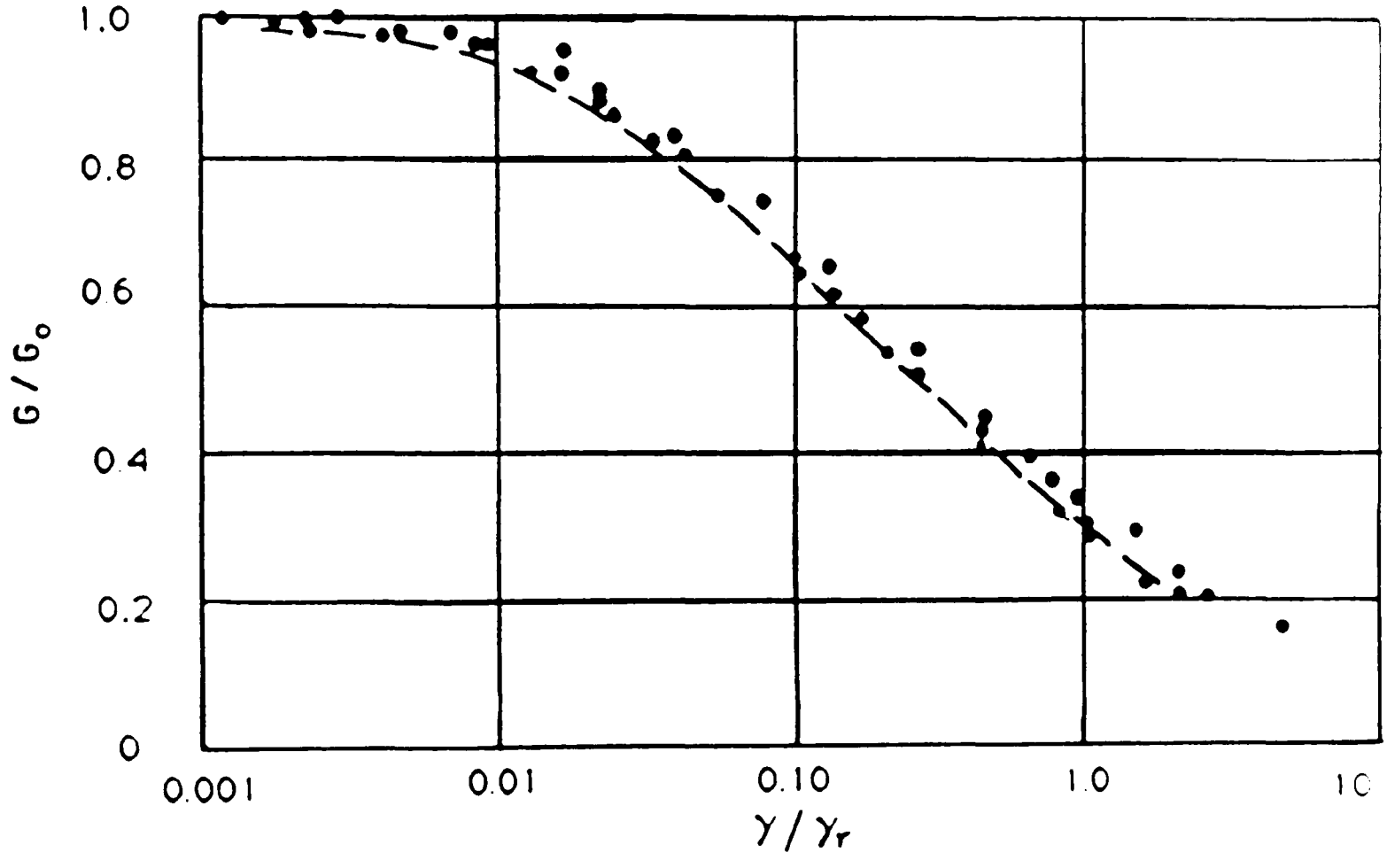

Figure (3.1): The variation of shear modulus ratio with shear strain (G is the shear or rigidity modulus, G_o is the initial tangent modulus, and the shear strain has been normalized for a reference strain) (after Woods, 1991 from Richart, 1987).

interlocking) and cementation. Along with porosity, intergranular stress is a significant property of the skeletal frame modulus (Ogushwitz, 1985c).

Domenico (1977) examined the affect of compressive stress and pore fluid properties on the elastic properties of fine grained sand and glass beads (porosity 38%). He noted: (1) the shear modulus increased non-linearly with differential pressure, (2) shear wave velocities generally decreased moderately with increasing brine saturation (as would be expected from the difference in bulk density), (3) the sand shear modulus increased more rapidly then that of the glass beads with increasing differential pressure. The sand frame becomes increasingly more rigid then the glass bead frame, probably as a result of the angular sand grains.

Work summarized by Hamilton (1971) shows that the well known effects on the shear strength (cohesion) of clay structure, inter-particle bonding, and thixotropic regain of strength after these bonds and structure have been broken, also applied to dynamic rigidity; in other words dynamic rigidity is due to cohesion in these clays.

Hamiltons (1971) conclusions on rigidity are that almost all marine sediments that have mineral to mineral contacts or flocculated clay structures will allow the transmission of shear waves if they have enough rigidity. This amount of rigidity may be small as long as it is significant. Thus any equation for elastic wave propagation in natural marine sediments that does not provide for rigidity, such as the Wood's equation (described below) should be abandoned.

When the rigidity is zero, no shear wave can be transmitted, and Poisson's ratio is that of a fluid or suspension: 0.50. Most natural marine sediments posses rigidity and transmit shear waves; therefore, most sediments have values of Poisson's ratio less than 0.50. Liquid saturation of porous rocks and sediments increases the velocity of compressional waves, and decreases the velocity of shear waves (Hamilton, 1971).

Bell and Shirley (1980) showed that even in highly porous clay material, there is enough rigidity to enable the propagation of a significant amount of shear wave energy. From data for low amplitude acoustic waves

in saturated sand and clay sediments it may be concluded that: shear wave speed is independent of temperature; compressional wave speed varies with temperature, but it can be determined if the speed in the pore fluid is known as a function of temperature; and compressional and shear wave attenuation are also insensitive of temperature. However Jones (1990) appeared to show that shear wave velocity will vary with temperature. These results seem to suggest that temperature gradients within the sample set up stresses which affect the intergranular forces, in turn affecting the shear wave velocity, with velocity changes only occurring on cooling and not on heating. However, the affect of the sample container contracting was not determined.

Hamilton (1971) confirms that either Hookean elastic or linear visco-elastic equations can be used to derive the same compressional and shear wave velocities and associated elastic constants. Shear wave velocities are more likely to show good correlation with strength parameters than compressional wave velocities (Nacci et al., 1974).

3.1.2. Suspensions.

Suspension of particles behave as fluids as long as the grains do not interact in any way, and as such the suspensions have a zero shear modulus, i.e. no shear strength. Woods (1930) produced an equation for compressional wave velocities in suspensions, in which the bulk density and compressibility are replaced by terms for the water and mineral fractions.

$$\rho = n\rho_w + (1-n)\rho_s \tag{3.10}$$

$$\beta = n\beta_w \pm (1 \pm n)\beta_s \tag{3.11}$$

where ρ_s is solid density, $ß_s$ is solid compressibility, ρ_w is fluid density, $ß_w$ is fluid compressibility and n is fractional porosity (Hamilton 1971). Substituting into (3.7) gives,

$$V_f = \left(\frac{1}{(n\beta_w + (1-n)\beta_s)(n\rho_w + (1-n)\rho_s)} \right)^{½} \tag{3.12}$$

This is Wood's emulsion equation and it predicts that the compressional wave velocity can be lower in dilute suspensions than in the individual water or mineral suspensions. Work carried out by Urick (1947; 1948) and Urick et al. (1949) on low concentration suspension of kaolinite has shown the equation to be true for these suspensions. The equation does not take into account any grain interactions and is therefore restricted to only true suspensions. This means that in all but high porosity sediments this equation will provide a lower velocity (Schultheiss, 1982).

Hay and Burling (1982) examined the scattering and attenuation of sound waves by elastic spheres. They assumed that the additional attenuation of a sound wave propagating in a dilute suspension results from scattering, and from heat conduction and viscous drag at the surface of the particle, and argued that the relative importance of thermal and viscous effects depends primarily on the difference in the bulk densities of the scatterer and the ambient fluid. In particular, for particles with the thermal and elastic properties of quartz and polystyrene, and densities greater than 1.3 and 1.7 g/cm^3, respectively, thermal losses can be ignored for frequencies at which the skin depths of the thermal and viscous waves are much less than the particle radius. Most particles composed of solid minerals should satisfy these conditions.

3.1.3. **Propagation of Elastic Waves in Saturated Sediments.**

The propagation of elastic waves in a saturated sediment is controlled by the dynamic response of the sediment, which in turn is determined by a number of parameters of which the following play a principal role; dynamic strain amplitude, porosity, static intergranular stress, degree of sorting and grain shape, material properties of individual grains, degree and kind of lithification and structure as determined by the mode of deposition (Stoll, 1980).

In a series of papers, Biot (1941; 1956a,b; 1962a,b) developed a theory to describe the propagation of stress waves in a porous elastic solid containing a compressible viscous fluid. This model has been developed

further by a number of authors, and it has been shown that it can satisfactory model the elastic constants of fine grained sediments, from very low frequencies of a few hertz, to very high frequencies of mega hertz (Geertsma and Smit, 1961; Stoll and Bryan, 1970, Stoll, 1974, 1976, 1977, 1980, 1985; Berryman, 1981; Attenbourgh, 1982; Hamidi and Taylor Smith, 1982; Hovem et al., 1991).

The theory assumes: The equations of motion are linear; The system can be divided into elements which are small in size relative to the wavelength of the elastic waves but are large compared to the pores (therefore the wavelength is large relative to the pores and dissipation due to scatter can be neglected); The system is defined in two parts: (i) a porous elastic solid containing (ii) a viscous fluid which is interconnected throughout the solid.

However, the theory is limited as it only applies to small strain amplitudes and macroscopic homogeneity is required. This means that a small element must be defined with a mean porosity, permeability, pore size, and a fairly narrow pore size distribution. If this cannot be defined then assumptions on inertial and viscous coupling will be invalid. This is likely to be the case with most natural marine sediments and therefore any sediment properties determined with the theory must take this into account (Jones, 1990).

The theory models the propagation of three types of body waves in a fluid-saturated porus medium; two dilatational waves and one shear wave. The first dilatational wave corresponds to the normal compressional wave with slow attenuation and slight dispersion as it propagates. The second dilatational wave, which is seldom observed in water-saturated sediments, has a lower velocity, attenuates very rapidly, has the form of a diffusion wave and its propagation is closely analogous to heat conduction. The theory shows that the rotational (shear) wave is uncoupled from the dilatational (compressional) waves and obeys independent equations of propagation. Nacci et al. (1974) defined the three types of elastic wave propagating through a saturated soil as: a dilatational wave through the pore fluid, a dilatational wave through the soil skeleton, and a shear wave through the soil skeleton (with an inertial contribution from the pore fluid

(Plona, 1980)). Due to viscous coupling between the fluid and the solid none of these waves are entirely independent, but the shear wave is probably least influenced by pore fluid coupling.

Yew and Jogi (1976) showed by comparing theoretical and experimental results, that the normally measured waves are in fact the fast waves as predicted by the Biot theory, and that it is possible to detected the slow wave. When the solid is modelled as a homogeneous elastic material the fast wave is equivalent to a dilatational wave. This fast wave shows little dispersion but the slow wave is highly dispersive and its amplitude decreases rapidly with distance, consequently making it difficult to detect except over short distances with short specimens. For both waves the amplitude decrement is frequency dependent with the amplitude of the slow wave decreasing much more rapidly than that of the fast wave.

The ability of a material to carry acoustic waves changes markedly as the material consolidates, ($\oint$ 3.1.1.) by changes to the frame moduli. Experiments on glass beads, carried out by Johnson and Plona (1982), show that (both experimentally and theoretically) in un-fused (unconsolidated) glass beads there is only one compressional wave, but after only light fusing of the glass beads into a consolidated elastic frame, both fast and slow compressional waves and a shear wave are observed, with the compressional waves having markedly different velocities from that of the un-fused case. This acoustic difference between un-fused and lightly fused glass beads is easily and quite naturally quantitatively described by the Biot theory (Johnson and Plona, 1982).

In earlier work Plona (1980), using porous sintered glass disks that act like the skeletal frame of the Biot model, had detected a slow compressional wave, which he deduced was a bulk wave and tentatively identified it as the Biot compressional wave of the second kind.

Berryman (1980) compared quantitatively this early work by Plona (1980) to the predictions of Biot's theory, with good results. The fast compressional wave and shear wave predictions lay inside the 3% experimental error bounds and the predictions of slow compressional wave speed fell within 10% of the experimental values.

Johnson and Plona (1982) have shown that slow waves exist as propagatory modes, above a frequency where the viscous skin depth is considerably less than the pore size of the material. At high frequencies the speed of the slow wave vanishes if the frame moduli vanishes, but at even higher frequencies with non-zero frame moduli, the slow wave may not be observable due to its short wavelength which leads to scattering and attenuation. In later work, Johnson and Plona (1984) defined the two compressional waves as first and second kinds, fast and slow respectively. The first kind has the fluid motion in phase with the frame and is propagatory in character. The second is propagatory or diffusive in character depending on frequency, frame stiffness, and properties of the pore fluid matrix; the fluid motion is out of phase with the frame. This change in mode of propagation with frequency for the compressional wave of the second kind, diffusive at low frequencies, has also be noted by Berryman (1981).

The shear wave velocity for a fluid-saturated frame is just the speed of the dry frame with a frequency-dependent correction for the inertia of the fluid (Berryman, 1981). For very high frequencies, the velocity will be higher mainly because the fluid mass is decoupled from the frame (Hovem and Ingram, 1979). At low frequencies the viscosity of the fluid causes the fluid motion to lock on to that of the solid for both fast compressional and shear modes (Gassman, 1951).

A number of investigations have shown a relationship between shear wave velocity, shear modulus and porosity (as well as other sediment properties). Although there is no theory for determining the rigidity modulus from sediment grain properties of size, shape and packing, a few empirical formulations have been made. Stoll (1980) gave the rigidity modulus in a two-component system of a fluid and a porous elastic frame as,

$$\mu = F_1 P_a \left(\frac{\sigma_o}{P_a} \right)^{2m} \qquad (3.13).$$

where P_a is the atmospheric pressure, σ_o is the mean effective stress and F_1 is a dimensionless factor that depends primarily on porosity. F_1 has various forms due to the efforts of different authors to find the best fit to

their experimental data. However the most common form is the one originally expressed by Hardin and Richart (1963),

$$F_1 = \frac{c(d-e)^2}{(1+e)} \qquad (3.14).$$

where e is the voids ratio, related to the porosity by e=n/(1-n), m, c and d are constants adjusted to fit the experimental data. The rigidity modulus can also be obtained directly from shear wave velocity measurements in dry sediments or at the extreme low frequency limit in saturated sediments, due to the assumption that μ is independent of pore-fluid and frequency (almost). Therefore for a saturated sediment at low frequency,

$$\mu = V_s^2 \rho \qquad (3.15)$$

and for a dry sediment,

$$\mu = V_s^2 \rho_s (1-n) \qquad (3.16).$$

The relationship between porosity and shear wave velocity is not simple, as it is related to grain shape, size, sorting and packing. With the shear wave velocity showing a marked sensitivity to grain shape, due to the nature of interlocking between grains. This was demonstrated by both Bell (1979) and Schultheiss (1983) with deposits of highly angular grains showing higher velocities then similar porosity deposits of well rounded grains.

The theory described above and its many adaptations can be used to describe a number of properties of acoustic wave propagation. Although McCann and McCann (1985) showed that Biot's model in non-cohesive saturated sediments needs some alteration, to allow it to predict the variation with frequency of the compressional wave attenuation coefficients.

The theory uses a number of parameters, some of which can be obtained directly; however some need to be inferred particularly the complex bulk and shear frame moduli. A number of authors have developed methods of determining the coefficients in Biot's model. For example Bedford et al. (1984) formulated a method for determining the drag and

virtual mass coefficients and concluded that the magnitudes and frequency dependence of both are determined by the microstructure of the porous medium.

Browen (1980) showed a connection between formation factor and fluid-solid coupling in Biot's equations. At low frequencies, fluid-solid coupling is due primarily to viscous forces and at intermediate frequencies, viscous forces increase inertial coupling and inertial forces increase viscous coupling. The connection was that the coefficient of inertial (fluid-solid) coupling is equal to or greater than the product of porosity and the low-frequency electrical-resistivity formation factor. This is equal when fluid viscosity affects are minimal, as at high-frequencies in high permeability and porosity media. Thus the product of formation factor and porosity can provide a lower limit to the coupling coefficients.

The Biot theory is frequently applied to two physically distinct situations. That of a fully consolidated frame and that of a partially consolidated frame or fluid suspension, where a rigid frame may exist but at least some of the solid particles are not connected to the frame (Berryman, 1981). The coefficients in Biot's strain energy function are related to the frame and fluid moduli and will vary for the two cases. Although the standard approximation of these coefficients gives good agreement to measured results, a more accurate determination of the frame moduli and inertia moduli is desirable, and may be possible analytically in the context of a macroscopic model.

3.1.3.1. **Attenuation, Energy Losses and Log Decrement.**

Attenuation and other viscous losses are determined by a number of sediment properties, the pore size (parameter), the mass coupling affect between the fluid and the solid, form and size distribution of grains, porosity and the mutual relationship of these factors to each other (Hovem and Ingram, 1979).

Hamilton (1976) concluded that at frequencies between a few hertz to at least 1MHz, there is no measurable compressional velocity dispersion;

the linear attenuation is approximately related to the first power of frequency; the log decrement and 1/Q (the specific attenuation factor) are independent of frequency; and theoretically the same should be true for low strain shear waves. These conclusions are supported by Kudo and Shima (1970) and McDonald (1958).

The compressional wave attenuations through carbonate sediments are found to be similar to those through some terrigenous sediments. This is because the compressional wave attenuation through sediments is mainly driven by the permeability and shear properties of the sediments. The pore size distribution has a more dominant effect on the acoustic wave attenuation in higher frequencies. For low frequencies, conventional Biot theory adequately predicts the acoustic wave attenuation. However, for higher frequencies, the variable pore size in the model shows a better agreement with the measured data. The permeability and shear properties of oolitic shallow water carbonate sediments are comparable to those of some terrigenous sediments (Badiey et al., 1988).

Movement of the fluid relative to the solid frame (and thus probable viscous fluid losses) are allowed for by the Biot theory. These losses will increase with frequency (f); proportional to f^2 for lower frequencies, when flow in the pores is laminar; and proportional to $f^{\frac{1}{2}}$ at higher frequencies when the flow pattern is more complex (Hovem and Ingram, 1979). However in the intermediate frequency range, both laboratory and in situ measurements show that viscous attenuation increases at roughly f^1, which may mean that viscous attenuation is important as attenuation increases linearly with frequency at intermediate frequency (Hovem and Ingram, 1979).

The work of Hovem and Ingrams (1979) was done at high frequencies in highly permeable sands. At lower frequencies and in less permeable media the viscous losses will be much smaller and other forms of losses are likely to be dominating.

In a particulate medium saturated with water, energy losses would occur in a number of ways: Frictional losses at grain to grain contacts; viscous losses in the fluid if there is significant relative motion between the

fluid field and skeletal frame; losses near grain contacts caused by local fluid motion from the relative approach between particles in contact; and dissipation resulting from the possible inelasticity of any particular bonds and of the frame. In granular sediments (sands and silts) inelasticity of the frame is primarily a function of frictional losses at grain to grain contacts. In fine sediments (clays and silty clays) losses during small frame distortions are attributed to a variety of rate-dependent processes related, to electrochemical bonds between particles (Stoll, 1976; 1980).

The fluid component of marine sediments causes various forms of viscous damping that are always frequency dependent. Most fluid losses are due to fluid motion caused by variations (with the same wavelength as the propagating wave) in the average pressure and inertial forces (the average movement of the fluid field with respect to the skeletal frame). This overall motion of the fluid field relative to the skeletal frame is the main form of viscous damping in coarse sediments, causing a strong frequency dependence, determined by the permeability and tortuosity of the intergranular pores. Other fluid losses are caused by the movement of fluid in and out of cracks as they open and close in a variable stress field and the motion of fluid caused by the relative approach of particles near the grain to grain contacts. This last case is termed "squeeze film" in lubrication theory (Stoll, 1980; 1985).

In general the theory predicts that, at low frequencies, skeletal frame losses will dominate while viscous losses due to motion of interstial water will dominate at high frequencies. Stoll (1980) predicted that if there is sufficient mobility of the fluid relative to the skeletal frame then attenuation is dominated overall by viscous losses in the fluid, even at low frequencies. However frequency must be used in a relative sense, as its actual value depends on the physical properties of the sediment. In sands and other coarse granular materials viscous losses dominate over a significant portion of the frequency range, even at frequencies as low as a few Hertz. However for finer and less permeable sediments, (frequency-dependent) viscous losses only dominate at very high frequencies, with skeletal frame losses dominant over most of the frequency range, resulting in a linear dependence on frequency. (Stoll and Bryan, 1970; Stoll, 1976; 1980) The parameters of the sediment which are significant to the losses

also change with frequency. At low frequency, intergranular stress and cementation are important, but at higher frequencies porosity and grain size become more significant, at least in coarser materials (in which they are the major controls of permeability).

When modelling the relationship between frequency and attenuation, two points must be included. The frequency dependence of the viscous resistance to fluid flow due to the deviation from Poiseuille flow at all but very low frequencies, and the inelastic nature of sediment frames (Stoll, 1976).

From research in the fields of soil mechanics and foundation engineering, the logarithmic decrement is favoured as a measure of shear wave energy damping. The logarithmic decrement is defined as the natural log of the ratio of successive amplitudes in an exponentially decaying sinusoidal wave (Hamilton, 1976).

Hamilton (1976), using a linear visco-elastic model and published measurements, produced a report on the attenuation of low-strain shear waves in surficial water-saturated sands and silty clays (mud). In near-surface sands, the logarithmic decrement of low-strain shear waves should vary between 0.1 to 0.6 and 0.2 to 0.4 for saturated sands. For shear waves in water-saturated silt clays (mud), the values are between 0.1 and 0.6 and probably most are between 0.1 and 0.3 (Hamilton, 1976).

Both kinds of viscous damping as well as frictional losses at the grain contacts can be included in the generalized Biot model which has been used to describe the acoustical response of marine sediments (Stoll, 1985).

3.1.4. **Summary**

As the theories show, it is possible to relate acoustic propagation characteristics to physical sediment properties. In particular, they can be used to determine the sediment elastic moduli. The shear wave velocity is more sensitive to sediment properties then compressional wave velocities, as it passes through the solid part of the sediment and is controlled by the

grain properties and the interaction between the grains (which will include bonding between grains, be it electrostatic, chemical, from biological influences or by any other means).

3.2. **Acoustic Measurements.**

3.2.1. **Piezo-electric Bender Development.**

There are a number of requirements that be must meet to make shear wave measurement possible:

(a) The shear transducer must generate and detect a shearing motion within the medium.

(b) The received signal should be of such a quality that either its signature or preferably its onset can be clearly determined.

When working in marine (saturated unconsolidated) sediments, it becomes more difficult to achieve these requirements . Schultheiss (1983) summarized some general sediment properties and transducer properties necessary for good shear wave measurements:

(1) The transducer stiffness must be close to that of the sediment to minimize any impedance mismatch.

(2) Shear waves exhibit high attenuation coefficients which increase rapidly with increasing frequency. The transducer must therefore work at a relatively low resonance frequency in order to allow transmission over reasonable distances.

(3) Compressional waves travel faster and are less highly attenuated than shear waves. If these compressional waves form a significant part of the received signal, then they can easily obscure the later arriving shear wave.

There are a number of methods that can be used to generate and receive shear waves in a solid. Figure 3.2 shows a schematic representation of one type of shear wave transducer. An electrical signal passing across the electrodes will cause the transducer to deform. If the top or bottom face is in contact with a solid medium, then a shear wave will propagate perpendicular to the motion of the face. This form of transducer can be constructed from a Y-cut quartz crystal or a piezoelectric ceramic that is

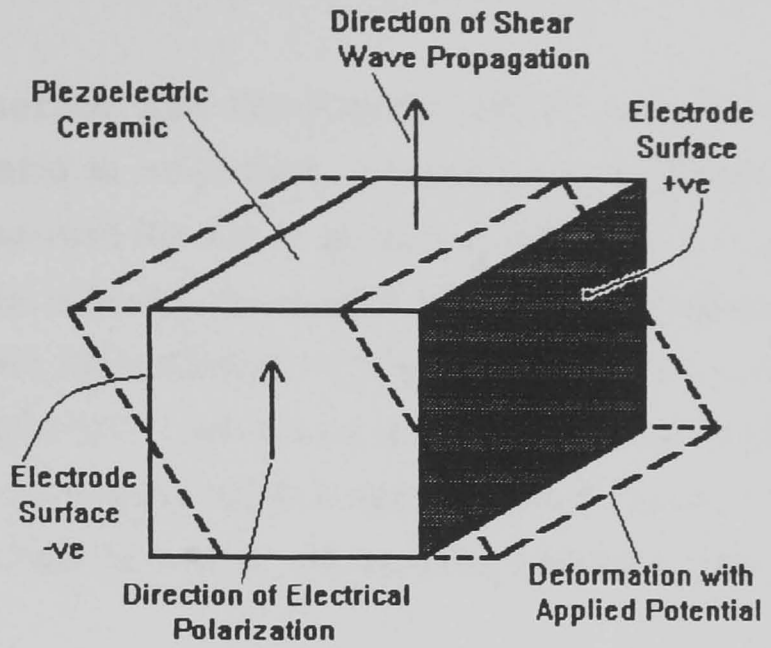

Fig (3.2): Principle of a Shear Wave Transducer.

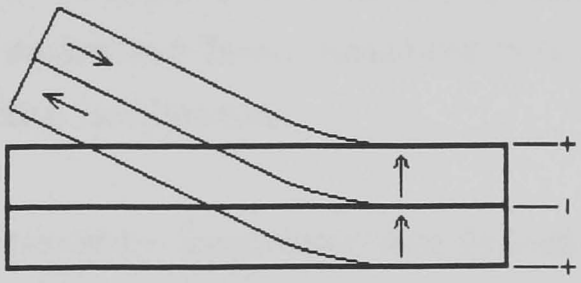

→ Direction of Polarization

Fig (3.3): Ceramic Bender Element.

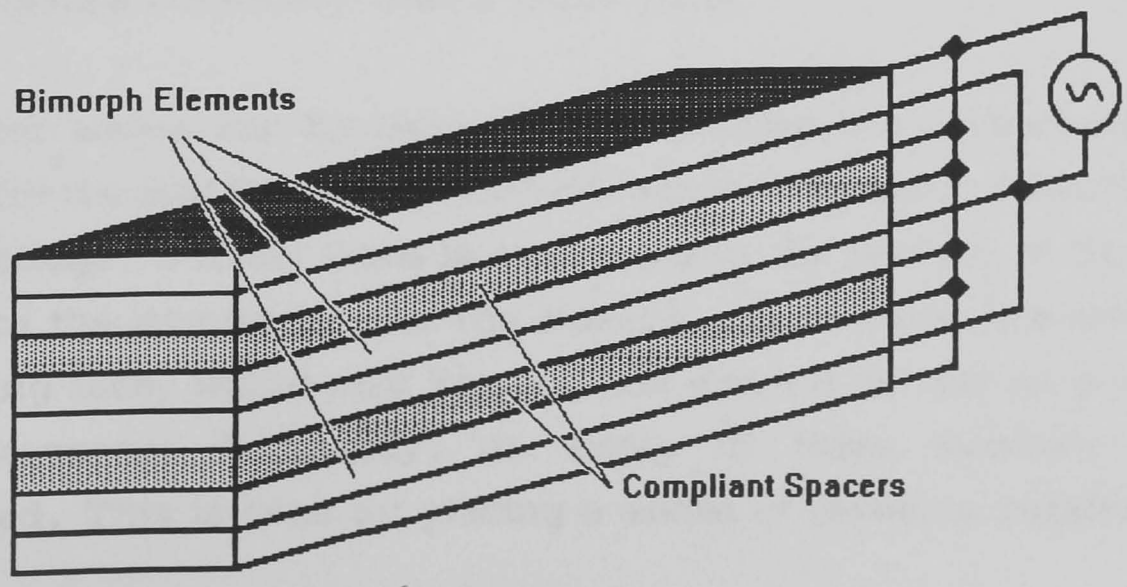

Fig (3.4): Array of Bender Elements.

polarized perpendicular to the applied field, and due to the reciprocity of the transducer it can be used both to transmit and receive shear waves. However for work in sediments this form of transducer has a few disadvantages:

(1) To generate low frequency shear waves a large length to thickness ratio is required, because the transducer behaves as a vibrating bar and its resonance is a function of the bar's stiffness.
(2) There is a large mismatch between the sediment and element characteristic impendence. (The element shows small motion with a large applied force, whereas the sediment is highly compliant and shows large movement with a small applied force, therefore resulting in only a small transfer of motion between the element and the sediment.

Some of these problems can be overcome by modifying the basic element by dividing it into thin slices, to reduce its stiffness and increase its compliance. A transducer of this type has an increased-amplitude shear wave than the standard element, due to the greater displacement of the modified element at its radiating face. However it is not an adequate tool for work in saturated marine sediments.

A further improvement - increased displacement and lower resonance frequency - can be made by using ceramic bender elements. This type of element is formed from two ceramic plates cemented together. The plates are polarized such that an electrical voltage applied across the element will cause one plate to contract and the other to expand, thus causing the element to bend if its length is significantly larger than its composite thickness (Figure 3.3). Elements of this type show large displacement and lower resonance frequency then a shear plate.

Shear waves can be generated by placing the desired medium in contact with the end face of the element. As the element is deformed by an applied voltage, a shear wave is generated in the portion of the medium adjacent to the moving face of the element. To increase the area of the transmitting face, whilst still keeping the element as thin as possible to reduce resonance frequency, an array of these elements can be constructed. This is done by placing a series of elements together, each

separate from its neighbour by a piece of high compliance material (Figure 3.4). This initial development outlined above was carried out at the Applied Research Laboratories (ARL), The University of Texas, where an array bender was developed with dimensions of 1.27x1.26x2.54cm with a resonance frequency of 4kHz.(Shirley and Hampton, 1978).

By totally immersing the element in the sediment, a large amount of acoustic energy can be transmitted to the sediment, because the medium is driven along the entire length of the element. The way in which the element deforms results in most of the mechanical motion being transferred to the sediment particles in a manner such that the particle motion will be perpendicular to the length dimension of the element. If the element is allowed to vibrate freely, then the motion at the ends of the element will be in phase and the motion in the middle of the element will have a phase of 180° with respect to the ends. If the sediment exhibits some rigidity then the sideways or shearing motion of the sediment will be propagated as a shear wave. The direction of propagation will be perpendicular to the particle motion, parallel to the length of the element, with only a small amount of energy being propagated perpendicular to the element length (Shirley, 1978).

3.2.2. **Bender Element properties.**

A bender element can be configured in two ways, either in series or in parallel. This relates to the direction in which the piezo-electric plates are polarized (Figure 3.5). In the parallel form, both plates are polarized in the same direction, but for the series form the plates are polarized in opposite directions. The wiring for each type is different, and they behave in slightly different ways. A series element develops twice the voltage of a parallel element, but provides only half the displacement of the parallel element for the same applied voltage. This means that a parallel element is the better transmitter but a series element is the better receiver. The manner in which an element is mounted can generally be described in two ways: (a) Unconstrained, in which the element can vibrate freely. (b) Cantilever, where one end is firmly clamped and the other allowed to vibrate freely (Figure 3.6).

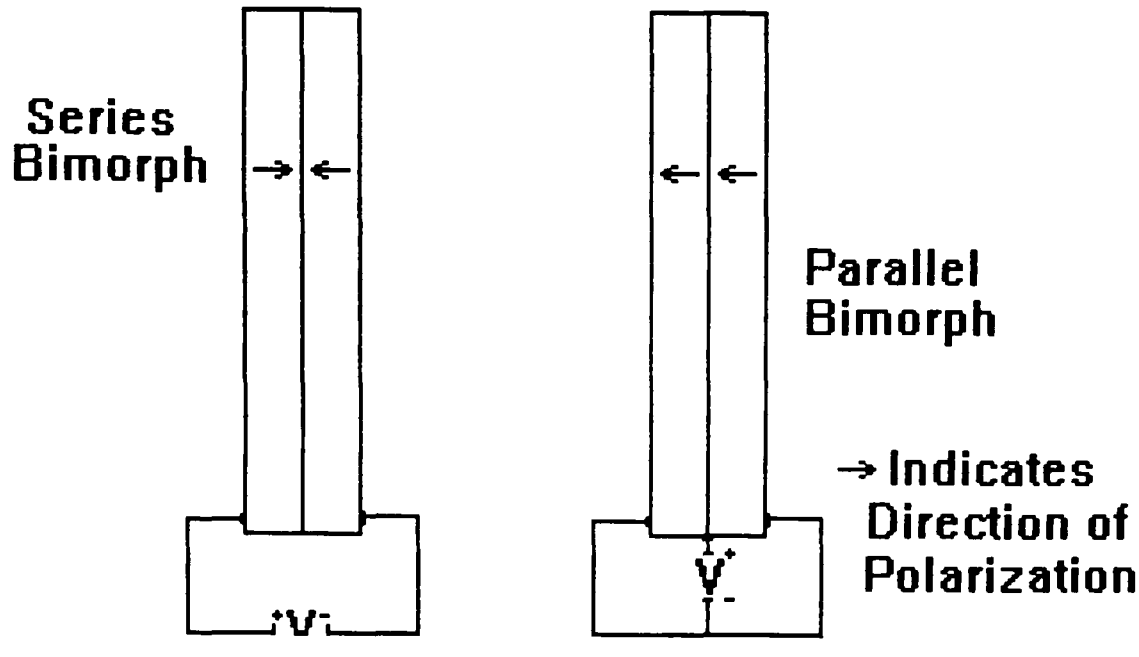

Fig (3.5): Bimorph Bender Element Configuration.

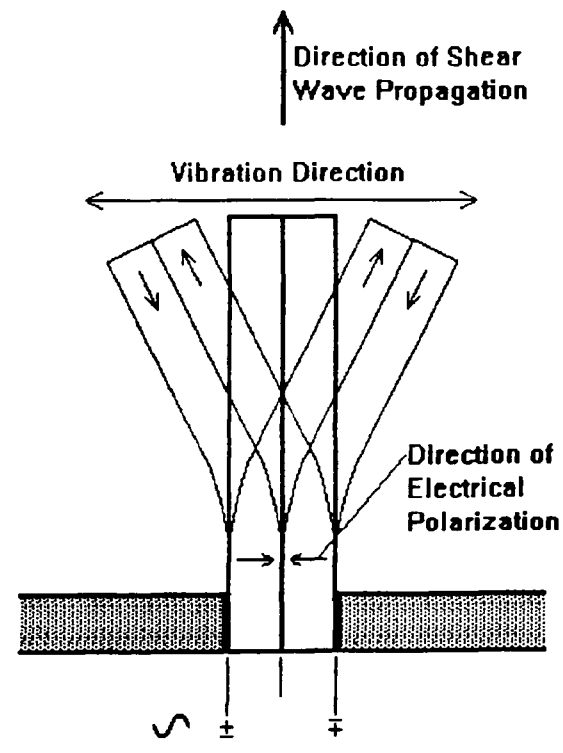

Fig (3.6): Schematic operation of a Bender Element in a Cantilever Mode.

In this investigation a single bender element was used. The type used was a VERNITRON PZT5BN bimorph element. One of the major improvements of the piezo-electric bender element over the shear plate is the reduction in resonance frequency. In a shear plate the resonance frequency is inversely proportional to its length, whereas it is inversely proportional to the square of its length for a bender element. The exact relationship of frequency to length depends on the material used to construct the bender element. The following definitions are from Vernitron product specification literature (Bulletin no., 66012/D) and apply to their PZT5BN bimorph mounted in cantilever mode and operating in air.

The mechanical compliance is given by,

$$C_m = 3.2x10^{-9}\frac{L^3}{WT^3} \qquad (3.17).$$

Where L, W and T are the length, width and thickness dimensions, given in inches, of the bender element respectively.

The resonant frequency is given by,

$$F_r = \frac{1}{2\pi\sqrt{MC_m}} \qquad (3.18).$$

M is the effective mass of the element given by,

$$M = 3.0x10^{-2}LWT \qquad (3.19).$$

Hence,

$$F_r = \frac{1}{2\pi\sqrt{9.6x10^{-11}\frac{L^4}{T^2}}} \qquad (3.20),$$

$$F_r = \frac{T}{\pi L^2}(5.1x10^4) \qquad (3.21).$$

The maximum free end displacement in air is given by,

$$D = 315\frac{L^2}{T^2}V \qquad (3.22)$$

Where V is the voltage applied across the bender element.

As already stated these equations relate to the behaviour of an element in air. They also give a guide to the change in behaviour of the element, with varying size, when it is encapsulated in some form of insulating material, and the effect of immersion in the sediment.

An increase in length of the element will, as shown in equation 3.21 and 3.22, result in a lower resonance frequency and an increase in displacement. Both of these are desired, as they give improved shear wave measurement, so long as the element remains coupled to the sediment. Due to the method in which the element is held, constrained along its width, changes in its width do not affect the displacement or resonance.

Encapsulation has the effect of increasing the element's thickness. Encapsulation is necessary to protect the element and insulate it from the conductive pore fluids, which would short out the electrical contacts. From equations 3.21 and 3.22, an increase in thickness of an order of magnitude will decrease free end displacement and increase resonance frequency. However, once encapsulated the above equations can only be used as a guide to the element's behaviour, because the encapsulating material will have different elastic moduli than those of the bender element.

Immersing the element into a sediment has a far more important affect than those described above. The expected effect is that the sediment will limit the movement of the bender element and therefore raise its resonant frequency. This does not take into account the behaviour of the sediment itself. With the element totally immersed in the sediment, then provided it is adequately coupled to the sediment and can respond at the correct frequency, it will be at its most sensitive when a half wavelength of the propagating shear wave corresponds to the length of the element (Shirley, 1978).

The sediment also determines the quality of the received signal due to the high attenuation of the transmitted signal. The attenuation is related to frequency. From values given by Shirley et al. (1979) for a transducer in saturated sand at low confining pressures, a 2kHz signal will suffer

attenuation of 100dB/m, at 1kHz the attenuation is only 25dB, and at 600Hz the attenuation is estimated at 10dB/m. Therefore any reduction in the transmitted signal frequency will improve the strength and quality of the received signal.

Two other common problems are; The detection of compressional wave components in the received signal, and the presence of energy transmitted between the transducers via the cell walls and mounts. The compressional wave components interfere with the shear wave onset and make its identification more difficult, but problems of this nature are more common in more rigid materials (e.g. sands) and at higher confining pressures. The problems of energy transmission can be reduced with better mounting techniques and the use of filtering which will also reduce any compressional component problems.

3.2.3. **Flume Bender Element Development.**

3.2.3.1. **Early Probes.**

The first probes for use in this study were designed with the constraint that they would have to be inserted into the bed from above. They were therefore made to give good clamping of the bender element and to give the least obstruction to the flow. The actual bender was 32mm long and 5mm high. This gives a resonant frequency of 200Hz for the un-potted element. A mould was also constructed to encapsulate the element with protective and water-proofing epoxy resin. The probes then had a resonant frequency of about 1000Hz. Figure 3.7 shows the probe and the mould. A difficulty that arose due to the mounting of these probes from above, was that any movement of the probe support would cause the sediment structure around the probe element to be weakened and the strength of contact between the element and the sediment reduced. This resulted in an apparent reduction in shear wave velocity.

Re-design of the probes was possible when it was decided that the probes did not need to be mounted from above but could be wall or floor mounted. This more secure mounting also alleviated the problem of reduced

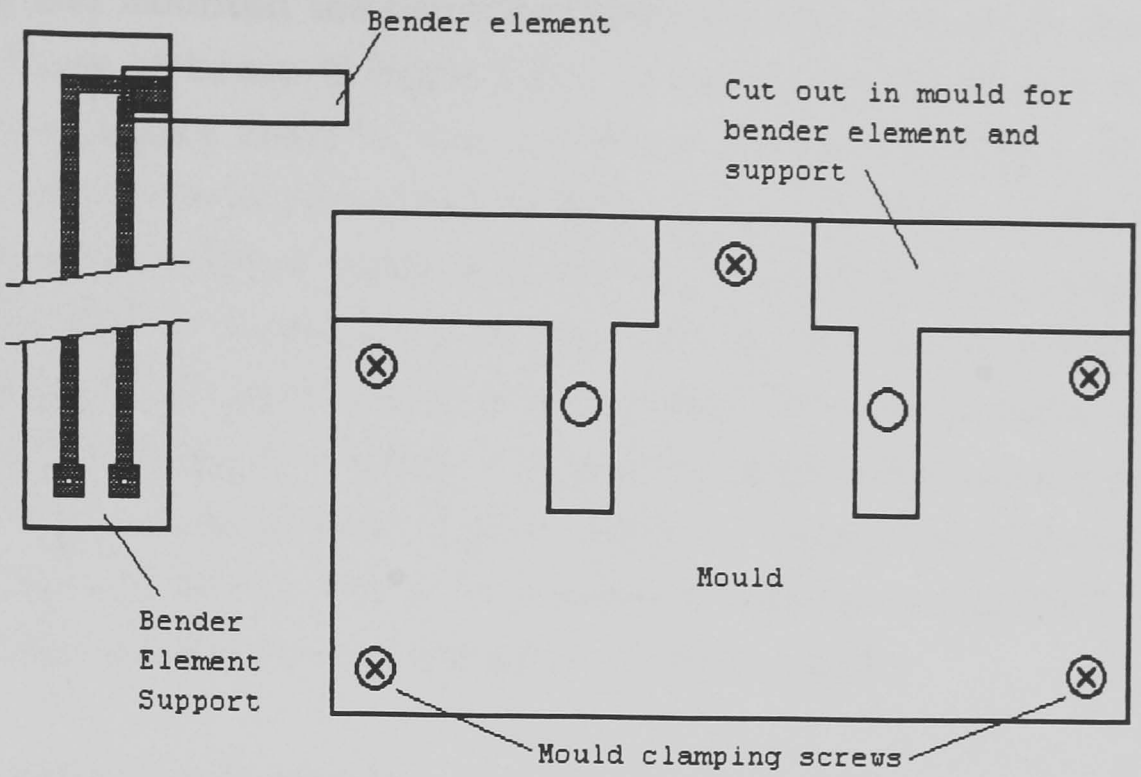

Fig (3.7): Bender Mark 1 and Mould.

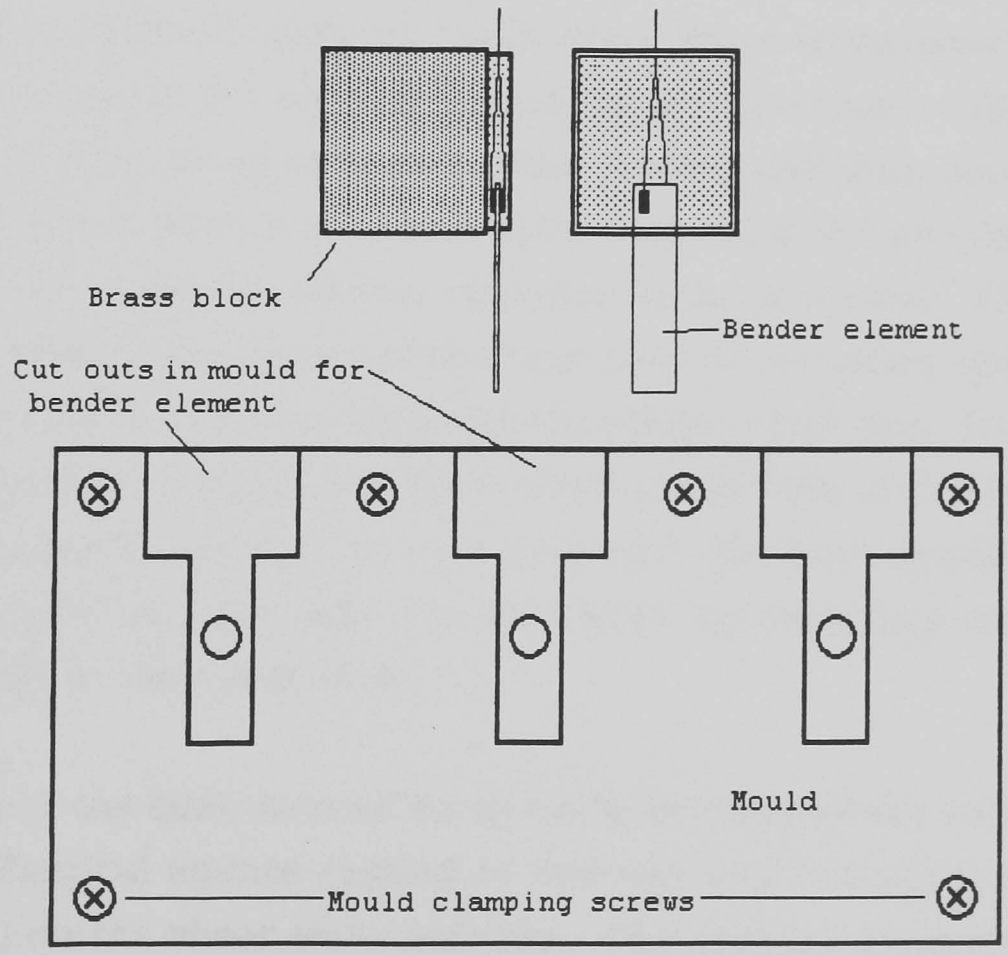

Fig (3.8): Bender Mark 2 and Mould.

shear wave velocities caused by the less secure mounting method of the first probe design. The re-design was based on a design by Richardson (1990) and mounted the bender elements (32mm long by 5.5mm high) on a small block of brass (Figure 3.8). A mould was first used to fix a small square of epoxy resin to the end of the element and then this square of epoxy resin was glued to the brass block (2x2x1.5cm, weighing 62grams). The element was then water-proofed by using an acrylic lacquer; this was used instead of epoxy resin as the need for the lowest possible resonant frequency outweighed the need for protection of the fragile element. The resonant frequency of the probes was found by mounting the probes 0.5cm apart, and driving one through a range of frequencies and using the other to the look at the amplitude of the bender element. Figure 3.9 shows the result and the resonant frequency of about 500Hz.

Initial Experiments.

The initial investigation of shear wave properties in cohesive sediments were carried out with these probe designs. The main property that was looked at was, the nature of shear wave velocity variation with time (i.e. during bed consolidation) and the affects of bleaching agents on the cohesive sediment samples (to destroy micro-organisms). The samples were of two types; (a) remoulded samples that had been collected from the mud flats of the Conwy estuary at Glan Conwy and then poured into a test tank, measuring 30cm x 13cm and 18cm deep: and (b) samples of powdered kaolinite that w ere mixed into seawater in the test tank. The first probes w ere mounted in the centre of the tank from above using retort stands and clamps with the probes vertical and the element tips 6cm. Later runs, with the second set of probes, had them fixed to the base of the tank again with the probe tips 6cm apart. In this case with the tank empty a frame wave could be detected, but this was alleviated by mounting the probes on a double layer of 4mm neoprene.

One of the main aims of these early investigations was to look at the affect of chemical agents (added to prevent any biological activity in the sediments) on the shear wave velocity. The primary question was whether the halt in biological activity caused a change in shear wave velocity and if any change was in fact due to changes in the mineralogical properties of the clay minerals caused by the chemical agent. In the initial experiments

Fig (3.9): Response of Bender Mark 2
to Variations in Driving Frequency.

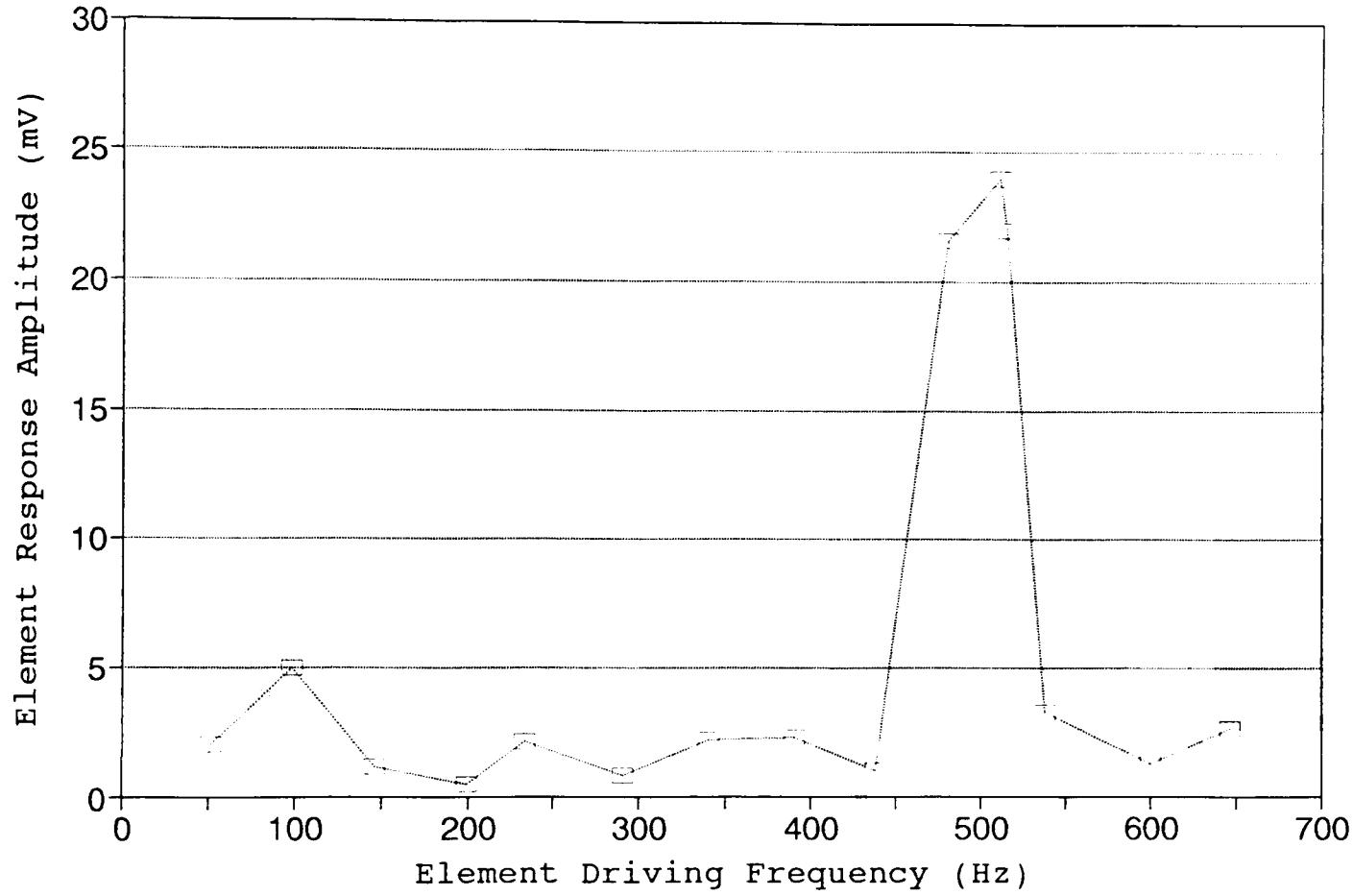

an ordinary domestic bleach was used but in the later experiments sodium azide was used. In both cases the chemical was added to both the field mud and the industrial kaolinite.

A Thander TG102 2MHz Function Generator was used to produce the 5Hz square wave that drives the bender element and provides the trigger for the Oscilloscope. The signal from the receiving bender element was passed through an amplifier and a band pass filter, set at 10Hz and 0.1MHz, and then to a Hewlett Packard 54200A Digitizing Oscilloscope.

The results of the initial experiments on the variation of shear wave velocity with time are depicted in Figure 3.10a,b and 3.11a,b. Figure 3.10a,b shows four individual runs using the later probe design. Figure 3.11a,b show the combined results of a number of individual runs. The main points that can be seen in Figure 3.10a,b more easily then in the more scattered appearance of Figure 3.11a,b are:

1) The velocity increases slowly to a constant value.

2) The kaolinite has a much higher velocity due to the lack of major particle flocculation and reduced electrical activity of the clay particles.

3) The chemical agent appears to affect the mineralogy. The chemical agent, both the bleach and the azide, affected the non-biologically active kaolinite, as well as the biologically active mud. It appears likely that the chemical alters the electro-chemical activity of the clay particles and therefore how they interact with each other. This means that any velocity changes that occur in a mud after the addition of a bleaching agent can be caused by both the changes in biological activity and changes in the behaviour of clay particles in the mud.

The more scattered appearance of Figure 3.11a,b is caused by the differences in actual velocity from run to run, although the general features of each run are the same. Points 2 and 3 above can also be seen in the total data, but point 1 can not be made out easily due to the variations in velocity between runs.

These results are similar to those of McDermott (1992) on the consolidation of soils. He observed small amplitude shear waves after a 20% degree of consolidation in the range of 1 to 11m/s with an increase or creep

Fig (3.10a): Individual Consolidation Runs, Bender Mark 2 in Kaolinite.

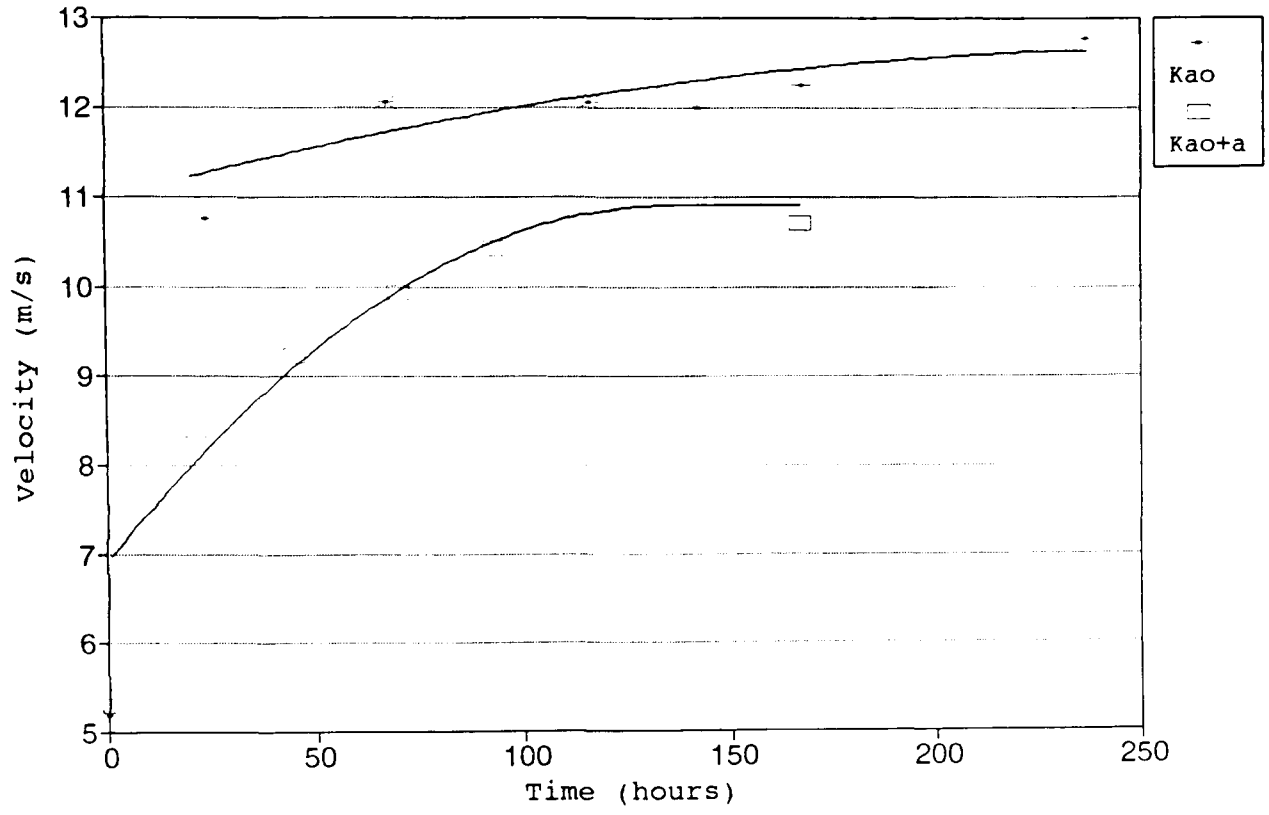

Fig (3.10b): Individual Consolidation Runs, Bender Mark 2 in Mud.

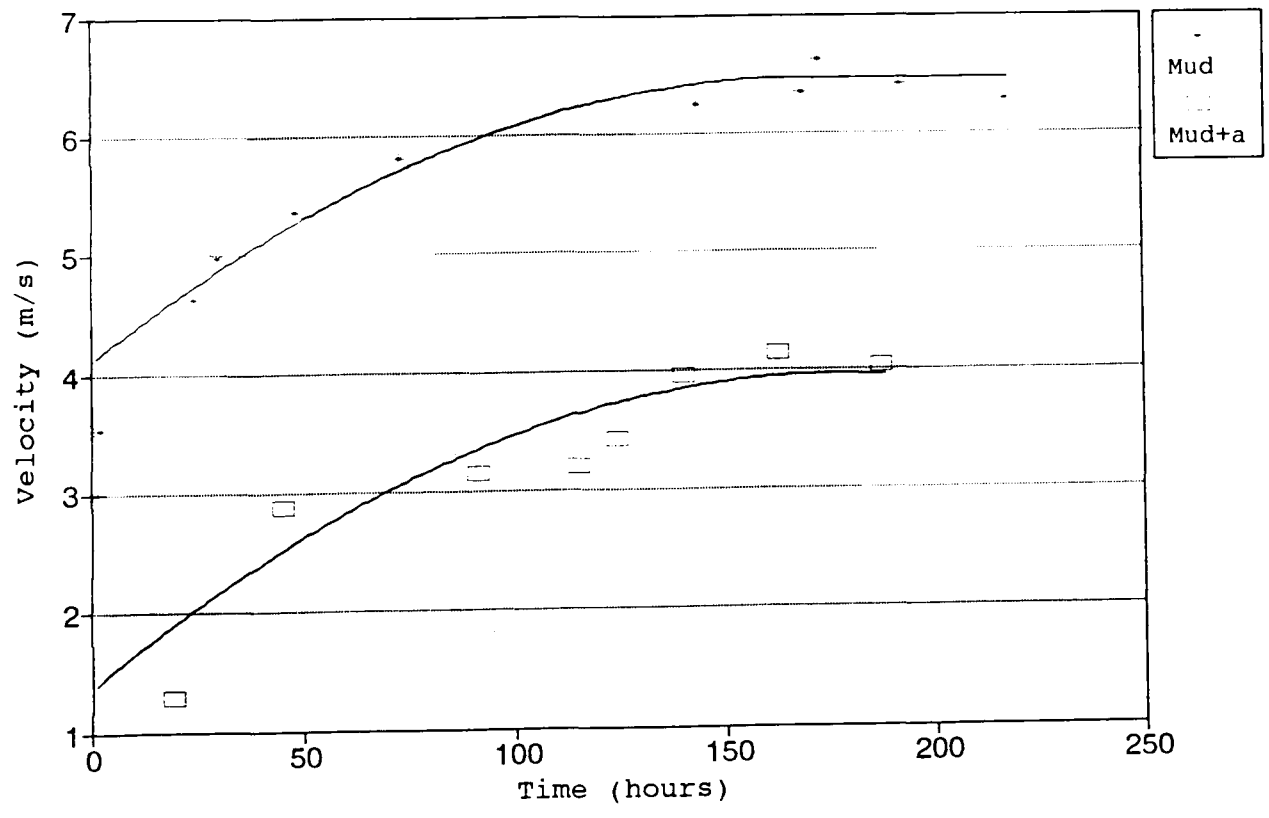

Fig (3.11a): Consolidation Runs on Kaolinite.

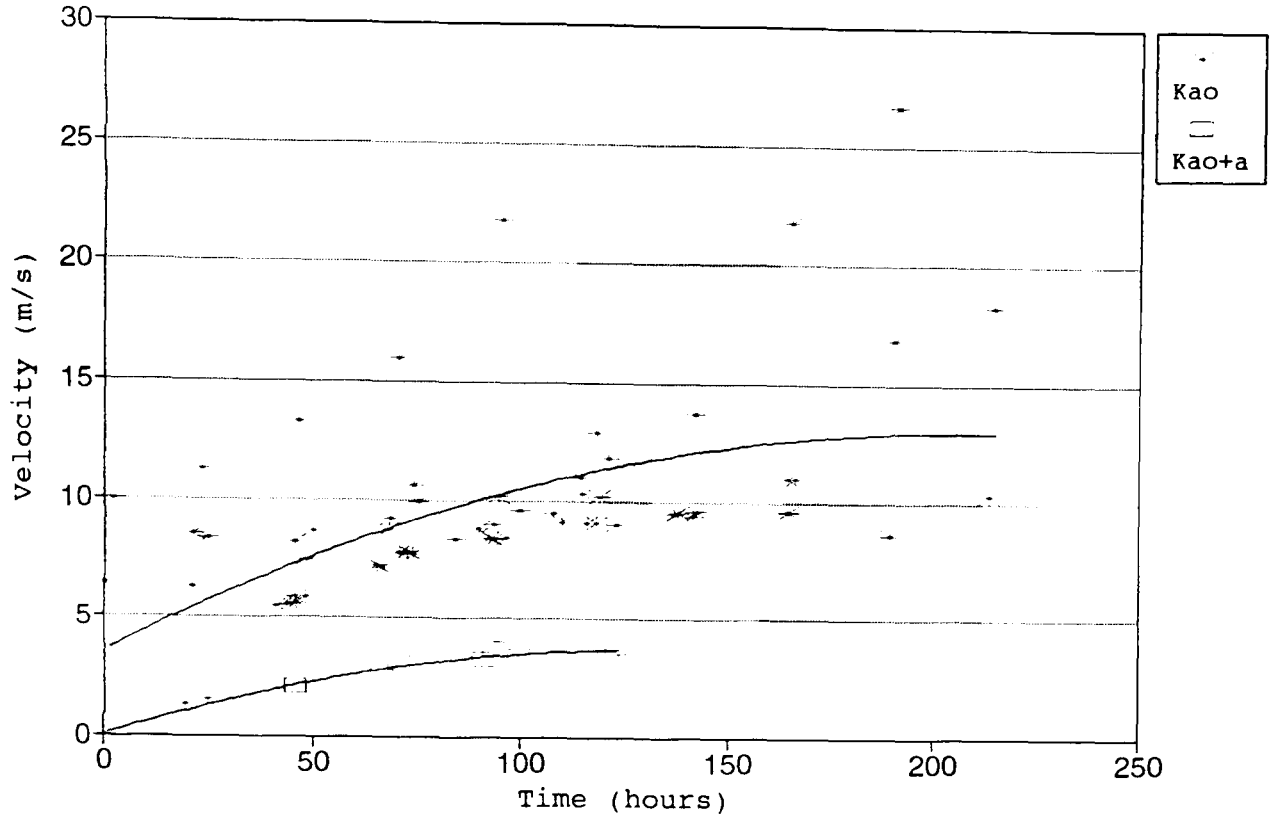

Fig (3.11b): Consolidation Runs on Natural Mud.

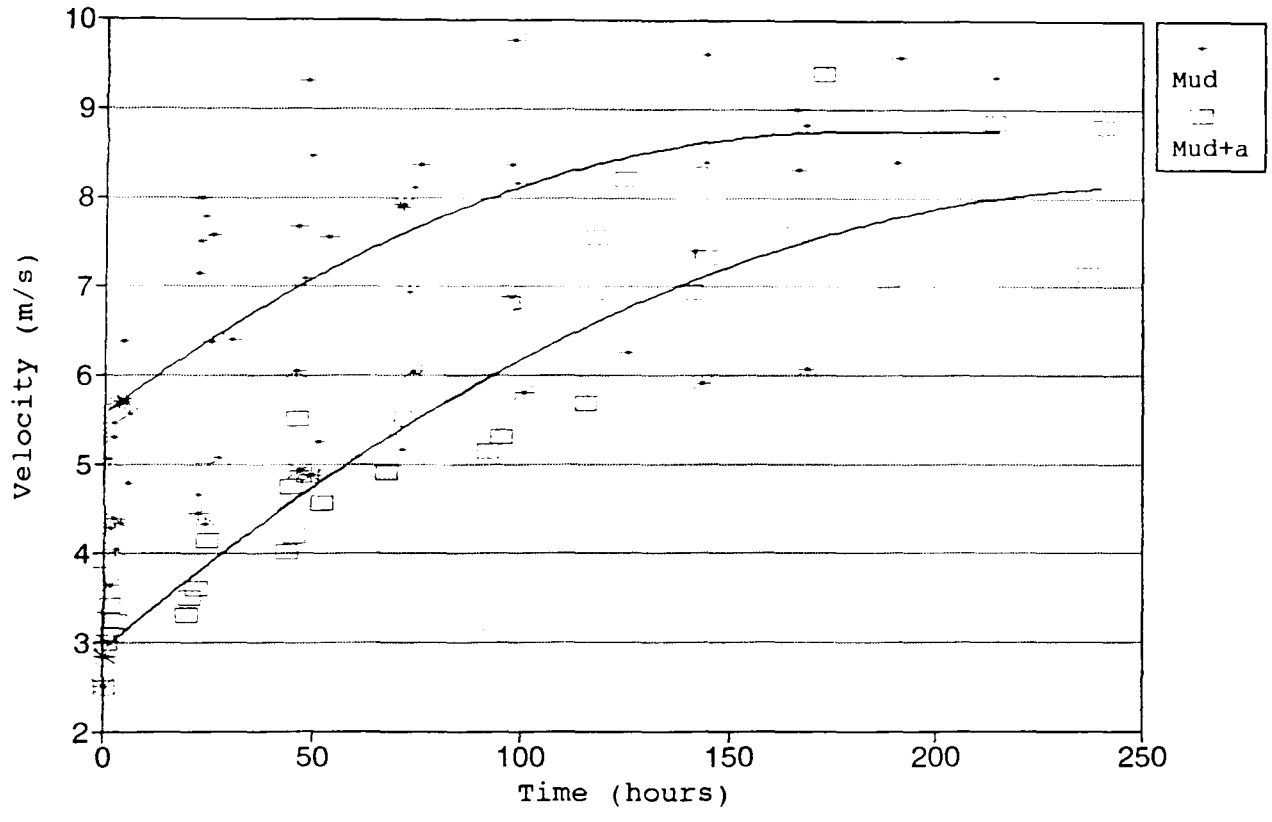

in velocity and rigidity with time caused by clay particle floc interaction during secondary consolidation. Since the consolidation behaviour of a rapidly deposited sediment is influenced by its initial input density and that by creep, the shear wave velocity to porosity relationship has a very complex form. This implies that shear wave velocity increases with decreasing porosity and with increasing overburden, as would be expected, but that no unique shear wave velocity - porosity relationship exists. So any porosity may be associated with a wide range of velocities (McDermott, 1992).

3.2.3.2. **Flume Probes.**

A new probe design, based on the McDermott (1992) design, was used for work in the flume (Figure 3.12). A mould was used to make sure that the probe was fixed into the perspex rod centrally and that the element was not leaning to any one side. For these probes, a more flexible potting compound was used than the hard epoxy resin used in the other probes to fix one end of the element into the recess in the perspex rod. The water proofing of the element was completed by coating it in an acrylic lacquer. In the flume a Thurlby DSA524 Digital Storage Adaptor was used instead of an oscilloscope, and this allowed the signal to be passed to a PC for storage on disk for later analysis.

An analysis of the element's resonant frequency in air was carried out in the same manner as that used on the earlier probes and this showed a peak at about 410Hz (Figure 3.13). The probes proved to work very well and Figure 3.14 shows the shear waves produced in boulder clay. The setup and testing of these probes in the recirculating flume is given below (§5.2.4.1. Acoustic Shear Wave Measurement).

3.3 **Summary and Conclusions.**

As already outlined the acoustic shear wave velocity and the rigidity modulus, which is a function of the shear wave velocity and sediment density (a measure of how densely packed the sediment is) give a measure

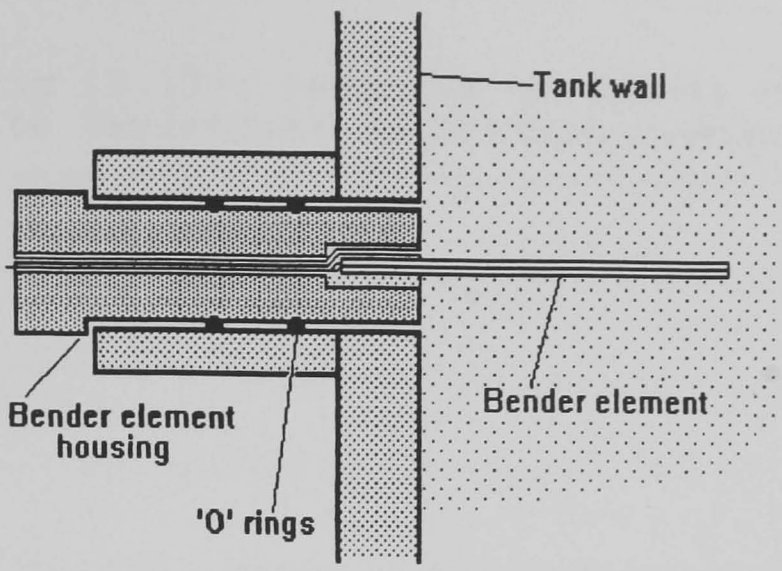

Shear Wave Transducer Construction

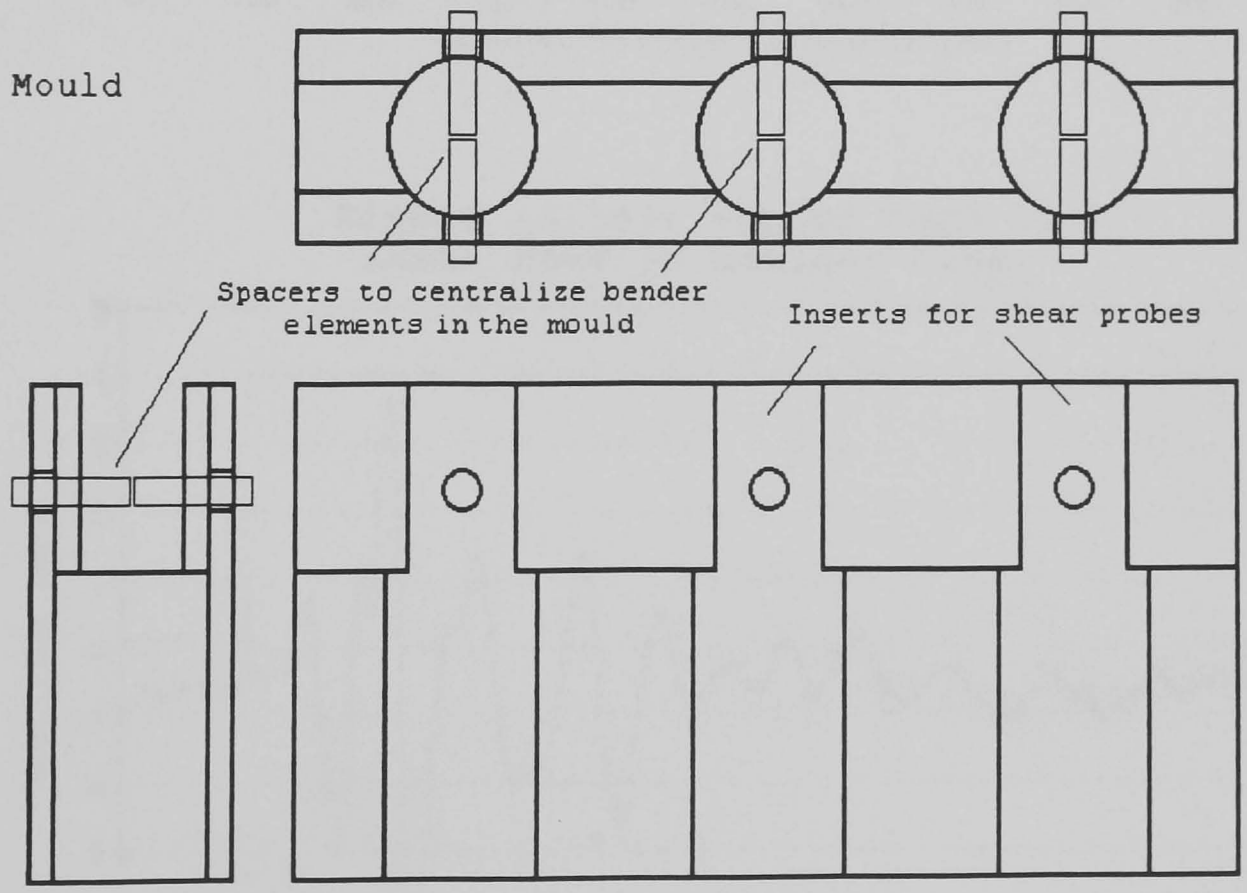

Fig (3.12): Bender Mark 3 and Mould.

Fig (3.13): Response of Bender Mark 3
to Variations in Driving Frequency.

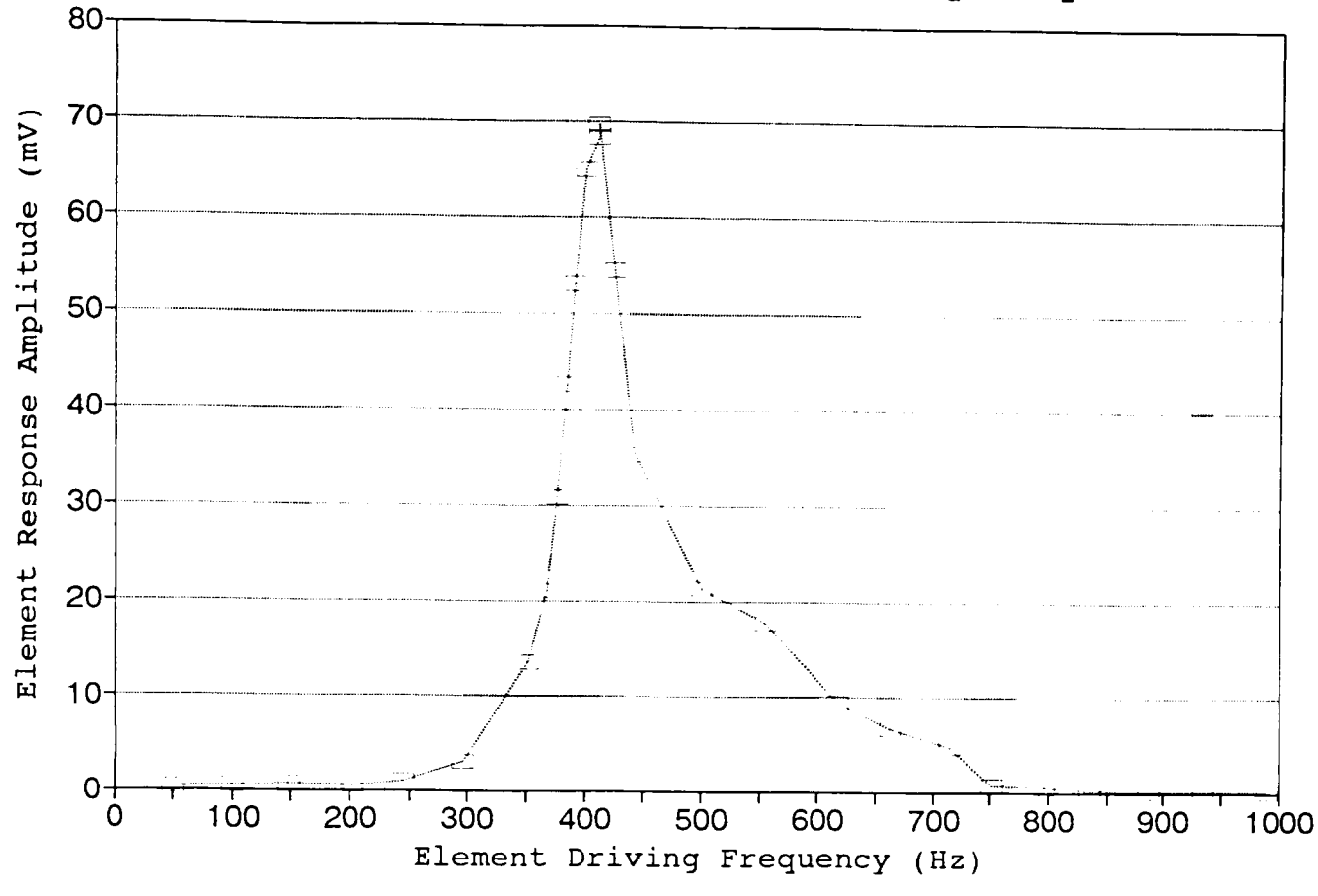

Figure (3.14): Bender Mark 3,
Shear Wave in Boulder Clay.

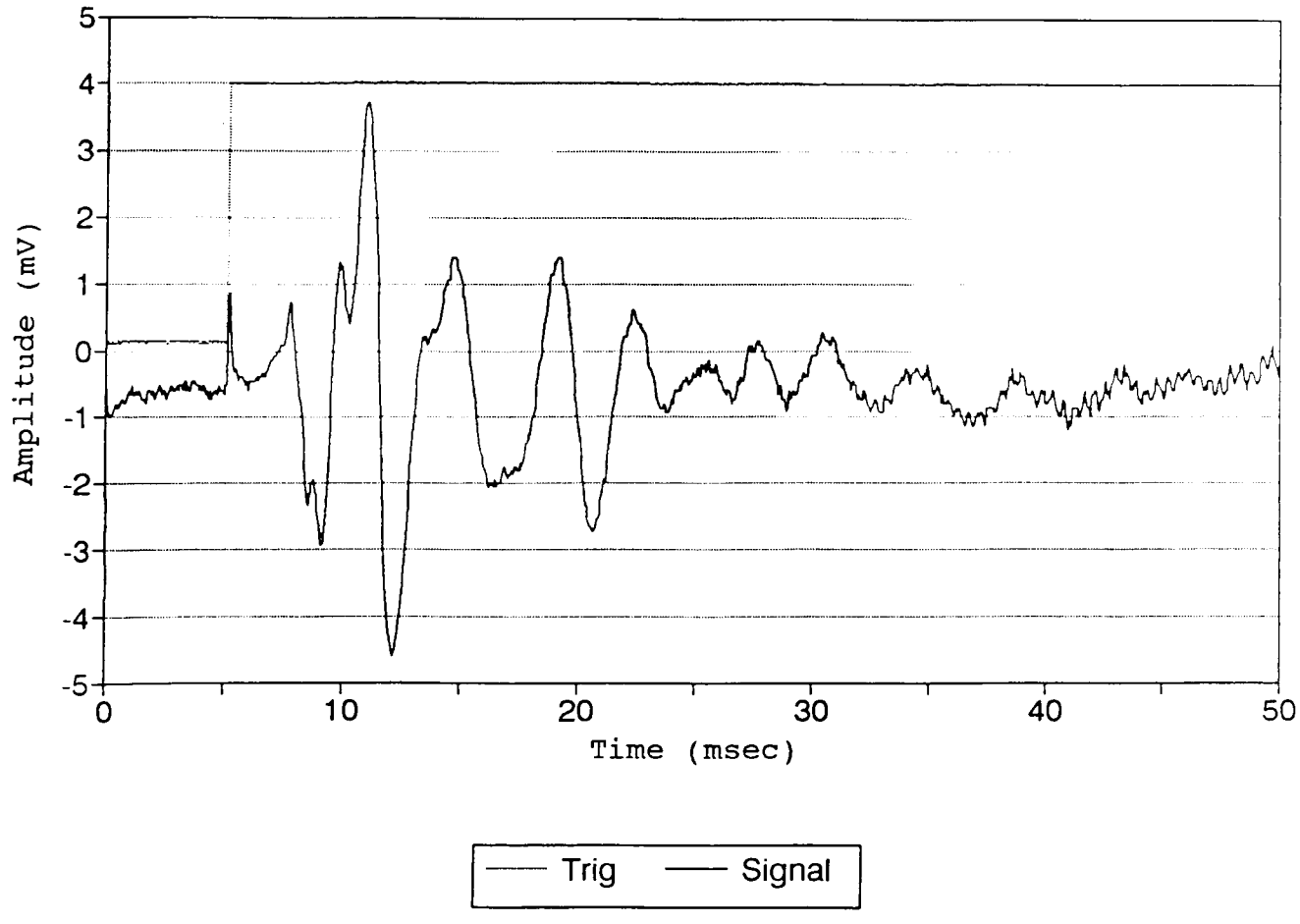

of the sediments strength, and can be correlated with other sediment properties. By the nature of its passage through the sediment the shear wave velocity and moduli derived from are more sensitive too and better measures of the degree and nature of inter-particle bonding then the compressional wave velocity. This interaction between rigidity modulus and other sediment properties can, with the use of correctly design piezo-electric and other shear wave transducers, be examined in highly saturated cohesive sediments, with good results. The use of this geophysical method allows measurements to be taken without any major disturbance to the sediment structure, and therefore allow other properties of the sediment to be measured as well. In this investigation where the erosion behaviour of the sediment is being examined, the need to reduce disturbance of the sediment structure prior to erosion is very important, and accordingly the use of this approach is crucial.

CHAPTER 4.

RESISTIVITY THEORY AND MEASUREMENT.

4.1. Electrical Properties of Sediments

4.1.1. Current Flow in a Homogenous Medium.

The place to start with a description of sediment electrical properties is with Ohm's Law.

$$R=\frac{V}{I} \tag{4.1}$$

where I is the current in a conducting body, V is the potential difference between two surfaces of constant potential and R is the resistance between the surfaces.

The bulk resistivity ρ_b of a conductor is related to its measured resistance R by a geometric factor F which accounts for the area available for conduction normal to the direction of current flow and for the current path length.

$$\rho_b=RF \tag{4.2}$$

For a cylindrical conducting wire of radius r and length L, F is,

$$F=\frac{L}{\pi r^2} \tag{4.3}$$

It follows from these equations that resistivity is reduced with increasing cross-sectional area and increased with increasing path-length (Griffiths and King, 1981).

Electrical conduction in sediments is via free ions in the saline pore fluid and/or free electrons in the solid. For most sediments the mineral structure acts as an insulator and conduction is through the pore fluid alone, except in clays and certain metallic ores.

The electrical resistivity is thus a function of the resistivity of the pore fluid (nature and distribution), the resistivity of the sediment grains (size and shape) and conductance along the solid/fluid interface. This surface conductance is related to the 'diffusive double layer' (§2.3.2.1.): the exposed ions on the surface of the solid attract counter ions, present in the fluid, which form a conductive layer of densely packed ions. The size of this layer is controlled by temperature and the salinity of the pore fluid; it increases in size with increasing salinity (increasing ion concentration). With increasing temperature, the thermal motion of the ions increases in magnitude and the ions are less strongly influenced by electrostatic fields (Dyer, 1986). However there is a minimum salinity below which the layer does not exist. This phenomenon is only significant in clays and other fine grained sediments at low salinities. It is negligible in sands and/or when the resistivity of the pore fluid has a magnitude similar to that of seawater (Brace et al., 1965; Urish, 1981 and Dyer, 1986).

The resistivity of the system can be expressed as the sum of the contributing factors.

$$\frac{1}{R_{app}} = \frac{1}{R_w} + \frac{1}{R_s} + \frac{1}{R_m} \qquad (4.4)$$

Where R_w is the resistance of the pore fluid matrix, R_s is the resistance of sediment matrix, R_m is the resistance of the surface layer of ions and R_{app} is the apparent (measured) bulk resistivity.

The bulk resistivity ρ_o can be reduced to a dimensionless form, by dividing by the pore water resistivity ρ_w, giving the formation factor FF original defined by Archie (1942).

$$FF = \frac{\rho_o}{\rho_w} \qquad (4.5)$$

The formation factor can be defined as either the apparent formation factor FF_{app}, which includes surface conductance and other inter-granular pore water contributions, or the intrinsic formation factor FF_i, for a perfectly nonconducting solid matrix (Urish, 1981), dependent only on the porosity and the tortuosity of the sediment (Jackson et al., 19).

The apparent formation factor is a function of many variables. For a saturated unconsolidated nonconductive sand it can be given by,

$$FF_{app}=f(k_s, k_w, k_m, n, T, S_p) \tag{4.6}$$

where k_s is the specific conductivity (reciprocal of the resistivity) of the sediment matrix, k_w is the specific conductivity of the fluid, n is the porosity and T is the sediment tortuosity. S_p is the specific internal pore area defined as the total interstitial surface area of the pores per unit pore volume of the sample; this term combines the effects of the grain size distribution, grain shape, and porosity. k_m is the specific surface conductivity of the grains dependent on the resistivity, ionic composition and pH of the pore water and the cation-anion exchange capacity of the matrix minerals.

Pfannkuch (1969) produced a model which can relate the apparent and intrinsic formation factor to each other, in terms of the geometry of the sediment grains.

$$FF_{app}=FF_i\left[1+\frac{k_s}{k_w}\frac{1-n}{n}T^2+\frac{k_m}{k_w}S_p\right]^{-1} \tag{4.7}$$

If the grain matrix is made up primarily of nonconducting grains, such as quartz, then the second term in the denominator of (4.7) -the matrix conductivity- becomes very small and can be neglected giving,

$$FF_{app}=\frac{FF_i}{1+(k_m/k_w)S_p} \tag{4.8}$$

This shows that when the pore fluid conductivity k_w becomes high, the ratio (k_m/k_w) will approach zero. Thus the apparent formation factor will approach the intrinsic formation factor in cases of high pore fluid conductance. This is the case when the pore fluid resistivity has a magnitude similar to that of sea water. However for sediments with highly

resistive pore fluid or significant amounts of clay, the affect of the surface conductance on the formation factor must be considered.

The surface conductivity and the pore water conductivity are both functions of C, the molar concentration of the pore-water. The ratio k_m/k_w can be expressed as $B\rho_w^{0.5}$, where B is a constant equated to $k_s\rho_w^{0.5}$ and defined as a surface conductance factor representing the magnitude of the double layer effect. For a given sediment matrix and porewater, B is assumed to be constant (Urish, 1981). Equation (4.9) can now be rewritten as,

$$FF_{app} = \frac{FF_i}{1 + B\rho_w^{0.5} S_p} \tag{4.9}$$

Archie's Law, which has been developed and adapted by a number of authors, shows that for most sediments the formation factor can be related to the porosity and a number of constants representing intrinsic properties of the grain matrix (Archie, 1942; Wensauer et al., 1952; Boyce, 1968; Kermabon et al., 1968; Taylor Smith, 1971; Erchal and Nacci, 1972; Jackson 1975, 1980; Lovell 1984). Archie (1942) originally defined it as,

$$FF = \frac{1}{nm} \tag{4.10}$$

This was expanded by Winsauer et al. (1952) to,

$$FF = \frac{a}{nm} \tag{4.11}$$

This can be combined with (4.5) and a term for the degree of saturation to give,

$$\rho_o = \frac{a\rho_w}{n^m S^o} \tag{4.12}$$

where n is the porosity, S is the fraction of pores containing fluid, $o \approx 2$, and a, m are constants, $0.5 < a < 2.5$, $1.3 < m < 2.5$. In a saturated sediment S=1, and the equation can be simplified to,

$$\rho_o = \frac{a\rho_w}{n^m} \tag{4.13}$$

The constants a and m can be determined graphically from calibration measurements in the laboratory of various porosities and formation factors. Most of the work has been carried out in sands and crystalline rocks on the affect of grain shape and packing, (Mendelson and Cohen, 1982; Sen et al., 1984; Jackson et al., 1978), but Taylor Smith (1971) produced a general result for sands and clays which uses only two Archie type equations,

$$FF=n^{-2} \qquad \textit{for clays} \quad (n>0.6) \tag{4.14}$$

$$FF=n^{-1.5} \qquad \textit{for sands} \quad (n<0.6) \tag{4.15}$$

Jackson et al. (1978) has determined a generalised relationship between formation factor and porosity showing variations caused by particle shape. Most results appear to agree with the use of an Archie's Law type equation to obtain the porosity from the formation factor. However, Kermabon (1969) found that a third degree polynomial,

$$n=171.2504-105.3899FF+40.0416FF^2-5.9021FF^3 \tag{4.16}$$

gave the best fit to his experimentally obtained data.

As stated above there has been some success in modelling formation factor and porosity in sands, but for systems in which surface conductivity has an affect there is no detailed model for the prediction of matrix conduction. Hill et al. (1956) related this surface effect to the cation exchange capacity of the sediment grains, and McCarter (1984) determined the resistivity of a clay as a function of moisture content and degree of saturation. Each sediment has a different relationship. As McCarter (1984) showed, for cohesive or any clayey sediments, there is a unique relationship between formation factor and porosity dependent on the particular properties of the individual sediments.

4.1.2. **Summary.**

The main limitations with Archie's Law is that it only really applies to clean sands. In sediments containing clays, an individual relationship between porosity and formation factor must be worked out. Also in order

to compare measurements, variations in temperature and other properties like salinity must be taken into account.

4.2. Resistivity Measurements

For measurements of sediment resistivity to be made, it is necessary to determine how current will flow in the sediment. A few basic ideas must first be defined.

Current Density C

This is the total current crossing any unit area perpendicular to the current flow. It may be resolved into components u, v and w parallel to the x, y and z coordinate axes.

Line of Current Flow

Defined as the path along which the transfer of charge takes place. No current can cross a line of flow.

Tube of Current Flow

Any cross sectional area at right angles to the current flow when summed gives rise to a tube flow. Inside the tube the current is a constant.

Ohm's Law for a Continuous Media

This law can be modified for a three dimensional media by considering a tube of current I in a medium of resistivity ρ_o. Over a length of tube Δl the potential difference is ΔV and the resistivity R. From Ohm's law $\Delta V = IR$. $I = Ca$ where C is the current density and a is the cross-sectional area of the tube. From the definition of ρ_o given by equation (4.2), the Potential Gradient can be defined as,

$$\frac{\Delta V}{\Delta l} = -\rho_o C \qquad (4.17)$$

The negative sign is due to the fact that the potential falls in the direction of current, hence the gradient is negative in the direction of current flow.

4.2.1. Current Flow due to Point Sources

Spherical Electrode in an Infinite Medium

Consider a current I passed into an infinite medium through a spherical electrode. The lines of flow will radiate outwards and the equipotential surfaces will form spheres centred on the electrode. The current density over the surface of an equipotential surface, distance r from the centre, is given by,

$$C=\frac{I}{4\pi r^2} \tag{4.18}$$

The potential gradient is given by $\partial V/\partial R$, using this and (4.17) gives,

$$-\frac{1}{\rho_0}\frac{\partial V}{\partial r}=\frac{I}{4\pi r^2} \tag{4.19}$$

This function can be integrated to give the potential value of an equipotential surface at a distance r from the centre of an electrode producing a current I,

$$V=\frac{\rho_0 I}{4\pi r} \tag{4.20}$$

The constant of this integral is zero, as at r=∞, V=0.

If the electrode is at the surface, no current will travel in the air, the electrode becomes a hemisphere, the equipotential surfaces are hemispheres and the function becomes,

$$V=\frac{\rho_0 I}{2\pi r} \tag{4.21}$$

The Affect of a Boundary

In order to establish the various features of the boundary separating two media of resistivities ρ_1 and ρ_2 and potential values of V_1 and V_2, the potential function must satisfy the following two conditions:

(1). The potential function V must be continuous across the boundary between the two media.

$$\frac{\partial V_1}{\partial l}=\frac{\partial V_2}{\partial l} \tag{4.22}$$

(2). The normal component of current flow through the boundary must be continuous. If a cylinder of cross-sectional area a is placed across the boundary such that its axis is perpendicular to the interface, then the current density entering the cylinder is U_{n1} and the current density leaving is U_{n2} plus a constant for the current leaving the curved sides of the cylinder. If the cylinder length decreases toward the boundary the area of the curved sides decreases to zero, therefore $U_{n1} = U_{n2}$ or,

$$\frac{1}{\rho_1}\frac{\partial V_1}{\partial n} = \frac{1}{\rho_2}\frac{\partial V_2}{\partial n} \tag{4.23}$$

A Point Source in the Vicinity of a Plane Boundary

It is possible to use an optical approach (method of 'images') to define the distribution of potential due to a point current source placed in a medium of resistivity ρ_1 and near to a boundary separating it from a medium ρ_2 (Figure 4.1).

If V_1 is the potential function for the region below the plane and V_2 for that above; I' is the image source seen from below the plane and I'' is the source of reduced intensity as viewed from above the plane.

Hence V_1 at P is given by,

$$V_1 = \frac{\rho_1}{4\pi}\left(\frac{I}{r} + \frac{I'}{r'}\right) \tag{4.24}$$

and V_2 at P is given by,

$$V_2 = \frac{\rho_2}{4\pi}\frac{I''}{r} \tag{4.25}$$

applying the boundary conditions:

(1)

$$\rho_1(I + I') = \rho_2 I'' \tag{4.26}$$

(2)

$$I - I' = I'' \tag{4.27}$$

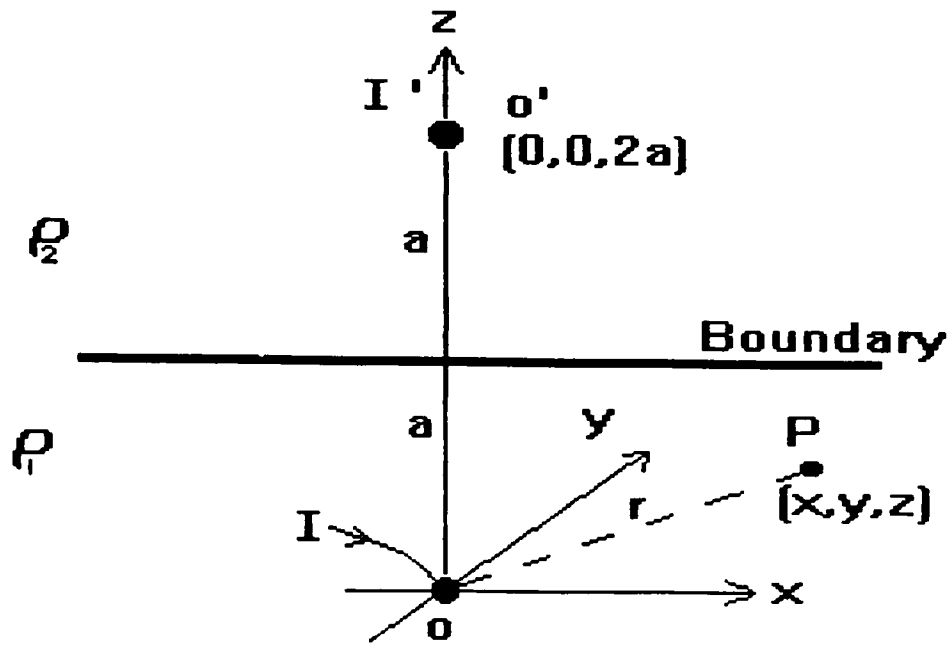

Fig (4.1): A Point Source Near a Plane Boundary.

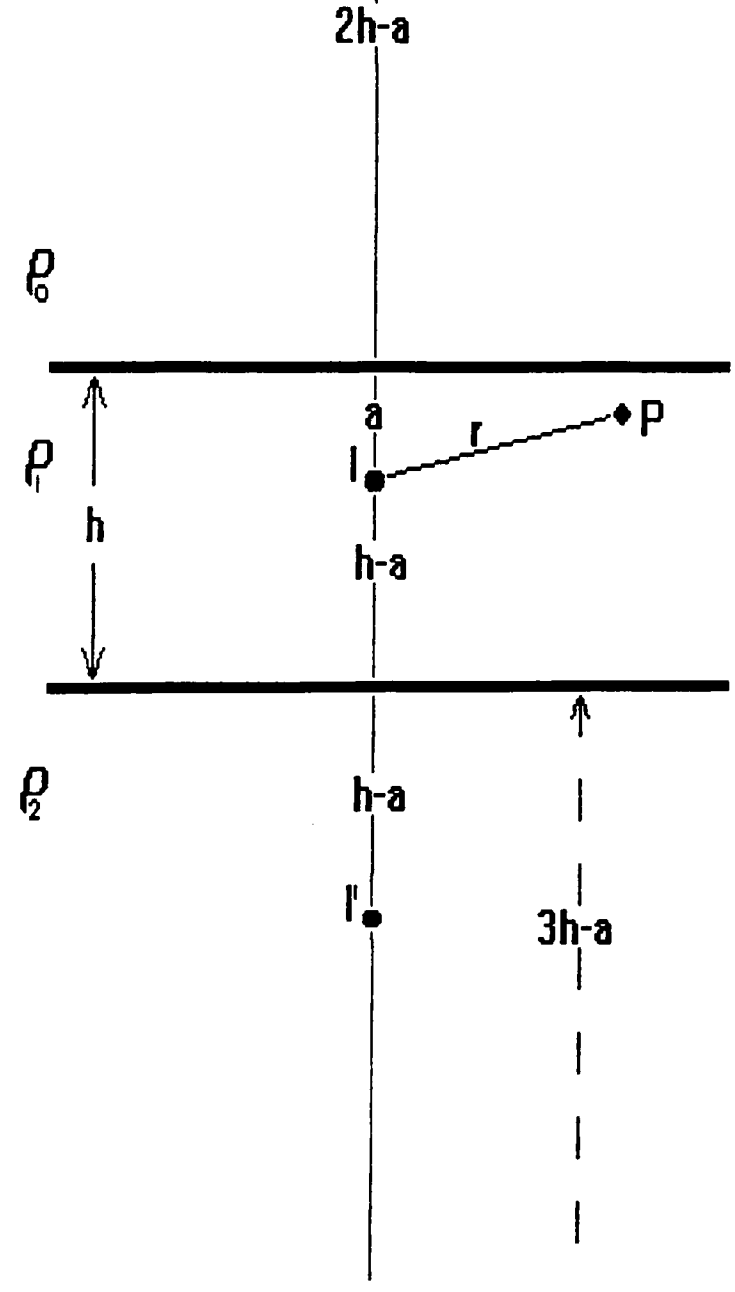

Fig (4.2): A Point Source Near Two Plane Boundaries.

Thus,

$$I'' = \frac{2\rho_1}{\rho_1+\rho_2} I \tag{4.28}$$

$$I' = \frac{\rho_2-\rho_1}{\rho_1+\rho_2} I \tag{4.29}$$

Substituting (4.24) and (4.25) into (4.28) and (4.29) respectively gives,

$$V_1 = \frac{\rho_1 I}{4\pi r}\left(1+\frac{\rho_2-\rho_1}{\rho_1+\rho_2}\right) \tag{4.30}$$

$$V_2 = \frac{2\rho_1\rho_2}{\rho_2+\rho_1}\frac{I}{4\pi r} \tag{4.31}$$

If $\rho_1 = \rho_2$ then both reduce to (4.20) as would be expected. If the boundary is the surface of the earth and the electrode is on the surface then a=0 and $\rho_2 = \infty$ and both will reduce to (4.21).

Point Source Distribution Related to Two Interfaces

The above theory can be expanded to consider the potential distribution of a point source related to two interfaces (Figure 4.2). This produces a complicated expression for the total potential P. However if the first boundary is the surface of the media and ρ_0 is that of the air, then the expression can be simplified to,

$$V_p = \frac{\rho_1 I}{2\pi r}\left(1-2\sum_{n=0}^{\infty}\frac{K_2^n}{\left[1+\frac{4n^2h^2}{r^2}\right]^{1/2}}\right) \tag{4.32}$$

This potential consists of two parts,

$$(A)\quad \frac{\rho_1 I}{2\pi r} \qquad (B)\quad \frac{\rho_1 I}{\pi r}\sum_{n=0}^{\infty}\frac{K_2^n}{\left[1+4n^2h^2/r^2\right]} \tag{4.33}$$

(A) is the potential function for a homogeneous isotropic half-space and is called the 'normal potential'. (B) is the potential function due to the infinite series and which is called the 'disturbing potential'.

Two Current Electrodes at the Surface

If the current electrodes are a finite distance apart, then any potential measured at the surface between the current electrodes will be affected by both current electrodes (Figure 4.3).

The potential due to C_1 at P_1 is,

$$V_1 = \frac{I\rho_0}{2\pi r_1} \qquad (4.34).$$

The potential due to C_2 at P_1 is,

$$V_2 = -\frac{I\rho_0}{2\pi r_2} \qquad (4.35)$$

(since the currents at the two electrodes are equal and opposite in direction).

Thus we have,

$$V_1 + V_2 = \frac{I\rho_0}{2\pi}\left(\frac{1}{r_1} - \frac{1}{r_2}\right) \qquad (4.36).$$

With another potential electrode at P_2, the potential difference between P_1 and P_2 will be,

$$\Delta V = \frac{I\rho_0}{2\pi}\left[\left(\frac{1}{r_1} - \frac{1}{r_2}\right) - \left(\frac{1}{r_3} - \frac{1}{r_4}\right)\right] \qquad (4.37).$$

This arrangement corresponds to the many four electrode spreads normally used in resistivity measurements. In the Wenner spread, which is used in this case, the electrodes are uniformly spaced along the line. Therefore $r_1=r_4=a$ and $r_2=r_3=2a$ and equation (4.37) simplifies to,

$$\rho_0 = 2\pi a \frac{\Delta V}{I} \qquad (4.38).$$

Using this equation the measured ratio $\Delta V/I$ can be used to obtain a resistivity ρ_0. In a homogeneous medium this value will be the actual resistivity, but for an inhomogeneous medium the value is termed the apparent resistivity.

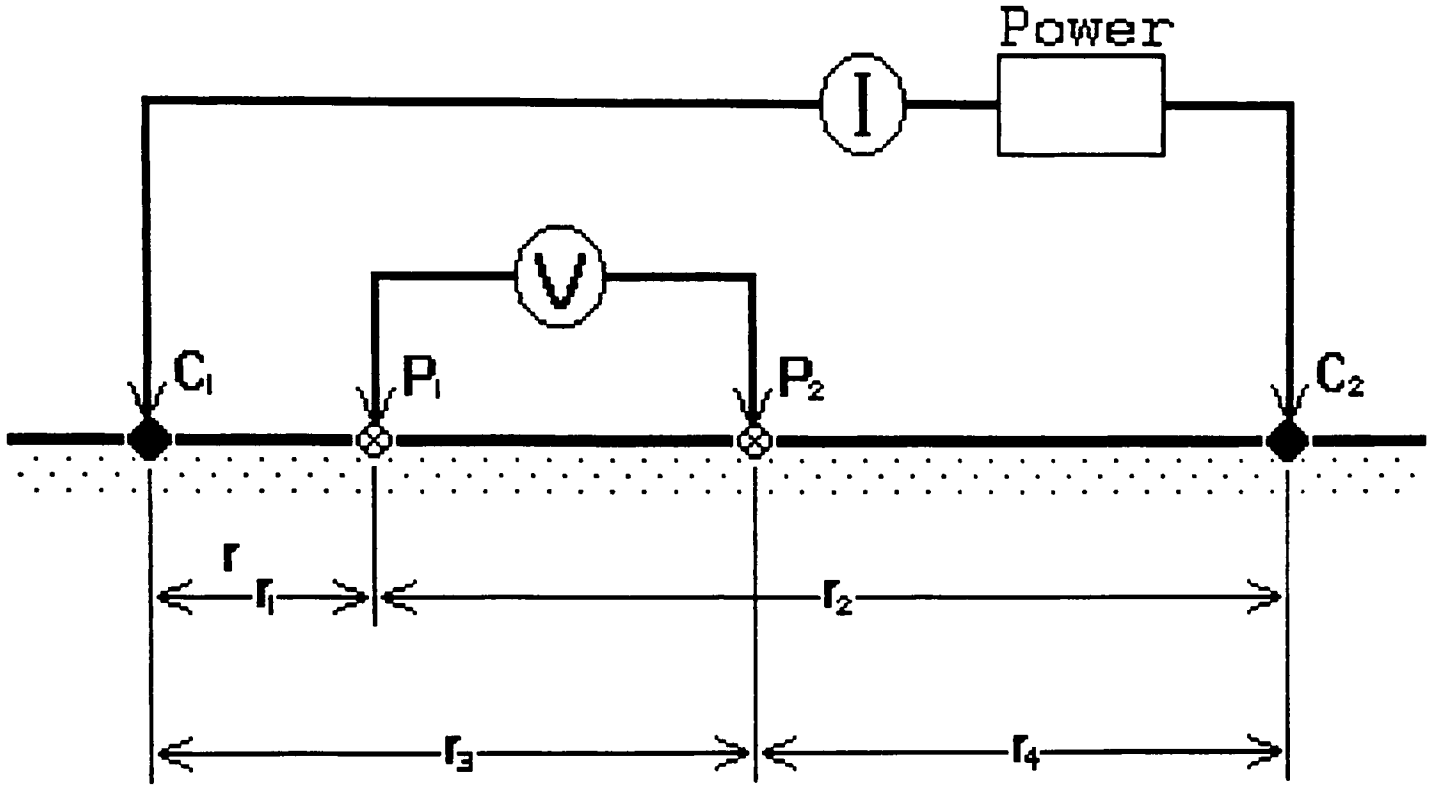

Fig (4.3): A Four Electrode System.

4.2.2. Pore Fluid Resistivity

The pore fluid resistivity, as described above, is a major control of a sediment's bulk resistivity. In most cases the pore fluid will be water, and the resistivity of water depends on its temperature, salinity and pressure. Its variation with these properties has been determined accurately and standardised as the Practical Salinity Scale (1980). Using this scale the variation of resistivity with temperature and salinity at one atmosphere of pressure can be determined (Figure 4.4). The equation used to define this relationship is given in appendix I.

4.2.3. Sediment Resistivity Measurements

As the equations above show, any measured resistance must be corrected by some factor to give a true resistance. This factor (k) will be a constant for each method of measurement. If resistances, measured by different methods, are to be compared then this constant must be calculated for each method. However if formation factors (FF) are being compared then the constant does not need to be calculated.

$$FF = \frac{\rho_s}{\rho_w} = \frac{kR_s}{kR_w} = \frac{R_s}{R_w} \qquad (4.39)$$

This means that formation factors (FF) measured in different cells can be compared. In this investigation the formation factor of a sediment has been used to determine porosity. Measurements in the flume used a Wenner array to measure sediment resistivity. However, as has been already stated, the relationship between formation factor and porosity for a cohesive sediment must be determined experimentally for each sediment. In this case a modified oedometer was used to calibrate the relationship for each sediment. The use of this cell allowed accurate measurement of porosity whilst allowing resistivity measurements on a sample of sediment.

Another important affect on resistivity measurements is the presence of boundaries close enough to disrupt the current distribution of the array. This was investigated by simply measuring the change in resistivity

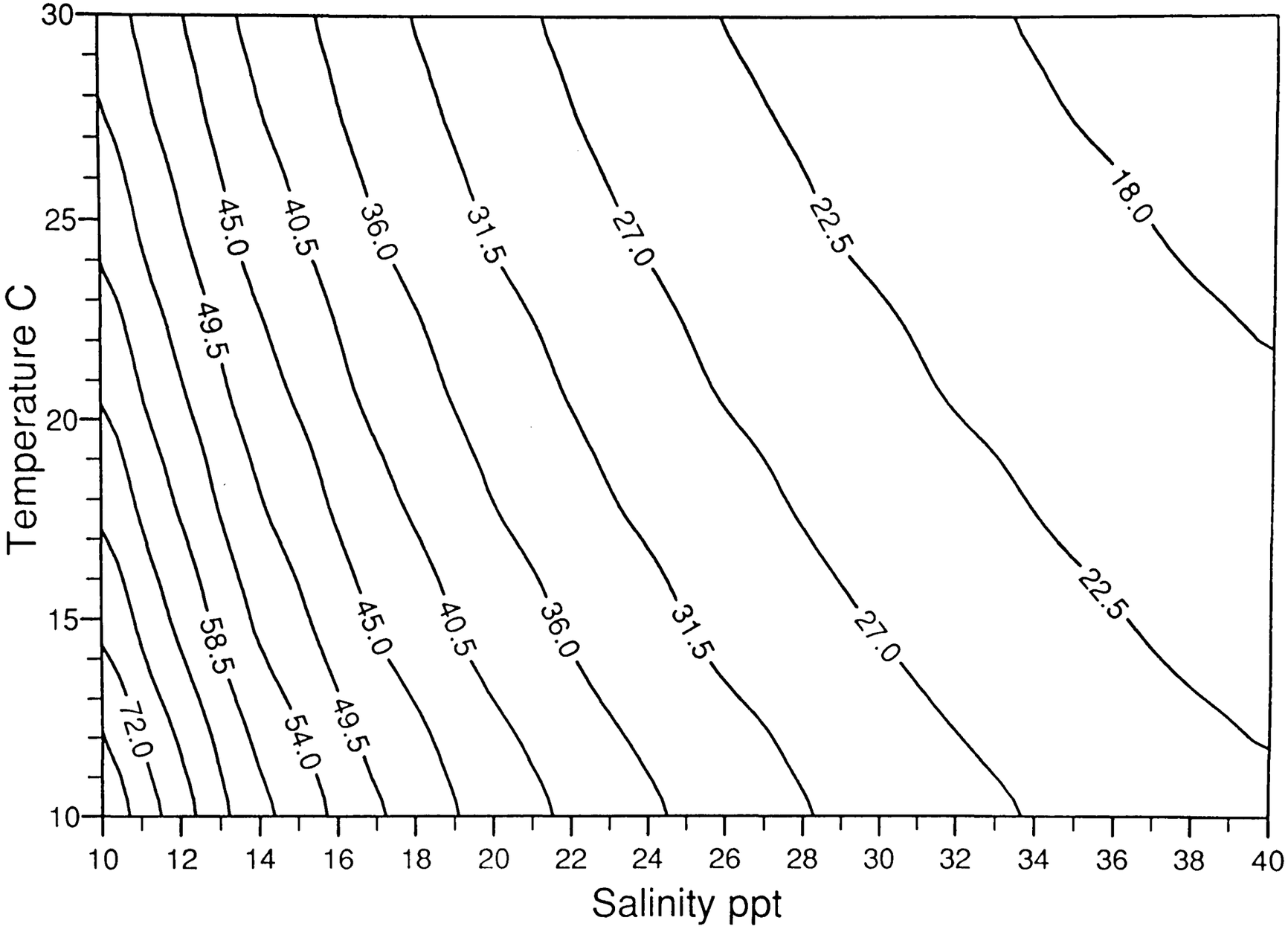

Figure (4.4): Variation of seawater resistivity with salinity and temperature.

as: (1) the array approached a partition in a tank of sea water and (2) the depth of water in the tank was varied. This showed that any boundary within 6cm of an array with an electrode spacing of 2cm will affect the result. This could be taken as a determination of the effective depth of penetration of the current. However seawater is a good conductor and this distance is reduced in sediments, due to poorer conduction. Normally the effective depth is defined as 0.17(AB/2), where AB is the distance between the current electrodes. Therefore for a 2cm electrode spacing this distance would be 0.51cm.

4.2.3.1. **Modified Oedometer Cell.**

This is based on a designed by Lovell (1983), which is similar to a standard cell but modified to allow resistivity measurements. The sample is contained as normal within a ring, a fixed porous disk below and a porous disk above which is free to move within the ring (Figure 4.5). The main variation from the standard oedometer cell is that the cell is constructed almost entirely out of electrically non-conductive PVC. This is to remove any conductive affects of the standard metal cell. The only metal part of the cell is the upper cap of stainless steal, which avoids any distortion due to loading. The sample ring is of the standard dimensions: diameter of 75mm and height of 20mm.

For resistivity measurements in this study, a standard four electrode system is incorporated into the cell. The inner surfaces of each of the two perspex disks, above and below the sample, are coated with electrically conducting silver paint to form the current electrodes. The potential electrodes are formed by wrapping the conducting wire around a ring of stainless steel wire which is then coated with the conductive silver paint; this is secured to the inner surface of the porous disk.

4.2.3.2. **Oedometer Technique**

As with normal oedometer experiments the sediment sample is placed into the sample ring and then into the cell. The cell is then filled with

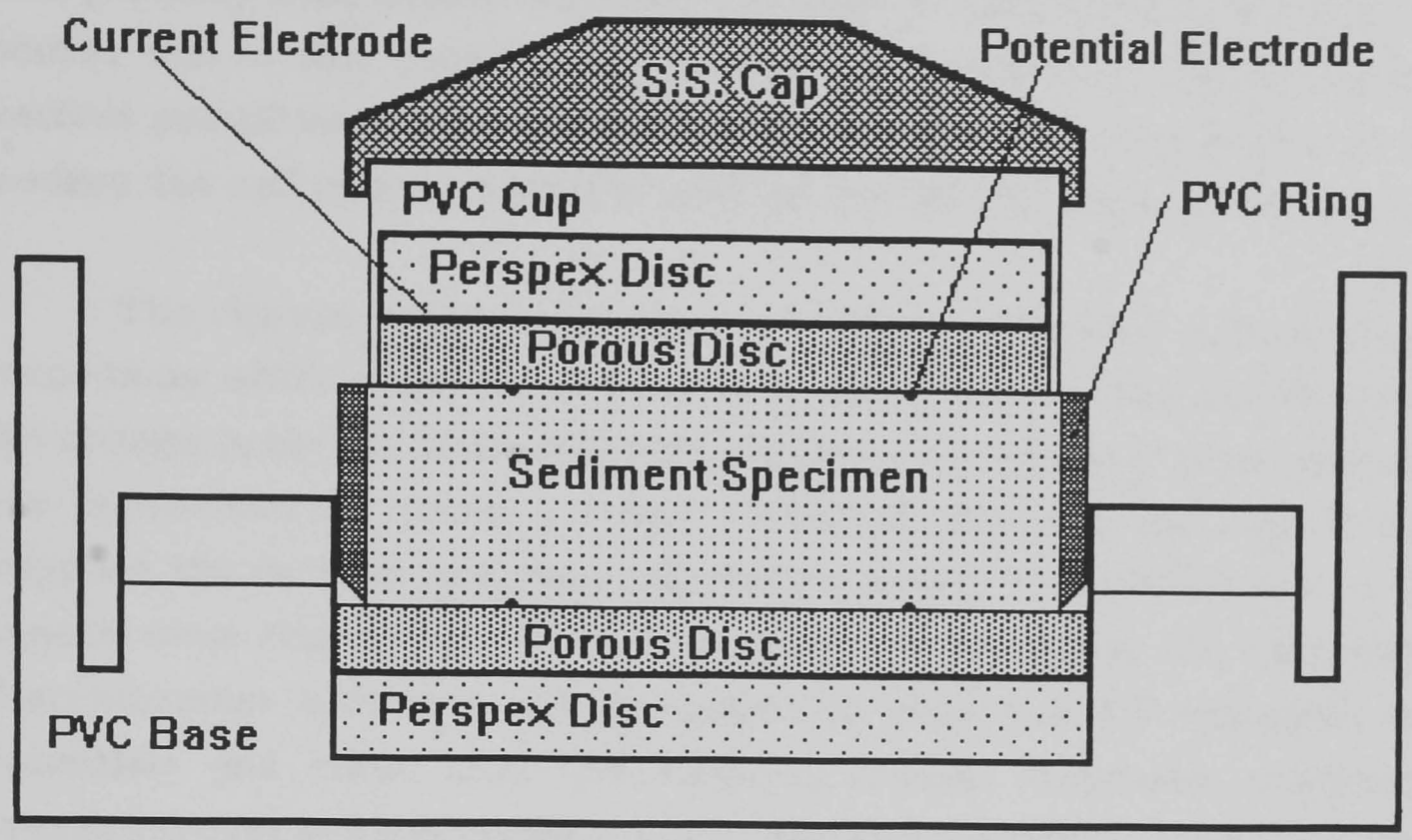

Fig (4.5): Modified Oedometer Cell.

Cell Height (mm)	Cell Constant
21.425	18.679
20.050	19.926
17.750	21.804
15.850	24.447
13.675	28.431

Table (4.1): Cell Constant Calibration Results for the Modifed Oedometer cell.

water. Normally this would be distilled water, but as the calibration is for marine sediments, this must be sea water, with a salinity of 35 ppt. The cell is placed in the oedometer and loaded every twenty four hours. The first load is that of the top cap alone and then five kilograms is added every twenty four hours. Normally the load is doubled every twenty four hours, but in this case the aim is to obtain resistivity measurement at various porosities and so gradual loading is required. Even with this slow loading the cell is compressed to half its size within three to four days.

The change in height of the cell is determined from a displacement transducer which measures the fall in height of the cell cap and therefore the change in height of the sediment sample. The resistivity measurements are determined by using a ABEM TERRAMETER SAS 300, which both supplies the current and measures the potential. The system uses a 4Hz square wave alternating current to avoid polarisation at the electrodes. Discrimination circuitry and programming separates DC voltages, self potentials and noise from the incoming signal. Automatic continuous averaging over several cycles is performed and the resistance is calculated and displayed as a digital readout.

4.2.3.3. Data Analysis

Porosity

The measured cell displacement is used to determine the cell height and therefore the cell volume (V_t). To calculate the sediment porosity (n), the mass of dry sediment (M_s) and the sediments specific gravity (G_s) are need. The dry mass of sediment is determined by washing the sediment in a Buchner funnel and drying in the oven, and the specific density is determined by standard soil analysis techniques (§5.2.4.2.). These measurements can be converted to a porosity by the equation,

$$n = 1 - \frac{M_s}{G_s \rho_w V_T} \qquad (4.40).$$

Resistivity

The formation factor can be obtained by simply dividing measured resistivity by the fluid resistivity. In this case the variation with

temperature and the change of the cell constant with height must be determined. It is possible to produce an equation relating cell height to cell constant. This is done by measuring the resistivity of seawater in the cell at various cell heights. The cell constant can then be found by dividing the resistivity determined from the Practical Salinity Scale by the measured resistance. This was done at four separate cell heights, with the resistance given by the average of ten separate measurements.

The data are shown in Table 4.1, and plotted in Figure 4.6, with a straight line fitted to the data. The variation of conductance with distance between two electrodes is described by a complicated function. However in this case the range of distances between the electrodes and the accuracy of the equipment means that a straight line provides the best fit to the data, giving,

$$Cell\ Constant = 44.421 - 1.236(Cell\ Height) \qquad (4.41)$$

(R^2=0.968)

The formation factor of the sediment in the oedometer is determined by,

$$FF = \frac{kR_s}{\rho_w} \qquad (4.42)$$

where R_s is the measured sediment resistivity, ρ_w is the water resistivity at the same temperature and k is the cell constant at that cell height.

Results

The formation factor and porosity are plotted on logarithmic scales and the relationship between them determined. For each of the mud samples used in the flume, three separate oedometer runs were made and then combined to give the porosity formation factor relationship.

4.2.3.4. Sediment Porosity / Formation Factor Results.

The results for the four muds used in this study are shown in Figure 4.7 and the equations fitted to each of the data sets are;

Figure (4.6): Modified Oedometer Cell.
Cell Constant Calibration Results

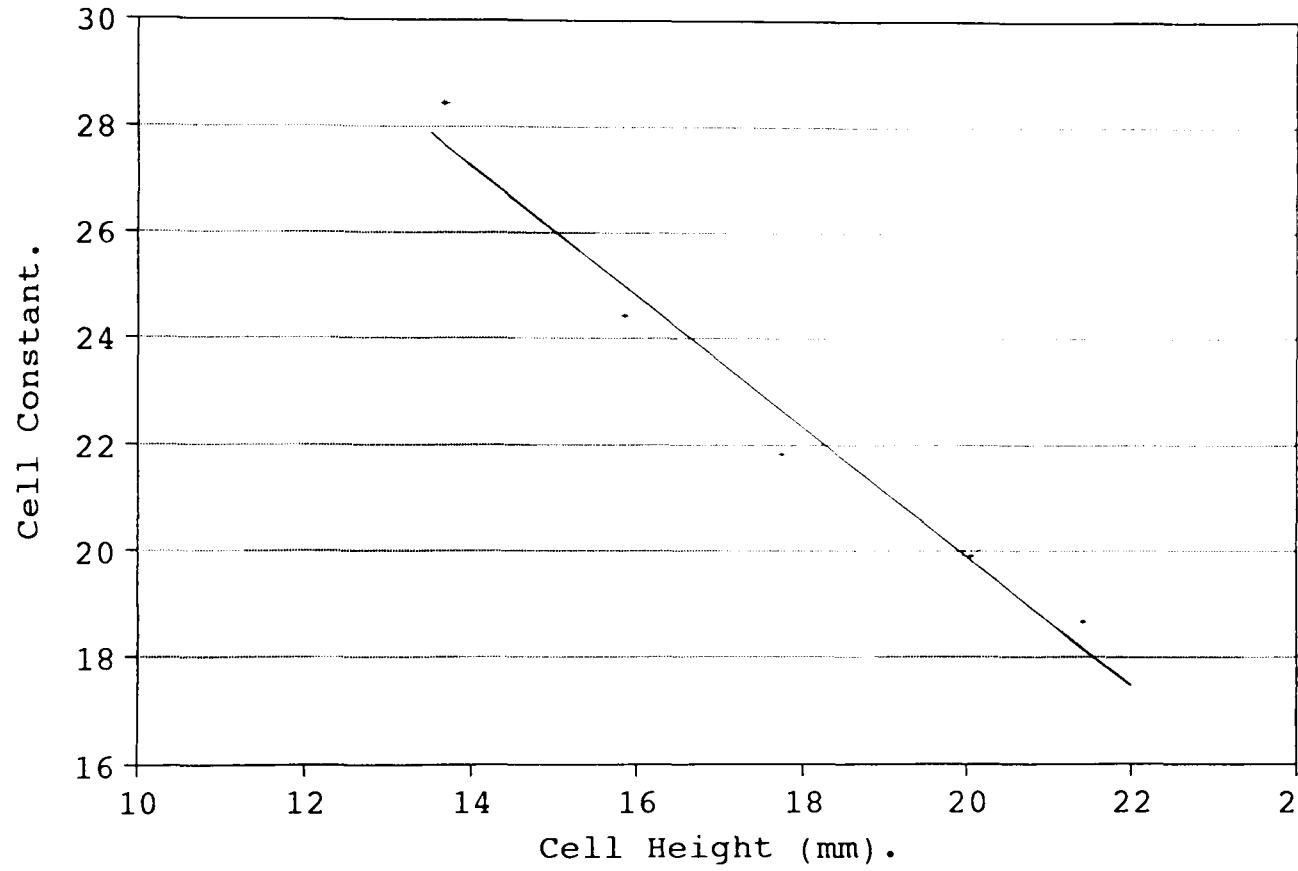

Fig (4.7): Data from Oedometer Cell Relating Formation Factor and Porosity.

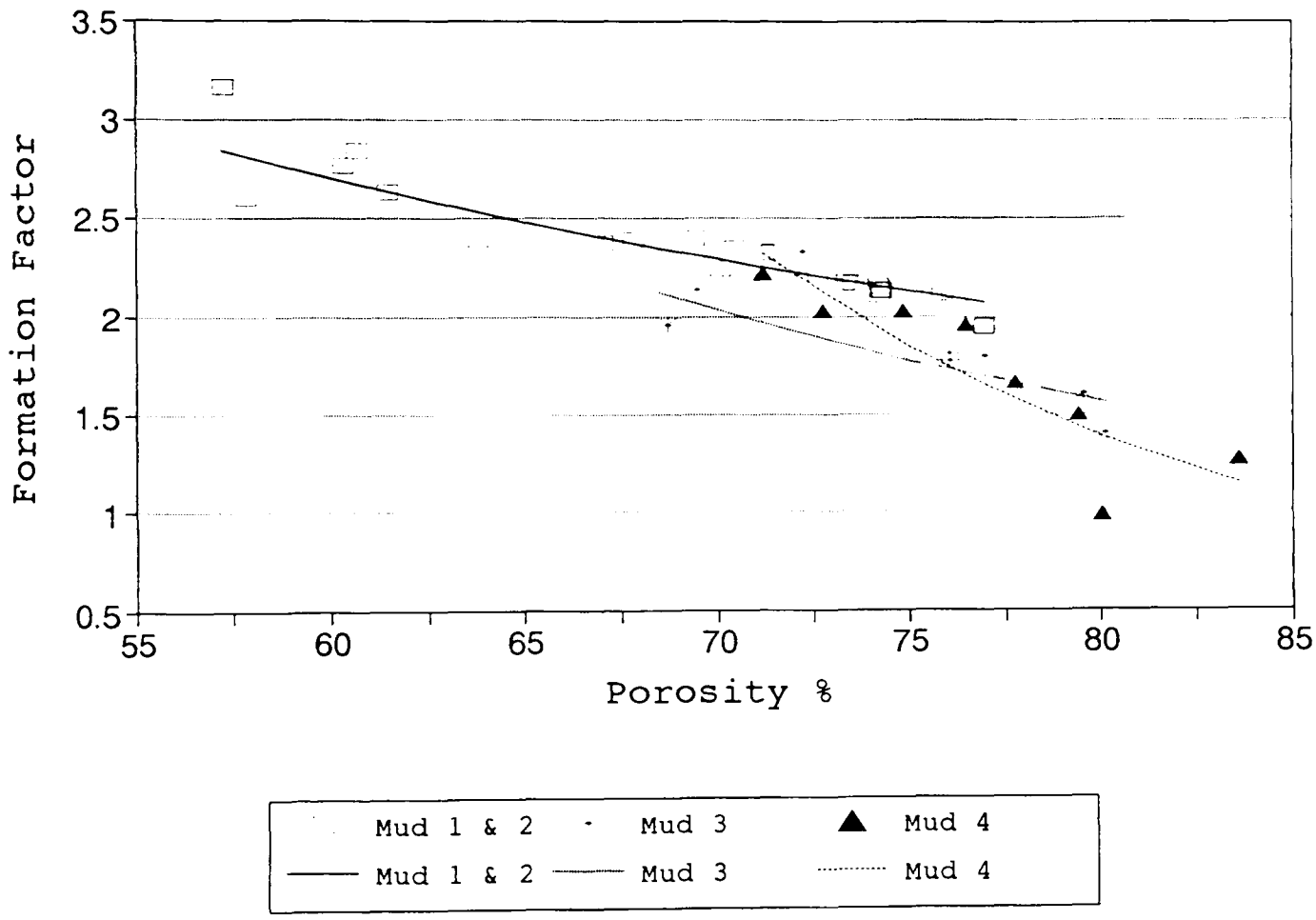

Mud 1 & 2,

$$FF = \frac{1.566}{n^{1.068}} \qquad (4.43)$$

(R^2=0.823)

Mud 3,

$$FF = \frac{1.017}{n^{1.941}} \qquad (4.44)$$

(R^2=0.771)

Mud 4,

$$FF = \frac{0.520}{n^{4.412}} \qquad (4.45)$$

(R^2=0.700)

4.3. **Summary and Conclusions.**

The measurement of the electrical formation factor is a tool that can be used to ascertain some feature of a sediment's structure in a non destructive manner. However the interpretation of the formation factor is not simple, and necessitates some form of calibration if its is going to be used to determine porosity. In this section the theory behind formation factor and its relationship to porosity have been outlined, and the individual relationship for the muds used in the flume study defined. The individual relationships for each mud are different due to other properties of mud that vary between the samples, which in this case is most probably due to changes in the organic content (§6.2.2.1.). The method and equipment set up used to measure the electrical resistivity and formation factor of sediment in the flume is given below (§5.2.4.2.).

CHAPTER 5.

INSTRUMENTED RECIRCULATING FLUME.

5.1. The Recirculating Flume.

The principal aim of a laboratory or field flume is to generate controlled and measurable flow conditions that can then be used to study a range of fluid dynamic and coupled fluid-sediment phenomena (Nowell and Jumars, 1987). In general the design of laboratory flumes can be divided into two main groups - annular flumes and straight flumes; both have advantages and disadvantages.

Annular flumes by their design can be approximated to infinitely long channels and therefore the boundary layer flow is allowed full development. The bed is preformed around the entire length of the flume base. The main problem with this design of flume is the presence of secondary circulations perpendicular to the main flow. These radial flows vary in strength in proportion to the main flow and their presence can generate erroneous erosion patterns that vary in appearance across the channel width. This complicates analysis of bed shear stress and erosion rate due to the lack of a uniform distribution of shear stress across the flow.

Straight or unidirectional flumes tend to have better hydrodynamic conditions but the length of the test section may be limited. Therefore the boundary layer may not be allowed to develop fully and this can invalidate use of the 'law of the wall' to calculate bed shear stress. Another problem is where to place the bed. A bed formed on the floor of the flume will change the flow regime, and the more usual method of placing the sediment bed in a box or well, mounted under the flume floor causes problems with

edge effects, especially as the sediment is eroded and a change in height forms at the lip of the box.

Another variable relating to straight flumes is the nature of the recirculation. For very long test sections large volumes of water are needed, which requires an efficient pump to generate higher velocities. The design of re-circulating flumes must try to minimise the deposition of sediment in parts of the flume other then the test section. The loss of material in this way can make measurements of suspended sediments difficult; also the greater the volume of water in the flume the more difficult it is to measure small changes in suspended sediment concentration.

To allow accurate and useful determinations of critical erosion velocity of sediment, accurate control of the flow is essential. It also needs to be considered that a boundary layer will develop on the walls of the flume as well as the floor; the only systematic study of flume wall effects (Williams, 1970) concluded that width had very little effect on the relation between bulk flow and net sediment transport, but that narrow flumes produce significant arrangements of bed forms (Muschenheim et al., 1986). However narrow flumes, especially smooth walled ones can still be of use, if it is ensured that the bottom boundary layer has developed in an unimposed fashion (Eckman and Nowell, 1984).

Before the flume in this study was design and constructed a number of criteria which had to be satisfied were established. These were:

- bilaterally symmetrical flow over the test bed.
- streamline flow rather than helical flow.
- low volumes of water (thus increasing capability to measure turbidity).
- accurate and reproducible control of water speed.

The flume that resulted from these criteria was a vertically arranged re-circulating channel (Fig 5.1 and Plate 1). There were two main reasons for giving the flume a vertical orientation: 1) it reduces the strength of any cross stream variability in the flow over the test section, giving rise to top to bottom azimuthal velocity gradients only. 2) it saves space. The

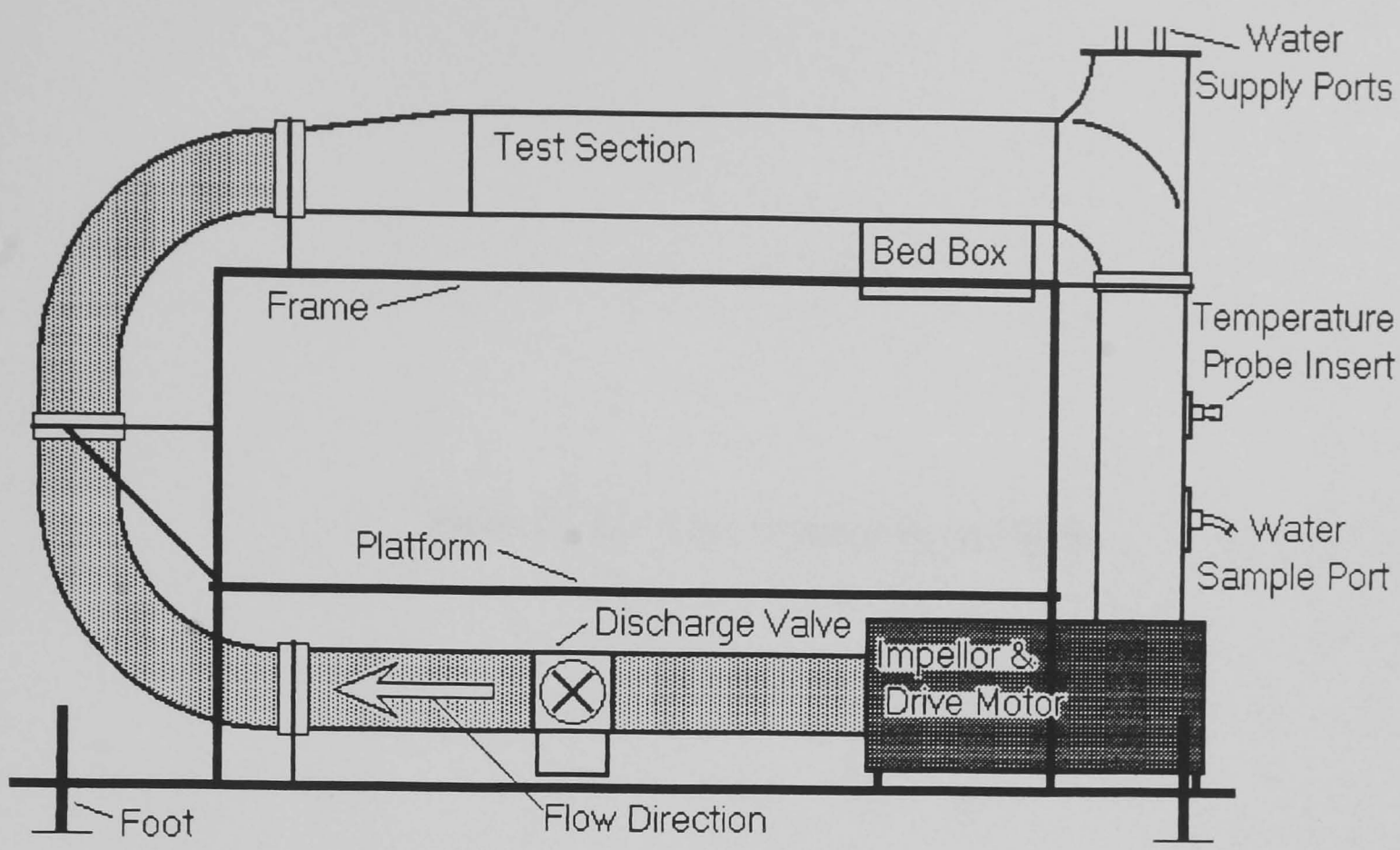

Fig 5.1: Schematic of the Recirculating Flume.

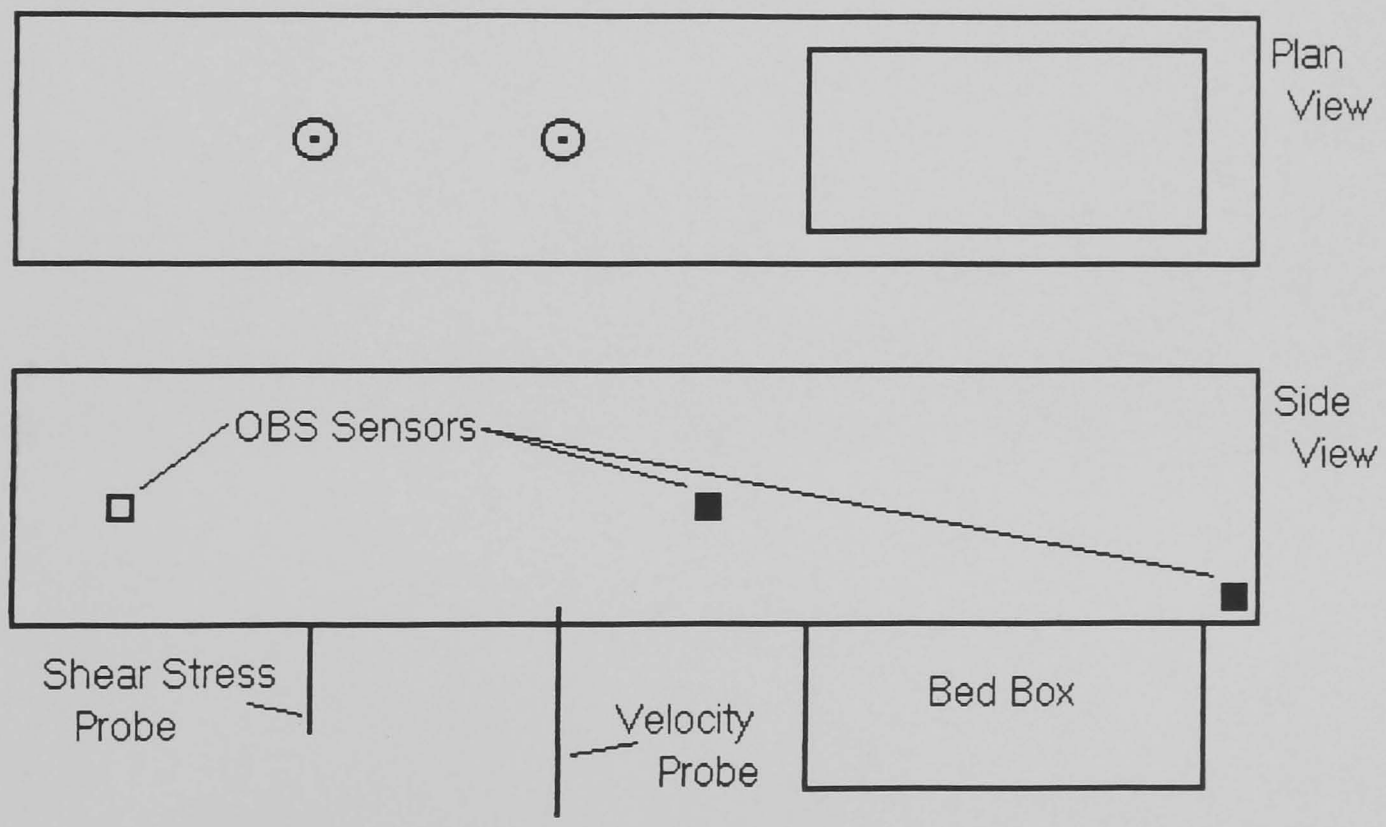

Fig 5.2: Schematic of the Recirculating Flume test section.

Plate (5.1): The recirculating flume.

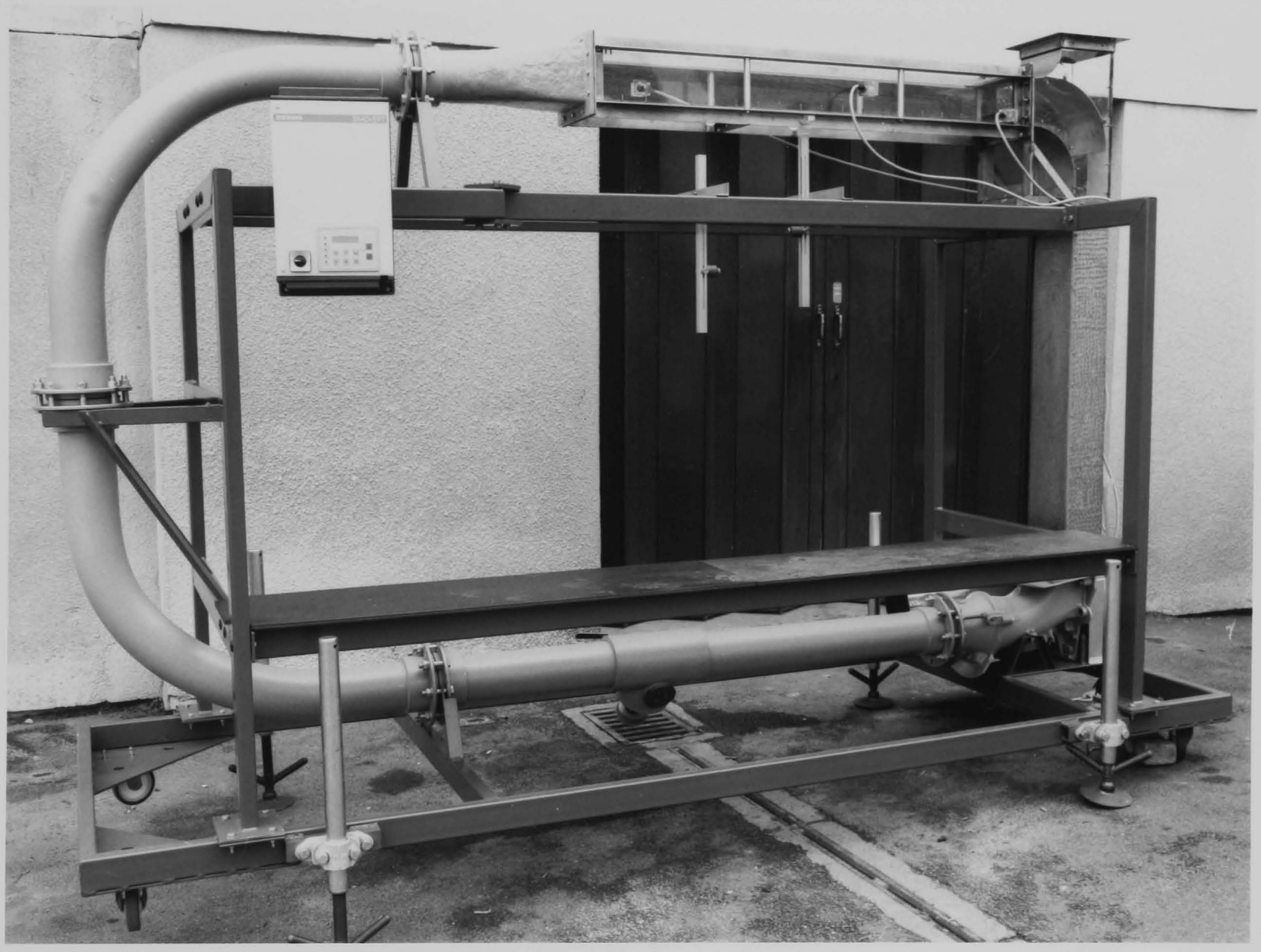

flow is driven by an impeller system, which is a P.P. 65 jet boat engine made by R.G. Parker (Engineering) Ltd, and this system produces a less turbulent output than that of a normal propeller. This is powered by a three phase 4KW 415V AC electric, force ventilated, inverter fed motor that can give 0 to 6000 RPM. This impeller and motor system produce very little un-wanted vibration. The motor is controlled by a Siemens Invertor Unit 6SE1207 2A100, an electronic control unit. This electronic control unit allows accurate, repeatable and constant output from the electric motor and displays the motor output frequency on a liquid crystal display on the front face of the unit. From the impeller, the water initially flows through a 5" non-corrosive PVC piping, along the base and around two bends before entering the perspex test section which forms the top horizontal limb of the flume. The clear perspex test section is 1.50m in length, 0.2m wide and 0.14m deep. The transition from the circular PVC pipe to the rectangular test section is made by a specially constructed fibre-glass moulding, which has been design to give a smooth transition, and reduce the generation of turbulent eddies. At the end of the test section the water returns to the impeller via a vertical rectangular stainless steel conduit. A sheet of curved stainless steel guides the flow around the top of this top bend, with gaps at both ends of this flow guide allowing any air to escape. Above the flow guide is a small vertical perspex section that allows a small head of water to form, which with the sealable lid of the test section allows the test section to be filled right to its roof. The flow is only open to the air in this header section.

The sediment is in a box located at the downstream end of the test section 1.02m from the start of the test section. The box is 0.3m long and 0.14m wide located centrally in between the side walls. The box is fixed to the underside of the perspex floor and can be removed if necessary. It also has a moveable base that can be raised and lowered at increments as small as 0.1mm. This moveable base allows the bed surface to be moved upwards as it erodes, keeping it level with the flume floor and therefore reducing the magnitude of any leading edge effects.

The flume is mounted on wheels so that it can be moved around the laboratory if necessary, but during all of the experiments it was secured by means of height adjustable feet at each corner. These gave rise to a

stable flume and more importantly, because each foot could be adjusted individually, it was possible to level the bed of the test section to with-in a 1mm variation at each corner. The flume is drained by means of a discharge valve built into the PVC pipe leaving the impeller and is filled by two valves built into the header section supplying sea or fresh water.

5.2. **Instrumentation.**

The flume has been instrumented to allow a number of parameters to be logged continuously by a PC whilst the flume is running. These parameters are flow velocity, bed shear stress, and suspended sediment concentration. The temperature is also measured but manually at regular intervals, by using a temperature probe accurate to 0.1°C inserted into the flow through a water proof connection in the stainless steel conduit.

Due to a constraint of the flume design, the measurement of bed shear wave velocity, electrical resistivity and, pore and total pressure are measured in the flume before the start of an erosion run. The sediment is placed in the box and a vertical profile is made of these four parameters as the sediment is raised to bring it level with the flume floor. The actual flume run is then started.

5.2.1. **Flow Measurement.**

Two flow properties are measured: flow velocity and wall shear stress. Both are measured by the same technique of hot film anemometry, but using slightly different probes. The probes consist of a small quartz-platinum coated resistance element which is heated electrically and then controlled at the elevated temperature. The resistance of the film is related to its temperature and the system uses this to keep the film at a constant temperature, by measuring its resistance and varying the voltage supplied to the film to keep its resistance and therefore its temperature constant. The sensor is cooled by the fluid flowing past it and therefore the supply voltage to the film, used to keep its resistance constant, is related to the cooling affect of the fluid. This cooling affect of the fluid is dependent on

both the mass flow of the fluid and the temperature difference between the sensor and the fluid. It is for this reason that the fluid temperature needs to be constant or any variation recorded.

Temperature differences between the actual flow temperature and calibration temperature can be corrected for by using a factor defined by the following equation,

$$\left[\frac{(t_s - t_{e_2})}{(t_s - t_{e_1})}\right]^n = \left[\frac{(66.7 - t_{e_2})}{(66.7 - t_{e_1})}\right]^n \qquad (5.1)$$

Where t_s is the sensor operating temperature (66.7°C for the probes used in this case), t_{e1} is the new flow temperature, t_{e2} is the calibration temperature and n is either $\frac{1}{2}$ or 2 for bridge or linearised voltage output corrections, respectively. The correction is carried out by simply multiplying the logged voltage by the correction factor.

Figure 5.2 shows the location of the two probes. The shear stress probe is 0.425m from the start of the test section and the velocity probe 0.285m further down stream. The flow sensor which measures the free stream flow velocity and its fluctuations protrudes about 13mm into the flow. This short protrusion reduces any wake shedding effects and allows the probe to be well secured, alleviating any vibration problems. The actual quartz-platinum coated film is located on the side of the probe just below the tip, (at a height of 10mm above the floor), and the probe is orientated so that the film faces across the flow. The other sensor is a cylindrical flush mounted, wall stress probe. It is mounted flush with the floor of the test section and is used to determine indirectly the shear stress acting on the flume floor.

The use of flush mounted hot-film gauges for measuring skin friction in steady laminar and turbulent boundary-layer flows has been proved effective with the theory behind these measurements extended in a more general form by Menendez and Ramaprian (1985) to include unsteady flows. Hot-film gauges have been used to give accurate measurement of the friction velocity and for smooth flows where the bottom stress is required, reduce elaborate profile measurements to a signal point measurement

(Cardoso et al., 1989). The error in measuring wall stress by hot-film sensors can be 2 to 6 times smaller than errors in wall stress values calculated from velocity profiles using the logarithmic layer technique, under the same flow conditions (Gust, 1988). However hot film sensors are sensitive only to the magnitude of the instantaneous skin friction and not its direction (Paola et al., 1986). To give accurate results, the probe must be mounted in the test section with its measuring face flush with the flume floor; if it is not then one of two problems will occur. Either the probe face is below the flume floor and a sediment trap is formed, or the probe face is above the flume floor, particles are deflected around the sensor and flow separation occurs (Gust and Southard, 1983).

For the velocity probe it is possible to record a choice of two outputs. One is the bridge voltage, which is approximately a quarter the power of the flow velocity (the square of the voltage corresponds to the square root of the flow velocity). Even in zero flow the bridge output is greater than zero, because the hot sensor is being cooled by free convection in the fluid and conduction to its support. The other output uses an electronic lineariser built into the anemometer hardware. The lineariser first subtracts a constant from the bridge output and then uses a function to convert it to a signal that is linear with the mass flow. The bed shear stress probe also gives a non-linear output, but it lacks a built in lineariser and so the voltage data is converted to a shear stress by means of a polynomial. Hence to relate the voltage outputs of both probes to known flow conditions and to optimise the range of the lineariser to give the best and most useful output, both probes were calibrated.

Gust (1982) recorded no change in the heat transfer coefficient between his hot-wire sensors and the fluid for various flows with and without sediment. Gust and Weatherly (1985) found no change in skin friction readings in flows with mud concentrations up to 320μgl^{-1}. The effect of suspended sediment on the hot-film sensors used in the flume is given in ($\oint$ 5.2.5.2.). However in flows containing sediment, care must be taken that the sensing film is not contaminated with sediment or air bubbles, because both cause a reduction in sensor output (Gust, 1982). Therefore access to the probe's faces was designed into the flume, in the form of small access ports built into the test section roof above each

sensor. This allows the probes to be cleaned with a small soft brush, to remove contamination by air bubbles and sediment whilst the flume is running.

Mathews and Poll (1985), in an investigation of hot film probes used as shear stress sensors cite a number of disadvantages, which include: (1) the calibration curve is such that errors in the measurement of voltage are magnified greatly when related to shear stress; and (2) a different probe response can be expected in laminar and turbulent flows. Mathews and Poll (1985) based these findings mainly on experiments involving air flow, but in water flows Gust (1988) and Graham et al. (1992) have obtained calibrations that agree for both laminar and turbulent flows.

5.2.1.1. **Velocity Probe Calibration.**

During the course of the flume work two velocity sensors were used. This was necessary because the original probe (termed probe 1) became damaged in use and had to be replaced by a new probe (termed probe 2). The two probes were calibrated in different ways. The reason for this was that experience and knowledge gained from the calibration and use of the first probe allowed the second probe to be calibrated more easily using calibration data supplied by the probe manufacturer.

Probe 1 Calibration.

The calibration of velocity probe 1 was carried out using a laser doppler anemometer set-up in back scatter mode in a ten meter Armfield recirculating flume. The calibration was done in separate runs, where the flume speed was stepped up slowly to a maximum of over $1.5ms^{-1}$ and then slowed down in the same manner, with output from the laser and hot film sensor recorded at each step. In fact a number of measurements were recorded at each increment to allow an average to be taken. A problem with this flume was that the water temperature increased slowly through the day and was therefore recorded for each velocity measurement and then corrected for by using equation 5.1.

As described later ($\oint$ 5.2.3.), the data logger takes voltages from -5 to +5 volts, and so it was therefore decided to set-up the linearisers with a range from 0 to +5 volts. Hence for each of the calibration runs the linearisers range was changed to cover a different velocity and bridge voltage range.

Table 5.1 shows the results of the calibration runs. As can be seen in run 2 the linearisers range was changed at the half way stage, when the flume was at maximum velocity. An interface box was used to scale the bridge output down from a range of 0 to 16 volts to a lower range of 0 to 5 volts so that it could be logged due to the data logger's voltage range as explained above. Figure 5.3 shows a plot of bridge output and Figure 5.4 shows the quarter power relationship between velocity and bridge output. Figures 5.5, 5.6 and 5.7 show the different linearisers ranges used, with the equations of the lines of best fit. The linearisers ranges were;

Fig.	Lin. Zero (Volts)	Bridge Voltage
All	0.021	6.9
	Lin. Max. (Volts)	Bridge Voltage
5.5	4.917	15.515
5.6	4.99	13.01
5.7	5.004	12.55

For subsequent flume experiments calibration run 3 was used. This gives a velocity to linearised voltage output relationship (at a calibration temperature of 13.5°C) of,

$$(Velocity\ (m/s)) = \frac{(Lin.\ Volts)}{3.66} \qquad (5.2)$$

(R^2=0.976)

Probe 2 Calibration.

The calibration data supplied with probe 2 is given in Table 5.2 and Figure 5.8. For use in the flume the linearisers range of 0 to +5 volts was set to a bridge output range of 5.627 to 13.700 volts. This gives a velocity to linearised voltage output relationship (at a calibration temperature of 25.4°C) of,

Figure (5.3): Bridge Output
Calibration Data

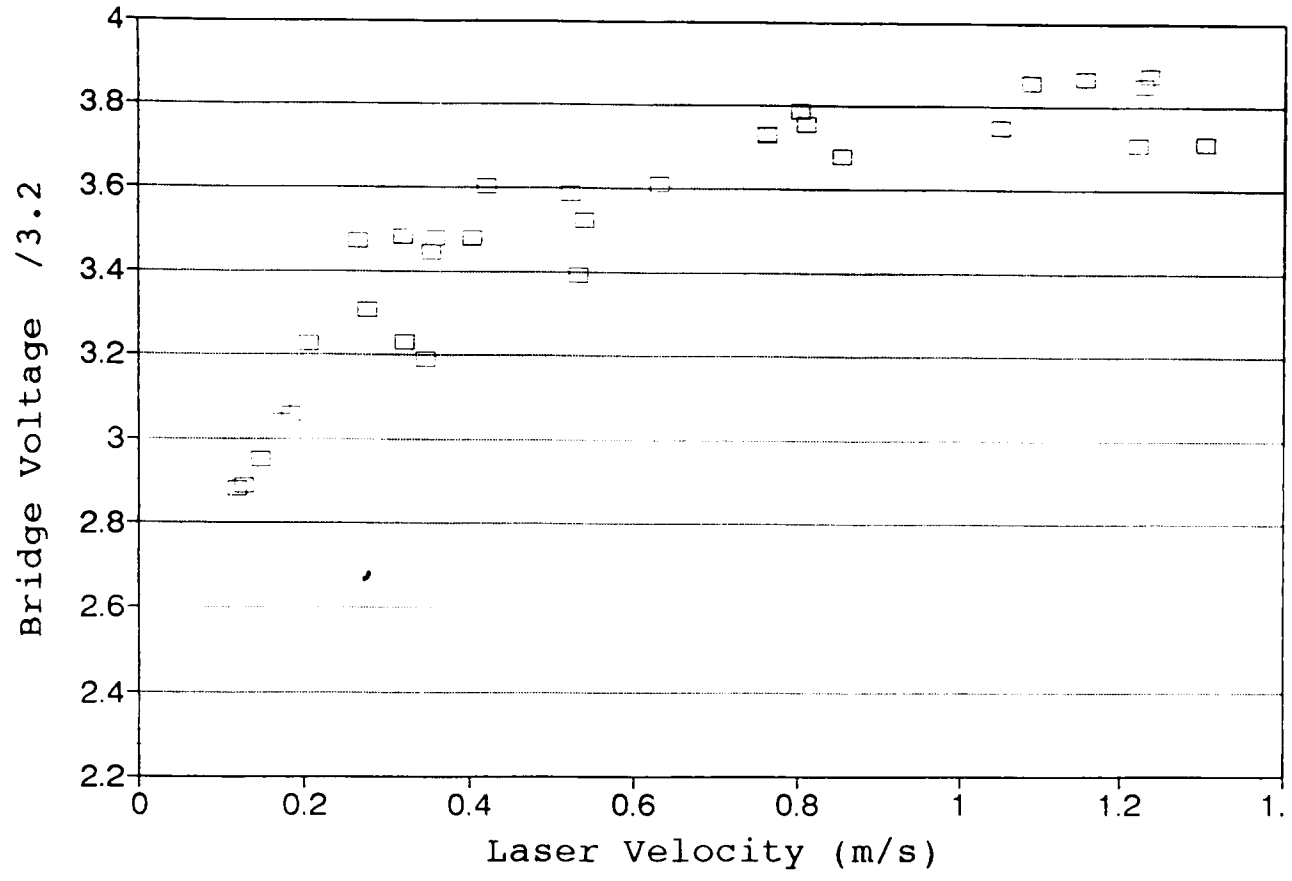

Run No.	Laser Vel m/sec	Linear Volts	Bridge Volts	Run No.	Laser Vel m/sec	Linear Volts	Bridge Volts
1:1	0.266	0.554	3.475	2:16	0.000	0.000	2.292
1:2	0.321	0.554	3.485	2:17	0.120	0.249	2.885
1:3	0.422	0.703	3.604	2:18	0.147	0.291	2.955
1:4	0.524	0.678	3.587	2:19	0.323	0.637	3.234
1:5	0.633	0.710	3.613	2:20	0.348	0.593	3.193
1:6	0.763	0.876	3.728	2:21	0.533	0.975	3.395
1:7	0.812	0.912	3.755	2:22	0.764	1.986	3.733
1:8	1.050	1.230	3.749	2:23	0.804	2.165	3.786
1:9	1.303	0.858	3.711	2:25	1.154	2.490	3.869
1:10	1.220	0.791	3.710	2:26	1.228	2.492	3.849
1:11	0.541	0.558	3.526				
1:12	0.354	0.471	3.448	3:27	1.235	4.449	3.876
1:13	0.277	0.360	3.309	3:28	1.087	4.223	3.858
1:14	0.207	0.319	3.230	3:29	0.856	2.746	3.680
1:15	0.128	0.153	2.890	3:30	0.404	1.721	3.482
				3:31	0.360	1.683	3.482
				3:33	0.173	0.469	3.078
				3:34	0.185	0.427	3.062

Table (5.1): Hot film velocity sensor calibration data, Probe 1.

Figure (5.4): Bridge/Laser Relationship

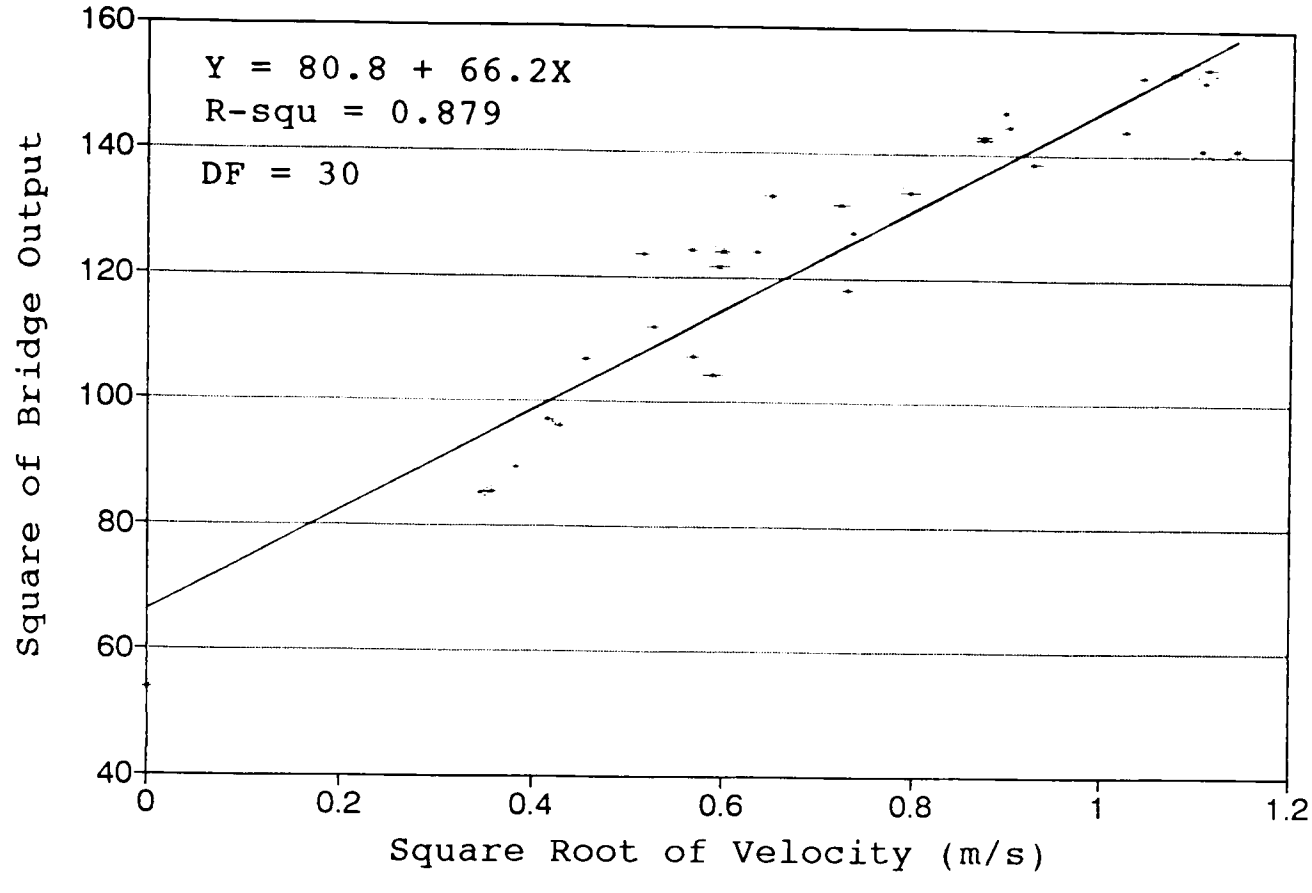

Figure (5.5): Calibration Run 1

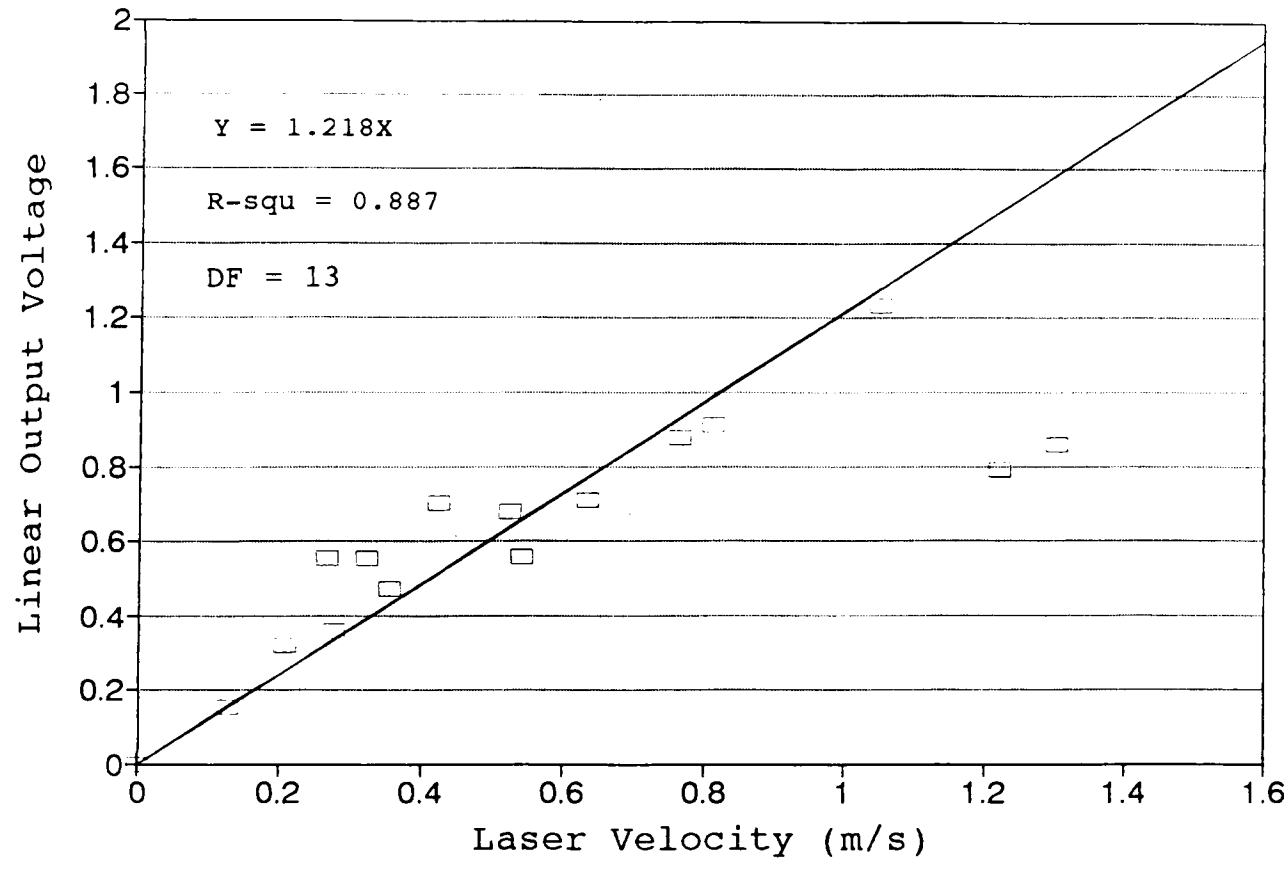

Figure (5.6): Calibration Run 2

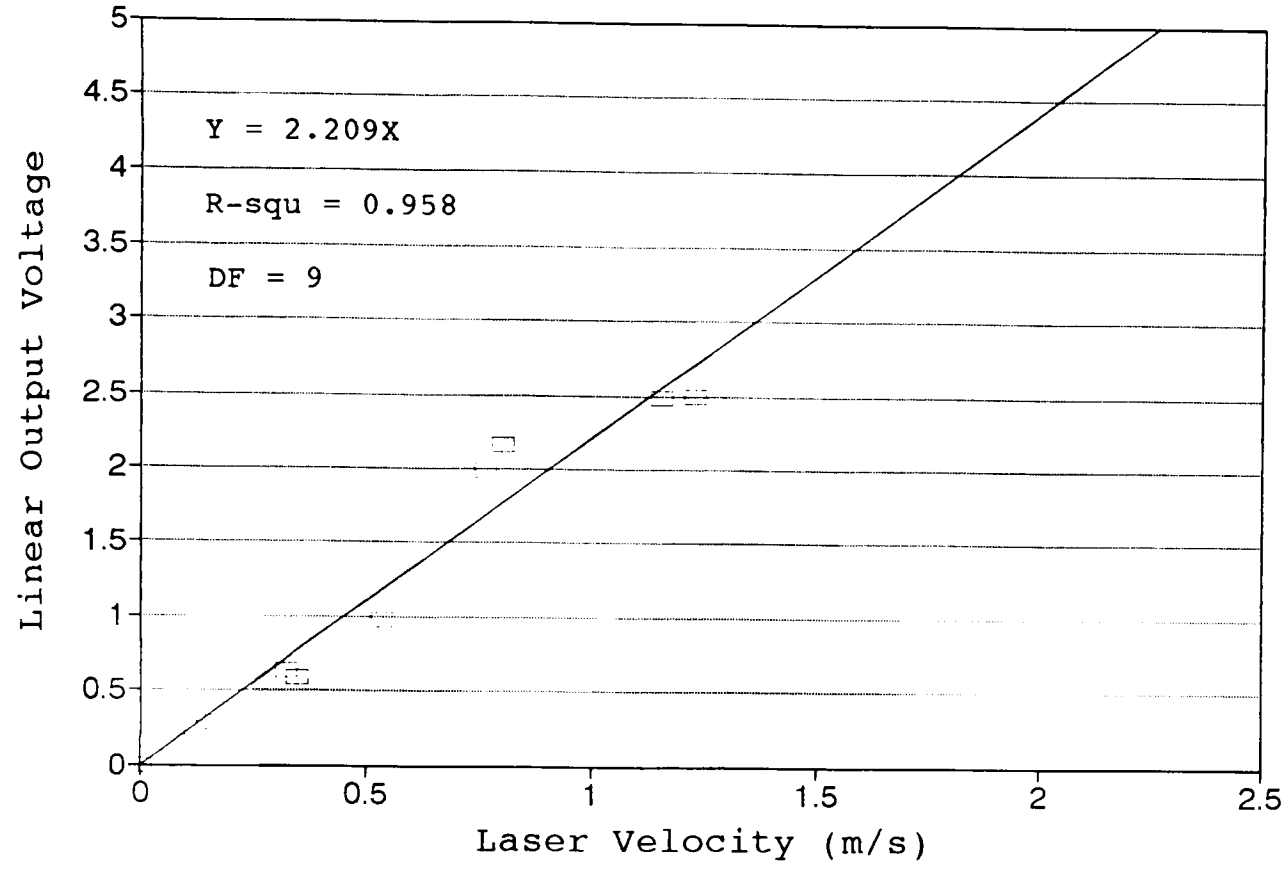

Figure (5.7): Calibration Run 3

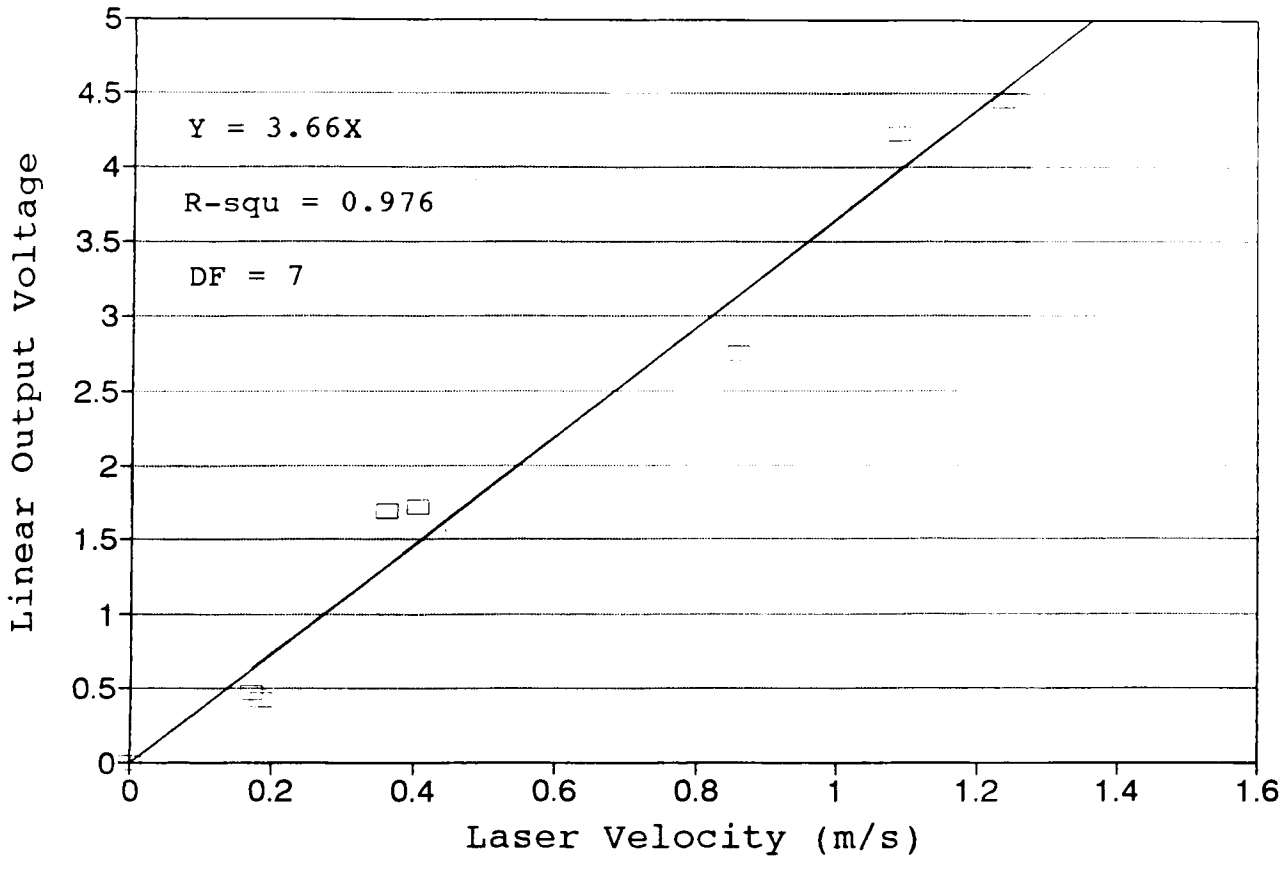

Figure (5.8): Velocity Probe 2,
Calibration Data.

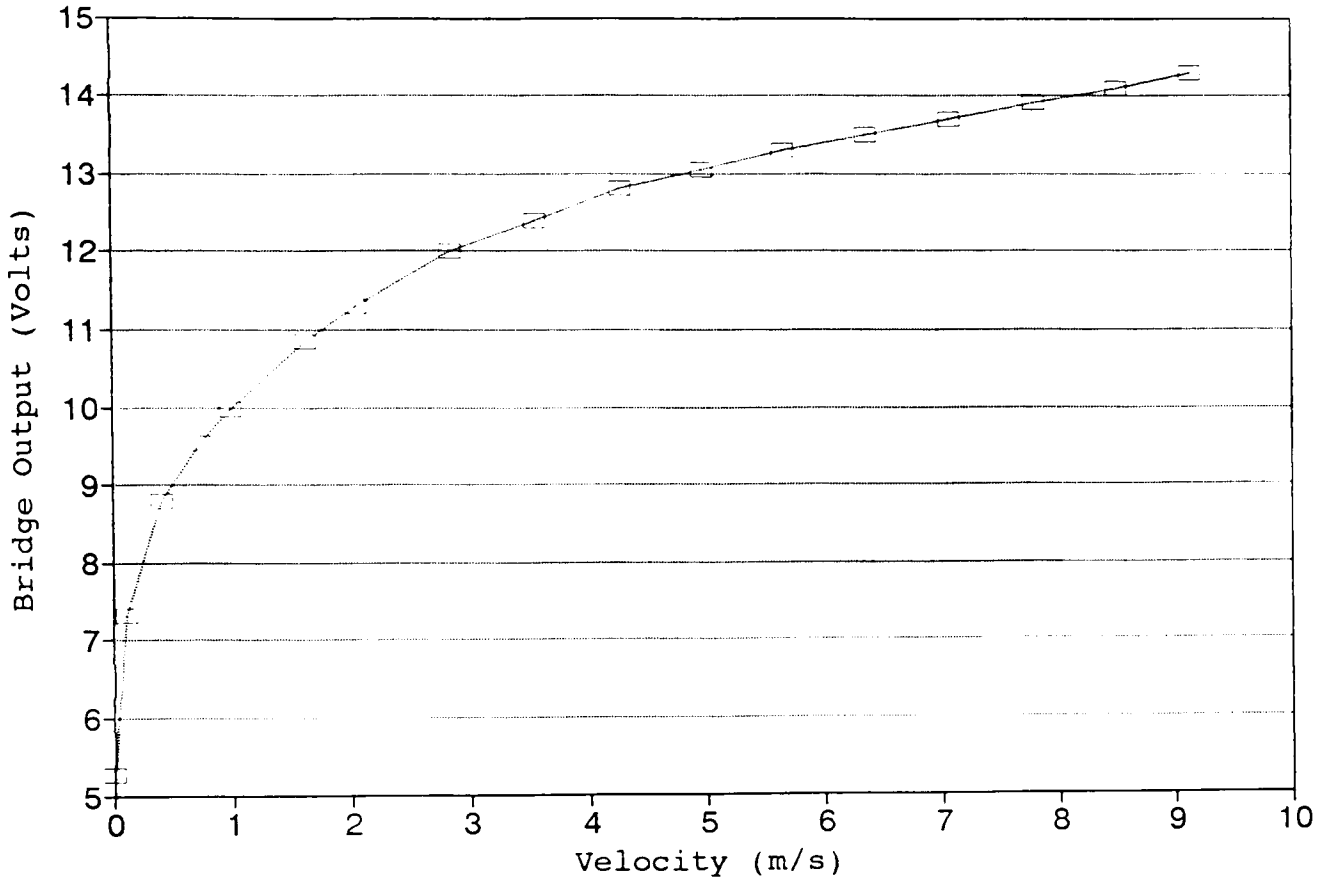

Bridge Ouput (Volts)	Flow Velocity (feet/s)	Flow Velocity (m ^ s)
5.267	0.000	0.000
7.330	0.400	0.122
8.800	1.371	0.418
9.550	2.421	0.738
9.980	3.242	0.988
10.850	5.312	1.619
11.300	6.703	2.043
12.000	9.334	2.845
12.400	11.680	3.560
12.800	14.070	4.289
13.050	16.340	4.980
13.300	18.600	5.669
13.500	20.890	6.367
13.700	23.210	7.074
13.900	25.610	7.806
14.100	27.900	8.504
14.300	30.000	9.144

Table (5.2): Calibration Date for Probe 2.

$$(Velocity\ (m/s)) = 1.41\ x\ (Lin.\ Volts) \tag{5.3}$$

Motor Control Calibration.

With the velocity sensor calibrated, it was therefore possible to calibrate the motor output frequency, as displayed on the motor control box, to the flow velocity. This then allowed the velocity in the flume to be varied by known amounts easily, whilst the actual flow velocity and its fluctuations were recorded by the data logger. This calibration was done by stepping up the motor output by increments of 5Hz from zero to 50Hz whilst logging the velocity sensor output at each point. During the course of the erosion runs in the flume the gearing on the motor was changed after Run 23, to give the possibility of higher flow velocities. Therefore two of these motor control calibrations where carried out. Table 5.3 and Figure 5.9 show the results for the motor to impeller gearing used on runs 1 to 23 (data was also collected at intermediate values as the motor was stepped down), which gave a derived equation between motor frequency in hertz and flow velocity in meters per second of,

$$(Motor\ Output\ Freq.(Hz)) = (Velocity\ (m/s))\ x\ 65.203 \tag{5.4}$$

$(R^2=0.995)$

The data for the motor to impeller gearing used in runs 23 to 40 is given in Table 5.4 and Figure 5.10 and the derived equation is,

$$(Motor\ Output\ Freq.(Hz)) = (Velocity\ (m/s))\ x\ 23.055 \tag{5.5}$$

$(R^2=0.971)$

5.2.1.2. Shear Stress Probe Calibration.

A number of methods for the calibration of flush mounted hot film sensors have been used. Brown and Davey (1971) calibrated their flushed mounted hot film sensors by use a rotating plate mounted over the sensors and calculating the shear stress from the distance between the plate and the sensor, and the angular velocity of the rotating plate. Gust and Southard (1983) used smooth return pipe flow to calibrate their sensor. Paola et al.'s (1986) calibration was done in situ, in the flume under smooth

Figure (5.9): Calibration of Motor Ouput to Flow Velocity, Probe 1.

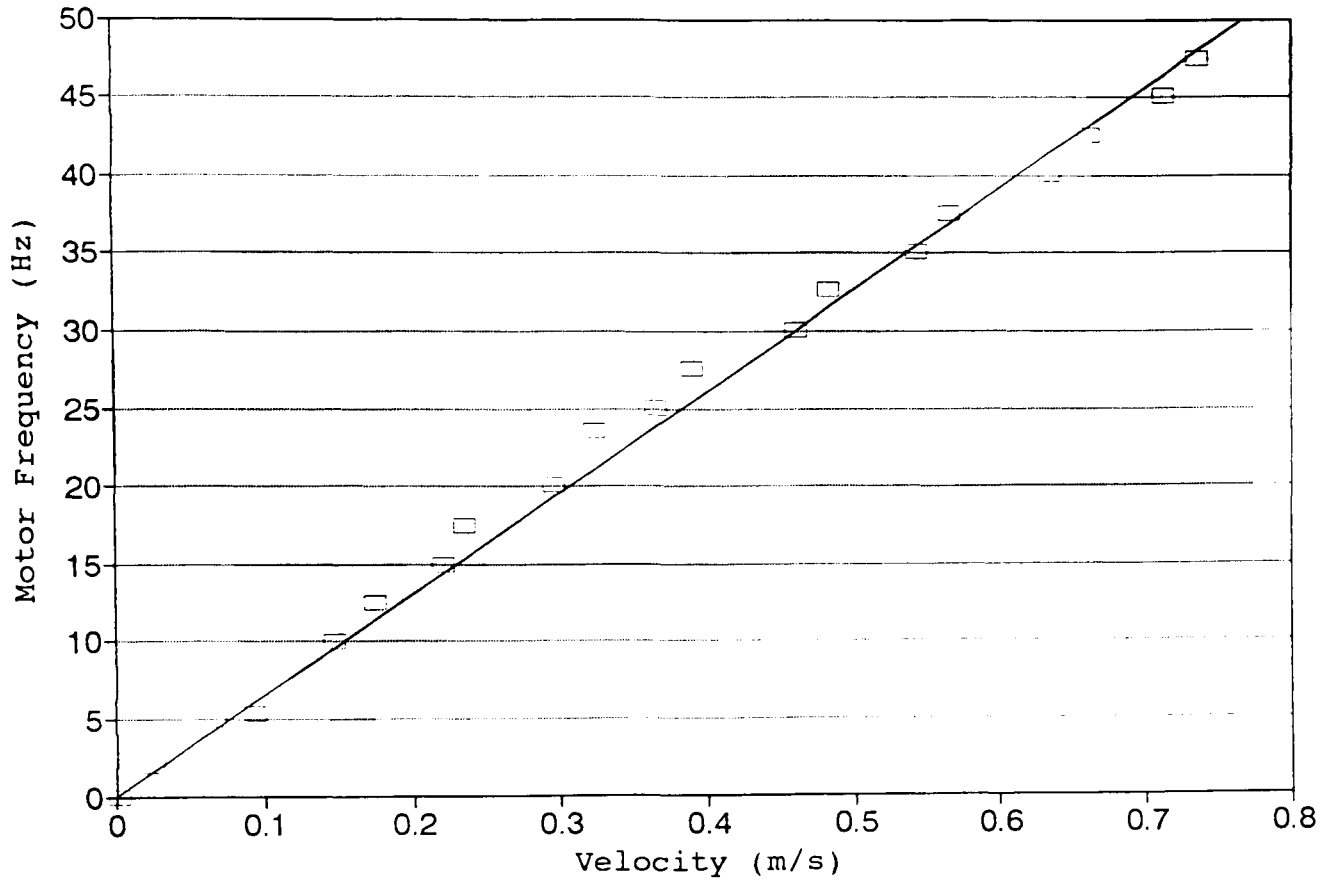

Motor Output Freq. (Hz)	Flow Velocity (m ^ s)	Motor Output Freq. (Hz)	Flow Velocity (m ^ s)
0.00	0.003	47.53	0.737
5.00	0.067	42.57	0.661
10.00	0.147	37.57	0.566
15.00	0.221	32.68	0.484
20.11	0.296	27.53	0.390
25.06	0.366	23.52	0.323
30.07	0.461	17.52	0.236
35.08	0.544	12.57	0.175
40.07	0.636	5.40	0.093
45.09	0.712	2.00	0.025
50.15	0.795	0.00	-0.002

Table (5.3): Motor calibration, Probe 1.

Figure (5.10): Calibration of Motor Ouput to Flow Velocity, Probe 2.

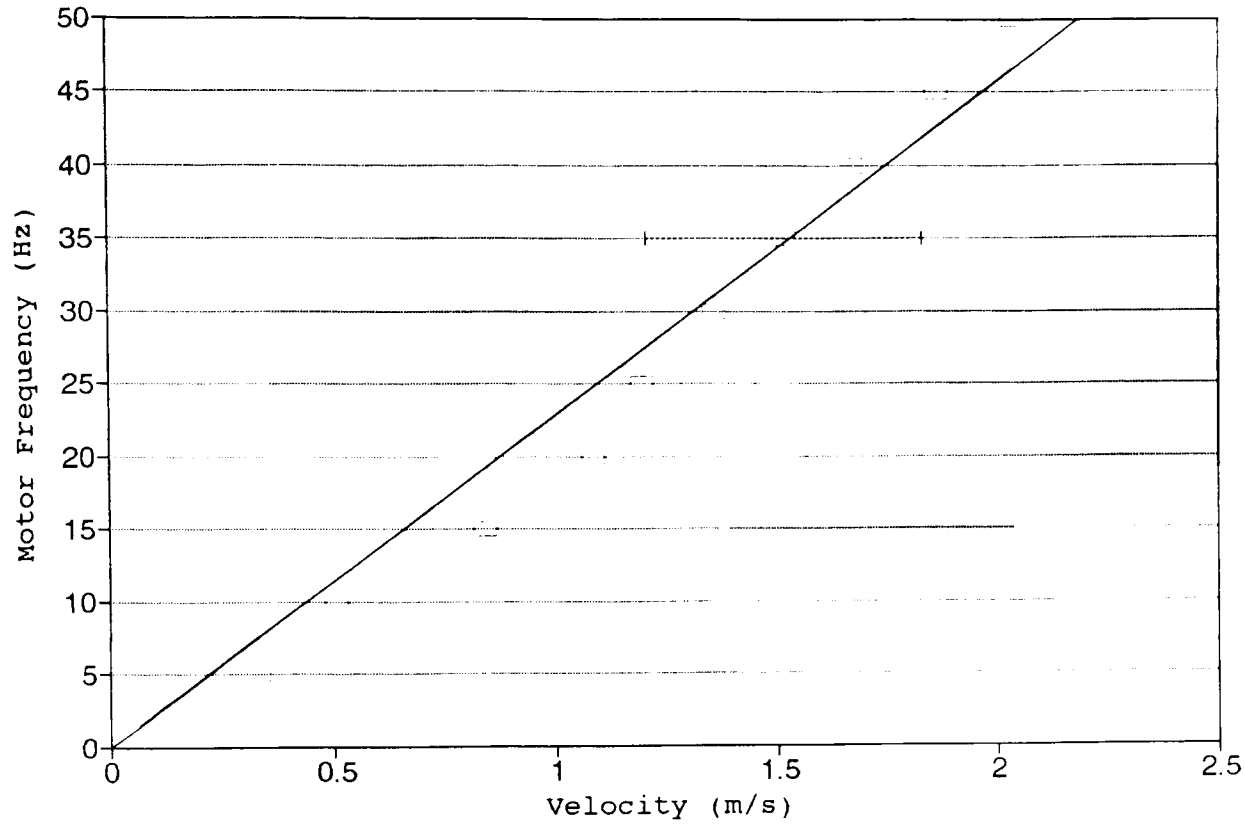

Motor Output Freq. (Hz)	Flow Velocity (m ^ s)
0	0.062
5	0.333
10	0.506
15	0.840
20	1.086
25	1.196
30	1.357
35	1.518
40	1.674
45	1.865
50	2.037

Table (5.4): Calibration of Motor

flow conditions, with the skin friction determined by measuring the water height surface slope over the middle 12.5m of the flume channel length.

Graham et al. (1992) used a calibration rig (Figure 5.11) in which water flows through a long, straight, horizontal channel under the influence of a pressure gradient generated by a header tank. The channel cross section is rectangular and of large aspect ratio, enabling edge effects to be neglected and the velocity field near the centre of the channel to be assumed to be the same as that between similarly spaced infinite plates. The probe is inserted along the axis of the bottom of the channel, at a distance 'x' from the header tank that is sufficiently far for the flow to be considered fully developed. The constant pressure gradient, dp/dx, is measured by means of manometer tubes and the wall shear stress at the probe location, τ_w, is calculated from,

$$\tau_w = \frac{h}{2}\frac{dp}{dx} \qquad (5.6)$$

where h=3.175mm (1/8in) and is the depth of the channel.

This method was used in this investigation, and utilised a 2m long and 0.11m wide channel (Plate 5.2). The four manometer tubes were connected at 0.5m intervals, with the first one 0.75m from the start of the channel. Different stresses were generated using a series of different water heights in the header tank, starting at zero flow and then stepping up to maximum flow and then back down to zero at the intermediate flow points. For each water height the flow was first allowed to stabilize and then the sensor output was logged at a rate of 10Hz for at least 120 seconds. Whilst the sensor output was logged the water height in the four manometer tubes was also recorded. To obtain the pressure gradient for each run to fit into equation 5.6, a regression line was fitted to the four manometer tube heights and the product (of the regression line's gradient and the unit weight of water) gave the pressure gradient. The results are shown in Table 5.5 and in Figure 5.12.

The behaviour of the probe can be predicted by theory (Ludwieg, 1949) according to the equation

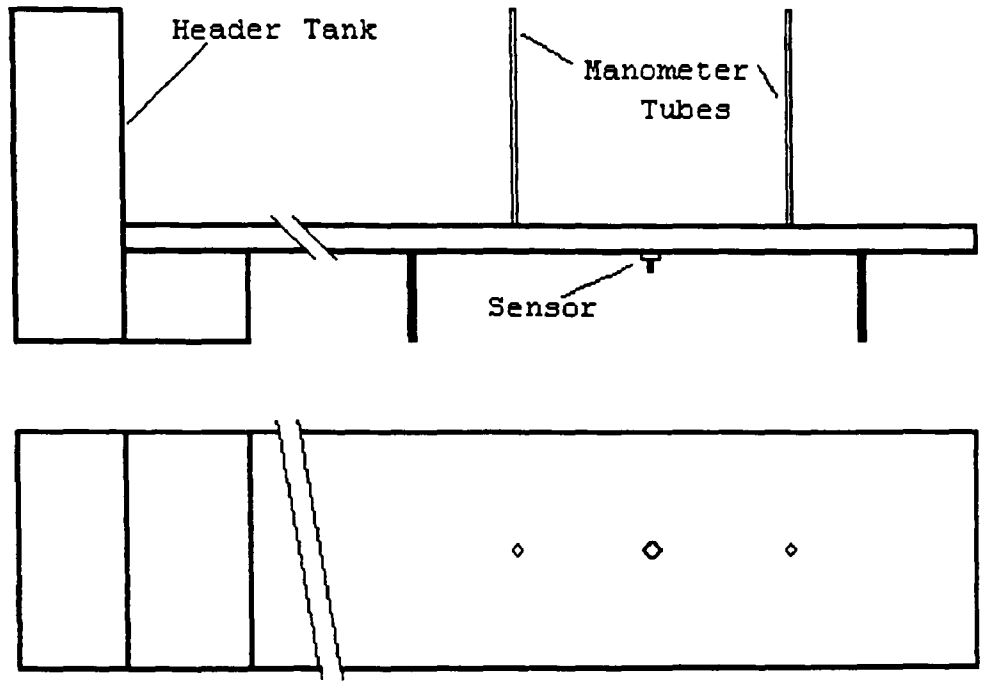

Figure (5.11): Flume used for calibration of Hot Film Shear Stress Sensors.

Plate (5.2): Shear stress sensor calibration rig.


FIRST AID

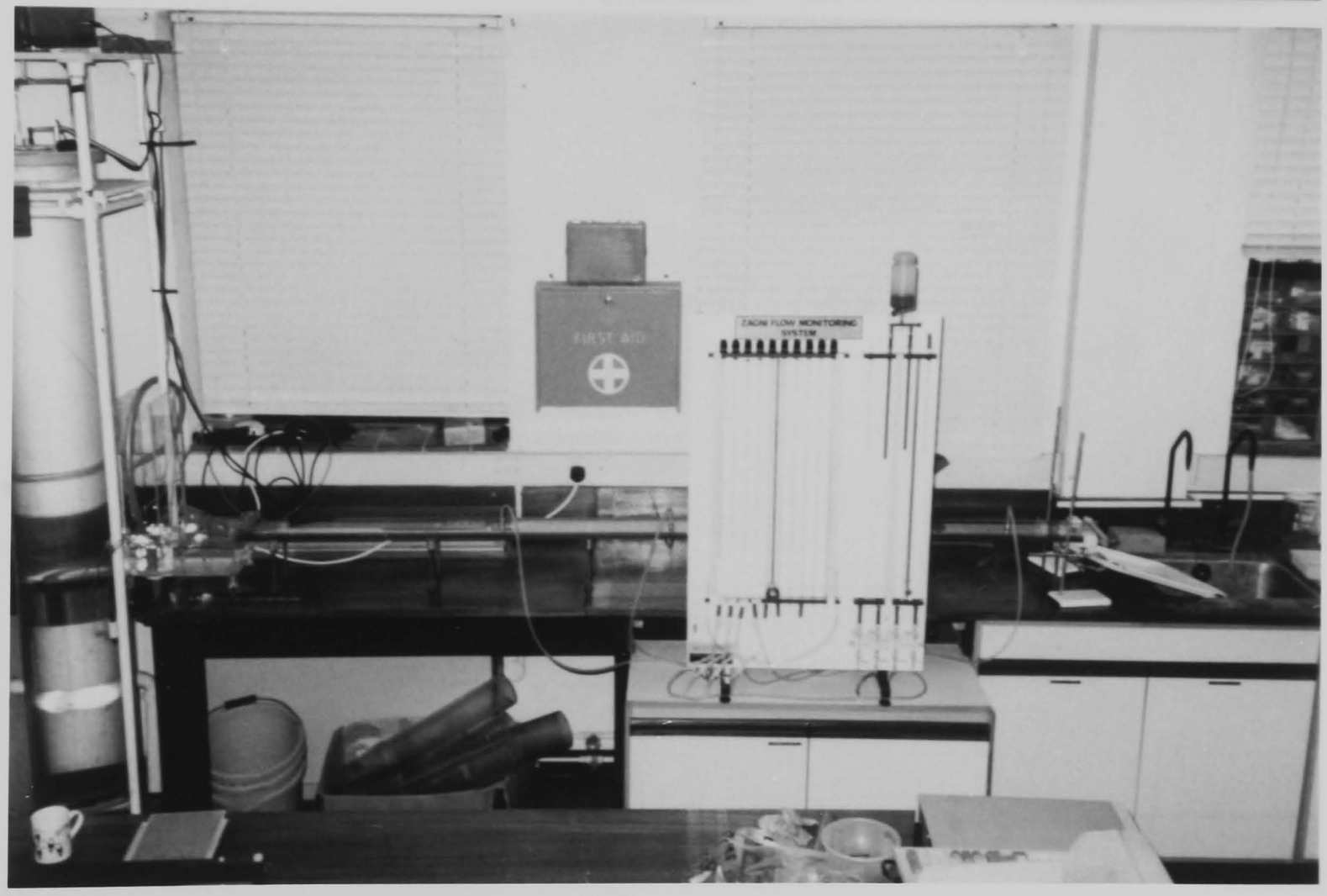
FIRST AID
ZAGNI FLOW MONITORING SYSTEM

Figure (5.12): Shear Stress Probe Calibration Results.

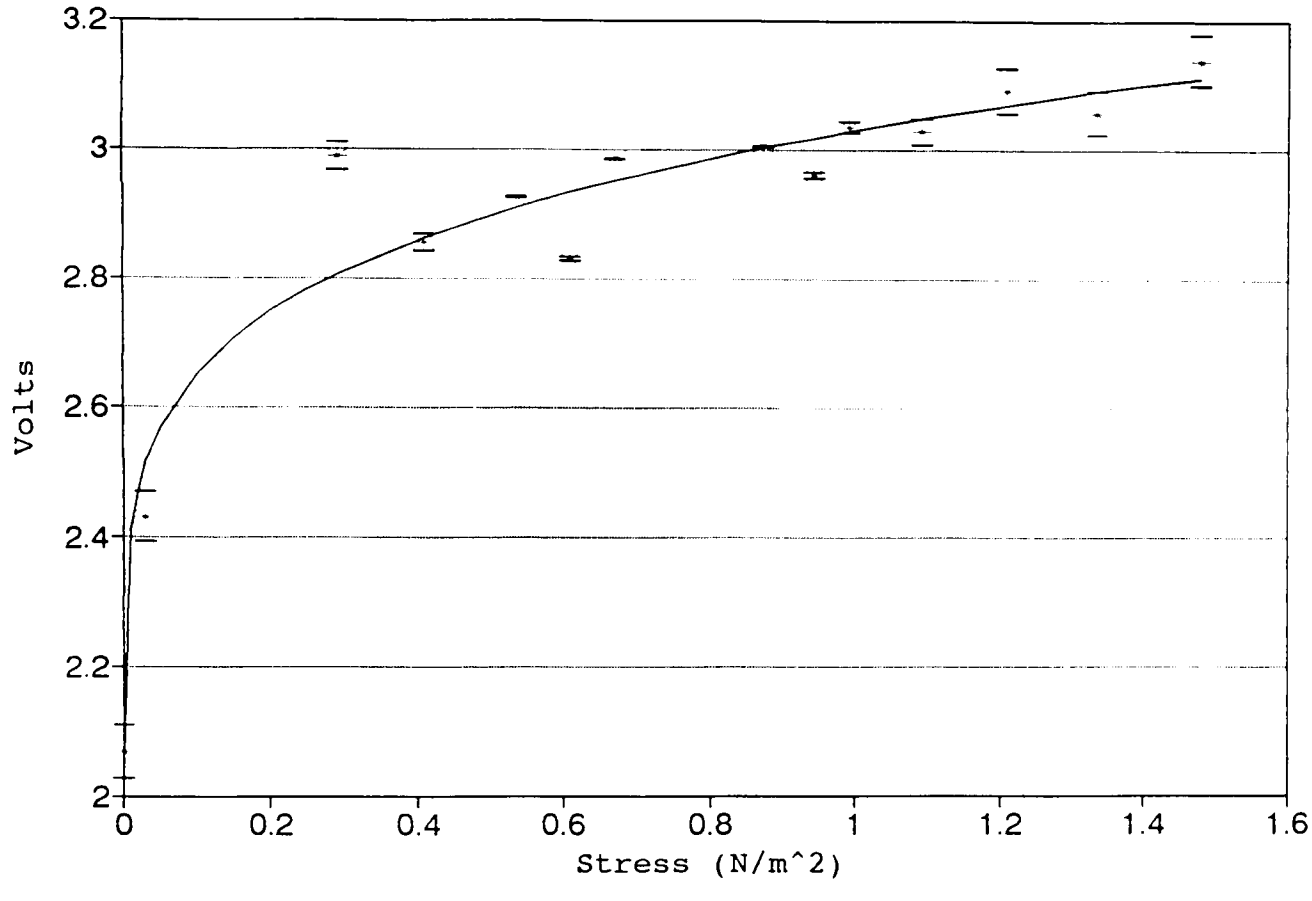

Sensor Output (Volts)	Temp. (C)	Temperat Corrected Sensor O (Volts)	Pressure Gradient	Bed Shea Stress (N/m ^ 2)
2.050	13.0	2.069	0.0000	0.000
2.427	12.2	2.431	-0.0020	0.031
2.947	11.8	2.941	-0.0166	0.258
2.869	11.5	2.856	-0.0264	0.411
2.939	11.5	2.926	-0.0345	0.537
2.999	11.5	2.986	-0.0431	0.671
3.022	11.4	3.006	-0.0562	0.875
3.055	11.3	3.035	-0.0639	0.995
3.121	11.0	3.092	-0.0778	1.211
3.174	10.8	3.139	-0.0950	1.479
3.092	10.8	3.058	-0.0858	1.336
3.062	10.8	3.029	-0.0702	1.093
2.994	10.8	2.962	-0.0606	0.943
3.112	10.8	3.078	-0.0508	0.791
2.861	10.8	2.831	-0.0392	0.610
2.970	10.6	2.933	-0.0305	0.475
3.027	10.6	2.989	-0.0188	0.293

Table (5.5): Bed Shear Stress Probe Calibration data.

$$Nu = B'(\tau_w)^{1/3} \tag{5.7}$$

where Nu is the Nusselt number, a dimensionless heat transfer number, τ_w a dimensionless wall shear stress and B' a constant. However this relationship is derived by considering only forced convection from the hot-film. If heat conduction into the probe mount is taken into account then equation 5.7 can be rewritten as (Tillmann and Schliper, 1979),

$$E^2 = A + B(\tau_w)^{1/n} \tag{5.8}$$

where E is the sensor voltage output and A, B and n are constants determined by calibration. Equation 5.7 was used by Graham et al. (1992) and the relationship $E^2 \propto \tau^{1/4}$ was given to relate sensor output to shear stress. Tillmann et al. (1981) used equation 5.8 and found that n=4 gave the best fit to their data. The relationship

$$E^2 \propto \tau^{1/4} \tag{5.9}$$

was found to provide the best fit to the calibration data for the sensor used in this investigation and produces a shear stress to voltage relationship (at a calibration temperature of 12°C) of

$$\tau^{1/4} = 0.190(E^2) - 0.757 \tag{5.10}$$

(R^2=0.937)

This is shown in Figure 5.13.

The relationship between flow velocity and bed shear stress as measured in the flume is shown in Figure 5.14. This is also a power relationship and defined as,

$$\tau^{1/2} = Velocity\, x\, 0.815 \tag{5.11}$$

(R^2=0.958)

To asses the accuracy and legitimacy of the stress measurements made in the flume using the hot film sensor, a simple experiment was devised to examine the threshold of motion of a non-cohesive sediment and to compare it to measurements made by other studies. This involved

Figure (5.13): The Relationship Between Shear Stress and Probe Output Voltage.

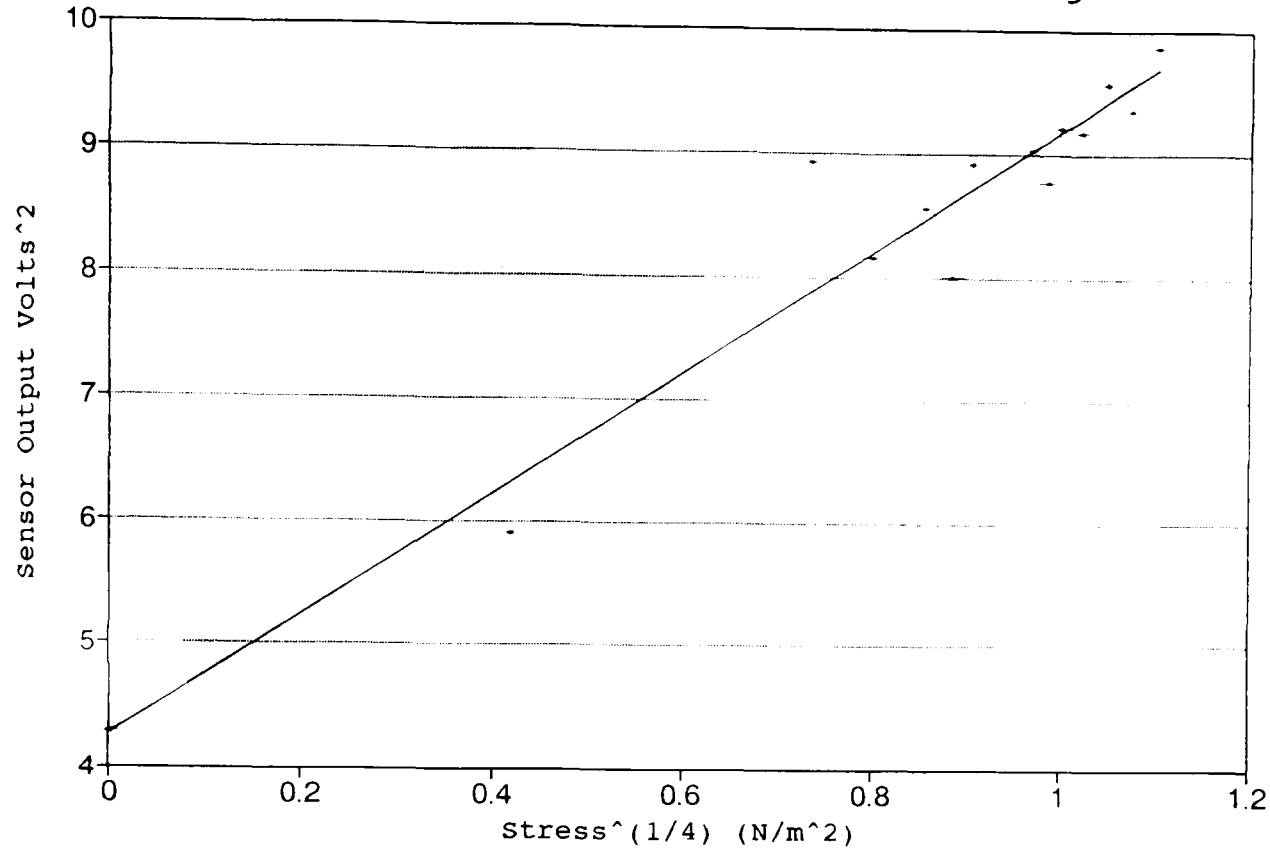

Fig (5.14): Flow Velocity and Bed Shear Stress Relationship in the Flume.

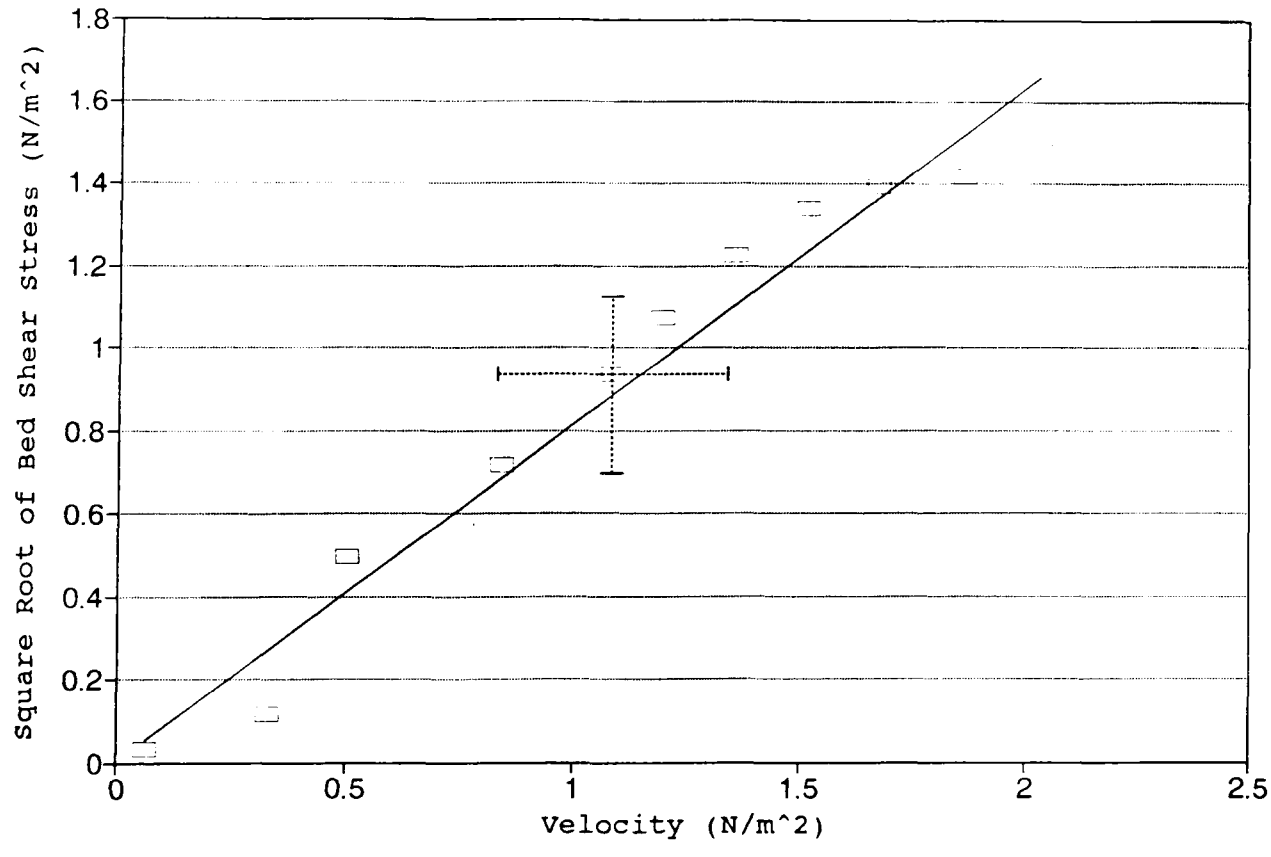

recording stress readings at the threshold of motion for a number of sieved sand samples. The sands had size ranges of; 90-125, 125-180, 180-250, 355-425, 425-510, 510-600, 600-710 microns. The results are shown in Figure 5.15 and compared to two previous studies. The main inaccuracy in this very simple study are; the low sample size, that each sample covers a range of sizes, and that the actual threshold of motion was judged by eye. Given these possible errors the results appear to show a good correlation to the two previous studies, which supports the accuracy and legitimacy of the stress measurements made by the hot film sensor in the flume.

5.2.2. **Measurement of Suspended Sediment Concentration.**

Three optical back scatter (OBS) sensors (Figure 5.16) have been built into the flume to measure the concentration of particulate material in suspension in the flume, by measuring the amount of back scattered infra-red radiation. OBS 2 is on one side of the test section with OBS 1 and 3 on the other, with all three looking diagonally across the flow. OBS 2 is 0.075m above the flume floor at the start of the test section looking downstream. OBS 1 is also 0.075m above the flume floor but it is positioned in the centre of the test section looking upstream. OBS 3 is fixed at the end of the test section, downstream of the sediment box, 0.02m above the flume floor and looking upstream. Figure 5.2 shows the location of sensors in the test section and Figure 5.17 the sensor mounting. The sensor consists of a high-intensity infra-red emitting diode, a detector comprising four silicon diodes, a linear solid state transducer and a gelatin filter to shield the detector from visible light.

The linear solid state transducer is used to correct the sensor for any temperature variations that may occur. This correction is performed by the electronic interface package supplied with the sensors (which was designed specially for this particular laboratory application). Each sensor connects directly to the interface which then supplies an output in the range 0 to +5 volts continuously to the data logger. Simultaneously the interface can display the voltage output from any individual sensor, continuously, averaged over two seconds to damp out large fluctuations, or frozen with the hold feature.

Fig (5.15): Shields-type Entrainment Experiment.Threshold of Motion.

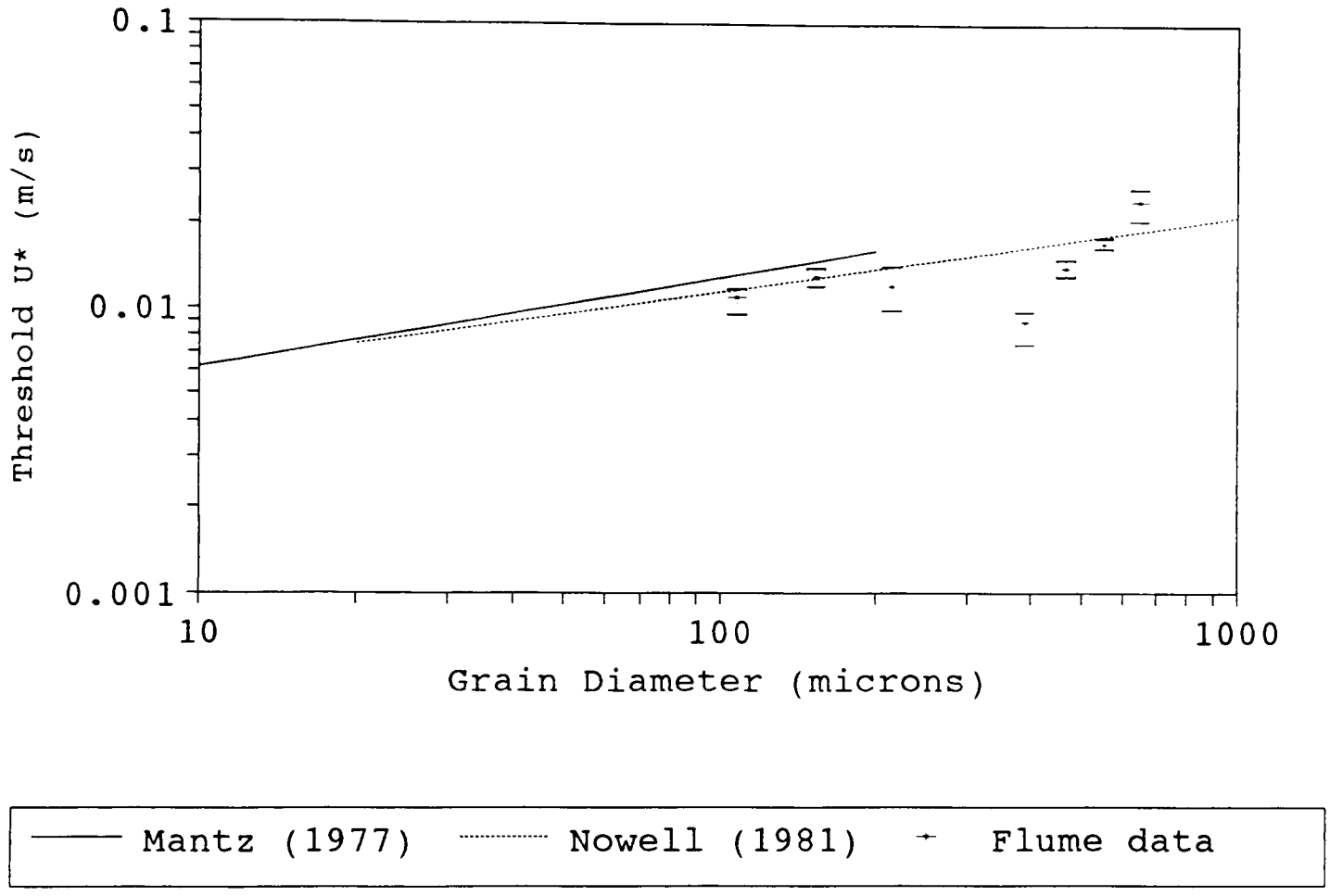

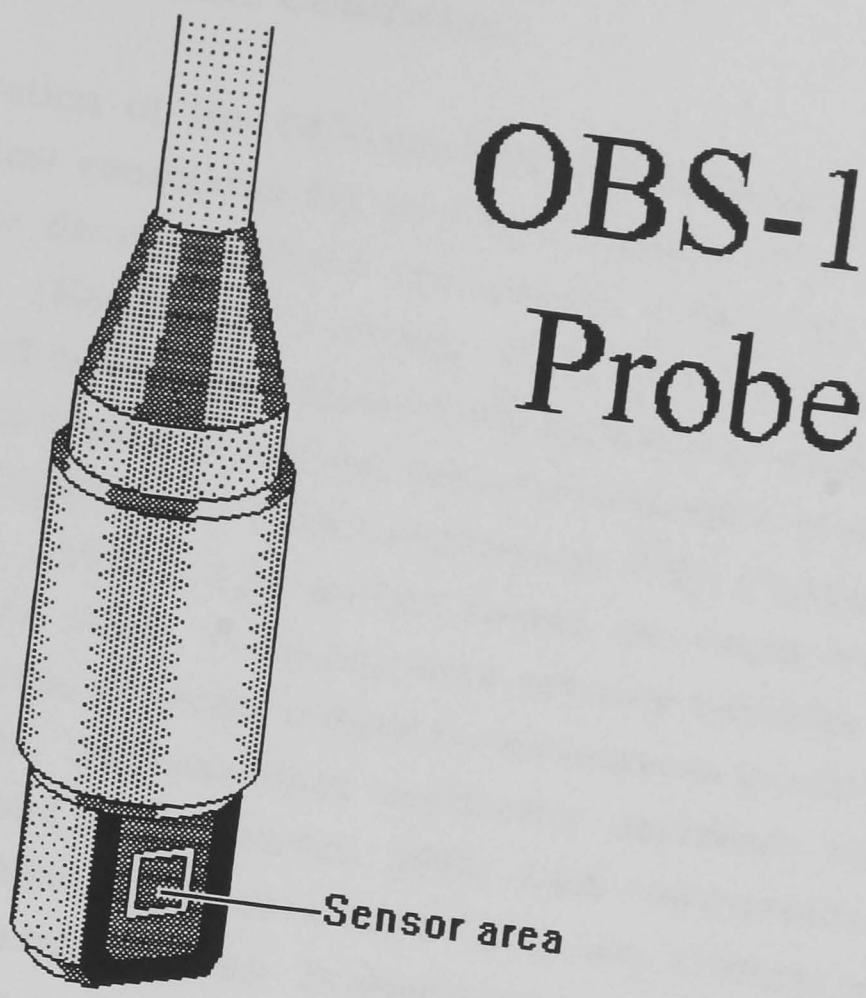

Fig 5.16: Schematic of an OBS sensor.

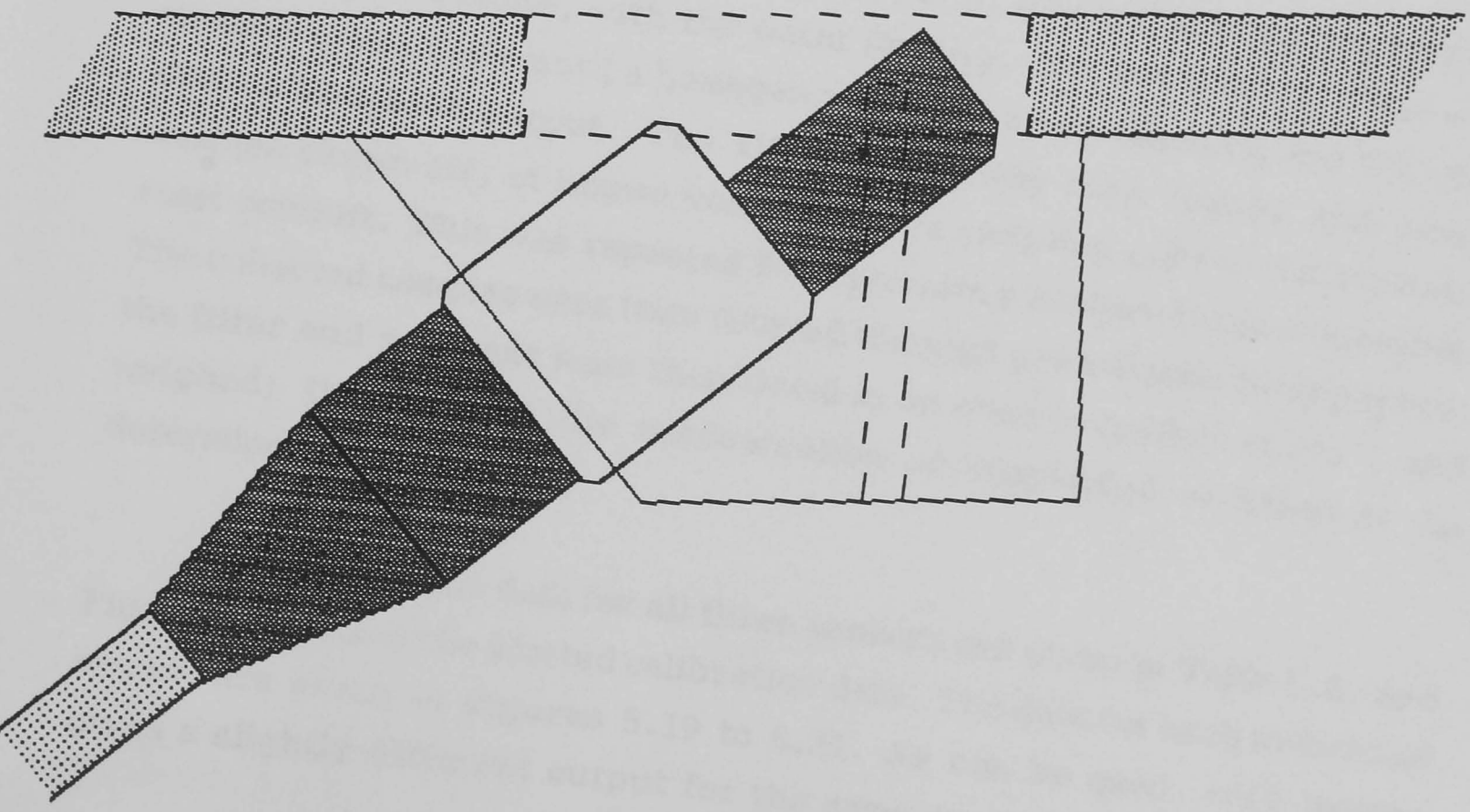

Fig 5.17: Schematic of the OBS sensor mounting.

5.2.2.1. OBS Sensor Calibration.

Calibration of the OBS sensors was necessary in situ or under equivalent flow conditions for two main reasons; (1) the orientation in terms of flow direction alters the sensor output for the same solids concentration (Hanes and Ludwig, 1990); and (2) size distribution, composition and refractive indices of the particles in suspension affect the response of the sensor to a given mass concentration of suspended solids (Downing and Beach, 1989; D&A Instruments, 1989; Conner and de Visser, 1992; Maa et al., 1992). This second reason can cause errors as flocs in suspension break down, releasing more primary particles into the flow, causing an increase in sensor output for no increase in the total amount of suspended solids, because back scattering decreases with increasing particle size(Gibbs and Wolanski, 1992; D&A Instruments, 1989). The volume of water that the sensors interrogate also changes with changing sediment concentration (D&A Instruments, 1989). Researchers have reported accurate response of OBS sensors to rapid temporal changes (Conner and de Visser, 1992) and a linear response in mud up to concentrations of approximately 3 or 4 g/l with sensitivity decreasing slightly after this (Hanes and Ludwig, 1989).

The OBS calibration was carried out in situ in the flume, by adding sediment to the flume, with the water flowing. The water in the flume was allowed to mix fully until a homogenous mixture was obtained and the OBS gave a constant output. The OBS output was then logged and water samples drawn off, of known volume, at the sampling port in the stainless steel conduit. This was repeated for increasing sediment concentrations. The collected samples were then filtered through pre weighed filter papers; the filter and sediment were then dried in an oven overnight at 105°C and weighed; this allowed the concentration of suspended sediment to be determined.

The calibration data for all three sensors are given in Table 5.6, and Figure 5.18 shows the plotted calibration data. The data for each individual sensor are given in Figures 5.19 to 5.21. As can be seen, each sensor gives a slightly different output for the same concentration, due to their

Figue (5.18): OBS Calibration Data.

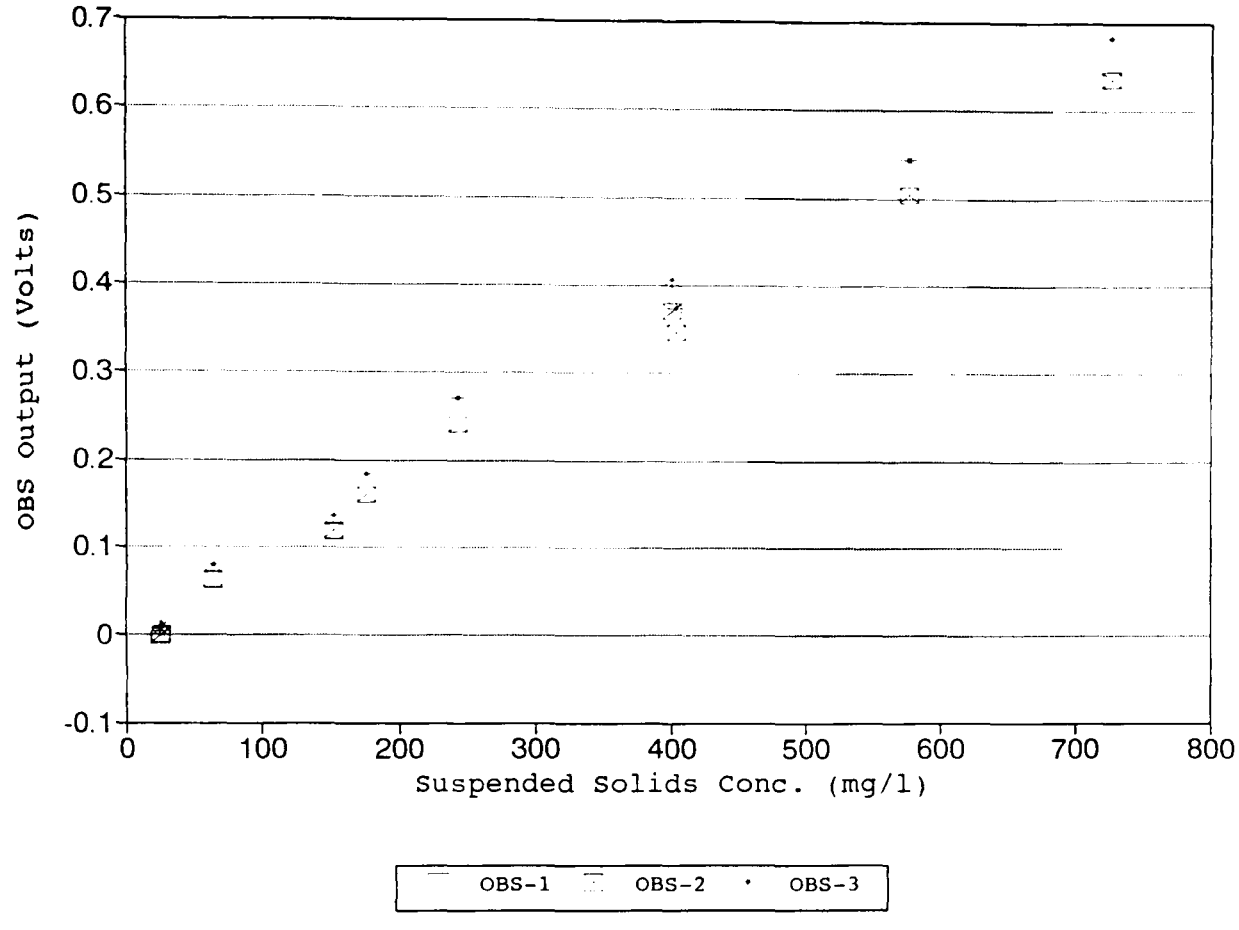

Sample	OBS1	OBS2	OBS3	Conc (mg/l)
T1	-0.00025	0.00112	0.01380	25.1
S1	-0.00455	-0.00202	0.00706	24.1
T2	0.06188	0.06298	0.08052	64.0
S2	0.11792	0.11937	0.13668	152.1
T3	0.15998	0.16036	0.18443	175.8
T4	0.24144	0.24159	0.27021	243.3
T5	0.37181	0.37177	0.40750	400.3
S3	0.34587	0.34607	0.37434	403.3
T6	0.50452	0.50354	0.54511	576.0
T7	0.63627	0.63542	0.68336	726.0

Table (5.6): OBS Calibration Data.

Figure (5.19): OBS-1 Calibration Data.

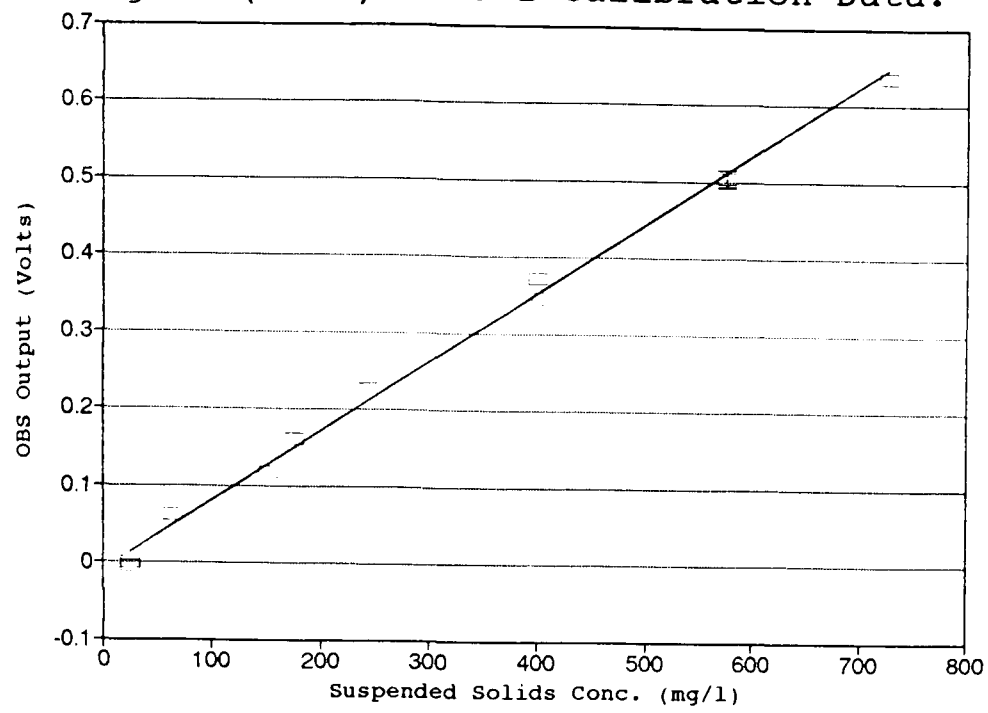

Figure (5.20): OBS-2 Calibration Data.

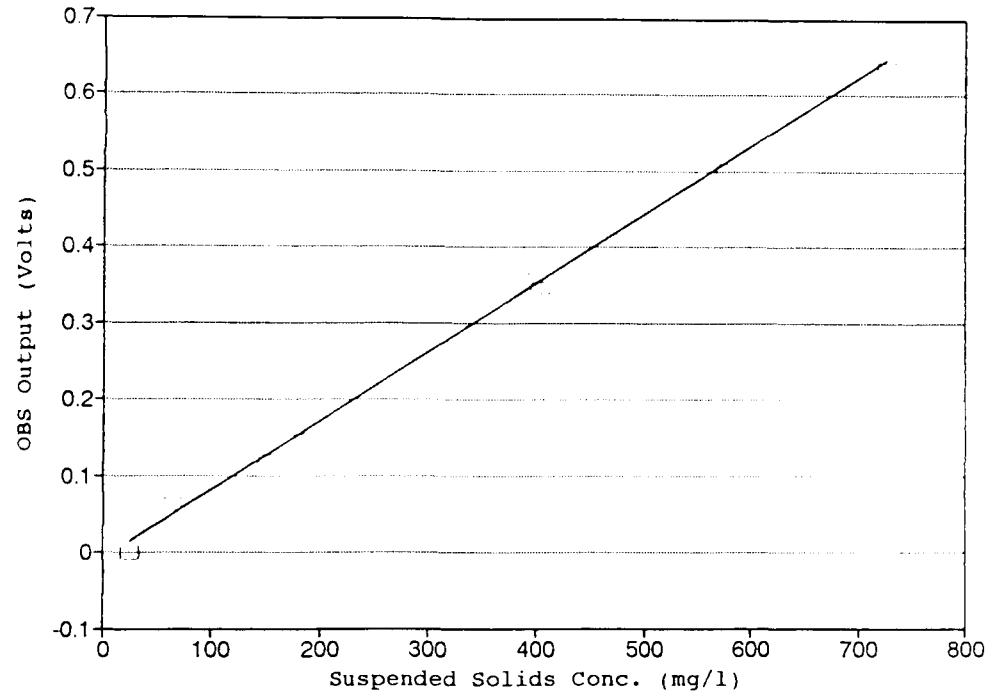

Figure (5.21): OBS-3 Calibration Data.

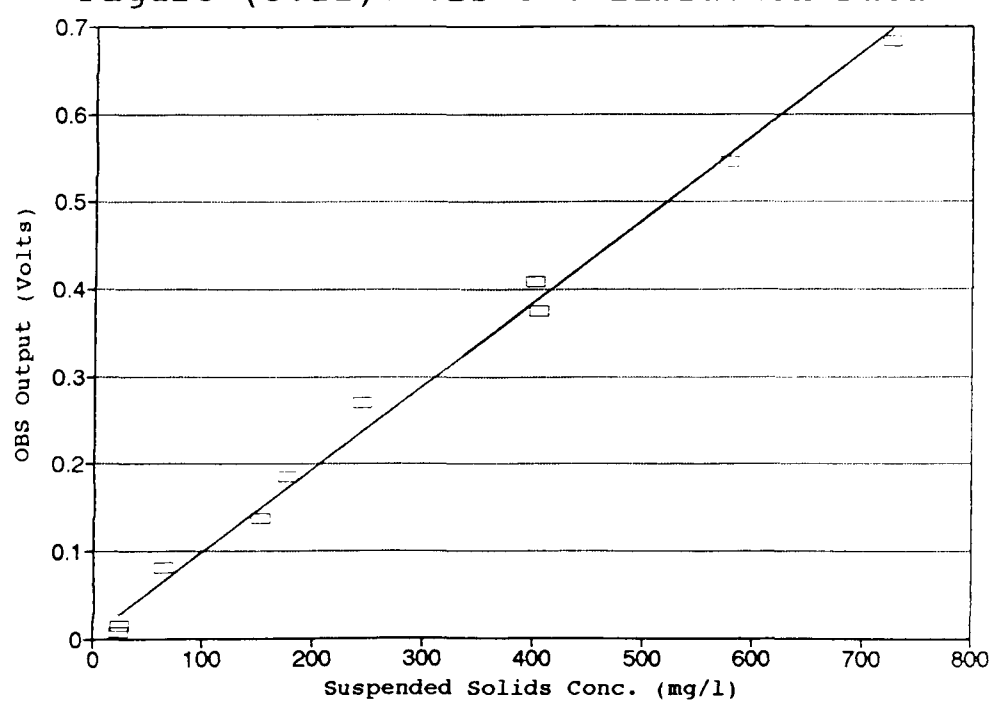

different positions in the flume test section (OBS-1 and -2 point in opposite directions and OBS-3 is close to the flume floor and has an output at zero suspended sediment concentration higher then the other two due to back-scattering from the flume floor. However they do all display a linear relationship between output voltage and concentration. For each sensor a calibration equation was obtained:

Sensor	Equation		
OBS-1	$C = 1103.682 \times V + 10.28601$	(R^2=0.994)	(5.12)
OBS-2	$C = 1108.862 \times V + 8.436744$	(R^2=0.994)	(5.13)
OBS-3	$C = 1047.835 \times V - 4.209589$	(R^2=0.993)	(5.14)

Where C is the suspended solids concentration in mg/l and V is the OBS output in volts.

5.2.2.2. **Acoustic Back-scatter Probe (Bed Level Monitor).**

The acoustic back-scatter probe (ABS), developed by Dr P. Thorne at P.O.L. (Proudman Oceanographic Laboratory) and normally used to measure suspended sediment concentrations, was modified slightly to allow it to be used as a bed level monitor. The probe was fixed in an upright position in a purpose-built mount on top of the flume lid pointing vertically downwards (Figure 5.22). The probe was controlled by an electronics package that triggered the probe to send out a 40µsec compressional wave signal every 4.4msec and then send any returning signals that the probe detected in between each transmission to the digital storage adaptor. The probe could be moved up and down the flume lid, allowing the position of the flume floor to be noted and then the sediment bed surface moved to correspond to this level.

During experimental runs, the probe was placed above the sediment bed three centimetres below its upstream end. As the bed eroded, its height was adjusted to keep it level with the floor of the flume. In this way any leading edge effects due to differences in level between the flume floor and the sediment bed were eliminated, up to the initial onset of erosion. However, once erosion started, the bed surface was no longer flat and

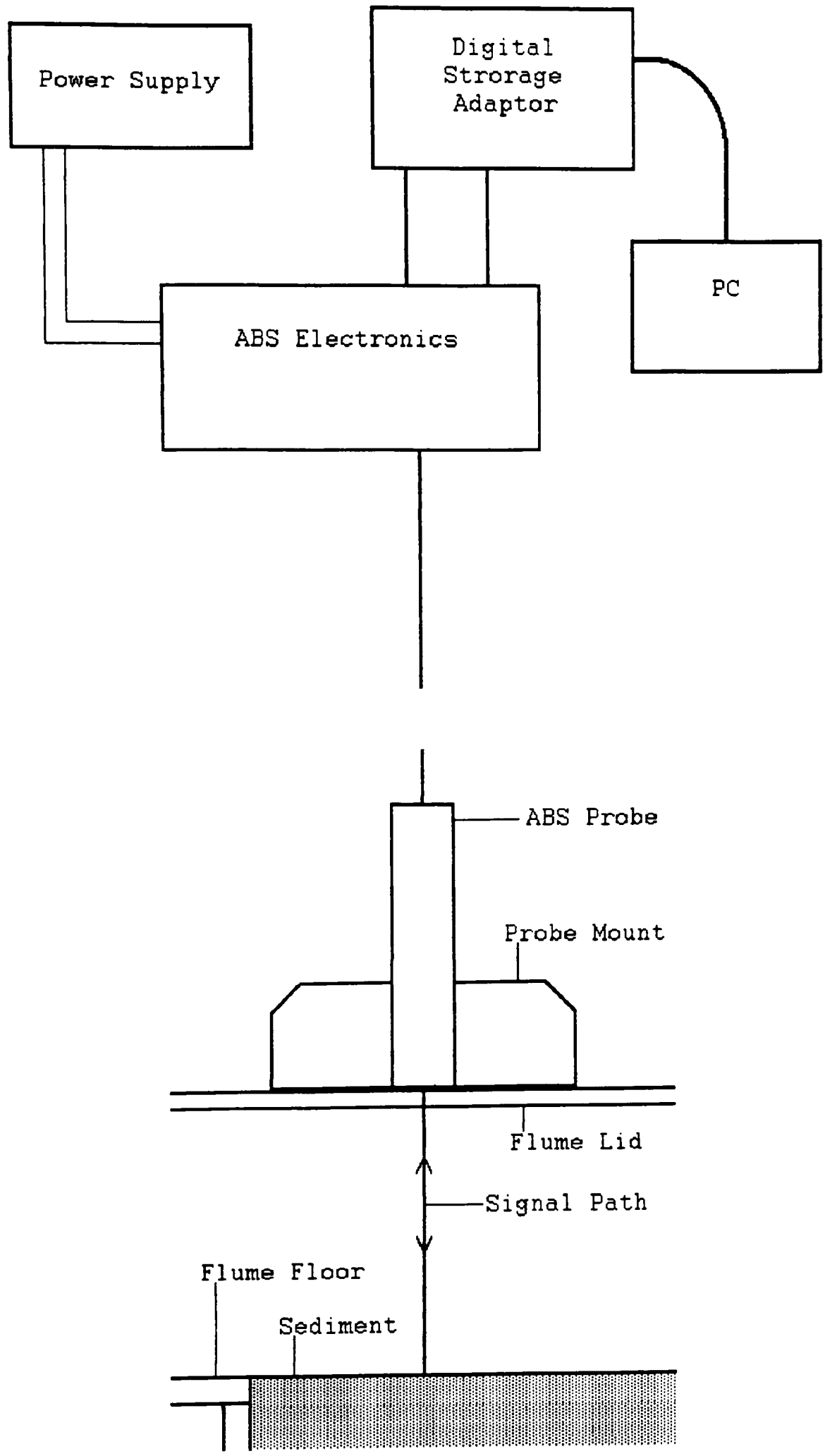

Fig (5.22): ABS Bed Level Monitor.

therefore a signal point on the bed was chosen and monitored in order to keep runs repeatable.

5.2.3. **Data Logging.**

As mentioned above, the output of the velocity, shear stress, OBS and pore pressure sensors was recorded on a PC. This was accomplished by utilising a Metrabyte DASH-8 data acquisition card, which was software driven, located inside the computer and capable of digitalizing continuously the analogue voltage output of the eight channels. The sensors were connected to the Dash-8 card via an interface box which converted the individual coaxial leads into one multi-cored lead to the Dash-8 card. Figure 5.23 shows the relationship between the voltage inputs into the Dash-8 card and the digitalized value that was stored on disk. As is clearly seen this is done accurately over the voltage range.

The software that controlled the logging program utilised sub-routines supplied by the Dash-8 manufacturer (see appendix II for a copy of the program). The data sampling rate of the Dash-8 is controlled by the program and can be easily changed, although in this case a sampling frequency of 1Hz was used for the flume erosion runs. This data is displayed as a time-series on the screen showing the previous two minutes data, and stored to disk in individual files each representing a one minute block of data. Each file was consecutively numbered allowing easy identification of the files for processing.

For processing of the data the files were loaded into a Quattro Pro spreadsheet that had been previously set up to convert the digitalization units back to voltages. Routines obtained from the calibration data then converted the voltage readings into their equivalent physical values. With the data in this state a despiking routine was applied. This was done by averaging each twenty seconds of data and then replacing any values that deviated from the mean by more then two standard deviations, by the previous value within two standard deviations of the mean. The means of this despiked data can then be displayed graphically. An erosion rate was also calculated using the already calculated flume volume ($0.186m^3$) and the

Fig (5.23): Calibration Check of the Dash-8 Card.

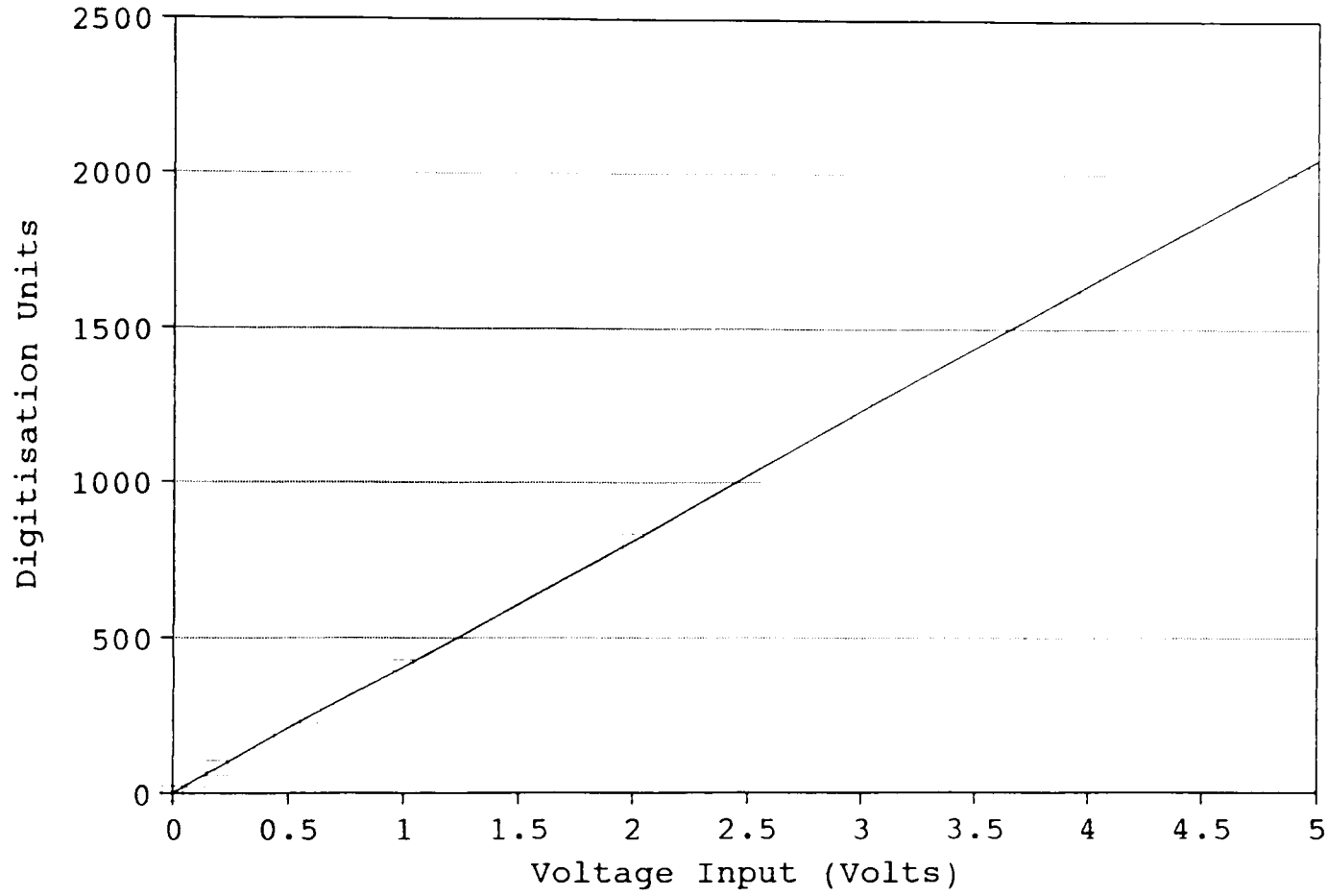

sediment surface area, as defined by the sediment box dimensions, ($0.0417m^2$).

5.2.4. Bed Properties and the Flume Sediment Box.

A number of bed properties were also measured:

- Grain size
- Specific density
- Moisture content
- Porosity
- Density wet/dry
- Organic carbon Content
- Acoustic shear wave velocity
- Electrical resistivity
- Pore and total pressure

All of these were measured on sediment samples before being placed in the flume, except for the last three which were measured in situ in the flume, prior to the starting of a flume run.

Plate 5.3 shows the flume sediment box. The pressure, acoustic shear wave and electrical resistivity sensors are all mounted in the same horizontal plane, which due to the stainless steel framework that supports the clear perspex test section of the flume is 65mm below the flume floor. This means that surface measurements cannot be made during a flume run (modifications have subsequently been made to correct for this limitation, but these were done after the experiments reported in this thesis). Therefore logging of these three parameters was made directly before the start of each flume run, in a way that produced a vertical profile. The bed box was filled with sediment until the acoustic shear probes were just covered. Once the bed box was fitted into the flume a reading of each measurement was first taken at the surface and then at one centimetre intervals as the bed was raised up past the sensors.

Plate (5.3): The sediment box, showing the arrangement of sensors.

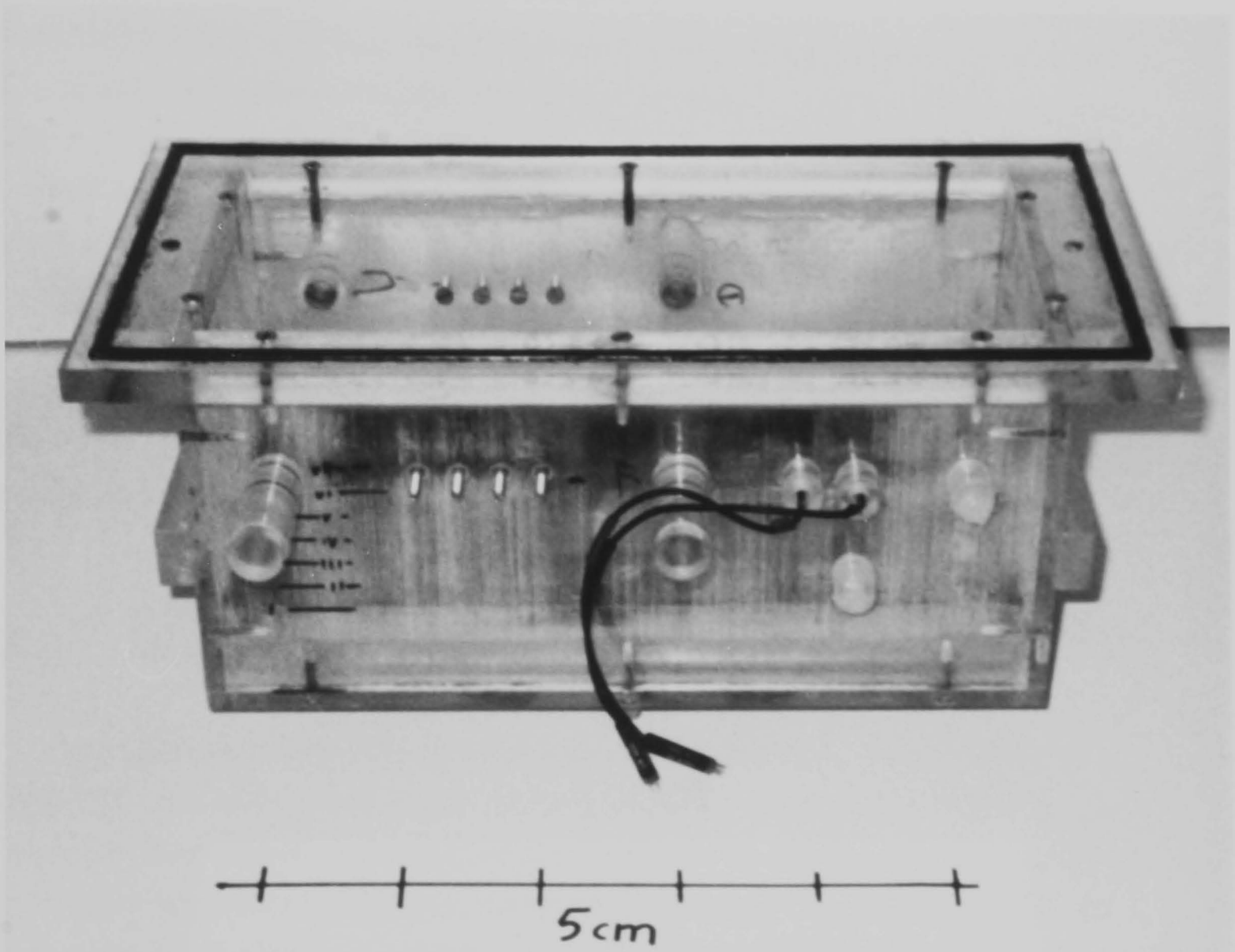
5cm

5.2.4.1. **Acoustic Shear Wave Measurement.**

The flume shear wave probes were installed in the sediment box to give three possible travel paths. These were A-B across the middle of the box (path length of 0.085m), C-D across the up-flow end of the box and E-F down the length of the box (path length of 0.246m). Initial test to see how the equipment worked were carried out on the bench. A small frame wave was generated by these probes (Figure 5.24). However with the box filled with water (Figure 5.25) the frame wave was altered, and modified even further when the box was filled with water saturated sand (Figure 5.26). It appeared that with the box full of sediment, and with appropriate filtering, the frame wave could be ignored and the signal produced in the saturated sand could be identified as a shear wave with a velocity of about 60m/sec. With cohesive sediment in the flume, a filter with a low-cut of 1Hz and a high cut of 50Hz was used. Figure 5.27 is an example of the type of signal received in the sediment box with cohesive material in it. It shows that the use of the filter and the slow velocity of the shear wave (3-4m/sec) allowed the signal onset to be resolved without any interference from a possible frame wave.

5.2.4.2. **Electrical Resistivity Measurement.**

The sediment box has two four electrode Wenner arrays built into it, with the two arrays arranged exactly opposite each other. This gives the facility for three separate measurements to be made, with each measurement covering a different volume of sediment. These measurements were achieved by using; (1) the array on the left (looking in the flow direction) of the sediment box on its own; (2) the array on the right of the sediment box on its own; and (3) by combining the two arrays so that the measurement was made across the whole width of the sediment box. However in this investigation only the single Wenner array on the right of the sediment box was utilised. This was due to equipment restraints and the wish to reduce the complexity of the electrical resistivity method.

The resistivity array in the flume was calibrated in the same manner as in the oedometer cell, e.g. measurement of water resistivity was used

Figure (5.24): Bender Mark 3 Frame Wave, Sediment Box Empty.

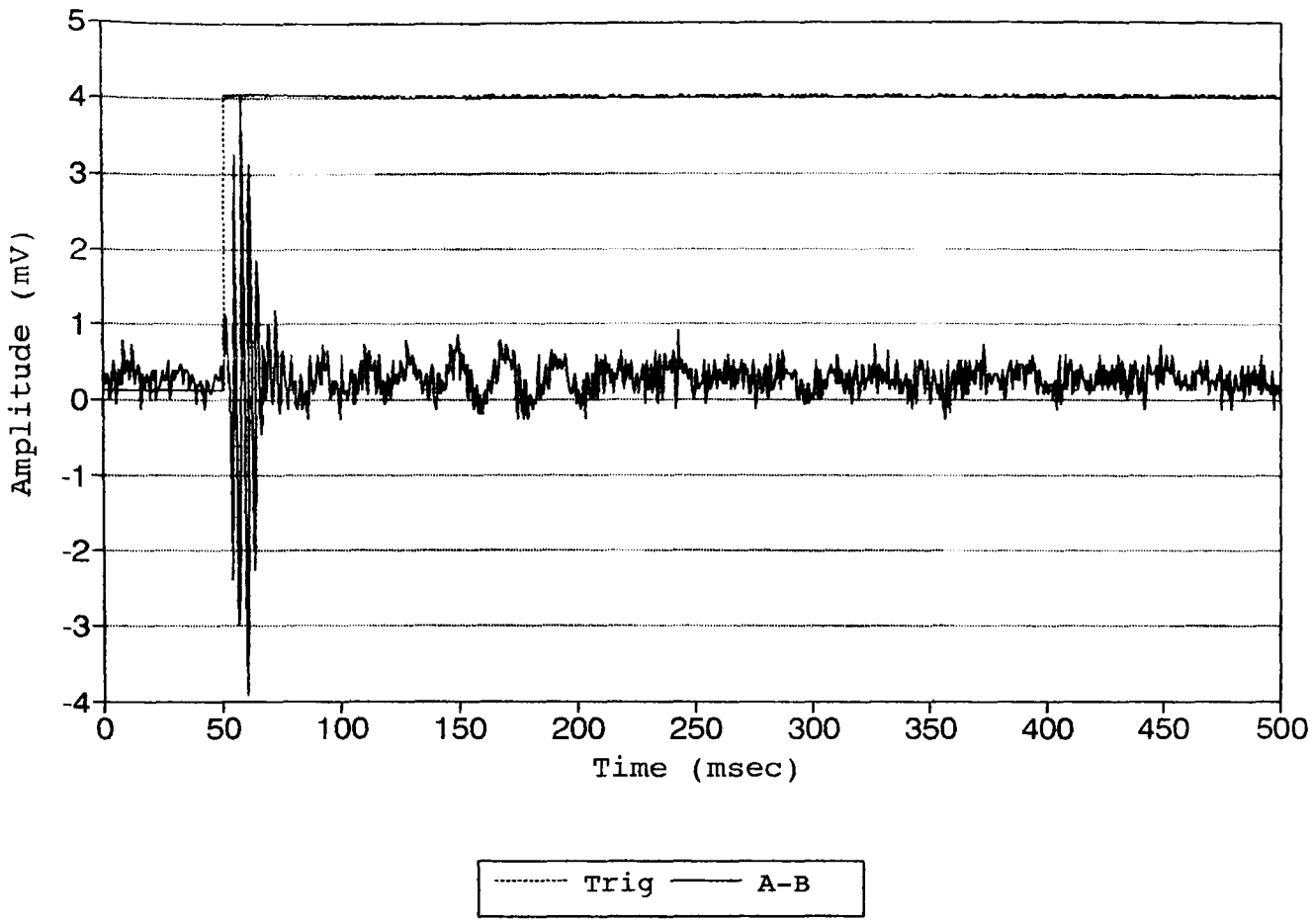

Figure (5.25): Bender Mark 3 Frame Wave, in Water Filled Sediment Box.

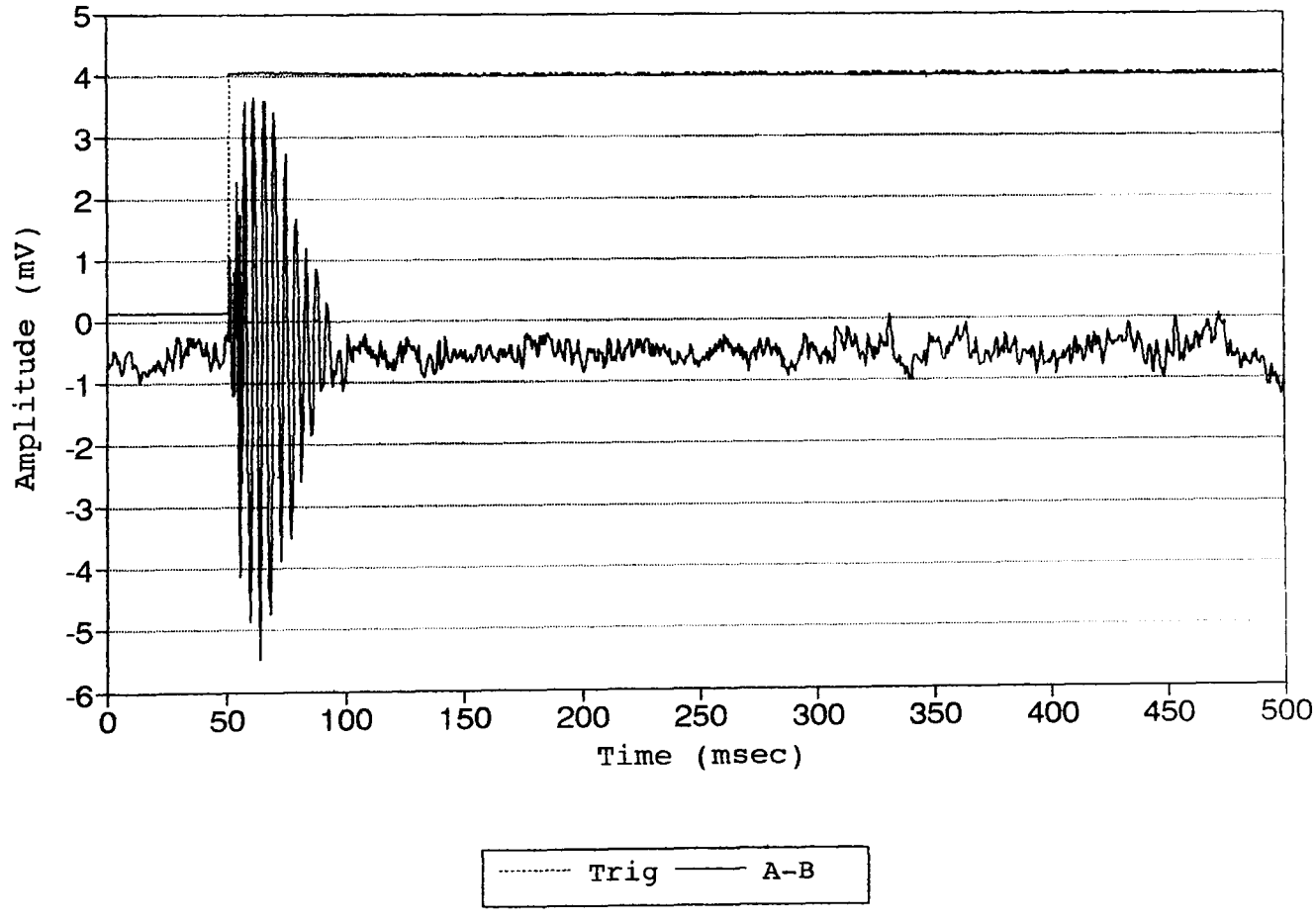

Figure (5.26a): Bender Mark 3 Signal
with Saturated Sand in the Sed. Box.

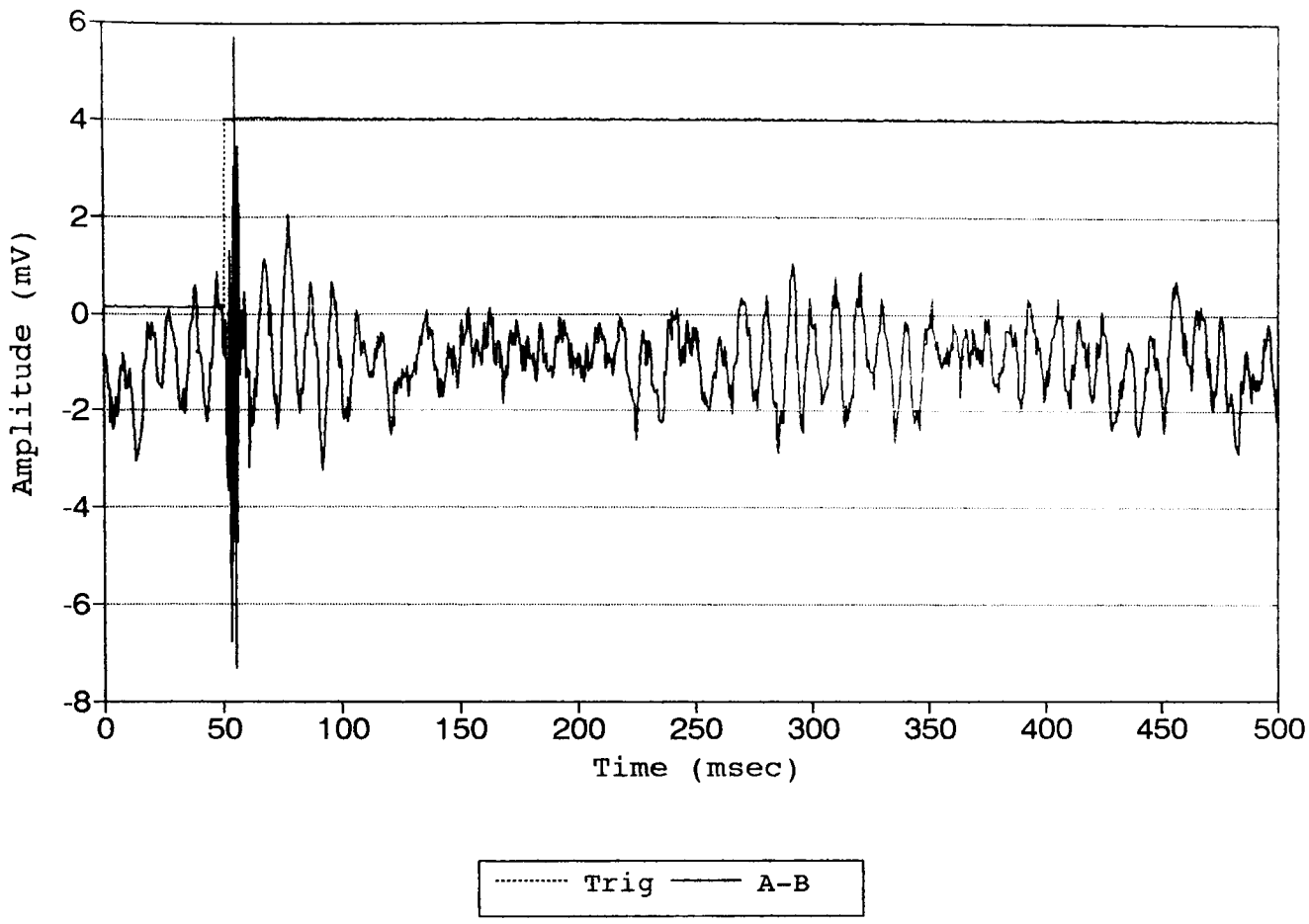

Figure (5.26b): Bender Mark 3 Signal
with Saturated Sand in the Sed. Box.

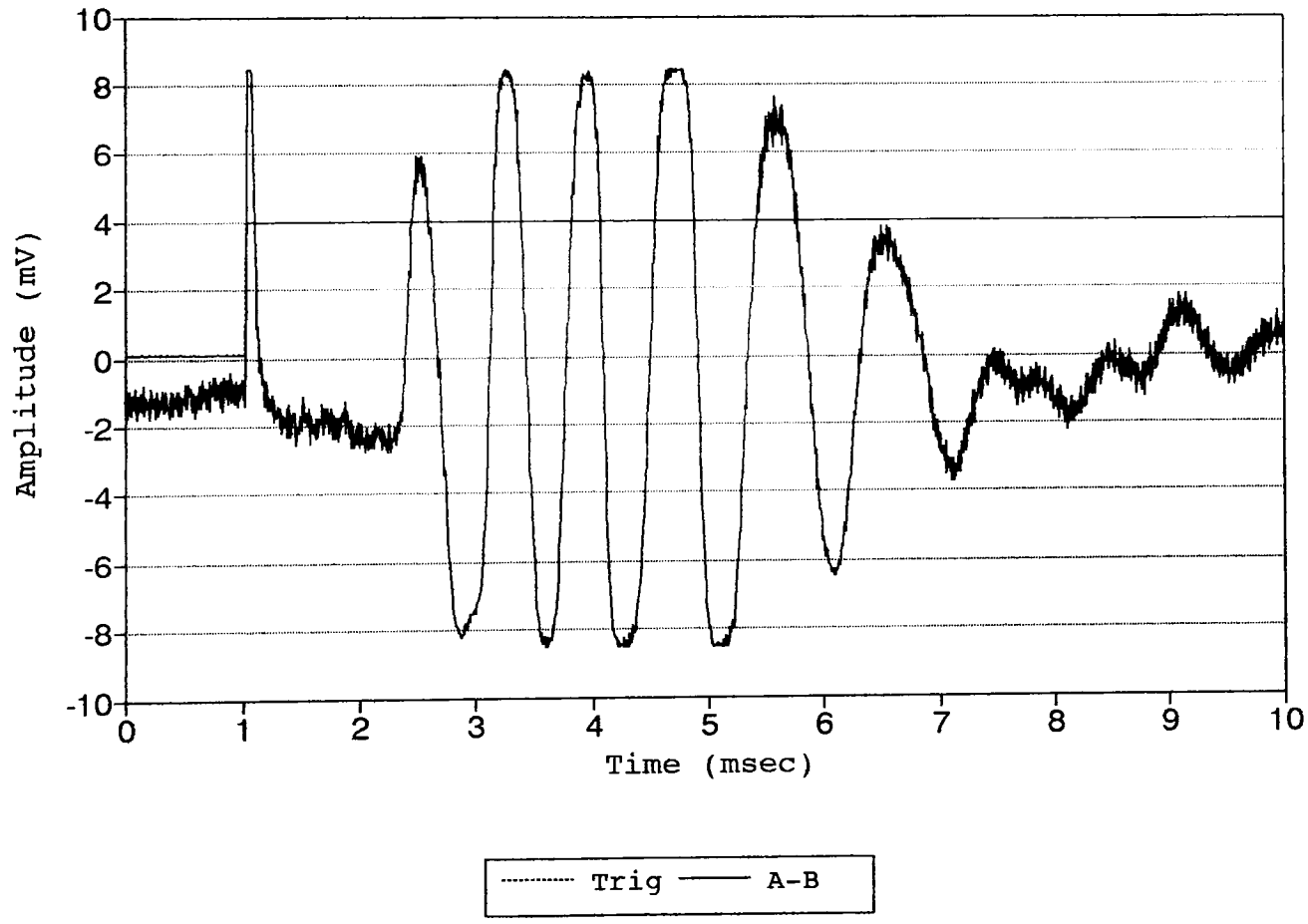

Fig (5.27): Bender Mark 3 Signal in Cohesive Sediment in Sed. Box.

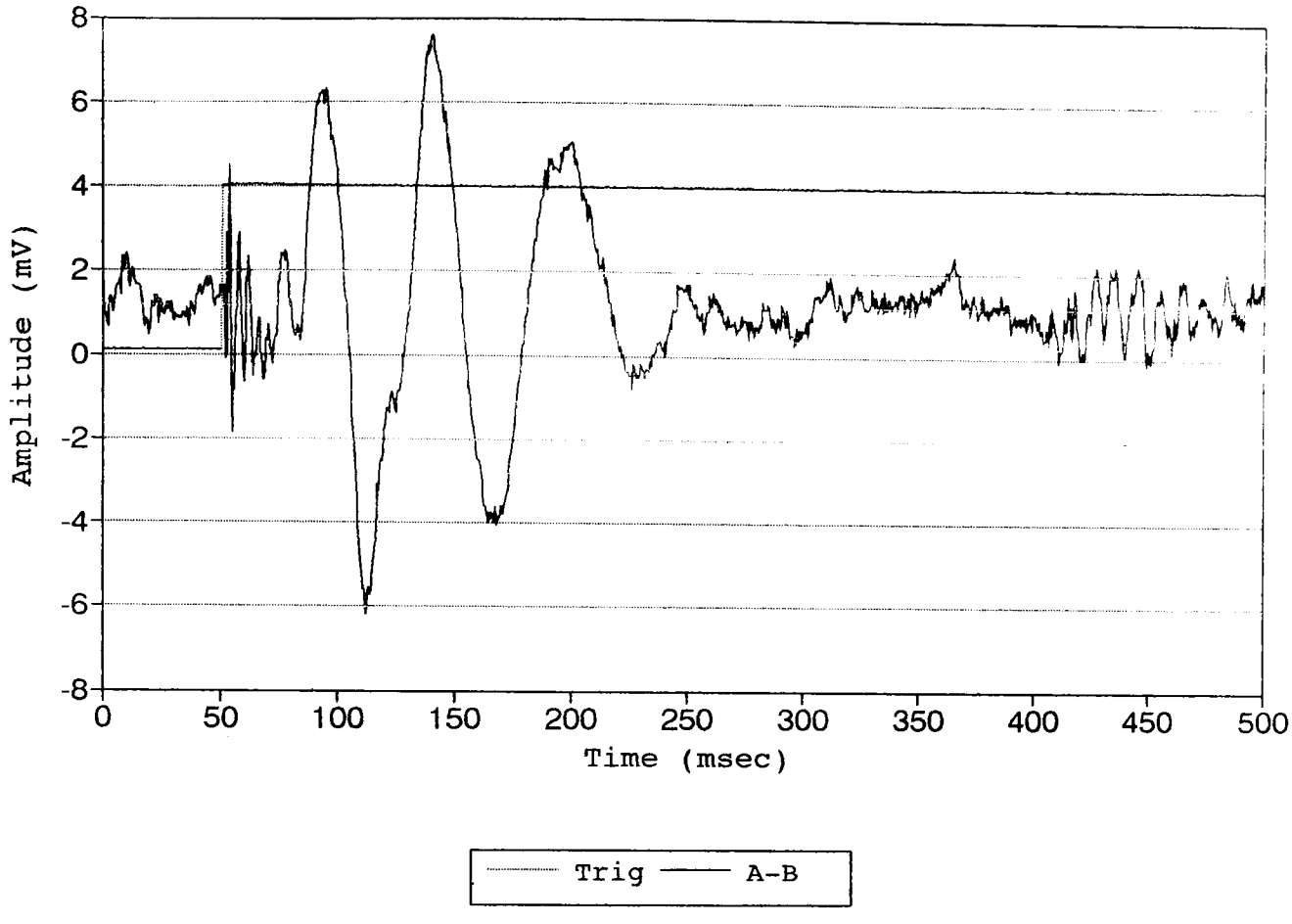

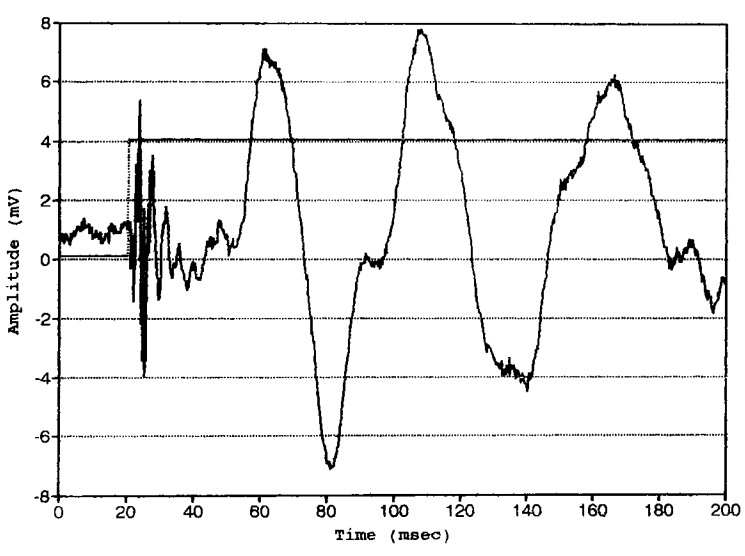

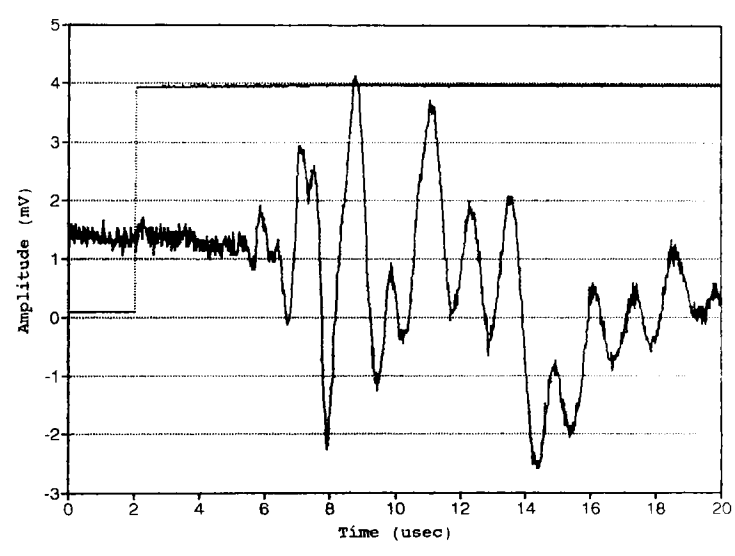

to calculate a cell constant that could then be used on the sediment resistivity measurements. Measurement of fluid resistivity was made in a similar manner to that used in the oedometer. Measurements were taken for various fluid heights and box base heights. These were then used in conjunction with the salinity and temperature measurements to calculate a equation for the cell constant in terms of the fluid level/sediment depth and box base height in the same way as in the oedometer. These are given below where k is the cell constant in each case:

Base Level	Equation	
iV	k = (sed.depth x 0.099294) + 0.7538	(5.15)
iii	k = (sed.depth x 0.129223) - 0.0335981	(5.16)
ii	k = (sed.depth x 0.165231) - 0.336672	(5.17)
i	k = (sed.depth x 0.203978) - 0.685501	(5.18)
B	k = (sed.depth x 0.153375) + 0.555708	(5.19)

With these equations a measured sediment resistivity could be converted into a formation factor by using equation 4.42.

5.2.4.3. **Pore and Total Pressure Measurements.**

The sediment box was designed so that four Druck Miniature series pressure transducers (PDCR 42) could be inserted into the wall; however only two sensors were actually used. Figure 5.28 shows the arrangement of the transducers, one measuring total pressure and the other measuring pore pressure mounted behind a porous membrane. The sensor measuring total pressure had no porous membrane across its face and was fitted so that its pressure sensing face was flush with the inner wall of the sediment box. The transducers are designed to give accurate linear measurements (a combined non-linearity and hysteresis of ±0.2%) and have their own in-built temperature sensing and compensation electronics (for the range 10° to 40°C there is thermal shift of ±0.05% of a reading per °C). An interface box was built in-house to supply the transducers with power and to amplify their output from a 0 to 75 millivolt range to the 0 to 5 volt range of the data logger.

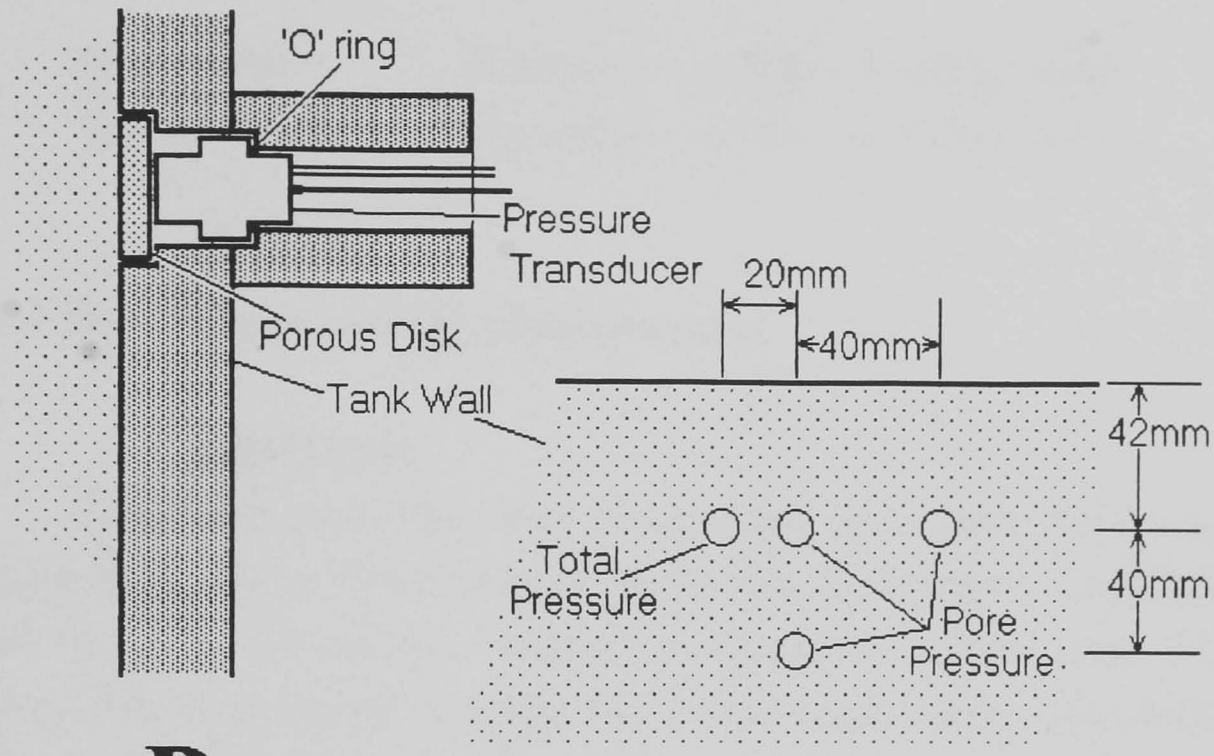

Pore Pressure Measurement

Fig 5.28: Pressure Transducer Array.

Calibration of the probes was easily carried out by fitting each transducer into the base of a burette from which the tap had been removed. With the burette vertical and the sensor at the bottom, sensor output was logged for various measured heights of water in the tube. The heights were then converted into pressures (in Nm^{-2}) and Figures 5.29 and 5.30 give the data and the plots for each sensor. The calibration gave the following equations for the two sensors;

Sensor 4812, Pressure = 0.090 + 1.629 x Volts (5.20)

Sensor 4825, Pressure = 0.412 + 1.632 x Volts (5.21)

5.2.4.4. **Geotechnical Measurements.**

Grain Size

Grain size analysis were carried out in the standard way, with the sample first being treated with hydrogen peroxide, overnight on a hot plate at 60°C (to remove organic matter), and then split into fine and coarse fractions by wet sieving through a 63µm sieve. The coarse fraction was then dried and analysed by using a fall tower (Larcombe, 1992), which uses fall velocity calibrated against sieve diameter to give an equivalent spherical diameter. The fine fraction was centrifuged and washed to remove any salt and the remains of the hydrogen peroxide and then analysed in a Micromeritics Sedigraph 5000ET (Sedigraph, 1986).

Specific Gravity

The specific gravity was determined by a standard soil engineering technique (B.S. 1377: 1961) using special density bottles. The process requires 10-15g of oven dried sample which has been ground into a fine powder and distilled water that has been de-aired and is kept at 20°C. Four weights are required, these are; W_1 the weight of the density bottle empty; W_2 the weight of the density bottle plus the dry sediment; W_3 the weight of the density bottle plus the dry sediment and distilled water; and W_4 the weight of the density bottle plus distilled water. The specific gravity, Gs, is then derived by the equation,

$$Gs = \frac{(W_2 - W_1)}{(W_4 - W_1) - (W_3 - W_2)} \qquad (5.22)$$

Fig (5.29): Calibration of Pressure Sensor 42/4812.

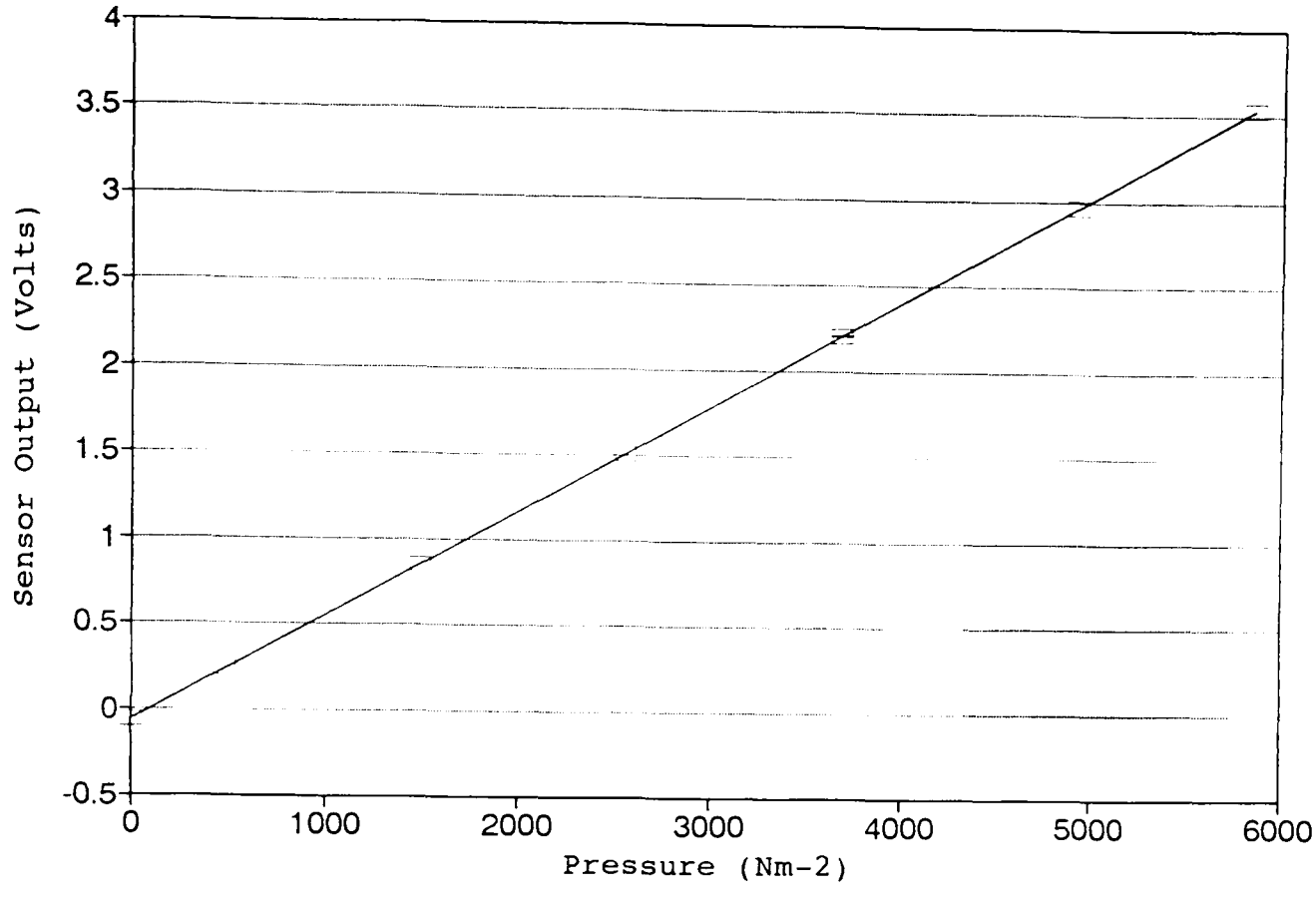

Fig (5.30): Calibration of Pressure Sensor 42/4825.

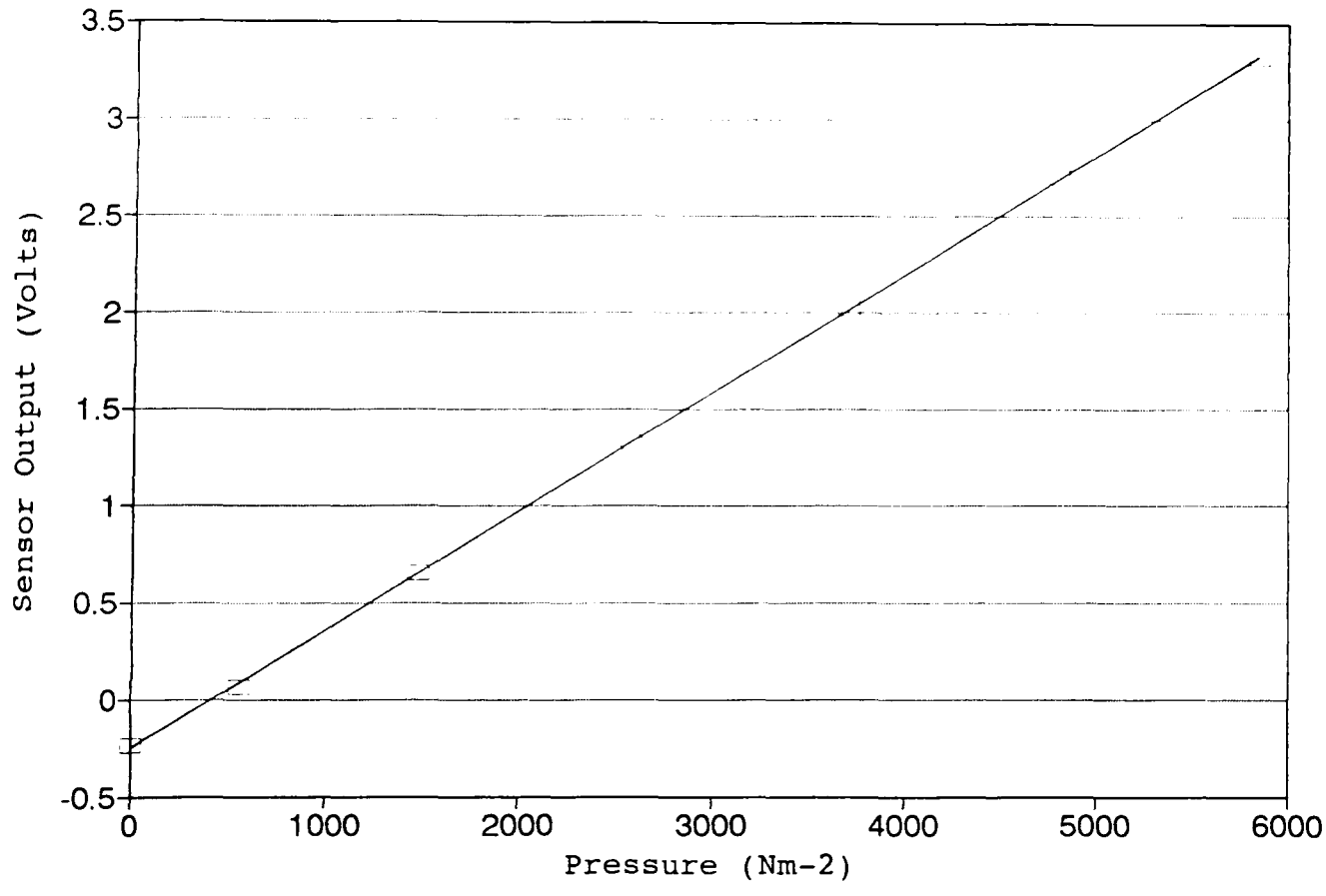

The analysis is done in triplicate and the result is the average of the three values. However the individual vales must not differ by more than 0.03 for the result to be valid.

Moisture Content

Moisture content is found by weighing a sediment sample before and after it is dried in an oven at 105°C overnight and then using the equation,

$$\omega = \frac{W_w}{W_s} = \frac{W_t - W_s}{W_s} \tag{5.23}$$

where ω is the moisture content, W_w is the weight of water in the sample, W_s is the weight of solids in the sample (its weight after drying) and W_t is the total weight of the sample (its weight before drying).

Porosity

The porosity can be derived from the moisture content and specific gravity if the sediment is assumed to be saturated. The porosity, n, and the voids ratio, e, are given by,

$$n = \frac{V_v}{V_t} \qquad e = \frac{V_v}{V_s} \tag{5.24}$$

where V_v and V_s are the volumes of the voids and solids in the sample respectively and V_t is the total sample volume. e for a saturated sediment is also the product of the moisture content and specific gravity ($e = \omega . Gs$). This can be substituted into the relationship,

$$n = \frac{e}{1+e} \tag{5.25}$$

to give,

$$n = \frac{\omega Gs}{1 + \omega Gs} \tag{5.26}$$

Density Wet/Dry

The wet and dry sediment densities, ρ_{wet} and ρ_d respectively, can be derived from measurements of the porosity and specific gravity, using the equations,

$$\rho_{wet} = \rho_w n + \rho_w Gs(1-n) \tag{5.27}$$

and

$$\rho_d = \rho_w Gs(1-n) \tag{5.28}$$

5.2.4.5. **Total Organic Matter (TOM).**

The method used to measure the TOM content of the sediment was that of loss of weight on ignition as described by Galle and Runnel (1960) and modified by Dean (1974). In a comparison of methods by Byers et al. (1978), this loss on ignition method yielded 100% of the TOM. The method is:

(a) A 2g powdered sample dried in an oven at 90-100°C for one hour in a preweighed ceramic crucible, after cooling in a desiccator is weighed. This gives the dry weight of sample that is the basis for all further calculations.

(b) The sample and crucible are paced in a muffle furnace and heated to 550°C for four hours. After cooling the sample is again weighed and the difference between this measurement and the dry weight is the amount of organic matter ignited.

5.2.5. **Flume Sensor Testing.**

5.2.5.1. **Sensor Drift.**

The drift of the sensors in the flume was measured by logging data at regular intervals over a period of a least one hour (which is the average length of the flume runs), with the flume full of water at zero flow and flowing with and without sediment. Figures 5.31 and 5.32 show the drift of the velocity and bed stress sensors, respectively, and as can be seen the stress sensor shows no obvious drift, but the velocity sensor appears to display a slow downward drift. However this drift is negligible when compared to the variation of the raw data as shown by the error bars. The apparent increase in the flow velocity sensor output at 160 minutes and that of the stress sensor at 60 minutes is caused by the formation of an air bubble on the face of the sensor during the data logging period. These bubbles form simply because the sensor warms the fluid around it and

Fig (5.31a): Hot Film Velocity Sensor Drift in Clear Still Water.

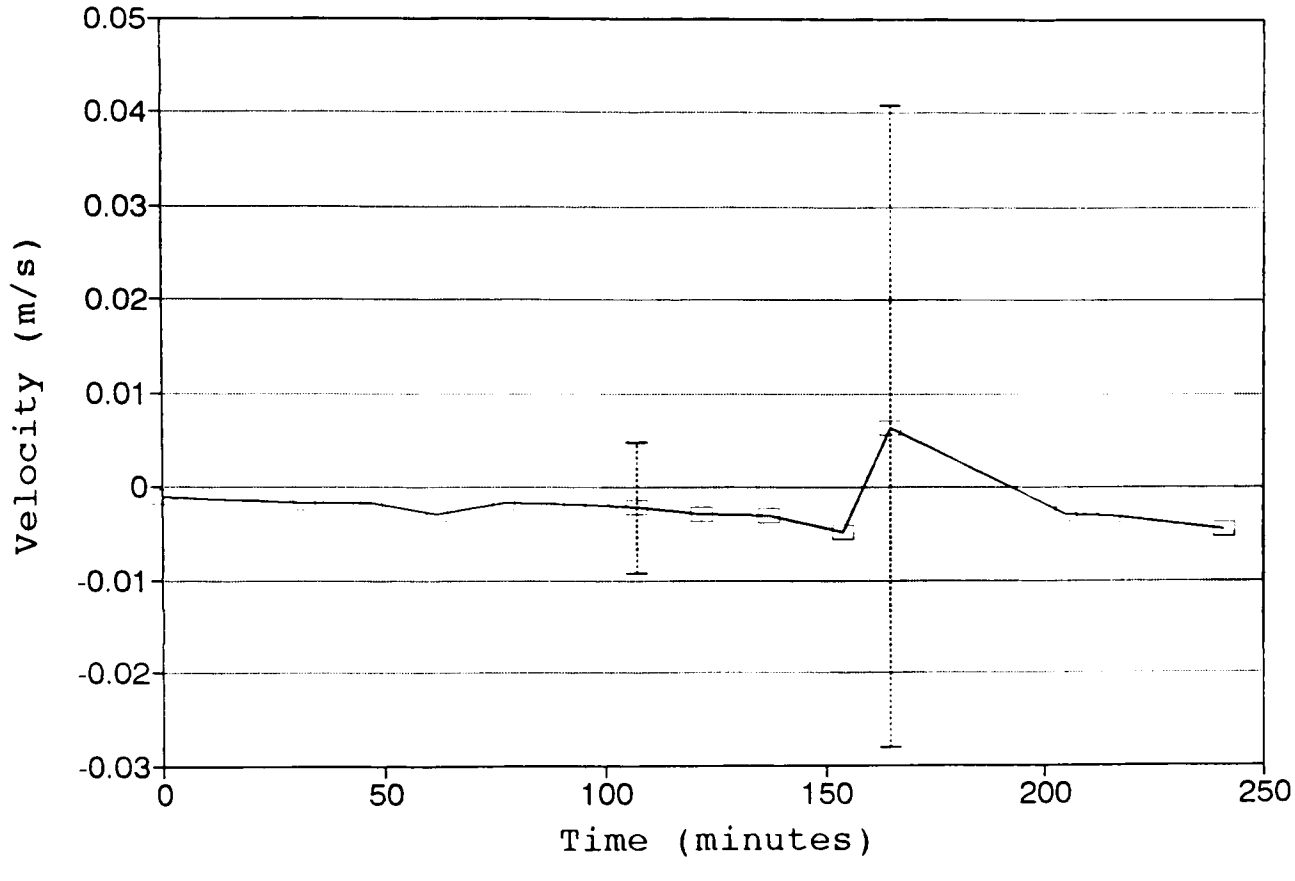

Fig (5.31b): Hot Film Velocity Sensor Drift in Clear Flowing Water.

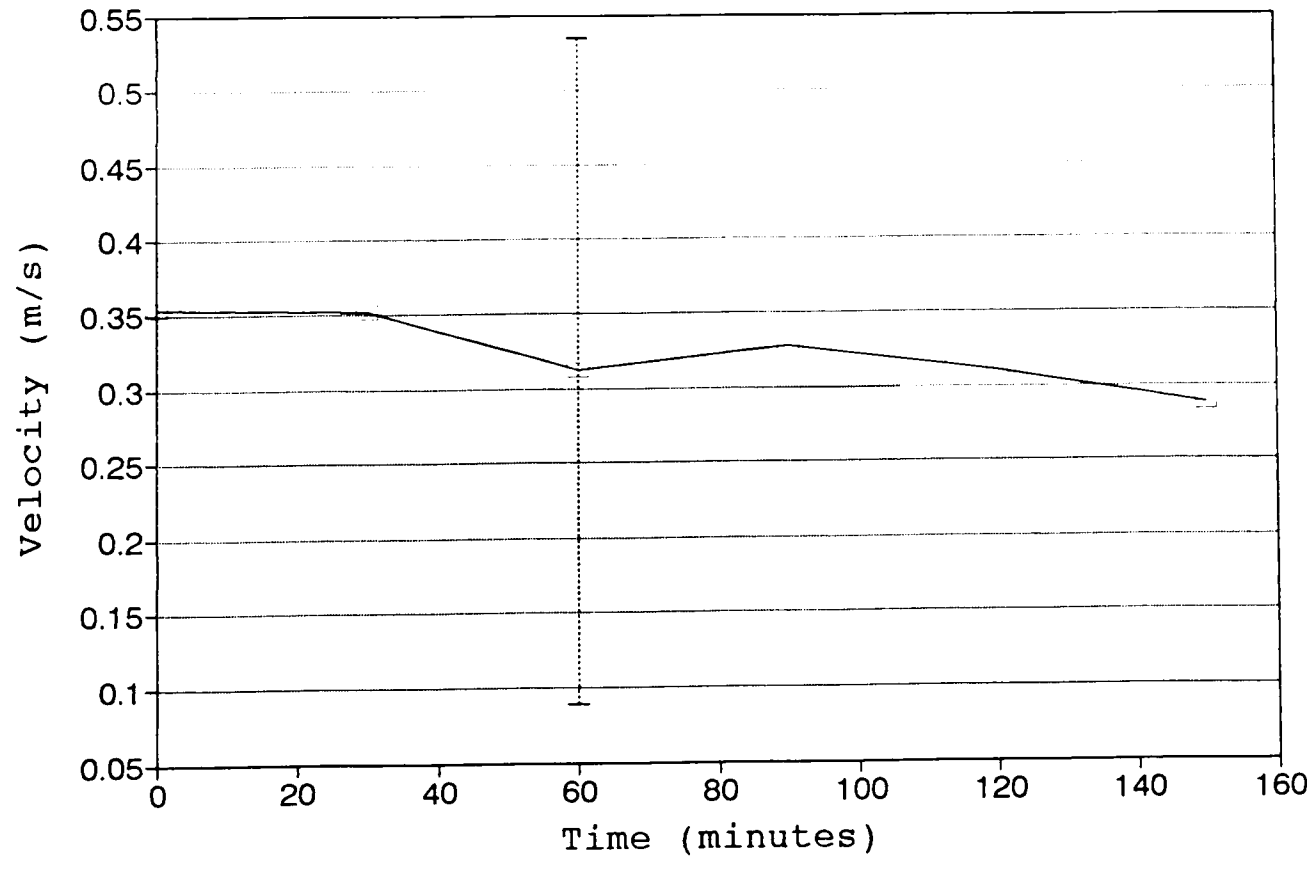

Fig (5.32a): Hot Film Shear Stress Sensor Drift in Clear Still Water.

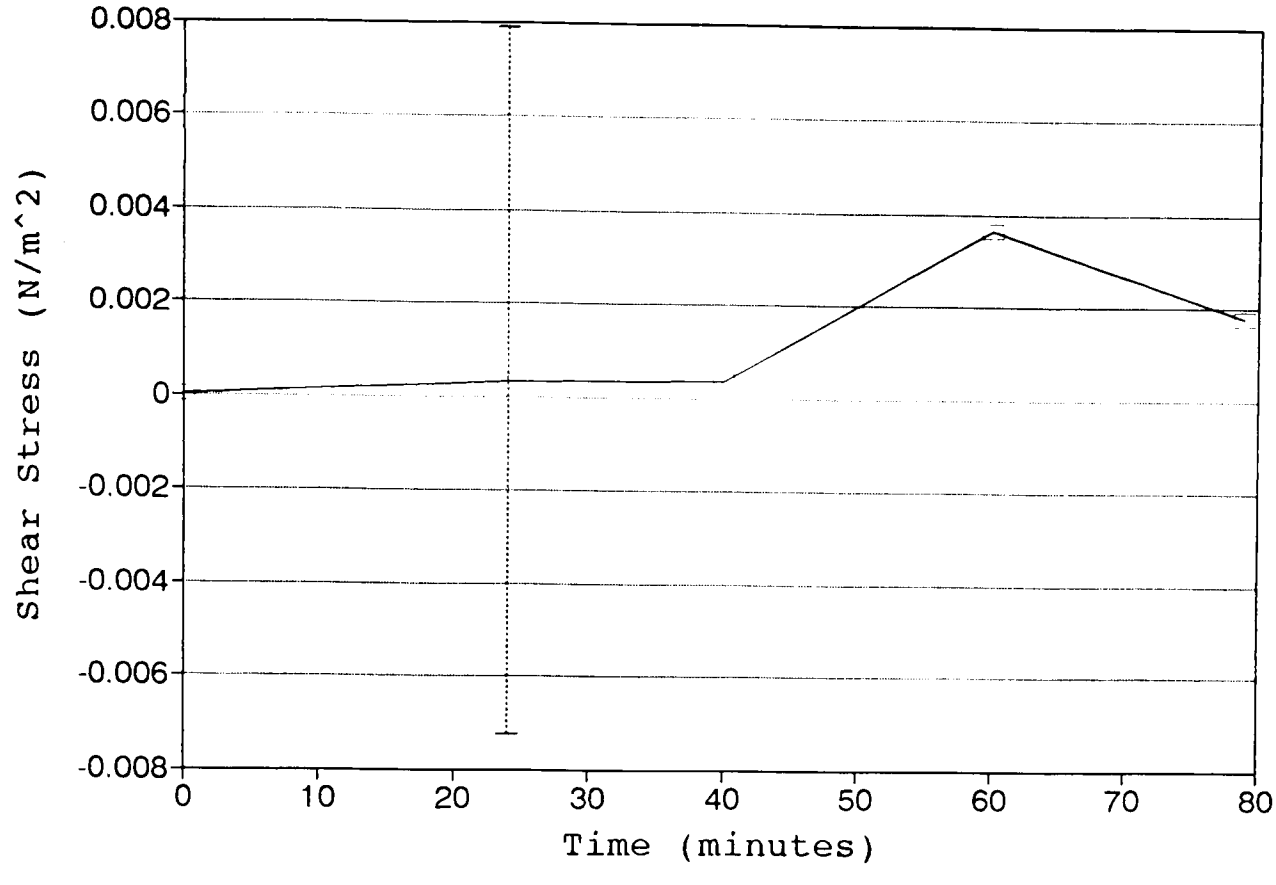

Fig (5.32b): Hot Film Shear Stress Sensor Drift in Clear Flowing Water.

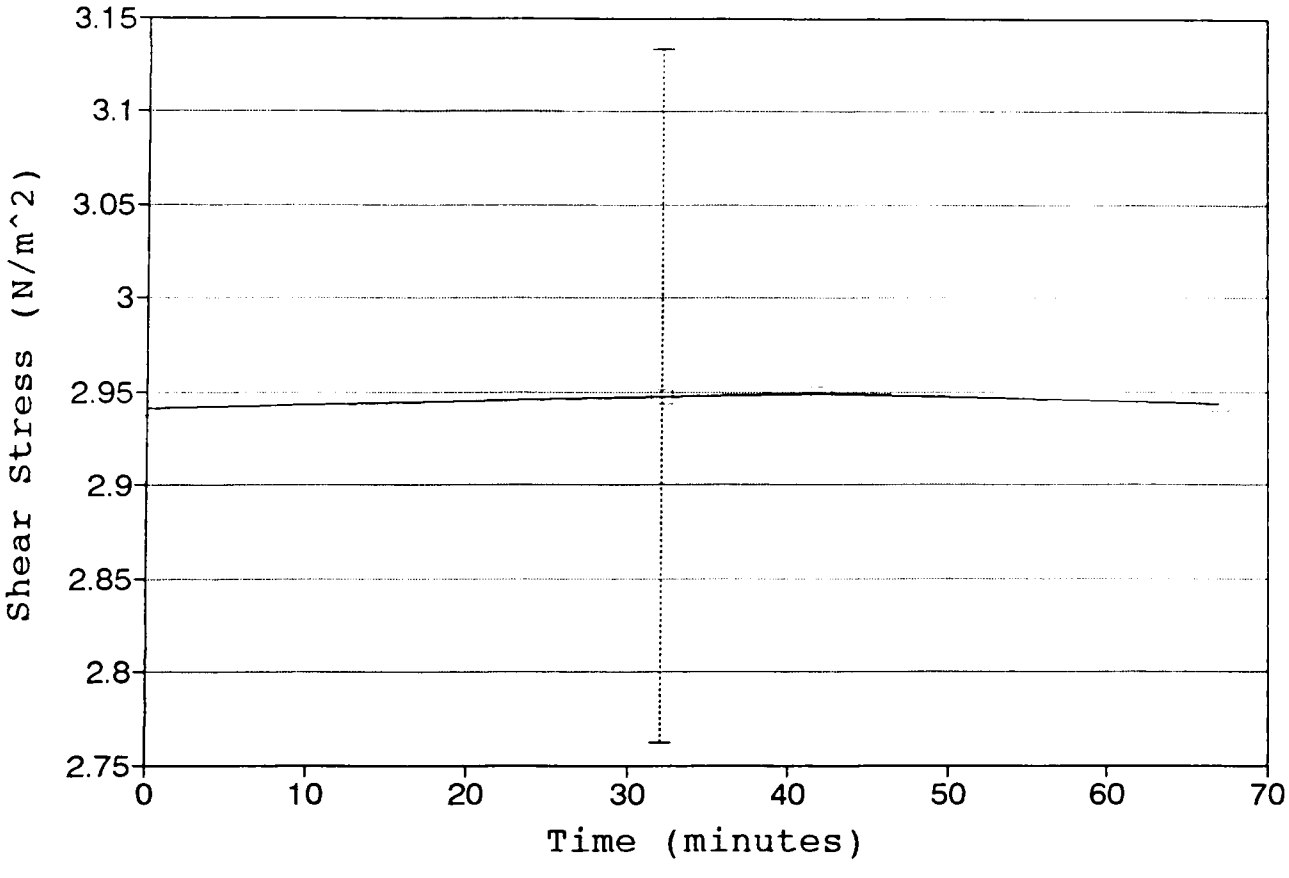

causes dissolved gas to come out of solution. However under normal flow conditions these air bubbles do not form, as the fluid is flowing past the sensor and is not heated to any degree.

The drift recorded on the OBS sensor is more complicated then that on the velocity and shear stress sensors. Figure 5.33a shows the drift on OBS-1 in clear water; this appears to be quite important, but as Figure 5.33b shows, once sediment is added the drift of a few millivolts is completely masked and no longer detectable. The apparent 100mg/l drift in suspended sediment concentration shown in Figure 5.32b is caused by the change in size of the particles in suspension. The possibility that sediment was being lost from the flume was ruled out by; (1) the apparent concentration increased rather then decreased and, (2) water samples taken at the same time as logged OBS data, demonstrated that the total amount of material in suspension was remaining constant. It appears that the size spectra of the material in suspension alters over a period of three hours before reaching a constant value, and this alteration in size spectra causes a shift in the OBS output, resulting in an apparent change in the suspended sediment concentration. An investigation of this problem was beyond the scope of this project. However the apparent variations in suspended sediment concentration caused by alteration of the size spectra is smaller and occur over a longer time period then the changes that occur in the suspended sediment concentration during an erosion run.

5.2.5.2. **Sediment Affect on Flow Sensors.**

Velocity Sensor.

Due to the way in which the velocity sensor measures the flow velocity, it could possibly be affected by increases in the concentration of suspended sediment in the water. Figure 5.34 shows the change in velocity sensor output in a constant velocity flow but with increasing concentrations of suspended sediment. It appears that as the concentration increases, the apparent velocity as measured by the sensor decreases (although the measured velocity variation is less then the variations of the raw data and is of the same magnitude as the variation due to drift, Figure 5.31b). There are two possible reasons why suspended sediments might alter the

Fig (5.33a): OBS Sensor Drift in Clear Still Water.

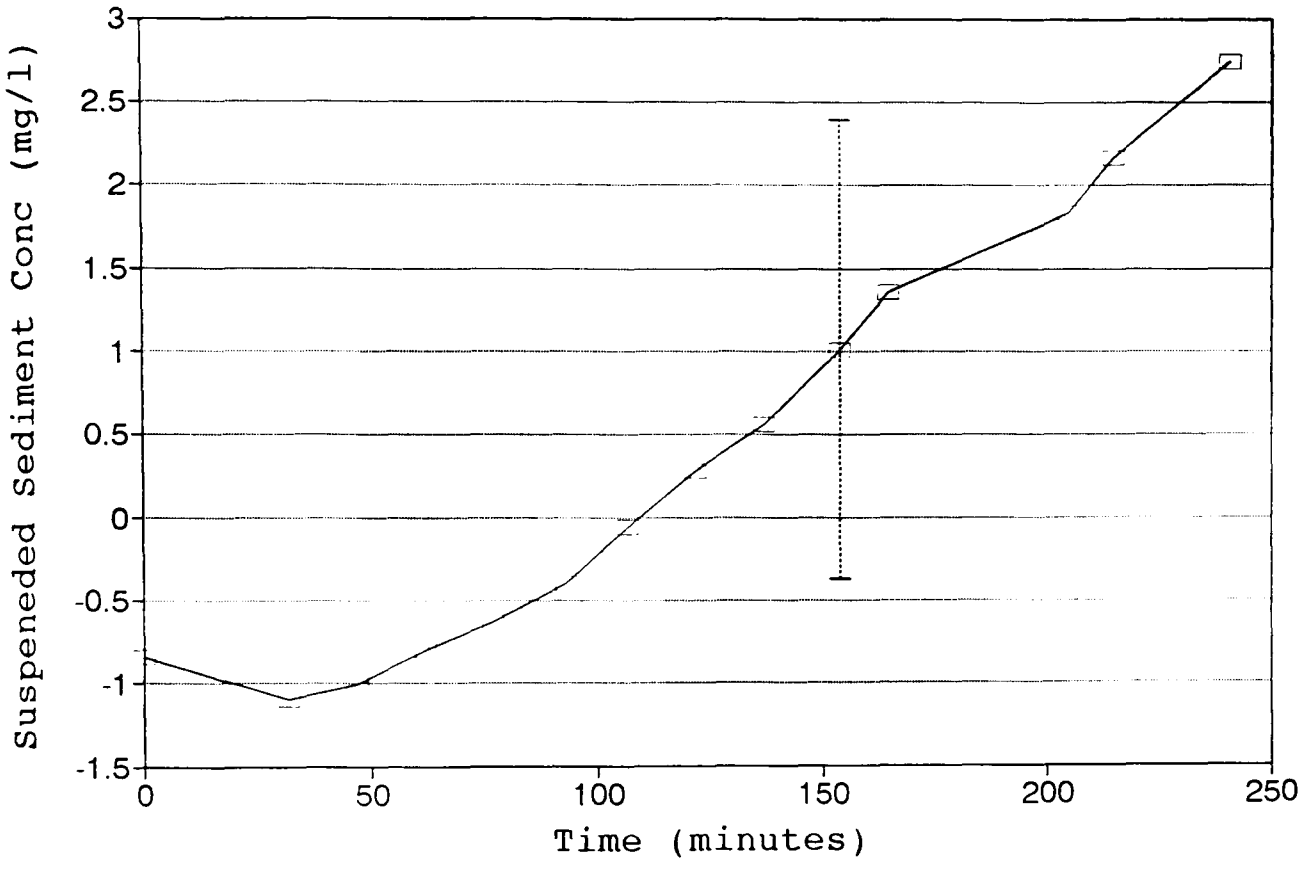

Fig (5.33b): OBS Sensor Drift in Flowing Turbid Water.

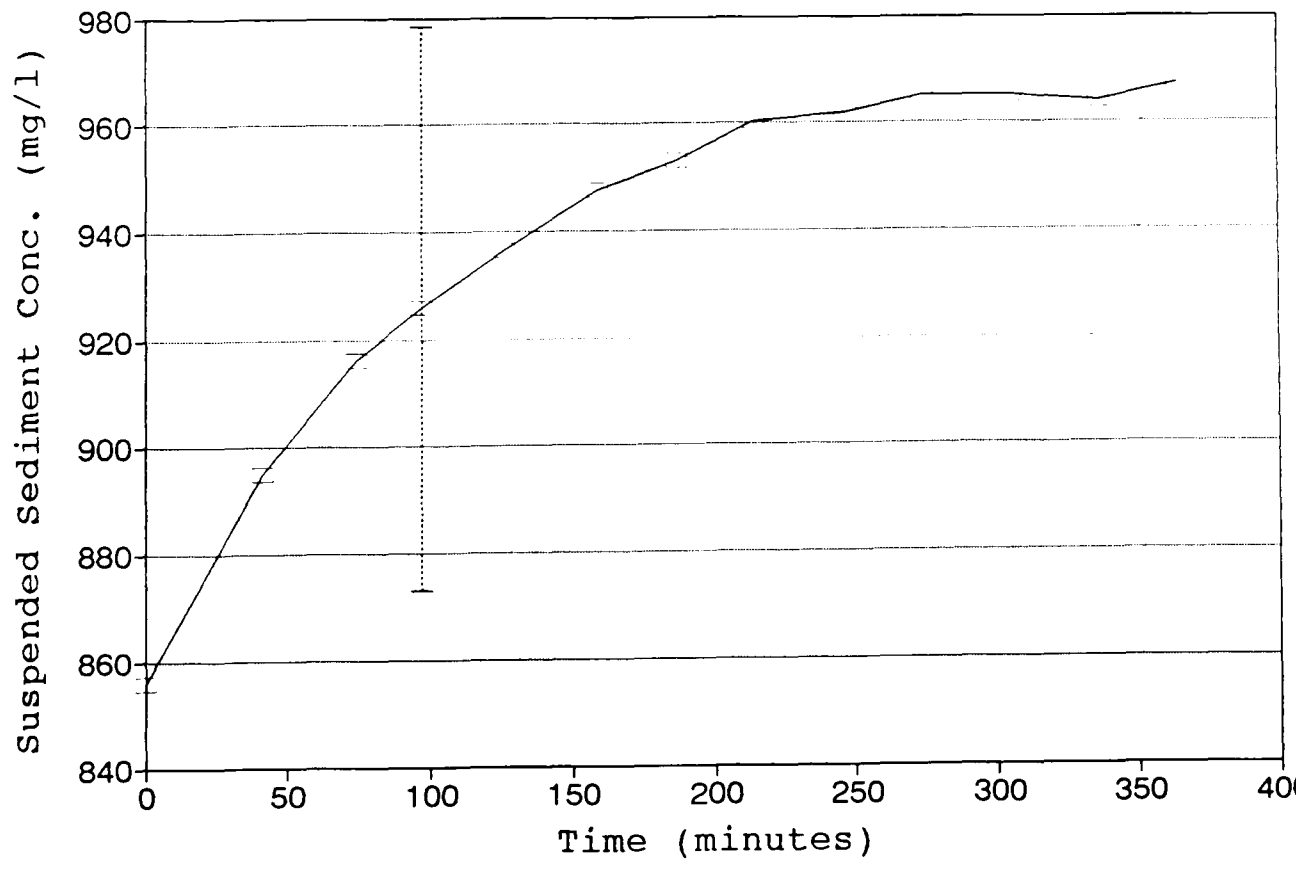

Fig (5.34): Suspended Sediment Affect on Hot Film Measured Velocity.

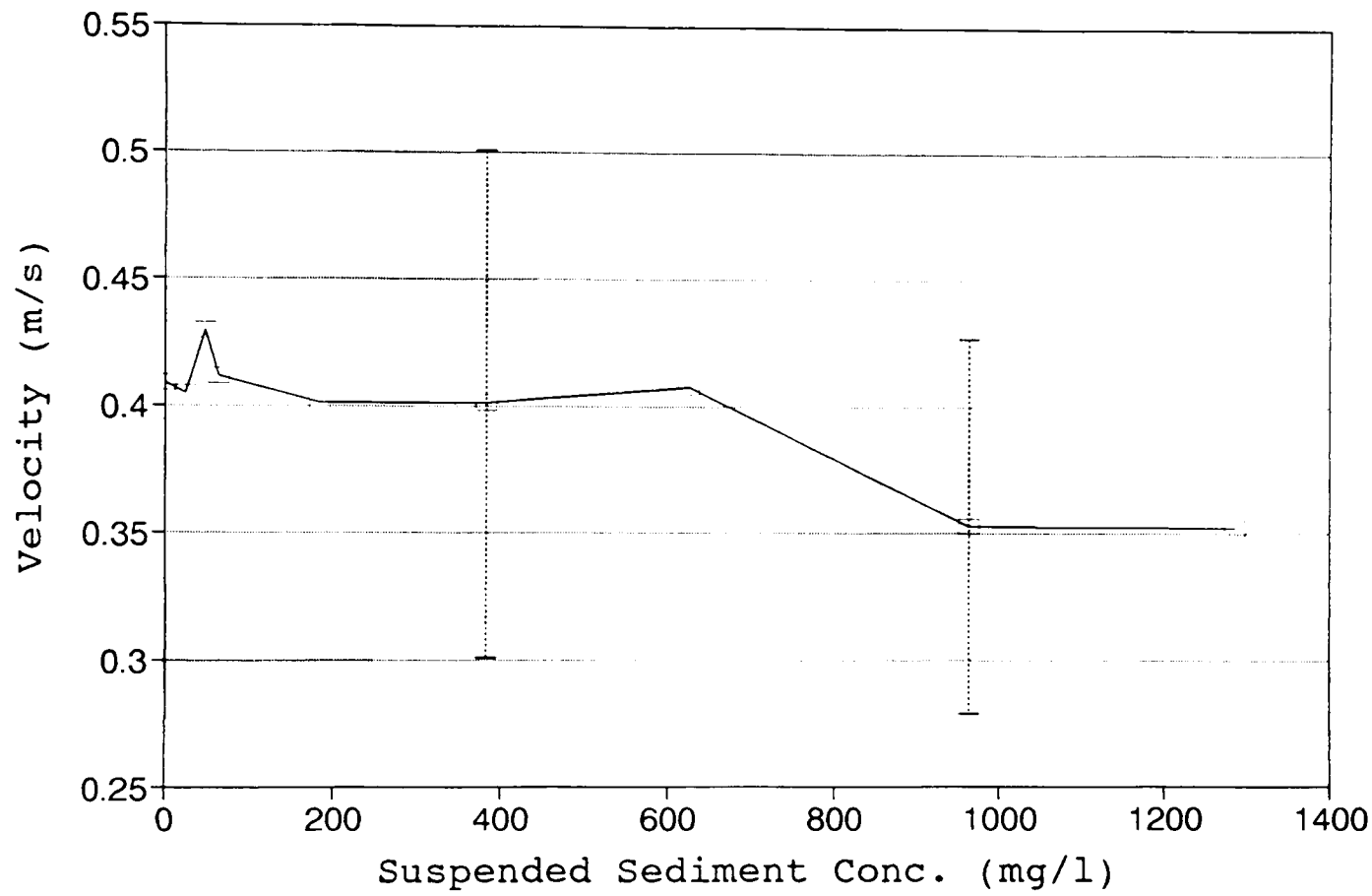

velocity sensor output. The first is that as the concentration of material increases, the number of particles colliding with the sensors increases. When a particle is in contact with the sensors it reduces the cooling affect on the sensor, because the particle is not able to conduct heat as well as the fluid. Therefore the cooling affect on the sensor decreases as the frequency of collisions increase, resulting in a lower apparent velocity. The other possible cause is that the structure and character of the boundary layer changes with increasing suspended solids concentration (Gust, 1976; Best and Leeder, 1993). Using Komar's (1978) equation for the thickness of the boundary layer in a turbulent flow,

$$\delta = 0.38x\left(\frac{\upsilon}{\bar{U}_{\infty} x}\right) \qquad (5.29)$$

where δ is the boundary layer thickness, x is the distance downstream, υ is the kinematic viscosity (at 10°C and 35ppt is $1.4 \times 10^{-6} m^2 s^{-1}$), and $\bar{U}_{\infty}$ is the mean free stream velocity, Figure 5.35 can be constructed to show the growth of the boundary layer with distance downstream from the start of the perspex test section (assuming that the boundary layer begins at the start of the perspex test section). This shows that the velocity sensor is located in the outer region of the boundary layer, in a trade of between measuring the velocity as far from the wall as possible while still having the sensor firmly mounted. Therefore any variation in velocity measured at the sensor due to changes in the boundary layer structure, are likely to be slight and probably masked by other changes including drift as already suggested. However the ability to differentiate between these two possible causes of apparent velocity variation or to investigate them further was beyond the scope of this project.

Bed Stress Sensor.

The affect on the stress sensor of increasing the sediment concentration is far more dramatic. Figure 5.36 shows the drop in measured shear stress with increasing suspended sediment concentration at the same motor setting. This also alters the relationship between shear stress and velocity in the flume (Figure 5.37). If it is assumed that the affect of sediment on the sensor is only slight, as demonstrated by the velocity data above, then this apparent reduction in stress caused by the increase in

Fig (5.35): Boundary Layer Growth with distance downstream.

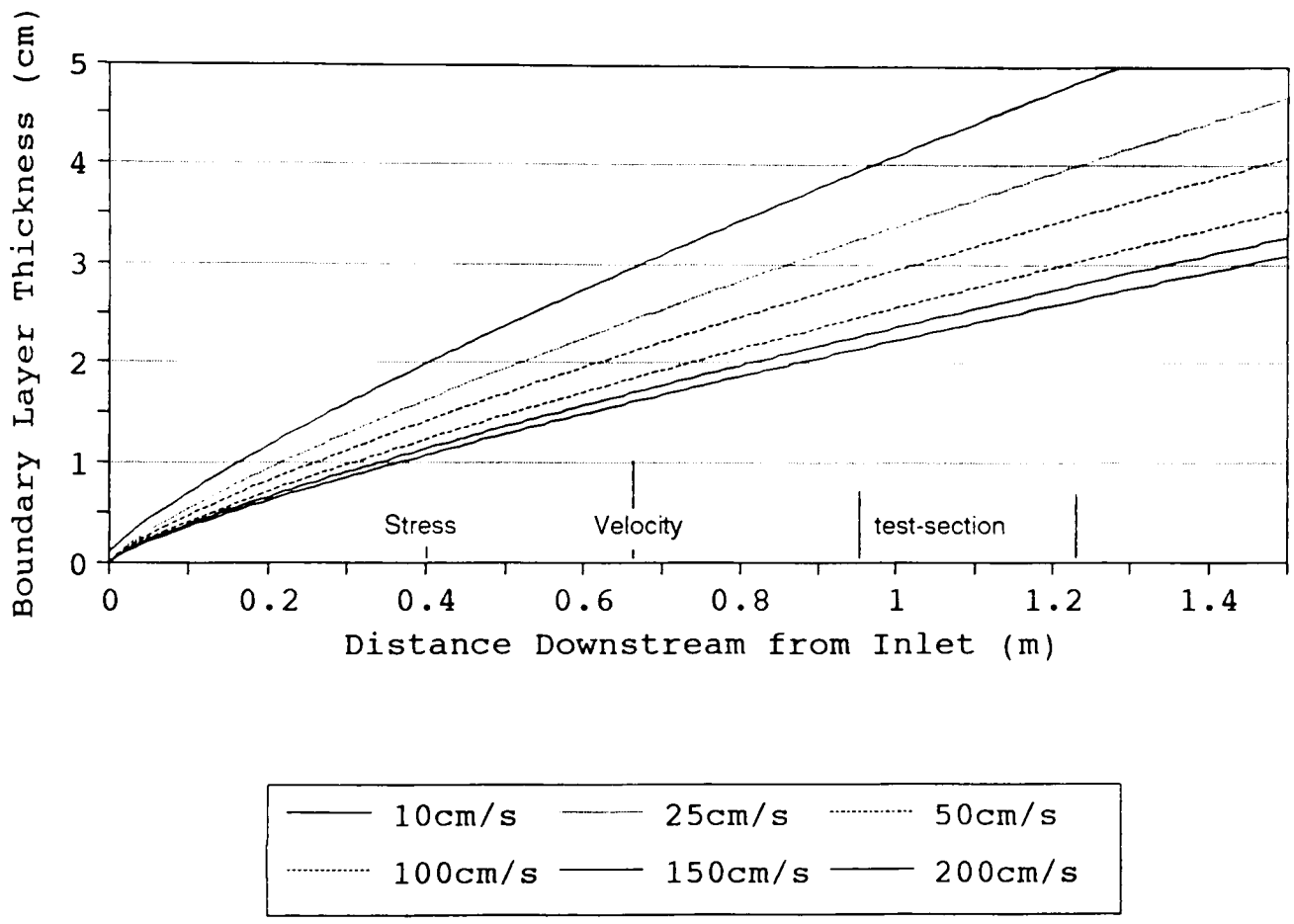

Fig (5.36): Suspended Sediment Affect on Hot Film Measured Shear Stress.

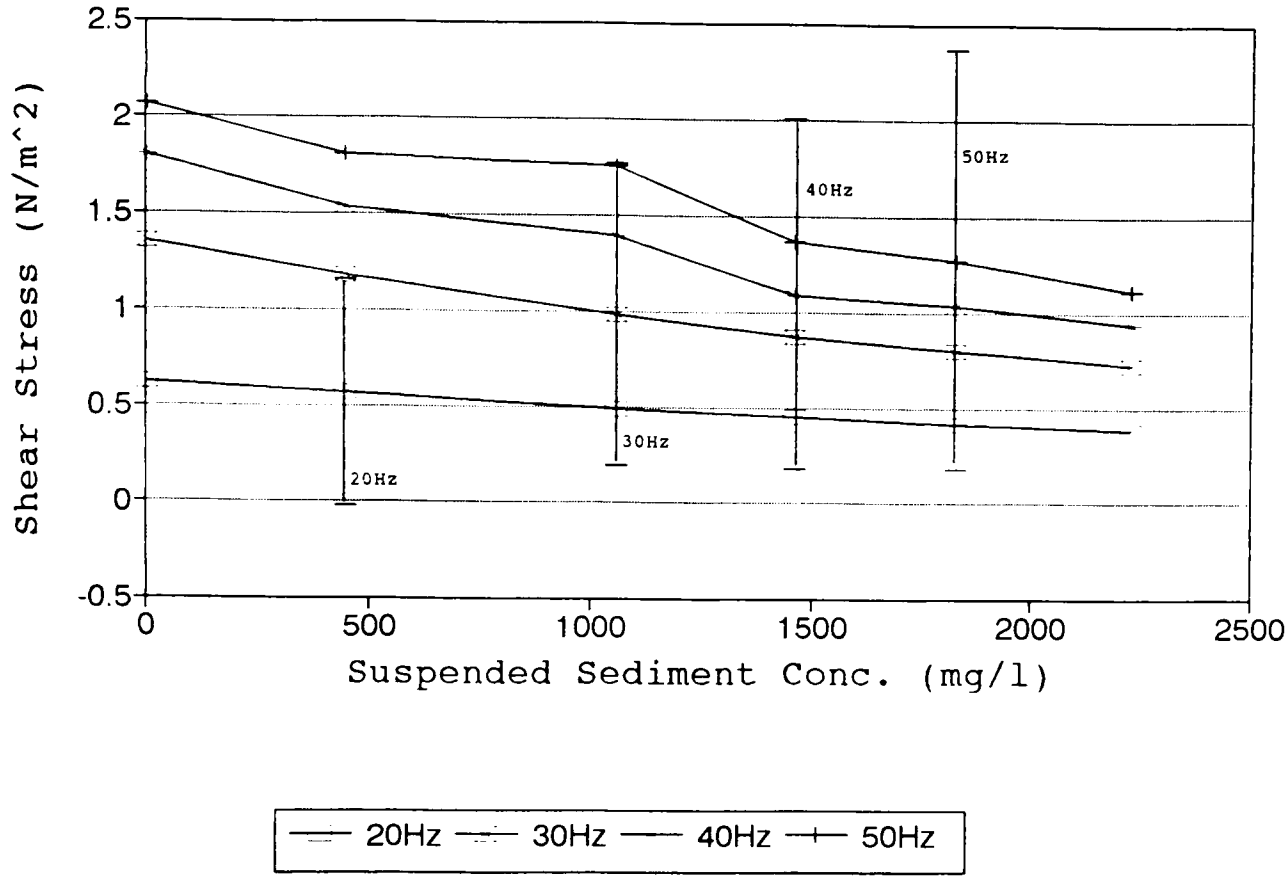

Fig (5.37): Suspended Sediment Affect on Stress/Velocity Relationship.

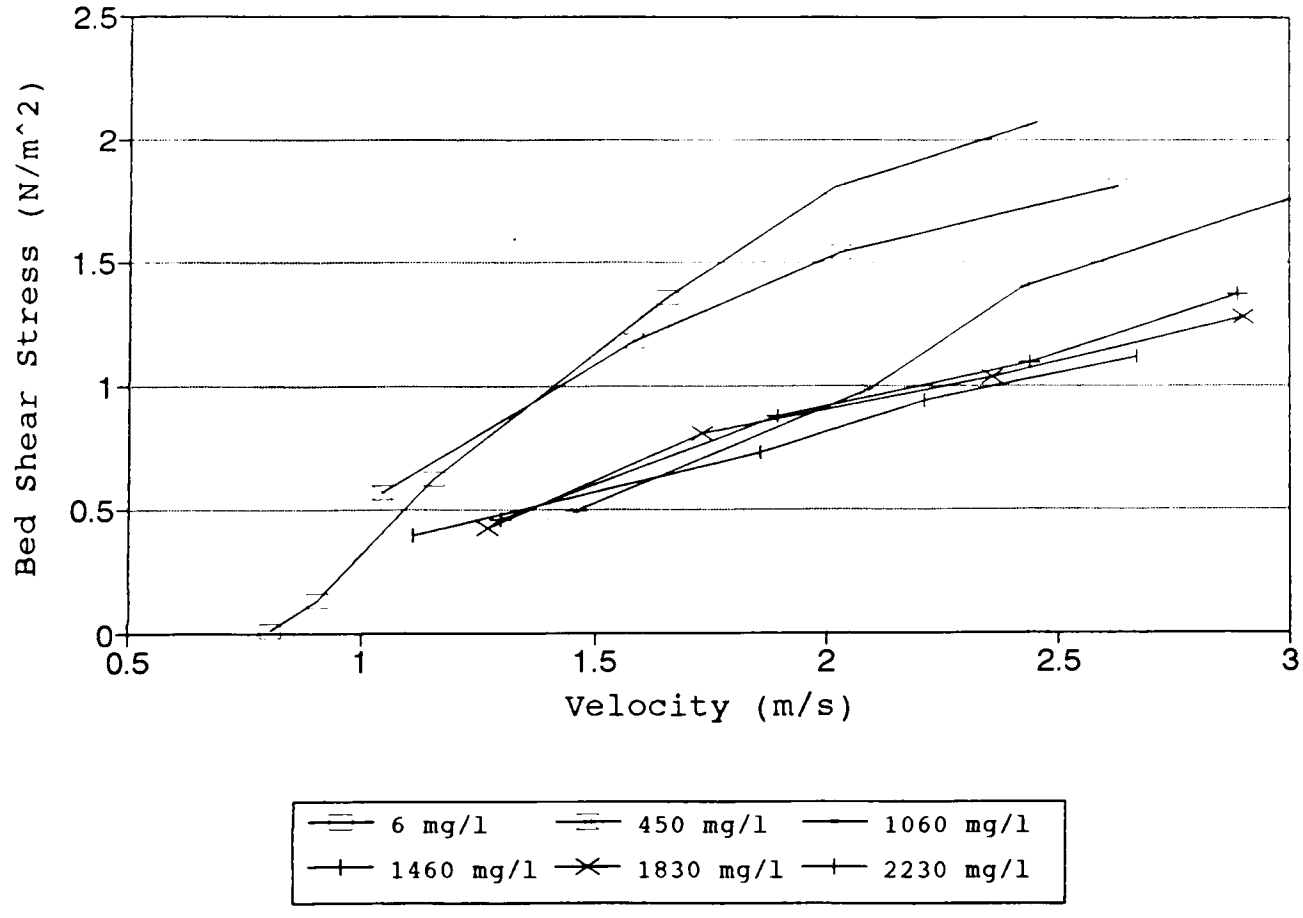

suspended solids is in fact a real reduction in the bed shear stress. This possibility is also supported by other work (Gust, 1976; Best and Leeder, 1993) which points to a change in the boundary layer structure and characteristics with variations of the suspended solids concentration. This means that the measured bed shear stress is correct and that no correction needs to be made for the increase in suspended solids concentration over the length of time of a flume run.

5.2.3.5. **Affect of Flow Velocity on OBS Output.**

Figures 5.38a,b shows the affect of velocity on OBS output at three suspended solids concentration. As would be expected the concentration rises sharply in the first half of the velocity range as material is suspended by the flow. The very small increase that appears with apparently clear salt water is caused by small volumes of sand (that remain in the flume even after flushing) and material that is present in the supplied seawater, which settle in the flume and are then suspended by the increasing flow velocities. At higher flow velocities there appears to be a very slight increase, which is possibly caused by the flow velocity rather then an actual change in suspended solids concentration. However this change of a few mg/l is small when compared to variation in the raw data and even smaller in comparison to actual changes that occur during an erosion run.

Figure (5.38a): Affect of Flow Velocity
on OBS Ouput, in clear Water.

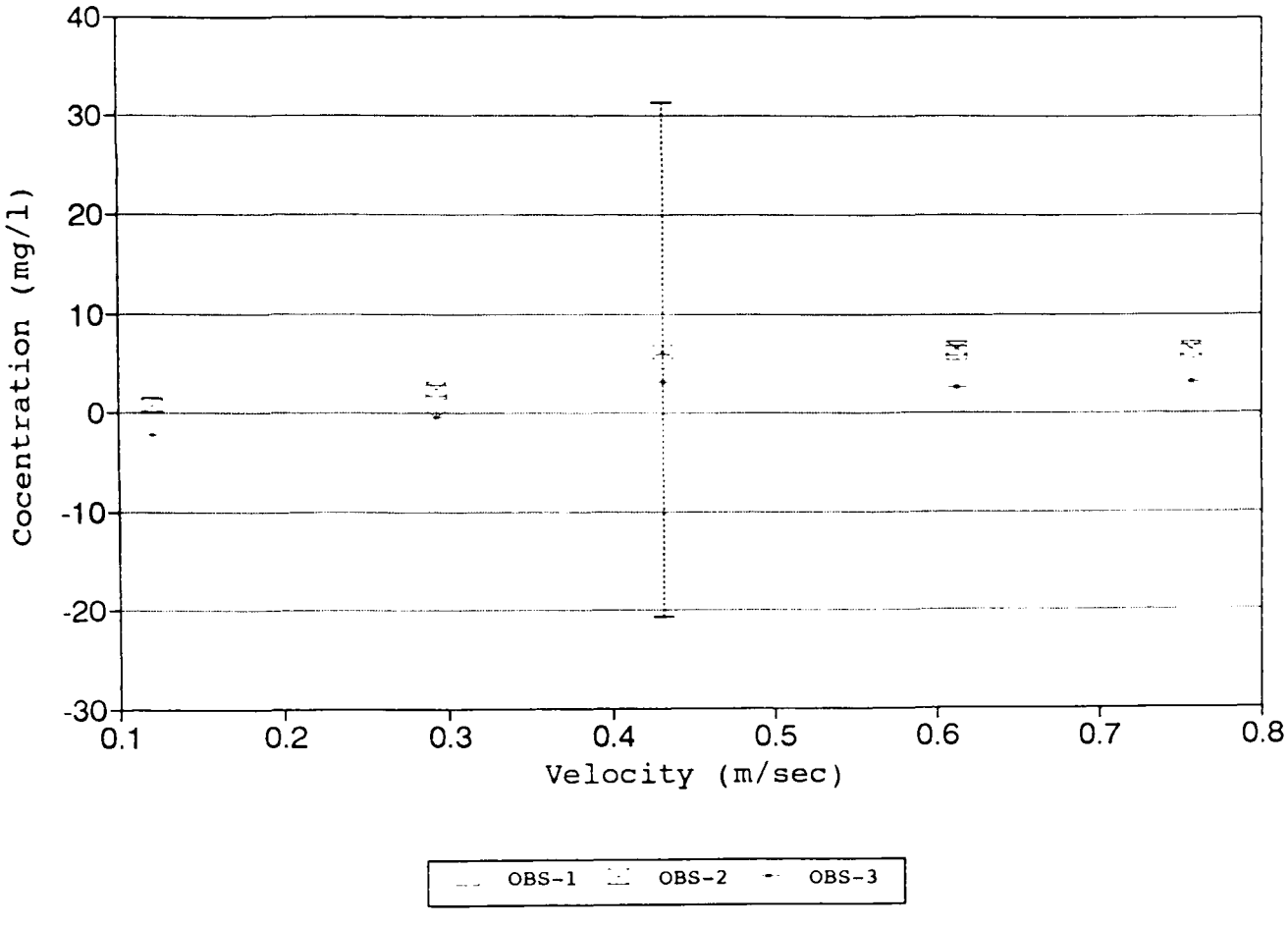

Figure (5.38b): Affect of Flow Velocity
on OBS Output, with suspended sediment.

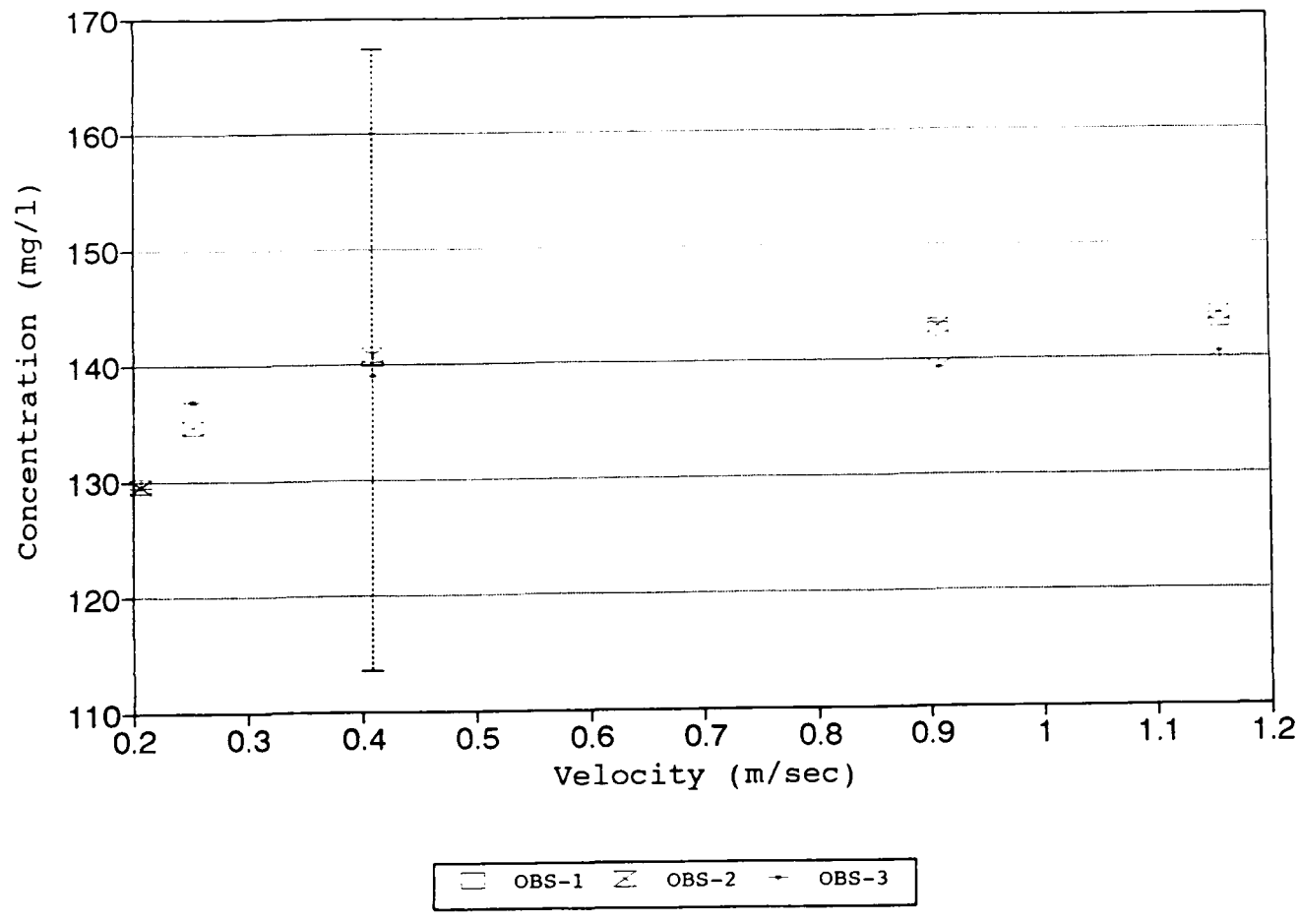

CHAPTER 6.

FLUME SEDIMENT EROSION EXPERIMENTS.

6.1 Experimental Strategy

The mud used in this investigation was collected from the mud flat at Glan Conwy, North Wales (Grid reference SH801763) (Figure 6.1). The upper part of the mud flat to a depth of 30 to 40mm was removed and placed into a 40 litre container and transported back to the laboratory. Small samples of this mud were used for analysis of: grain size distribution, clay mineralogy, specific density, total organic matter; for oedometer calibration of formation factor/porosity relationship; and the flume runs. Four mud collections were made, which from now on will be termed; Mud 1 collected 18/7/93, Mud 2 collected 26/8/93, Mud 3 collected 22/10/93 and Mud 4 collected 19/11/93. The decision to use remoulded mud was made to simplify the initial work, with the idea that further work would be carried out latter on real muds. Using remoulded muds allowed repeatable flume runs to be made and gave greater control over the properties of the mud (fluid could be added to the mud to increase its moisture content). Using the remixed mud made the identification of any relationships between bed properties and sediment erodibility easier without the complication of the more varied nature of real muds. One box core of a field mud was collected and run in the flume (run 34), but further development of the method of collecting the core and then inserting it in to the flume could not be made due to time restraints (the method used to insert the core into the flume meant that no bed property measurements could be made, only flow velocity, bed shear stress and OBS data were collected and therefore the data from this run is not used in the comparisons of the inter-relationships between bed properties and the relationships between bed properties and erosion threshold).

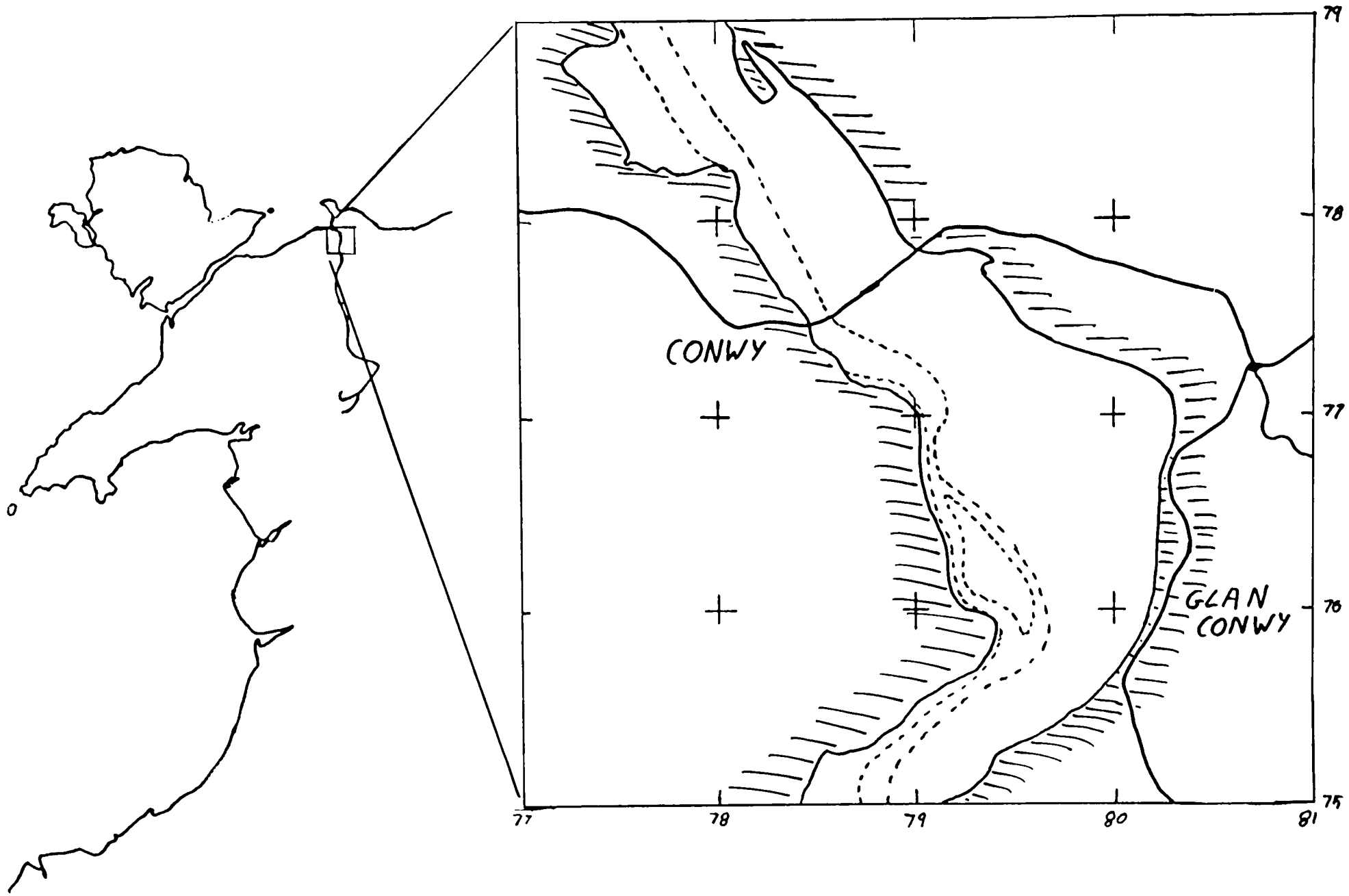

Figure (6.1): Location of the Glan Conwy mud flat.

For each flume run a small subsample of mud, about 4-5l was taken from the large field sample and mixed thoroughly in a bucket to a homogenous consistency and then poured in to the flume sediment box. Three smaller subsamples were then taken from the mud remaining in the bucket and used for the moisture content and density determinations. The temperature of the remaining mud in the bucket was measured and taken to be equal to the temperature of the mud in the sediment box. The temperature is needed for the computation of the formation factor. The pore fluid salinity is needed for the same reason, and this was obtained by taking a sample of the surface water of the field sample in the 40 litre container. This free surface water arises from the consolidation of the mud, and is mixed back into the mud prior to the mud being poured into the flume sediment box. With the sediment in the bed box, the three bed properties were measured at four levels in the mud; at the surface and then at three points down the bed at 10mm intervals. The reason for only measuring at four points was due to the constraint of the flume design which meant that the pressure, shear wave and electrical resistivity sensors were located in the middle of the bed box, thereby resulting in a maximum bed thickness of 60mm.

Once these bed properties had been measured the bed could be raised to bring its surface roughly level with the flume floor; the flume was then filled with sea water. The bed had to be raised to this level before the test section was filled with water, because water cascading over the edge of the bed box would generate scour pits at the edge of the sediment if the sediment was below the flume floor. Once the flume was completely full the bed level monitor could be used to adjust the bed height accurately to bring it level with the test section floor of the flume.

The flow could then be started and stepped up in 5Hz or 10Hz steps. The 10Hz steps were used at low velocities below the erosion threshold; 5Hz steps were used just below and above the threshold. At each step the velocity was kept constant for at least 10 minutes. The data from the velocity, stress and OBS probes was logged constantly and any temperature changes recorded. A record was also kept of the time at which each velocity increase occurred and notes were made of the bed behaviour.

Once the bed had started to erode it was kept level with the flume floor by using the bed level monitor. However erosion tended not to occur evenly across the bed and although the sensor was normally located a third of the way down the bed box, an indication of the overall erosion pattern was obtained by moving the bed level monitor over the flume lid in order to scan the mud surface.

Erosion continued until the flume reached maximum velocity, or the base of bed had reached it maximum height (this maximum point was 20mm below the flume floor). Data logging was then discontinued and the flume emptied and flushed out with saltwater to remove all sediment, leaving it clean for the next run. Data was not collected for the total erosion of the bed, because this would have involved the generation of a pit with complex flow conditions in order for the material below the level of the flume floor to be removed, and once the flow reached the base of the box any remaining material would be removed rapidly as the flow worked its way along the boundary and lifted the sediment up from underneath.

6.2. **Results.**

6.2.1. General Results

6.2.1.1. Specific Gravity

The specific gravity of the mud from Glan Conwy was measured by the previously described method (§5.2.4.4.) on four separate samples and the average was 2.67 with a maximum and minimum of 2.68 and 2.65, respectively.

6.2.1.2. Grain Size Distribution.

Grain size analysis was carried out using the previously defined method (§5.2.4.4.), and Figure 6.2 shows the cumulative frequency

Figure (6.2): Glan Conwy Grain Size Distribution.

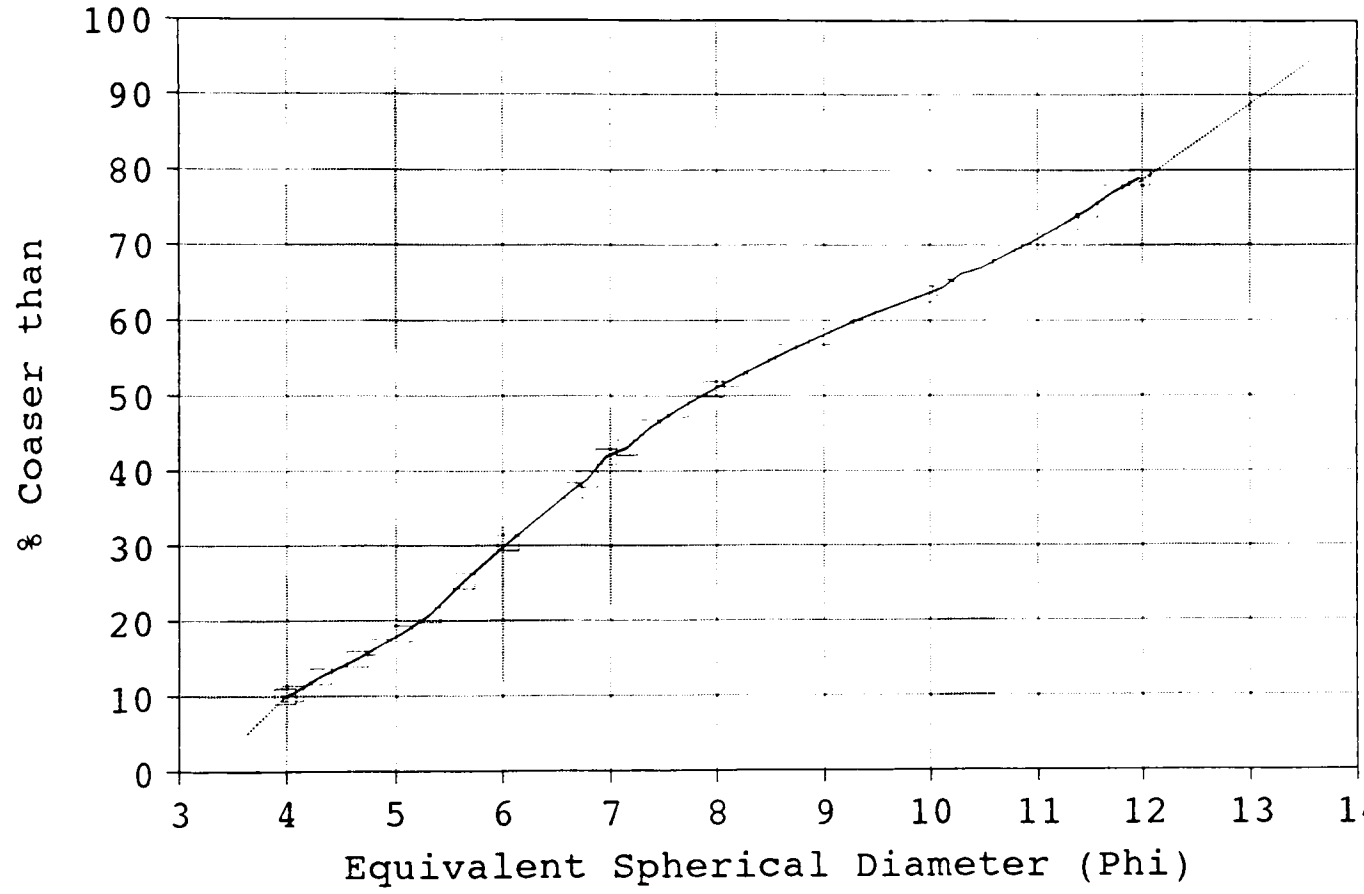

distribution for the mud from Glan Conwy. Using the graphical measures of distribution proposed by Folk and Ward (1957), the mean is 8.62φ units, standard deviation (sorting) is 3.45φ units and skewness is 0.10φ units. Because the extremes of the distribution w ere not analysed and the 95 and 5 percentiles had to be determined by extrapolation a more central measure of the skewness (Inman, 1952) may be more appropriate; this gave a skewness value of 0.19φ units. These parameters imply that the sediment can be defined as a very poorly sorted silty clay with a fine tail.

6.2.1.3. **Clay Mineralogy.**

X-ray diffraction analysis was carried out on the finer than 2 micron fraction of the sample and showed that the clay size fraction was mainly kaolinite, chlorite, vermiculite, and hydrous micas. Figure 6.3 displays the traces produced by the different treatments; untreated, Potassium chloride (K^+), Magnesium acetate (Mg^{+2}), Potassium chloride and heating to 500°C (K^+/500°C), Magnesium acetate and ethylene glycol (Mg^{+2}/Ethy), and Dimethyl sulphoxide (DMSO). These treatments are standard methods in clay mineralogical analysis (Jackson, 1964), although the DMSO treatment is less commonly used then the others and is specifically designed to aid the identification of kaolinite; it expands the kaolinite from 7.2Å to 11.2Å (Lim et al., 1981).

6.2.1.4. **Total Organic Matter, (TOM).**

The total organic matter (TOM) content of the four muds used in this study was determined by the method given previously (ϕ5.2.4.5.), and expressed as a percentage of the total dry weight of the sediment, were:

Mud 1	erosion runs 1 to 7	TOM = 7.3%	range 7.09%-7.52%
Mud 2	erosion runs 8 to 20	TOM = 6.4%	range 6.11%-6.57%
Mud 3	erosion runs 21 to 33	TOM = 7.2%	range 6.80%-7.87%
Mud 4	erosion runs 34 to 40	TOM = 8.4%	range 8.36%-8.52%

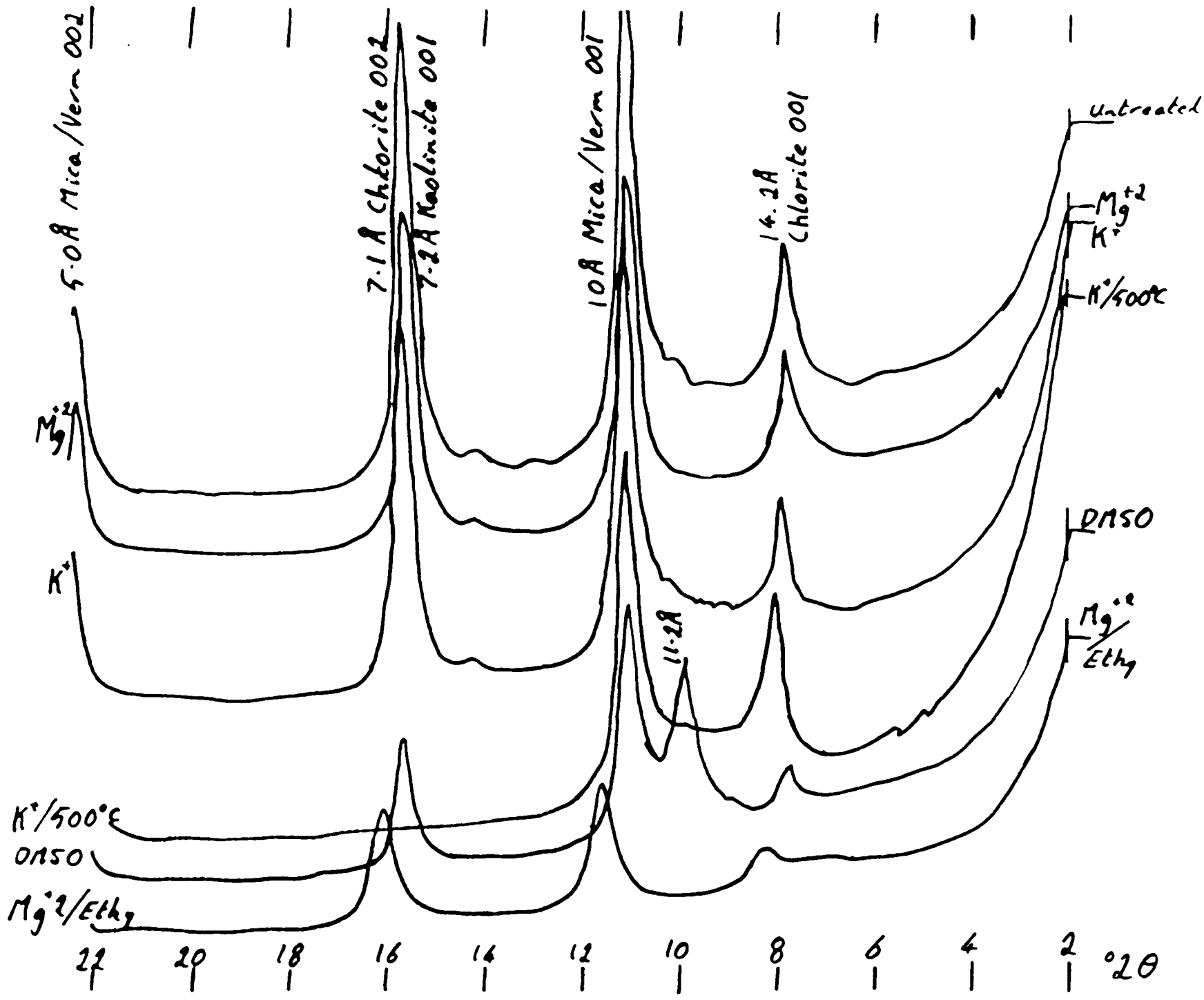

Figure (6.3): X-ray diffraction plots of the analysis carried out on the finer then 2 micron fraction of the mud from Glan Conwy.

Although the differences are small it appears that in terms of the TOM content muds 2 and 4 can be considered as distinctly different muds. However muds 1 and 3 although different from 2 and 4, could be regarded as the same mud in terms of the TOM content (mud 3 shows a range of values that includes those of mud 1). The TOM only represents the amount of organic material in the mud and not the nature of biological activity in the mud and in this sense although muds 1 and 3 have common TOM values the actual biological activity of the two muds may be different and therefore their physical properties may also be different. It may therefore be best to considered all of the muds as being different.

6.2.2. **Bed Property Results.**

Four bed properties (formation factor, shear wave velocity, pore pressure and moisture content) were measured on each sample of mud placed into the sediment bed box, prior to commencement of an erosion experiment. As already explained, a profile of these properties was made down each sample. The exception to this was the moisture content measurement which was made on a small subsample and is presumed to be representative of the average moisture content of the mud in the bed box. The pressure transducers did not work well and it was impossible to interpret the results meaningfully, therefore their results are not given.

The individual profiles of each run vary widely in their general format. However in general, shear wave velocity and formation factor would be expected to increase with decreasing porosity as the sediment becomes more densely packed, pore spaces are compressed and particle to particle contacts increase. It would be surmised that shear wave velocity and formation factor would increase down the profile in the sediment box due to the weight of sediment above. The degree of this compaction will vary with time and initial moisture content. In comparing different samples' shear wave velocity and formation factor data, they should show a positive correlation to each other (high formation factor corresponds to high shear wave velocity) and they should both show a negative correlation with moisture content (low formation factor and shear wave velocity to high moisture content). This is a very simplified view and would be presumed

to occur if formation factor is only controlled be porosity and shear wave velocity is solely determined by the number of particle to particle contacts. However, this is not strictly true and, as already explained in earlier chapters, formation factor and shear wave velocity are affected by other properties of the bed as well.

Table 6.1a,b shows two examples of the profiles that were generally obtained. These show a general increase in both shear wave velocity and formation factor with depth, although the deepest values (level iv) are apparently anomalous.

Table 6.2a,b,c,d are examples of some other more complex profiles that were obtained. Table 6.2a has an increase in shear wave velocity with depth but no correlation between velocity and formation factor. Table 6.2b also displays no correlation between velocity and formation factor but it does have an increase in formation factor with depth (the level B in Table 6.2b and 6.2c is the surface level, prior to an alteration of the sediment box which reduced the allowable bed thickness and made level I the surface level from then on). Table 6.2c shows no depth variation but a good positive correlation between velocity and formation factor (significant at a 5% level). On the other hand Table 6.2d shows an apparent negative correlation and an increase in velocity with depth.

The possible causes of the variations in the bed properties can be separated into two main parts; errors in the measurements, and changes in the mud properties. Errors in the measurement of the shear wave velocity are dominated by the accuracy with which the onset of the shear wave can be discerned from the noise in the signal. In general the higher the porosity the more difficult the onset is to see, as the greater the attenuation of the shear wave signal is. The other possible error is that the distance the signal was assumed to have travelled was the shortest distance between the tips of each bender element. Although the same distance was used in all cases, the path length of the signal could vary, due to changes in mud properties (the quickest path may not have been by the shortest distance). The errors in the measurement of formation factor are far more numerous. Two major errors are errors in the salinity and temperature measurement, both of which will affect the calculated formation factor,

Profiles

Run 40		
Level	Shear Wave Velocity (m/s)	Formation Factor
I	----------	1.121
II	0.580	1.133
III	0.755	1.203
IV	0.717	1.122

(a)

Run 31		
Level	Shear Wave Velocity (m/s)	Formation Factor
I	0.995	2.042
II	1.336	2.068
III	1.466	2.178
IV	1.375	2.042

(b)

Table (6.1): General bed profile examples.

Run 28		
Level	Shear Wave Velocity (m/s)	Formation Factor
I	0.751	1.710
II	0.988	1.649
III	1.161	1.770
IV	1.194	1.699

(a)

Run 22		
Level	Shear Wave Velocity (m/s)	Formation Factor
B	2.088	1.221
I	6.693	1.497
II	1.889	1.524
III	2.174	----------
IV	----------	1.577

(b)

Run 26		
Level	Shear Wave Velocity (m/s)	Formation Factor
B	2.485	1.420
I	2.742	1.761
II	2.522	1.741
III	2.769	1.946
IV	3.243	1.839

(c)

Run 38		
Level	Shear Wave Velocity (m/s)	Formation Factor
I	1.308	1.324
II	1.341	1.250
III	1.389	1.317
IV	1.540	1.236

(d)

Table (6.2): More complex examples of bed profiles.

although the salinity has a far greater affect then the temperature. The other main error is due to inaccuracies in determining the cell constants used to determine the formation factor, but this error will be constant for all measurements as the same set of cell constant equations was used for all of the data.

The other cause of variation in the data relates to changes and heterogeneity in the mud itself. These include:

a) The remixing of the mud before it was placed into the box was not absolutely consistent and some variation could occur. Although every effort was made to make sure that the mud was fully mixed, contained no lumps and was homogenous, possible differences on a microscopic structural scale between the different mixes cannot be ruled out.

b) These structural variations may be related to the time that the mud had been left undisturbed and able to consolidate in the container used for collecting the mud from the field and then storing it in before it was use in the flume.

c) The rate and way in which a mud consolidates and expels excess pore fluid is affected by the initial moisture content of the mud. The bed property measurements were made as quickly as possible after the mud had been pored into the box. However in some cases the mud displayed a gradient from top to bottom but in other cases it did not, and this was possibly due the manner of consolidation that was occurring in the mud.

d) The biological activity does not remain constant. Within a few days of the mud being brought to the laboratory, no visible activity could be seen, although activity on a microscopic scale was definitely occurring. These changes in the biological activity will alter the properties and characteristics of the sediment.

Given these variations and discrepancies between individual profiles, it was decided to compare bed property profiles of different runs in two ways; 1) using the average of the profile measurements (the average is of all measurements in the profile including the surface value): and 2) using only the individual surface measurements. The reason for this, is that the average values represent the general properties of the bed, whilst the surface property should be the more important in relation to initiation of erosion. These vales are given in Tables 6.3 and 6.4 for muds 1 & 2 and

Flume Run	Moisture Content %	Vss (m/s)	Vsa (m/s)	FFs	FFa
1	----------	5.313	3.031	1.846	1.746
2	127.26	2.408	2.681	0.754	1.246
3	120.46	4.315	4.315	----------	1.351
4	113.14	1.771	1.910	1.629	1.749
5	----------	4.359	4.359	----------	----------
6	117.76	1.133	1.133	----------	----------
7	111.51	0.899	1.049	1.970	2.219
8	114.55	1.589	1.176	1.737	1.960
9	116.17	2.073	1.250	1.705	1.827
10	115.97	1.232	1.201	1.903	2.208
11	105.76	0.966	1.301	1.893	2.129
12	137.04	----------	0.386	1.838	2.207
13	123.76	----------	0.620	1.984	2.362
14	109.14	1.574	1.740	2.103	2.452
15	114.03	0.859	0.993	1.694	2.189
16	115.54	0.919	1.467	2.139	2.338
17	111.31	1.667	4.235	2.084	2.356
18	111.55	4.474	9.748	1.558	1.977
19	111.16	1.717	1.903	2.077	2.410
20	107.09	2.408	3.088	1.552	2.277

Table (6.3): Results of Flume Runs for muds 1 and 2.

Flume Run	Moisture Content %	Vss (m/s)	Vsa (m/s)	FFs	FFa
21	131.94	2.576	3.913	1.407	1.621
22	136.15	2.088	2.472	1.221	1.455
23	121.88	1.995	2.035	1.393	1.591
24	115.54	1.793	2.339	1.355	1.615
25	114.41	3.795	2.870	1.294	1.594
26	116.16	2.485	2.738	1.420	1.741
27	110.82	2.628	2.781	1.532	1.711
28	113.87	0.751	0.990	1.710	1.707
29	118.43	0.777	1.289	----------	----------
30	148.42	----------	0.610	1.552	1.473
31	131.51	0.995	1.265	1.525	1.555
32	145.38	----------	0.750	1.468	1.493
33	156.81	----------	0.907	1.614	1.508
34	----------	----------	----------	----------	----------
35	142.57	1.130	1.604	1.160	1.066
36	142.57	1.042	1.329	1.088	1.053
37	147.14	1.111	1.403	1.179	1.130
38	147.14	1.308	1.389	1.324	1.282
39	137.93	1.451	1.517	1.266	1.196
40	162.10	----------	0.675	1.121	1.145

Table (6.4): Results of Flume Runs for muds 3 and 4.

Vsa & Vss - Average and Surface sediment Shear Wave velocity respectively.

FFa & FFs - Average and Surface sediment Formation Factor respectively.

muds 3 & 4, respectively. Using the results of the oedometer work (§4.2.3.4.) the formation factors were converted into porosities and these are compared, in Figures 6.4a,b to the porosity values determined (assuming 100% saturation) from the moisture content analysis results (Tables 6.3 and 6.4). In these two graphs each mud is represented by a different symbol and the straight line gives the ideal relationship where the porosity derived from formation factor is equivalent to porosity obtained by moisture content analysis.

These figures show two main features. 1) The average results although scattered do relate better to the sampled porosity than the surface results which have a higher degree of scatter. 2) The results can be split into two main groups; group A containing muds 1 and 2 whose formation factor porosities do not correspond well with the sample porosities, and group B containing muds 3 and 4 whose formation factor porosities do correspond well to the sample porosities. Nearly all of the formation factor porosities for muds 3 and 4 over-estimate the porosity by one or two percent. This is most likely due to the profiling method used, which only measures bed properties in the upper three quarters of sediment in the box (in order to avoid damage to the shear wave bender elements from the moveable base of the box), therefore the average is weighted in favour of the higher porosity near-surface sediments and is a representative average value of the upper three-quarters of the bed (as already stated this was the part of the bed that was eroded with a the bottom quarter of the bed remain at the end of a run). However the surface values appear to show no relation to the measured porosity and only approach the measured porosity at the higher moisture contents. This could be due to changes in the rate of consolidation of the mud with changing moisture content. Another problem with the measurement of surface formation factor, is that pore fluid expelled as the sediment consolidates forms a layer at the surface of the mud and will alter the measured resistivity. Also any errors in the equations used to generate the cell constants (used in the resistivity measurement to correct the measured resistance to a true resistance) will be greatest at the surface due to its proximity to a boundary (the surface).

Fig (6.4a): Porosity from average FF
and porosity from samples.

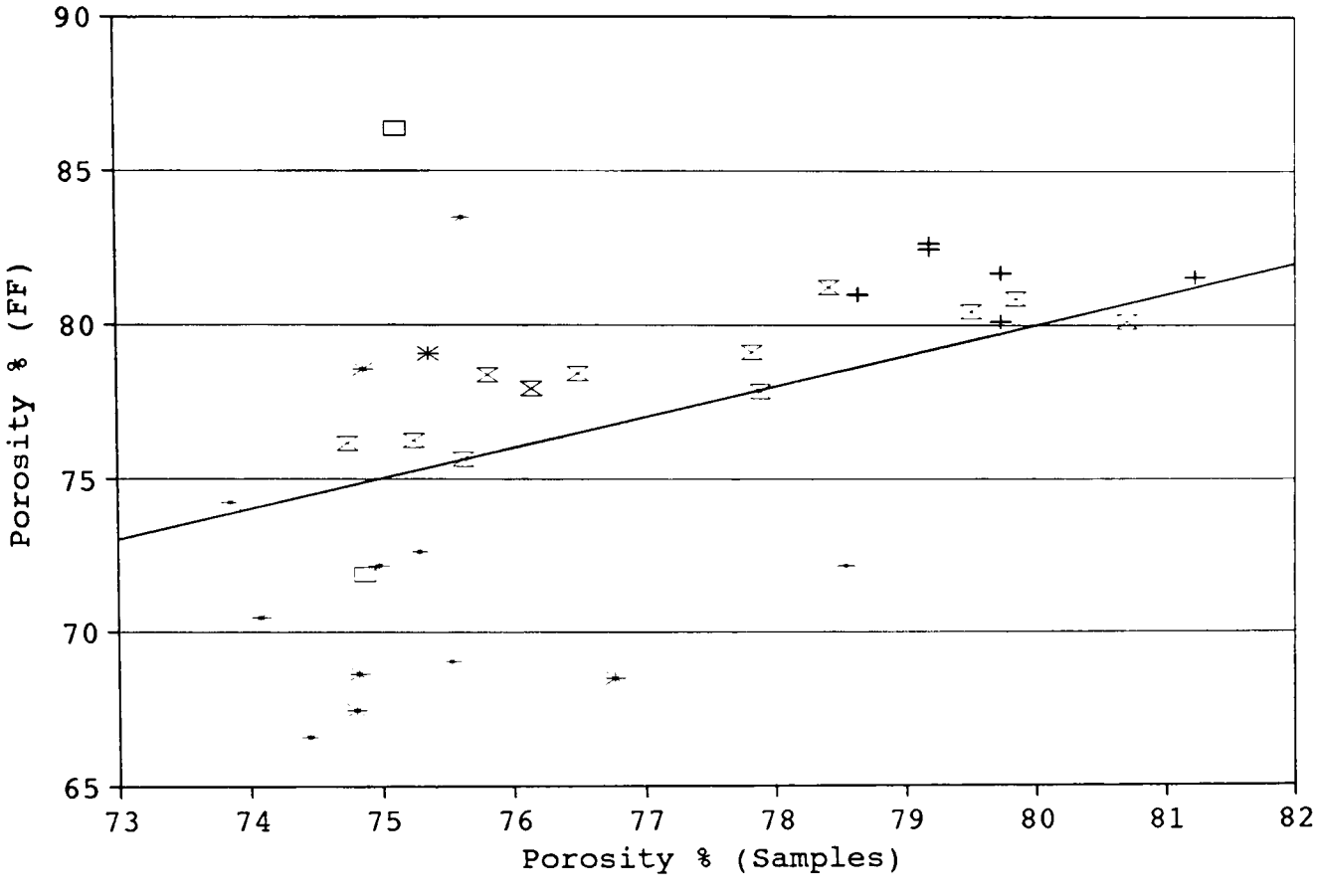

Fig (6.4b): Porosity from surface FF
and porosity from samples.

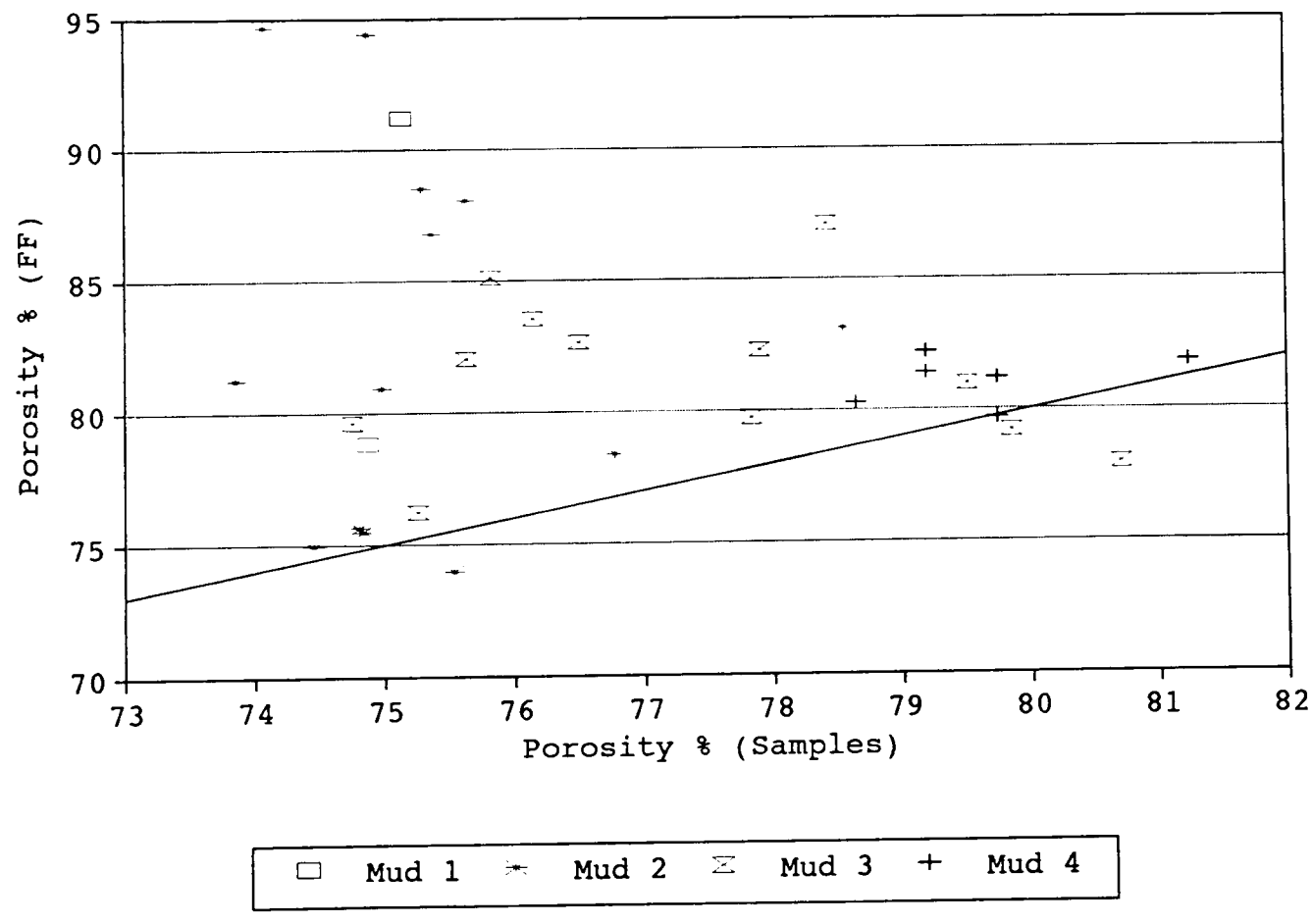

Using these plots and the other bed property data, it was decided to concentrate in more detail on muds 3 and 4 rather than muds 1 and 2. The reason that muds 3 and 4 have better quality data than muds 1 and 2 is due to improvements in experimental technique and equipment. During the experiments on muds 1 and 2, the techniques of mud preparation, insertion of mud into the flume, how the bed properties were measured, salinity and temperature measurement were all improved and refined, so that a good and repeatable method was used on muds 3 and 4. Minor changes were also made to the flume in order to improve it and a better filtering system was used for the shear wave measurements, for muds 3 and 4.

6.2.2.1. **Interrelationship of Bed Properties.**

For muds 3 and 4 the bed property interrelationships of the average and surface results are shown in Figures 6.5 and 6.6, respectively. Spearman's rank correlation coefficient was used to measure the significance of the correlation between individual bed properties for muds 3 and 4, and Table 6.5 shows the results for the individual muds and for the two muds combined (This is a nonparametric test of association used for data which is known not to be bivariate normally distributed like the data in this study (Sokal and Rohlf, 1981)). The lines in Figures 6.5 and 6.6 are there to show the trends of the significant relationships, although the actual relationships are unlikely to be linear. However the shear wave velocity values of runs 28-29 were not used in these calculations (the shear wave data for runs 28 and 29 are shown in the two figures as a cross within a square) due to their low shear wave velocity values (run 29 also had no formation factor data). The anomalous results of runs 28 and 29 are more likely due to experimental error in observing the onset of the shear wave (caused by external vibrations), than to a variation in the mud properties. These external vibrations were caused by heavy construction work that was going on in close proximity to the laboratory at the time of these runs and the shear wave sensors were affected by these vibrations.

The average results of mud 3 show significant correlations, but mud 4 average results do not. This arises because mud 3 covers a wide moisture

Fig (6.5a): Average Formation Factor and Shear Wave velocity.

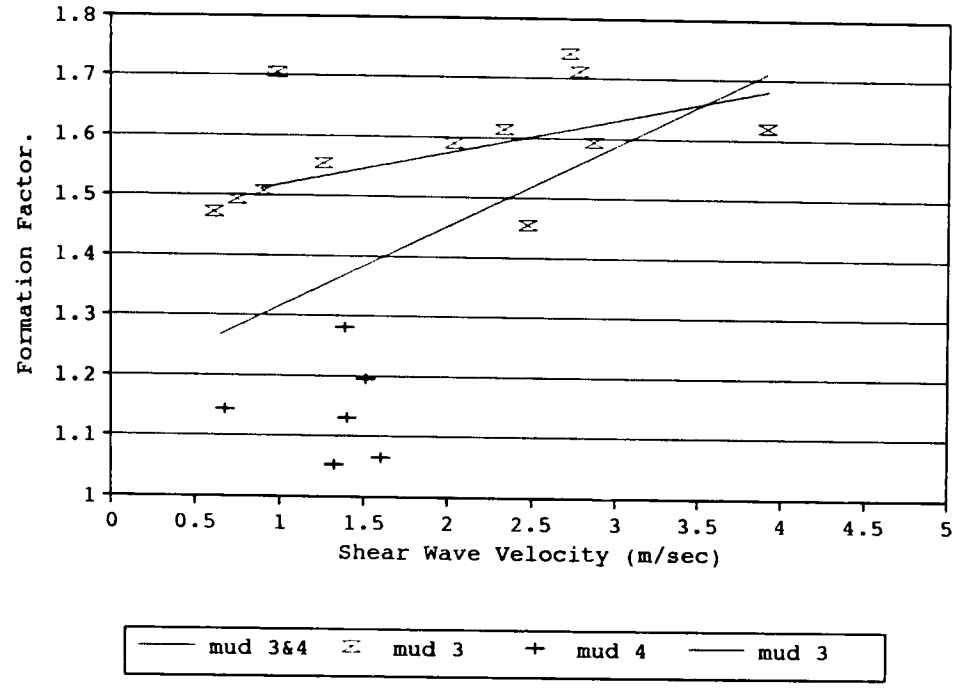

Fig (6.5b): Moisture Content and Average Shear Wave Velocity.

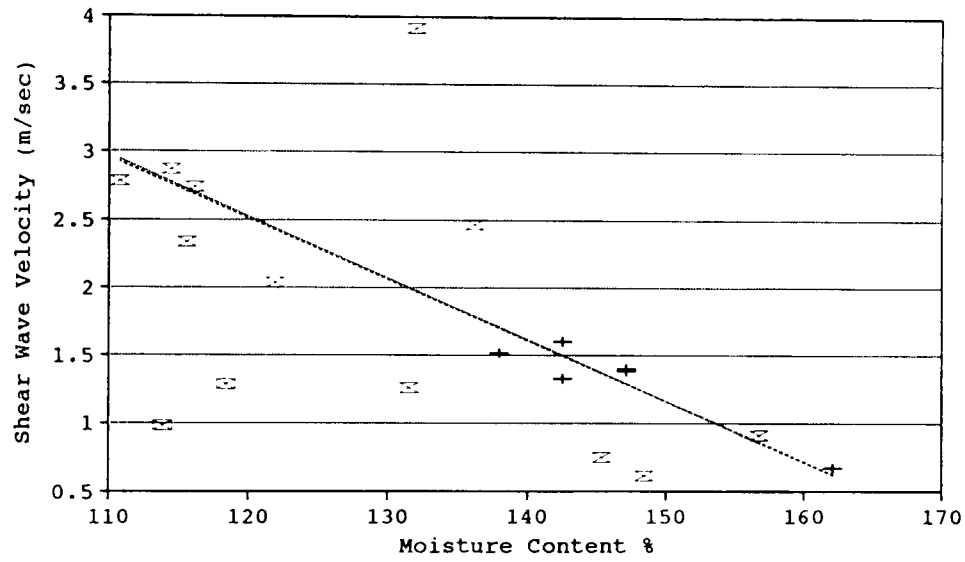

Fig (6.5c): Moisture Content and Average Formation Factor.

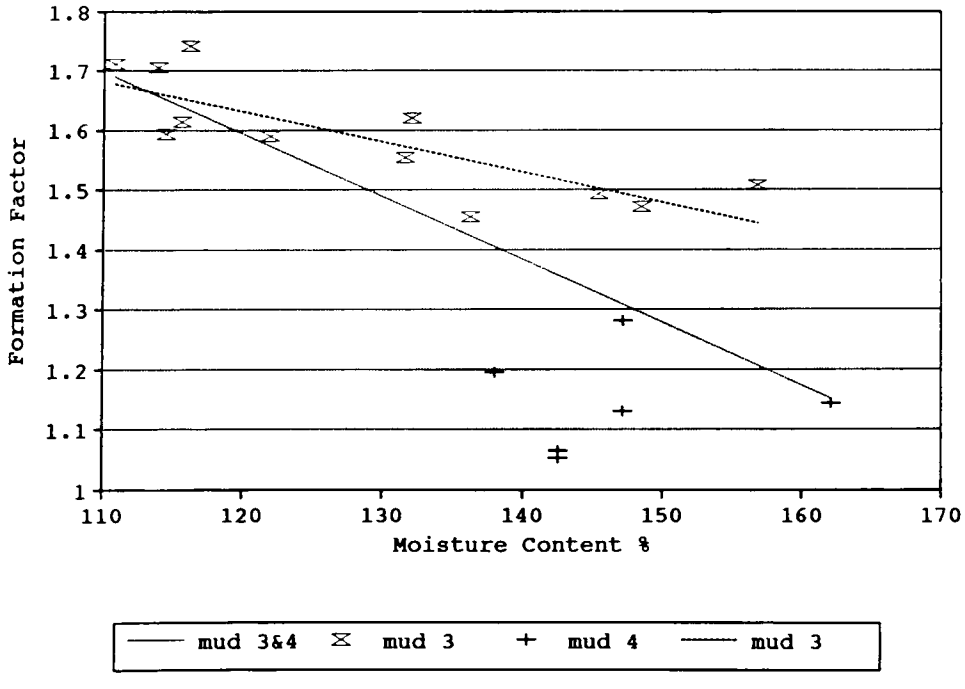

Fig (6.6a): Surface Formation Factor and Surface Shear Wave velocity.

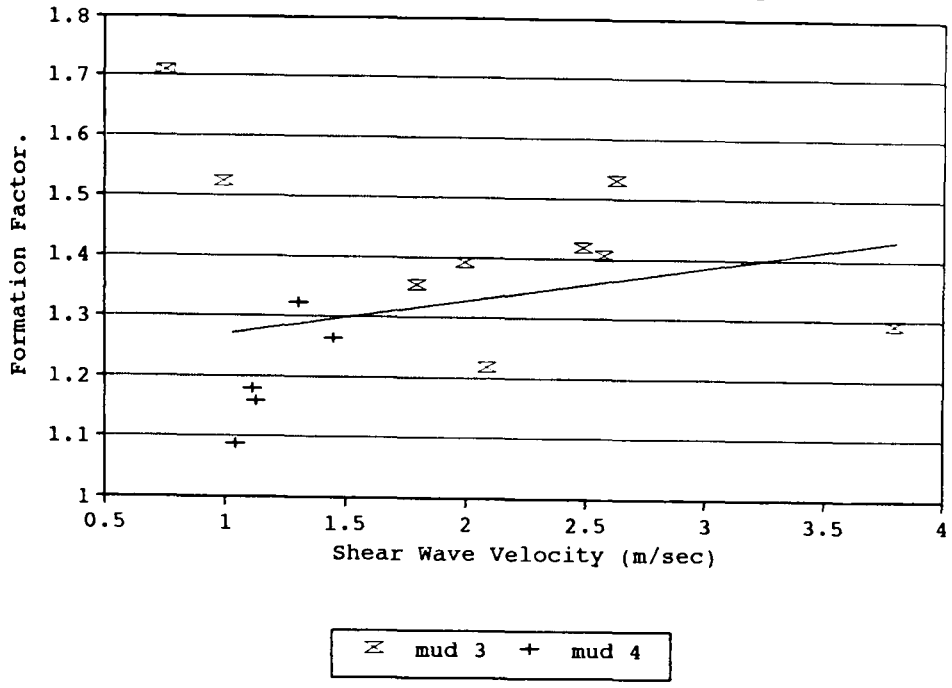

Fig (6.6b): Moisture Content and Surface Shear Wave velocity.

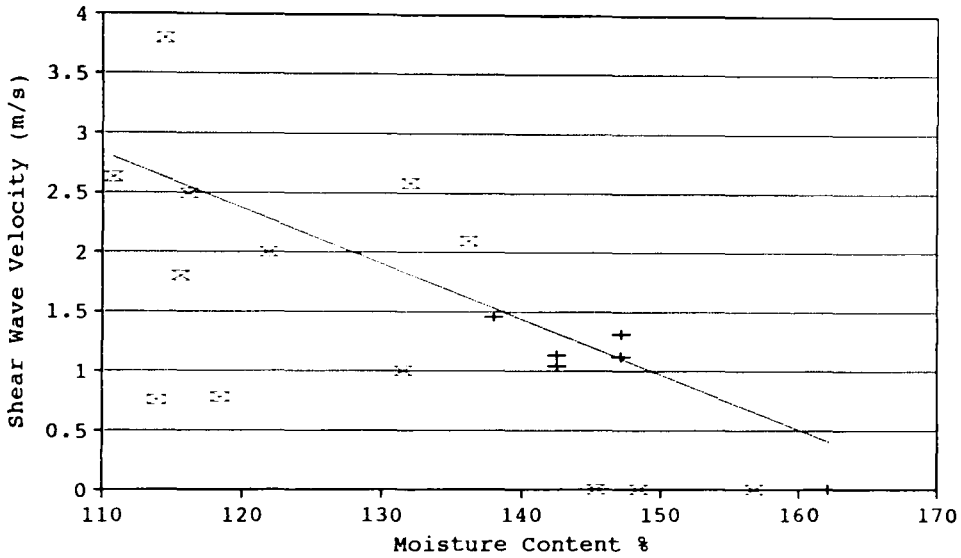

Fig (6.6c): Moisture Content and Surface Formation Factor.

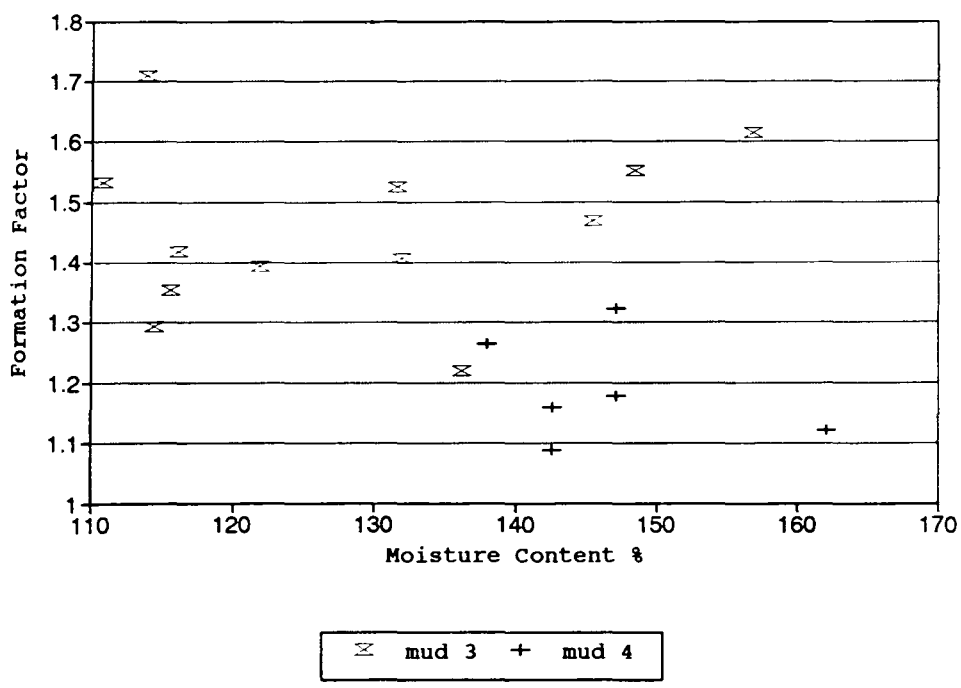

Mud 3

	Average Values			Surface Values		
	Correlation coefficent	No. of Values	Significance %	Correlation coefficent	No. of Values	Significance %
Vs - FF	0.691	11	10	-0.024	8	n/s
Vs - w	-0.673	11	10	-0.429	8	n/s
FF - w	-0.776	12	2	0.105	12	n/s

Mud 4

	Average Values			Surface Values		
	Correlation coefficent	No. of Values	Significance %	Correlation coefficent	No. of Values	Significance %
Vs - FF	-0.029	6	n/s	0.800	5	n/s
Vs - w	-0.647	6	n/s	-0.316	5	n/s
FF - w	0.206	6	n/s	-0.088	6	n/s

Mud 3/4

	Average Values			Surface Values		
	Correlation coefficent	No. of Values	Significance %	Correlation coefficent	No. of Values	Significance %
Vs - FF	0.564	17	10	0.423	13	20
Vs - w	-0.809	17	2	-0.694	13	2
FF - w	-0.737	18	2	-0.280	18	n/s
n(FF)-w	0.771	18	2	-0.240	18	n/s
Vs-n(FF)	-0.623	17	2	0.363	13	n/s

Table (6.5): Spearman's Rank Correlation Coefficients of the bed property relationships of Muds 3 & 4.

Vs - Sediment Shear Wave velocity.
w - Sediment Moisture Content.
FF - Sediment Formation Factor.
n/s - Not Significant.
n(FF) - Sediment Porosity derived from Formation Factor.

content range (110%-157%) but mud 4 only covers a small range of moisture contents (137%-162%), and as Figure 6.5 and 6.6 demonstrate it is only over a significant moisture content range that any trends in the data become visible. The combined average results cover a wider spread of moisture content values (110%-162%) and there is some improvement in the significance of the correlation coefficients.

The combined shear wave data appear to show that muds 3 and 4 could be considered as one mud, but the formation factor data point to the two muds being different. The only other property measured that varies between the two muds is the TOM. The change in biological activity that causes this change in the TOM could alter the electrical formation factor, by affecting the behaviour of the diffuse double layer of the clay minerals, by altering the conductivity on the surface of the other particles in the mud, or by changing the proportions of the different dissolved ions in the pore fluid and thereby changing the pore fluid conductivity. These will affect the formation factor without necessarily affecting the shear wave velocity, although a variation in shear wave velocity would be expected as alteration of the diffuse double layer would probably change the character of the particle to particle contacts, which are an important control of shear wave velocity. By converting the formation factor values to porosity (using the corrections determined by the oedometer experiments) the correlations with shear wave velocity and moisture content for the combined data are improved. This reinforces the idea that the two muds are different in terms of resistivity measurements, as different equations are used for the two muds to convert the electrical formation factor data to porosity.

The surface results only show any significant correlations when the two muds are grouped together. Although the formation factor results do not correlate with moisture content, they do correlate with the shear wave velocity. This again appears to show that a bed property other than moisture content is affecting the formation factor. This could relate to changes that occur in the mud with time, and one of the major changes that occurs to the mud once it has been brought in to the laboratory is the shift in biological activity. Within a few days of the mud being collected activity on a meso scale stops and the organisms die, leaving only activity on a microscopic scale, and this microscopic activity can alter the electrical

conductivity of the mud in the ways outlined above. This would be expected to affect the average results as well. As already suggested a change in the manner of consolidation could be occurring with the changing moisture content, but what ever the effect is, it does not appear to be affecting the surface shear wave velocity measurements which do show a significant correlation to moisture content.

6.2.3. Erosion Runs, Flume Results

The collected data of flow velocity, bed shear stress and suspended sediment concentration logged during each flume run at a frequency of 1HZ, were initially converted from the recorded digitalization units into volts and then using the calibration equations (Chapter 5) transformed into equivalent physical units of meters per second, Newtons per square meter and milligrams per litre, respectively. Once this had been completed further analysis could be preformed with the principal aim of using the suspended sediment data to determine erosion rates (ε), and then using this and the bed stress data to calculate a threshold shear stress for the initiation of erosion.

6.2.3.1. Analysis of Results

The raw data (data that have already been converted into physical units) collected from each flume run had to be further manipulated to make analysis and comparison of all flume runs possible. This manipulation involved; correcting the hot film data for temperature variations, despiking the data, and averaging the data.

Affect of Temperature Correction

As already stated above ($\oint$5.2.1.), it is necessary to correct the hot film data for changes in the water temperature of the flume over the time period of an erosion run. The temperature during a run only ever increased and never decreased. This was because the sea water that was used was stored outside and was always at a lower temperature than the

laboratory in which the flume work was conducted. The water therefore slowly warmed up towards room temperature over the course of a flume run. There may also of been some warming due to friction generated by the circulation, but direct warming by the motor was unlikely, as the motor drove the impeller via a toothed belt and a forced fan connected to the motor stopped it from running at an elevated temperature.

The temperature correction is given by equation 5.1 and is different for the three sensors used, due to their various calibration temperatures. Below is an example of the different corrections required for each sensor at a water flow temperature of 10°C.

Probe	Calibration Temperature	Flow Temperature	Correction factor
1	13.5	10	0.8804
2	25.4	10	0.5366
Stress	12.0	10	0.9822

A change in the flow temperature of ±1°C, increases or decreases the correction factor correspondingly by 3.5% for the velocity sensors (1 and 2) and 0.9% for the stress sensor. Figure 6.7 shows the affect of temperature correction on the first 1600 seconds of flume run 39. As can be seen in both the velocity and stress data (although more easily in the velocity data) the correction is very significant and without it the data obtained would be wholly inaccurate.

In the case of the velocity data, the temperature correction could be carried out after transforming the data from volts to physical units, because of the linear relationship between voltage output (from the lineariser) of the sensor and velocity. However the relationship between shear stress and sensor output voltage is nonlinear and therefore the temperature correction must be carried out on the voltage data before it is transformed into Newtons per square metre. The suspended sediment concentration measured by the optical back-scatter sensors requires no temperature correction, as the sensor itself contains a temperature compensation unit.

Fig (6.7a): Raw Data before Temperature Correction, Run 39.

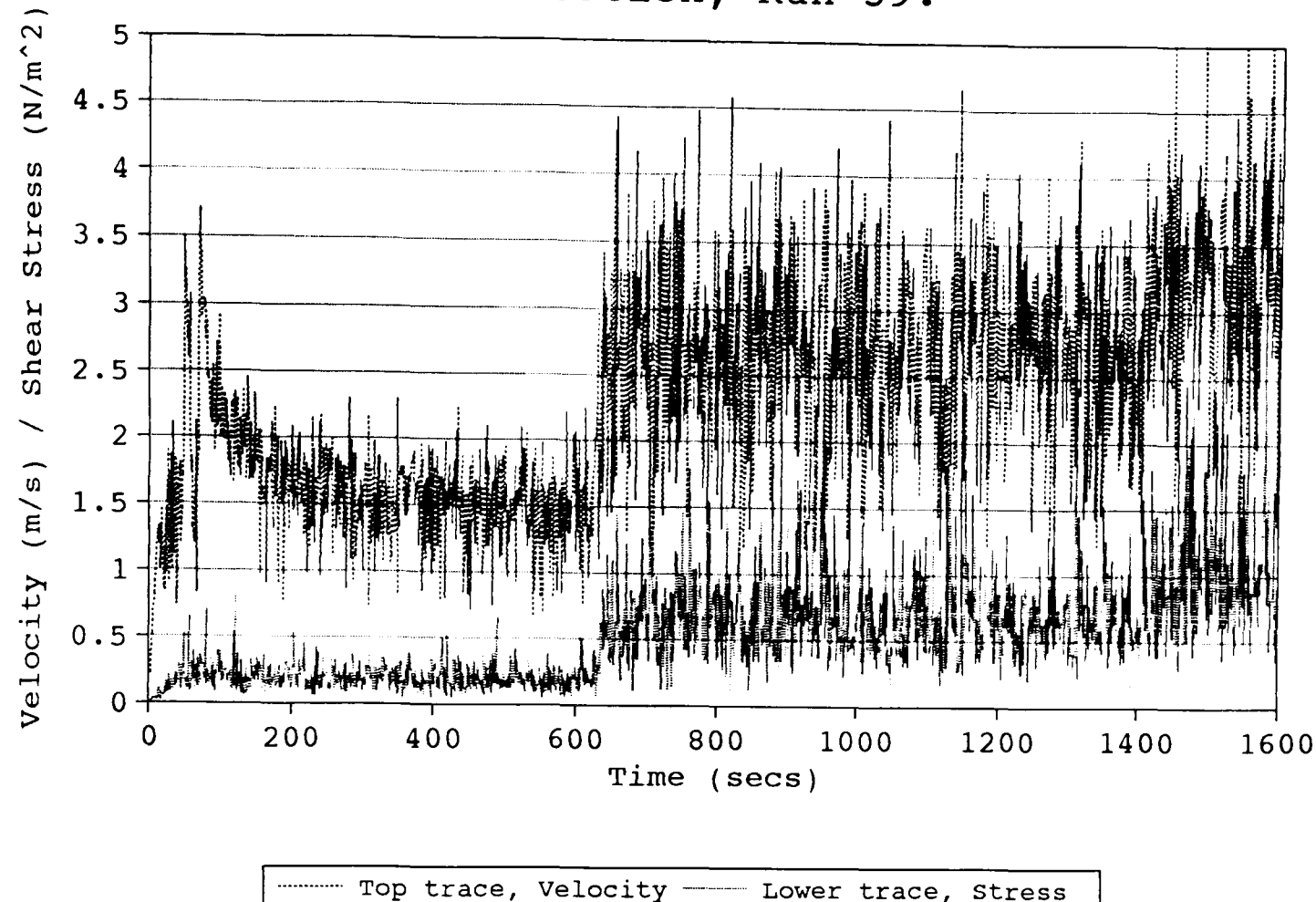

Fig (6.7b): Temperature Corrected Data, Run 39.

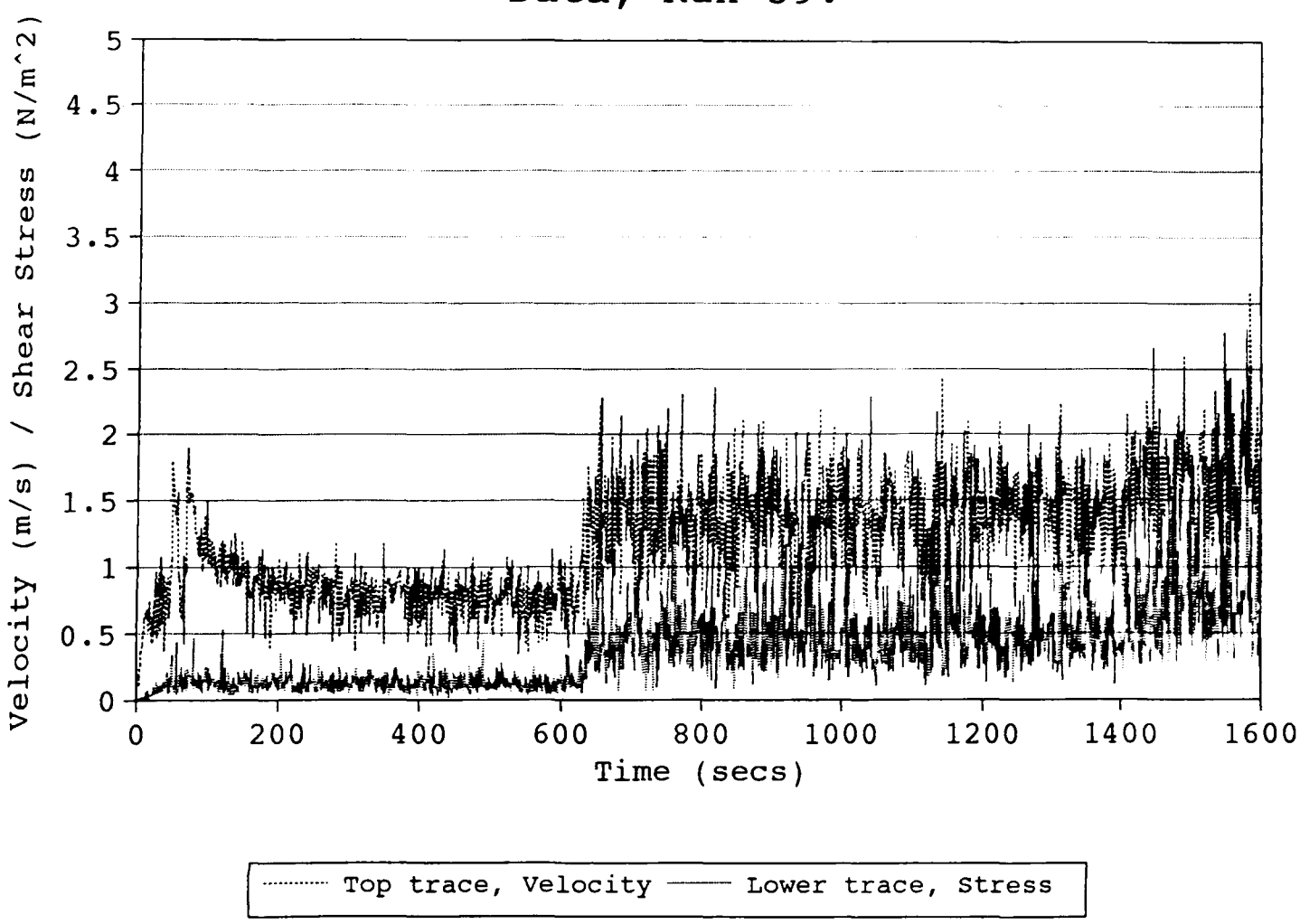

Despiking of Data

After being corrected for temperature variations the data was then despiked to remove any extreme high or low values. The same method as Amos et al. (1992) was applied, in which each twenty seconds of data was averaged and then any values that deviated from the mean by more then two standard deviations were replaced by the previous value within two standard deviations of the mean. The affect of this on the data set is minimal and very difficult to see graphically, Figure 6.8 (the affect of despiking can be seen by the absence in Figure 6.8b of some of the larger spikes visible in Figure 6.8a). The suspended sediment data was also despiked but due to the few erroneous values the affect is impossible to see graphically.

Data Averaging

Both operations of temperature correction and despiking have been carried out on the total data set. However to make the data more manageable and clearer to see, twenty second averages were obtained. As well as making the data clearer, this also removed the short timescale rapid changes that are indicative of the turbulent nature of the flow, and gives an average flow rate and bed shear stress. The character of the suspended sediment data was already fairly smooth due to the rapid mixing of eroded material by the flow. Nevertheless averaging did remove the wave-like features of the suspended sediment data (Figure 6.9) that occurred at low concentrations when erosion of the bed occurred suddenly and then halted, e.g a sizeable lump of the bed surface was eroded and then erosion halted or continued at a very low level. The result of this was that a parcel of water would circulate around the flume with a higher than average suspended sediment concentration, until after about 8 to 16 circulations (depending on initial maximum concentration) the suspended sediment had been dispersed throughout the water in the flume. It is this circulating packet of higher turbidity water that generates the wave like appearance in the suspended sediment data. Averaging the data, although not fully removing this feature, did reduce its magnitude, so that the suspended sediment data better reflected the total amount of material in suspension in the flume over the twenty second time period.

Fig (6.8a): Temperature Corrected Data
Prior to Despiking, Run 39.

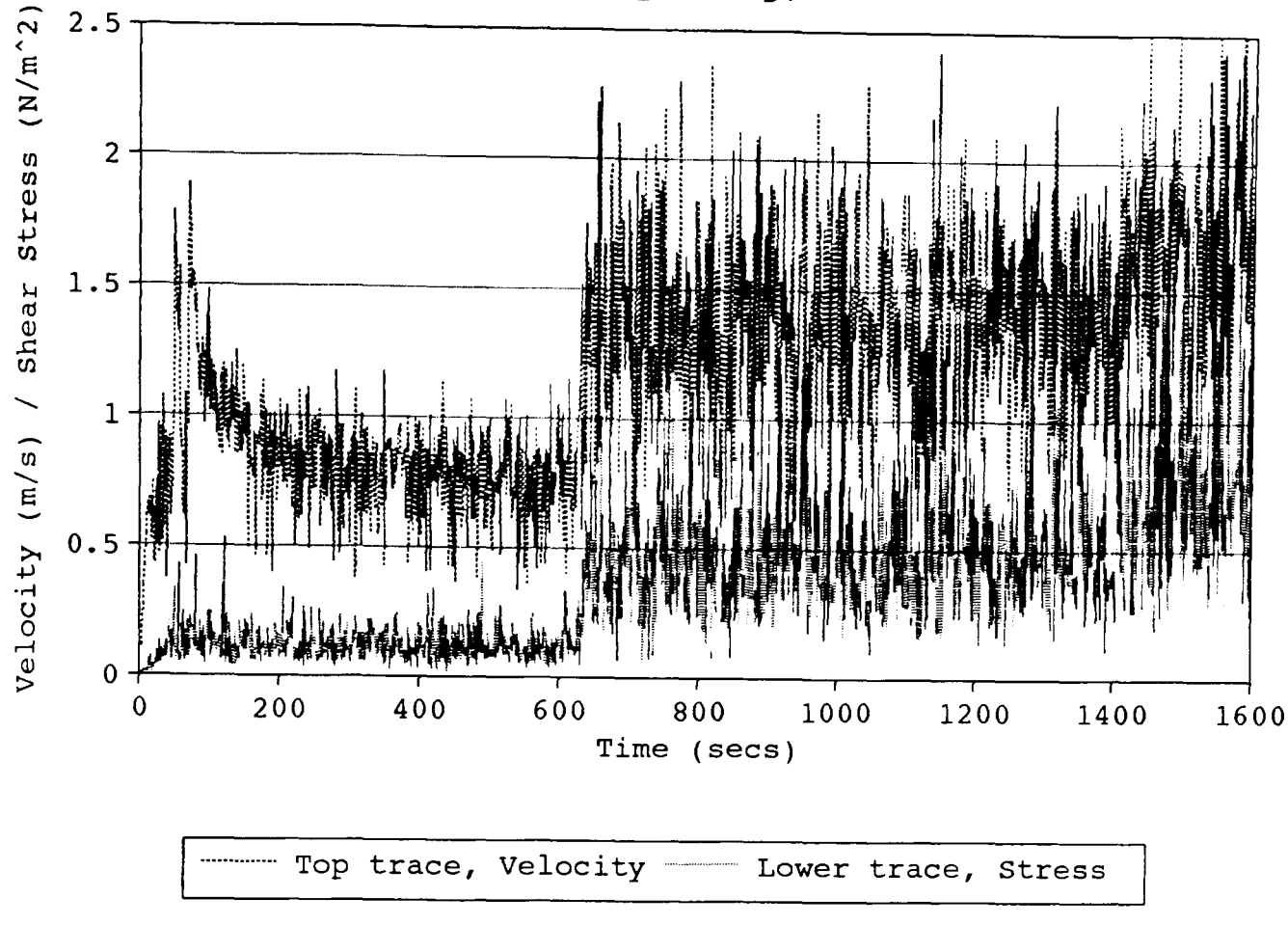

Fig (6.8b): Despiked Data,
Run 39.

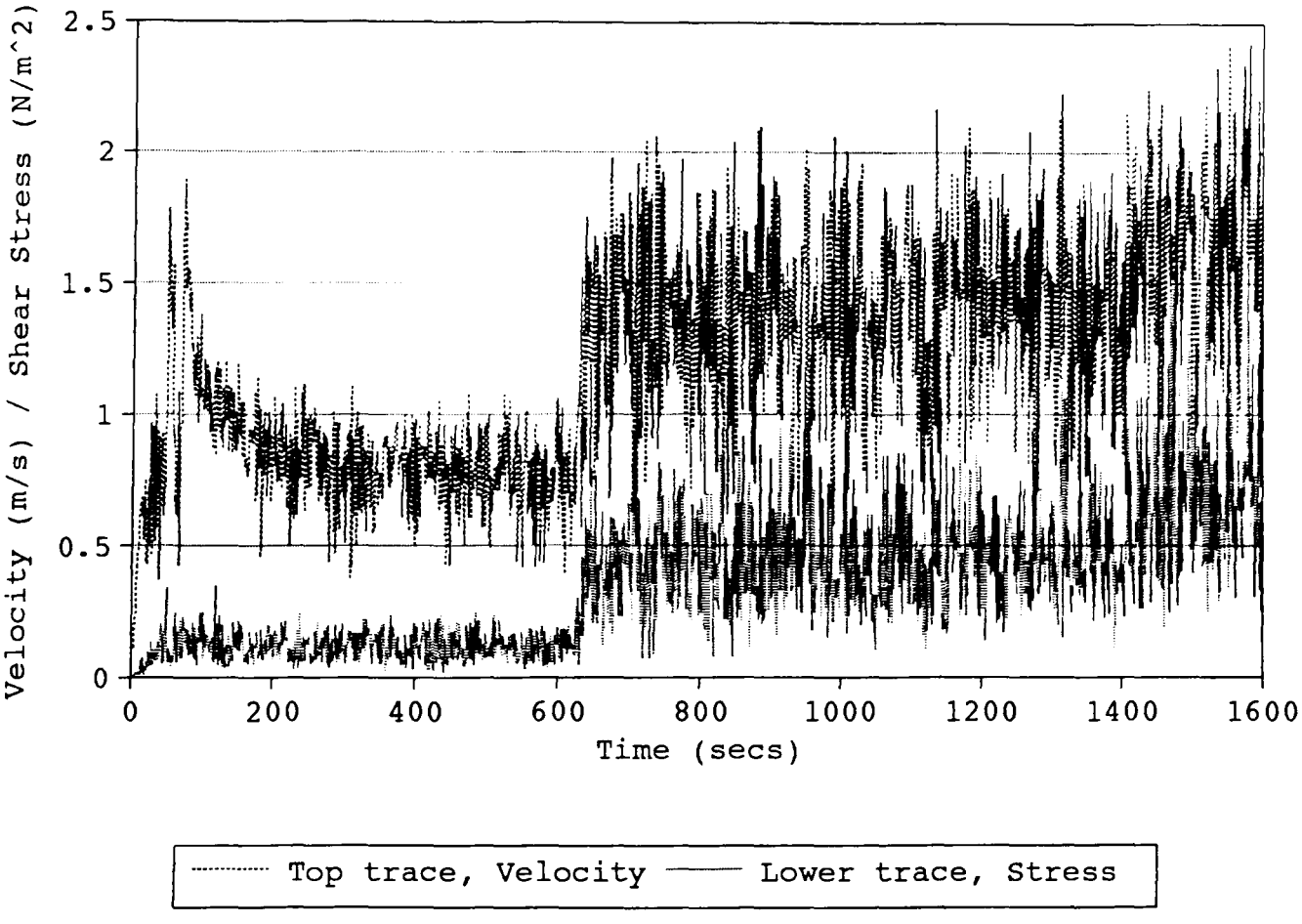

Fig (6.9): Affect of Averaging on the OBS-1 Data.

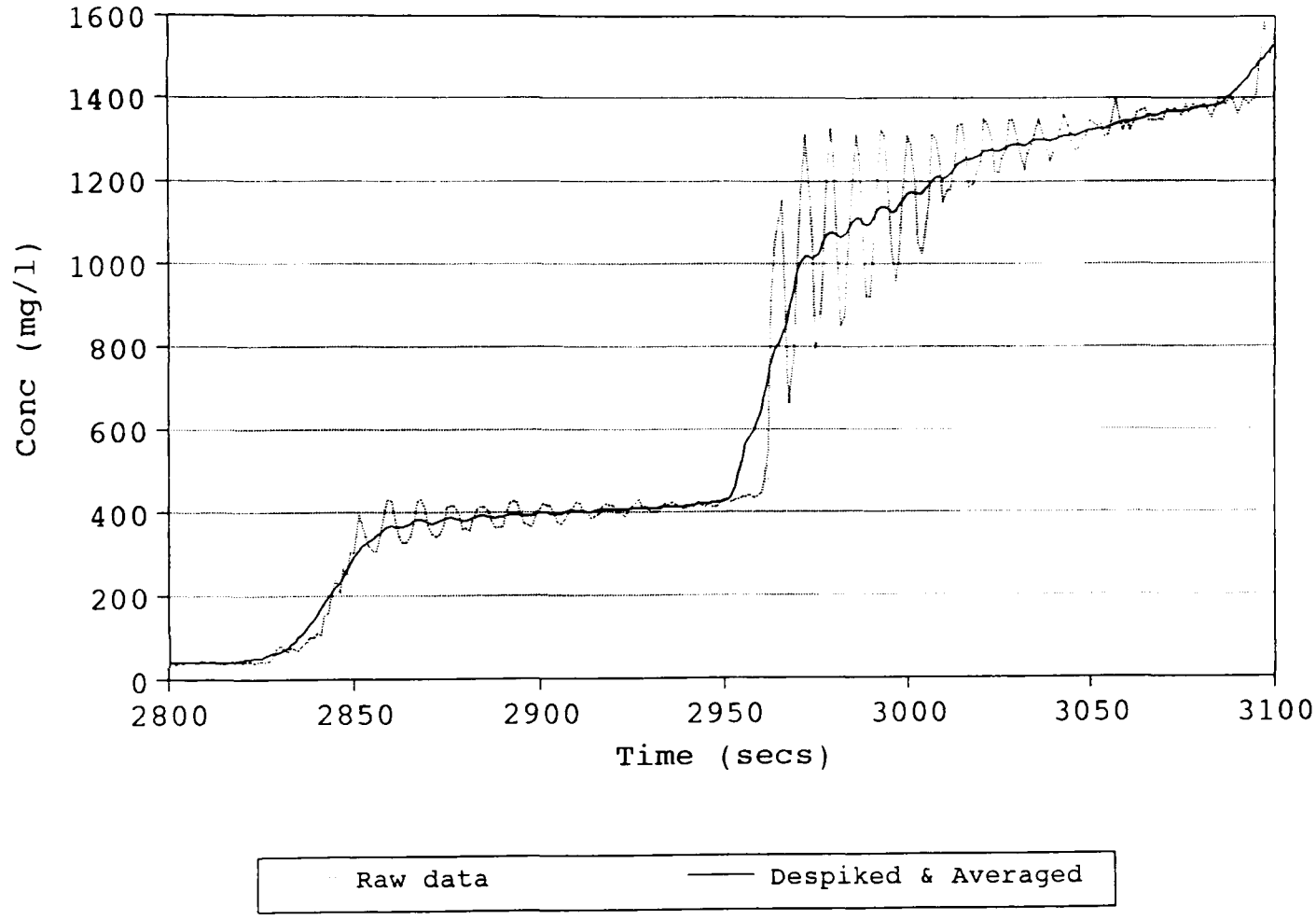

The total affect of these three data processing methods (temperature correction, despiking and averaging) are shown in Figures 6.10 and 6.11. Figure 6.10 presents the results of despiking and averaging on temperature corrected data and Figure 6.11 displays the fully processed data in relation to the raw data. These demonstrate that the temperature correction has the greatest affect on the magnitude of the data and that despiking and averaging improve the clarity of the data set.

Determining a Rate of Erosion

The total amount of sediment in suspension was derived from the suspended concentration values using the flume volume of 186l. An erosion rate was then calculated from the difference between successive twenty second time averaged sediment masses and then corrected for the size of the sediment surface as defined by the sediment box dimensions, ($0.0417m^2$). The method of calculating the erosion rate gives another reason for averaging the data. If the sometimes wavy appearance of the suspended sediment data (§6.2.3.1. Data Averaging) had not been reduced by averaging, negative erosion rates would have been produced at these features in the record.

6.2.3.2. **Flow Results**

The results of all of the flume runs are displayed in Appendix IV. In general all of the runs show an increase in bed shear stress, velocity and suspended sediment concentration with time. As with the measurement of the bed properties improvements were made to the flume over the early runs and the quality of data improved. This is most obvious in the shear stress data, which show a number of erroneous measurements in some of the early runs and only become consistent in the later runs 21-40. The velocity data was not collected on runs 4-27; this was due to the malfunction of the first sensor (probe 1) and a replacement sensor (probe 2) was not available until run 28. The suspended sediment data was of good quality over all of the runs. Below is outlined some of the more interesting points about the flume runs.

Fig (6.10a): Despiked Velodity Data, Run 39.

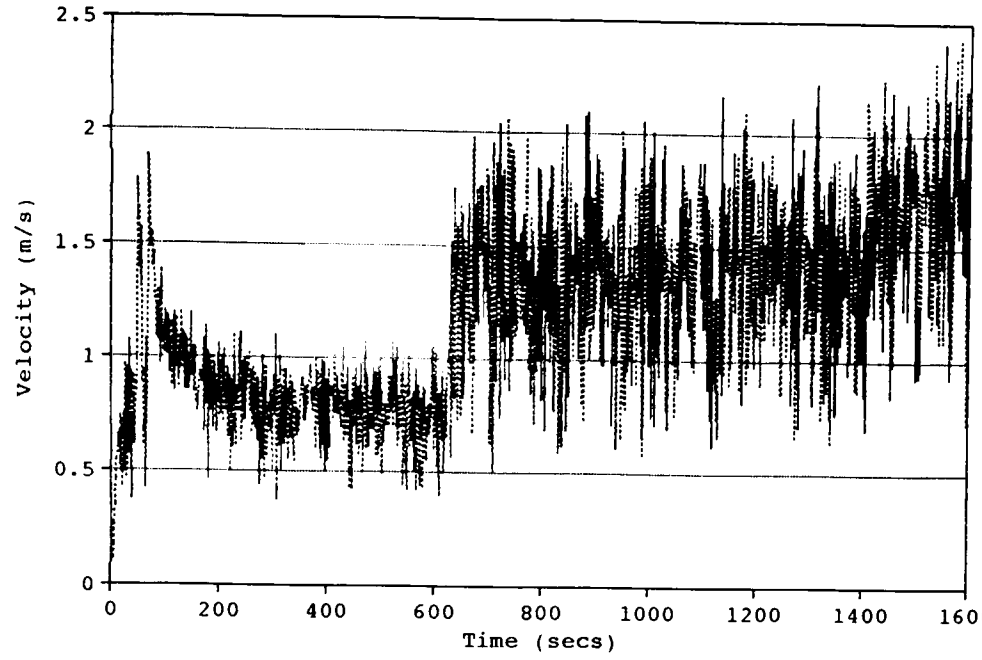

Fig (6.10b): Despiked Shear Stress Data, Run 39.

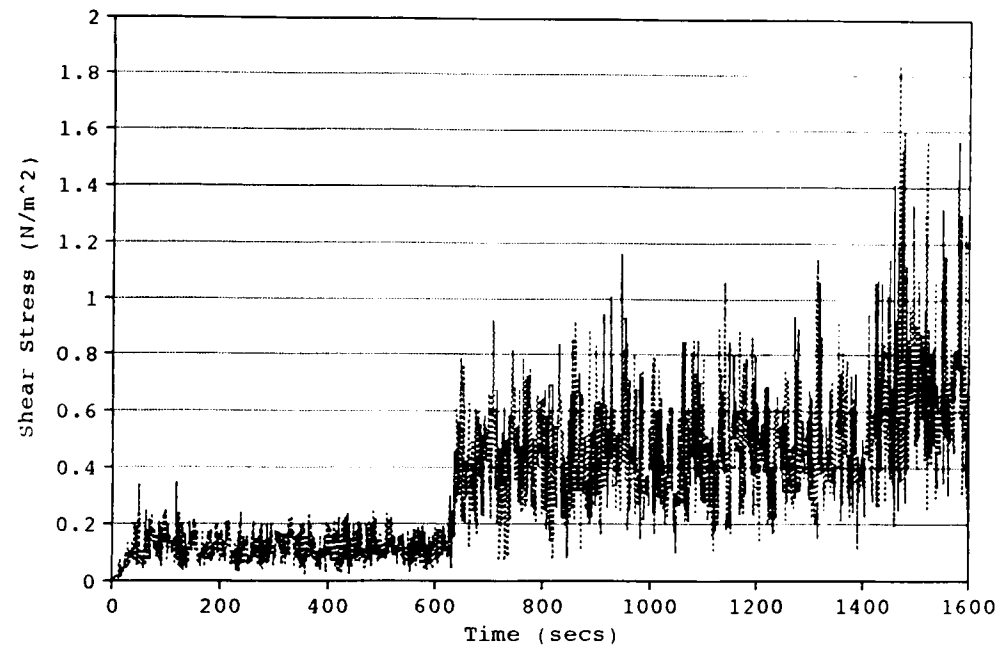

Fig (6.10c): Affect of Averaging on Temperature Corrected Data, Run 39.

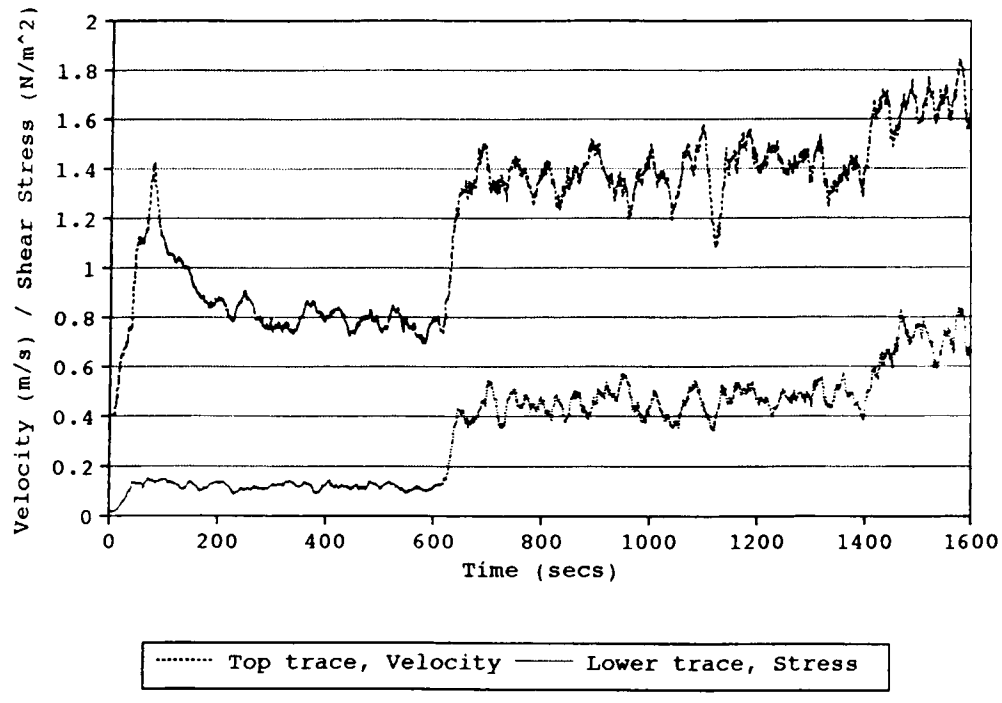

Fig (6.11a): Affect of Initial Data Processing on Velocity Data, Run 39.

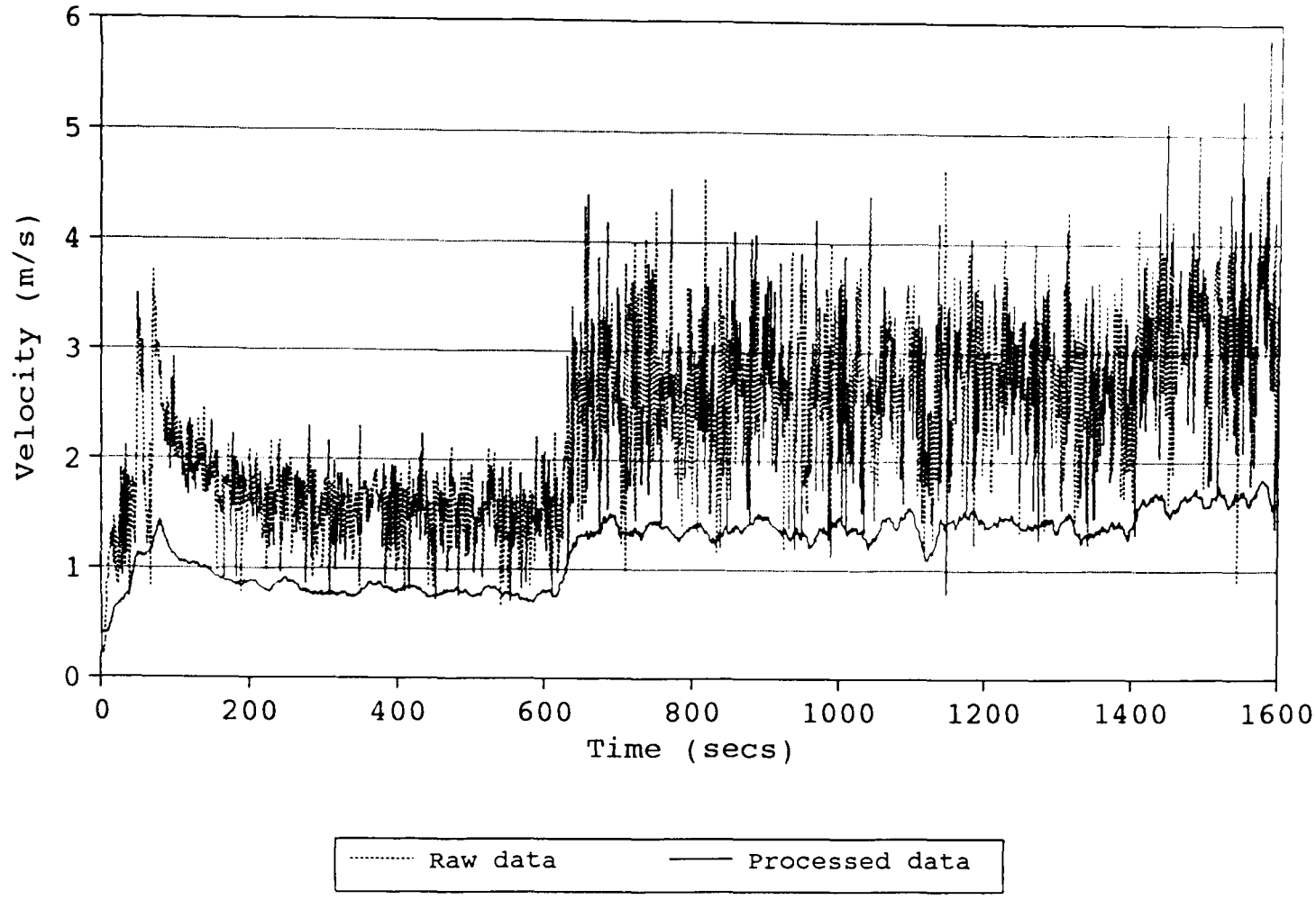

Fig (6.11b): Affect of Initial Data Processing on the Shear Stress Data.

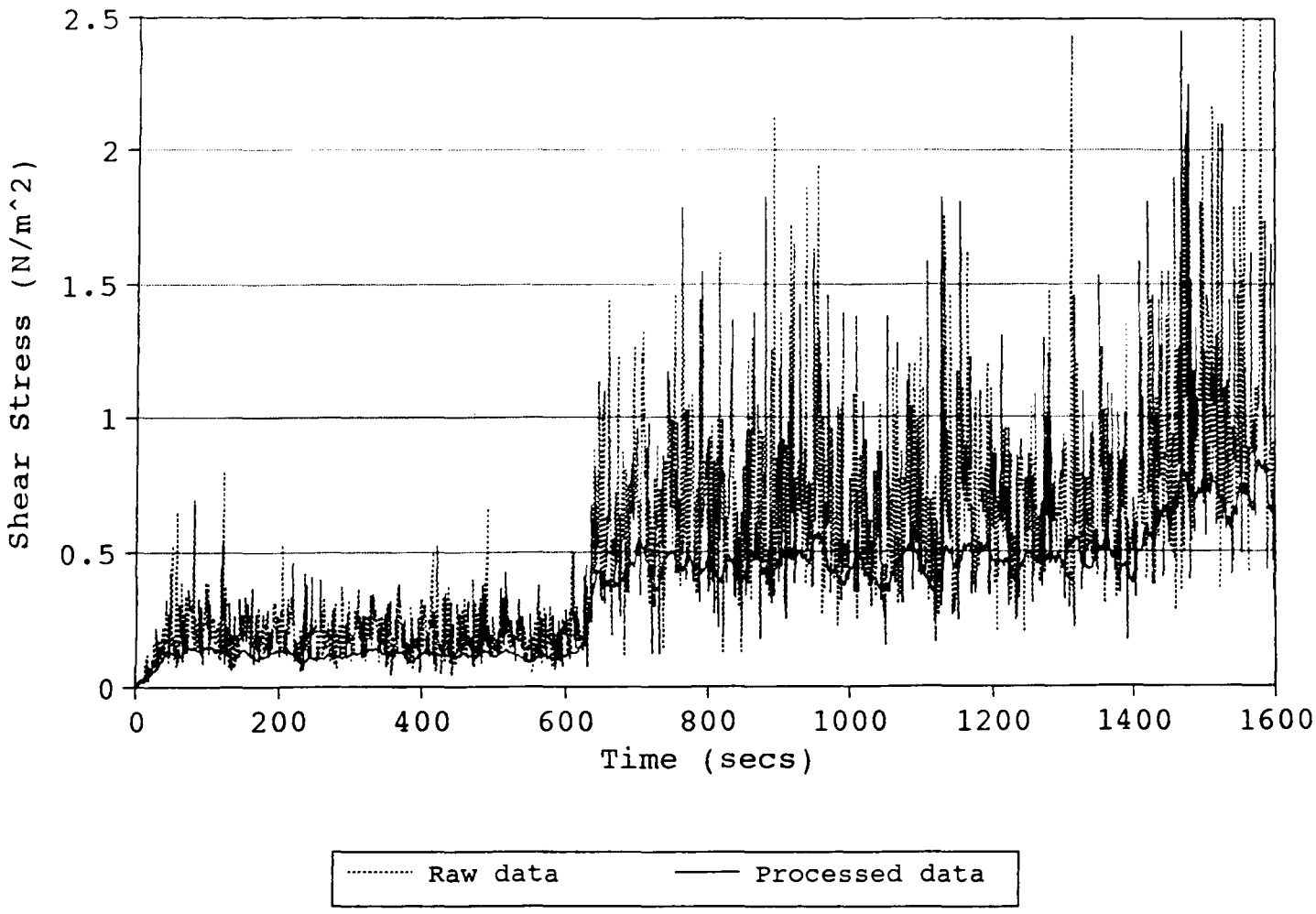

Velocity and Shear Stress Data

The main point of interest in the velocity and bed shear stress data is that the affect of suspended sediment on these two parameters, as discussed above (§5.2.5.2.), which can be seen in a few of the runs where a rapid and large rise in suspended sediment occurs. Figure 6.12 displays the processed data for flume run 32 and the velocity and shear stress data can be seen to fall over the last stress increment as the bed rapidly erodes and material is entrained into suspension. The heavy solid lines on this graph are lines of best fit, calculated from the data to show the trend across each stress interval.

Suspended Sediment Data

The suspended sediment data was more varied from run to run, as this is the parameter related to the bed characteristics and these varied from run to run. Figure 6.13 shows the general appearance of the OBS-1 data and ε calculated from this data. The ε variation is very irregular, but it tends to peak at the start of a stress increment and then fall off over the duration of the stress increment. The appearance of the OBS data also changes: after the initial erosion the OBS data increases but appears to be approaching a constant, but after the next erosion event the OBS data increase constantly at roughly the same rate. This could be related to Type I and Type II erosion as described by Mehta and Partheniades (1982). Mehta (1985) and Sheng and Villaret (1989) defined Type I (or 'floc' erosion rate) as: bed erosion rate under an applied fluid bed stress is eventually balanced by an increase in bed shear strength with depth as erosion takes place. With this process being independent of particle settling rate or mass deposition and implies a time-variable erosion rate and an increase in bed strength with depth (Mehta 1989). In Type II erosion, erosion is constant and continuous and erosion rate is a function of excess bed stress and shows no time dependency. (Simply for Type I the erosion rate (ε) decays with depth as the threshold increases and for Type II the ε remains constant with depth.) It would be expected that the mud bed used in this case should display Type II erosion, as the mud bed is made from well mixed (homogenous) samples that have not been allowed to settle for any length of time. However the results of the flume runs are varied,

Fig (6.12): Processed Data for Flume Run 32.

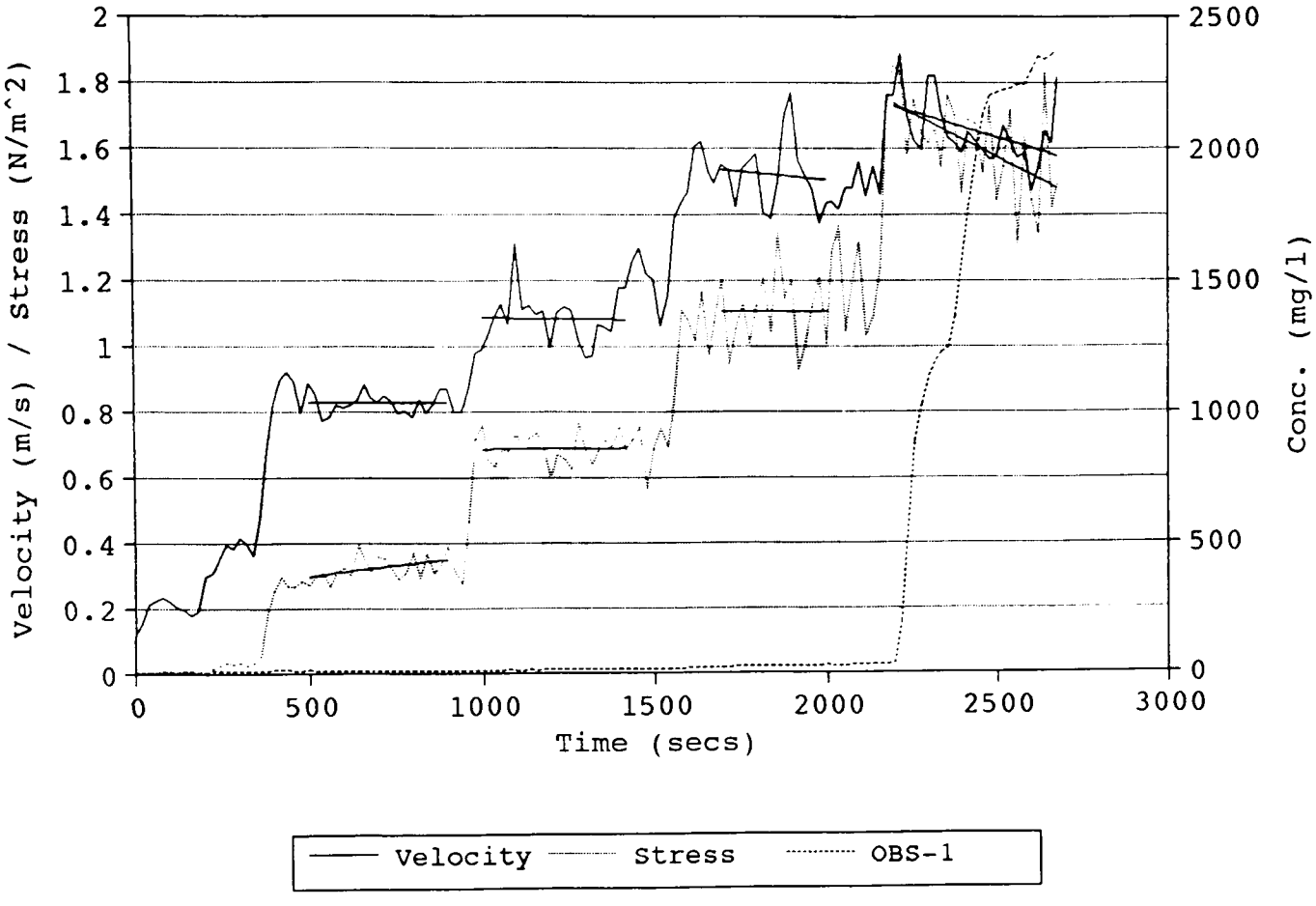

Fig (6.13): Run 38, Suspended Sediment Concentration and Rate of Erosion.

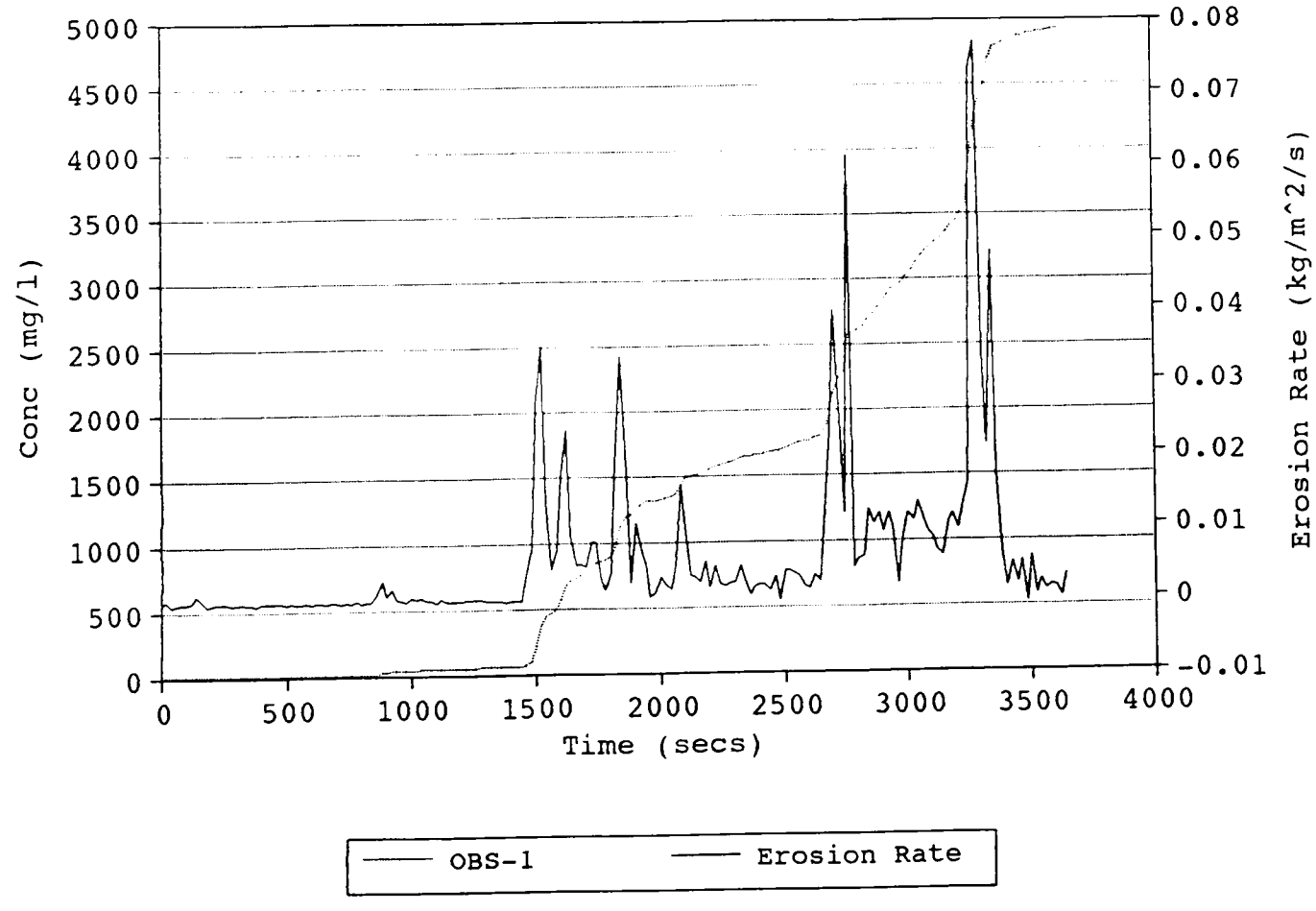

some show Type I, some Type II, some both and others more complex examples that cannot easily be defined. This reflects the complexity of bed structures shown by the muds used in the flume and this is supported by geophysical measurements made of the bed properties.

Figures 6.14 and 6.15 are flume runs that show erosion Types I and II. Figure 6.14 is of flume run 6 and as can be seen very little erosion occurred over the first twenty five minutes of the run, and then with the next stress increment the bed erodes and continues to erode at a constant rate. The heavy solid lines represent best fit lines that can be calculated from the OBS data and then used to give an erosion rate. This appears to be an example of Type II erosion. However this can not strictly be termed Type II erosion, because the time period from 1500 to 4800 seconds represents four stress increments and therefore τ_{cr} must have been increasing with depth resulting in the apparently constant rate of erosion.

Figure 6.15 is of flume run 34 in which a box core of mud taken from the field was inserted into the flume, instead of the normal mixed mud. This box core represented a reasonably undisturbed core although some disturbance had occurred due to the coring process. The plot is similar to those of Amos et al. (1992), with ε peaking at the start of each increment and the falling off as the OBS data approaches a constant (although due to a time constraint this was not allowed to develop fully over the last few increments). It demonstrates that the flume is generating results that can be related to other work and that the use of remixed muds can produce basic work which can be developed on for future work with real muds. This shows Type I erosion occurring at the surface and possibly type II erosion occurring with depth, although due to time constraints the latter events are not so well defined. The three stress increments between 4000 to 5000 seconds may have shown Type I erosion if they had been allowed to develop fully, and this may also be true for the last two stress increments after 5000 seconds although these appear to be following a different trend then those of the previous stress increments.

Figures 6.16 and 6.17 show flume runs 30 and 32 respectively, and they show complete and rapid bed failure. These runs ended when the bed could no longer be raised. In both of these cases the bed failed suddenly

Fig (6.14): Run 6, Suspended Sediment Concentration and Rate of Erosion.

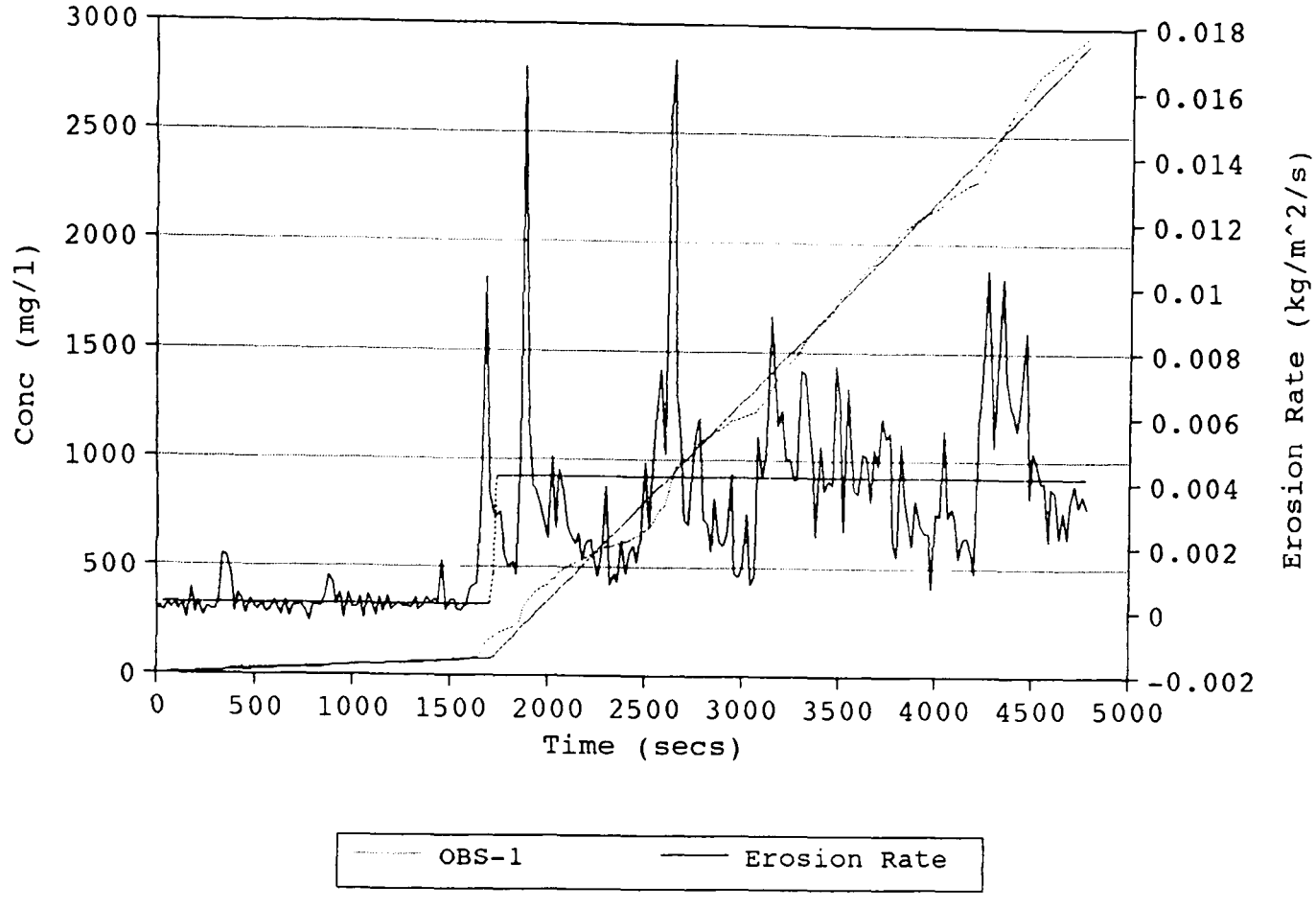

Fig (6.15): Run 34, Suspended Sediment Concentration and Rate of Erosion.

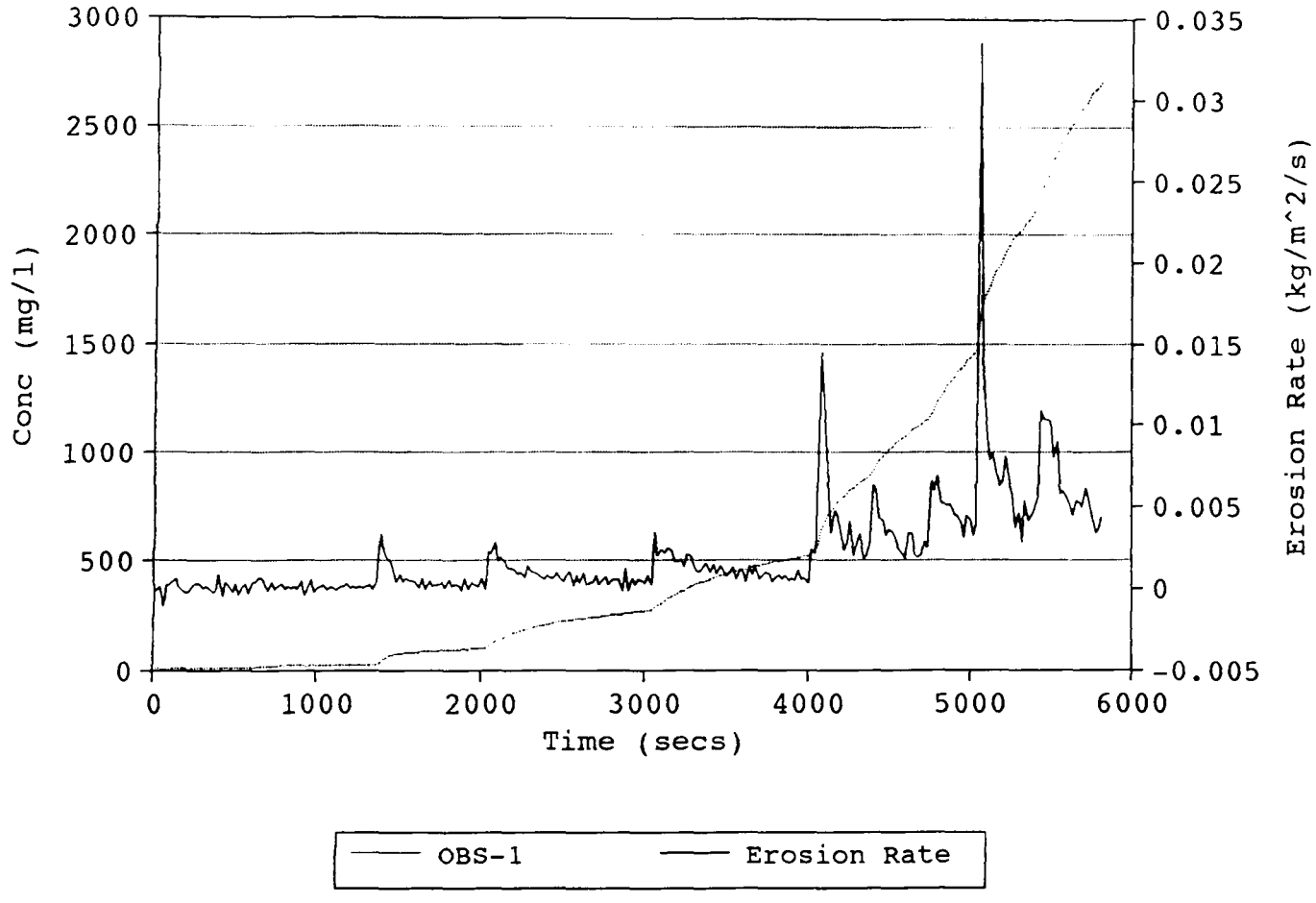

Fig (6.16): Run 30, Suspended Sediment Concentration and Rate of Erosion.

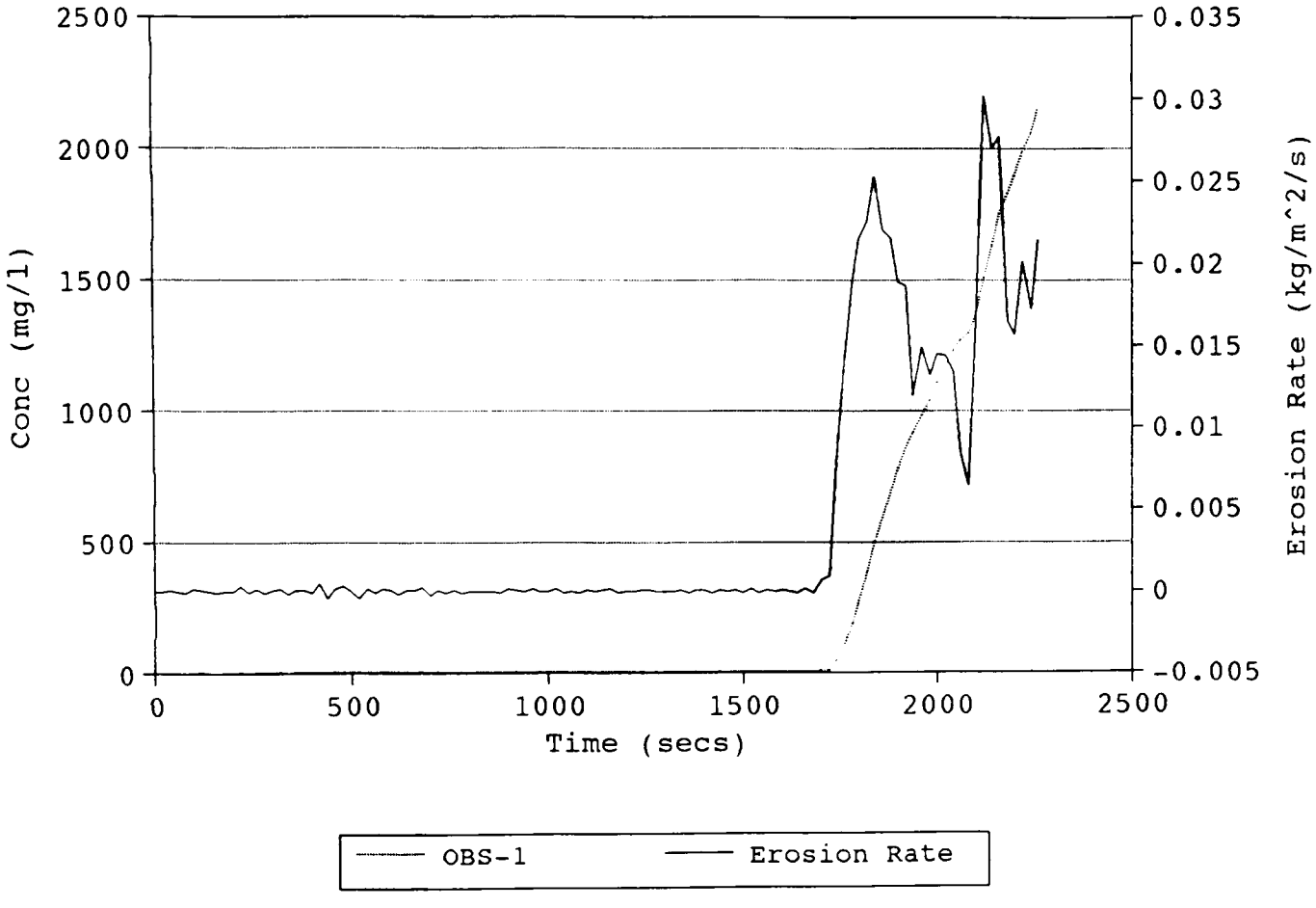

Fig (6.17): Run 32, Suspended Sediment Concentration and Rate of Erosion.

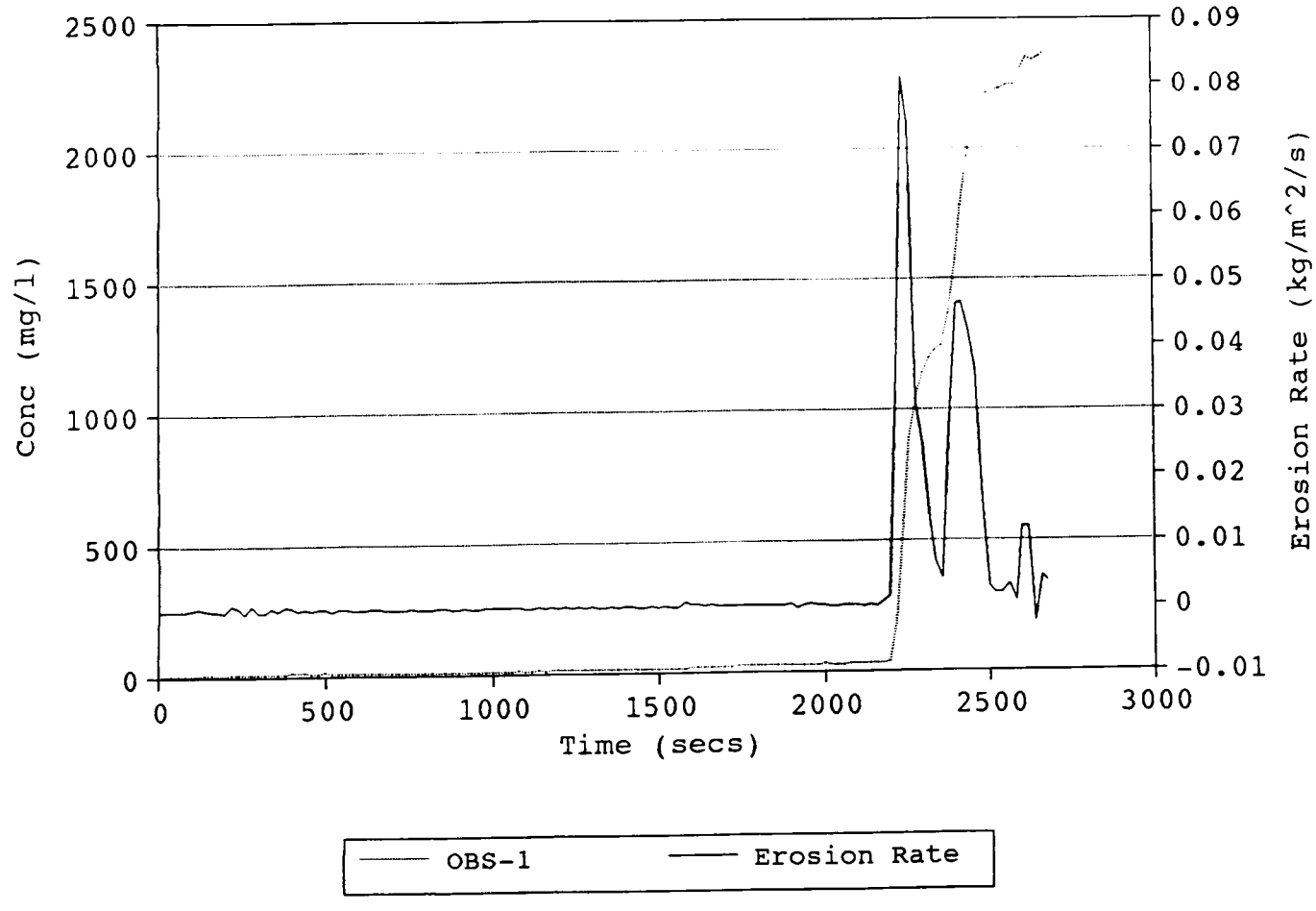

and erosion continued until all of the bed had been removed. It was under these circumstances were the bed was being rapidly eroded that the rule of leaving the flume for ten minutes at each stress increment had to be waived in order to obtain erosion data (of the bed being eroded) at more then one stress increment before all of the bed was totally removed.

Figures 6.18 and 6.19 (flume runs 21 and 22) show the other extreme where erosion occurred continuously over the period of the flume run. These muds still had a large amount of biological activity. Although erosion was occurring continuously, it was not very rapid and is believed to be related to the biological activity which increased bed roughness, and allowed sediment to enter suspension at low velocities. Because the muds in flume runs 21 and 22 did not fail catastrophically, the maximum flow speed of the flume was increased for later runs. This lack of bed failure means that the threshold values calculated for runs 21 and 22 (§6.2.3.3.) are in fact not the true stress values at bed failure as calculated for the other muds, but signify some other change in the erosion behaviour of the bed.

Another possibility is that the biological activity has increased the threshold shear stress of the bed to above that of the maximum flume shear stress, and that the erosion that was occurring could be termed sub-critical erosion (erosion occurring below the critical shear stress required to erode the bed fully). This is supported by Figures 6.20 and 6.21 which also show low rates of erosion. Figure 6.20 is of flume run 20, in which the bed had been left for two days (it was not allowed to become desiccated on its surface) and showed a higher resistance to erosion. Figure 6.21 is of a normal flume run (run 25) where the bed was not allowed to settle. However this is only the first half of the run, the end of the plot is where catastrophic erosion of the bed starts (the whole plot is given in appendix IV), and it shows that erosion was occurring at a low rate on the freshly poured muds below the stress values where erosion of the bed became more dramatic and visible.

Fig (6.18): Run 21, Suspended Sediment Concentration and Rate of Erosion.

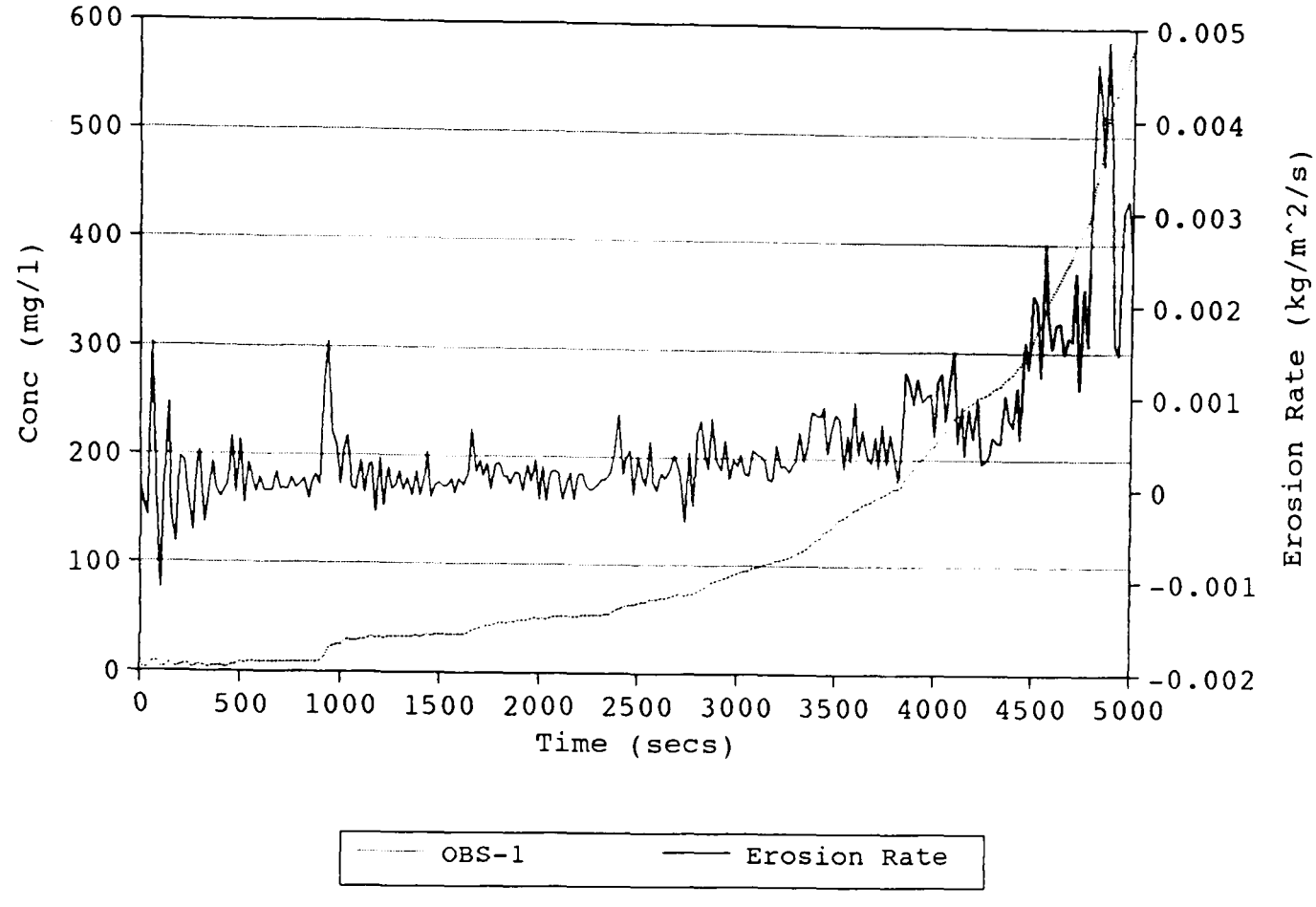

Fig (6.19): Run 22, Suspended Sediment Concentration and Rate of Erosion.

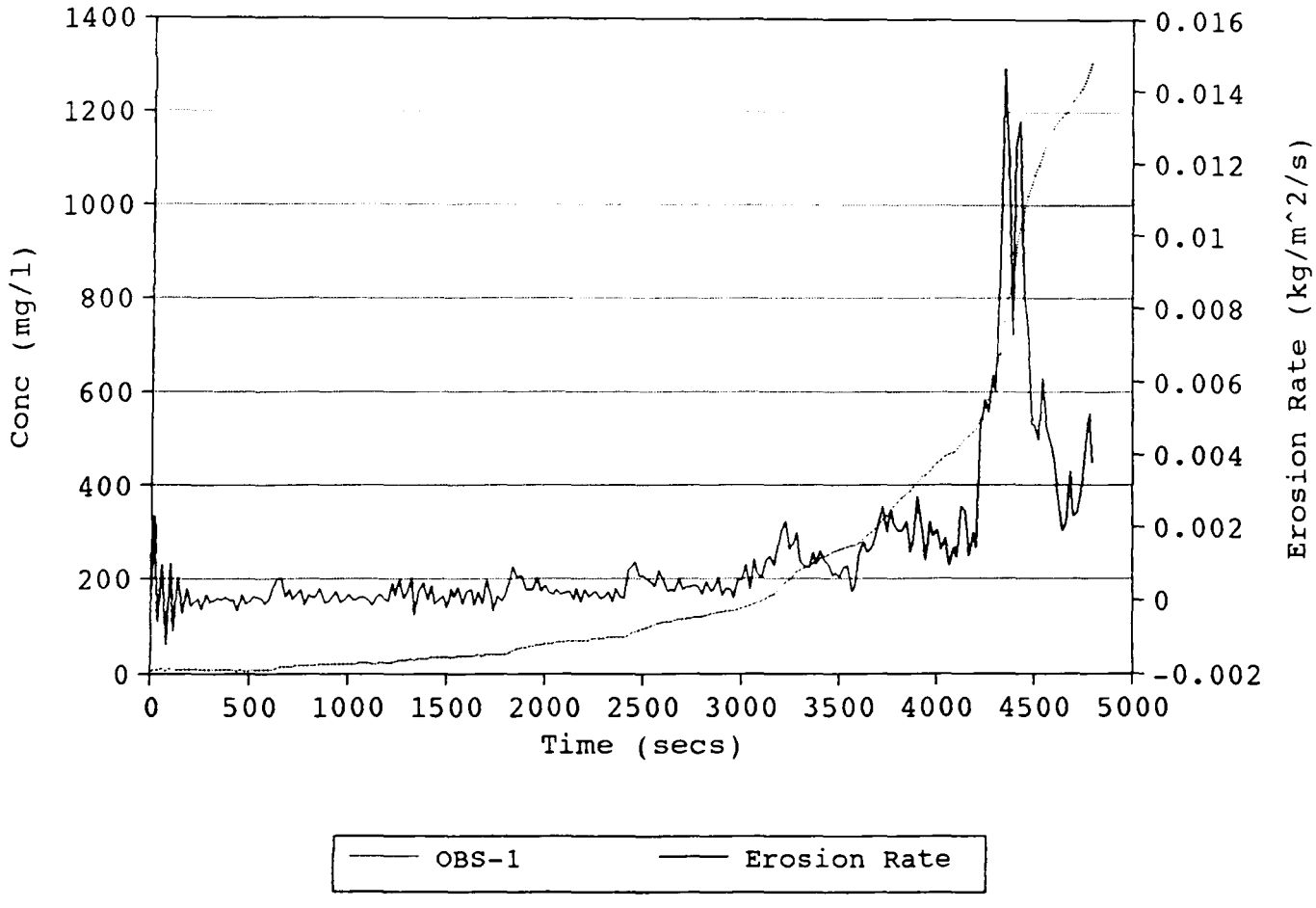

Fig (6.20): Run 20, Suspended Sediment Concentration and Rate of Erosion.

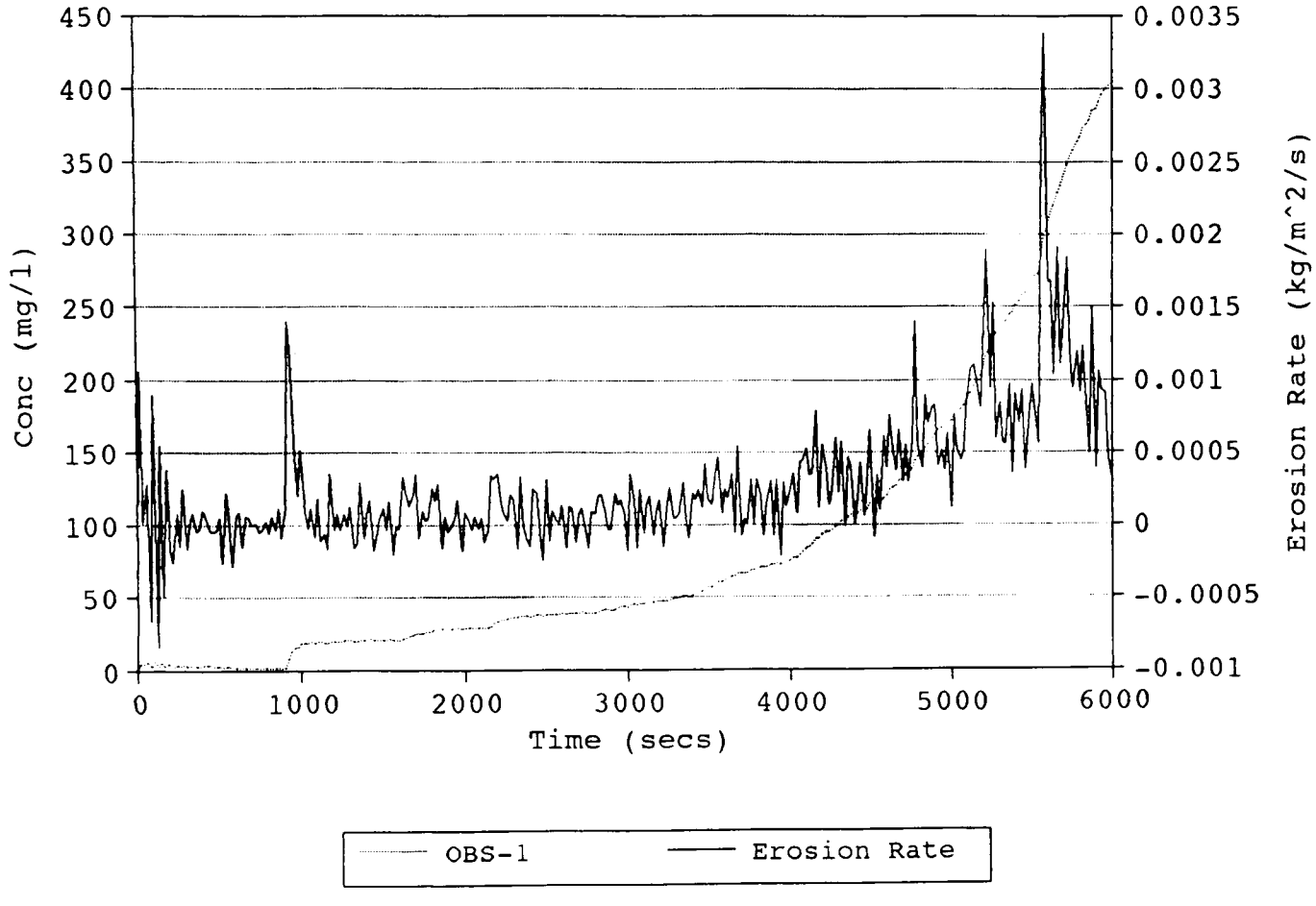

Fig (6.21): Run 25, Suspended Sediment Concentration and Rate of Erosion.

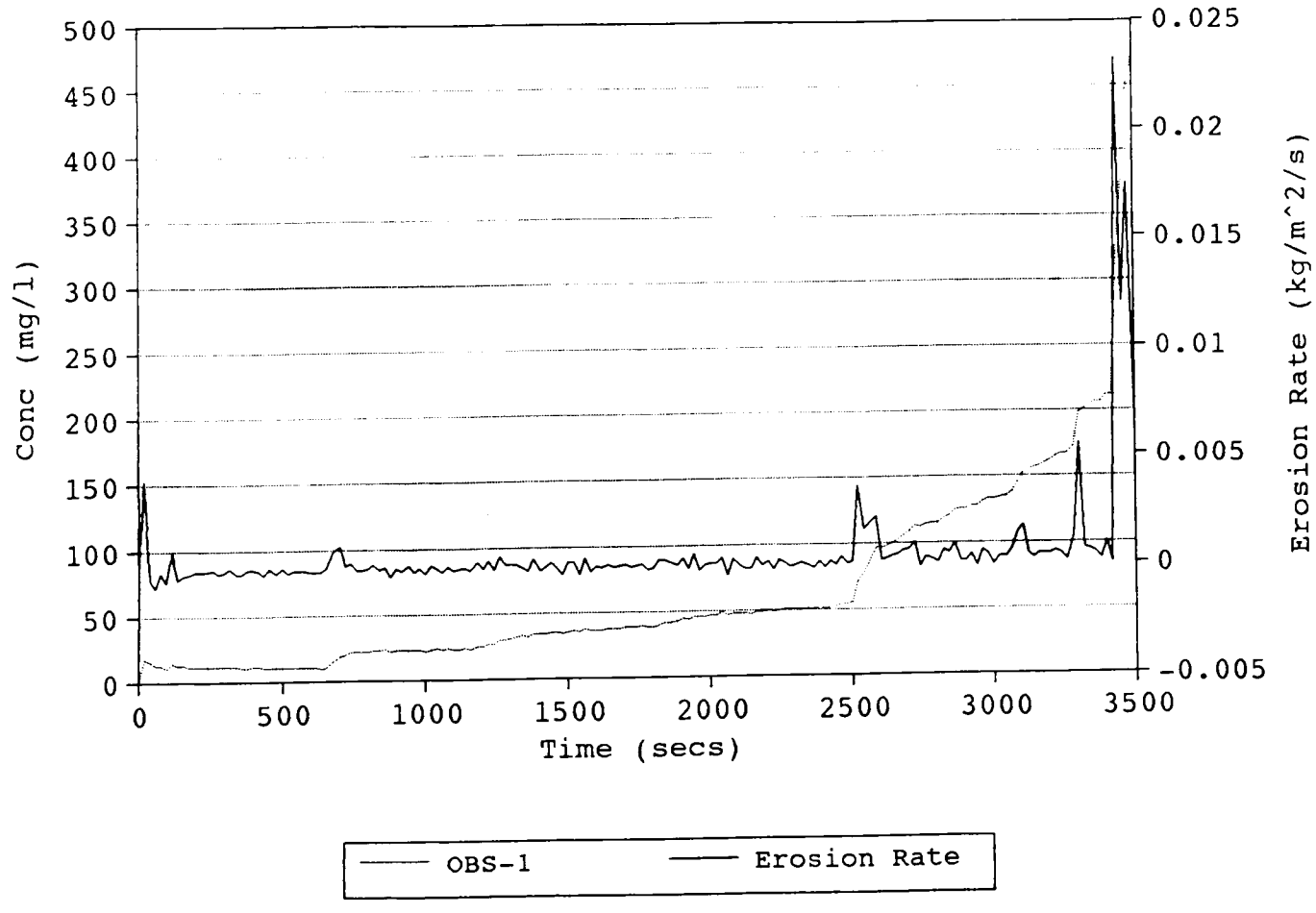

6.2.3.3. Determining Erosion Threshold

As can be seen from the flume results (Appendix IV) the muds have a shear stress value at which the erosion changes from a minor to a major regime. This shear stress can be termed the characteristic bed stress (τ_{ch}) and is equivalent to the critical bed shear stress (τ_{cr}). All of the muds exhibit this bi-linear form (as described by Mehta (1981) and as outlined earlier §2.3.6.3.) and when the erosion rate is plotted against bed shear stress plots similar to Figure 2.18 are generated.

Figures 6.22 and 6.23 are plots of erosion rate and bed shear stress for runs 34 and 35 respectively; the erosion rate and shear stress are averaged over each stress increment. Figure 6.22 shows the normal bi-linear form, but Figure 6.23 can also be considered as bi-linear as the M_1 line is on the x-axis or zero erosion line (ε=0). Most of the flume runs produced plots like Figure 6.23. From these plots the data points which are in the major erosion regime can be selected and then a line of best fit calculated, this best fit line is the M_2 line. For the plots where the M_1 line is the ε=0 line, the intercept of the best fit line and the ε=0 line is the τ_{ch} value. However for plots that show a true bi-linear form like run 34 (Figure 6.22) best fit lines for the minor and major erosion regimes must be calculated and then the stress value at their intercept is the τ_{ch} value. The τ_{ch} value found using this intercept method on data averaged over a stress increment will be termed τ_{chA} from now on.

For some of the muds it was not possible to obtain a value of τ_{ch} using the method outline above, with one data point for each stress increment. However for these muds it is possible to obtain a value of τ_{ch} by using the twenty second average data without any further averaging. Figure 6.24 is a plot of the twenty second averages of erosion rate and bed shear stress for run 31. The plot shows that the flow is turbulent and that each stress increment covers a range of stress values. In order to determine τ_{ch} the data is first sorted into ascending order of bed shear stress and then peak erosion rate values are selected (Figure 6.25). This selected data is then treated in the same way as the longer time average data, with a line of best fit being calculated and used to determine τ_{ch}. The τ_{ch} value obtained in this way from the twenty second averaged data is termed τ_{chS} from now on.

Fig (6.22): Run 34, Determination of Characteristic Bed Stress.

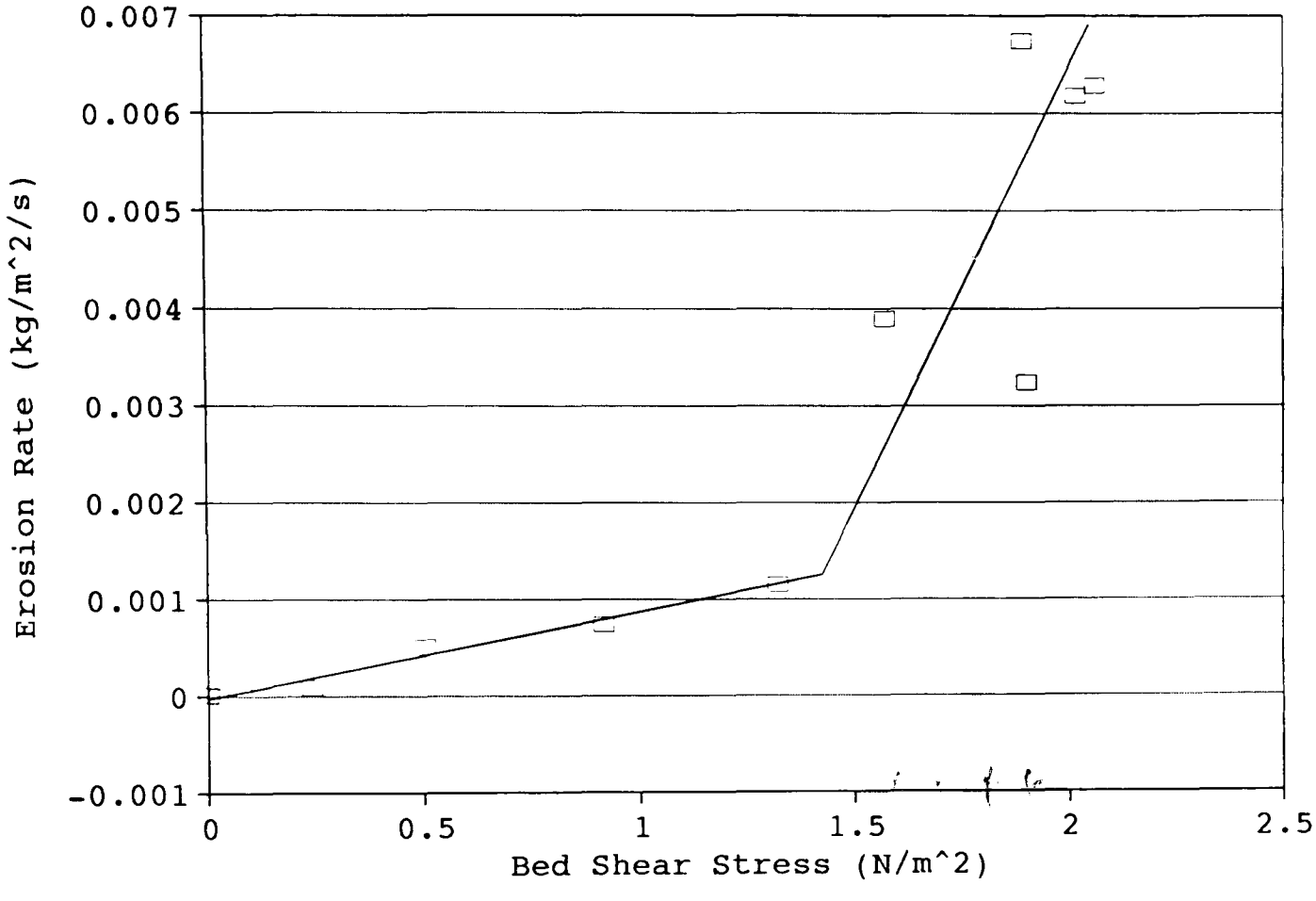

Fig (6.23): Run 35, Determination of Characteristic Bed Stress.

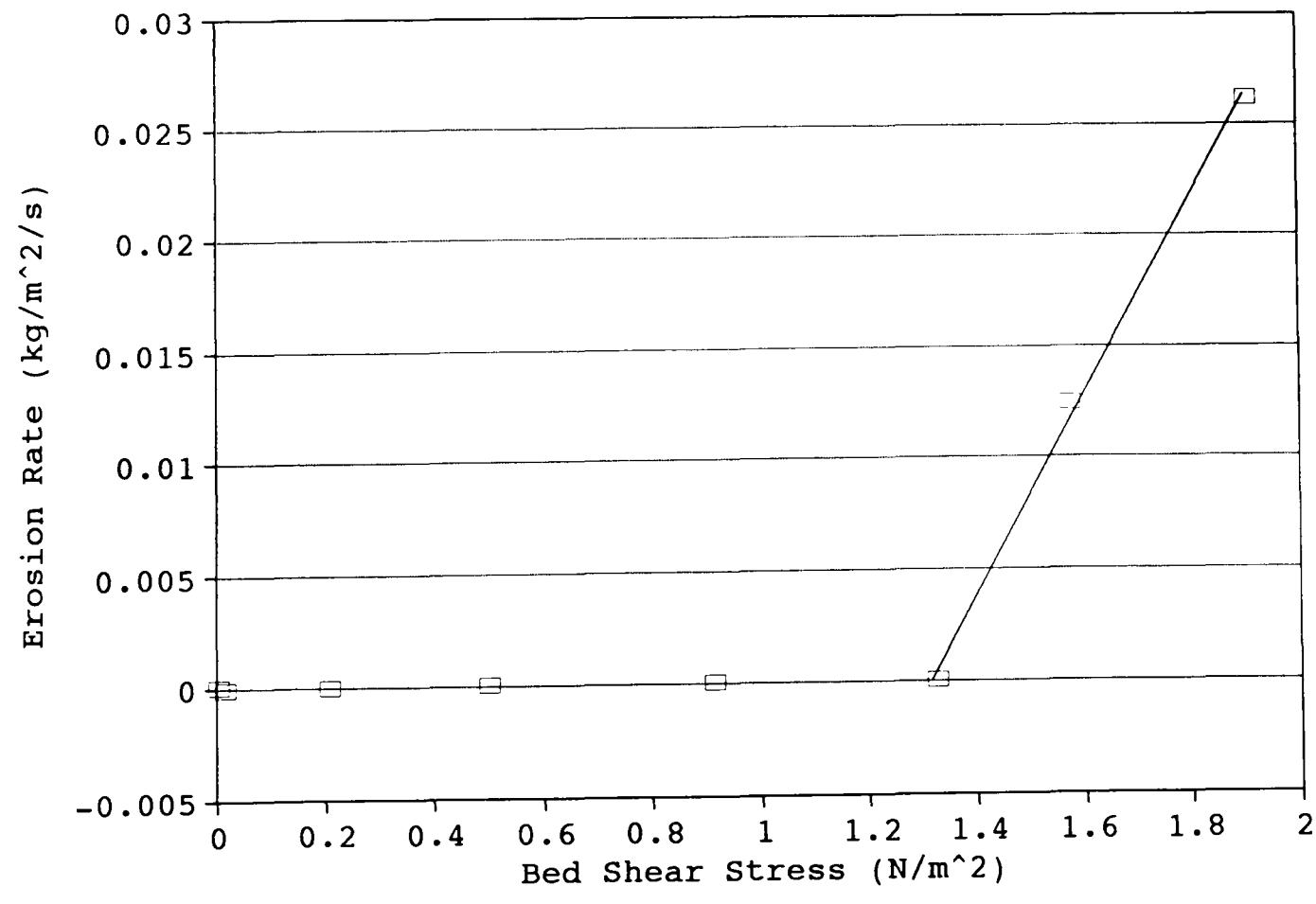

Fig (6.24): Run 31, 20sec Average Data of Erosion Rate and Bed Shear Stress.

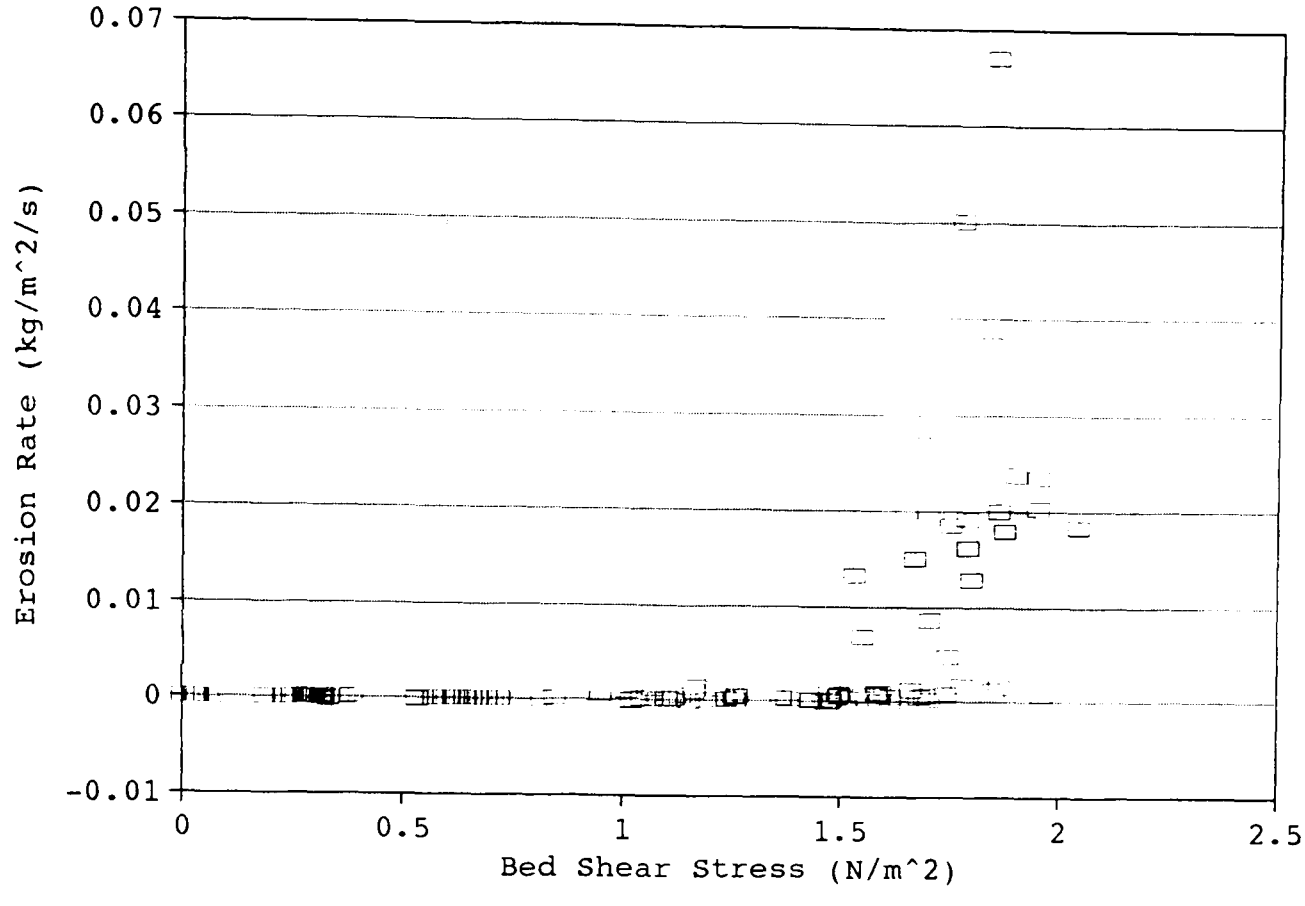

Figure (6.25): Run 31, Selected 20sec Average Data.

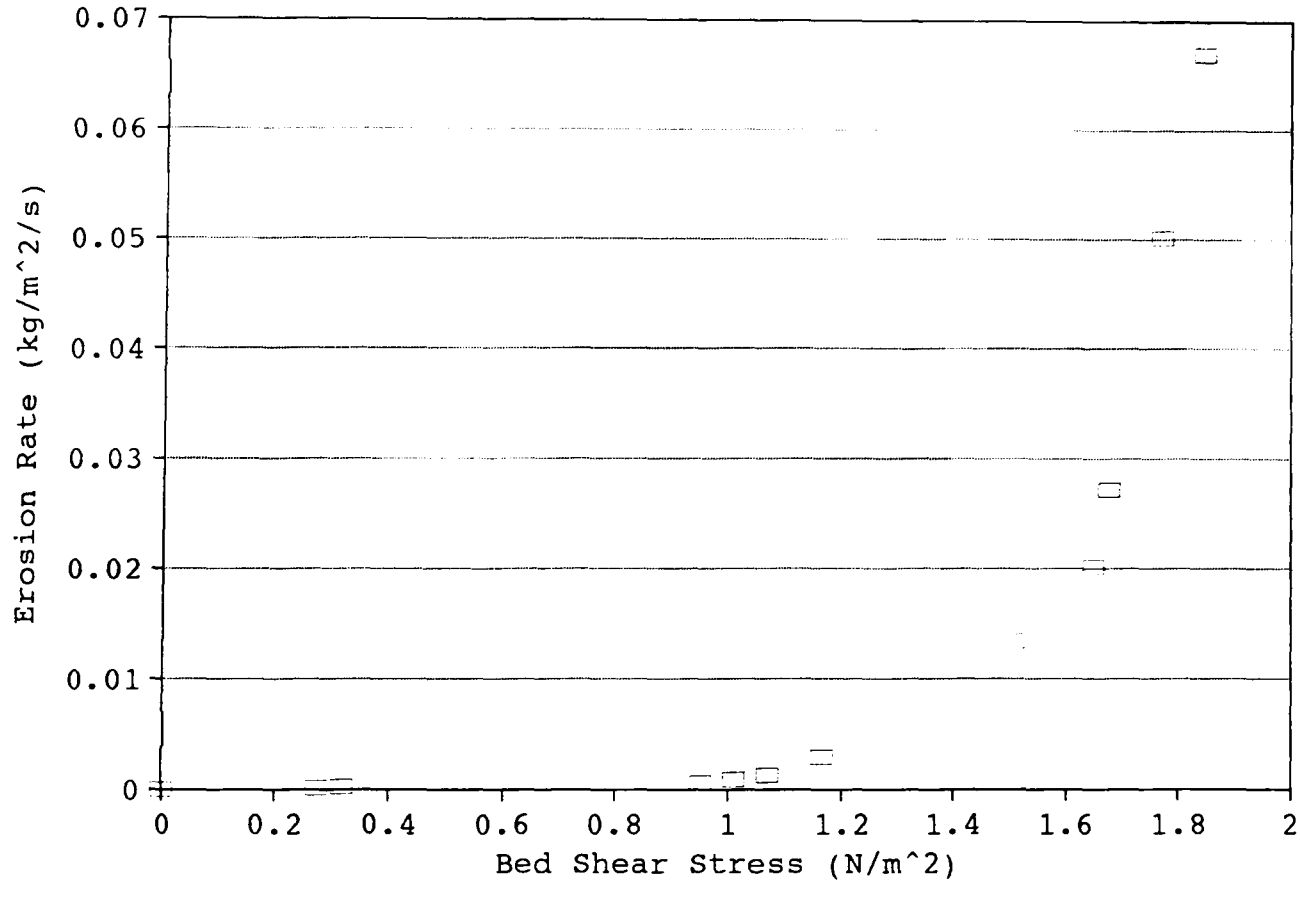

6.2.3.4. Erosion Threshold Results

The method outline above for calculating τ_{chA} produces different τ_{ch} values depending on the time period over which the erosion rate and bed stress are averaged. A value of τ_{ch} can be calculated from the twenty second average data, from the data averaged over the whole stress increment and from the data averaged over the first 60 seconds, the first 120 seconds, the first 180 seconds, the first 300 seconds, and the first 600 seconds of each stress interval. For each time period used a slightly different τ_{ch} is obtained. Figures 6.26 and 6.27 are of runs 30 and 38 respectively and show the reduction in τ_{ch} as the time period is increased (the value at 900 seconds is the value obtained with averaging over the entire stress increment). All of the muds produced similar plots,

Table 6.6 gives the τ_{ch} values calculated using the method of averaging the data over the whole of each stress increment and the method of using the twenty second average data, and then this is displayed graphically in Figure 6.28. It was possible to use both methods on a few of the runs and the results from these are shown in Figure 6.29. The different methods compare well, with both giving reasonable results, but because different methods are used to calculate them and they are likely to be measuring slightly different bed thresholds then they should be and are treated separately.

6.2.3.5. Relationship between Erosion Threshold and other Bed Properties

Erosion rate can now be compared to bed properties using the same method as that used to look at the inter-relationships of bed properties. As with the comparisons between the bed properties it is possible to presume what general form the relationship between τ_{ch} and the bed properties should be. In relation to the moisture content, the characteristic bed stress would be expected to decrease with increasing moisture content as the sediment becomes less rigid and more easily deformed, and the same should be true for porosity. In relation to the two measured geophysical

Fig (6.26): Affect of Time Averaging on Characteristic Bed Stress, Run 30.

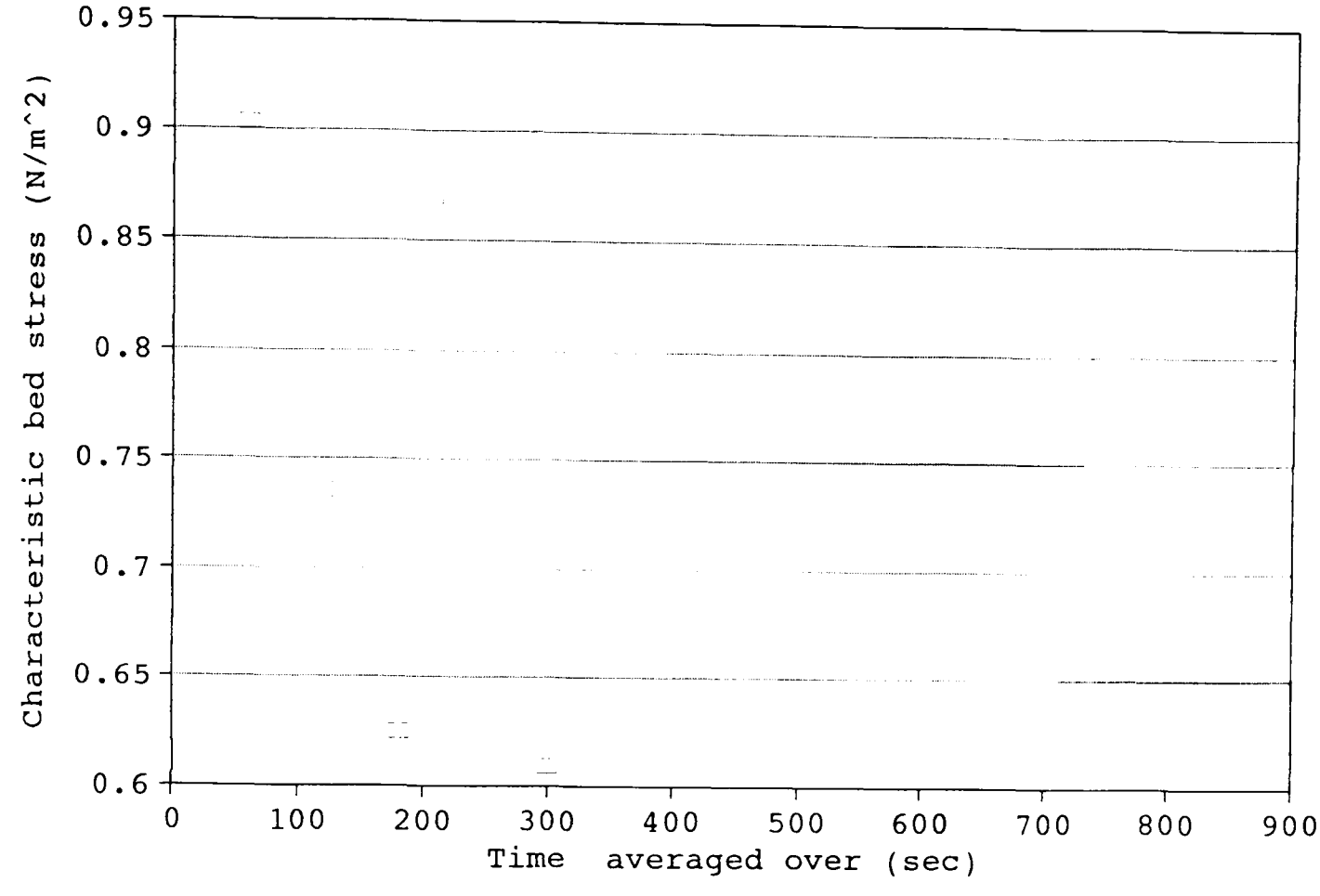

Fig (6.27): Affect of Time Averaging on Characteristic Bed Stress, Run 38.

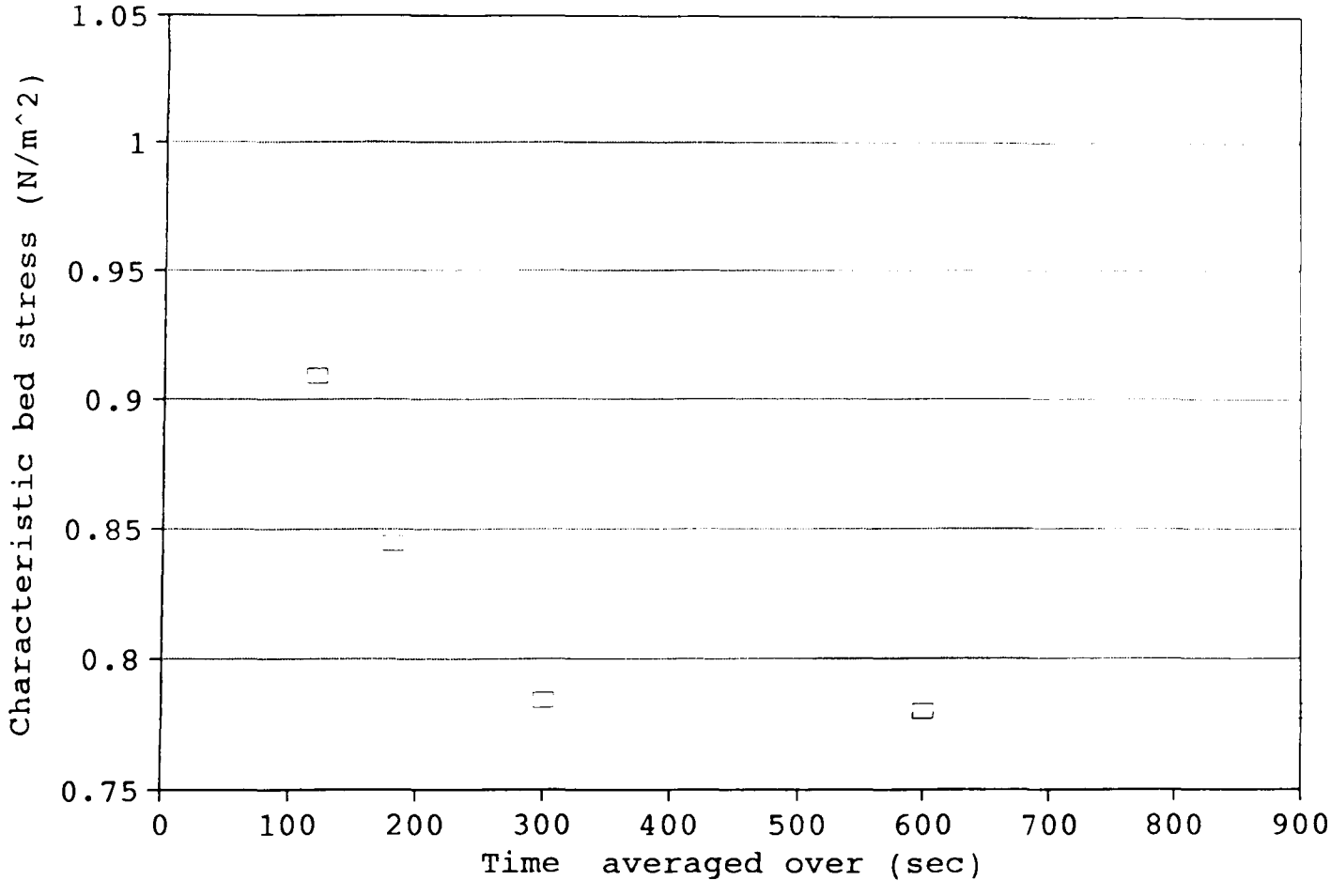

Flume Run	Characteristic Bed Stress (N/m^2)	
	A	S
21	0.2794	----------
22	0.2815	0.2619
23	1.4087	----------
24	----------	1.1149
25	1.6804	----------
26	1.5859	----------
27	1.6818	----------
28	1.0078	0.9243
29	1.2868	1.5403
30	0.6135	0.9248
31	1.5340	1.5096
32	----------	1.2998
33	----------	0.9000
34	1.4270	1.0843
35	1.3147	1.2363
36	0.9825	----------
37	----------	0.5795
38	0.7796	0.9151
39	0.7431	0.8301
40	0.5463	0.6693

Table (6.6): Characteristic Bed Stress Results of Flume Runs for muds 3 and 4.

A - Stress value obtained from data averaged over each stress increment.

S - Stress value obtained from twenty seconds average data.

Fig (6.28): Characteristic Bed Stress Results.

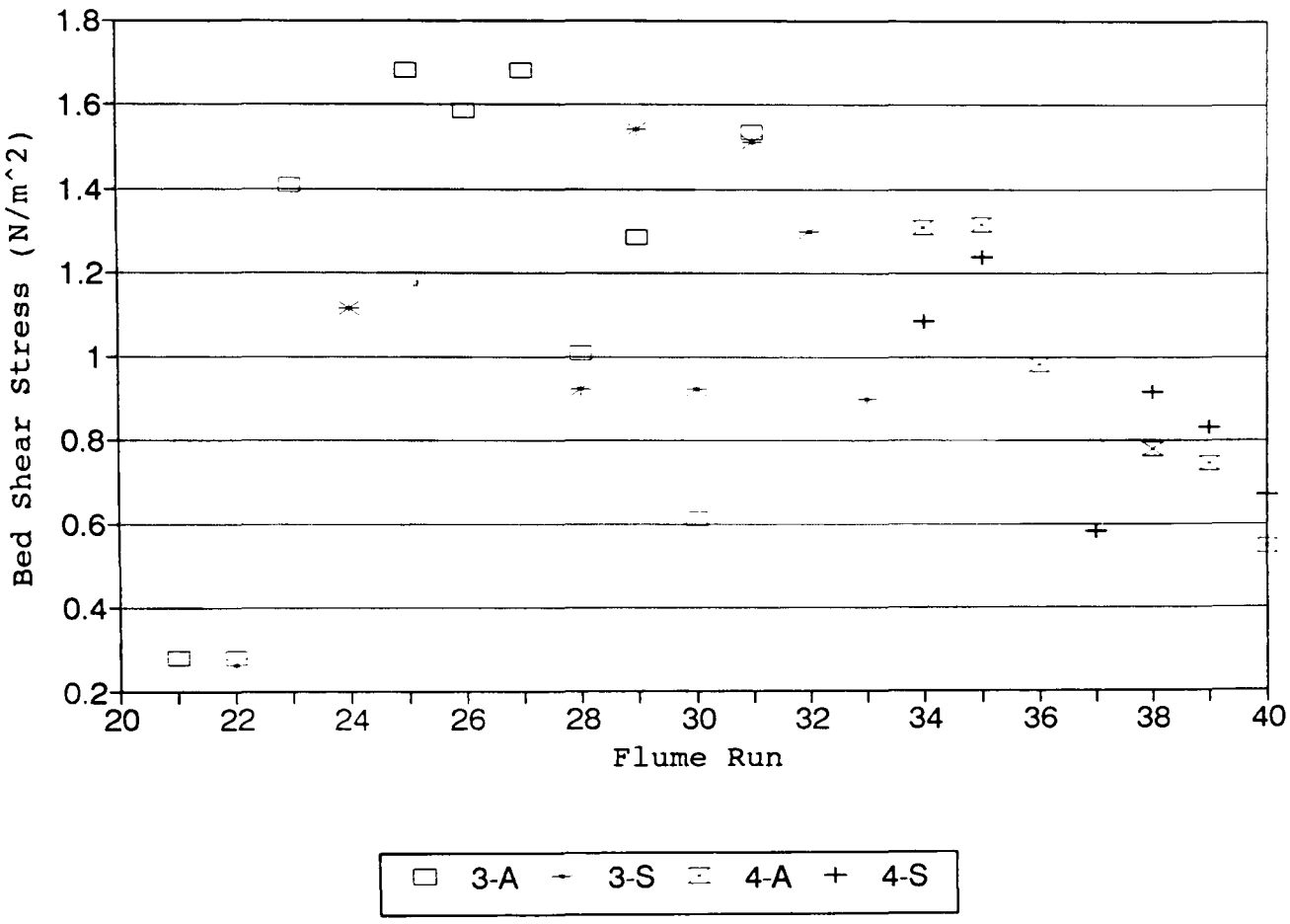

Fig (6.29): Comparison of the Different Characteristic Bed Stress Results.

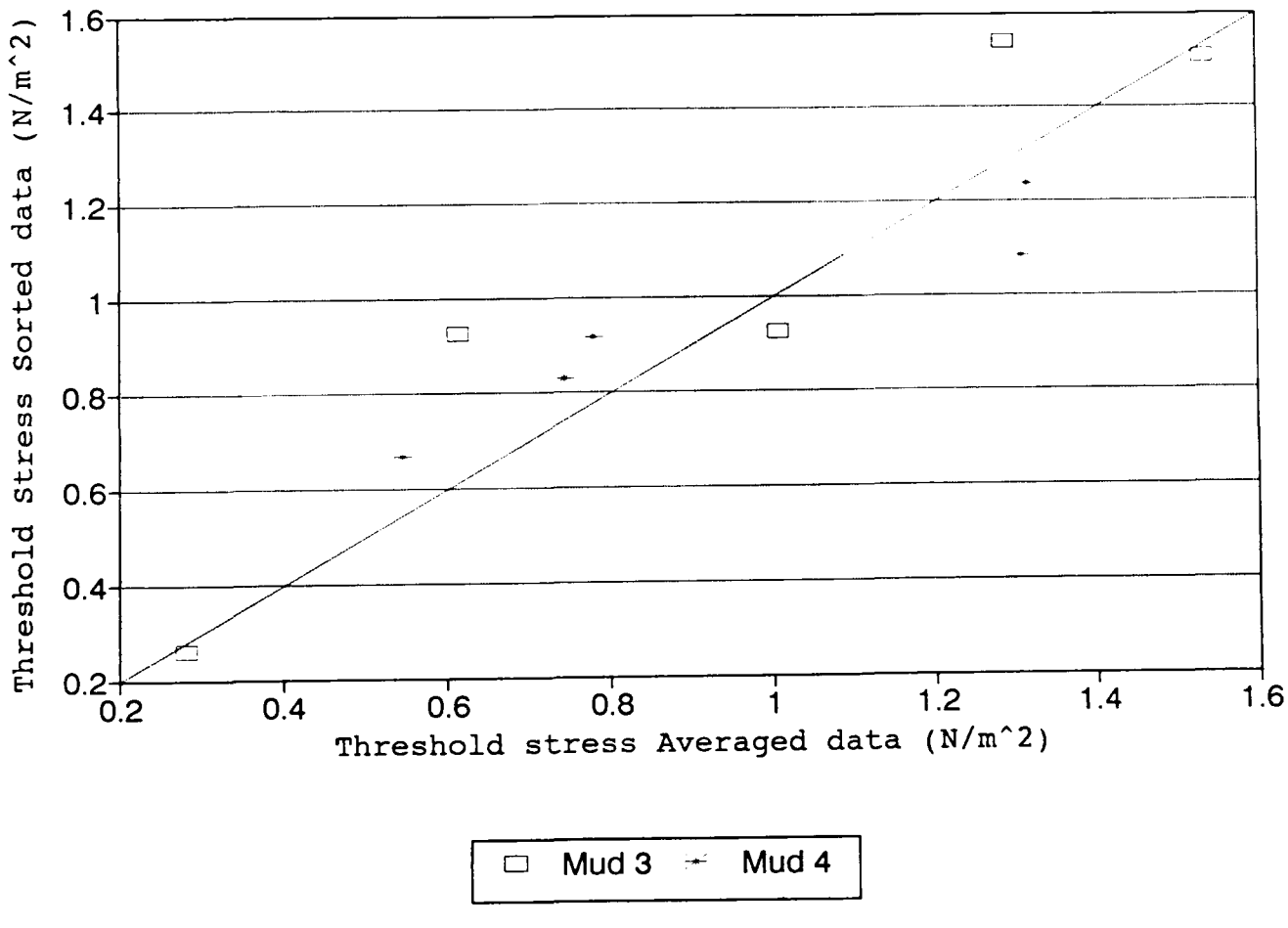

parameters, τ_{ch} would be expected to show increases with both increasing formation factor and shear wave velocity, as both of the latter would be expected to increase as the sediment becomes more rigid and moisture content falls.

Figure 6.30 shows the relationship between τ_{ch} and the moisture content (in all of the interrelationship graphs 3-A are the τ_{chA} values for mud 3, 3-S are the mud 3 values of τ_{chs}, and 4-A and 4-S are the corresponding values for mud 4). The lines fitted to the data are regression lines (calculated from the combined data sets of muds 3 and 4) which show that, as anticipated there is an increase in τ_{ch} with decreasing moisture content.

To investigate if the relationships between τ_{ch} and formation factor, shear wave velocity and porosity derived from formation factor are significant, Spearman's rank correlation coefficients have been calculated and are given in Table 6.7 for the results of mud 3 and in Table 6.8 for the combined results of mud 3 and 4. Figures 6.31 to 6.36 show these relationships graphically. The dashed lines on these graphs are regression lines to demonstrate the general nature of the correlation between τ_{ch} and the particular bed property (these are calculated from the combined data of muds 3 and 4, and only depicted for Spearman's rank correlation coefficients of 10% significance or more). The data for mud 4 showed no significant correlations due to the small number of data points and the small range that they represent, and therefore their correlation values are not shown. The results for mud 3 show only two correlations and once again this is due most probably to the small range of the data and the lack of data points available. Once the two sets of data (muds 3 and 4) are combined the number of correlations greatly increases.

It is noteworthy that the τ_{chA} values show a greater number of significant correlations than the τ_{chs} values. This is related to the different methods used to calculate the two values. The τ_{chA} value uses the erosion rate and corresponding stress data average for each stress increment, whereas the τ_{chs} values uses peak erosion rates and their corresponding stress values. This the τ_{chs} data more susceptible to variations in both the flow and the bed, where as the other τ_{chA} value is indicative of average flow

Mud 3						
	Correlation coefficent	No. of Values	Significance %			
Ta - w	0.548	8	n/s			
Ts - w	-0.250	7	n/s			

Mud 3						
	Average Values				Surface Values	
	Correlation coefficent	No. of Values	Significance %	Correlation coefficent	No. of Values	Significance %
Ta - FF	0.607	7	n/s	0.893	7	2
Ts - FF	-0.086	8	n/s	-0.714	6	n/s
Ta - Vs	0.886	6	10	0.800	5	n/s
Ts - Vs	0.300	5	n/s	----------	----------	----------

Table (6.7): Spearman's Rank Correlation Coefficients of the characteristic bed stress and bed property relationships of Mud 3.

Vs - Sediment Shear Wave velocity.

FF - Sediment Formation Factor.

n(FF) - Sediment Porosity derived from Formation Factor.

Ta - Stress value obtained from data averaged over each stress increment.

Ts - Stress value obtained from twenty seconds average data.

w - Sediment Moisture Content.

n/s - Not Significant.

Mud 3/4

	Correlation coefficent	No. of Values	Significance %
Ta - w	-0.795	13	2
Ts - w	-0.539	12	10

Mud 3/4

	Average Values			Surface Values		
	Correlation coefficent	No. of Values	Significance %	Correlation coefficent	No. of Values	Significance %
Ta - FF	0.678	12	10	0.301	12	n/s
Ts - FF	0.427	11	20	0.355	11	n/s
Ta - Vs	0.809	11	2	0.583	9	10
Ts - Vs	0.042	10	n/s	-0.257	6	n/s
Ta-n(FF)	-0.406	12	20	0.189	12	n/s
Ts-n(FF)	-0.642	11	10	-0.445	11	20

Table (6.8): Spearman's Rank Correlation Coefficients of the characteristic bed stress and bed property relationships of Muds 3 & 4.

Vs - Sediment Shear Wave velocity.

FF - Sediment Formation Factor.

n(FF) - Sediment Porosity derived from Formation Factor.

Ta - Stress value obtained from data averaged over each stress increment.

Ts - Stress value obtained from twenty seconds average data.

w - Sediment Moisture Content.

n/s - Not Significant.

Fig (6.30a): Charateristic Bed Stress and Moisture Content, Averaged Data .

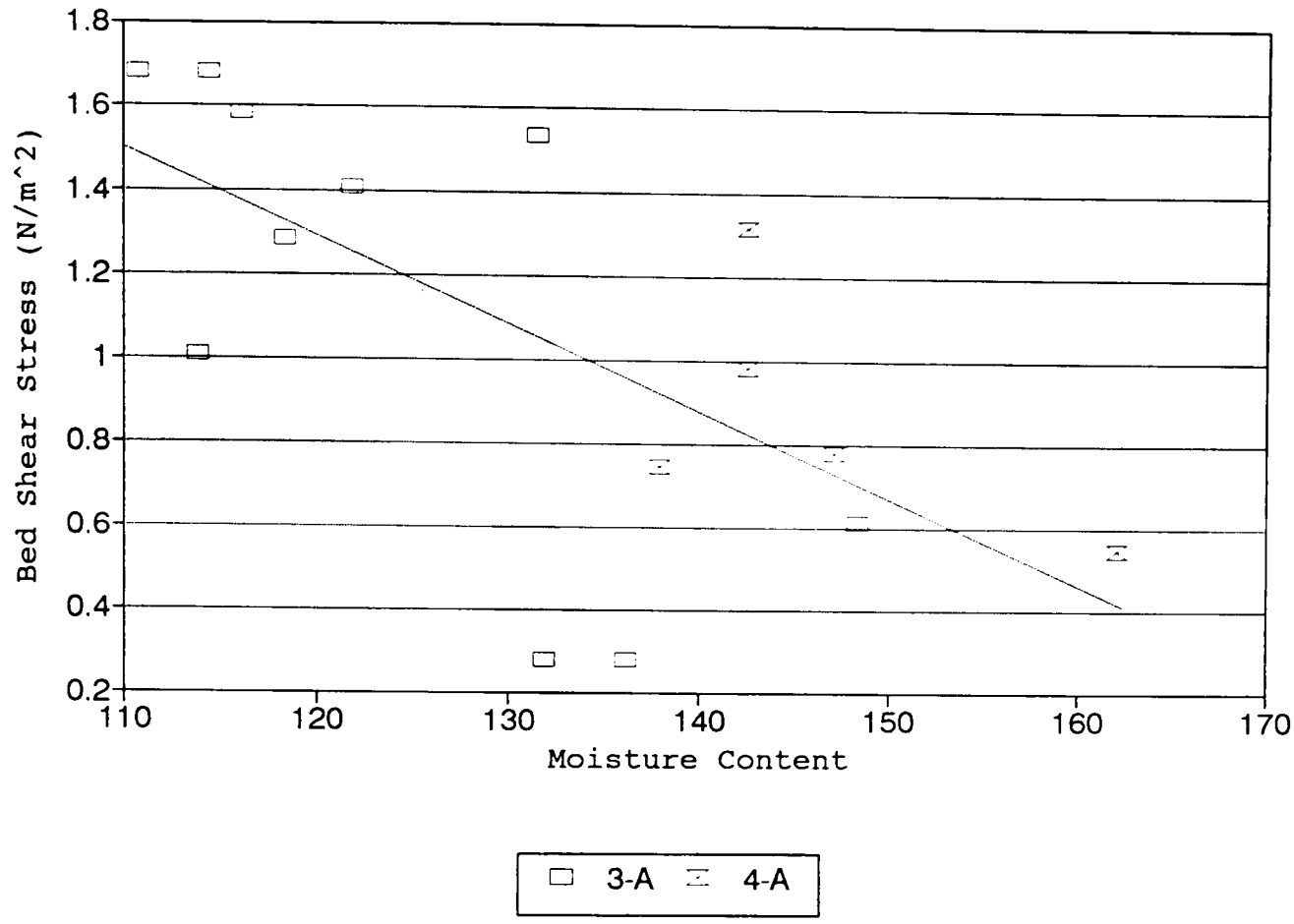

Fig (6.30b): Charateristic Bed Stress and Moisture Content, Sorted Data.

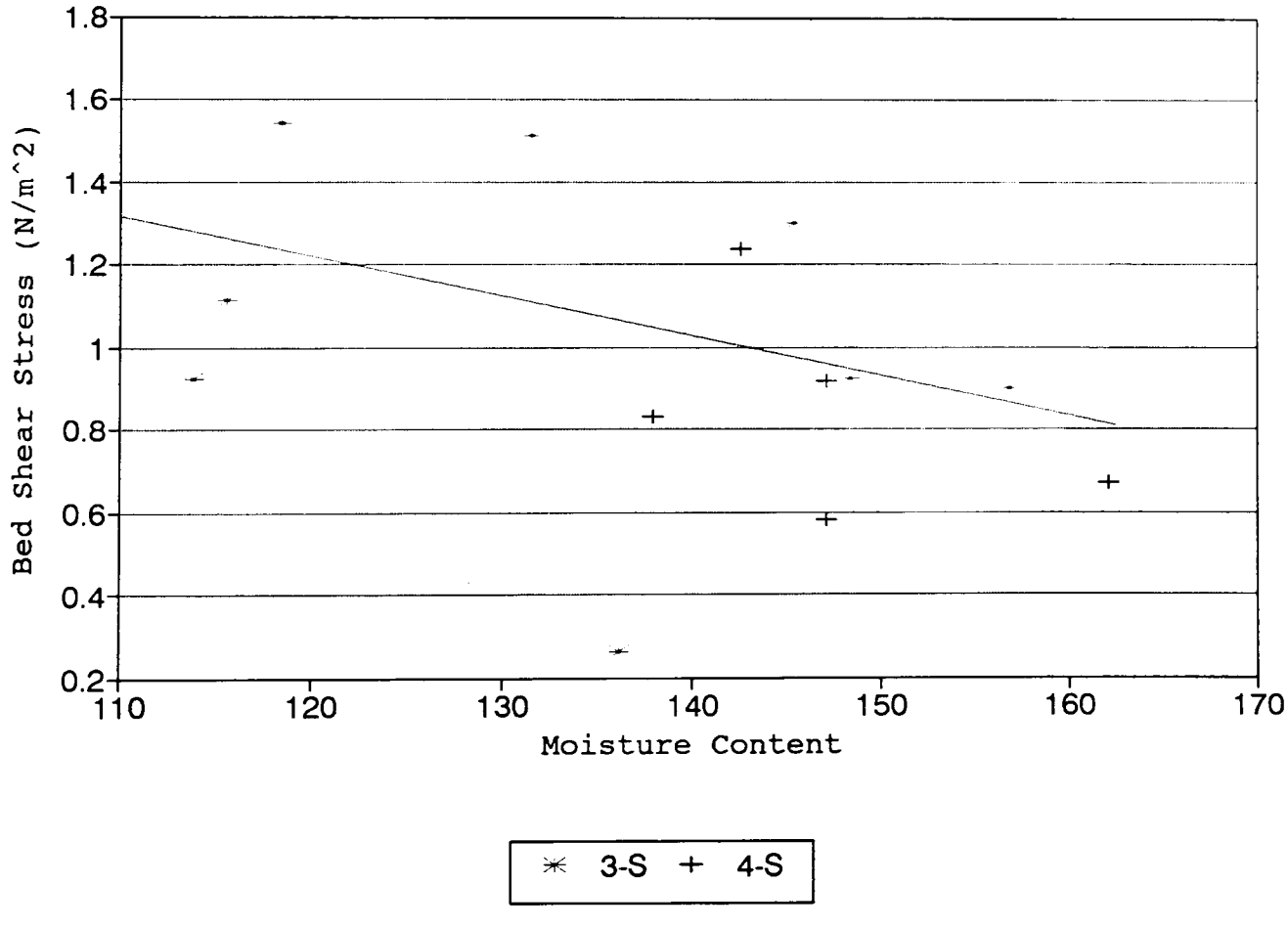

Fig (6.31a): Characteristic Bed Stress and Surface FF.

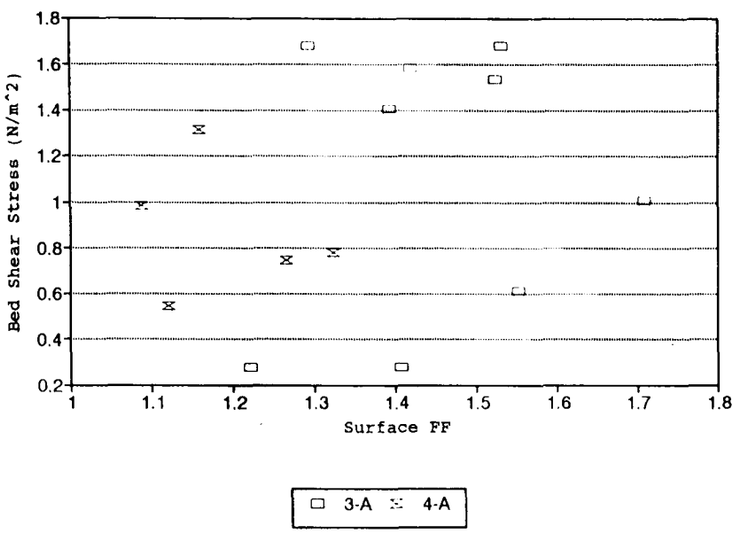

Fig (6.32a): Characterisitc Bed Stress and Average FF.

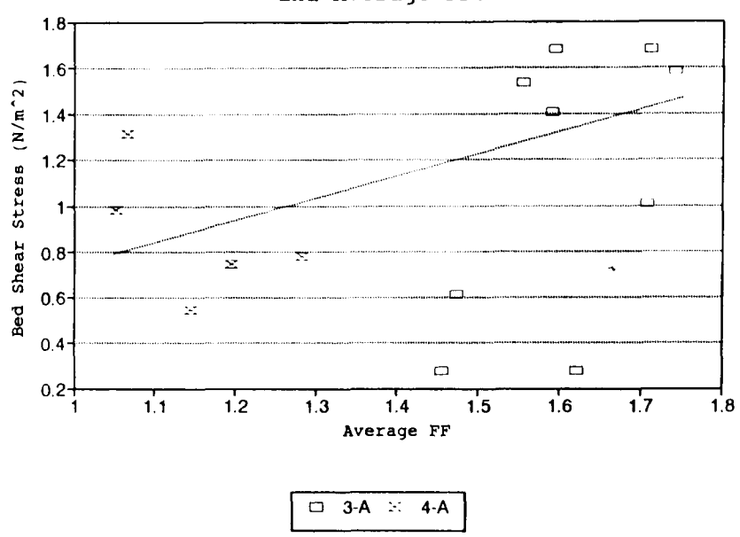

Fig (6.31b): Characteristic Bed Stress and Surface FF.

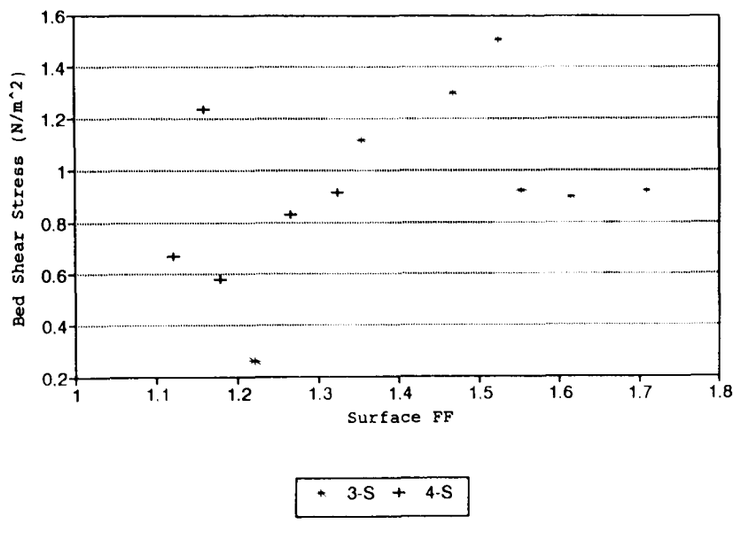

Fig (6.32b): Characterisitc Bed Stress and Average FF.

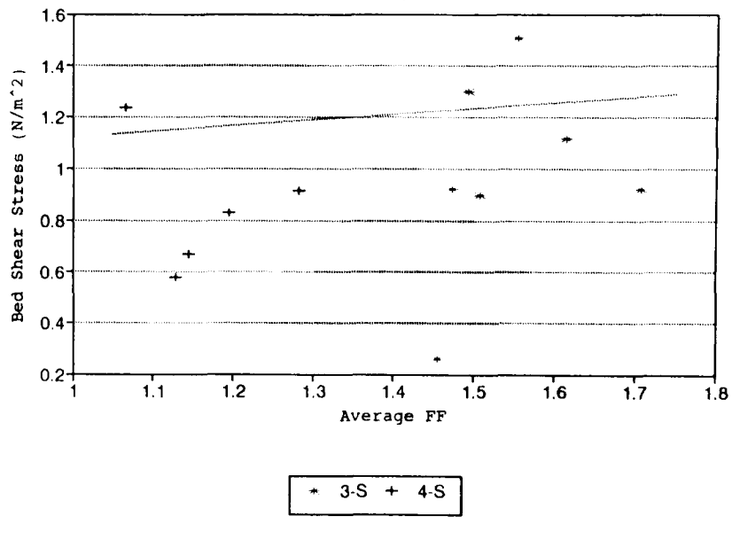

Fig (6.33a): Characteristic Bed Stress
and Surface Shear Wave Vel.

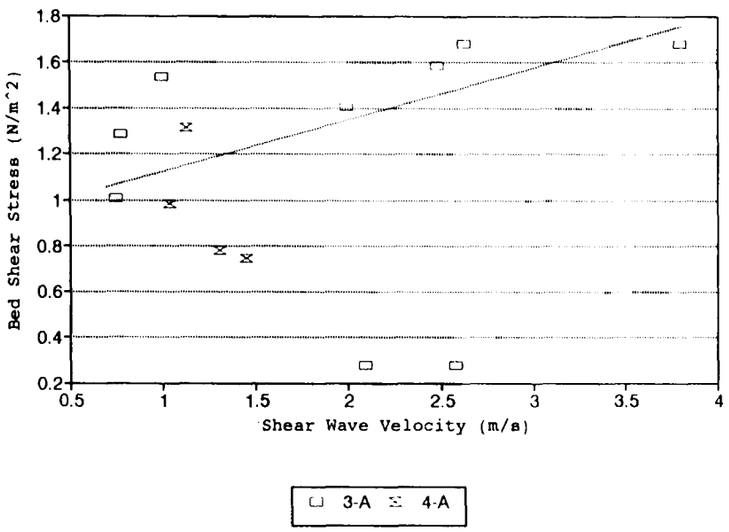

Fig (6.34a): Characterisitc Bed Stress
and Average Shear Wave Vel.

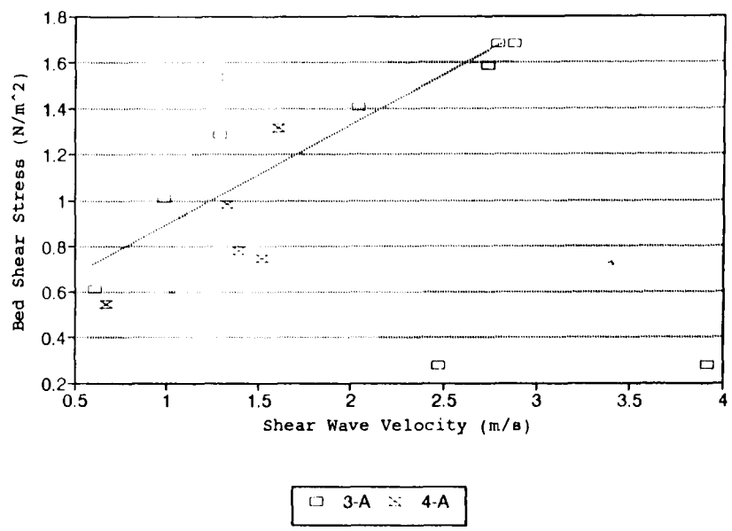

Fig (6.33b): Characteristic Bed Stress
and Surface Shear Wave Vel.

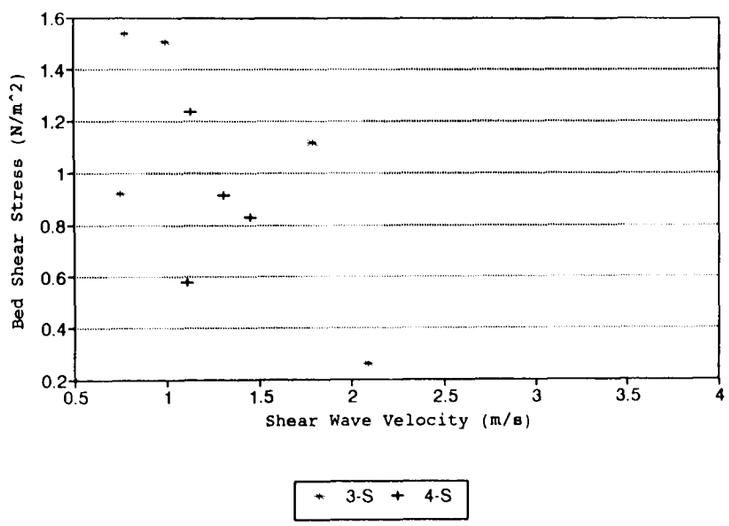

Fig (6.34b): Characterisitc Bed Stress
and Average Shear Wave Vel.

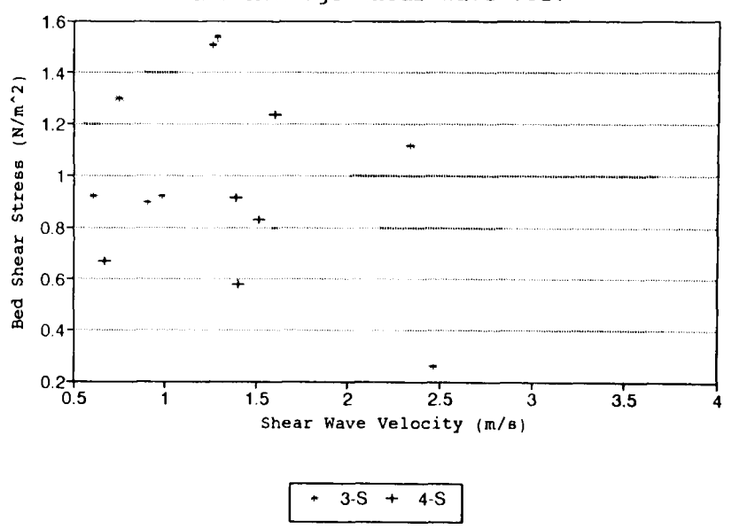

Fig (6.35a): Characteristic Bed Stress
and Surface (FF)Porosity.

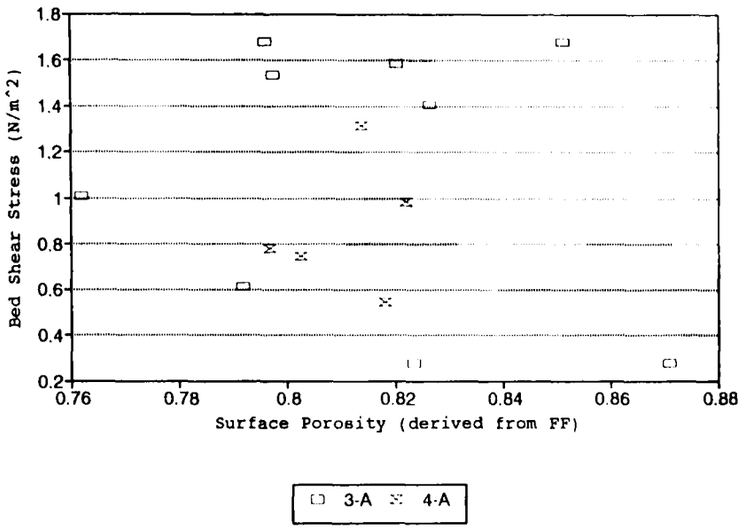

Fig (6.36a): Characteristic Bed Stress
and Average (FF) Porosity.

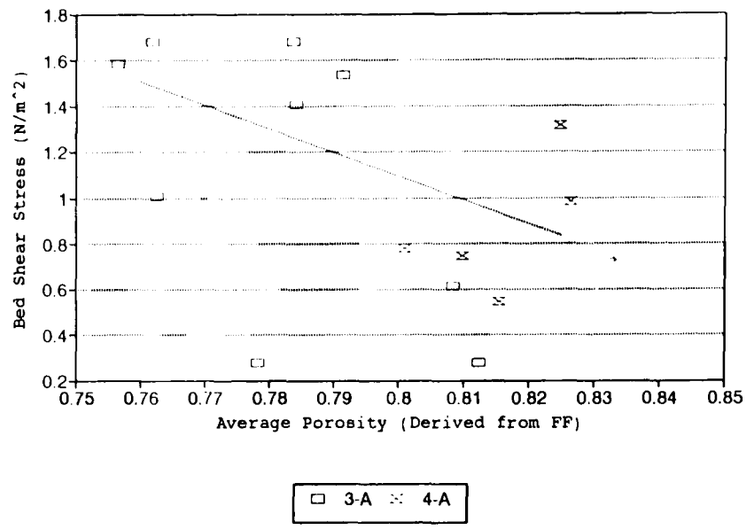

Fig (6.35b): Characteristic Bed Stress
and Surface (FF)Porosity.

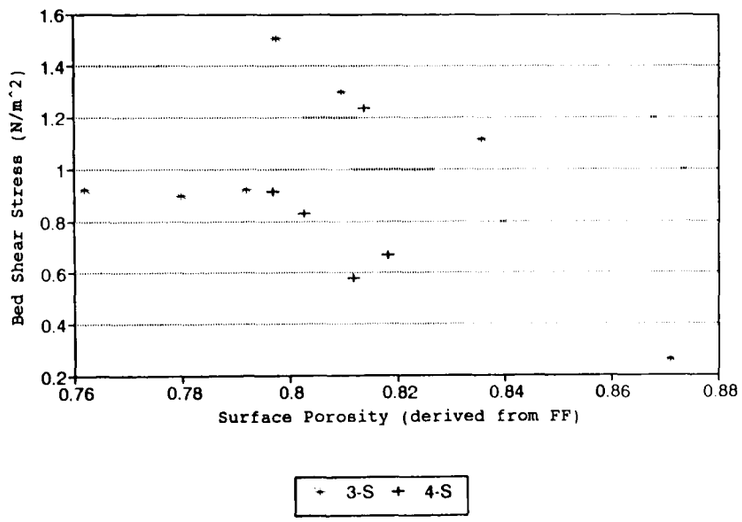

Fig (6.36b): Characteristic Bed Stress
and Average (FF) Porosity.

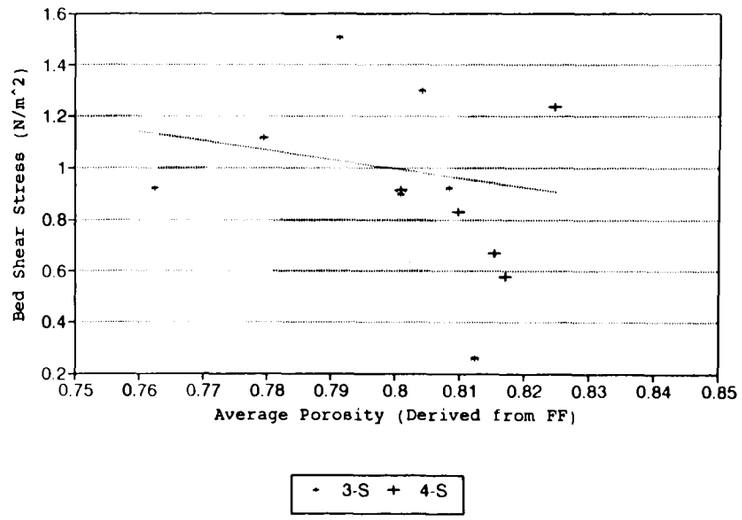

conditions and average bed erosion rate under those flow conditions. Thus the τ_{chs} data are likely to incorporate more noise then the τ_{chA} data.

For the combined data of muds 3 and 4, τ_{chA} show significant correlations with the depth averaged bed properties and with some of the surface bed properties. As with the bed property interrelationships the depth averaged results show the most correlations. There are two main reasons for this greater correlation to the depth averaged rather then the surface values: 1) As shown above (§6.2.2.) the surface measurements have greater variation than the average measurements. 2) The surface results would be expected to correlate best as erosion is initiated at the surface; but the beds do not show very great vertical heterogeneity (since no major vertical structural variations were allowed to form) and the threshold is calculated from erosion data at the bed surface and at depth, so the threshold value is an average threshold of all of the eroded bed material and should therefore relate best to the average bed property (as is often the case).

The most significant correlations are between τ_{ch} and the shear wave velocity data, which implies that shear wave velocity is a better indicator of bed erodibility then the other bed properties. The variation between the data collected for the two muds (muds 3 and 4) is less for the shear wave velocity data then it is for the formation factor data, and this is also shown on the graphs of shear wave velocity (Figure 6.5b) and formation factor (Figure 6.5a) to moisture content. This appears to suggest that the muds are different in terms of the relationship between formation factor and τ_{ch}, but are the same in terms of the relation between shear wave velocity and τ_{ch}. The correlations also show this, with the correlations between τ_{ch} and shear wave velocity for both the surface and average data improving when the data of mud 4 is added to the data of mud 3, but with the correlations to formation factor the changes are not all good. The average data do show a correlation when the mud 3 and mud 4 data are combined, but for the surface data the correlation of mud 3 are no longer significant when mud 4 data are added.

This similarity in terms of shear wave velocity behaviour but difference in terms of formation factor behaviour for muds 3 and 4 is due

to the inherent differences of these two parameters. The shear wave velocity is affected by the nature of particle contacts, as is the threshold. The formation factor is also measuring the nature of packing but because clays are present in the mud and biological material is on the particle surfaces, the formation factor will also measure surface conductance. This surface conductance means that the electrical resistance measured in the flume is an apparent resistance and not a true resistance and is one of the reasons why muds 3 and 4 need separate calibrations for the calculation of porosity from formation factor. Although this surface conductance will affect the formation factor, it appears to have less affect on the erosion threshold. However any affect that it may have on the threshold, will probably be caused by changes in the characteristics of particle contacts, which will also affect the shear wave velocity.

The possibility that shear wave velocity is a better indicator of erosion threshold can also be explained by the actual properties of the bed that formation factor and shear wave velocity are measuring. The formation factor is a measure of the bed's resistance to an electric current, and as this current can only flow in the fluid the formation factor is predominately a measure of the size and interconnection (tortuosity) of the pore space. As already shown it is possible to relate formation factor to porosity. Therefore the formation factor could be termed as a measurement of particle packing, and like moisture content and density, relate to the bed threshold in by virtue of being a measure of the number of particle contacts; as the sediment becomes less dense the porosity and moisture content(for a saturated sediment) will increase, the number of contacts between solids will decrease and the threshold of erosion of the bed will decrease. However the threshold is not solely dependent on the number of contacts between the particles of the sediment, but also on the nature of these contacts (how they behave under stress and how strong they are) as well as other properties. The shear wave velocity is affected by the degree of packing; work on sands has demonstrated that as the density of the sediment increases the shear wave velocity also increases; from acoustic theory (§3.1.) the velocity is determined by the number of particle contacts and also by their characteristics, i.e. by the nature of particle contacts. Thus shear wave velocity is controlled by more then just the sediment packing and since the additional controls are also likely to

determine τ_{ch}, shear wave velocity could give a better indication of erosion threshold then density and other packing measurements.

6.2.4. **Rigidity Results**

One of the major aims of this work was to look at the possible use of rigidity modulus as an indicator of cohesive sediment erodibility. The rigidity modulus (μ) can be determined from equation 3.5, using measured shear wave velocity and with the density value calculated from the formation factor (density can be derived from porosity assuming saturation, equation 5.28). This allows both an average and surface rigidity to be determined. Before rigidity and τ_{ch} were compared, the correlation between rigidity and moisture content was examined and as would be expect a negative correlation was obtained with rigidity increasing as the moisture content decreases and the bed becomes more solid. Table 6.9 shows Spearman's rank correlation coefficients of this relationship. Although the significance of this relationship is no greater then that between formation factor and moisture content on the one hand and shear wave velocity and moisture content on the other, the significance is the same but with fewer values. This may signify that a combination of formation factor and shear wave velocity produces a rigidity modulus that incorporates more useful information on the sediment than formation factor and shear wave velocity on their own do.

Figures 6.37 and 6.38 show the relationships between rigidity and the threshold. Spearman's rank correlation has again been carried out on this data and is displayed in Table 6.10. The τ_{chS} data showed no significant correlations to the rigidity, but the τ_{chA} data did show significant correlations. So once again, the time averaged data display the more significant correlations. Although of more importance it that a relationship between bed rigidity (measured by geophysical methods) and erosion threshold has been demonstrated.

Mud 3/4							
	Average Values				Surface Values		
	Correlation coefficent	No. of Values	Significance %		Correlation coefficent	No. of Values	Significance %
w	-0.868	15	2		-0.767	11	2

Table (6.9): Spearman's Rank Correlation Coefficients of the moisture content and bed rigidity relationships of Muds 3 and 4.

w - Sediment Moisture Content.

Mud 3/4							
	Average Values				Surface Values		
	Correlation coefficent	No. of Values	Significance %		Correlation coefficent	No. of Values	Significance %
Ta	0.809	11	2		0.583	9	10
Ts	----------	----------	n/s		----------	----------	n/s

Table (6.10): Spearman's Rank Correlation Coefficients of the characteristic bed stress and bed rigidity relationships of Muds 3 and 4.

Ta - Stress value obtained from data averaged over each stress increment.

Ts - Stress value obtained from twenty seconds average data.

n/s - Not Significant.

Fig (6.37a): Bed Stress at Erosion Threshold and Surface Rigidity.

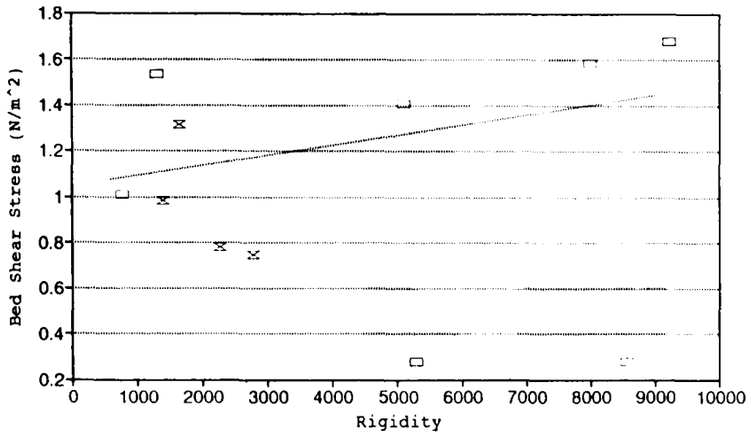

Fig (6.37b): Bed Stress at Erosion Threshold and Surface Rigidity.

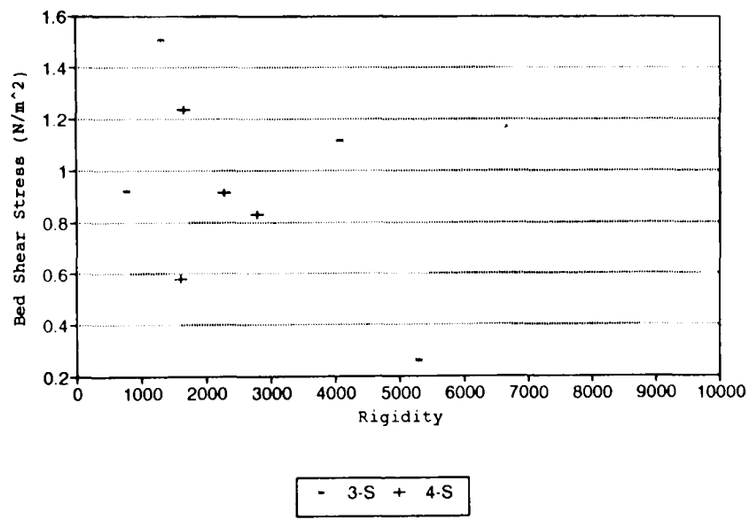

Fig (6.38a): Bed Stress at Erosion Threshold and Average Rigidity.

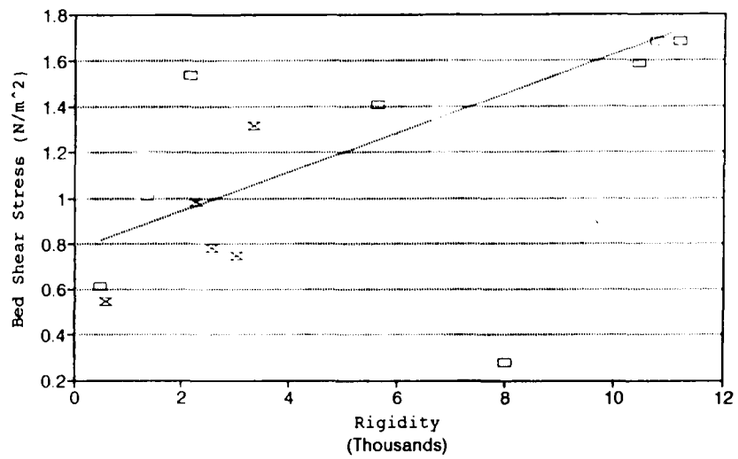

Fig (6.38b): Bed Stress at Erosion Threshold and Average Rigidity.

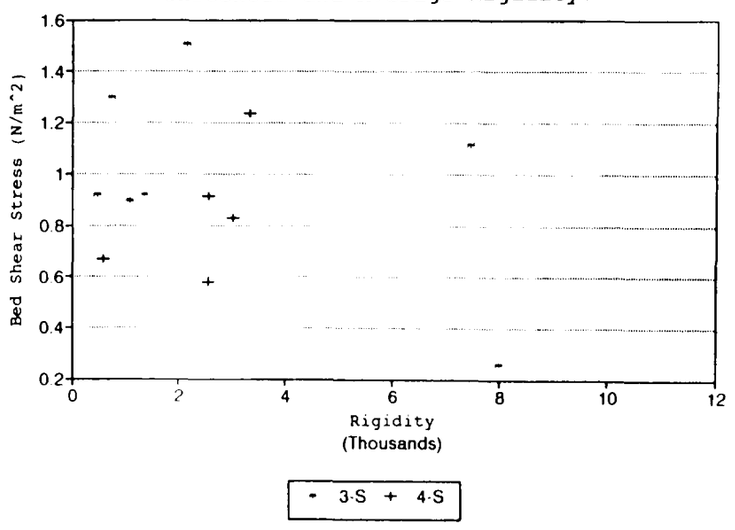

6.2.5. General Observations

Whilst a flume run was under way the perspex construction of the test section allowed visual observations of bed behaviour to be made. Due to the nature of these observations they are qualitative rather then quantitative but some interesting points should be raised.

A significant observation is that the nature of the initial erosion of the bed varied with moisture content. Although in all of the runs erosion started at some bed feature, be it a track caused by biological activity or a tiny crack from slight bed settlement, the erosion that followed varied. At low moisture contents small pieces of bed (a few millimetres in size at the most) were removed with erosion and then slowly moved down the bed in very much a straight line. The small pieces of the bed could be seen to move before they entered suspension, but the rest of the bed did not deform and these erosion points increased in number and size with time and increasing stress. Visual observation of the bed was then lost either on that stress increment as erosion proceeded or on the next stress increment when the erosion rate would increase. With high moisture content beds, the bed surface could be seen to flex before any initial erosion occurred, and once erosion had started it was very rapid and sight of the bed was quickly lost. However before sight of the bed was lost it could be seen that the site of erosion would move rapidly down the bed from its starting place, with the flow deforming the bed into a wave like appearance with material being suspended at the front of this feature (Figure 6.39).

As already stated it was observed that the flume runs on freshly collected mud that was still active biologically (i.e. visible tracks and topographic features were generated between the sediment being placed in the box and the start of a flume run) behaved differently form mud that was no longer biologically active. With active beds, erosion was occurring at all stress increments although at a very low rate in the early stress increments, and this erosion was occurring evenly across the bed at the surface features formed by the organisms. These organisms as well as generating topography also produced very small surface particles that could be easily entrained by the flow. The none active mud did not have

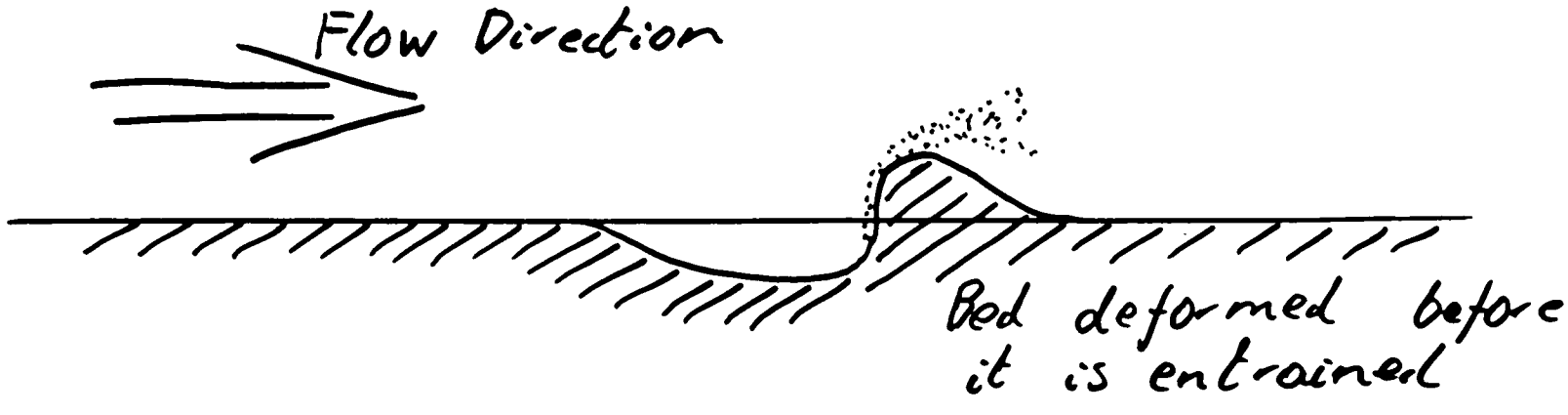

Figure (6.39): Deformation of eroding high porosity bed.

this surface topography and erosion did not occur at the low stress values; once it did start, bed failure was far more rapid.

A minor problem with the method used in this investigation to determine threshold is that it does not take into account any time-weakening of the bed; that is to say a time delay between the increase in bed stress and the initiation of erosion. Although this time delay only occurred on a few of the beds and then only at the low stress increments with low erosion rates, it was observed. However for a few of the beds this delay was apparent for the stress increment where major erosion of the bed started. This problem cannot easily be solved and it is a feature of erosion behaviour which can lead to over estimation of the erosion threshold.

A variable that was not considered in this investigation, is the affect of consolidation and strengthening of the bed with time and bed armouring from exposure to sub-threshold flows. The mud bed formed for run 20 was allowed to settle for about 48 hours before a flume run was started. This produced results very different from the freshly eroded muds; the bed was more resistant to erosion with only slight surface erosion occurring and no major failure of the bed surface even at the higher velocities which had completely remove the bed on earlier runs. However this was one of the early muds for which calculated results are not wholly reliable, and (and once again) due to time constraints further investigation of time varying bed properties and their affect on erosion behaviour was not investigated any further.

6.3. **Summary**

The bed properties and τ_{ch} data, show some form of relationship. For two of the most significant correlations τ_{chA} to average shear wave velocity and τ_{chA} to average rigidity modulus of the combined data of muds 3 and 4 a possible power relationship can be generated. For each one two slightly different results can be obtained depending on weather the fitted curve is forced through the origin or not.

τ_{chA} to average shear wave velocity (Vs)

$$\tau_{chA} = m_1 Vs^{1/5} + c_1 \qquad (6.1)$$

(Data points 13, R^2 = 0.685)

$$\tau_{chA} = m_2 Vs^{1/2} \qquad (6.2)$$

(Data Points 13, R^2 = 0.664)

τ_{chA} to average rigidity modulus (μ)

$$\tau_{chA} = m_3 \mu^{1/5} + c_3 \qquad (6.3)$$

(Data points 12, R^2 = 0.717)

$$\tau_{chA} = m_4 \mu^{1/3} \qquad (6.4)$$

(Data points 12, R^2 = 0.711)

where m and c are constants. Figures 6.40 and 6.41 show the results of this for the shear wave and rigidity data, respectively. In each plot the solid line is calculated only from the data and the dashed line is calculated from the data and forced through zero.

However these equations are only for the mud used in this study and are unlikely to be the same for other muds or for this mud in an undisturbed form in the field. Even if these equations are not useable for other muds, a relationship between two geophysical bed properties and the characteristic erosion threshold has been demonstrated and the general form of these relationships (a power relationship) has been shown.

Fig (6.40): Best Fit Relationship of Shear Wave Velocity and Shear Stress.

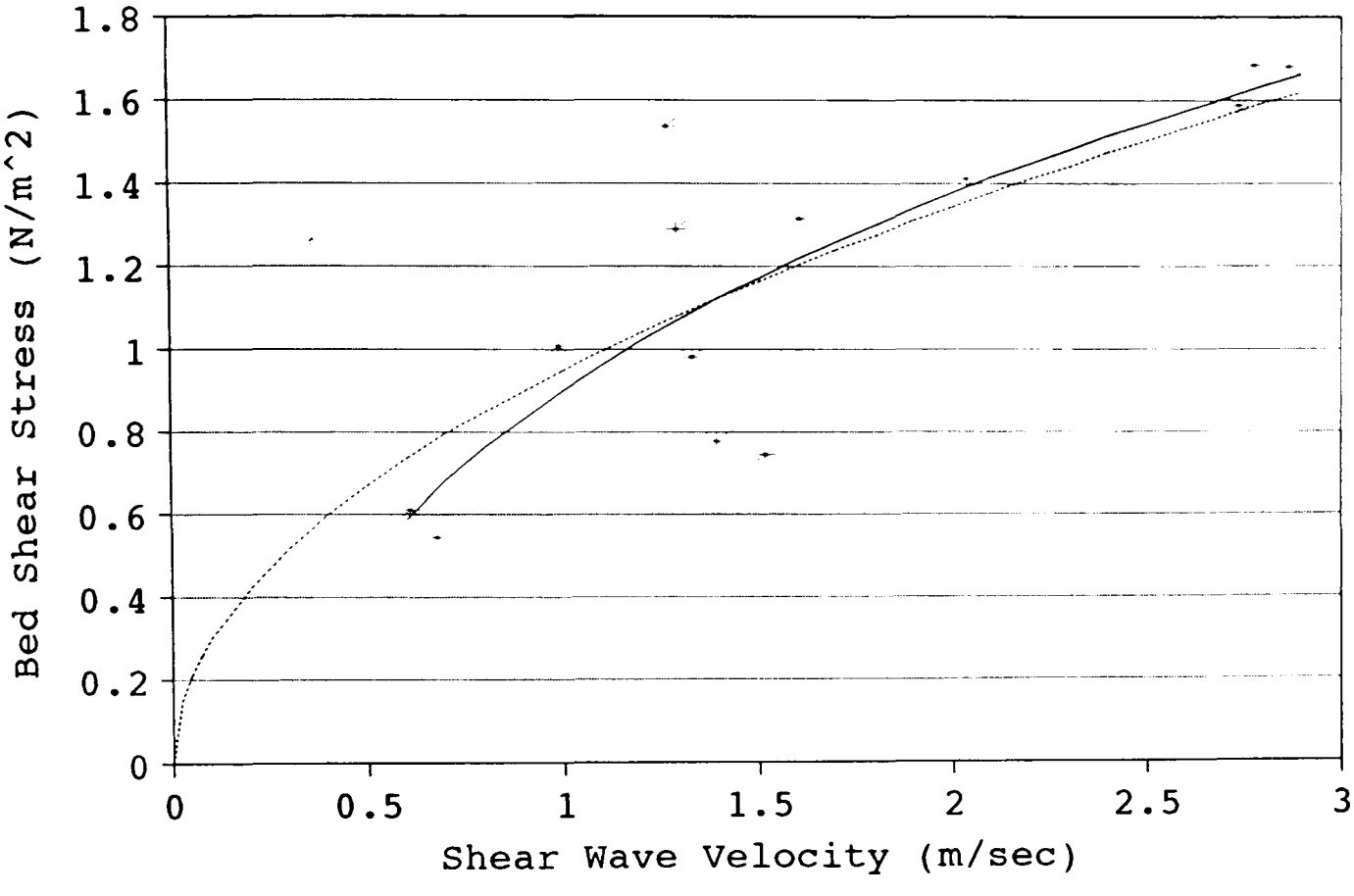

Fig (6.41): Best Fit Relationship of Rigidity and Shear Stress.

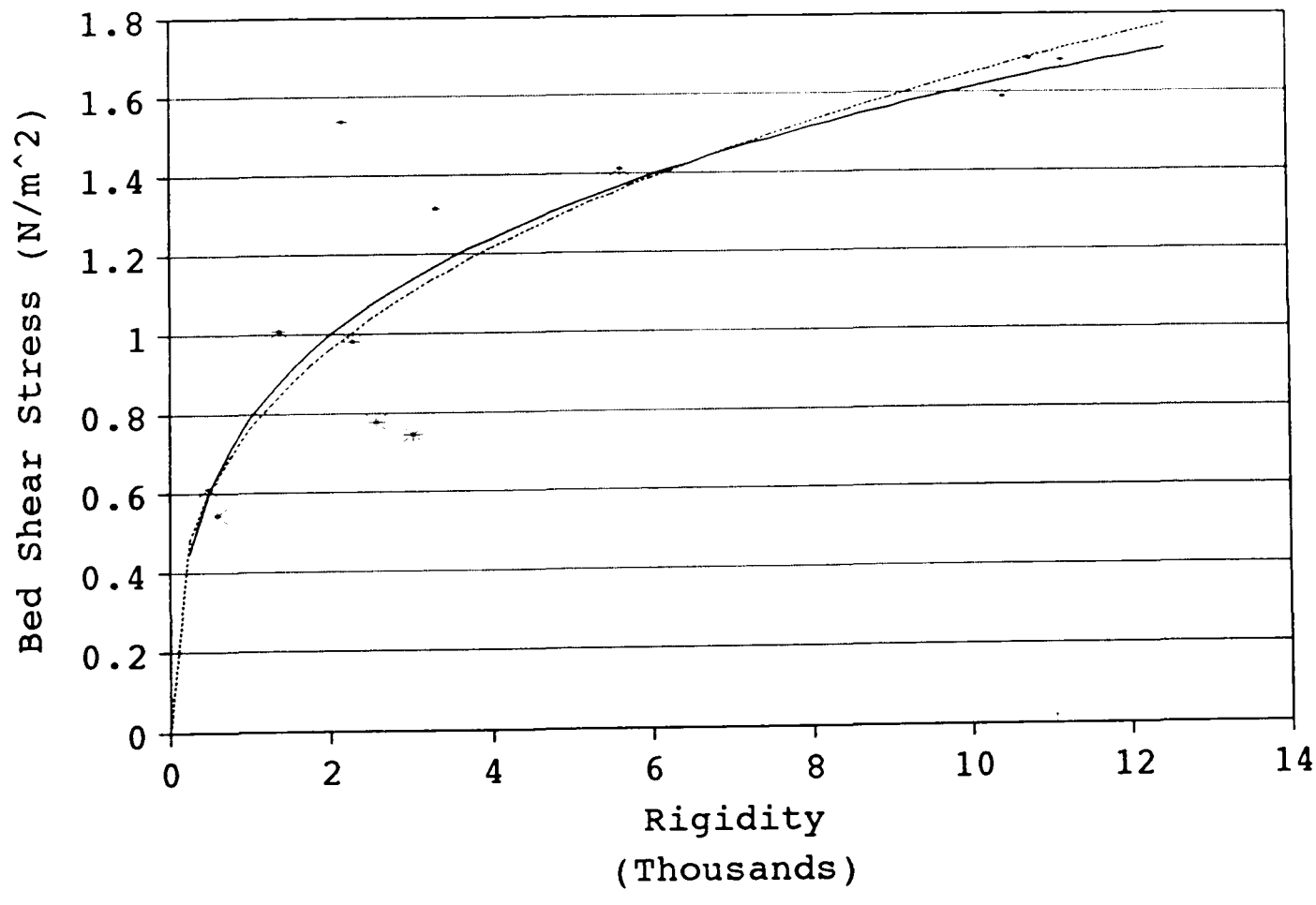

CHAPTER 7.

CONCLUSIONS.

7.1. Conclusions

(1) A recirculating laboratory flume has been constructed, and using this flume meaningful measurements of flow velocity, bed shear stress and suspended sediment concentration have been made.

(2) The flume has produced good data on the erosion behaviour of re-moulded cohesive sediments.

(3) Measurements of electrical formation factor have been made in high porosity clay-rich sediments, and these have been used to derive porosity data using calibration equations obtained from work in an instrumented oedometer cell.

(4) Shear wave velocity measurements have also been carried out successfully in these high porosity cohesive sediments using custom-built pezo-electric bender elements.

(5) Certain bed properties - moisture content, formation factor and shear wave velocity - have been shown to correlate significantly with the characteristic bed stress, τ_{ch}.

(6) Of these bed properties, shear wave velocity appears to be a better indicator of cohesive sediment erodibility then the other two (moisture content and electrical formation factor).

(7) The rigidity modulus, calculated using the non-destructive measurement techniques of shear wave velocity and formation factor (from which density was derived) has been correlated significantly with the characteristic bed stress, τ_{ch}.

(8) The relationships of rigidity modulus μ and shear wave velocity Vs to characteristic bed τ_{ch}, can be described by power relationships, $\tau_{ch} \propto \mu^{0.2}$ and $\tau_{ch} \propto Vs^{0.2}$, respectively.

7.2. **Further Work**

The work on the flume done as part of this investigation has given rise to a number of areas in which further work could be conducted.

A) The affect of suspended sediment on the hot film measuring sensors.

B) The affects of changes in particles size on the output from the optical back scattering sensors.

C) The use of filters to reduce noise and aliasing of the data logged by the DASH-8 card.

D) Improve the calibration method of the pressure sensors, with the aim of making the measurements more meaning full and understandable.

E) Develop an electronics package that would allow the acoustic backscatter to be used looking along the length of the flume test section to monitor the behaviour of the bed and the nature of re-suspension.

F) Improve the acoustic bed level monitor and its data logging.

G) Replace the present temperature probe with one that can have its output logged by computer.

H) Improve the method of collecting field cores and their insertion in the flume, to allow data to be collected on less disturbed sediment samples.

I) Investigate the nature of erosion, the size of particles that are being eroded, and the affects of changing bed roughness.

J) Investigate other muds to determine how universal the relationships found in this study may be.

REFERENCES

Abdel-Rahman, N.M., 1962. The effect of flowing water on cohesive beds. **Unpub. Ph.D. thesis, Swiss Federal Institute of Technology, Zurich, Switzerland.**

Al Ani, S., Dyer, K.R. and Huntley, D.A., 1991. Measurement of the influence of salinity on floc density and strength. **Geomarine Letters 11**, 154-158.

Alexis, A., Le Hir, P. and Teisson, C.., 1992. Study of consolidation of soft marine soils: unifying theories and numerical modelling. **MAST-I Section G6-M Coastal Morphodynamics Book of Extended Abstracts, Report 4.10.**

Alizadeh, A., 1974. Amount and type of clay and pore fluid influences an the critical shear stress and swelling of cohesive soils. **Unpub. Ph.D Thesis, Univ. of California, Davis, CA.**

Allen, J.R.L., 1970. **Physical Processes of sedimentation.** Allen & Unwin, 248pp.

Allen, J.R.L., 1971. Transverse erosional marks of mud and rock: their physical basis and geological significance. **Sed. Geol. 5(3/4)**, 167-385.

Allen, J.R.L., 1984. **Sedimentary Structure: their character and physical basis.** Elseveir, 663pp.

Allen, J.R.L., 1985. **Principals of physical sedimentology.** George Allen & unwin.

Aller, R.C., 1978. Experimental studies of changes produced by deposit feeders on pore water, sediment, and over lying water chemistry. **Am. J. Sci., 217**, 1185-1234.

Aller, R.C., 1980. Relationship of tube-dwelling benthos with sediment and overlying water chemistry, in: **Marine Benthic Dynamics** (eds. K.R.Tenrore and B.C.Coull), 285-308, Uni. South Carolina Press, Columbia.

Aller, R.C. and Yingst, J.Y., 1978. Biogeochemistry of tube-dwellings: A study of the sedimentary polychaete Amphitrite ornata (Leidy). **J. Mar. Res., 36**, 201-254.

Amos, C.L., 1991. Erodibility of the Starrs Point tidal flats. In: (Daborn et al., Eds.) **Littoral Investigation of Sediment Properties, Minas Basin, Bay Of Fundy, Compiled Final Report. Acadia Centre for Estuarine Research, Publ. No.17**, 145-182.

Amos, C.L. and Mosher, D.C., 1985. Erosion and deposition of fine-grained sediments from the Bay of Fundy. **Sedimentology, 32**, 815-832.

Amos, C.L., Grant, J., Daborn, G.R., and Black, K.S., 1992a. Sea Carousel - a benthic annular flume. **Estuarine Coastal Shelf Sci. 34,** 557-577.

Amos, C.L., Christian, H.A., Grant, J. and Paterson, D.M., 1992b. A comparison of in situ methods to measure mud flat erodibility. **Proc. 2nd. Inter. Conf. of Modelling Coastal, Est. and River Waters, Bradford, England,** September (in press).

Anderson, F.E., 1972. Re-suspension of estuarine sediments by small amplitude waves. **J. Sed. Petrol. 42,** 602-607.

Anderson, F.E., 1983. The northern muddy intertidal: a seasonally changing source of suspended sediment to estuarine waters - a review. **Can. J. Fish. Aquat. Sci. 40(Suppl.1),** 143-159.

Archie, G.E., 1942. The electrical resistivity log as an aid in determining some reservoir characteristics. **Petroleum Tech.,** 54-62.

Ariathurai, R. and Arulanandan, K., 1978. Erosion rates of cohesive soils. **J. Hydraul. Div. ASCE., 104, HY2,** 279-283.

Ariathurai, R. and Krone, K.B., 1976. Finite element model for cohesive sediment transport. **J. Hydraul. Div. ASCE., 102, HY3,** 323-338.

Arulanandan, K., 1975. Fundamental aspects of erosion of cohesive soils. **J. Hydraul. Div. ASCE, 101, HY5,** 635-639.

Arulanandan, K. and Heinzen, R.J., 1977. Factors influencing erosion in dispersive clays and methods of identification. **Proc. of the Paris Symp. on erosion and solid matter transport. International Association for Hydraulic Research,** 404-416.

Arulanandan, K., Sargunam, K. Loganathan, P. and Krone, R.B., 1973. Application of chemical and electrical parameters to the prediction of erodibility. In: **Soil Erosion: causes and mechanisms, prevention and control. Special Report No.135, Highways Research Board,** 42-51.

Arulanandan, K., Loganathan, P. and Krone, R.B., 1975. Pore and eroding fluid influences on the surface erosion of a soil. **J. Geotechnical Eng. Div. ASCE., 101 No. GT1. Proc paper 11078,** 51-66.

Arulanandan, K., Gilogley, E. and Tully, R., 1980. Development of a quantitative method to predict critical shear stress and rate of erosion of natural undisturbed cohesive soils. **Civil Engineering Dept., Univ. of California, Davis. Final Report to the U.S. Army, Waterways Experiment Station, Vicksburgh, Mississippi, Tech. Rep. GL-80-5,**54pp.

Attenborough, K., 1982. Acoustical characteristics of porous materials. **Physics Reports (Review Section of Physics Letters), 82(3),** 180-227.

Ashley, G.M. and Grizzle, R.E., 1988. Interactions between hydrodynamics, benthos and sedimentation in a tidal-dominated coastal lagoon. **Marine Geology 82(1/2)**, S61-81.

Babcock, K.l., 1963. Theory of chemical properties of soil colloidal systems at equilibrium. Section III: Double-layer theory. **Hilgardia 34(11)**, 471-480.

Badiey, M., Yamamoto, T., Turgut, A., Bennett, R. and Conner, C. S., 1988. Laboratory and in situ measurements of selected geoacoustic properties of carbonate sediments. **J. Acoust. Soc. Am., 84(2)**, 689-696.

Bagnold, R.A., 1946. Motion of waves in shallow water, interaction between waves and sand bottoms. **Proc. R. Sco. Lond., A 187**, 1-16.

Baier, R.E., 1973. Influence of the initial surface condition of materials in bioadhesion. In: **Proc. 3rd Inter. Congress on Corrosion and Fouling (eds. R.F. Acker, B.F. Browen, J.R. DePalma and W.D. Iverson)**, 633-639, National Bureau of Standards, Washington, D.C..

Bailey-Brock, J.H., 1979. Sediment trapping by chaetopterid polychaetes on a Hawaiian fringing reef, **J. Mar. Res. 37**, 643-656.

Bain, A.J., 1981. Erosion of Cohesive Sediments. **Unpub MSc. Thesis, Dept. Engineering, Manchester Univ**, 111pp.

Bassoulett, P. and Le Hir., P., 1992. Mud characterisation on intertidal flats: in situ experiments. **MAST-I Section G6-M Coastal Morphodynamics Book of Extended Abstracts, Report 4.3.**

Batchelor, G.K., 1970. **An Introduction to Fluid Dynamics**, Cambridge.

Beckett, A. and Read, N.D., 1986. Low-temperature scanning electron microscopy. In: **Ultrastructure Techniques for Micro-organisms** (Aldrich, H. and Todd, W., Eds.), Plenum, 45-86.

Been, K. and Sills, G.C., 1981. Self weight consolidation of soft soils: an experiment and theoretical study. **Geotechnique, 31**, 519-535.

Bell, D.W. and Shirley, D.J., 1980. Temperature variation of the acoustical properties of laboratory sediments. **J. Acoust. Soc. Am., 68(1)**, 227-231.

Bell, S.S. and Sherman, K.M., 1986. A field investigation of meiofaunal dispersal: tidal resuspension and implications. **Mar. Ecol. Prog. Ser. 3**, 245-249.

Bennet, R.H., 1976. Clay fabric and geotechnical properties of selected submarine cores from the Mississippi. **Ph.D thesis, Texas A&M Univ.**, 269.

Bennet, R.H. and Hulbert, M.H., 1986. **Clay Microstructure**. International Human Resources Development Corporation Press, Prentice Hall, Boston, Mass., 161.

Bennet, R.H., Bryant, W.R. and Keller, G.H., 1981. Clay fabric of selected submarine sediments: fundamental properties and models. **J. Sed. Petrol. 51(1)**, 217-232.

Bennet, R.H., O'Brien, N.R. and Hulbert, M.H., 1990. **Microstructure of Fine-grained Sediments. Frontiers in Sedimentary Geology**, Springer-Verlag, 582pp.

Berghager, D. and Ladd, C.C., 1964. Erosion of cohesive soils. **Research report R64-1, Dept. of Civil Eng., Massachusetts Institute of Tech., Cambridge, Mass.**.

Berryman, J.G., 1980. Confirmation of Biot's Theory. **Appl. Phys. Lett., 37(4)**, 382-384.

Berryman, J.G., 1980. Long-wavelength propagation in composite elastic media. I.Spherical inclusions. **J. Acoust. Soc. Am., 68(6)**, 1809-1819.

Berryman, J.G., 1980. Long-wavelength propagation in composite elastic media. II.Ellipsodial inclusions. **J.Acoust. Soc. Am., 68(6)**, 1820-1831.

Beutelspacer, H. and van der Marel, H.W., 1968. **Atlas of electron microscopy of clay minerals and their admixtures**. Elsevier, Amsterdam.

Biddle, P. and Miles, J.H., 1972. The nature of contemporary silts in British estuaries. **Sedimentary Geol., Vol.7**, 23-33.

Biot, M.A., 1941. General theory of three-dimensional consolidation. **J. Applied Physics, 12**, 155-164.

Biot, M.A., 1956. Theory of propagation of elastic waves in a fluid-saturated porous solid. I. Low-frequency range. **J. Acoust. Soc. Am., 28(3)**, 168-178.

Biot, M.A., 1956. Theory of propagation of elastic waves in a fluid-saturated porous solid. II. Higher frequency range. **J. Acoust. Soc. Am., 28(3)**, 179-191.

Biot, M.A., 1962. Mechanics of deformation and acoustic propagation in porous media. **J. Applied Physics, 33**, 1482-1489.

Biot, M.A., 1962. Generalized theory of acoustics propagation in porous dissipative media. **J. Acoust. Soc. Am., 34(9)**, 1254-1264.

Black, K.S., 1991. The Erosion Characteristics of Cohesive Estuarine Sediments: some in situ experiments and observations. **Unpublished Ph.D. Thesis, Univ. Wales**, 313pp.

Black, K.S., 1993. The erosion of cohesive marine sediments in shallow water environments: a review. **Unpublished**

Bokuniewicz, H.J., Gordon, R.B. and Rhoads, D.C., 1975. Mechanical properties of the sediment-water interface. **Mar. Geol. 18**, 263-278.

Bordovsky, O.K., 1965. Accumulation and transformation of organic substances in marine sediments 3. Accumulation of organic matter in bottom sediments. **Marine Geology 3**, 33-82.

Booth, J.S. and Dahl, A.H., 1984. A note on the relationships between organic matter and some geotechnical properties of a marine sediment. **Mar. Geotechnol. 6(No.3)**, 281-297.

Bowles, F., Bryant, W.R. and Wallin, C., 1969. Microstructure of consolidated and unconsolidated marine sediments. **J. Sed. Petrol. 39**, 1546-1551.

Bowles, J.E., 1979. **Physical and Geotechnical Properties of Soils.** McGraw-Hill, New York.

Boyce, R.E., 1968. Electrical resistivity of modern marine sediments from the Bearing Sea. **J. Geophys. Res., 73**, 4759-4766.

Boyce, R.E., 19. Determination of the relationships of electrical resistivity, sound velocity, and density/porosity of sediment and rock by laboratory techniques and well logs from deep sea drilling project. **Initial Rep. Deep Sea Drilling Project, 50(4)**, 305-318.

Boyer, L.F., 1980. Production and preservation of surface traces in the intertidal zone. **Ph.D. Thesis, Univ. of Chicago, Chicago, Illinois.**

Brace, W.F., and Orange, A.S. and Madden, T.k., 1965. The effect of pressure on the electrical resistivity of water-saturated crystalline rocks. **J. Geophys. Res., 70(22)**, 5669-5678.

British Standard, 1377: 1961. Methods of Testing Soils for civil Engineering Purposes. **British Standards Institution.**

Brodkey, R.S., Wallace, J.M. and Eckelmann, H., 1974. Some properties of truncated turbulence signals in bounded shear flows. **J. Fluid Mech., 63**, 209-224.

Browen, G.L. and Davey, R.F., 1971. The calibration of Hot Films for skin friction measurements. **Rev. Sci. Instrum., 42(1)**, 1729-1731.

Brown, J.S., 1980. Connection between formation factor for electrical resistivity and fluid-solid coupling in Biot's equations for acoustic waves in a fluid-filled porous media. **Geophysics, 45(8)**, 1269-1275.

Brown, S.L., 1984. Benthic invertebrate faeces and nutrient recycling on an intertidal sandflat: Loughor Estuary, S.Wales. **Unpub. Ph.D thesis, Univ. Wales**, 333pp.

Bryant, W.R., Bennett, R.H., Burkett, P.J. and Rack, F.R., 1990. Microfabric and physical properties characteristics of a consolidated clay section. In: (Bennet, R.H., O'Brien, N.R. and Hulbert, M.H., Eds.) **Microstructure of Fine-grained Sediments. Frontiers in Sedimentary Geology**, Springer-Verlag, 73-92.

Buchan, S., Floodgate, G.D. and Crisp, D.J., 1967. Studies on the seasonal variations of the suspended matter in the Menai Straits. I. The inorganic fraction. **Limnol. Oceanogr., 12**, 419-431.

Bull, M.K. and Willis, J.L., 1961. Some results of experimental investigations of the surface pressure field due to turbulent boundary layer. **Univ. Southampton, Dept. Aronautic Astrpnautics, Report No. 199**, 1-27.

Burrel, D.C., 1983. Patterns of carbon supply and distribution and oxygen renewal in two Alaskan fjords. **Sediment. Geol. 36**, 93-115.

Butman, C.W. and Wheatcroft, 1991. Field measurements of fine-scale sediment grading at the STRESS site: Implications for the interpretation of light transmission records. **Sec. 021C(-8)** p.241 American Geophysical Union Fall Meeting (abstract only).

Byers, S.C., Eric, L.M. and Stewart, L.P., 1978. A comparison of methods of determining organic carbon in marine sediments, with suggestions for a standard method. **Hydobiologia, 8(1)**, 43-47.

Cadee, G.C., 1979. Sediment reworking by the polychaete Heteromastus filiformis on a tidal flat in the Dutch Wadden Sea. **Neth. J. Sea Res. 13**, 441-456.

Cadee, G.C., 1984. Biological activity and sediments. In: (Molinari, J., Ed) **Sediments and Pollution in Waterways**, IAEA, Vienna, Tech. Documents, IAEA-TECDOC-302, 111-126.

Cardoso, A.H., Graf, W.H. and Gust, G., 1989. Uniform flow in a smooth open channel. **J. Hydraul. Res. 27(5)**, 603-616.

Carson, B., Carney, K.F. and Meglis, A.J., 1988. Sediment aggregation in a salt-marsh complex, Great Sound, New Jersey. **Marine Geology 82**, 83-96.

Casagrande, A., 1932. The structure of clay and its importance in foundation engineering. **J. Boston Soc. Civ. Engrs. 19**, 168-221.

Chan, K.W., Baird, M.H.I. and Round, G.F., 1972. Behaviour of beds of dense particles in horizontal oscillatory liquid. **Proc. R. Soc. London, A 330**, 537-559.

Chapman, G.A., 1949. The thixotropy and dilatancy of a marine soil. **J. Mar. Biol. Assoc. U.K. 28**, 123-140.

Chapuis, R., 1986. Quantitative measurements of the scour resistance of natural solid clays. **Can. Geotech. J. 23**, 132-141.

Chapuis, R. and Gatien, T. 1986. An improved rotating cylinder technique for the quantitative measurements of scour resistance of clays. **Can. Geotech. J. 23**, 83-87.

Characklis, W.D., 1984. Biofilm development: a process analysis. In: **Microbial adhesion and aggregation** (Marshall, K.C., Ed.), Springer-Verlag, 137-158.

Christian, H.A., 1991. Geomechanics of Starrs Point tidal flat. In: (Daborn et al, Eds.) **Littoral Investigations of Sediment Properties, Minas Basin, Bay of Fundy, Compiled Final Report**. Acadia Centre for Estuarine Res., Publ.No.17, 113-144.

Christensen, R.W. and Braja M.Das, 1973. Hydraulic erosion of remoulded cohesive soils. In: **Soil Erosion: Causes Mechanisms, Prevention and Control Spec. Rep. No.135, Highways Research Board**, 52-74.

Chriss, T.M. and Caldwell, D.R., 1984. Universal similarity and the thickness of the viscous sub-layer flow at the ocean floor. **J. Geophys. Res., 89**, 6403-6414.

Clifford, N.J., 1990. The formation, nature and maintenance of riffle-pool sequences in gravel-bed rivers. **Unpub. PH.D Thesis, Univ Cambridge.**

Cole, P. and Miles, G.V., 1983. Two dimensional model of mud transport. **J. Hydraul. Engng. ASCE., 109(1)**, 1-12.

Collins, K. and McGowen, A., 1974. The form and function of microfabric features in a variety of natural soils. **Geotechnique, 24**, 223-254.

Conner C.S. and de Visser, A.M., 1992. A laboratory investigation of particles size effects on an optical back scatter sensor. **Mar. Geol. 108**, 151-159.

Corino, F.R. and Brodkey, R.s., 1969. A visual investigation of the wall region in turbulent flow. **J. Fluid Mech. 37**, 1-30.

Cormault, P., 1971. Determination exerimentale du debit solide d'erosion de sediments fins cohesifs. **Proc. 14th. Congress of the IAHR, 4**, 9-16.

Costerton, J.W., Irvin, R.T. and Cheng, K.-J., 1981. The bacterial glycocallyx in nature and disease. **Ann. Rev. Microbiol. 35**, 299-324.

Cratchley, C.R., Davis, A.M. and Taylor Smith, D., 1982. Enhancement of the role of geophysics in marine geotechnical investigations. **Oceanology International Conf. Brighton.**

Creutzberg, F. and Postma, H., 1979. An experimental approach to the distribution of mud in the North Sea. **Neth. J. Sea Res. 13(1)**, 99-116.

Croad, R.N., 1981. Physics of erosion of cohesive soils. **Ph.D. thesis, Depy. Civil Engineering, Univ. Auckland, N. Zealand.**

Cullen, D.J., 1973. Bioturbation of superficial marine sediments by interstitial meiobenthos. **Nature 242**, 323-324.

D&A Instruments, 1989. Optical methods for measuring turbidity and suspended particles in water. Some notes for users of OBS^{tm} sensors. **D&A Instruments, Technote (3/89).**

Daborn, G.R., 1991. Laboratory flume studies on sediment erodibility. In: (Dabron et al, Eds.) **Littoral Investigation of Sediment Properties, Minas Basin, Bay of Fundy**, Compiled Final Rep. Acadia Cen. Estur. Res., Publ. No.17, 191pp.

Daborn, G.R., et al, 1991. **Littoral Investigation of Sediment Properties, Minas Basin, Bay of Fundy**, Compiled Final Rep. Acadia Cen. Estur. Res., Publ. No.17, 239pp.

Dade, W.B. and Nowell, A.R.M., 1991. Moving muds in the marine environment. **Coastal Sediments 1991**, 54-71.

Dade, W.B., Nowell, A.R.M. and Jumars, P.A., 1992. Predicting the erosion resistance of muds. **Marine Geology 105**, 285-297.

Das, B.M., 1983. **Advanced Soil Mechanics**. MacGraw-Hill Book Company, N.Y., 520pp.

Dauphine, J.M. and Klein, H.P., 1977. The effect of temperature on the electrical conductivity of seawater. **Deep-Sea Res., 24**, 891-902.

Davies, A.G., 1980. Field observations of the threshold of sand motion in a transitional wave boundary layer. **Coastal Eng., 4**, 23-46.

Dean, W.E., Jr., 1974. Determination of carbonate and organic matter in calcareous sediments and sedimentary rocks by loss on ignition: comparison with other methods. **J. Sed. Petrol., 44**, 242-248.

Devries, J., 1992. Field measurements of the erosion of cohesive sediments. **J. Coastal Res. 8(2)**, 312-318.

Domenico, S.N., 1977. Elastic properties of unconsolidated porous sand reservoirs. **Geophysics, 42(7)**, 1339-1368, (Discussion, Geophysics, 44(4), 830-833).

Downing, J.P. and Beach, R.A., 1989. Laboratory apparatus for calibrating optical suspended solids sensors. **Mar. Geol. 86**, 243-249.

Drake, D.E. and Cacchinone, D.A., 1986. Field observations of bed shear stress and sediment re-suspension on continental shelves, Alaska and California. **Continental Shelf Res. 6(3)**, 415-429.

Duck, R.W. and McManus, J., 1991. Cohesive sediments in Scottish Freshwater Lochs and Reservoirs. **Geomarine Letters 11**, 127-131.

Dunn, I.S., 1959. Tractive resistance of cohesive channels. **J. Soil Mech. Foundations Div. ASCE., Vol.85, No.SM3.**

Dyer, K.R., 1986. **Coastal and estuarine sediment dynamics**. Wiley.

Dyer, K.R., 1989 Sediment Processes in Estuaries: Future Research Requirements. **J. Geophys. Res. 94 (C10)**, 14,327-14,339.

Eckman, J.E., 1983. Hydrodynamic processes affecting benthic recruitment. **Limnol, Oceanogr. 28**, 241-257.

Eckman J.E. and Nowell, A.R.M., 1980 Boundary skin friction and sediment transport about an animal tube mimic. **Sedimentology 31**, 851-862.

Eckman J.E., Nowell, A.R.M. and Jumars, P.A., 1979. The influence of animal motility on sediment entrainment. **EOS 60**, p847 (abstract only).

Eckman J.E., Nowell, A.R.M. and Jumars, P.A., 1981. Sediment destabilisation by animal tubes. **J. Mar. Res. 39**, 361-374.

Einstein, H.A. and Krone, R.B., 1962. Experiments to determine modes of cohesive sediment transport in salt water. **J. Geophys. Res., 67**, 1451-1461.

Eisma, D., 1986. Flocculation and deflocculation of suspended matter in estuaries. **Neth. Jour. Sea Res. 20(2/3)**, 183-199.

Enger, P.F., 1964. Canal erosion and tractive force study - analysis of data taken on a boundary shear flume. **Hydraul. Branch Report No. Hyd- 532, Bureau of Reclamation, Denver, Cole.**.

Enger, P.F. and Carlson, E., 1985. Canal erosion and tractive force study - analysis of data from a boundary shear flume. **Breau of reclamation, Denver, Hydraulic Branch Rep. HYD-532.**

Erchul, R.A. and Nacci V.A., 1972. Electrical resistivity measuring system for porosity determination of marine sediments. 47-53.

Evans, G. 1965. Intertidal flat sediments and their environments of deposition in the wash. **Q. J. Geol. Soc. Lond. 121**, 209-245.

Faas, R.W., 1991. Rheological boundaries of mud: where are the limits? **Geomarine Letters 11**, 143-146.

Fazio, S.A., Uhlinger, D.G., Parker, J.H. and White, D.C., 1982. Estimations of uronic acids as quantitative measures of extracelluar polysaccharide and cell wall polymers from environmental samples. **Appl, Env, Microbiol, 43**, 446-450.

French, J.R. and Clifford, N.J., 1992. Characteristics and 'event structure' of near bed turbulence in a macrotidal saltmarsh channel. **Estuar. Coastal Shelf Sci. 34(1)**,46-69.

Featherstone, R.P. and Risk, M.J., 1977. Effects of tube-dwelling polychaetes on intertidal sediments of the Minas Basin, Bay of Fundy, **J.Sediment. Petrol. 47**, 446-450.

Fukuda, M.K., 1978. The entrainment of cohesive sediments in freshwater. **Unpub. Ph.D. thesis, Case Western Reserve Univ., Cleveland, Ohio.**

Fukuda, M.K. and Lick, W., 1980. The entrainment of cohesive sediments in fresh water. **J, Geophys. Res., 85**, 2813-2824.

Galle, K.O. and Runnels, R.T., 1960. Determination of CO_2 in carbonate rocks by controlled loss on ignition. **J. Sed. Petrol. 30(4)**, 613-618.

Gibbs, R.J. and Konwar, L., 1986. Coagulation and settling of Amazon River suspended sediment. **Cont. Shelf Res. 6(1/2)**, 127-149.

Gibbs, R.J. and Wolanski, E., 1992. The effect of flocs on optical back scattering measurements of suspended material concentrations. **Mar. Geol. 107**, 289-291.

Glogger, B. and Hanselman, K.W., 1985. Microstructure of lake sediments: sediment aggregates a microbiol habitat. **Experientia 41**, 555.

Gordon, C.M., 1974. Intermittent momentum transport in a geophysical boundary layer. **Nature 248**, 392-394.

Graham, D.I., James, P.W., Jones, T.E.R., Davies, J.M. and Delo, E.A., 1991. Measurement and prediction of surface shear stress in annular flume. **J. Hydrul. Engng. 118(No.9)**, 1270-1216

Granboulan, J., Feral, A., Villerot, M. and Jouanneau, J.M., 1989. Study of the sedimentological and rheological properties of fluid mud in a fluvio-estuarine system of the Gironde Estuary. **Ocean Shoreline Manag. 12(1)**, 23-46.

Grant, J., Bathmann, U.V. and Mills, E.L., 1986. The interaction between benthic diatom films and sediment transport. **Estuar. Coastal. Mar. Sci. 23**, 225-238.

Grant, J., Griswold, A. and Daborn, G.R., 1990. Flume measurements of erosion in bioturbated intertidal mud. **13th Int. Sedimentological Congress, Nottingham, England**, p.197 (Abstract only).

Grant, W.D., Boyer, L.F. and Sanford, L.P.,1982. The effects of bioturbation on the initiation of motion of intertidal sands. **J. Mar. Res. 40**, 659-677.

Grass, A.J., 1970. Instability of a fine sand bed. **J. Hydraulics Division, Porc. ASEC 96(Hy 3)**, 619-632.

Gray, J.S., 1974. Animal-sediment relationships. **Ann. Rev. Oceanogr. Mar. Biol. 12**, 223-261.

Grass, A.J., 1971. Structural features of turbulent flow over smooth and rough boundaries. **J. Fluid Mech., 50**, 233-255.

Grenon, J.-F. and Walker, G., 1980. Biochemical and rheological properties of the pedal mucus of the limpet Patella vulgata L. **Comparative Biochem. Physiol 66B**, 451-458.

Grim, R.E., 1962. **Applied clay mineralogy**. McGraw-Hill book company, Inc..

Grim, R.E., 1968. **Clay mineralogy**, 2nd ed.. McGraw-Hill book company, New york.

Grissinger, E.H., 1966. Resistance of selected clay systems to erosion by water. **Water Resources Res., Vol.2 No.1**, 131-138.

Grissinger, E.H., Little, W.C. and Murphey, J.B., 1981. Erodibility of stream bank materials of low cohesion. **Trans. ASCE 24(3)**, 624-630.

Gross, T.F. and Dade, W.B., 1991. Suspended sediment storm modelling. **Marine Geology 99**, 343-360.

Gucinski, H. and Baier, R.E., 1983. Estuarine bacterial slime film: relation of biophysical properties to hydrodynamic drag. **Estuaries 6(3)**, 237 (Abstract only).

Gularte, R.C., 1978. Erosion of cohesive marine sediments as a rate process. **Unpub Ph.D Thesis, Univ. Rhode Island.**

Gularte, R.C., Kelly, W.E. and Nacci, V.A., 1980. Erosion of cohesive sediments as a rate process. **Ocean. Engng., 7**, 539-551.

Güst, G., 1976. Observations on turbulent drag reduction in a dilute suspension of clay in sea water. **J. Fluid Mech., 75**, 29-47.

Güst, G., 1982. Tools for oceanic small scale, high frequency flows: Metal-clad hot wires and epoxy-sealed hot films. **J. Geophys. Res., 87**, 445-447.

Güst, G., 1988. Skin friction probes for field applications. **J. Geophys. Res., 93(C11)**, 14121-14132.

Güst, G. and Morris, M.J., 1989. Erosion threshold and entrainment rates of undisturbed in situ sediments. **J. Coastal Res. Special Issue No.5: High Conc. Cohesive Sediment Trans.**, 87-100.

Güst, G. and Southard, J.B., 1983. Effects of week bed load on the universal law of the wall. **J. Geophys. Res., 88(C10)**, 5939-5952.

Gust, G. and Walger, E., 1976. The influence of suspended cohesive sediments on boundary- layer structure and erosive activity of turbulent sea water flow. **Marine Geol., 22**, 189-206.

Güst, G. and Weatherly, G.L., 1985. Velocities, turbulence and skin friction in a deep sea logarithmic layer. **J. Geophys. Res., 93(C3)**, 4779-4792.

Halka, J., Panageotou, W. and Sanford, L.P., 1991. Consolidation and erosion of deposited cohesive sediments in Northern Chesapeake Bay, USA. **Geomarine Letters 11**, 174-178.

Hamblin, A.P. and Davis, D.B., 1977. Influence of organic matter on the physical properties of some East Anglian soils of high silt content. **J. Soil Sci. 28**, 11-22.

Hamdi, F. and Taylor Smith, D., 1982. The influence of permeability on compressional wave velocity in marine sediments. **Geophys. Prospecting, 30**, 622-640.

Hamilton, E.L., 1970. Sound velocity and related properties of marine sediments, North Pacific. **J. Geophys. Res. 75**, 4423-4446.

Hamilton, E.L., 1971. Elastic properties of marine sediments. **J. Geophys. Res., 76**, 579-604.

Hammond, T.M. and Collins, M.B., 1979. On the threshold of transport of sand-sized sediment under the combined influence of unidirectional and oscillatory flow. **Sedimentology, 26**, 795-812.

Hanes, M.D. and Ludwig, K.A., 1990. A laboratory evaluation of optical back scatterance suspended solids sensors exposed to sand mud mixtures. **Mar. Geol. 94**, 173-179.

Hardin, B.O. and Richart, Jr., 1963. Elastic wave velocities in granular soils. **J. Soil Mech. Found. Div. Amer. Soc. Civil. Eng., 89(SM1)**, 33-65. Discussions **SM5**, 103-118.

Harrison, W. and Waas, M.L., 1965. Frequencies of infaunal invertebrates related to water content of Chesapeake Bay sediments. **Southeast. Geol. 6**, 177-187.

Hay, A.E. and Burling, R.W., 1982. On sound scattering and attenuation in suspensions, with marine applications. **J. Acoust. Soc. Am., 72(3)**, 950-959

Hayes, F.R., 1964. The mud consolidation during a short time interval. **Geo-marine Letters 1**, 7-10.

Hawley, N., 1981. Mud consolidation during a short time interval. **Geo-marine Letters 1**, 7-10.

Head, M.R, and Bandyopadhyay, P.H., 1981. New aspects of boundary-layer structure. **J. Fluid. Mech., 107**, 297-338.

Heathersaw, A.D., 1979. The turbulent structure of the bottom boundary layer in a tidal current. **J. R. Astronom. Soc., 58**, 395-430.

Heatherson, A.D. and Thorne, P.D., 1985. Sea bed noises reveal role of turbulent bursting phenomena in sediment transport by tidal currents. **Nature, 316**, 339-342.

Hesse, R. and Chough, S.K., 1980. The North-West Atlantic Mid-Ocean Channel of the Labrador Sea II: Deposition of parallel laminated levee-muds from the viscous sublayer of low density turbidity flows. **Sedimentology 27**, 693-711.

Hollick, M., 1976. Towards a routine test for the assessment of critical tractive forces of cohesive soils. **Trans. ASCE 19(6)**, 1076-1081.

Hill, H.J. and Milburn,J.D., 1956. Effect of clay and water salinity on electrochemical behaviour of reservoir rocks. **Petroleum Transactions, AIME, 207**, 65-72.

Hjülström, F. 1935. The morphological activity of rivers as illustrated by the river Fyris. **Bull. Geol. Inst., Upsala, 25**, 221-527.

Hobbie, J.E. and Lee, C., 1980. Microbial production of extracelluar material: importance in benthic ecology. In: **Marine Benthic Dynamics** (Tenore, K.R., and Coull, B.C., Eds.), 341-346, Univ, S.Carolina Press, Columbia.

Hovem, J.M., Richardson, M.D. and Stoll, R.D., 1991. **Shear Waves in Marine Sediments,** Kluwer Academic Publ., 29-39.

Hughes, T.G., 1979. Studies on the sediment of St. Magarets Bay, Nova Scotia. **J. Fish. Res. Board Canada 36,** 529-536.

Hunt, J.R., 1980. Prediction of oceanic particle size distribution from coagulation and sedimentation mechanisms. In: (Kavanaugh, M.C. and Leckie, J.O., Eds.) **Particulates in Water,** American Chemical Society, Advances in Chemistry Series No. 189, 243-257.

Hydraulics Research Station (HRS) 1979. Port Brisbane siltation study. **5th Report: Properties of Brisbane mud. HRS Rep. No.EX86.**

Jackson, M.L., 1964. Soil Clay Mineralogical Analysis. In: (Rich, C.I. and Kunze, G.W., Eds.) **Soil Clay Mineralogy**. Chapel Hill. pp 245-293.

Jackson, P.D., 1975. An electrical resistivity method for evaluating the in-situ porosity of clean marine sands. **Marine Geotec., 1(2),** 91-115.

Jackson, P.D., Taylor Smith, D. and Stanford, P.N., 1978. Resistivity-porosity-particle shape relationships for marine sands. **Geophys., 43,** 1250-1268.

Jackson, P.D., Baria, R. and McCann, D.M., 19. Geotechnical assessment of superficial marine sediments using in-situ geophysical probes. **Oceanology International 80,** 33-40.

Jackson, R.G., 1976. Sedimentological and fluid-dynamic implications of the turbulent bursting phenomena in geophysical flows. **J. Fluid Mech.,** 77, 531-560.

Jensen, F.B. and Schmidt, H., 1986. Shear properties of ocean sediments determined from numerical modelling of scholte wave data. In: **Ocean Seismo Acoustics** (ed. T.Akal and J.M.Berkson). Plenum Press.

Johnson, D.L., 1982. Acoustic slow waves and the consolidation transition. **J. Acoust. Soc. Am., 72(2),** 556-565.

Johnson, R.G., 1974. Particulate matter at the sediment-water interface in coastal environments. **J. Mar. Res. 33,** 313-330.

Johnston, J.W., 1943. Laboratory investigations of bedload transportation and bed roughness. **U.S. Dept. Agric. Soil Conserv. Service, SCS-TP-50,** 115pp.

Jonsson, I.G., 1966. Wave boundary layers and friction factors. **Coastal Engng., 1966, Proc. 10th Conf.,** 127-148.

Jonsson, I.G., 1978. A new approach to oscillatory rough turbulent boundary layers. Copenhagen polytenisk laereanstalt, Instituttet for stroeming-smekanick of andbygning, series paper 17, 87pp..

Jumars, P.A. and Nowell, A.R.M., 1984. Effects of benthos on sediment transport: difficulties with functional grouping. **Continental Shelf Res. 3(2)**, 115-130.

Jumars, P.A. and Nowell, A.R.M., 1984. Fluid and sediment dynamic effects on marine benthic community structure. **Am. Zool. 24**, 45-55.

Kamphuis, J.W., 1974. Determination of sand roughness for fixed beds. **J. Hydraul. Res., 12**, 193-203.

Kamphuis, J.W., 1983. On erosion of consolidated clay material by a fluid containing sand. **Can. J. Civ. Eng., 109(N0.1)**, 49-61.

Kamphuis, J.W. and Hall, K.R., 1983. Cohesive material erosion by unidirectional current. **J. Hydraul. Engng. ASCE., 109, 1**, 49-61.

Kandiah, A., 1974. Fundamental aspects of surface erosion of cohesive soils. **Unpub. Ph.D thesis, Univ. of California, Davis, CA.**

Kandiah, A. and Arulanandan, K., 1974. Hydraulic erosion of cohesive soils. **Soil Properties, Proc. 53rd. Annual Meeting Trans Res. Record 497**, 60-68.

Karcz, I. and Shanmugam, G., 1974. Decrease in scour rate of fresh deposited muds **J. Hydraulics Division, Proc. ASCE 100(Hy 11)**, 1735-1738.

Kermabon, J., Gehin, C. and Blavir, P., 1969. A deep sea electrical resistivity probe for measuring porosity and density of unconsolidated sediments. **Geophysics, 34**, 554-571.

Khailov, K.M. and Finenko, Z.Z., 1970. Organic macromelecular compounds dissolved in sea-water and their inclusion into food chains. In: **Marine Food Chains** (ed. J.H.Steele), 6-18, Univ. California Press, Berkeley.

Kirchener, J.W., Dietrich, W.E., Iseya, F. and Ikeda, H., 1990. The variability of critical shear stress, friction angle and grain protrusion in water-worked sediments. **Sedimentology 37**, 647-672.

Kline, S.J., Reynolds, W.C., Schraub, F.A., and Rundstadler, P.E., 1967. The structure of turbulent boundary layers. **J. Fluid Mech. 30**, 741-773.

Komar, P.D. and Miller, M.C., 1973. Sediment threshold under oscillatory waves. **Proc. 14th Coastal Eng. Conf.**, 756-775.

Komar, P.D. and Miller, M.C., 1975a. One the comparison between the threshold of sediment movement under oscillatory waves and unidirectional currents with a discussion of the practical evaluation of the threshold. **J. Sedimentary Petrol., 45(3)**, 362-367.

Komar, P.D. and Miller, M.C., 1975b. The initiation of oscillatory ripple marks and the development of plane-bed at high shear stresses under waves. **J. Sedimentary Petrol., 45(3)**, 697-703.

Kraeuter, J.N. and Wetzel, R.L., 1986. Surface sediment stabilisation-destabilisation and suspended sediment cycles on an intertidal mud flat. In: **Estuarine Variability** (Wolfe, D.A., Ed.) Academic Press, 203-223.

Kranck, K., 1984. The role of flocculation in the filtering of particulate matter in estuaries. In: **The Estuary as a Filter** (Kennedy, V.S., Ed.) 159-175.

Kranck, K. and Milligan, T., 1980. Production of marine snow in the laboratory. **Mar. Ecol. Prog. Ser., 4**, 19-24.

Krauskopf, K.B.,1982. **Introduction to geochemistry**, 2nd ed. McGraw-Hill Book Company.

Krone, R.B., 1962a. Flume studies of the transport of sediment in estuarial shoaling processes. **Final Report, Hydraulic. Engng. Lab. and Sanitary Engng. Res. Lab., Univ. Calif. Berckeley**, 110 pp.

Krone, R.B., 1962b. Silt transport studies utilizing radioisotopes. **Final report Inst. of Engng. Res., Univ. of Calif., Berckeley.**

Krone, R.B., 1963. A study of the rheological properties of estuary sediments. **Tech. Bulletin No. 19, US Army Corps of Engineers Committee on Tidal Hydraulics, Wes, Vicksburg, Miss.**, 62pp

Krone, R.B., 1976. Engineering interest in the benthic boundary layer In: **The Benthic Boundary Layer** (McCave, I.N., Ed.), Plenum Press, New York, 143-156.

Krumbein, W.C., 1934. Size frequency distributions of sediments. **J. Sediment. Petrol., 4**, 65-77.

Kudo, K. and Shima, E., 1970. Attenuation of shear waves in soil. **Bull. Earthquake Res. Inst. Univ. Tokyo., 40**, 145-158.

Kuijper, C., Cornelisse, J.M. and Winterwerp, J.C., 1989. Research on erosion properties of cohesive sediments. **J. Geophys. Res., 94**, 14341-14350.

Kuo, A., Nichols, M.N. and Lewis, J., 1978. Modelling sediment movement in the turbidity maximum of an estuary. **Publ. Office of Water Research and Technology**, 80pp.

Kusuda, T., Umita, T., Koga, K., Futawatari, T. and Awaya, Y., 1984. Erosional process of cohesive sediments. **Wat. Sci. Tech. 17**, 891-901.

Kuti, E.Q. and Yen, C., 1976. Scouring of cohesive soils. **J. Hydraulic. Res., 14(3)**, 195-206.

Lamb, H., 1932. **Hydrodynamics**, 6th ed. Cambridge University Press, 738 pp.

Larcombe, P., 1992. The post glacial evolution and present day sedimentary processes of the Mawddach estuary. **Unpb. Ph.D. thesis Univ. Wales, U.K..**

Lavelle, J.W. and Mofjeld, H.O., 1987. Do critical erosion stresses for incipient motion and erosion really exist? **J. Hydraul. Eng. 113(No.3)**, 370-393.

Lavelle, J.W., Mofjeld, H.O. and Baker, E.T., 1987. An in situ erosion rate for a fine-grained marine sediment. **J. Geophys. Res. 89(No.C4)**, 6543-6552.

Lee, H.J. and Chough, S.K., 1987. Bulk density void ratio and porosity determined from average grain density and water content: an evaluation of errors. **Marine Geotech 7**, 53-62.

Lee, D., Lick, W. and Kang, S.W., 1981. The entrainment and deposition of fine-grained marine sediments. **J. Geophys. Res. 89(No.C4)** 6543-6552.

Leeder, M.R., 1982. **Sedimentology: Processes and Products**. George Allen and Unwin Ltd., 344pp.

Lee II, H, and Swartz, R.C., 1980. Biological processes affecting the distribution of pollutants in marine sediments. In: (Baker, R.A., Ed.) **Contaminants and Seds. Vol.II**, Sci. Publ. Ann Arbour, MI, 555-605

Leithold, E.L., 1989. Depositional processes on an ancient and modern muddy shelf North California. **Marine Geology 36**, 179-202.

Lick, W., 1982. Entrainment, deposition and transport of fine-grained sediments in lakes. **Hydrobiologia 9**, 31-40.

Lick, W., 1986. Modelling the transport of fine-grained sediments in aquatic systems **Sci, Total. Env. 55**, 219-228.

Lim C.H., Jackson, M.L. and Higgins, T., 1981. Interaction of soil clays with dimethyl sulphoxide **Soil Soc. Am. J. 45**, 433-436.

Lonsdale, P. and Southard, J.B., 1974. Experimental erosion of North Pacific red clay. **Marine Geology 17**, M51-M60.

Lovell, M. A., 1985. Thermal conductivity and permeability assessment by electrical resistivity measurements in marine sediments. **Marine Geotec, 6(2)**, 205-240.

Ludwieg, H., 1949. Ein Gerat zur Messung der Wanschubspannung turbulent Reibungsschichten. **Ingenieurarchiv, 17**, 207.

Lynch, M. and Harrison, W., 1970. Sedimentation caused by a tube-building amphipod. **J. Sediment. Petrol., 40**, 434-435.

Lyle, M.W. and Smerdon, E.T. 1965. Relation of compaction and other soil properties to erosion resistance of soils. **Trans. ASAE 8**, 419-422.

Maa, P.-Y. and Mehta, A.J., 1987. Mud erosion by waves: a laboratory study. **Continental Shelf Res. 7(11/12)**, 1269-1284.

Maa, P.-Y., Shannon, W.T., Lee, C.H. and Li, C., 1991. In situ measurements of the critical shear stress for erosion using an annula seabed flume. **Sec. 021C(-4) p.241 Amer. Gephys. Union Fall Meeting (abstract only)**.

Maa, J.P.-Y., Xu. J. and Victor, M., 1992. Notes on the performance of an optical back scattering sensor for cohesive sediments. **Mar. Geol. 104**, 215-218.

MacIlvaine, J.C. and Ross, D.A., 1979. Sedimentary processes on the continental slope of New England, **J. Sediment. petrol. 49**, 565-574.

Mahohar, M., 1955. Mechanics of bottom sediment movement due to wave action. **U.S. Army Corps Engineers Coastal Eng. Res. Centre, Tech. Paper No.78-5**, 101pp.

Mallik, T.K., Mukherji, K.K. and Ramachandran, K.K., 1988. Sedimentology of the Kerala mud banks (fluid mud?). **Marine Geology 80**, 99-118,

Mantz, P.A., 1977. Incipient transport of fine grains and flakes by fluid-extended shields diagrams. **J. Hydraul. Div., 103, HY6**, 601-615.

Mantz, P., 1978. Bedforms produced by fine, cohesionless, granular and flaky sediments under subcritical water flow. **Sedimentology, 25**, 83-103.

Martin, R.T., 1962. Discussion of experiments on the scour resistance of cohesive sediments by Moore, W.L. and Mash,F.D., **J. Geophys. Res., Vol.67**, 1447-1449.

Mathews, J. and Poll, D.I.A., 1985. The theory and application of heated films for the measurement of skin friction. **Report CoA 8515, Cranfield Inst. of Tech., England**.

McCall, P.L., 1977. Community patterns and adaptive strategies of the infaunal benthos of Long Island Sound. **J. Mar. Res. 35**, 221-266.

McCall, P.L. and Tevesz, M.J.S., 1982. The effects of benthos on physical properties of freshwater sediments. In: **Animal-Sediment Relations: the biogenic alteration of sediments** (Tevesz, M.J.S., and Mcall, P.L., Eds.), Plenum Press N.Y., 105-176.

McCann, C., and McCann, D.M, 1985. A theory of compressional wave attenuation in noncohesive sediments. **Geophysics, Vol 50(8)**, 1311-1317.

McCarter, W.J., 1984. The electrical resistivity characteristics of compacted clays. **Geotechnique, Vol.34**, 263-267.

McCave, I.N., 1981. Location of coastal accumulation of fine sediments around the southern North Sea. In: **Proc. of a Workshop on Sed. and Pollutant Exchange. Rapp. Processverbaux Reun. Cons. Int. Explor. Mer. 181**, 15-27.

McCave, I.N., 1984. Erosion, transport and deposition of fine-grained marine sediments. In: **Fine-Grained Sediments: Deep Water Processes and Facies** (Stow, D. and Piper, D.J.W., Eds.). Geol. Soc. Lond. Spec. Publ. 15, 35-69.

McCave, I.N., 1985. Sedimentology and stratigraphy of box cores from the HEBBLE site on the Nova Scotian continental rise. **Marine Geology 66**, 59-90.

McClean, S.R., 1985. Theoretical modelling of deep ocean sediment transport. **Marine Geology 66**, 243-266.

McDermott, I.R., 1992. Seismo-acoustic investigations of consolidation phenomena. **Unpub. Ph.D. Thesis, University of Wales**.

McDonald, F.J., Angona, F.A., Mills, R.L., Sengbush, R.L., Van Nostrand, R.G. and White, J.E., 1958. Attenuation of shear and compressional waves in Pierre shale. **Geophysics, 23**, 412-439.

McDowell, D.N. and O'Connor, B.A., 1977. **Hydraulic behaviour of estuaries**. MacMillan, London, 292pp.

McTiernan, L., 1989. The erosion potential of fine grained sediments in Long Island Sound. **Unpub. MSc Thesis, Marine Sci. Res. Centre, State Univ.**, New York, Stoney Brook, New York, 103pp.

Meadows, P.S. and Tufail, 1986. Effects of microbial and macrobenthic secretions on stability to erosion and sedimentation at the sediment-water interface. **NERC Progress Report on Estuarine Processes, Special Topic Grant GST/02/54**, 19pp.

Meadows, P.S. and Tait, R.F., 1989. Bioturbation geotechnics and microbiology at the sediment water interface in deep sea. **Proc. 19th European Mar. Bio. Symp.** (Gibbs, P.E., Ed.), Cambridge Univ. Pres, Cambrdige, 191-199.

Meadows, P.S. and Tait, R.F. and Hussain, S.A., 1985. Burrowing animals affect sedimentation and stability of marine sediments. **Experientia**.

Mehta, A.J., 1981. Review of the erosion function for cohesive sediment beds. **Proc. 1st. Indian Conf. on Ocean Engng, Madras, India, 1**, 122-130.

Mehta, A.J., 1989. On estuarine cohesive sediment suspension behaviour. **J. Geophys. Res., Vol.94**, 14303-14314.

Mehta, A.J., 1991. Review notes on cohesive sediment erosion. **Coastal Sediments 1991**, 40-53

Mehta, A.J. and Lott, J.W., 1987. Sorting of fine sediment during deposition. In: **Proceedings of Specialty of Coastal Sediment Processes, ASCE.**, New York, 348-362.

Mehta, A.J. and Partheniades, E., 1982. Re-suspension of deposited cohesive sediment beds. **18th Conf. Coastal Engineering**, 1569-1588,

Mehta, A.J., Parchure,T.M., Dixit,J.G. and Ariathurai, R., 1982. Re-suspension potential of deposited cohesive sediment beds. In: (Kennedy, V., Ed.), **Estuarine Comparisons**. Academic Press, New York, 591-609.

Mehta, A.J., Hayter, E.J., Parker, R., Krone, R.B. and Teeter, A.M., 1989. Cohesive sediment transport I. Process description. **J. Hydraulic Engng, 115(No.8)**, 1076-1093.

Mendelson, K.S. and Cohen, M.H., 1982. The effect of grain and anistropy on the electrical properties of sedimentary rocks. **Geophysics 47(2)**, 257-263

Menendez, A,N, and Ramaprian, B.R., 1985. The use of flush-mounted hot-film gauges to measure skin friction in unsteady boundary layers. **J. Fluid Mech. 161**, 139-159.

Middleton, G.V. and Southard, J.B., 1977. **Mechanics of Sediment Movement. SEPM Short Course Notes No.3**, 240pp.

Mignoit, C., 1968. Etudes des properties physiques de differents sediments tres fins et de leur comportement sous des actions hydrodynamics. **La Houille Blanche, 7**, 591-620.

Miller, M.C., McCave, I.N. and Kromar, P.D., 1977. Threshold of sediment motion under unidirectional currents. **Sedimentology, 24**, 507-527.

Mills, E.L., 1967. The biology of an ampeliscid amphipod crustacean sibling species pair. **J. Fish. Res. Board Can. 24**, 305-355

Mills, E.L., 1969. The community concept in marine zoology, with comments on continua and instability in some marine communities: A Review. **J. Fish. Res. Board Can. 24**, 305-355

Mimura, N., 1989. Recent Japanese studies on cohesive sediment transport. **J. Coastal Res. 5(Special Issue No.5)**, 101-115.

Mirtskhoulava, T.E., 1969. Erosional stability of cohesive soils. **J. Hydr. Res. 4(1)**, 37-50.

Mirtskhoulava, T.E., 1991. Scouring by flowing water of cohesive and non-cohesive beds. **J. Hydr. Res. 29(3)**, 341-354.

Mitchell, J.K., 1976. **Fundamentals of Soil Behaviour**. John Wiley and Sons, N.Y., 42pp.

Montague, C.L., 1986. Influence of biota on the erodibility of sediments. In: **Estuarine Cohesive Dynamics** (Mehta, A.J., Ed.) Springer-Verlag, Berlin, 251-268.

Moody, L.F., 1944. Friction factor for pipe flow. **Trans ASME., Vol.66**, 671-684.

Moon, C.F. and Hurst, C.W., 1984. Fabric of muds and shales: an overview. In: **Fine-Grained Sediments: Deep Water Processes and Facies** (Stow, D. and Piper, D.J.W., Eds.). Geol. Soc. Lond. Spec. Publ. 15, 579-593.

Moore, R., 1991. The chemical and mineralogical controls on the residual strength of pure natural clays. **Geotechnique 41(1)**, 35-47.

Moore, W.L. and Mash,F.D., 1962. Experiments on the scour resistance of cohesive sediments. **J. Geophys. Res., Vol.67**, 1437-1449.

Morris H.M., 1955. A new concept of flow in rough conduits. **Trans. Am. Soc. Civ. Eng. 120**, 373-398.

Murdoch, J. and Barnes, J.A., 1986. **Statistical Tables**, Macmillan Press, 60pp.

Muschenheim, D.K., Grant, J. and Mills, E.L., 1986. Flumes for benthic ecologists: theory, construction and practice. **Mar. Ecol. Prog. Ser., 28**, 185-196.

Myers, A.C., 1977. Sediment processing in a marine subtidal sandy bottom community. **I. Physical aspects. J. Mar. Res., 35**, 609-632.

Nakagawa, H. and Nezu, I., 1977. Prediction of the contributions to the Reynolds stress from bursting events in open-channel flow. **J. Flid Mech., 70**, 209-228.

Nakagawa, H. and Nezu, I., 1981. Structure of space-time correlations of bursting phenomena in an open-channel flow. **J. Flid Mech., 104**, 1-43.

Neihof, R.A. and Leob, G.I., 1972. The surface charge of particulate matter in seawater. **Limnol. Oceanorgr. 17**, 7-16.

Neihof, R.A. and Leob, G.I., 1973. Molecular fouling surfaces in seawater. In: **Proc. 3rd Inter. Congress on Corrosion and Fouling** (eds. R.F.Acker, B.F.Browen,J.R.DePalma and W.D.Iverson), 710-718, National Bureau of Standards, Washington, D.C..

Nelson, B.W., 1959. Transport of colloidal sediment in the freshwater-marine transition zone. **1st. Inte. Oceanography Congress**, 640-641.

Newton, A.J. and Gray, J.S., 1972. Seasonal variations of the suspended solid matter off the coast of North Yorkshire. **J. Mar. Biol. Assn. U.K. 52**, 33-47.

Nichols, M.M., 1986. Effects of fine sediment re-suspension in estuaries. In: **Estuarine Cohesive Sediment Dynamics** (Mehta, A.J., Ed.),

Lecture Notes on Coastal and Estuarine Studies Volume 14, Springer-Verlag, Berlin, FRG, 5-42

Nowell, A.R.M. and Church, M., 1979. Turbulent flow in a depth-limited boundary layer. **J. Geophys. Res. 84**, 4816-4824.

Nowell, A.R.M. and Jumars, P.A., 1987. Flumes:theoretical and experimental consideration for simulation of benthic environments. **Oceanogr Mar. Biol. Ann. Rev. 25**, 91-112.

Nowell, A.R.M., Jumars, P.A. and Eckman, J.E., 1981. Effects of biological activity on the entrainment of marine sediments. **Mar. Geol. 42**, 133-153.

Nowell, A.R.M., McCave, I.N. and Hollister, C.D., 1985. Contributions of HEBBLE to understanding of marine sedimentation. **Marine Geology 66**, 397-409.

Nychas, S.G., Hershey, H.C. and Brodkey, R.S., 1973. A visual study of turbulent shear flow. **J. Fluid Mech., 61**, 513-540.

O'Brien, N.R., 1985. The effects of bioturbation on the fabrics of shale. **J. Sed. Petrol. 57(3)**, 449-455.

Ockenden, M.C. and Delo, A.E., 1991. Laboratory testing of muds. **Geomarine Letters 11(3/4)**, 138-142.

Odd, N.V.M., 1988. Mathematical modelling of mud transport in estuaries. In: **Physical Processes in Estuaries** (Donkers, J. and van Leussen, W., Eds.) Springer-Verlag, 503-531.

Offen, G.R. and Kline, S.J., 1975. A proposed model of the bursting process in turbulent boundary layers. **J. Fluid. Mech., 70**, 209-228.

Ostubo, K. and Muraoka, K., 1985. Re-suspension rate function for cohesive sediments in stream. **J. Hydroscience and Hydraulic Engng, JSCE 3(2)**, 1-13.

Ostubo, K. and Muraoka, K., 1986a. Re-suspension of cohesive sediments by currents. In: **River Sedimentation, Vol.3: Proc. 3rd. Inter. Symp. on River Sedimentation** (Wang, S.Y., Sheng, .H. and Ding, L.Z., Eds.), 1680-1689.

Ostubo, K. and Muraoka, K., 1986b. Estimation of re-suspension rate of cohesive sediments by currents. **Proc. JSCE 375/II-6** 43-52.

Ostubo, K. and Muraoka, K., 1988. Critical shear stress of cohesive bottom sediments. **J. Hydraul. Eng. 114(No.10)**, 1241-1256.

Owen, M.W., 1975. Erosion of Avonmouth mud. **Hydraulics Research Station, Report INT150.**

Owen, M.W., 1976. Problems in the modelling of transport, erosion and deposition of cohesive sediments. In: (Golberg, E.D., et al., Eds.). **The Sea, Vol.6**, Wiley-Interscience, N.Y, 515-537.

Paaswell, R.E., 1974. Causes and mechanisms of cohesive soil erosion: The State of the Art. **Highway Research Board Special Report 135, Soil Erosion: Causes Mechanisms, Prevention and Control**, 52-72

Paintel, A.S., 1971. Concept of critical shear stress in loose boundary open channels. **J, Hydraul. Res. 9(1)**, 91-113.

Paola, C., Gust, G. and Southard, J.B., 1986. Skin friction behind isolated hemispheres and the formation of obstacle marks. **Sedimentology, 33**, 279-293.

Parchure, T.M. and Mehta, A.J., 1985. Erosion of soft cohesive sediment deposits. **J. Hydraul. Engng. ASCE., 111(10)**, 1308-1326.

Parker, D., Kaufman, W. and Jenkins, D., 1972. Floc breakup in turbulent flocculation processes. **J. Hydraul. Eng. 111(No.10)**, 1308-1326.

Parker, G. and Klingemand, P.C., 1982. On why gravel bed streams are paved. **Wat. Resour. Res. 18**, 1409-1423.

Parker, W.R., 1987. Observations on fine sediment transport phenomena in turbid coastal environment. **Continental Shelf Res. 7(11/12)**, Dynamics of Turbid Coastal Environments (16th. Annual EBSA Symposium), 1285-1300.

Parker , W.R., 1991. Quality control in mud coring. **Geomarine Lett. 11(3/4)**, 132-137.

Partheniades, E., 1964. A summary of present knowledge of the behaviour of fine sediments in estuaries. **Tech. Note No.8, Hydrodynamics Lab. M.I.T., Cambridge. Mass.**.

Partheniades, E., 1965. Erosion and deposition of cohesive soils. **J. Hydraul. Div. ASCE., 91, HY1**, 105-139.

Partheniades, E., 1971. Erosion and deposition of cohesive materials, In: **River Mechanics**, Shen, H.W.(ed.), Colorado State Univ. Press, Vol.II, 25.1-25.91.

Partheniades, E., 1984a. The present state of knowledge and needs for future research on cohesive sediments dynamics. **Proc. 3rd. Int. Symp. River Sedimentation**. School of Engng. Univ. Mississippi, 3-25.

Partheniades, E., 1984b. 2-dimensional model of mud transport. Discussion by EP. **J. Hydraul. Eng. 110(3)**, 364-366.

Partheniades, E., 1990. The effect of bed shear stress on the deposition and strength of deposited cohesive muds. In: (Bennet et al., Eds.) **Microstructure of fine-grained sediments: from mud to shale**, Frontiers in Sedimentary Geology, Springer-Verlag, 175-183.

Partheniades, E. and Kennedy, J.F., 1966. The depositional behaviour of fine sediment suspension in a turbulent fluid motion. **Coastal Engng. 10th Conf, Vol.1**, 707-729.

Partheniades, E. et al., 1986. Further results on the deposition of cohesive sediments. **Coastal Engng. 11th Conf, Vol.1**, 723-742.

Paterson, D.M., 1989. Short-term changes in the erodibility of intertidal cohesive sediments related to the migratory behaviour of epipelic diatoms. **Limnol. Oceanogr. 34**, 233-234.

Paterson, D.M., Crawford, R.M. and Little, C., 1986. The structure of benthic diatom assemblages: a preliminary account of the use and evaluation of low-temperature scanning electron microscopy. **J. Exp. Mar. Biol. Ecol. 96**, 279-289.

Paulic, M.J., Montague, C.L. and Mehta, A.J., 1986. The influence of light on sediment erodibility. In: **3rd Int. Symp. River Sedimentation** (Shen, H.W., Ed.), Univ. of Mississippi, 1758-1764.

Peirce, T.J. et al, 1970. An experimental study of silt scouring. **Proc. Inst. Civl. Engng., 45**, 231-243.

Pierce, J.W., 1990. Microstructure of suspensates: from stream to shelf. In: (Bennet et al., Eds.) **Microstructure of fine-grained sediments: from mud to shale**, Frontiers in Sedimentary Geology, Springer-Verlag, 139-145.

Pethick, J., 1981. **An Introduction to Coastal Geomorphology**. Edward Arnold Ltd, 260pp.

Poisson, A., 1980. Conductivity/salinity/temperature relationship of diluted and concentrated standard seawater. **IEEE. J. Oceanic Eng., OE-5(1), Special Issue on the Practical Salinity Scale 1978**, 41-50.

Pond, S. and Pickard, G.L., 1978. **Introductory dynamic oceanography**. Pergamon Press.

Postma, H., 1967. Sediment processes in estuaries: some evaluating remarks. In: **Physical Processes in Estuaries** (Dronkers, J. and van Leussen, W., Eds.) Springer_verlag, Closure, 547-550.

Pryor, W.A., 1975. Biogenic sedimentation and alteration of argillaceous sediments in shallow marine environments. **Geol. Soc. Am. Bull. 86**, 1244-1254.

Puls, W., 1984. Erosion characteristics of estuarine muds. **Hydraulic Res. Rep. No.It 265**.

Pusch, R., 1970. Clay Microstructure. **Document D8:1970**. National Swedish Building Res. Summaries, Stockholm, Sweden.

Quinn, M.J., 1980. A scanning electron microscope study of the microstructure of dispersed and flocculated kaolinite clay taken out of suspension. **Unpub. MSc. Thesis, Univ. Florida, Gainsville.**

Ranz-Guerra, C., 1991. Some soft mud properties' evaluation by acoustics. **Geomarine Lett. 11(3/4)**, 172-173.

Rashid, M.A. and Browen, J.D., 1975. Influence of marine organic compounds on the engineering properties of a remoulded sediment. **Eng. Geol. 9**, 141-154.

Rauch, D., 1986. On the role of bottom interface waves in ocean seismo-acoustics: a review. In: **Ocean seismo-acoustics** (eds T.Akal and J.M.Berkson), Plenum Press.

Raudkivi, A.J., 1990. **Loose Boundary Hydraulics**, 2dn. Edition, Pergamon.

Raudkivi, A.J. and Hutchinson, D.L., 1971. Erosion of cohesive soils. In: **Proc. 4th Australian Conf. on Hydraul. and Fluid Mech.**, 360-366.

Raudkivi, A.J. and Hutchinson, D.L., 1974. Erosion of kaolinite clay be flowing water. **Proc. Royal Soc. Lond. A337**, 537-554.

Raudkivi, A.J. and Tan, S.K., 1984. Erosion of cohesive soils. **J. Hydraul. Res. 22(No.4)**, 217-233.

Rees, A.I., 1965. The use of anisotropy of magnetic susceptibility in the estimation of sediment fabric. **Sedimentology, 4**, 4257-271.

Rees, A.I., 1966. Some flume experiments with fine silt. **Sedimentology, 6**, 209-240.

Reimers, C., 1982. Organic matter in anoxic sediments off Central Peru: relations of porosity, microbiol decomposition and deformation properties. **Marine Geology 46**, 175-197.

Reineck, H.E. and Singh, I.B., 1980. **Depositional Sedimentary Environments**, 2nd edition, Springer-Verlag, N.Y., 439pp.

Reynolds, S. and Grosline, D.S., 1992. Clay microfabric of deep-sea detrital mud(stone)s, California Continental Borderland. **J. Sedim. Petrol. 62**, 41-53.

Rezak, R. and Lavoie, D.L., 1990. Consolidation related fabric change of periplatform sediments. **Geomarine Letters 10**, 101-109.

Rhoads, D.C., 1967. Biogenic reworking of intertidal and subtidal sediments in Barnstable Harbor and Buzzards Bay, Massachusetts. **J. Geol. 75**, 461-476.

Rhoads, D.C., 1970. Mass properties, stability and ecology of marine muds related to burrowing. In: **Trace Fossils** (Crimes, T.P. and Harper, J.C., Eds.) Seel House Press, Liverpool, 391-406.

Rhoads, D.C., 1973. The influence of deposit-feeding benthos on water turbidity and nutrient recycling. **Am. J. Sci. 273**, 1-22.

Rhoads, D.C., 1974. Organism-sediment relations on the muddy sea floor. **Oceanogr. Mar. Biol. Rev., Vol.12**, 263-300.

Rhoads, D.C. and Boyer, L.F., 1982. The effects of marine benthos on physical properties of sediments a successional perspective, in:

Animal Sediment Relations, (ed. P.L.McCall and M.J.S.Tevesz), pp3-52, Plenum press, New York.

Rhoads, D.C., and Stanley, D.J., 1964. Biogenic graded bedding, **J.Sediemnt. Petrol. 35**, 956-963.

Rhoads, D.C. and Young, D.K., 1970. The influence of deposit-feeding organisms on sediment stability and community trophic structure. **J. Mar. Res., Vol.28**, 150-178.

Rhoads, D.C., McCall, P.L. and Yingst, J.Y., 1978a. Disturbance and production on the estuarine seafloor. **Am. Sci. 66**, 577-586.

Rhoads,D.C., Yingst, J.Y. and Ullman, W., 1978b. Seafloor stability in central Long Island Sound. Part I. Temporal changes in erodibility of fine-grained sediment. In: **Estuarine Interactions** (ed. M.L.Wiley), 221-224, Academic press, New-York.

Richardson, M.D., Briggs, K.B. and Young, D.K., 1985. Effects of biological activity on abyssal benthic macroinvertabrates and sediment structure in the Venezuela Basin. **Marine Geology 68**, 243-267.

Richardson, M.D., Muzi, E, Troiano, L. and Miaschi, B., 1990. Sediment shear waves: A comparison os in situ and laboratory measurement. In **Microstructure of fine-grained sediments, frome mud to shale. Frontiers in Sedimentary Geology** (eds. Bennett et al). Springer-Verlag.

Richart, A.F., Jr. **Foundation Dynamics - 1987**. The art and science of geotechnical engineering, A volume honoring Ralph B. Peck, Prentice-Hall, Englewood Cliffs, N.J., 1989.

Riemann, F. and Schrage, R.N., 1985. Depositional facies of a mud shoreface in Surinam, S.America: A mud analogue to sandy shallow marine deposits. **J. Sed. Petrol. 55(5)**, 633-652.

Ross and Mehta, A.J., 1990. Fluidisation of soft estuarine mud waves. In: (Bennet, R.H., O'Brien, N.R and Hulbert, M.H., Eds) **Microstructure of Fine-grained Sediments. Frontiers in Sedimentary Geology**, Springer-Verlag, 185-191.

Round, F.E., 1981. **The Ecology of the Algae**. Cambridge Univ. Press., Cambridge.

Rowe. G.T., 1974. The effects of the benthic fauna on the physical properties of deep-sea sediments, in: **Deep-sea Sediments: Physical and Mechanical Properties**, (ed. A.L.Inderbitzen), pp.381-400,Plenum press, New York.

Sahl, L.E., Merrel, W.J., McGrail, D.W. and Webb, J.A., 1987. Transport of mud on continental shelves: evidence from the Texas shelf. **Marine Geology 76**, 33-43.

Sanford, L.P., Panageotou, W. and Halka, J., 1991. Tidal re-suspension of sediments in Northern Chesapeake bay. **Marine Geology 97**, 87-103.

Sargunam, A., 1973. Influence of mineralogy, pore fluid composition and structure on the erosion of cohesive soils. **Unpub. Ph.D. Thesis, Univ. California, Davis, CA.**

Sargunam, A., Riley, P., Krone, B.R. and Arulanandan, K., 1973. Physio-chemical factors in erosion of cohesive soils (technical notes). **J. Hydraul. Div. Proc. ASCE., 99, HY3**, 555-558.

Schünemann, M. and Kühl, H., 1991. A device for erosion measurements on naturally formed muddy sediments: the EROMES-System. **Internal repo., GKSS, 91/E/18**, 28pp.

Sedigraph - **Instruction Manual Sedigraph 5000ET, particle size analyzer**, 1986. Micromeritics Instrument Corporation, Sales Service Department, 5680 Goshen Springs Road, Norcross, Georgia, USA.

Self, R.L., and Jumars, P.A., 1978. Factors controlling critical shears for deposition and erosion of individual grains. **Marine Geology 86**, 181-199.

Sen, P.N., 1984. Grain shape effects on dielectric and electrical properties of rocks. **Geophysics, 49(5)**, 586-587.

Sheng, Y.P., 1983. Transport, entrainment and deposition of cohesive sediments. In: **Mathematical modelling of 3-D. coastal currents and sediment dispersals**, 125-173. Tech. Rep. CERC-83-2 Vicksburg, Miss.;US Army WES.

Sheng, Y.P. and Villaret, C., 1989. Modelling the effect of suspended sediment stratification on bottom exchange processes. **J. Geophys. Res. 94(C10)**, 14,429-14,444.

Sheng, Y.P. and Lick, W., 1979. The transport and re-suspension of sediments in a shallow lake. **J. Geophys. Res. 84(C4)**, 1809-1826.

Shields, A. 1936. Anwending der ahnlickeitsmechanik und der turbulenz forshung auf die geschiebebewegung. Mitteitungen der Preuss. Versuchsanst. F. Wasserbu U. Schiffbau, Heft 26, Berlin Germany.

Singer, J.K. and Anderson, J.B., 1984. Use of total grain size distributions to define bed erosion and transport for poorly sorted sediment undergoing simulated bioturbation. **Marine Geology 57**, 335-359.

Smart, P., 1991. Microstructural classification of clayey sediments. **Geomarine Letters 11**, 170-171.

Smerdon, E.T. and Beasley, R.P., 1959. Tractive force theory applied to stability of open channels in cohesive soils. **Res. Bulletin No.715, Agricultural Experiment Station, Univ. of Missouri, Columbia, Mo.**.

Smith, G.N., 1982. **Elements of soil mechanics for civil and mining engineers**, 5th edn., Collins.

Sokal, R.R. and Rohlf, F.J., 1981. **Biometry**, W.H. Freeman and Company New York, 860pp.

Soulsby, R.L., 1983. The bottom boundary layer of shelf seas. In Johns, B. (Ed.), **Physical Oceanography of Coastal and Shelf Seas**, Elsevier Science Publishers, Amsterdam, Chapter 5.

Soulsby, R.L., Davies, A.G. and Wilkinson, R.H., 1983. The detailed processes of sediment transport by tidal currents and by surface waves. **Institute of Oceanographic Sciences, Report, No.152**, 80pp.

Southard, J.B., 1974. Erodibility of fine abyssal sediment. In: **Deep Sea Sediments: physical and mechanical properties** (Inderbitzen, A.L., Ed.), 367-380.

Southard, J.B., Young, R.A. and Hollister, C.D., 1971. Experimental erosion of calcareous ooze, **J. Geopghys. Res. 76(C24)**, 5903-5909.

Stanton, T.K., 1988. Sound scattering by cylinders of finite length. I. Fluid cylinders. **J. Acoust. Soc. Am., 83(1)**, 55-63.

Stanton, T.K., 1988. Sound scattering by cylinders of finite length. II. Elastic cylinders. **J. Acoust. Soc. Am., 83(1)**, 64-67.

Stanton, T.K., 1989. Sound scattering by cylinders of finite length. III. Deformed cylinders. **J. Acoust. Soc. Am., 86(2)**, 691-705.

Sternburg, R.W., 1968. Friction factors in tidal channels with differing bed roughness. **Mar. Geol., 6**, 243-260.

Stoll, R.D. and Bryan, G.M., 1970. Wave attenuation in saturated sediments. **J. Acoust. Soc. Am., 47(5)**, 1440-1447.

Stoll, R.D., 1977. Acoustic waves in ocean sediments. **Geophysics, 42(4)**, 715-725.

Stoll, R.D., 1980. Theoretical aspects of sound transmission in sediments. **J. Acoust. Soc. Am., 68(5)**, 1341-1350.

Stoll, R.D., 1985. Marine sediment acoustics. **J. Acoust. Soc. Am., 77(5)**, 1789-1799.

Stoll, R.D., 1991. Shear waves in marine sediments - Bridging the gap from theory to field applications. **Shear Waves in Marine Sediments**, (eds. J.M. Hoven, M.D. Richardson and Stoll, R.D.), Kluwer Academic Publ, 3-12.

Stow, D.A.V. and Bowen, A.J., 1978. Origin of laminations in deep-sea fine-grained sediments. **Nature 274**, 324-328.

Stow, D.A.V. and Bowen, A.J., 1980. A physical model for the transport and sorting of fine-grained sediments by turbidity currents. **Sedimentology 27**, 31-46..

Sumer, B.M. and Oguz, B., 1978. Particle motions near the bottom in turbulent flow in an open-channel. **J. Fluid Mech., 86**, 109-127.

Sumer, B.M. and Deigaared, R., 1981. Particle motions near the bottom in turbulent flow in an open-channel, part 2. **J. Fluid Mech., 109**, 311-337.

Sundborg, A., 1956. The river Klaralven, A study of fluvial processes. **Geograiska Annaler, Arg.XXXVIII, Hafte 2-3**, 127-316.

Sutherland, A.J., 1966. Entrainment of fine sediments by turbulent flows. **W.M. Keck Lab. of Hydraul, and Water Resources. Div. of Engng and Appl. Sci., California Inst. of Tech., Pasadena, CA. Repo. No.KH-R-13**, 199pp.

Sutherland, A.J., 1967. Proposed mechanism for sediment entrainment by turbulent flows. **J. Geophys. Res., 72**, 6183-6194.

Task Committee on Erosion of Cohesive Materials, 1968. Erosion of Cohesive Sediments. **J. Hydraul. Div., ASCE., 4(94)**, 1017-1049.

Taylor, A.W., 1961. Ion exchange phenomena. **Trans. ASCE., Vol.126 Pt.1**, 718-728.

Taylor, B.D. and Vanoni, V.A., 1972. Temperature effects in low flow flat bed flows. **J. Hydraulics Div. Proc. ASCE 98(Hy 8)**, 1427-1445.

Taylor Smith, D., 1971. Acoustic and electric techniques for sea-floor sediment identification.

Teisson, C., 1991. Cohesive suspended sediment transport: feasibility and limitations of numerical modelling. **J. Hydraulic Res. 29**, 755-769.

Tenore,K.R., Boyer,L.F., Corral,J., Garcia-Fernandez,C., Gonzalez,N., Gurrian,E.G., Hanson,R.B., Iglesias,J., Korm,M., Lopex-Jamar,E., McClain,J., Pamatmat,M., Perez,A., Rhoads,D.C., Rodriguez,R.M., Santiago,G., Tietjen,J., Westrich,J. and Windom,H.L.,1982. Coastal up-welling in the Rias Bajas, N.W. Spain: Contrasting the benthic regimes of the Ria de Arosa and de Muros. **J. Mar. Res. 40**, ******.

Terwindt, J.H.J. and Breusers, H.N.C., 1972. Experiments on the origin of flaser, lenticular and sand-clay alternate bedding. **Sedimentology 19**, 85-89.

Terwindt, J.H.J., Breusers, H.N.C. and Svasek, J.n., 1968. Experiments investigations on the erosion sensitivity of a sand-clay lamination. **Sedimentology 11**, 105-114.

Thimakon, P., 1980. An experiment on clay suspensions under water waves. **Coastal Engng. 17th Conf., Vol.II**, 2894-2906.

Thompson, R.W., 1968. Tidal flat sedimentation of the Colorado River delta, N.W. Gulf of California. **Geol. Soc. Am. Memoir No.107**, 133pp.

Thorn, M.F.C. and Parsons, J.G., 1980. Erosion of cohesive sediments in estuaries: an engineering guide. **Proc. 3rd Int. Symp. Dredging Tech.**, BHRA. Fluid engineering Bedford UK.. 349-358.

Thorne, C.R., 1981. Field measurements of rates of bank erosion and bank material strength. **Erosion and Sediment Transport Measurement (Proc. Florence Symp.), IAHS Publ. No.133**, 503-512

Thorne, M.C.F., 1981. Physical processes of siltation in tidal channels. In: **Hydraulic Modelling Applied to Maritime Engng**. Problems, Inst. Civil Engng., Lond., 47-55.

Thorne, P.D., Williams, J.J. and Heathershaw, A.D., 1989. In situ acoustic measurements of marine gravel threshold and transport. **Sedimentology 36**, 61-74.

Tillmann, W. and Schliper, H., 1979. A device for the calibration of hot-film wall shear probes in liquids. **J. Physics E: Sci. Instrum. 12**, 273.

Tillmann, W., Waschmann,W., Herold, M. and Haustinger, G., 1981. Hot-film wall shear probe for measurement at flexible walls. **J. Physics E: Sci. Instrum. 14**, 692-694.

Toorman, E.A., and Berlamont, J.E., 1991. A hindered settling model for the prediction of settling and consolidation of cohesive sediment. **Geomarine Letters 11**, 179-183.

Tsai, C.-H. and Lick, W., 1986. A portable device for measuring sediment re-suspension. **J. Great Lakes Res.**12, 314-321.

Tubman, M.W. and Suhayda, J.N., 1976. Wave action and bottom movement in fine sediments. In **Proc. 15th Coastal Eng. Conf., 2**, 1168-1183.

Unita, T., Kusuda, T., Futawatara, T., Awaya, T. and Onuma, M., 1986. A model of erosion of soft cohesive sediments. In: **River Sedimentation Vol.3: Proc. 3rd Int. Symp. River Sedimentation**, (Wang, S.Y., Shen, H.W. and Ding, L.Z., Eds.), 1658-1667.

Unita, T., Kusuda, T., Futawatara, T. and Awaya, T., 1987. Simulation of behaviour of suspended solids and muds in an estuary. **Proc. Specialised Conf. on Coastal and Estuarine Pollution**, Kyushu Univ./IAWPRC/JSWPR, 219-227.

Ünsold, G. and Walger, E. 1987. Critical entrainment conditions of sediment transport. In: **Seawater-Sediment Interactions in Coastal Waters: an interdisciplinary approach** (Rumohr et al, Eds.), Springer-Verlag, 338.

Urish, D.W., 1981. Electrical resistivity-hydraulic conductivity relationships in glacial outwash aquifers. **Water Resources Res., 17(5)**, 1401-1408.

van Leussen, W., 1988. Aggregation of particles, settling velocity of mud flocs: a review. In: **Physical Processes in Estuaries** (Dronkers, J. and van Leussen, W., Eds.) Springer-Verlag 347 403.

van Leussen, W. and Dronkers, J., 1988. Physical processes in estuaries: An introduction. In: **Physical Processes in Estuaries** (Dronkers, J. and van Leussen, W., Eds.), Springer-Verlag, 347-403.

van Leussen, W. and Winterwerp, J.C., 1990. Laboratory experiments on sedimentation of fine grained sediments: a state-of-the-art review in the light of experiments with the Delft tidal flume. In: **Residual Currents and Long-term Transport** (Cheng, R.T., Ed.) Springer-Verlag: 241-259.

van Olphen, H., 1977. **An Introduction to clay Colloid Chemistry**. 2nd. edition, John Wiley, N.Y..

van Straaten, L.M.J.U., 1952. Biogene textures and the formation of shell beds in the Dutch Wadden Sea. **I-II, Koninkl. Nederl. Arkad. Wet. Proc. Ser. B 55**, 500-516.

Villaret, C. and Paulic, M., 1986. Experiments on the erosion of deposited and placed cohesive sediments in an annular flume and a rocking flume. **Rep UFL/COEL-86/007, Coastal Oceanographic and Engineering Dept., Univ. Florda, Gainsville.**

Villaret, C. and Latteux, B., 1992. Long-term simulation of cohesive sediment bed erosion and deposition by tidal currents. **MAST-I Section G6-M Coastal Morphpdynamics Book of Extended Abstracts, Rep. 4.1.**

Vincent, C.E., Swift, D.J.P. and Hillard, I.E.P., 1981. Sediment transport in the New York Bight. **Marine Geology 42**, 369-398.

Vos, P.C., de Boer, P.L. and Misdop, R. 1988. Sediment stabilisation by benthic diatoms in intertidal sandy shoals: qualitative and quantitative observations. In: **Tidal Influenced Sedimentary Environments and Facies** (de Boer, P.L. et al., Eds.), Reidel Pub. Company, 511-526.

Webb, J.E., 1969. Biologically significant properties of submerged marine sands. **Proc. R. Soc. London Ser. B 174**, 355-402.

Webb, J.E., 1991. Hydrodynamics, organisms and pollution of coastal sands. **Ocean and Shoreline Management 16**, 23-51.

Wells, J.T., 1988. Accumulation of fine-grained sediment in a periodically energetic clastic environment, Cape Lookout Bight, N. Carolina. **J. Sedim. Petrol. 58(4)**, 589-606.

Wells, J.J. and Coleman, J.M., 1981. Physical processes and fine grained sediment dynamics, coast of Surinam, South America. **J. Sed. Petrol., 51**, 1053-1068.

Wentworth, C.K., 1922. A scale of grade and class terms for clastic sediments. **J. Geol., 30**, 377-392.

Wetzel, A., 1987. Sedimentological significance of strain and sonic velocity in fine-grained turbiditic and hemi-pelagic deep sea sediments: an example from the Mirs Fan. **Marine Geology 74**, 191-207.

Wetzel, A., 1991. Interrelationships between porosity and other geotechnical properties of slowly deposited fine-grained marine surface sediments. **Marine Geology 92**, 105-113.

Wiberg, P.L. and Butman, C.A., 1991. Bed response during storms at the STRESS Inner Shelf Site. **Section O22C(-6) p.245 Am. Geophys. Union Fall Meeting** (abstract only).

Williams, G.P., 1970. Flume width and water depth effects in sediment transport experiments. **U.S. Geol. Surv. Prof. Paper 562-H,P.**, 1-37.

Williams, P.R. and Williams, D.J.A., 1989. Rheometry for concentrated cohesive suspensions. **J. Cost. Res. 5**, 151-164.

Willmarth, W.W., 1975. Structure of turbulence in boundary layers. **Adv. Appl. Mech. 15**, 159.

Woodin, S.A., 1976. Adult-larval interactions in dense infaunal assemblages: Patterns of abundance. **J. Mar. Res. 34**, 24-41.

Woods, R.D., 1991. Soil properties forshear wave propagation. **Shear Waves in Marine Sediments**, (eds. J.M. Hoven, M.D. Richardson and Stoll, R.D.), Kluwer Academic Publ, 29-39.

Wright, L.D. and Krone, R.B., 1989. Aggregate structure in hyper-concentrated mud flows. **J. Coast. Res. 5**, 117-125.

Yalin, M.S., et al, 1979. Inception of sediment transport. **J. Hydraul. Div., 105, HY11**, 1433-1443.

Yeh, H.Y., 1979. Re-suspension properties of flow deposited cohesive sediment bed. **Unpub. MSc. thesis, Univ. Florida, Gainesville, Florida**, 118pp.

Yew, C.H. and Jogi, P.N., 1976. Study of motions in fluid-saturated porous rocks. **J. Acoust. Soc. Am., 60(1)**, 2-8.

Yingst, J.Y. and Rhoads, D.C., 1978. Seafloor stability in central Long Island Sound Part II. Biological interactions and their potential importance for seafloor erodibility. In: **Estuarine Interactions** (Wiley, M.L., Ed.), Academic Press, 221-244.

Yingst, J.Y. and Rhoads, D.C., 1980. The role of bioturbation in the enhancement of microbial turnover rates in marine sediments. In: **Marine Benthic Dynamics** (eds. K.R.Tenrore and B.C.Coull), 407-421, Uni. South Carolina Press, Columbia.

Young, D.K., Jahn, W.N., Richardson, M.D. and Lehanik, A.W., 1985. Photographs of deep sea lebenspuren: a comparison of sedimentary provinces in the Venezuela Basin, Carribean Sea. **Marine Geology 68**, 269-301.

APPENDIX I.

Conductivity/Salinity/Temperature Relationship of Seawater.

The equations below were defined by Poisson 1980, and used to elaborate the Practical Salinity Scale. The measurements where carried out in a salinity range from 0 to 42ppt and a temperature range of -1 to 30°C, and then a polynomial fitted to the data.

$$X_{t,}S=\frac{S}{35}(0.042933R_d)+$$

$$S(S-35)\left(B_0+B_1S^{1/2}+B_2t+B_3S+B_4tS^{1/2}+B_5t^2+B_6S^{3/2}+B_7tS+B_8t^2S^{1/2}\right)$$

where $X_{t,s}$ is the conductivity at temperature t and salinity S, and the coefficients are,

$B_0 = -8.647\text{x}10^{-4}$
$B_1 = 2.752\text{x}10^{-6}$
$B_2 = -2.70\text{x}10^{-7}$
$B_3 = -4.37\text{x}10^{-7}$
$B_4 = -5.29\text{x}10^{-8}$
$B_5 = -1.08\text{x}10^{-9}$
$B_6 = 2.61\text{x}10^{-8}$
$B_7 = -3.9\text{x}10^{-9}$
$B_8 = 1.2\text{x}10^{-10}$

R_D is a polynomial produced by Dauphine and Klien 1977, and is given by,

$$R_D=0.6765836+2.005294(t/100)+1.110990(t/100)^2-$$

$$0.726684(t/100)^3+0.13587(t/100)^4$$

APPENDIX II.

Basic Program used to Convert Hexadecimal Output Files into Decimal for a Quattro Spreadsheet.

```
CLS
TYPE header
date AS STRING * 8
space1 AS STRING * 4
time AS STRING * 8
space2 AS STRING * 2
range AS STRING * 6
space3 AS STRING * 2
tbase AS STRING * 7
space4 AS STRING * 90
END TYPE
DIM parameter AS header
INPUT "Input data filename "; a$
a$ = "c:\equip\dsa524\" + a$
OPEN a$ FOR BINARY AS #1
GET #1, 2, parameter
d$ = parameter.date
t$ = parameter.time
r$ = parameter.range
b$ = parameter.tbase
PRINT "File created on "; d$; " at "; t$
PRINT "Voltage range "; r$; " /Div"
PRINT "Timebase "; b$; " /Div"
INPUT "Output File Name "; out$
out$ = "c:\equip\dsa524\abs\" + out$
PRINT "Writing data to "; out$
OPEN out$ FOR OUTPUT AS #2
PRINT #2, d$; " ,"; t$; " ,"; b$; " ,"; r$
DIM d(1050)
l = LOC(1)
FOR i = 1 TO 1050
  GET #1, l + i, d%
  l% = d% AND 255
  PRINT #2, USING "####.###"; i / 100 * VAL(b$);
  PRINT #2, " ,";
  PRINT #2, USING "####.####"; (l% - 128) / 30 * VAL(r$)
NEXT i
CLOSE
PRINT "FINISHED"
END
```

APPENDIX III.

Basic Program used to run the DASH-8 card and data logging.

```
'-------------------------------------------------------------
' D A S H - 8  D A T A L O G G E R
'-------------------------------------------------------------
' T.J.O'Hare, School of Ocean Sciences, University of Wales,
'  Bangor
'-------------------------------------------------------------
' Written in Microsoft Quickbasic 3.0
' Requires DAS8.OBJ, INT86.OBJ and DAS8.ADR
'-------------------------------------------------------------
' Compile with command QB DATALOG;
' Link with command LINK DATALOG DAS8 INT86;
'-------------------------------------------------------------
' The datalogger reads up to 8 data channels
' Data is read in blocks of user-defined length at a
'  specified sampling rate.
'-------------------------------------------------------------
' When altering the block length or sampling rate it is
'  important to bear in mind the time required by the
'  datalogger to store and display a block of data.
' This block length must be at least double this storage
'  time.
' The product of the sampling rate, the number of channels,
'  and the block length must not exceed 5000
'-------------------------------------------------------------
' The data is stored on a floppy disc (Drive A) and is ' displayed on
two graphs which are updated whenever a new
'   data block is read
' These graphs display the following information :-
' Upper graph : Channels 1, 2, 6, 7 & 8
' Lower graph : Channels 3, 4 & 5
'-------------------------------------------------------------

' Set up maximum sizes and fixed frequencies
      CONST BufferSize% = 5000
      CONST HalfBufferSize% = 2500
      CONST Clock = 1400000
      CONST Pulse% = 4000

' Set limits for graphs (Volts)
      DIM Max(1),Min(1)
' Upper graph
      Min(0) = 0
      Max(0) = 5
' Lower graph
      Min(1) = -1
      Max(1) = 3
```

```
' Set Maximum channel number to plot
     MaxChannel% = 8

' Set values for digitization parameters
     BlockTime% = 30
     NumChannel% = 8
     Samp% = 10

' Display title and get data filename
     CALL text(3,1,31,"DASH-8 DATA-LOGGER")
     CALL text(15,2,30,STRING$(20,"-"))
     CALL text(2,4,2,"Enter filename (max 8 chars) : ")
          DO
           LOCATE 4,33
           PRINT STRING$(LEN(Name$)," ")
           LOCATE 4,33
           LINE INPUT "",Name$
          LOOP UNTIL LEN(Name$) < 9
     FileName$ = "a:"+Name$+"."

     IF Name$ <> "" THEN
      CALL text(18,8,2,
           "INSERT FORMATTED DISKETTE IN DRIVE A:")
     END IF
     CALL text(4,12,2,"HIT <SPACE BAR> TO START LOGGING")

' Wait until <SPACE> is pressed before starting logging
     DO
     LOOP UNTIL INKEY$ = " "

' Set screen mode for graphics
     SCREEN 8

' Define arrays buffer arrays
     DIM Buffer%(BufferSize%),Sample%(HalfBufferSize%),
BufferEnd%(1), Dio%(2)

' Calculate buffer variables
     NumScan% = BlockTime% * Samp%
     NumSamp% = NumChannel% * NumScan%
     NumByte% = 2 * NumSamp%
     BufferEnd%(0) = NumByte% / 2 - 1
     BufferEnd%(1) = NumByte% - 1

' Plot step
     Pstep = 300 / NumScan%
' Half screen width
     Hscreen% = 300

' Define storage arrays
     DIM Store%(NumChannel%,NumScan%), Oldstore%(NumChannel%,
NumScan%)
     DIM LastStore%(NumChannel%, NumScan%)

' Retrieve DASH-8 memory address
     OPEN "DAS8.ADR" FOR INPUT AS #1
```

```
      INPUT #1, BaseAddress%
      CLOSE #1

' Calculate segment address of buffer array
      CALL PTR86(BufferSegment%,BufferOffset%,
VARPTR(Buffer%(0)))
      SegmentAddress% = BufferSegment% + BufferOffset% / 16 + 1

' Clear half buffers
      FOR HalfBuffer% = 0 TO 1
       CALL clearbuffer(SegmentAddress%, BufferEnd%(HalfBuffer% ))
      NEXT HalfBuffer%

' Perform DASH-8 cals to set up and start digitization
      CALL Das8(0, BaseAddress%, Flag%)
      CALL Das8(14, 1, Flag%)
      FOR Counter% = 2 TO 0 STEP -1
            Dio%(0) = Counter%: Dio%(1) = 0
            CALL Das8(10, Dio%(0), Flag%)
      NEXT Counter%
      Dio%(0) = 0: Dio%(1) = NumChannel% - 1
      CALL Das8(1, Dio%(0), Flag%)
      CALL Das8(17, 1, Flag%)
' Set Dio%(0) to interrupt level set on das-8 board
      Dio%(0) = 2: Dio%(1) = 1
      CALL Das8(6, Dio%(0), Flag%)
      Dio%(0) = NumSamp%: Dio%(1) = SegmentAddress%
      CALL Das8(8, Dio%(0), Flag%)
      Dio%(0) = 0: Dio%(1) = 1
      CALL Das8(10, Dio%(0), Flag%)
      Dio%(0) = 0: Dio%(1) = NumChannel%
      CALL Das8(11, Dio%(0), Flag%)
      Dio%(0) = 1: Dio%(1) = 3
      CALL Das8(10, Dio%(0), Flag%)
      Dio%(0) = 1: Dio%(1) = (Pulse% / Samp%)
      CALL Das8(11, Dio%(0), Flag%)
      Dio%(0) = 2: Dio%(1) = 3
      CALL Das8(10, Dio%(0), Flag%)
      Dio%(0) = 2: Dio%(1) = INT(Clock / Pulse%)
      CALL Das8(11, Dio%(0), Flag%)

' Perform digitization until user prompts stop (capital S to stop)
      StopInput% = 0
      Pass% = -1
      Ctr%=1
      DO

       Pass% = Pass% + 1
' Read in a data block
       FOR HalfBuffer% = 0 TO 1
        CALL waitbuffer(SegmentAddress%, BufferEnd%(HalfBuffer% ))

        Dio%(0) = VARPTR(Sample%(0))
        Dio%(1) = NumSamp% / 2
        Dio%(2) = HalfBuffer% * NumSamp% / 2
        CALL Das8(9, Dio%(0), Flag%)
```

```
        CALL clearbuffer(SegmentAddress%, BufferEnd%( HalfBuffer%))
        CALL writebuffer(NumScan%, NumChannel%, HalfBuffer%,
Sample%(), Store%())
             print "Updating Graphics"
       NEXT HalfBuffer%

' Update graphs
       CLS
       FOR Graph% = 0 TO 1
' Compute graph origin (x0,y0)
        x0% = 20
        y0% = 50+100*Graph%
' Draw graph borders, axes and limits
' Top graph border
        LINE (x0%,y0%-45)-(x0%+2*Hscreen%,y0%-45)
' Maximum Value
        LINE (x0%,y0%-40)-(x0%+2*Hscreen%,y0%-40),,,&HF0F0
' Minimum Value
        LINE (x0%,y0%+40)-(x0%+2*Hscreen%,y0%+40),,,&HF0F0
        y0inc% = 80*Max(Graph%)/(Max(Graph%)-Min(Graph%))
' Zero
        LINE (x0%,y0%-40+y0inc%)-(x0%+2*Hscreen%,y0%-40+y0inc%)
,,,&HF0F0
' Base
        LINE (x0%,y0%+45)-(x0%+2*Hscreen%,y0%+45)
' Left Edge
        LINE (x0%,y0%-45)-(x0%,y0%+45)
' Right Edge
        LINE (x0%+2*Hscreen%,y0%-45)-(x0%+2*Hscreen%,y0%+45)
' Center Line
        LINE (x0%+Hscreen%,y0%-45)-(x0%+Hscreen%,y0%+45) ,,,&HF0F0
' Plot data on graph
        Scale = 4096*(Max(Graph%)-Min(Graph%))/800
        FOR Counter% = 0 TO (NumScan% - 1)
         IF Graph% = 0 THEN
' Upper graph : Channels 1 and 2
          FOR Channel% = 1 TO 2
' Plot old data in left half of graph
            IF LastStore%(Channel%,Counter%) > 2048*Max(Graph%) /5
THEN y% = 2048*Max(Graph%)/(5*Scale)
            ELSE
             IF LastStore%(Channel%,Counter%) < 2048*Min(Graph%) /5
THEN y% = 2048*Min(Graph%)/(5*Scale)
             ELSE
              y% = LastStore%(Channel%,Counter%)/Scale
             END IF
            END IF
            PSET (x0%+(Counter%*Pstep),y0%-40+y0inc%-y%),
1+Channel%
' Plot new data in right half of graph
            IF Store%(Channel%,Counter%) > 2048*Max(Graph%)/5 THEN
             y% = 2048*Max(Graph%)/(5*Scale)
            ELSE
             IF Store%(Channel%,Counter%) < 2048*Min(Graph%)/5 THEN
              y% = 2048*Min(Graph%)/(5*Scale)
             ELSE
```

```
                y% = Store%(Channel%,Counter%)/Scale
               END IF
              END IF
              PSET (x0%+Hscreen%+(Counter%*Pstep),
y0%-40+y0inc%-y%), 1+Channel%
' Set old data = new data
              LastStore%(Channel%,Counter%) =
Store%(Channel%,Counter%)
           NEXT Channel%
' Upper graph: Channels 6, 7 and 8
           FOR Channel% = 6 TO 8
' Plot old data in left half of graph
              IF LastStore%(Channel%, Counter%) > 2048*Max(Graph%) /5
THEN y% = 2048*Max(Graph%)/(5*Scale)
              ELSE
               IF LastStore%(Channel%,Counter%) < 2048*Min(Graph%) /5
THEN y% = 2048*Min(Graph%)/(5*Scale)
               ELSE
                y% = LastStore%(Channel%,Counter%)/Scale
               END IF
              END IF
              PSET (x0%+(Counter%*Pstep),y0%-40+y0inc%-y%),
1+Channel%
' Plot new data in right half of graph
              IF Store%(Channel%,Counter%) . 2048*Max(Graph%)/5 THEN
               y% = 2048*Max(Graph%)/(5*Scale)
              ELSE
               IF Store%(Channel%,Counter%) < 2048*Min(Graph%)/5 THEN
                y% = 2048*Min(Graph%)/(5*Scale)
               ELSE
                y% = Store%(Channel%,Counter%)/Scale
               END IF
              END IF
              PSET (x0%+Hscreen%+(Counter%*Pstep),
y0%-40+y0inc%-y%), 1+Channel%
' Set old data = new data
              LastStore%(Channel%,Counter%) = Store%(Channel%
Counter%)
           NEXT Channel%
          ELSE
' Lower graph : Channels 3, 4 and 5
           FOR Channel% = 3 TO 5
' Plot old data in left half of graph
              IF LastStore%(Channel%,Counter%) > 2048*Max(Graph%) /5
THEN y% = 2048*Max(Graph%)/(5*Scale)
              ELSE
               IF LastStore%(Channel%,Counter%) < 2048*Min(Graph%) /5
THEN y% = 2048*Min(Graph%)/(5*Scale)
               ELSE
                y% = LastStore%(Channel%,Counter%)/Scale
               END IF
              END IF
              PSET (x0%+(Counter%*Pstep),y0%-40+y0inc%-y%),
1+Channel%
' Plot new data in right half of graph
              IF Store%(Channel%,Counter%) > 2048*Max(Graph%)/5 THEN
```

```
             END IF
            END IF
            PSET (x0%+(Counter%*Pstep),y0%-40+y0inc%-y%),
1+Channel%
' Plot new data in right half of graph
            IF Store%(Channel%,Counter%) > 2048*Max(Graph%)/5 THEN
             y% = 2048*Max(Graph%)/(5*Scale)
            ELSE
             IF Store%(Channel%,Counter%) < 2048*Min(Graph%)/5 THEN
              y% = 2048*Min(Graph%)/(5*Scale)
             ELSE
              y% = Store%(Channel%,Counter%)/Scale
             END IF
            END IF
            PSET (x0%+Hscreen%+(Counter%*Pstep),
y0%-40+y0inc%-y%),1+Channel%
' Set old data = new data
            LastStore%(Channel%,Counter%) = Store%(Channel%,
Counter%)
          NEXT Channel%
         END IF
        NEXT Counter%
       NEXT Graph%
' Plot lines to show colour code of data channels
       FOR Channel% = 1 TO MaxChannel%
        x0% = 20+(Channel%-0.9)*600/MaxChannel%
        x1% = 20+(Channel%-0.1)*600/MaxChannel%
        LINE (x0%,100)-(x1%,100),Channel%+1
       NEXT Channel%
       PRINT "Screen Number"; ctr%

' Incrementing screen number
       ctr%=ctr%+1

' Write data to floppy disc
       print "Writing data to drive a:"
       IF Name$ <> "" THEN
        Ext$ = STR$(Pass%)
        IF LEN(Ext$) = 2 THEN Ext$ = "00"+RIGHT$(Ext$,1)
        IF LEN(Ext$) = 3 THEN Ext$ = "0"+RIGHT$(Ext$,2)
        IF LEN(Ext$) = 4 THEN Ext$ = RIGHT$(Ext$,3)
        OPEN FileName$+Ext$ FOR OUTPUT AS #1

        FOR Counter% = 0 TO (NumScan% - 1)
         PRINT #1, USING " ####### ";Counter%+Pass%*NumScan%;
         FOR Channel% = 1 TO NumChannel%
          PRINT #1, USING " +#### ";Store%(Channel%,Counter%);
         NEXT Channel%
         PRINT #1,""
        NEXT Counter%
        CLOSE #1
       END IF

' Check for stop input
       IF INKEY$ = "S" THEN StopInput% = 1
```

```
        LOOP UNTIL StopInput% = 1

' Perform DASH-8 calls to switch off digitization
        CALL Das8(7, 0, Flag%)
        FOR Counter% = 0 TO 2
                Dio%(0) = Counter%: Dio%(1) = 0
                CALL Das8(10, Dio%(0), Flag%)
        NEXT Counter%

        DO
        IN$ = INKEY$
        LOOP UNTIL IN$<>"" AND IN$<>" "

        END

'-------------------------------------------------------

SUB waitbuffer(SegmentAddress%, Pointer%) STATIC

        DEF SEG = SegmentAddress%
        DO WHILE PEEK(Pointer%) = &HFF
        LOOP

END SUB

'-------------------------------------------------------

SUB readbuffer(Pointer%, Length%, HalfBuffer%) STATIC
        REDIM Tran%(2)
        Tran%(0) = Pointer%
        Tran%(1) = Length%
        Tran%(2) = HalfBuffer% * Length%
        CALL Das8(9, Tran%(0), 0)
END SUB

'-------------------------------------------------------

SUB clearbuffer(SegmentAddress%, Pointer%) STATIC
        DEF SEG = SegmentAddress%
        POKE (Pointer%), &HFF
END SUB

'-------------------------------------------------------

SUB writebuffer(NumScan%, NumChan%, HalfBuffer%, Sample%(1),
Store%(2)) STATIC
        FOR Counter% = 0 TO (NumScan% / 2) - 1
         StartElement% = NumChan% * Counter%
         EndElement% = StartElement% + (NumChan% - 1)
         FOR Element% = StartElement% TO EndElement%
          Channel% = ((Sample%(Element%) AND &H7000) / 4096) + 1
          Value% = (Sample%(Element%) AND &H87FF)
          IF Value% AND &H8000 THEN Value% = Value% OR &H7800
                        Store%(Channel%, Counter% + HalfBuffer% * NumScan%
/ 2) = Value%
         NEXT Element%
        NEXT Counter%
```

```
END SUB

'-------------------------------------------------------------

SUB text(Colour%,y%,x%,words$) STATIC
      COLOR Colour%
      LOCATE y%,x%
      PRINT words$
END SUB

'-------------------------------------------------------------
```

APPENDIX IV.

Flume run results.

Fig (a.1a): Processed Data for Flume Run 1.

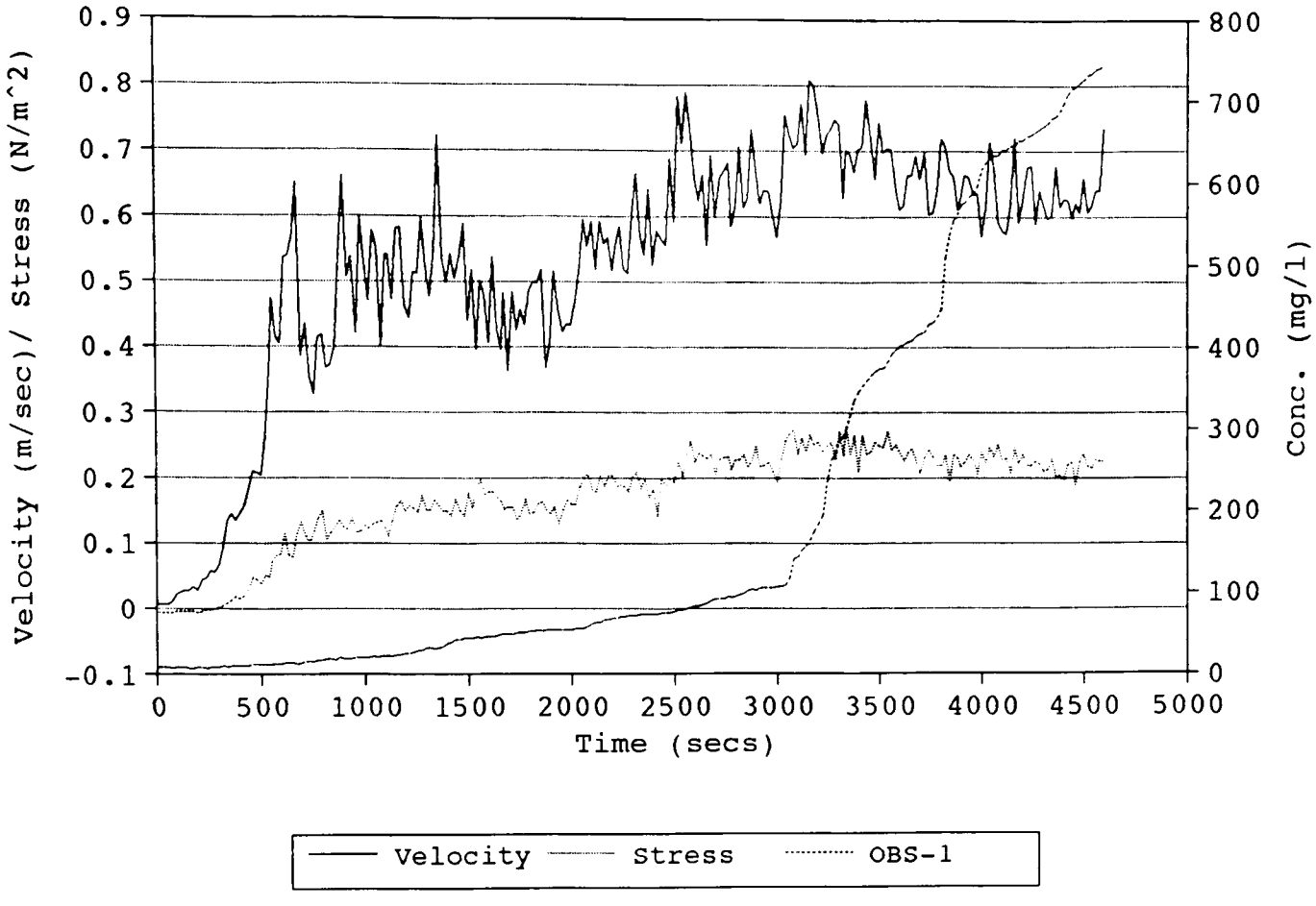

Fig (a.1b): Suspended Sediment Concentration and Rate of Erosion.

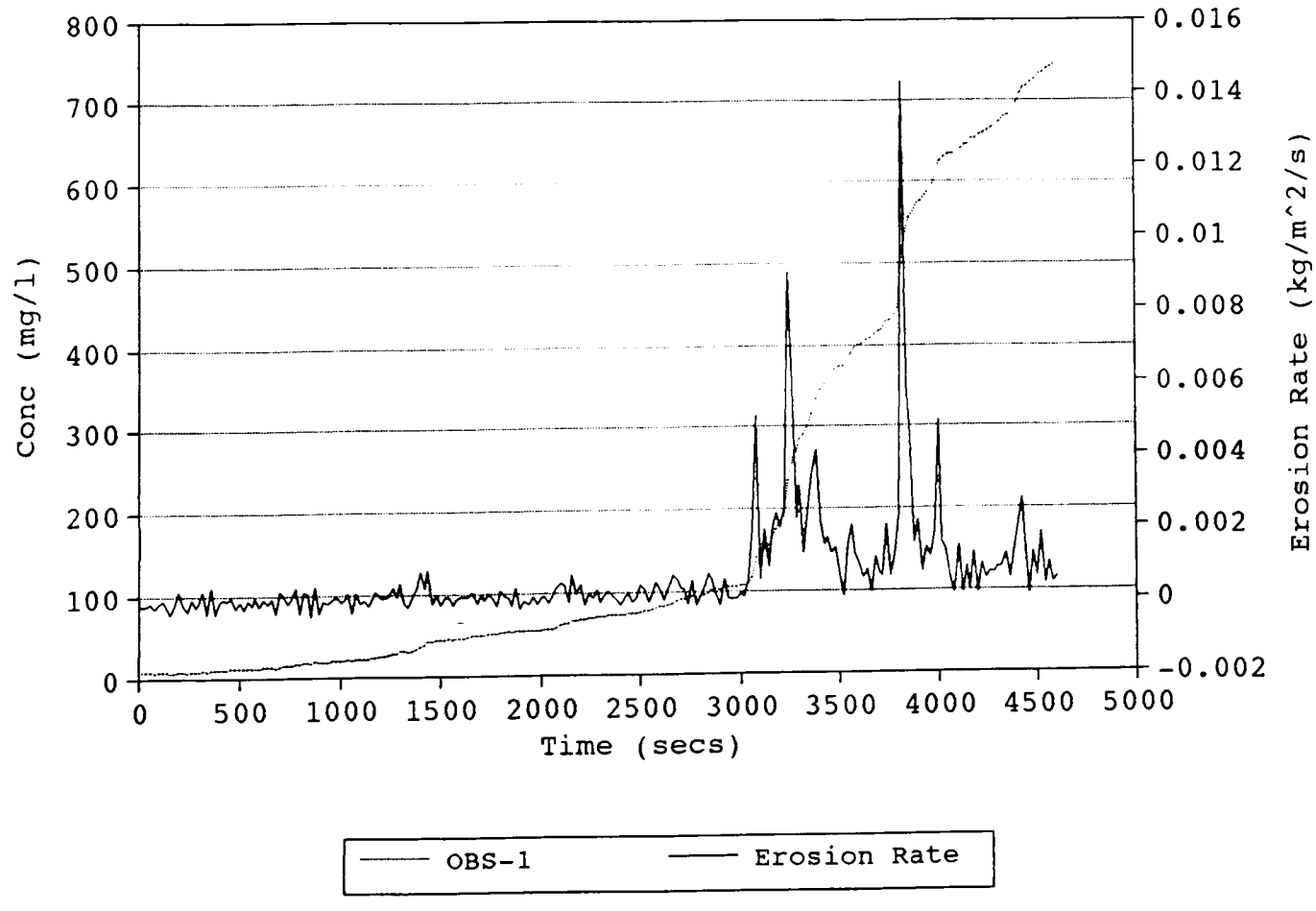

Fig (a.2a): Processed Data for Flume Run 2.

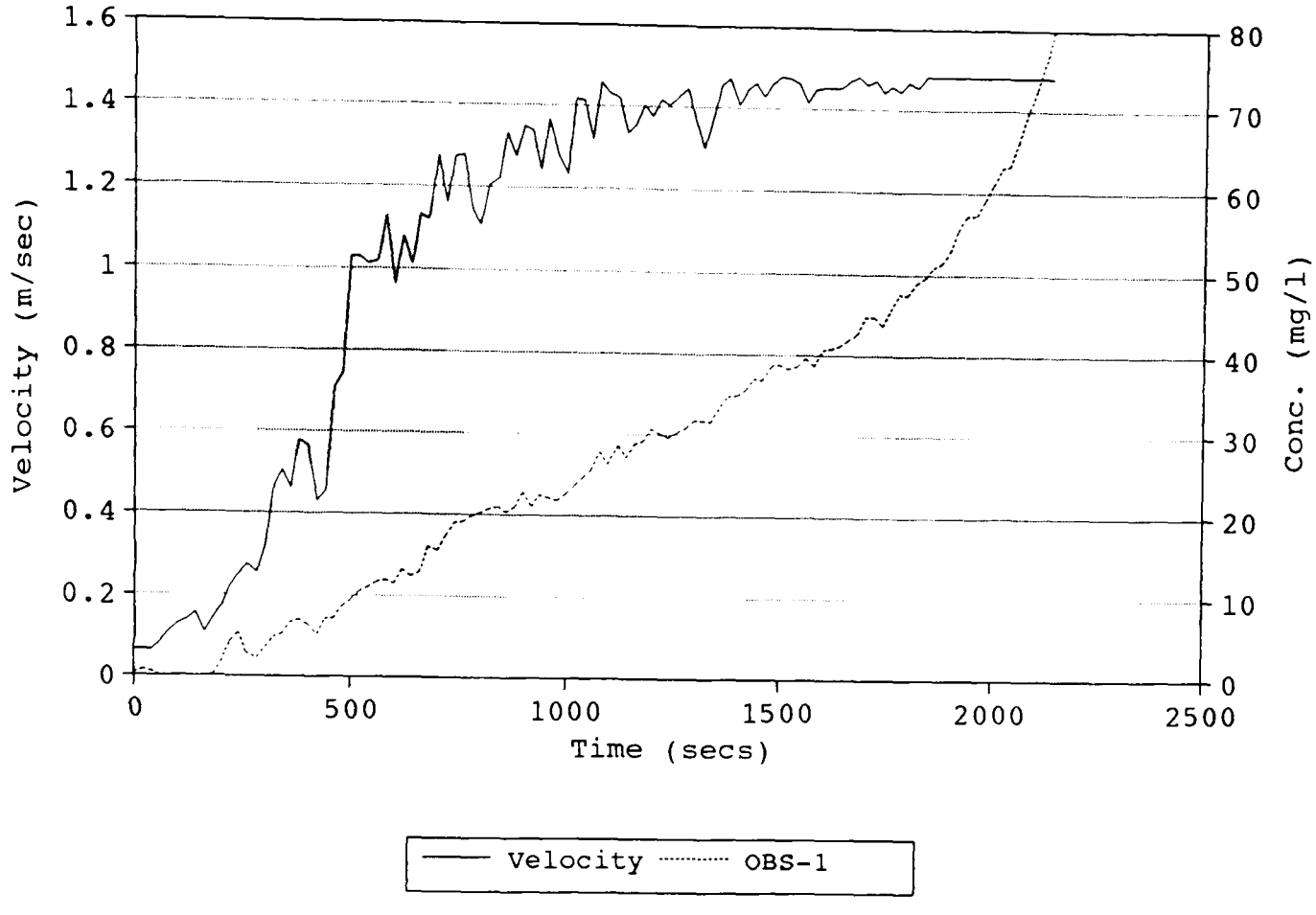

Fig (a.2b): Suspended Sediment Concentration and Rate of Erosion.

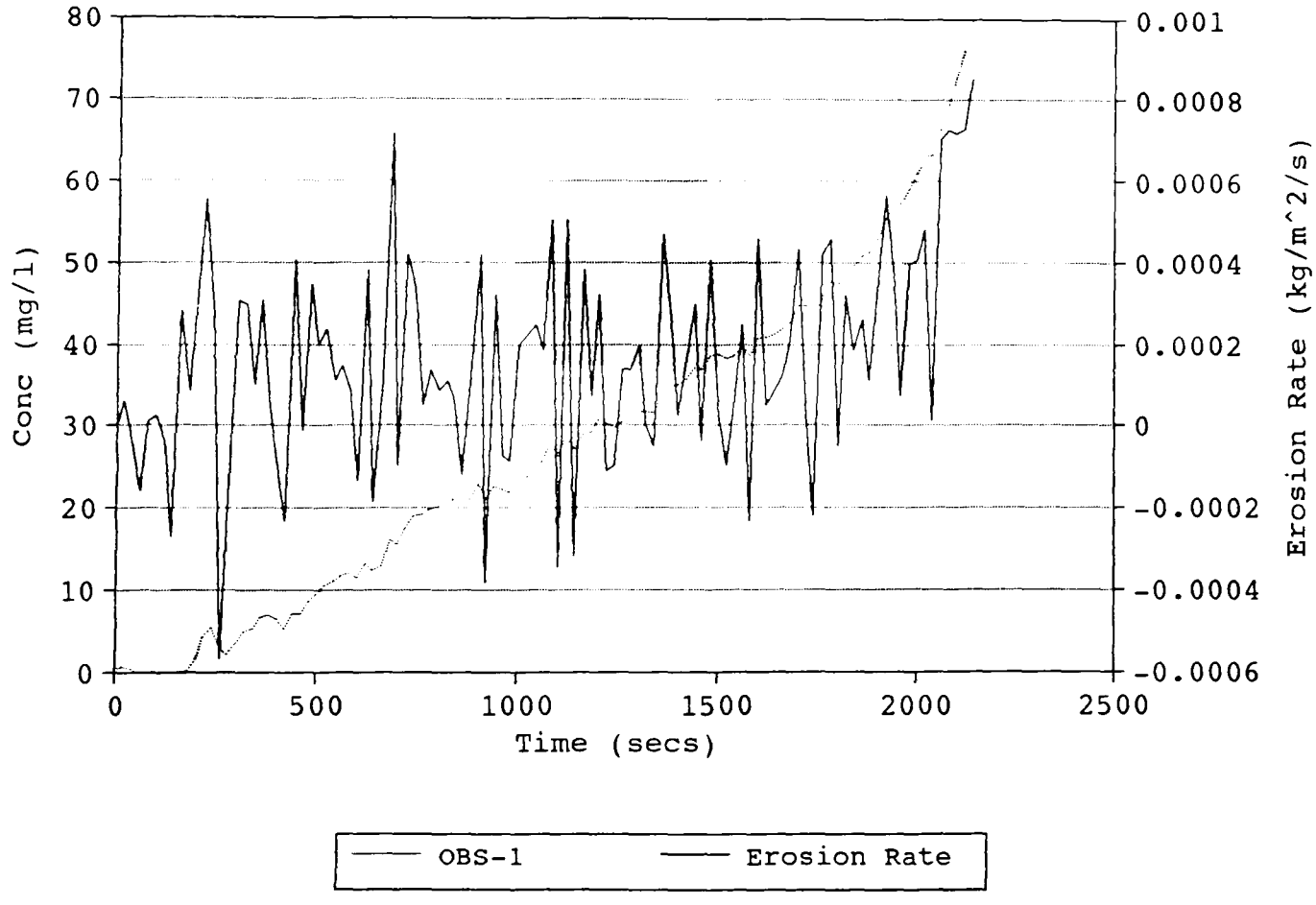

Fig (a.3a): Processed Data for Flume Run 3.

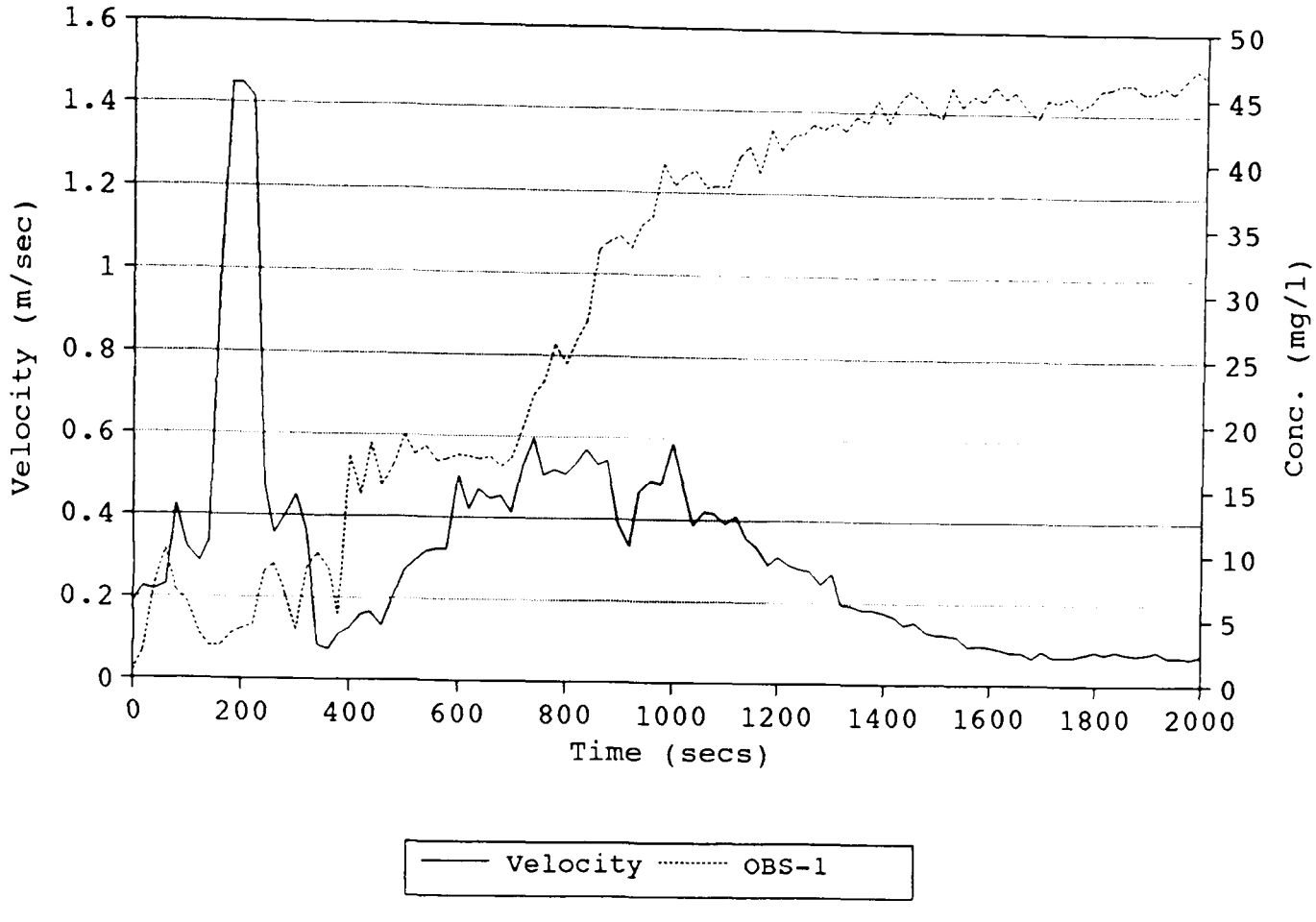

Fig (a.3b): Suspended Sediment Concentration and Rate of Erosion.

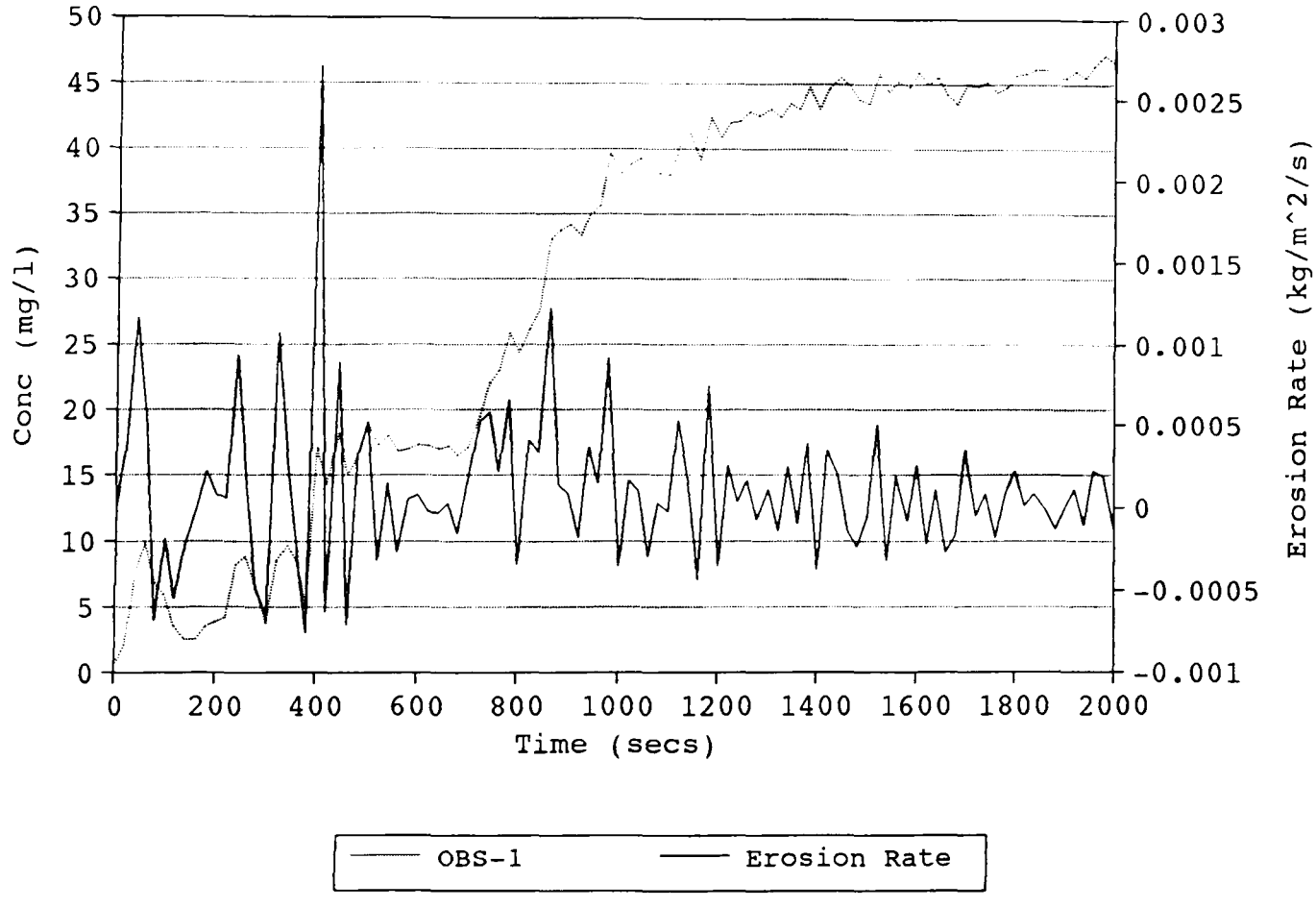

Fig (a.4a): Processed Data for Flume Run 4.

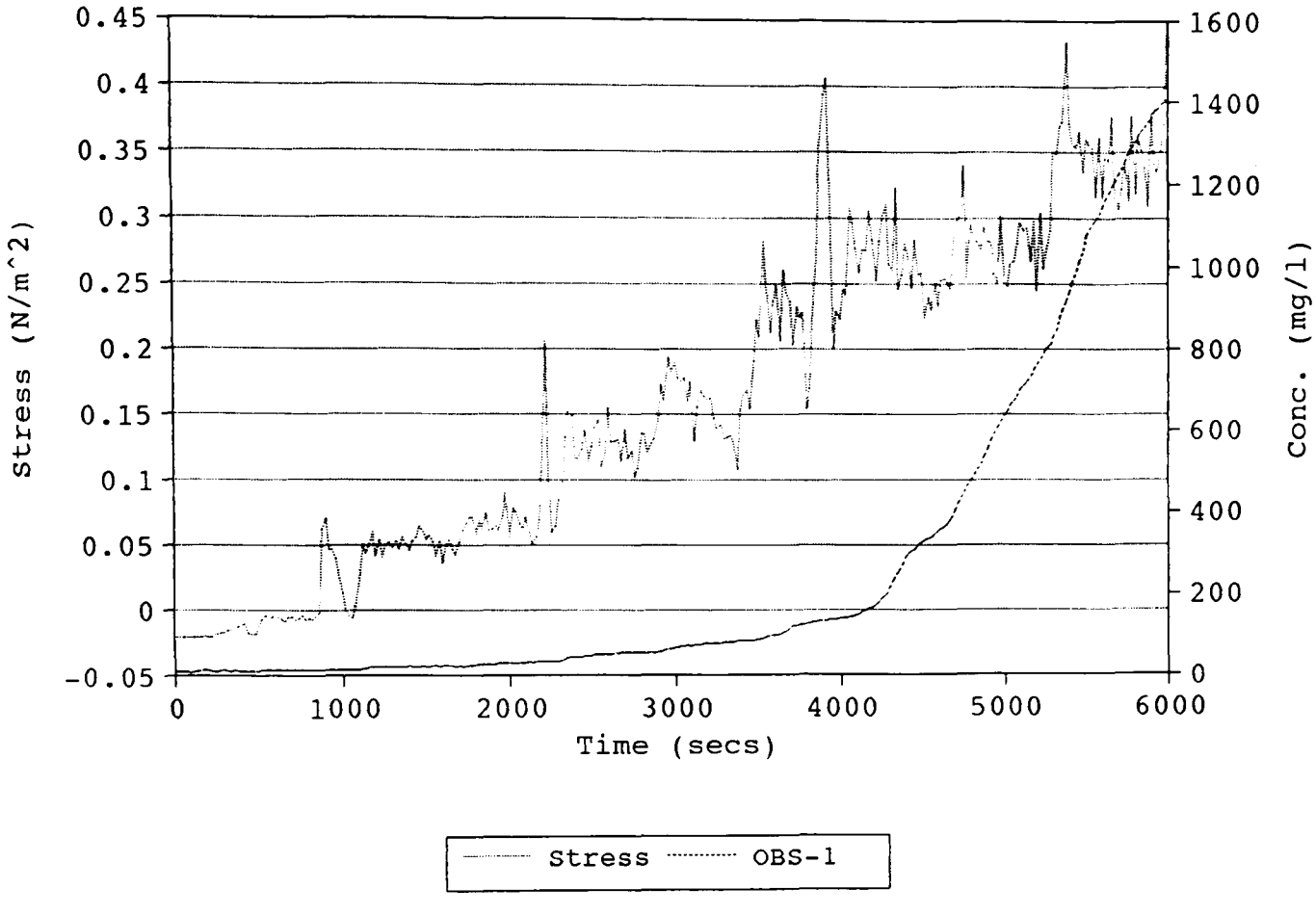

Fig (a.4b): Suspended Sediment Concentration and Rate of Erosion.

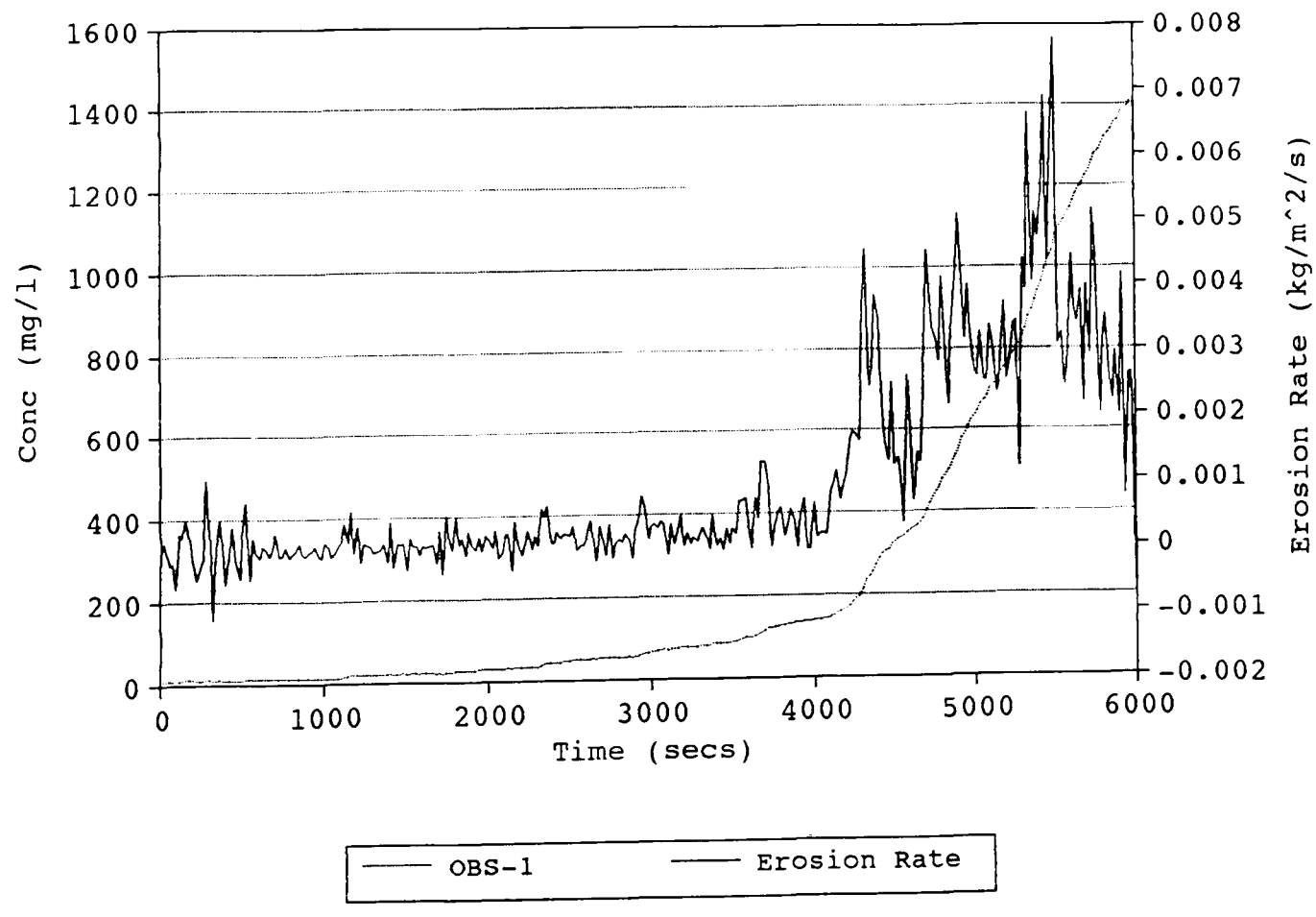

Fig (a.5a): Processed Data for Flume Run 5.

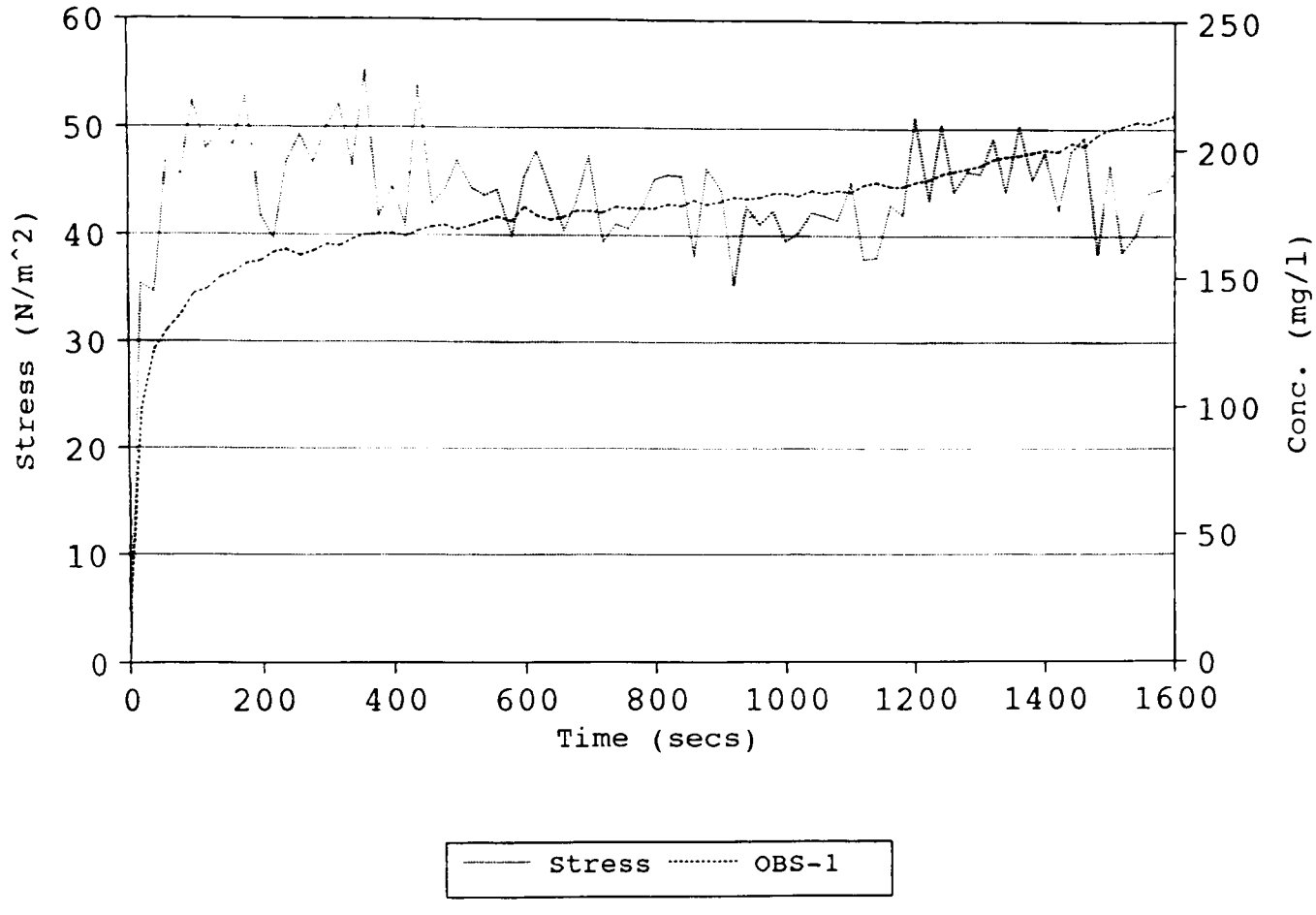

Fig (a.5b): Suspended Sediment Concentration and Rate of Erosion.

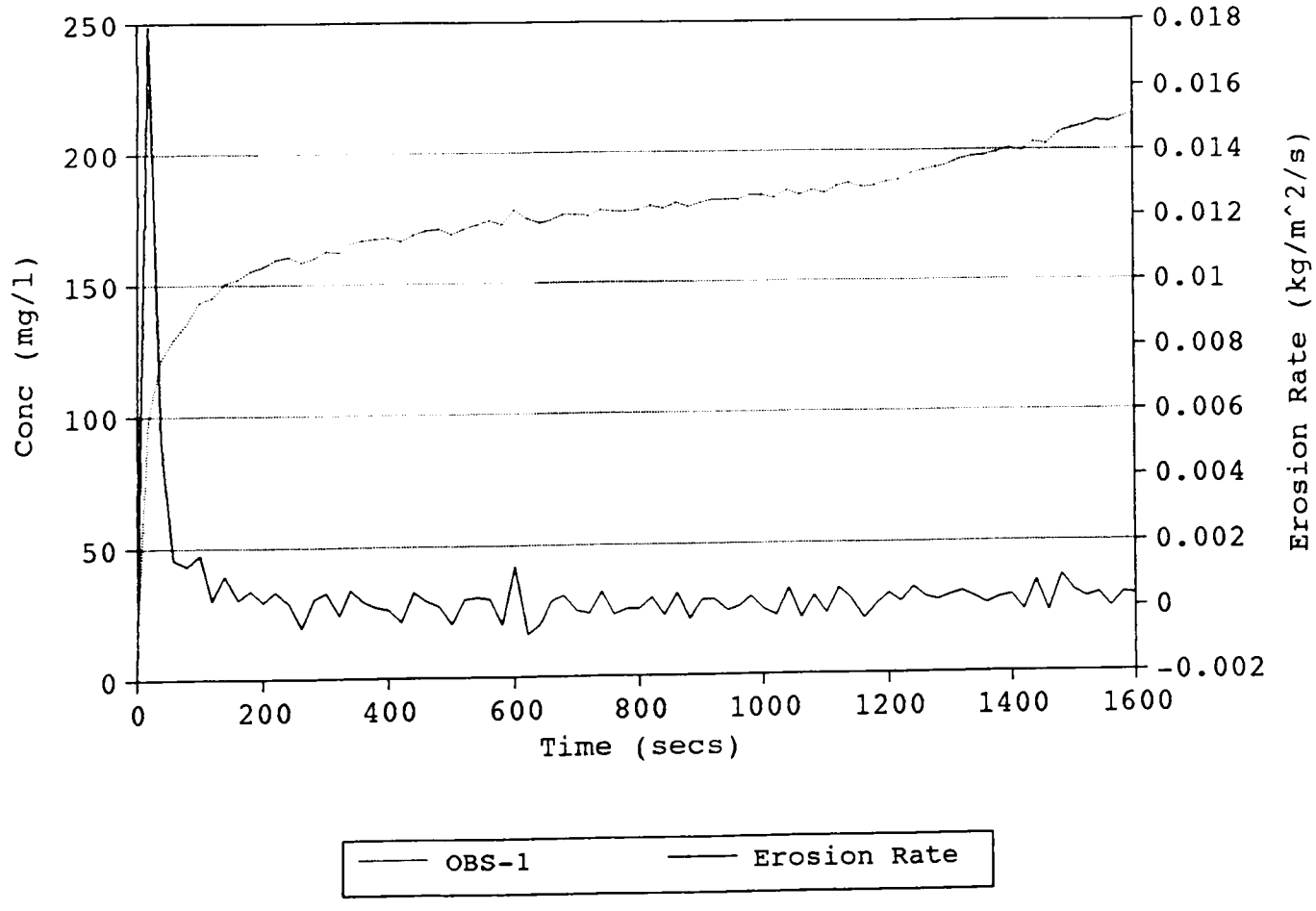

Fig (a.6a): Processed Data for Flume Run 6.

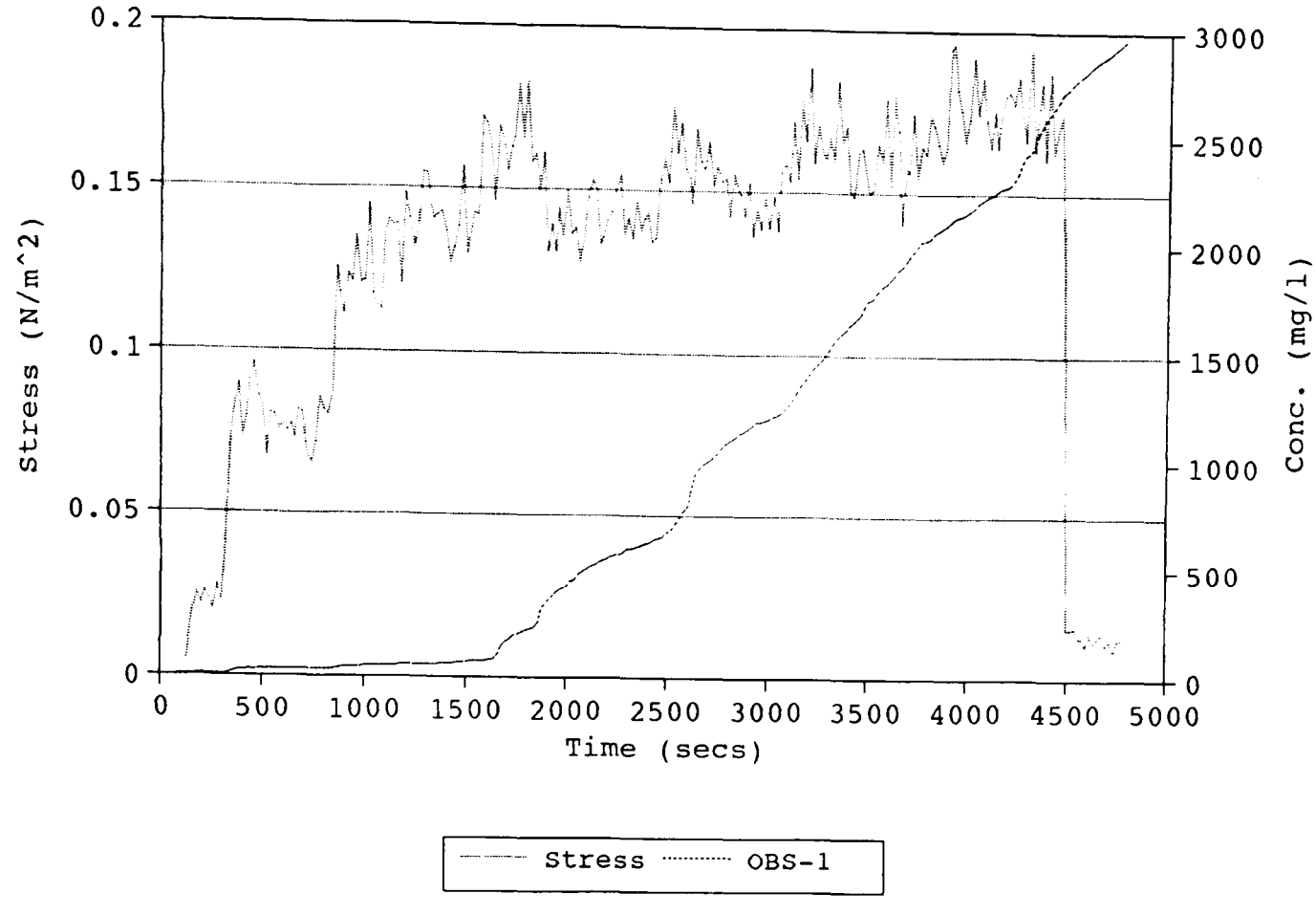

Fig (a.6b): Suspended Sediment Concentration and Rate of Erosion.

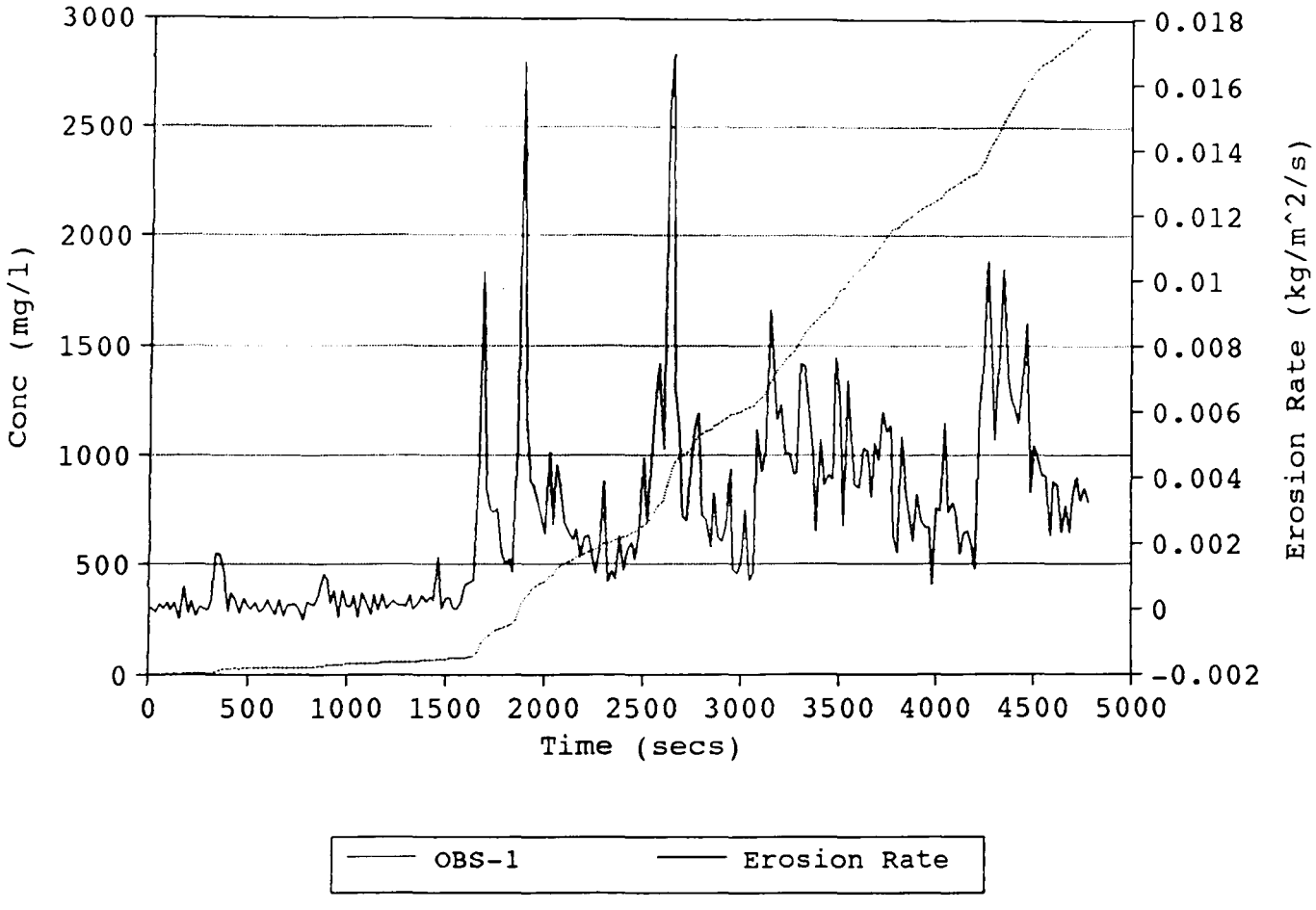

Fig (a.7a): Processed Data for Flume Run 7.

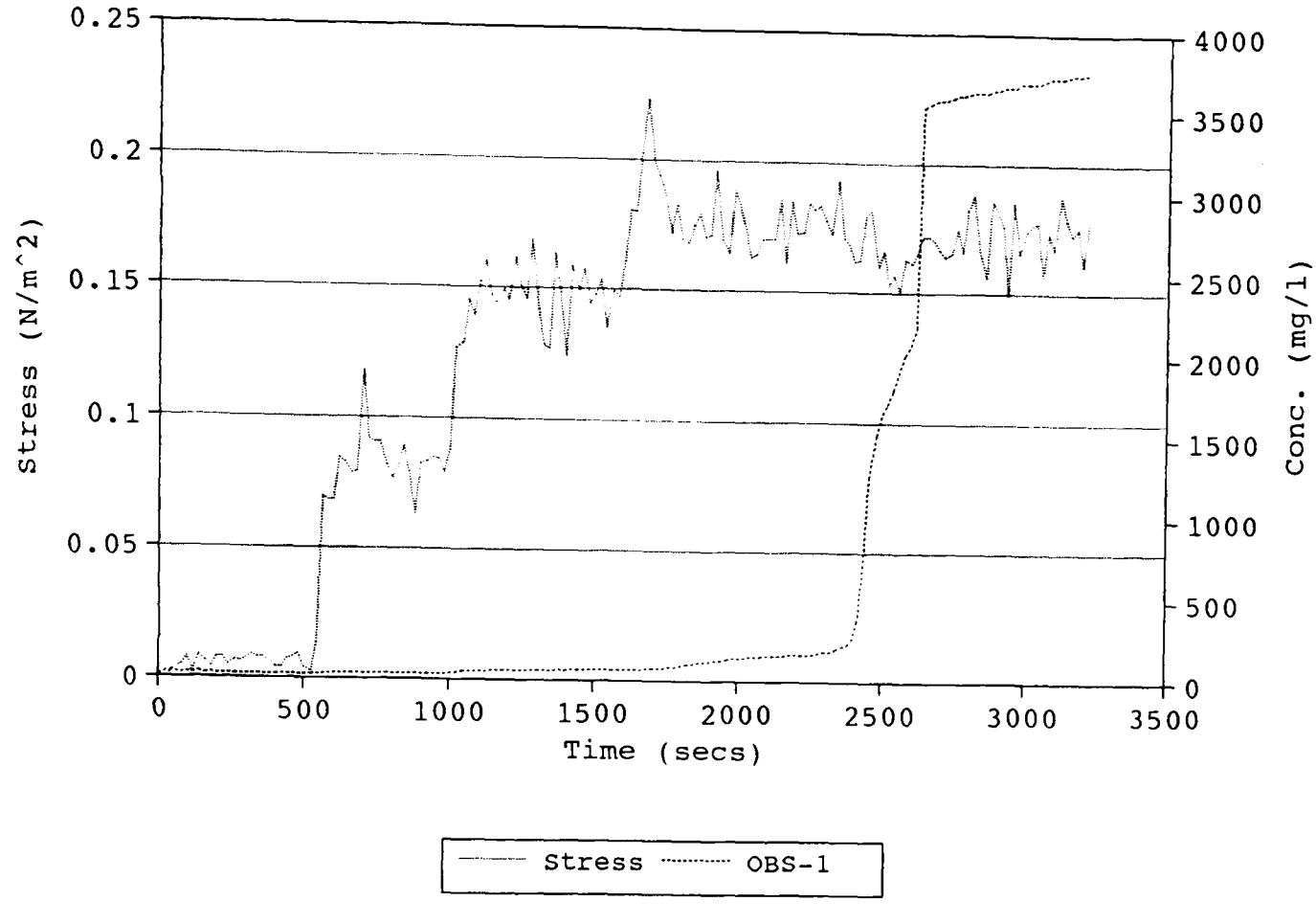

Fig (a.7b): Suspended Sediment Concentration and Rate of Erosion.

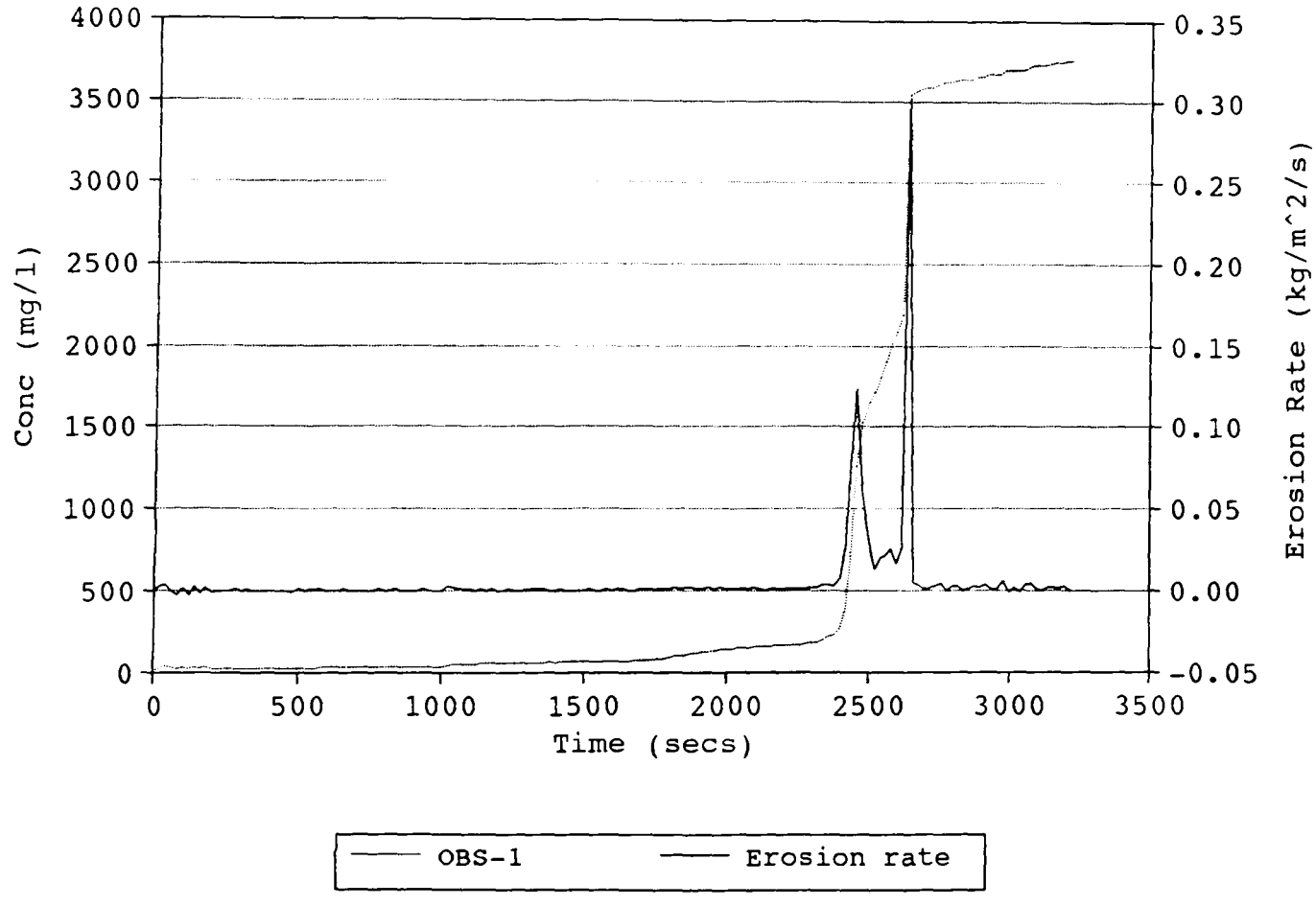

Fig (a.8a): Processed Data for Flume Run 8.

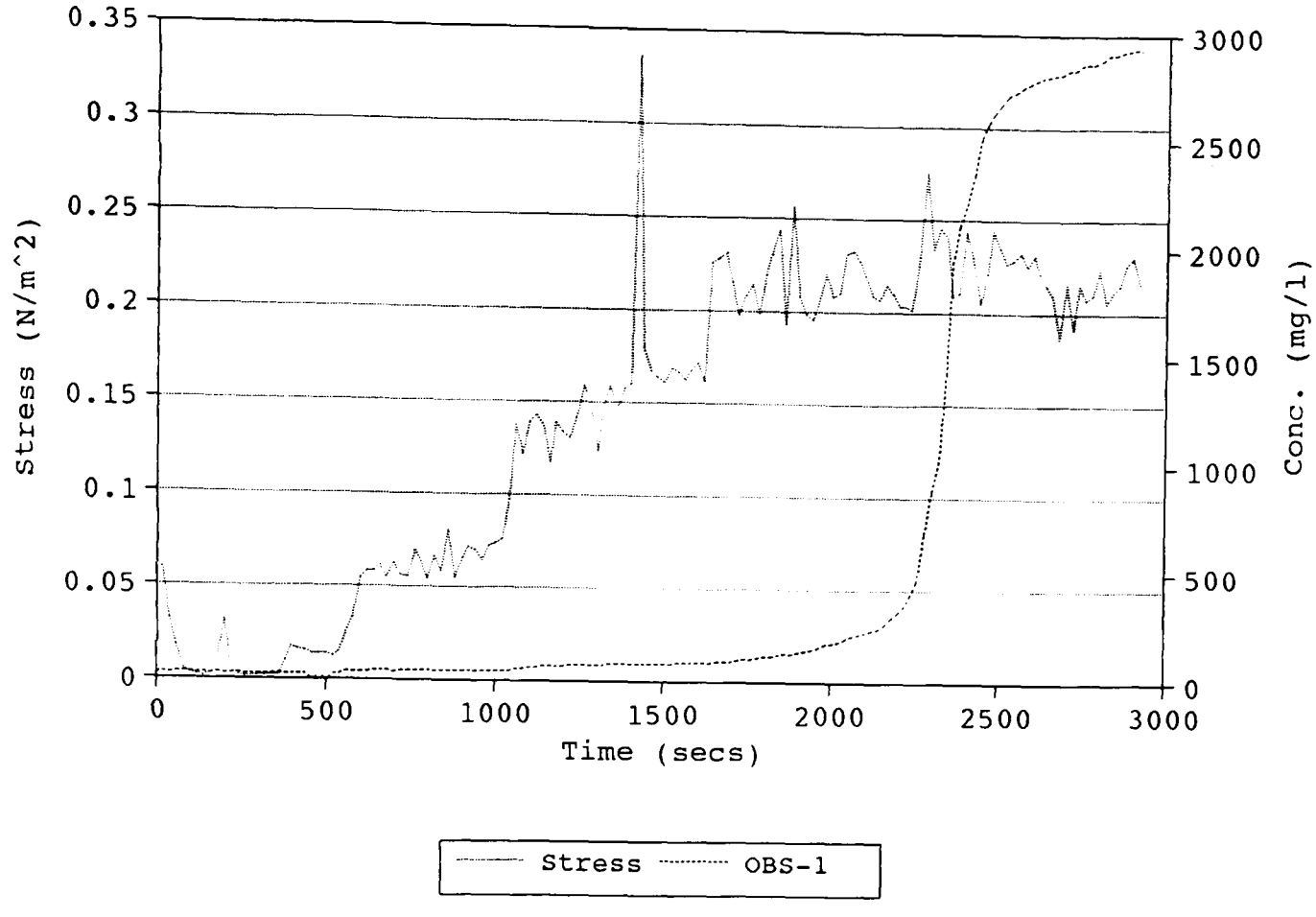

Fig (a.8b): Suspended Sediment Concentration and Rate of Erosion.

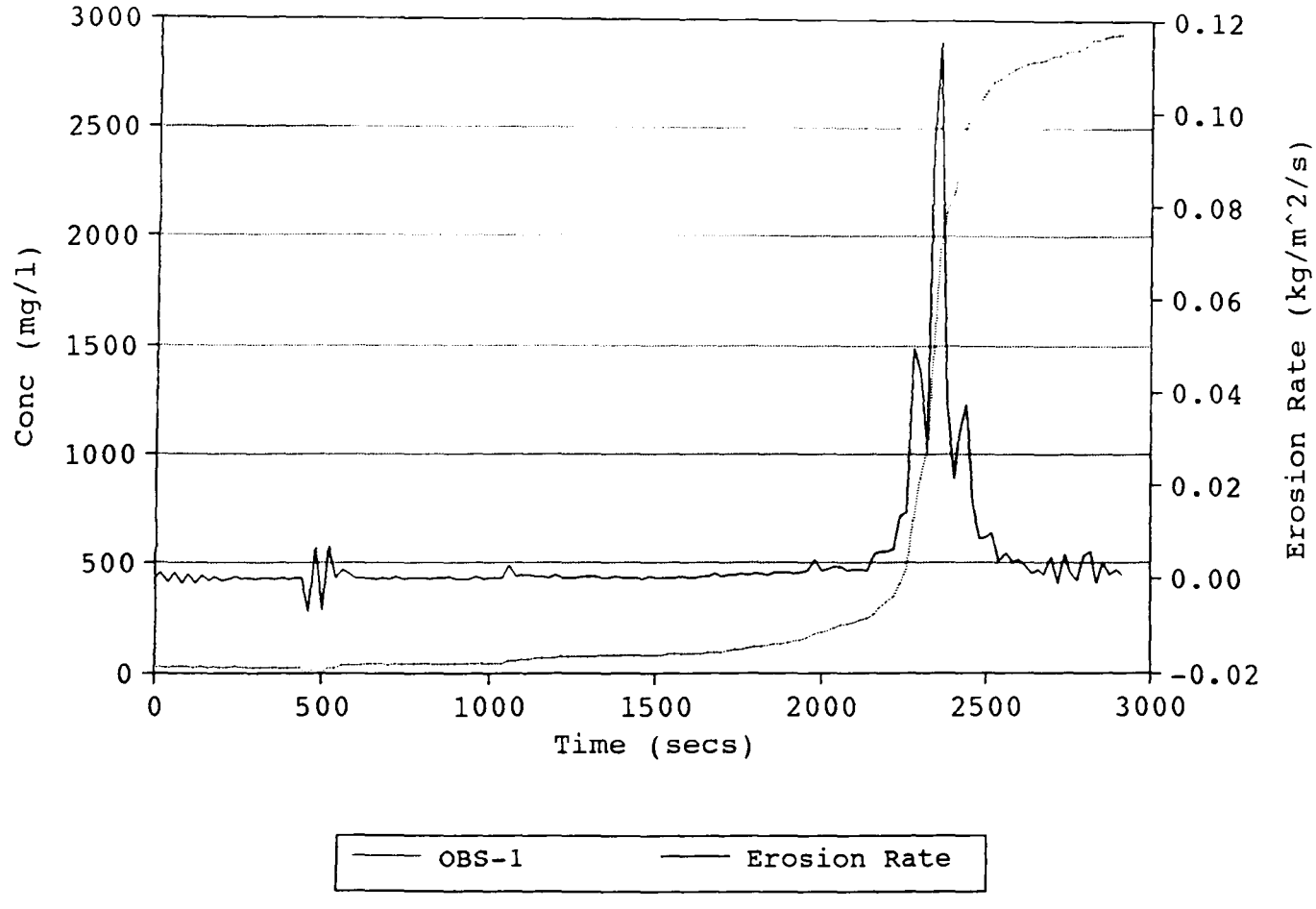

Fig (a.9a): Processed Data for Flume Run 9.

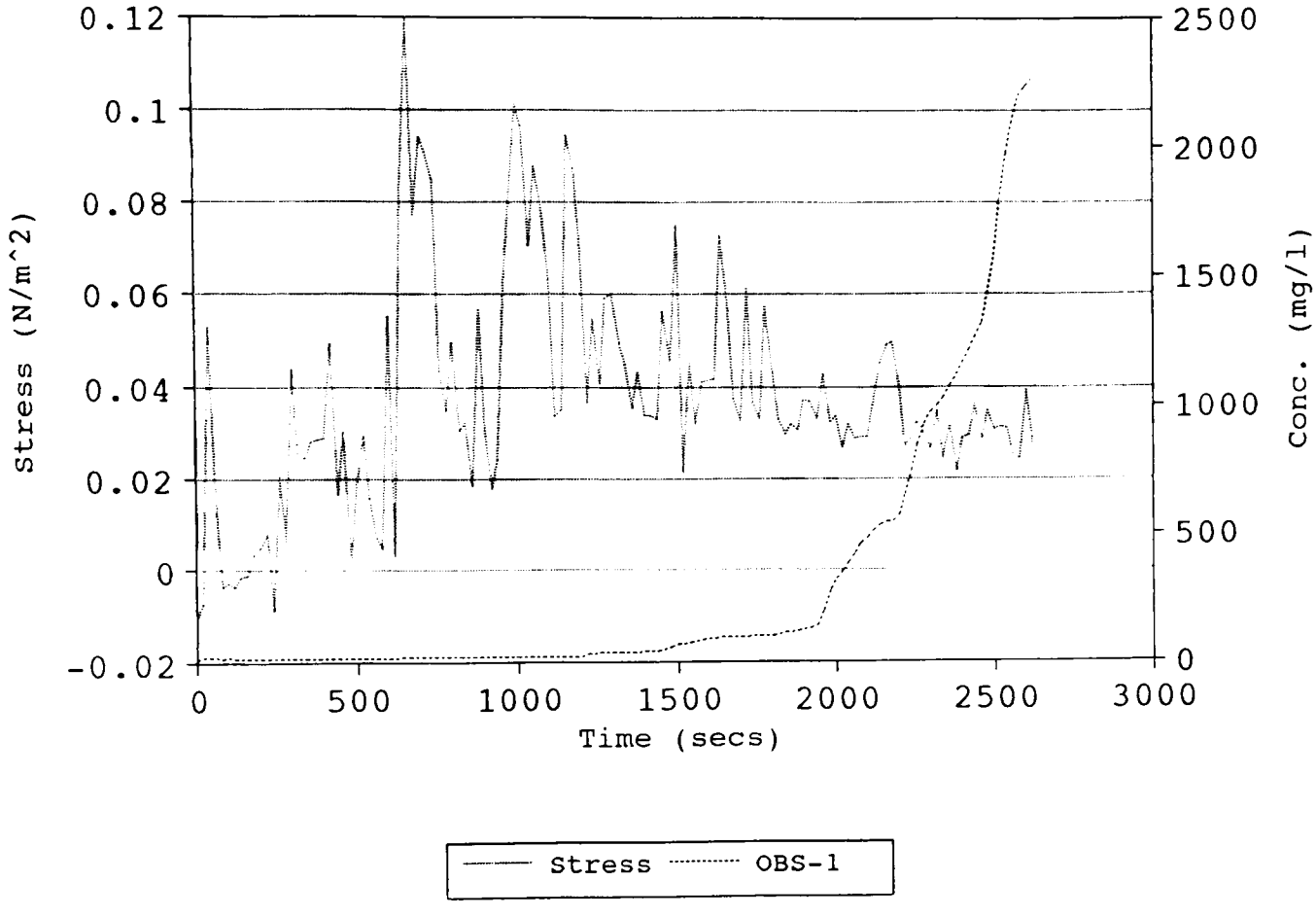

Fig (a.9b): Suspended Sediment Concentration and Rate of Erosion.

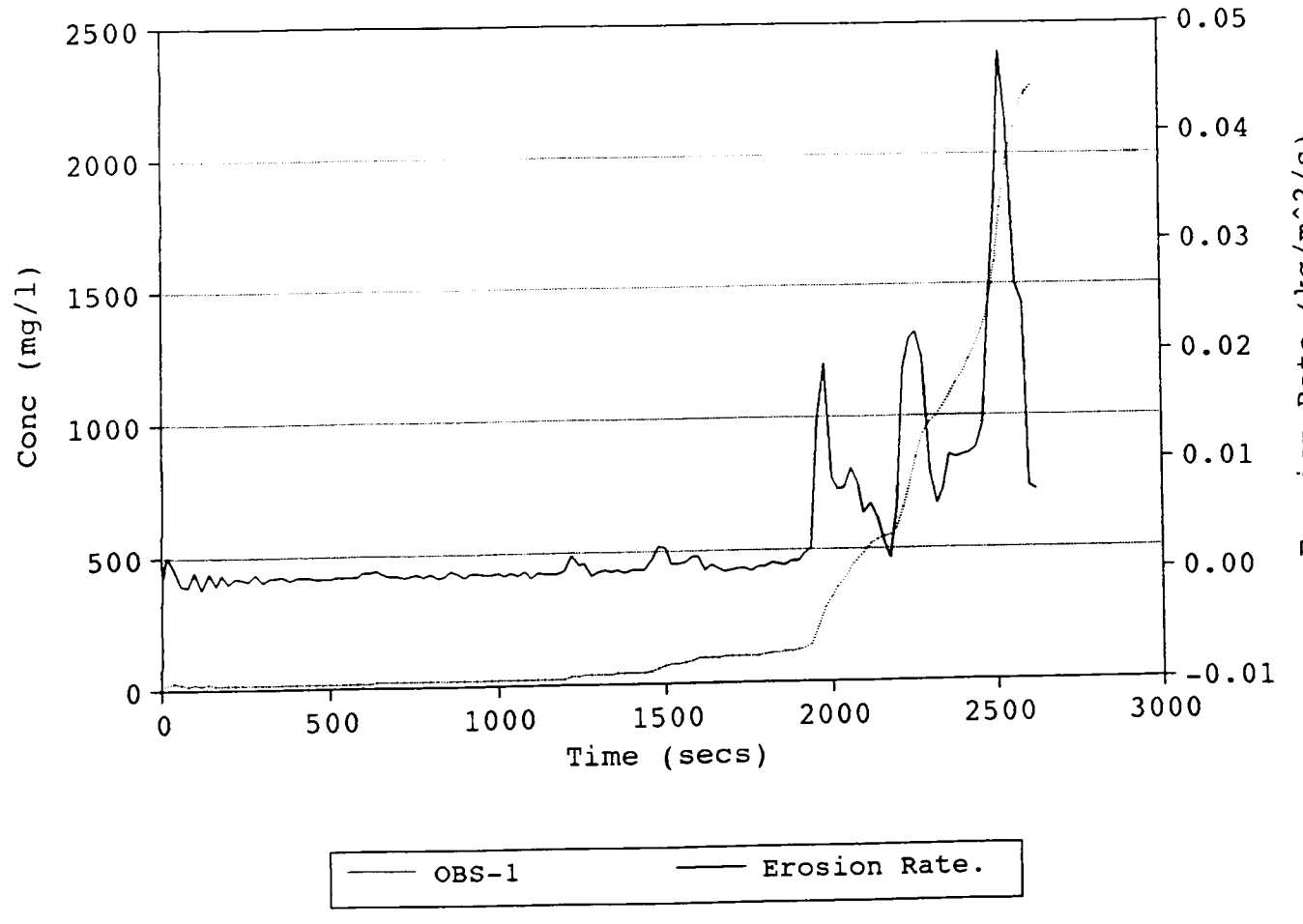

Fig (a.10a): Processed Data for Flume Run 10.

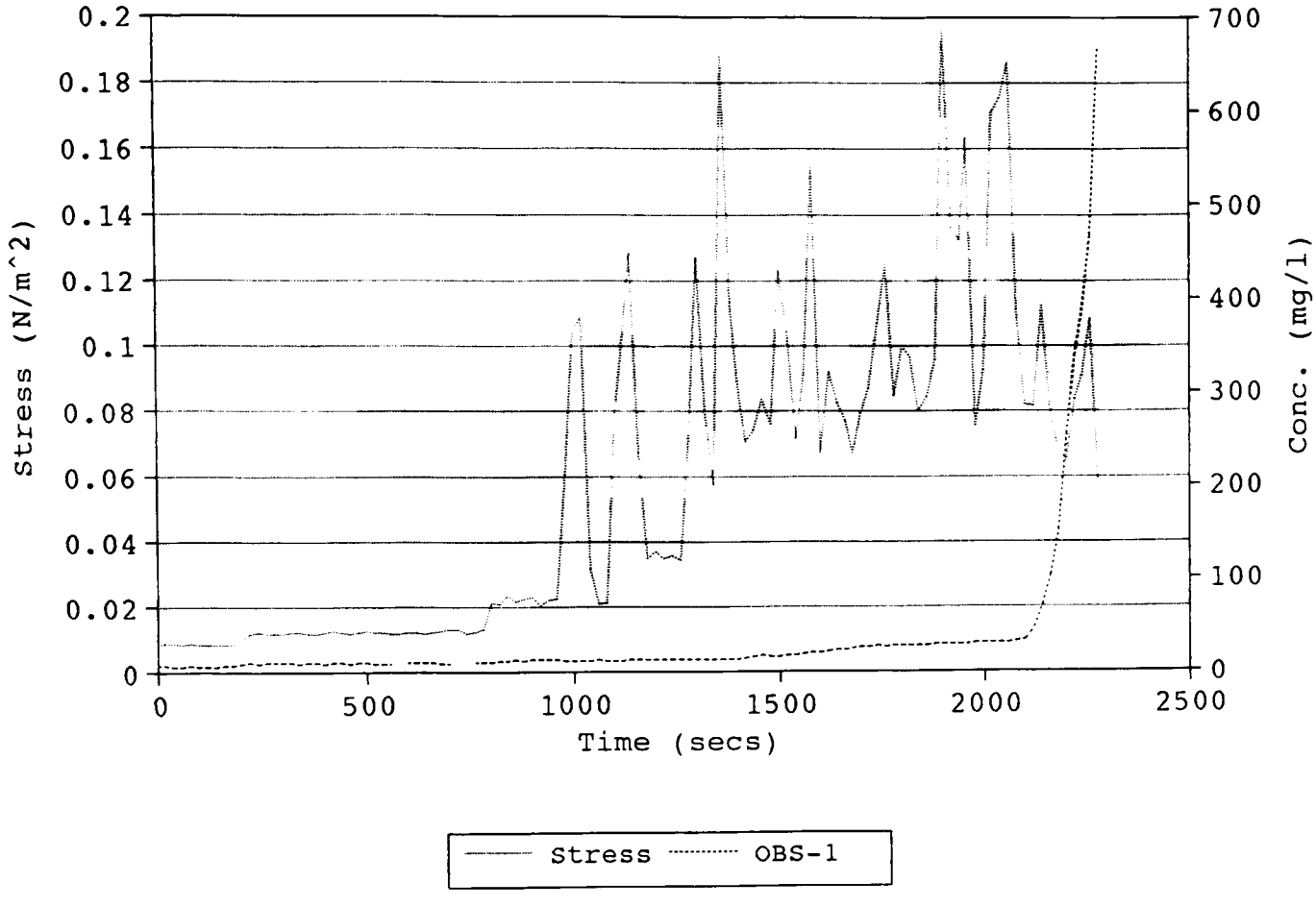

Fig (a.10b): Suspended Sediment Concentration and Rate of Erosion.

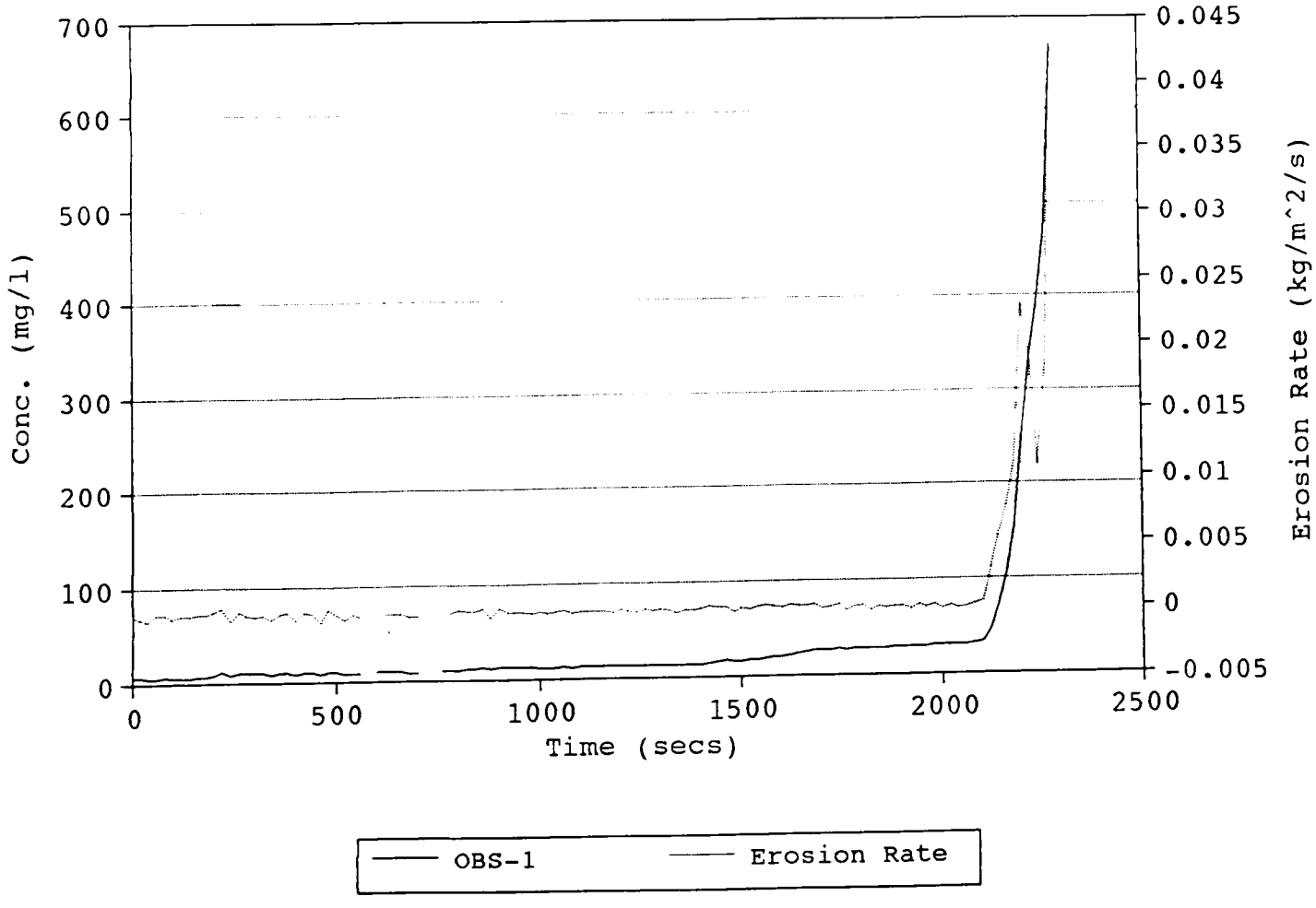

Fig (a.11a): Processed Data for Flume Run 11.

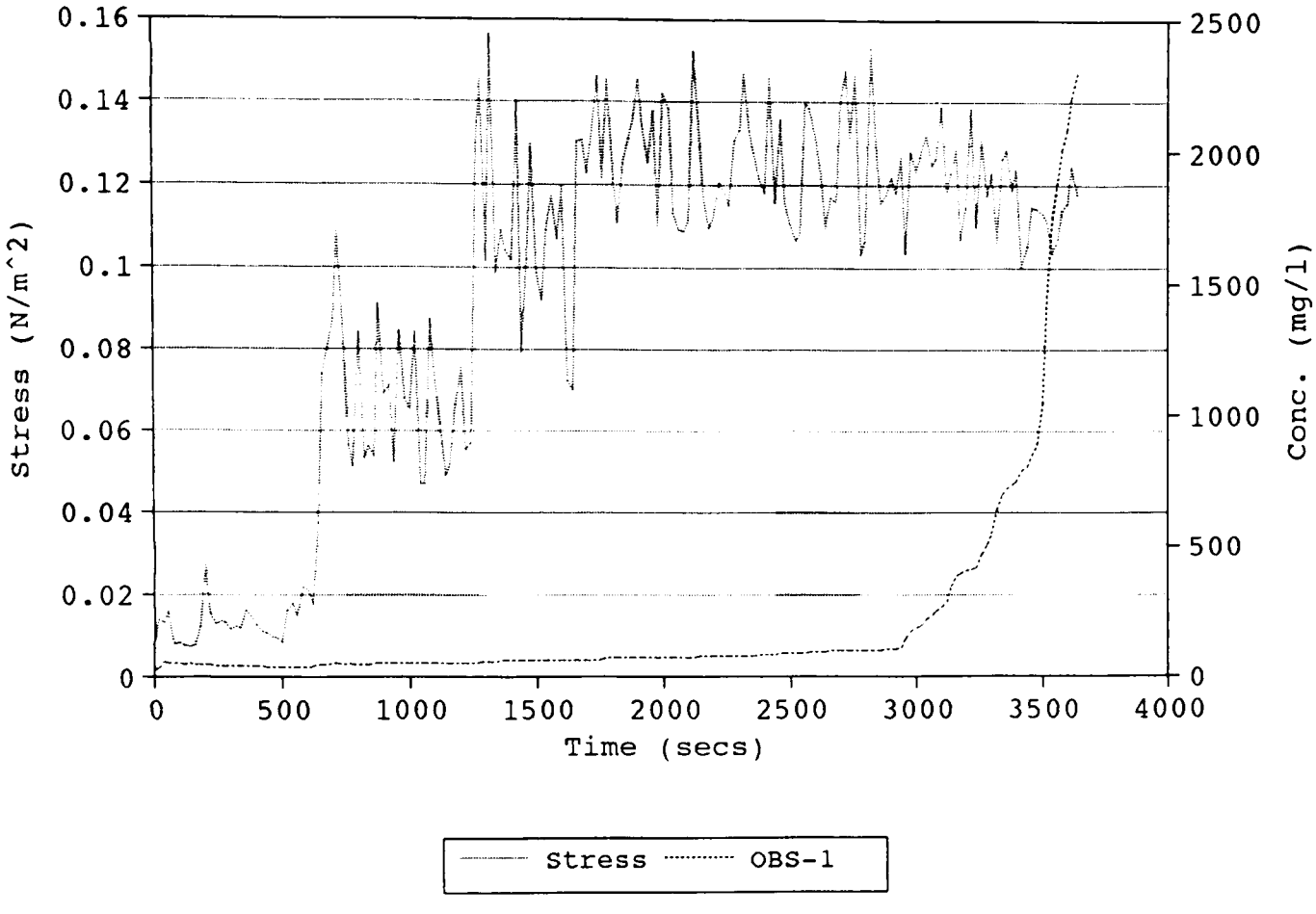

Fig (a.11b): Suspended Sediment Concentration and Rate of Erosion.

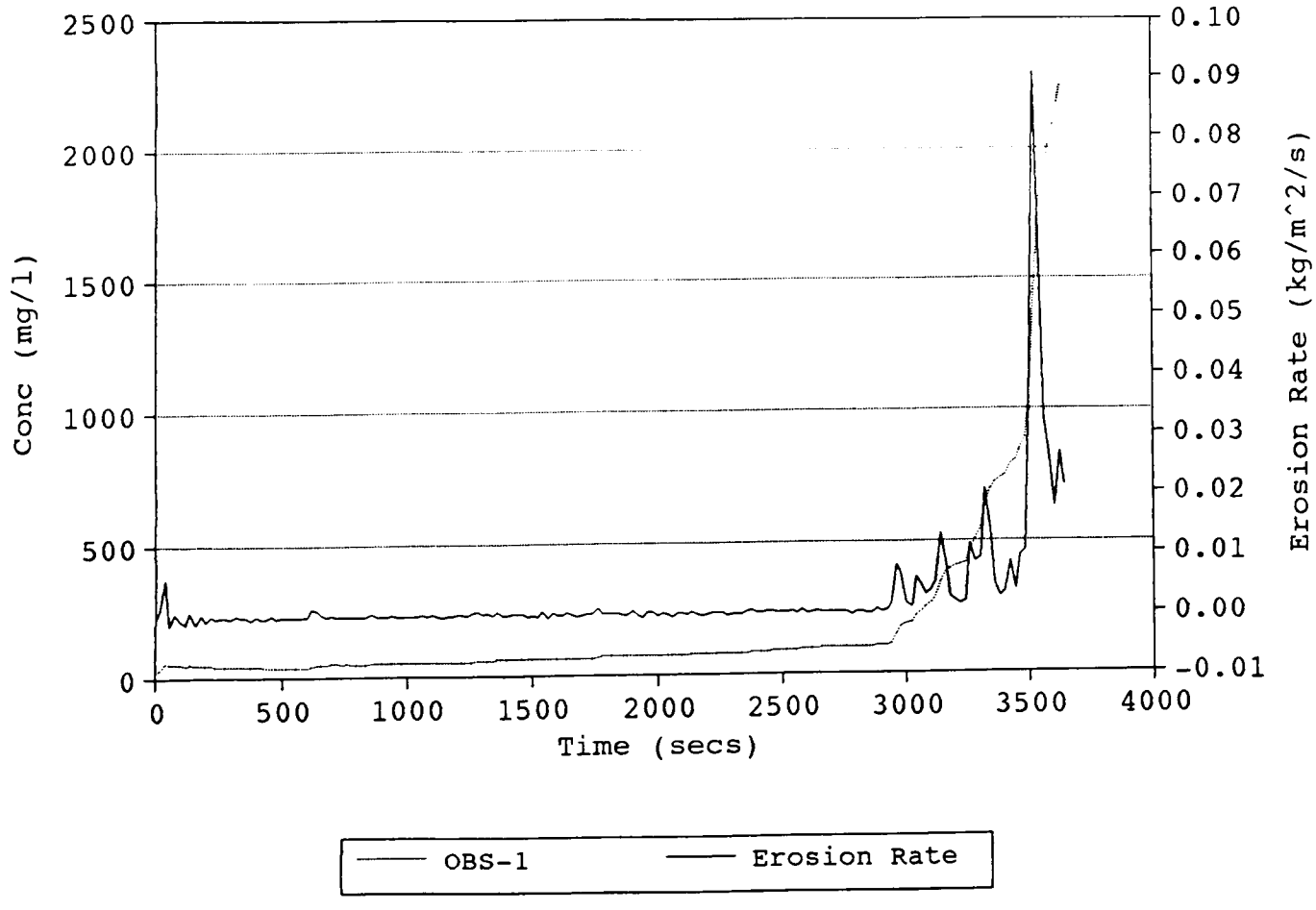

Fig (a.12a): Processed Data for Flume Run 12.

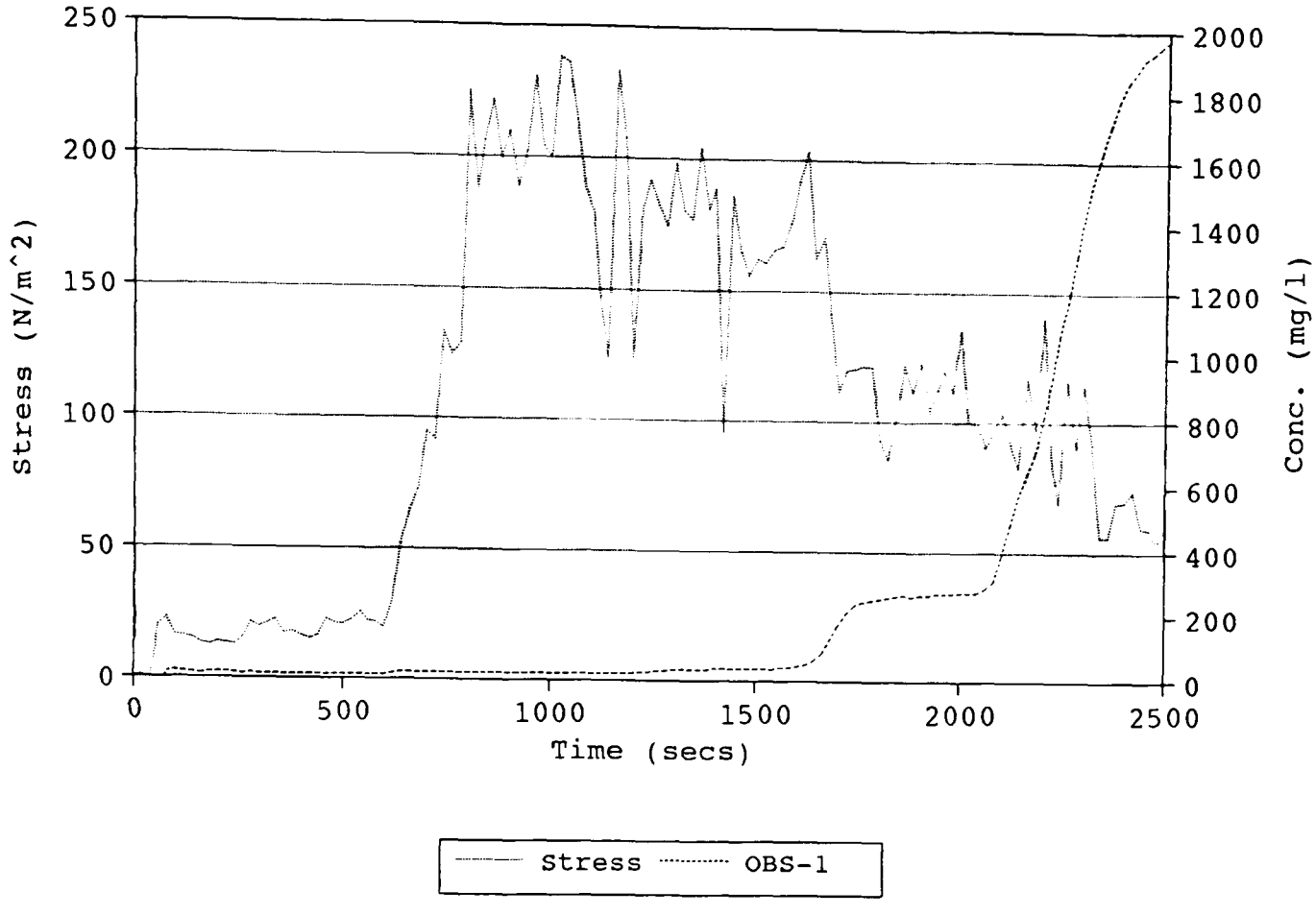

Fig (a.12b): Suspended Sediment Concentration and Rate of Erosion.

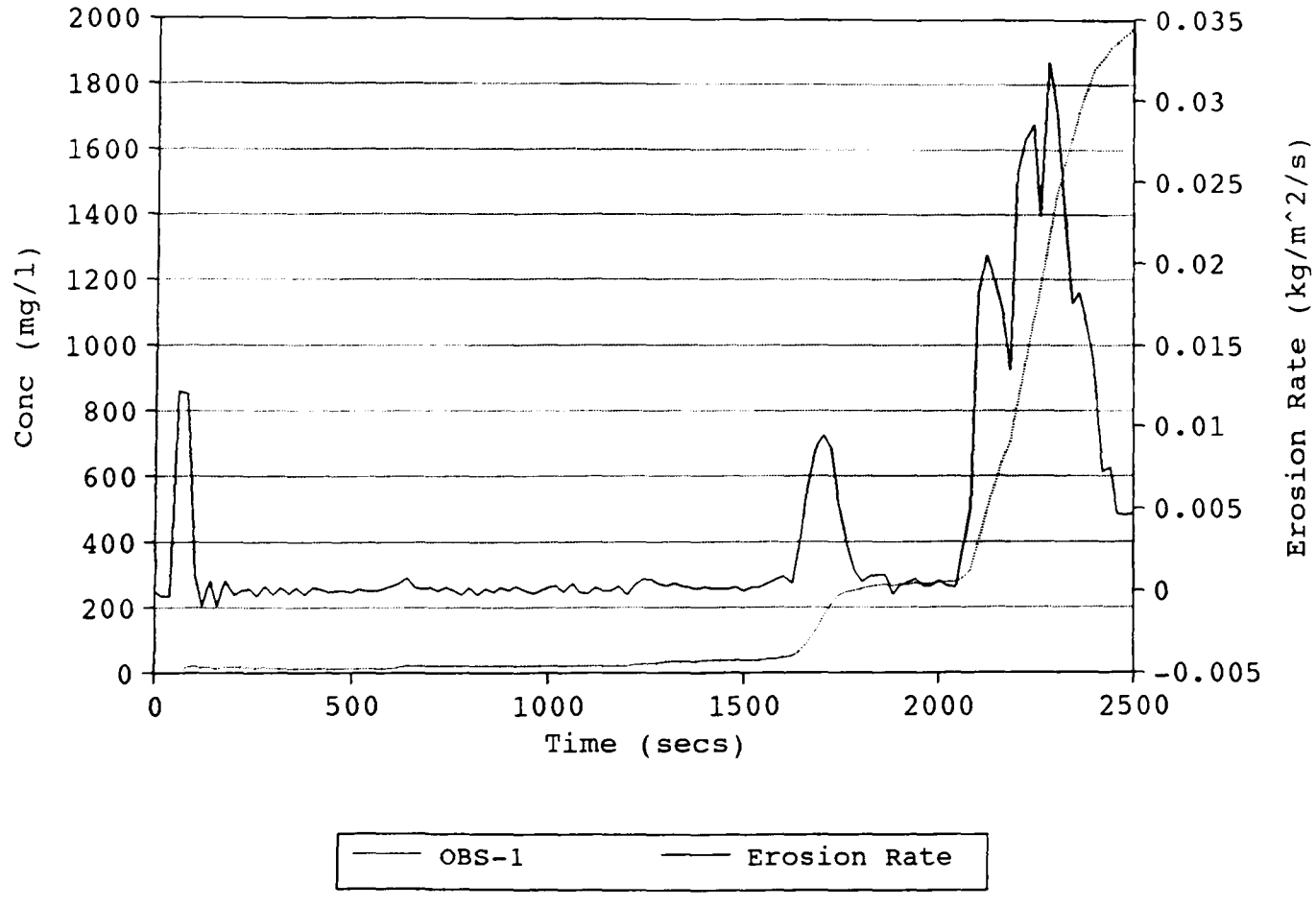

Fig (a.13a): Processed Data for Flume Run 13.

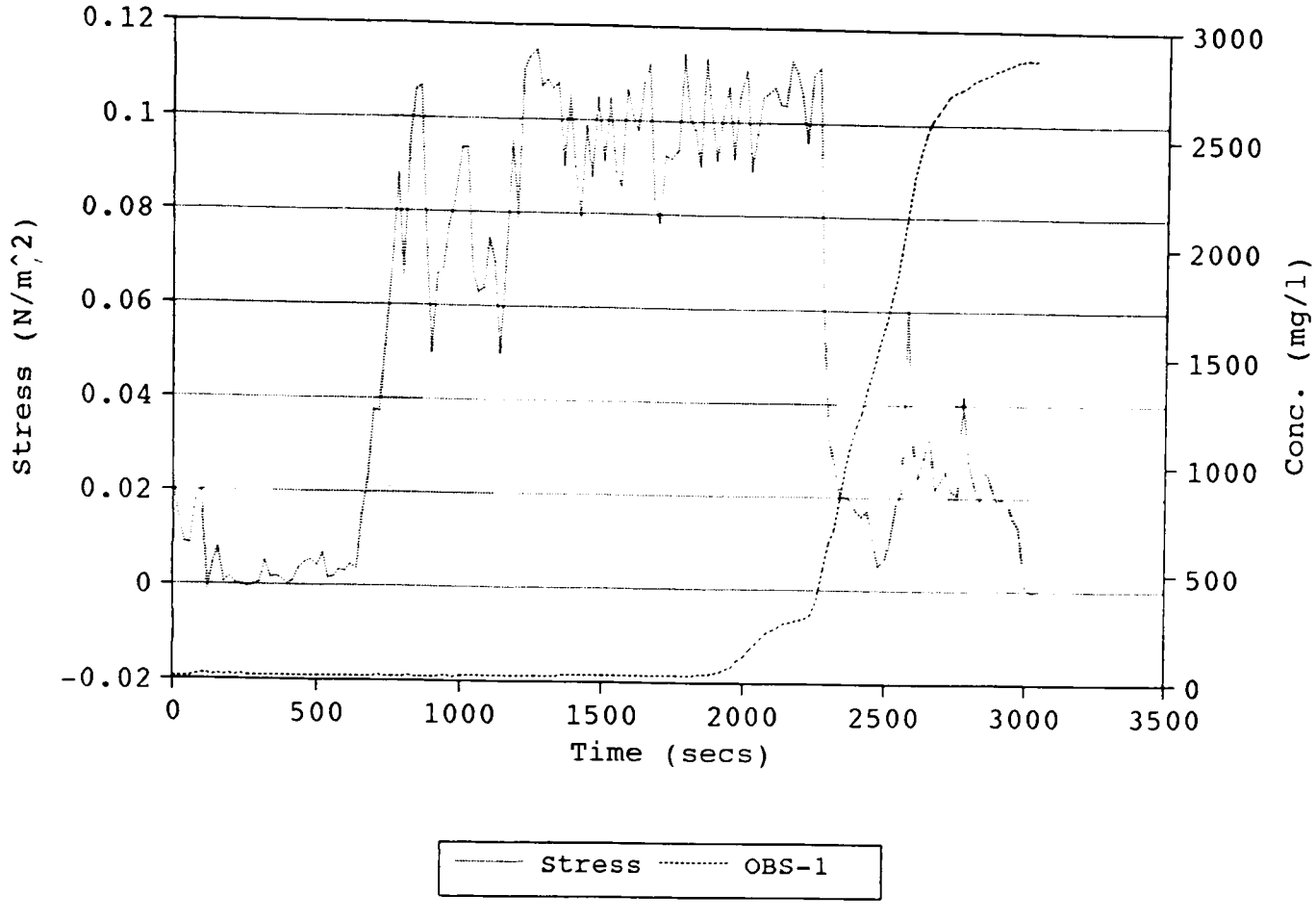

Fig (a.13b): Suspended Sediment Concentration and Rate of Erosion.

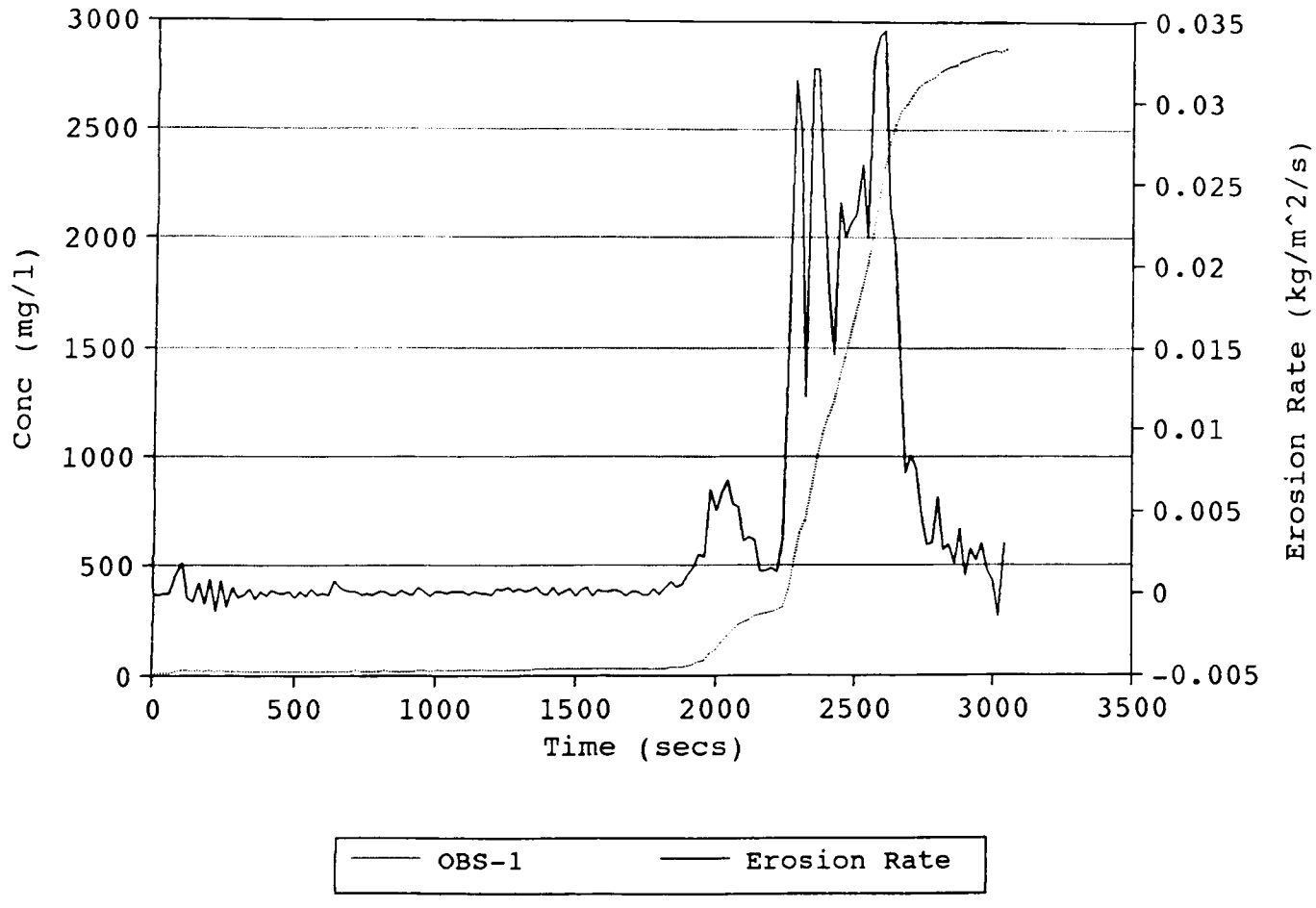

Fig (a.14a): Processed Dat for Flume Run 14.

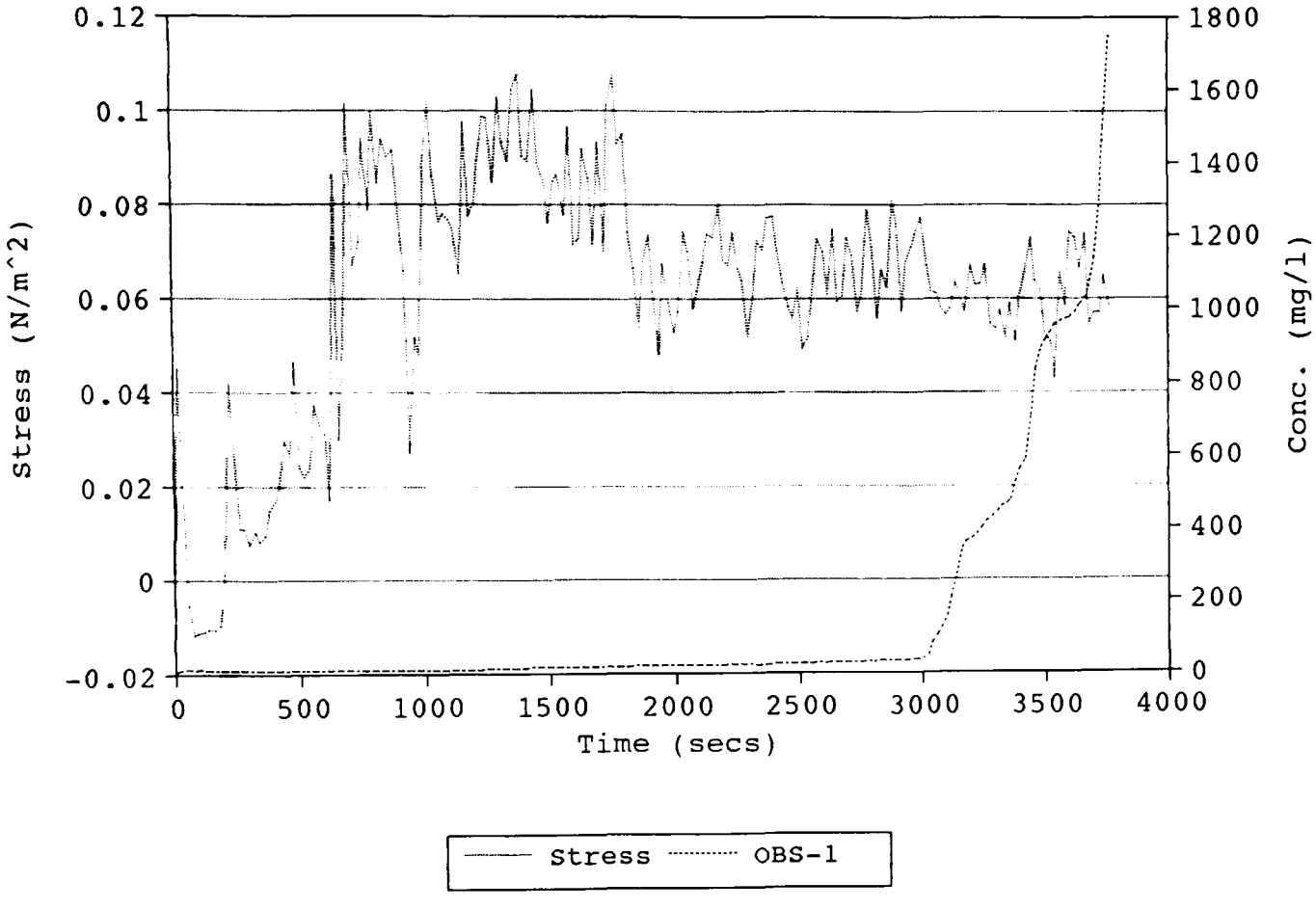

Fig (a.14b): Suspended Sediment Concentration and Rate of Erosion.

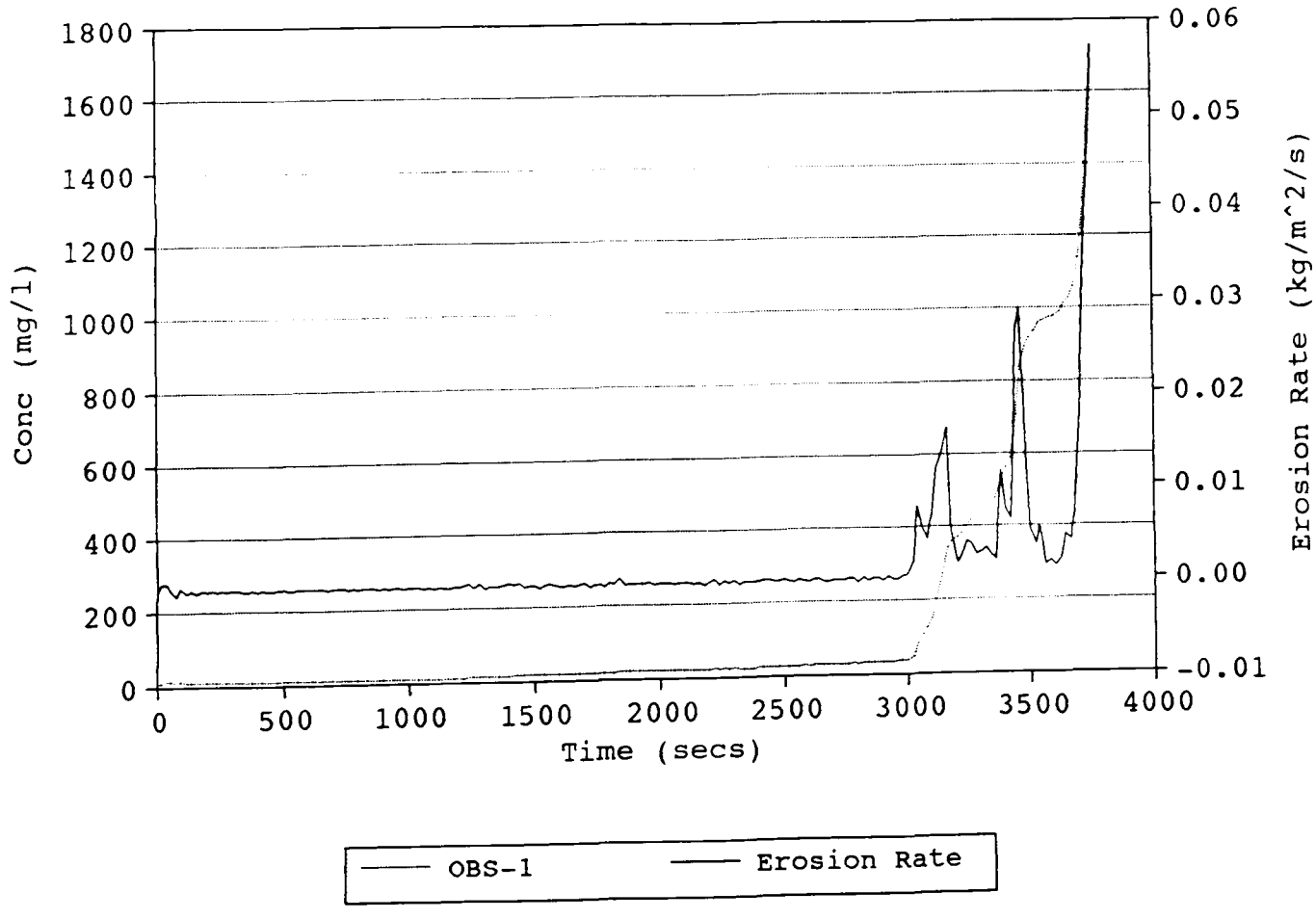

Fig (a.15a): Processed Data for Flume Run 15.

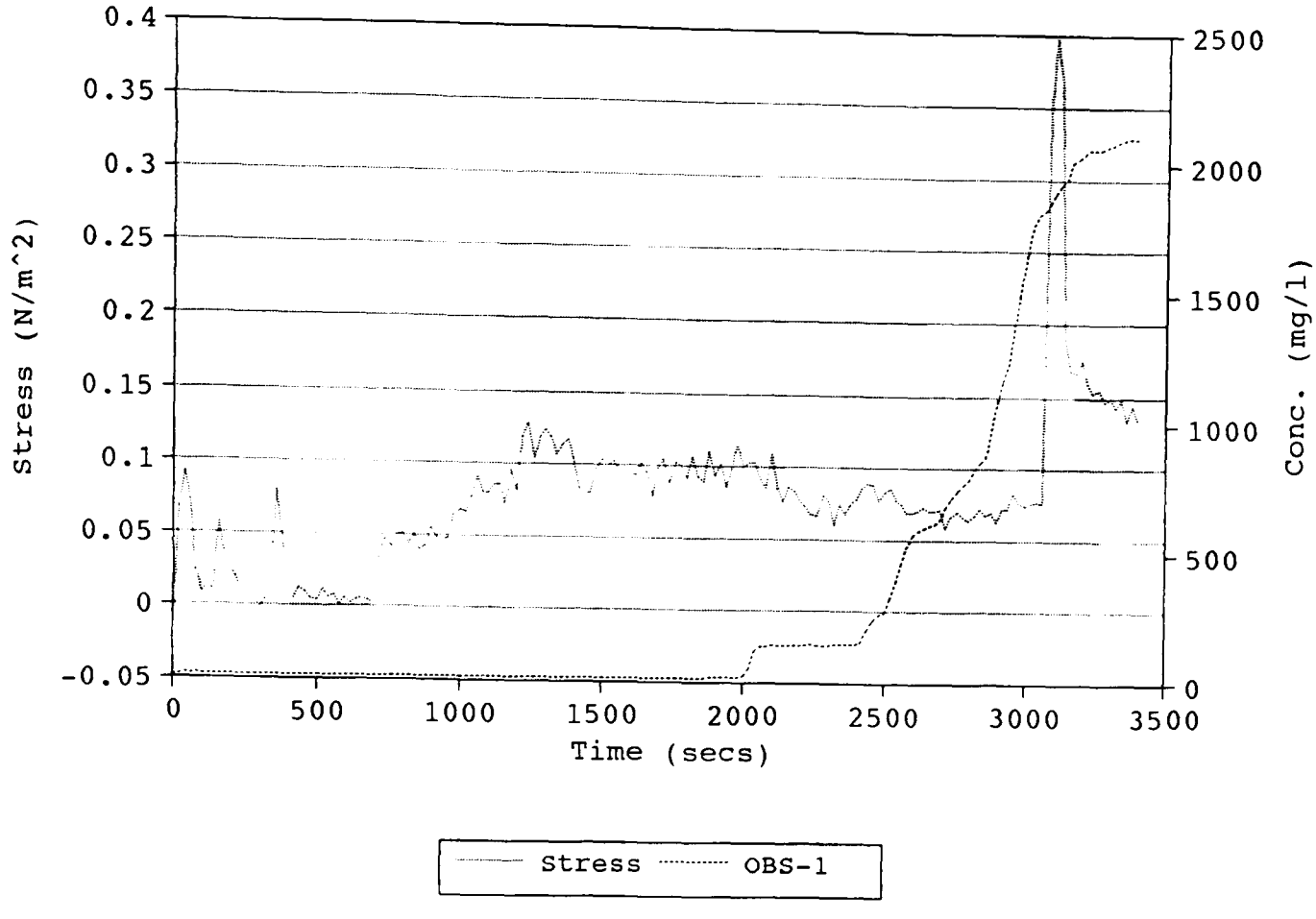

Fig (a.15b): Suspended Sediment Concentration and Rate of Erosion.

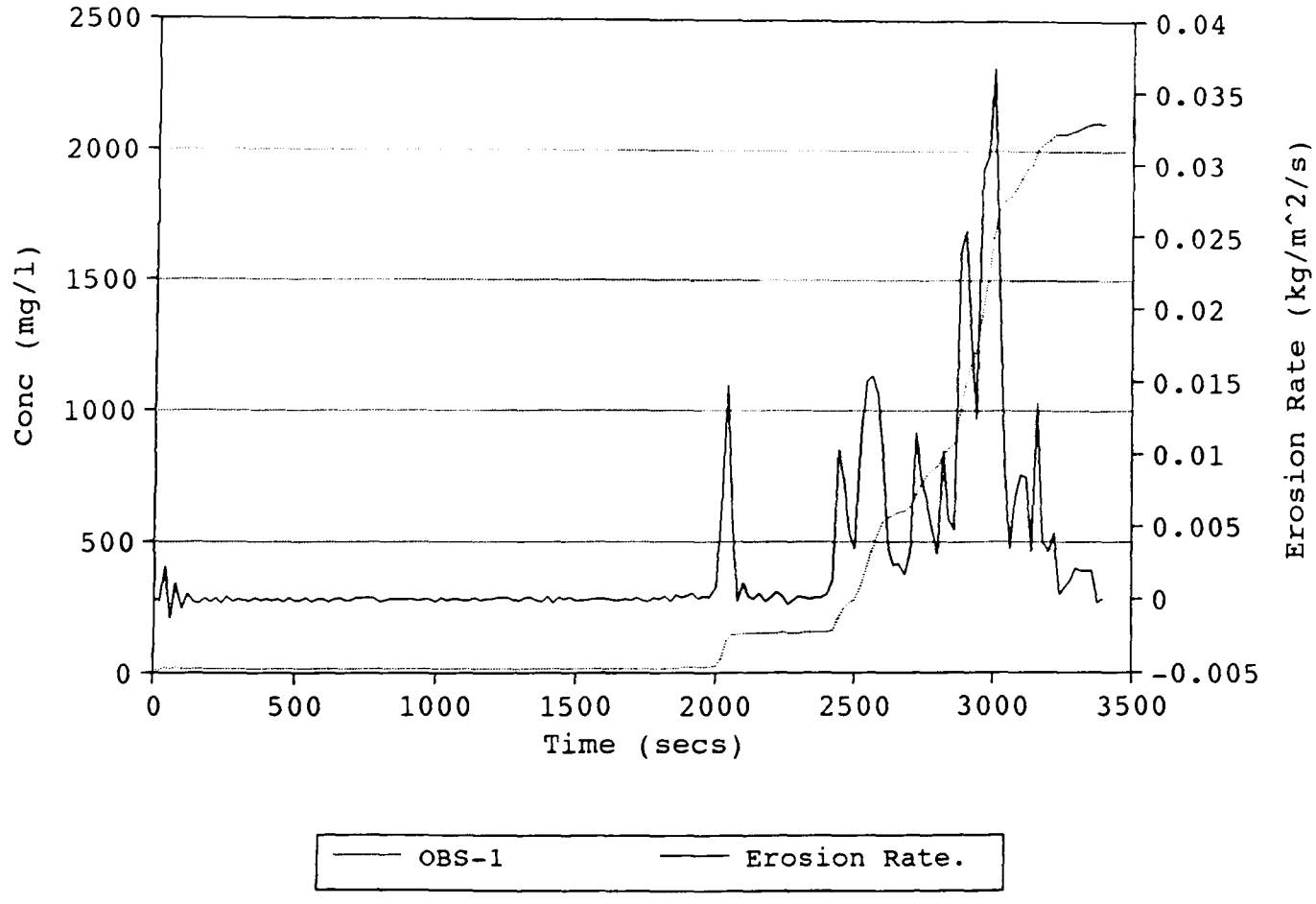

Fig (a.16a): Processes Data for Flume Run 16.

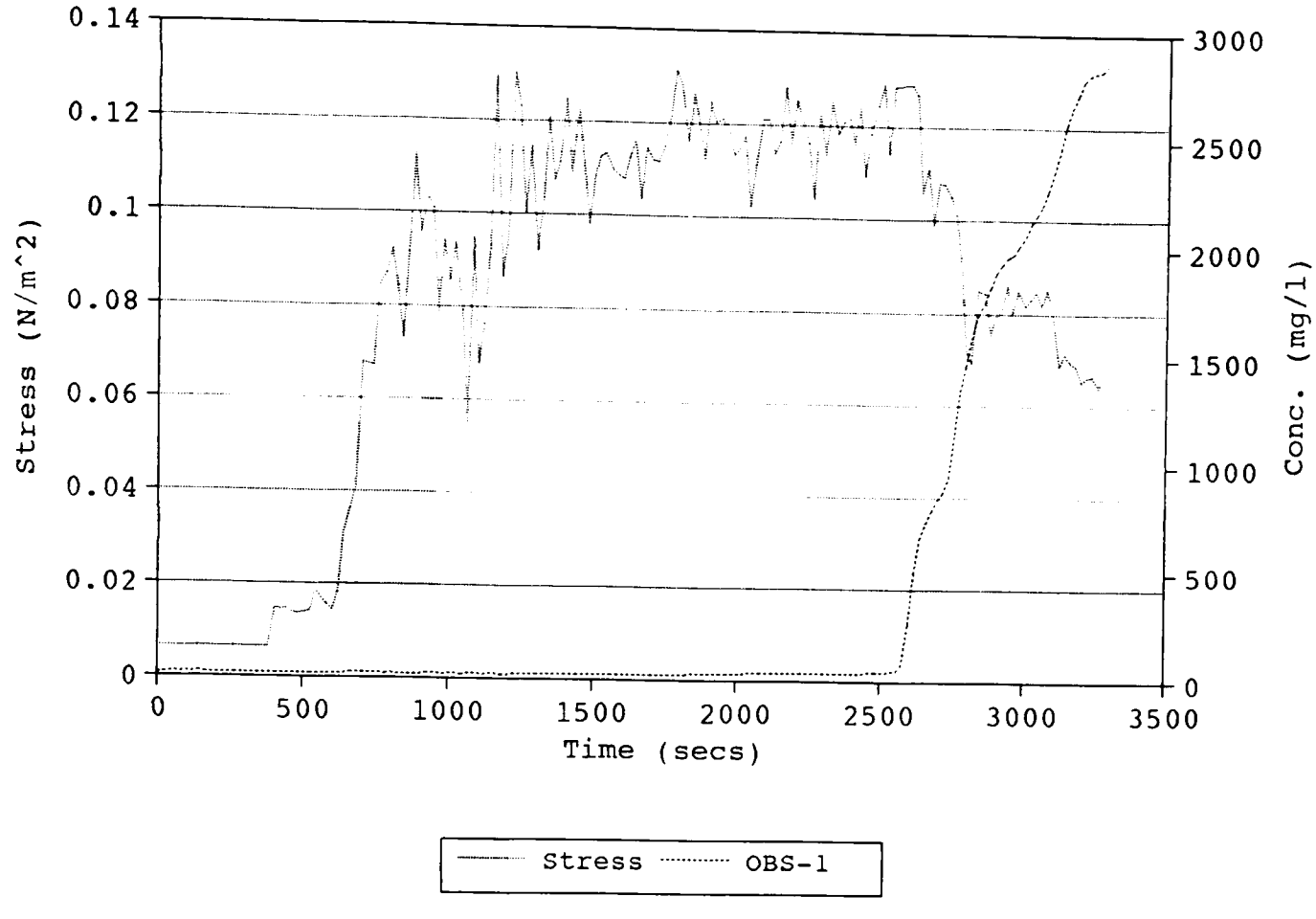

Fig (a.16b): Suspended Sediment Concentration and Rate of Erosion.

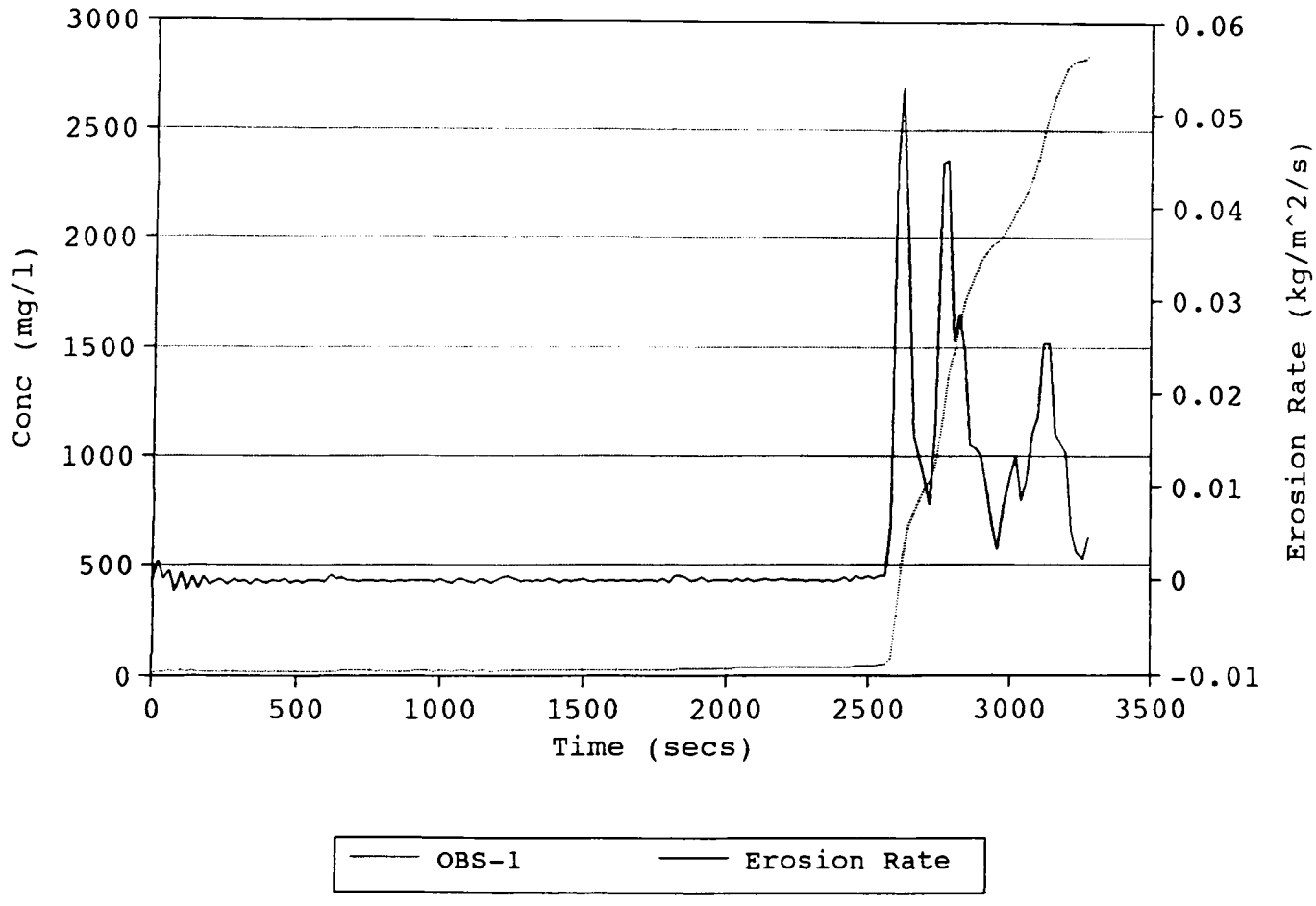

Fig (a.17a): Processed Data for Flume Run 17.

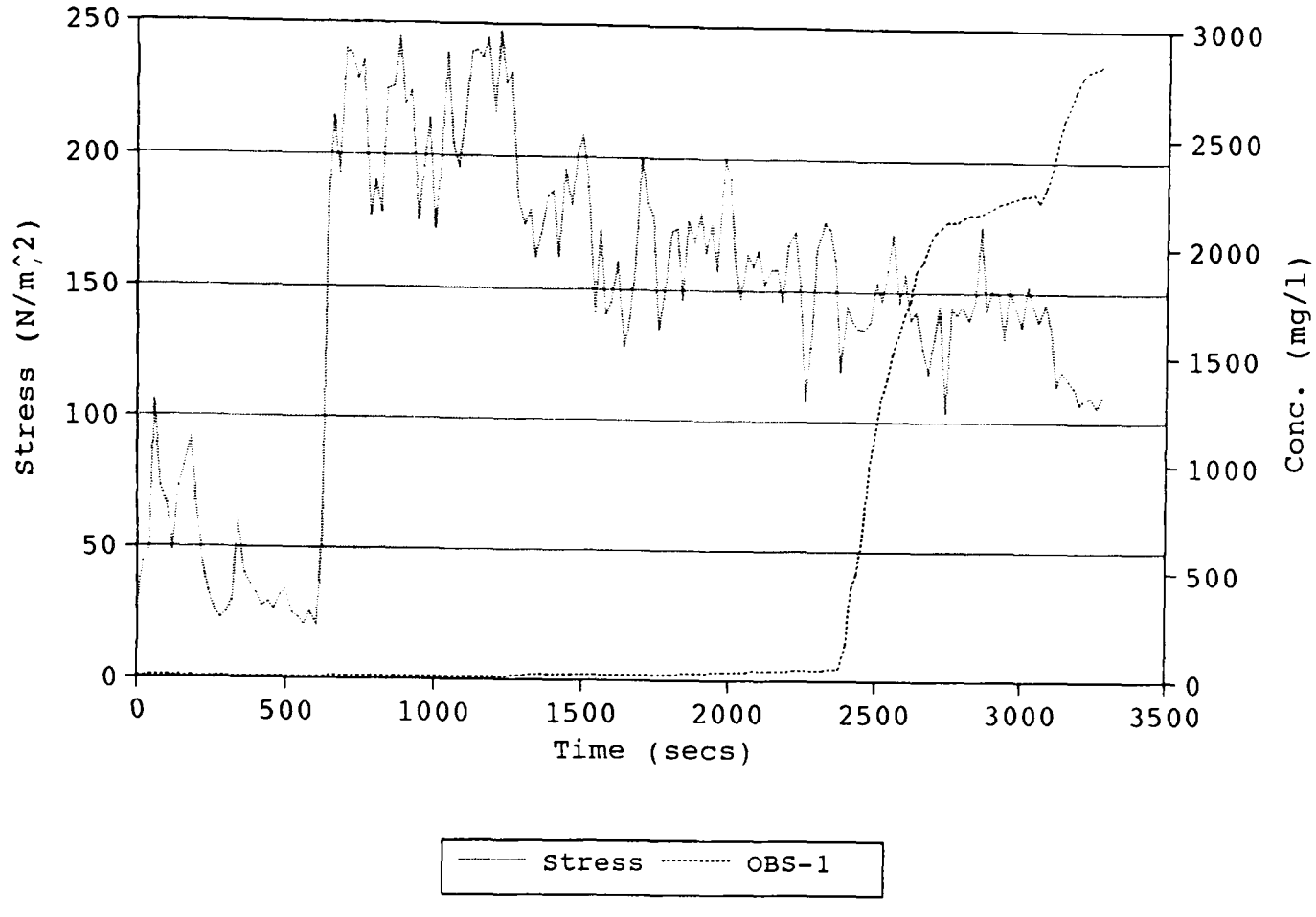

Fig (a.17b): Suspended Sediment Concentration and Rate of Erosion.

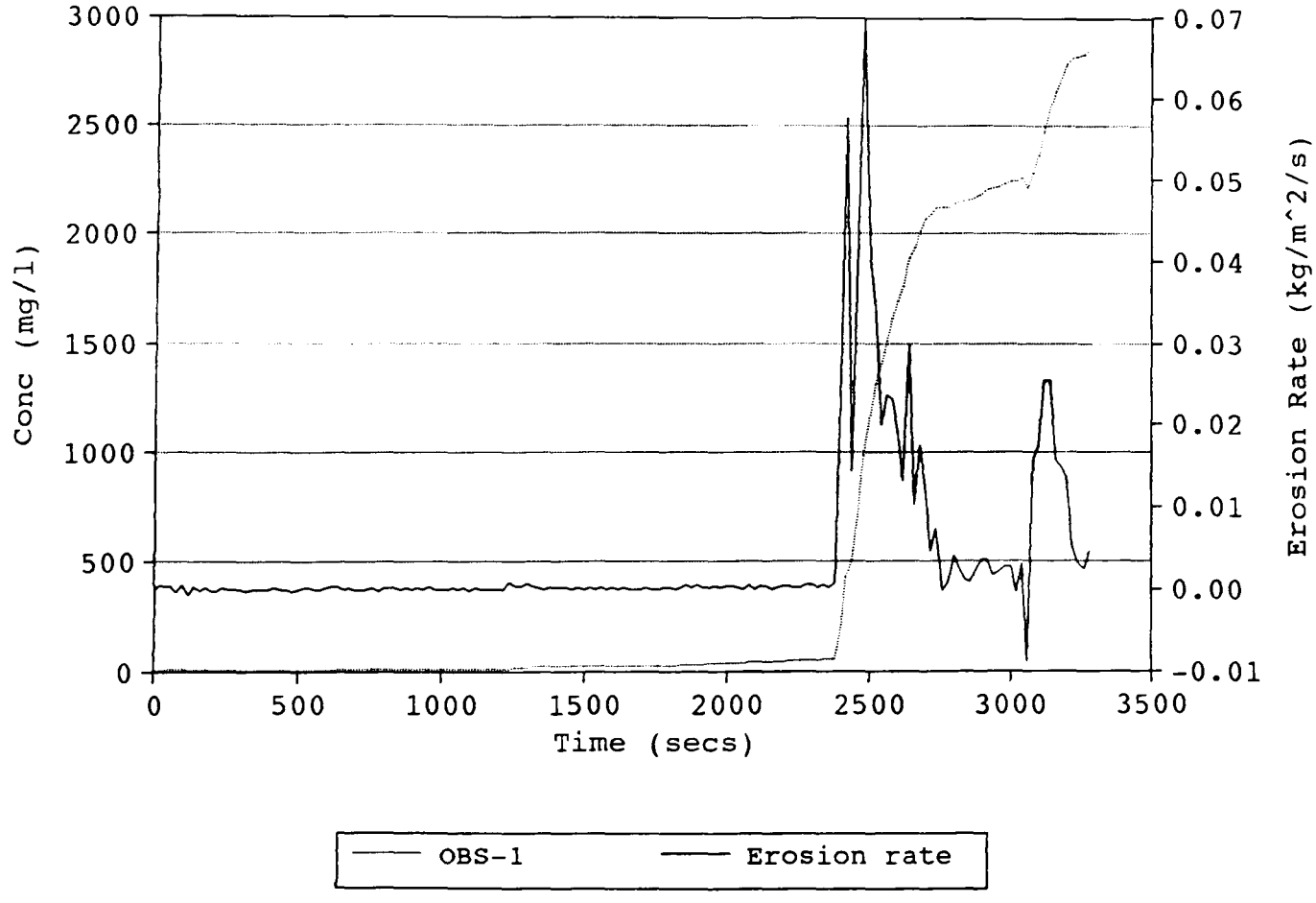

Fig (a.18a): Processed Data for Flume Run 18.

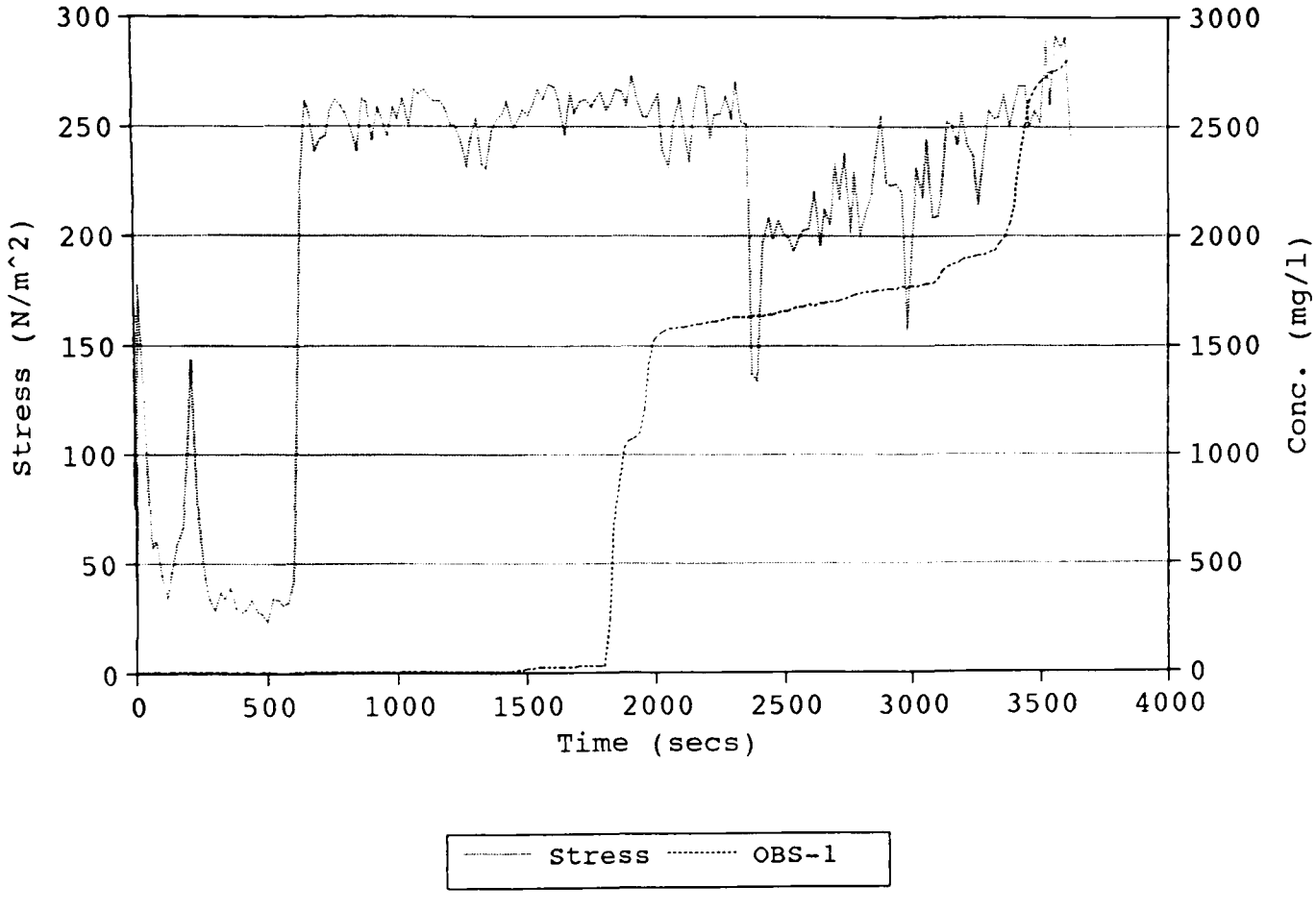

Fig (a.18b): Suspended Sediment Concentration and Rate of Erosion.

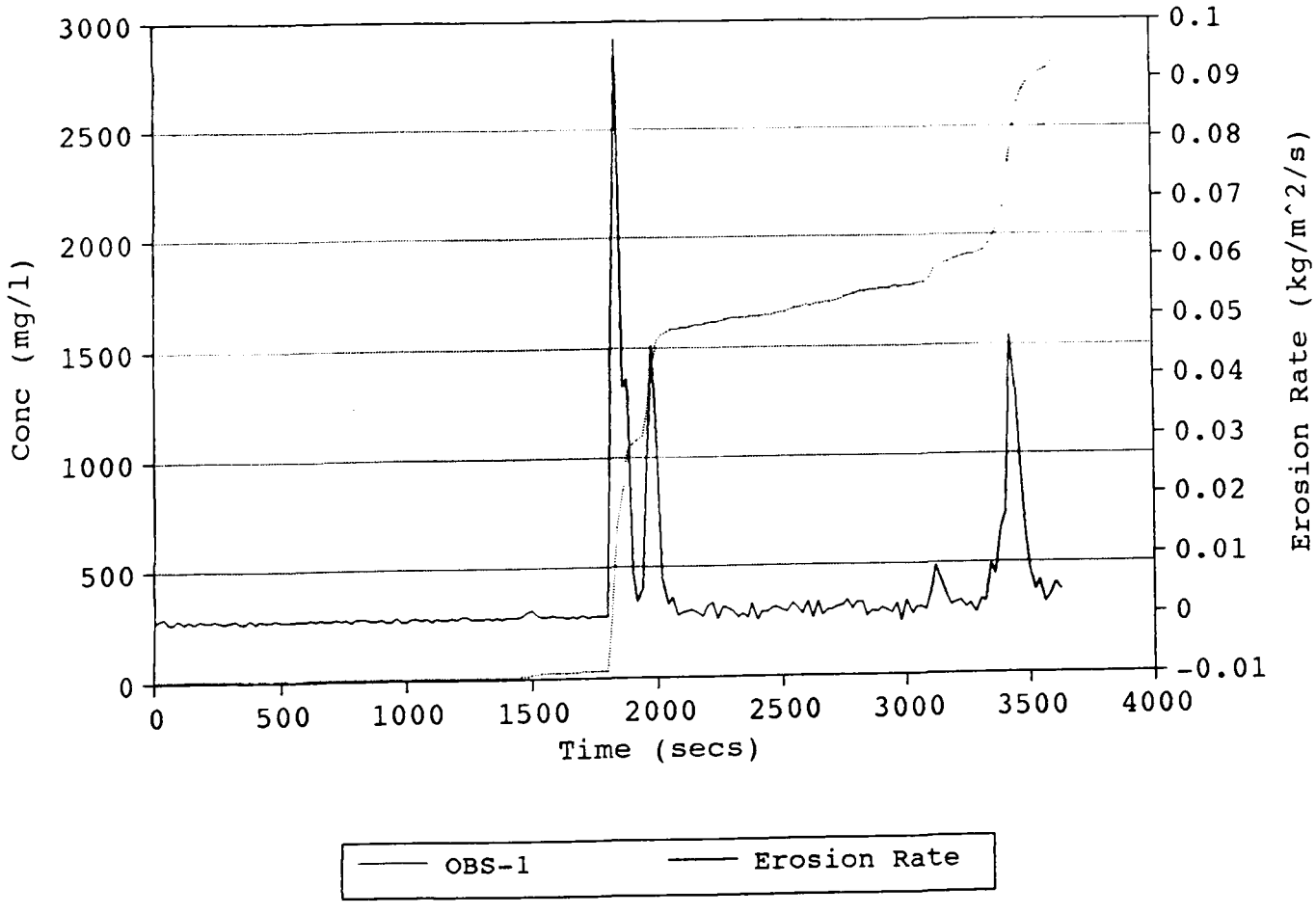

Fig (a.19a): Processed Data for Flume Run 19.

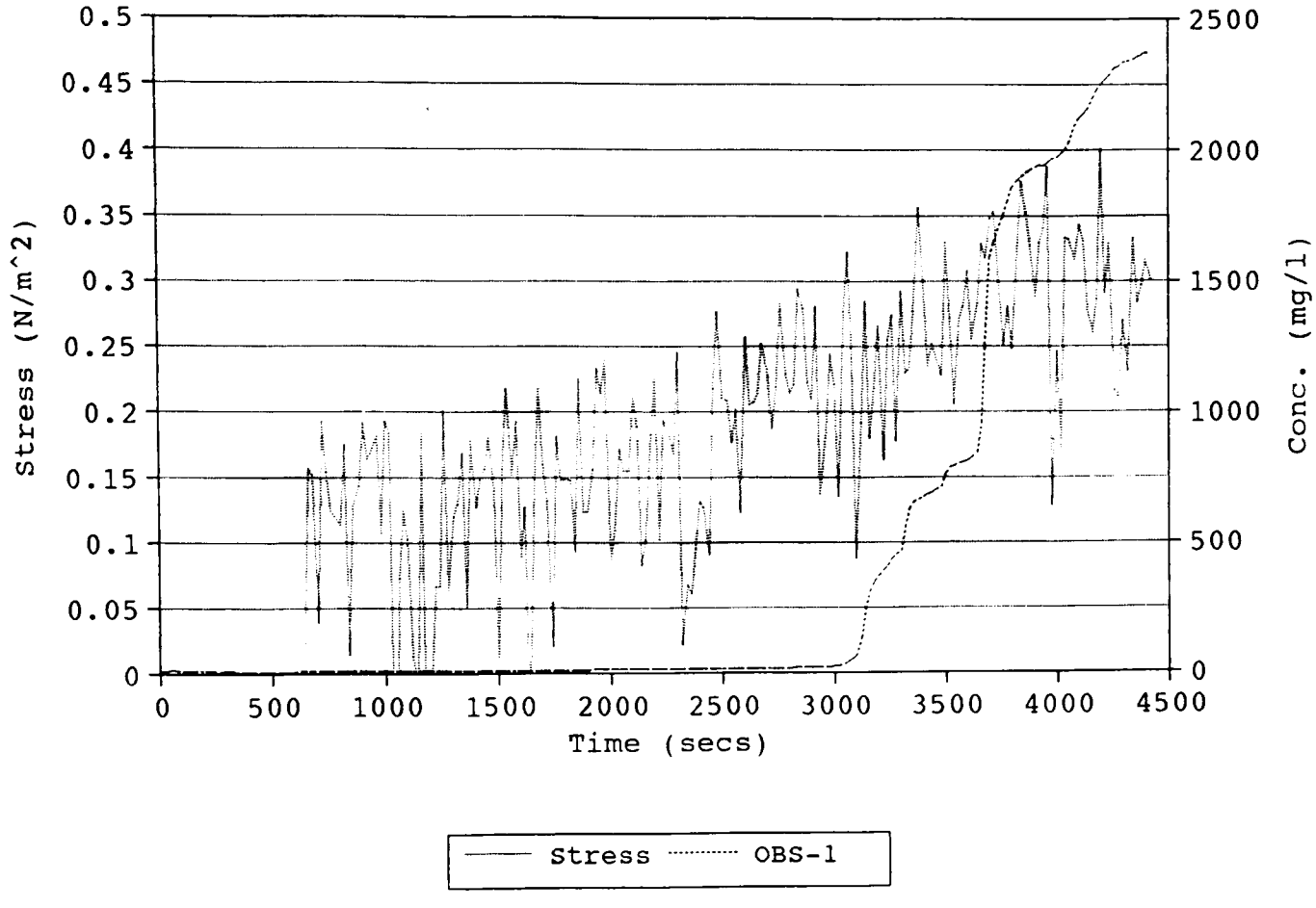

Fig (a.19b): Suspended Sediment Concentration and Rate of Erosion.

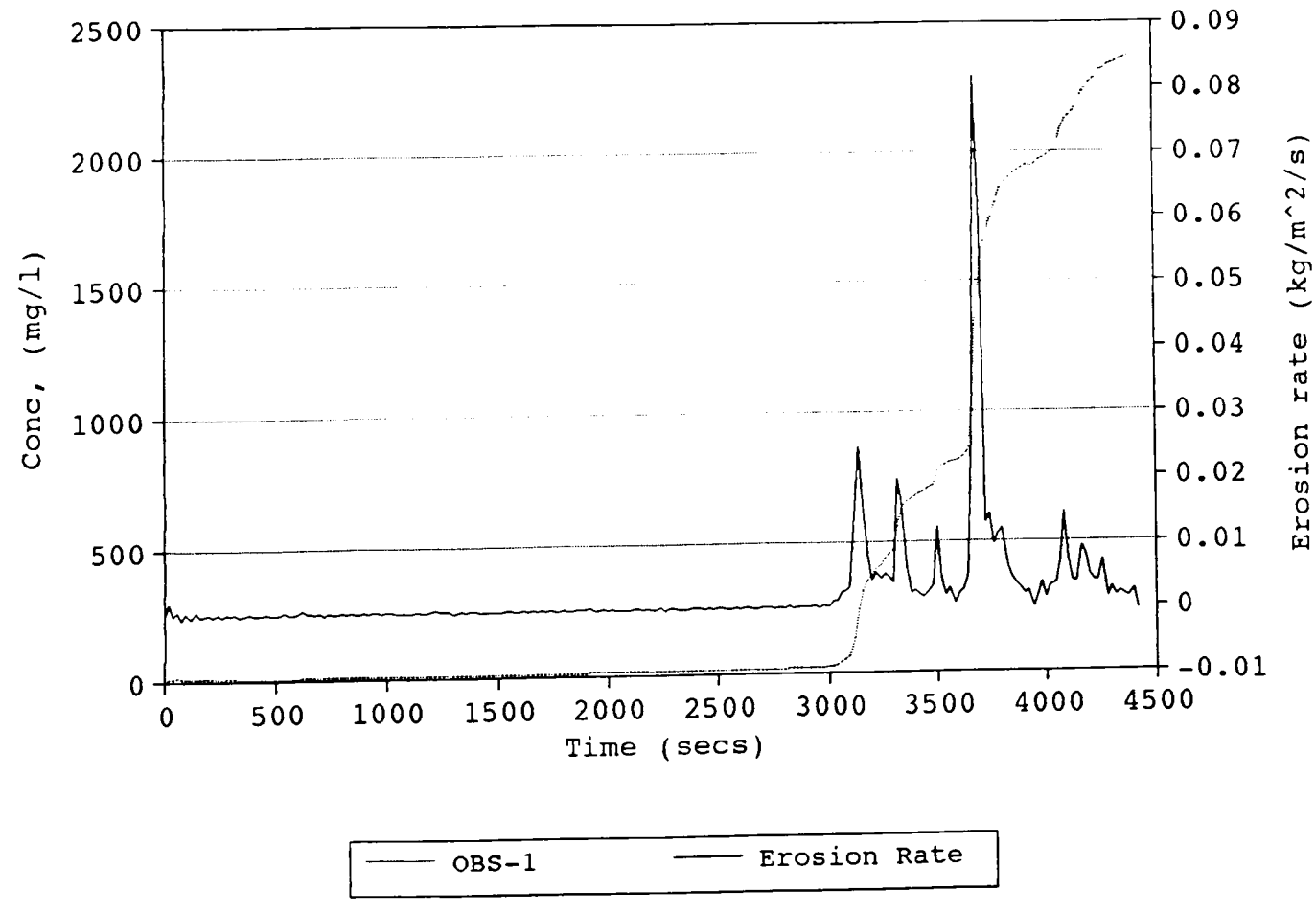

Fig (a.20a): Processsed Data for Flume Run 20.

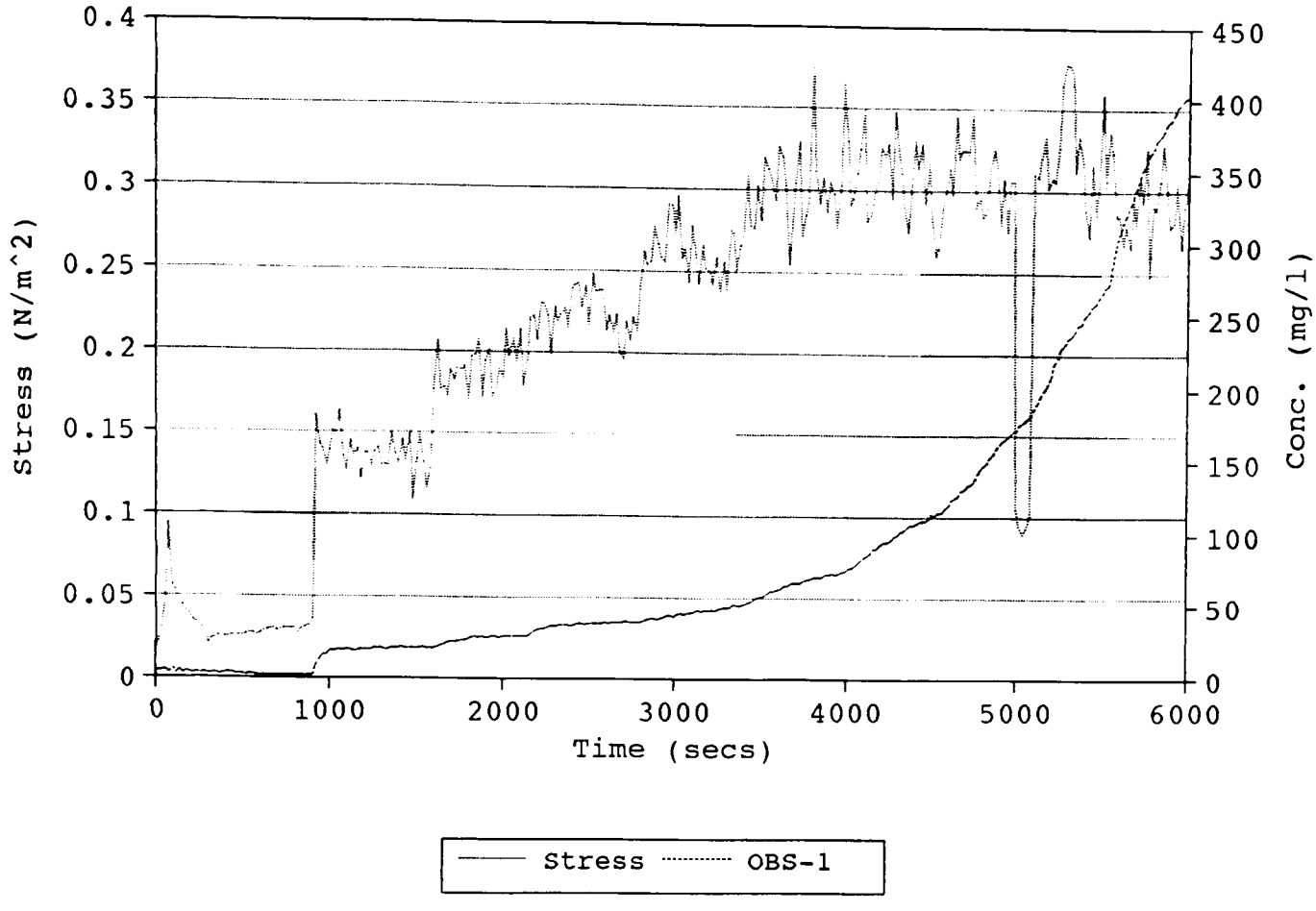

Fig (a.20a): Suspended Sediment Concentration and Rate of Erosion.

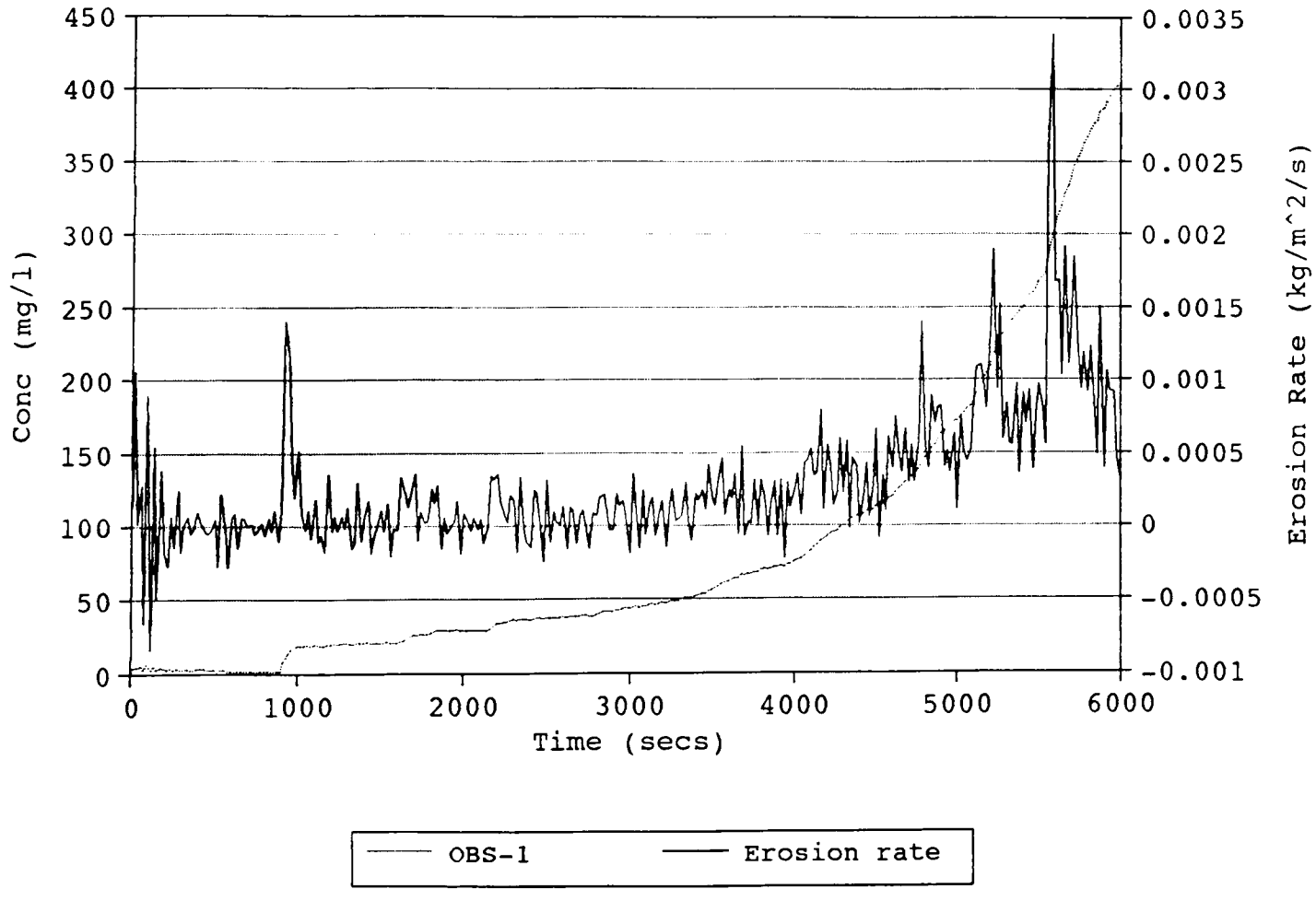

Fig (a.21a): Processed Data for Flume Run 21.

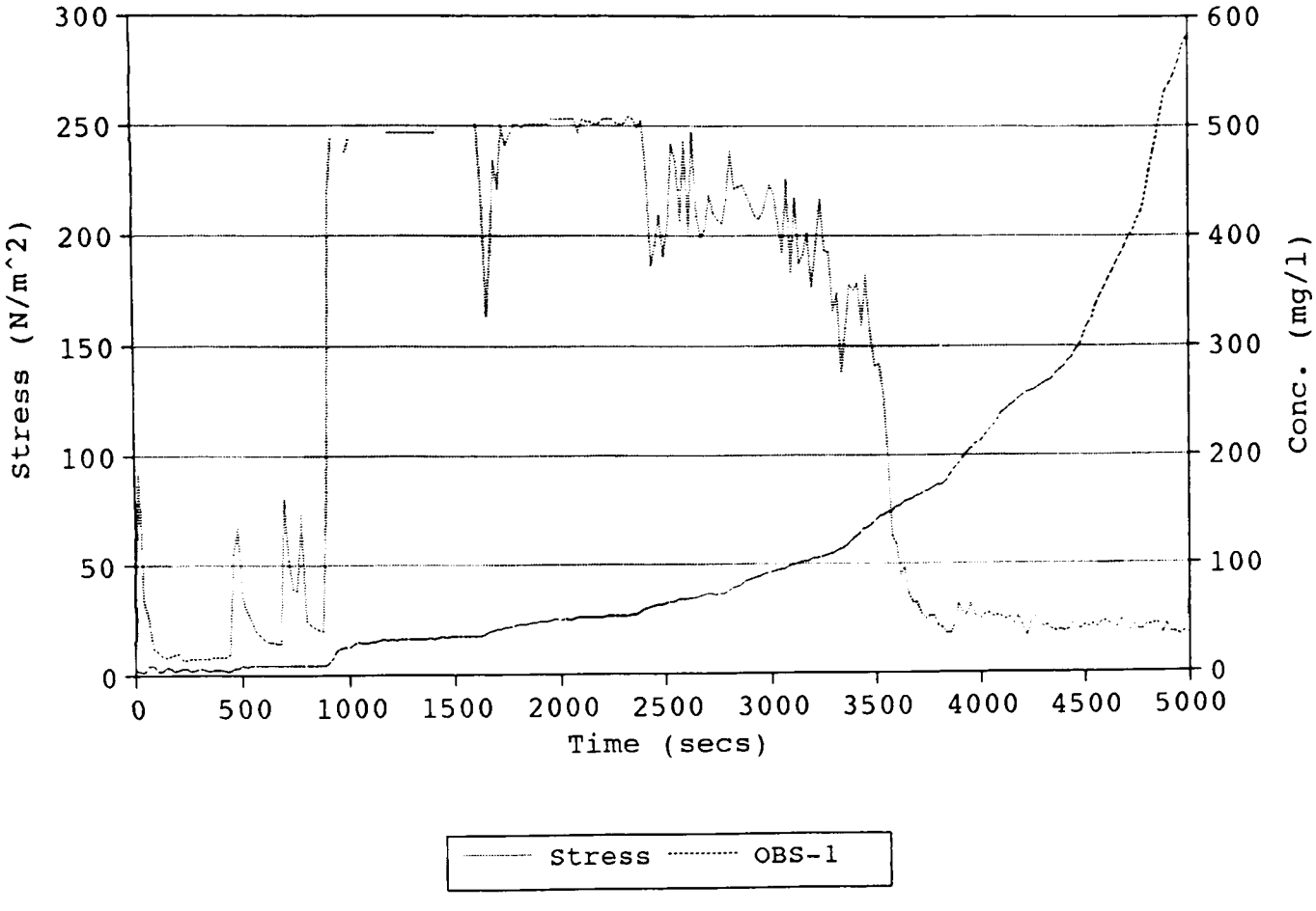

Fig (a.21b): Suspended Sediment Concentration andRate of Erosion

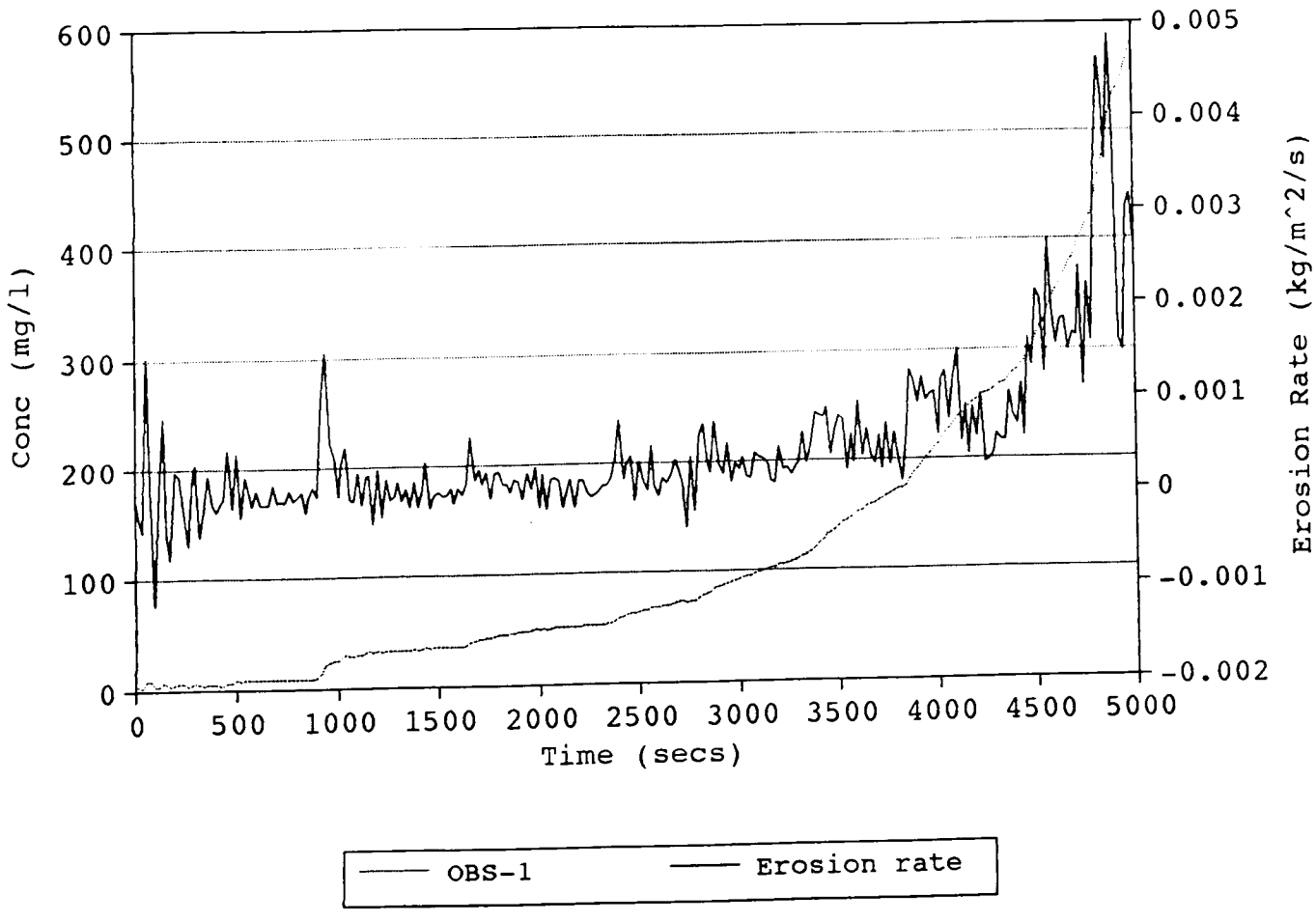

Fig (a.22a): Processed Data for Flume Run 22.

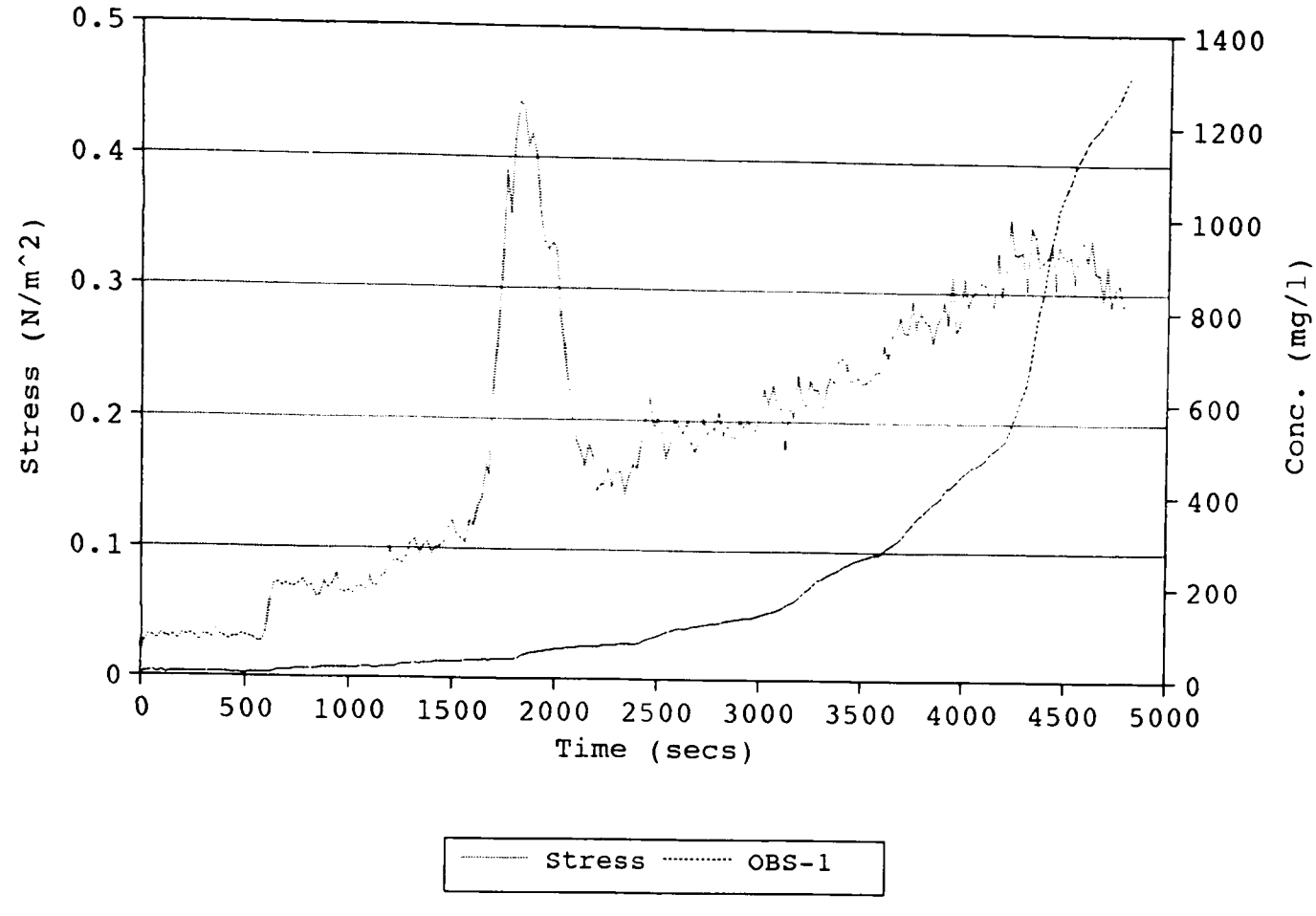

Fig (a.22b): Suspended Sediment Concentration and Rate of Erosion.

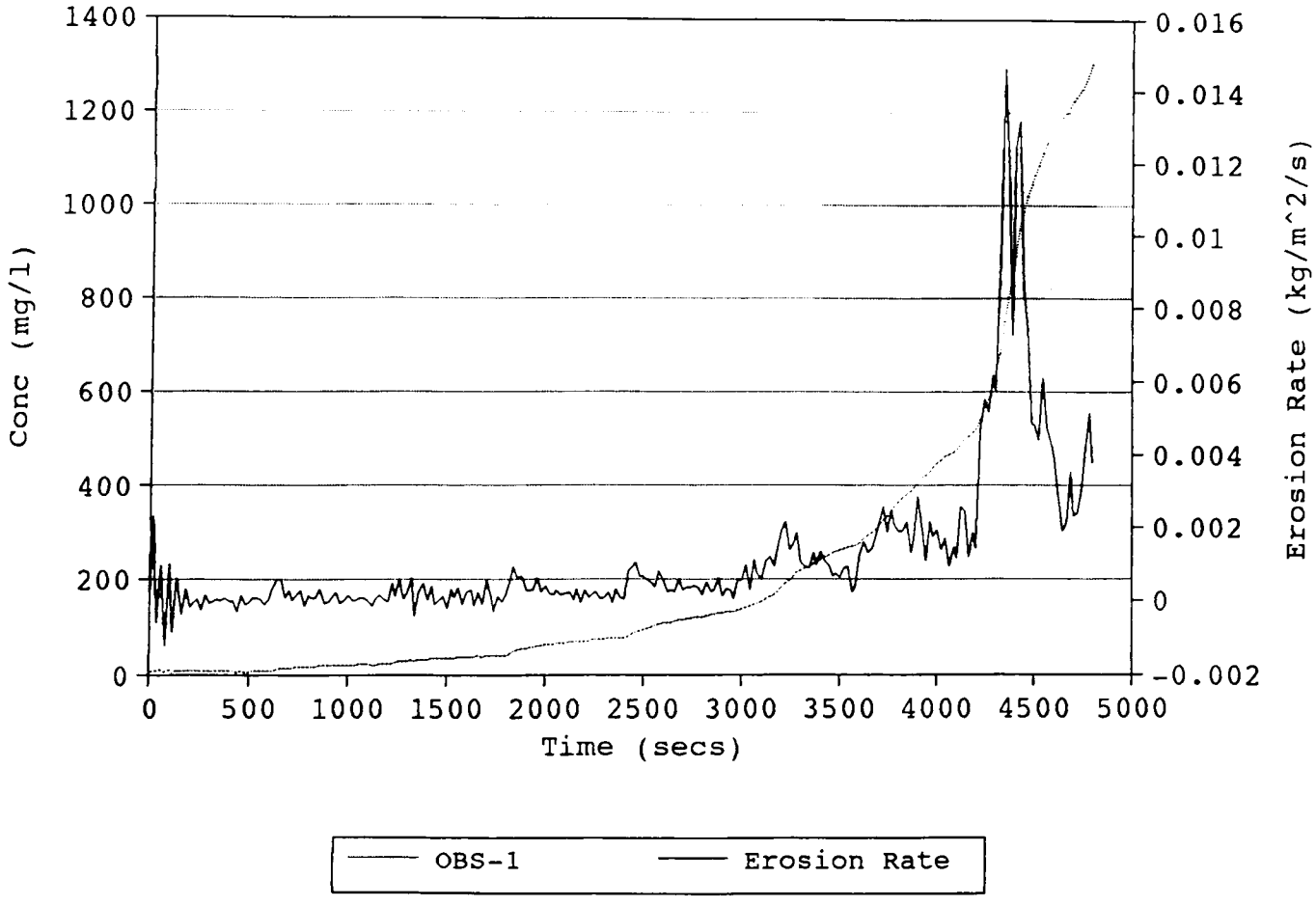

Fig (a.23a): Processed Data for Flume Run 23.

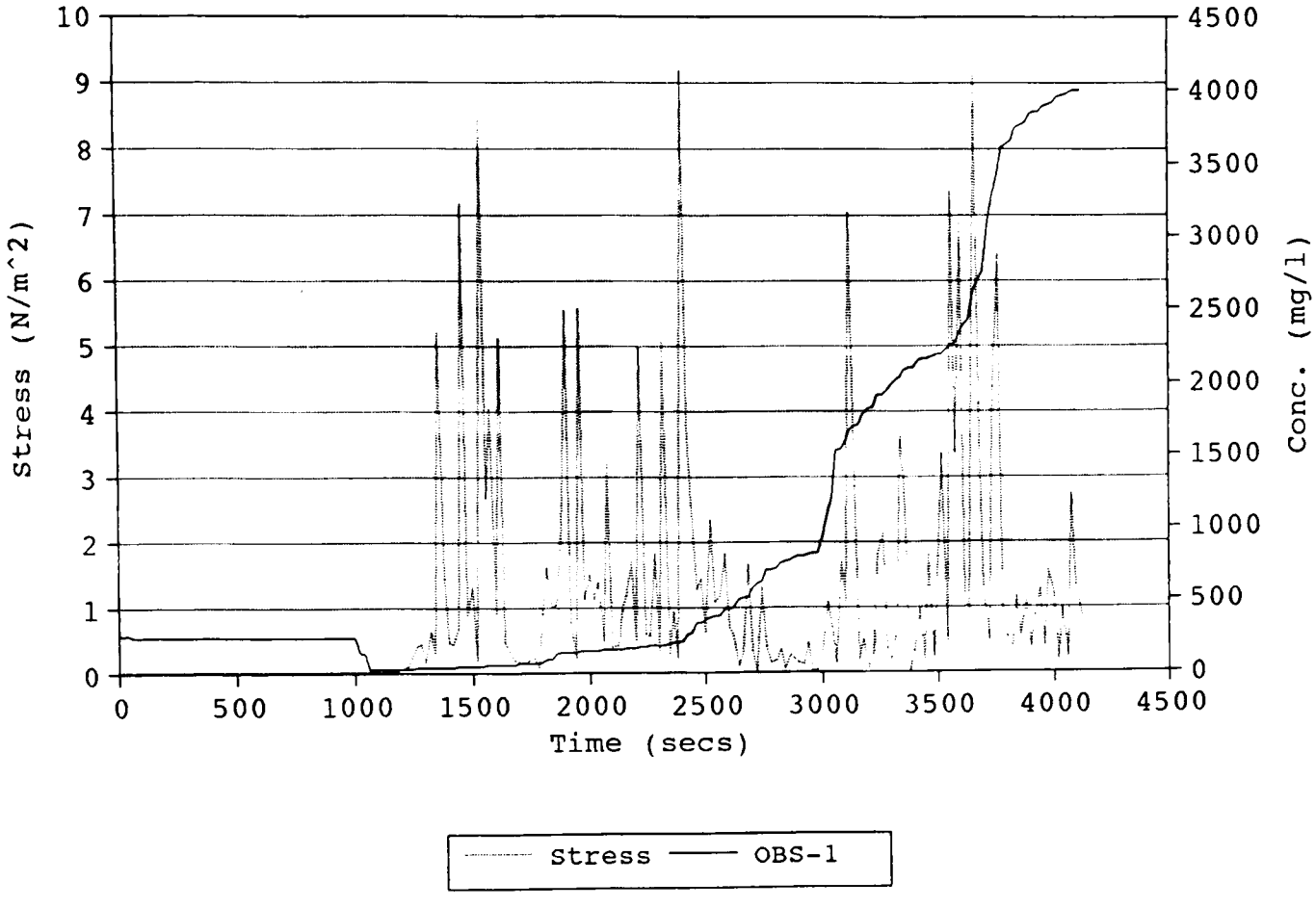

Fig (a.23b): Suspended Sediment Concentration and Rate of Erosion.

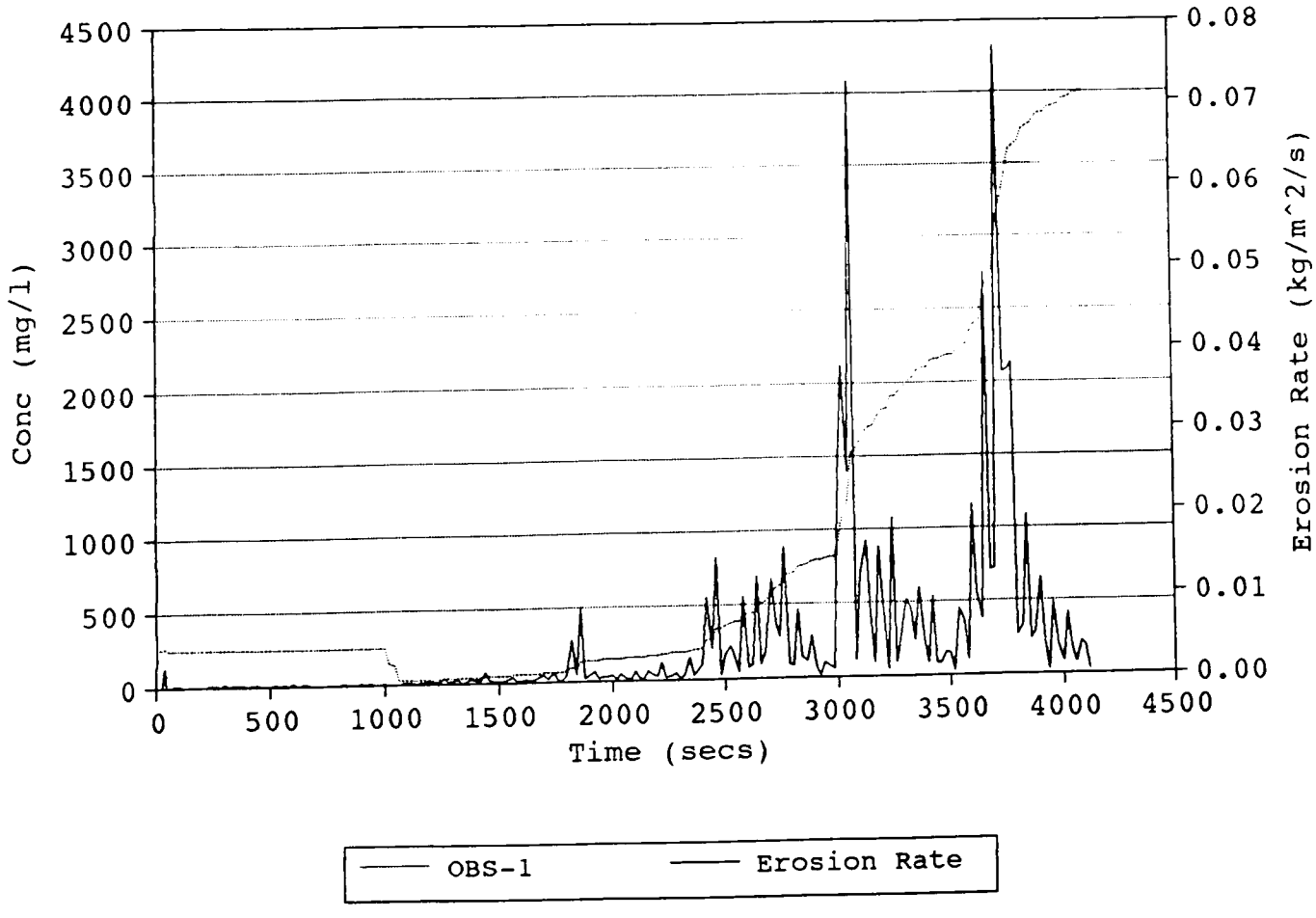

Fig (a.24a): Processed Data for Flume Run 24.

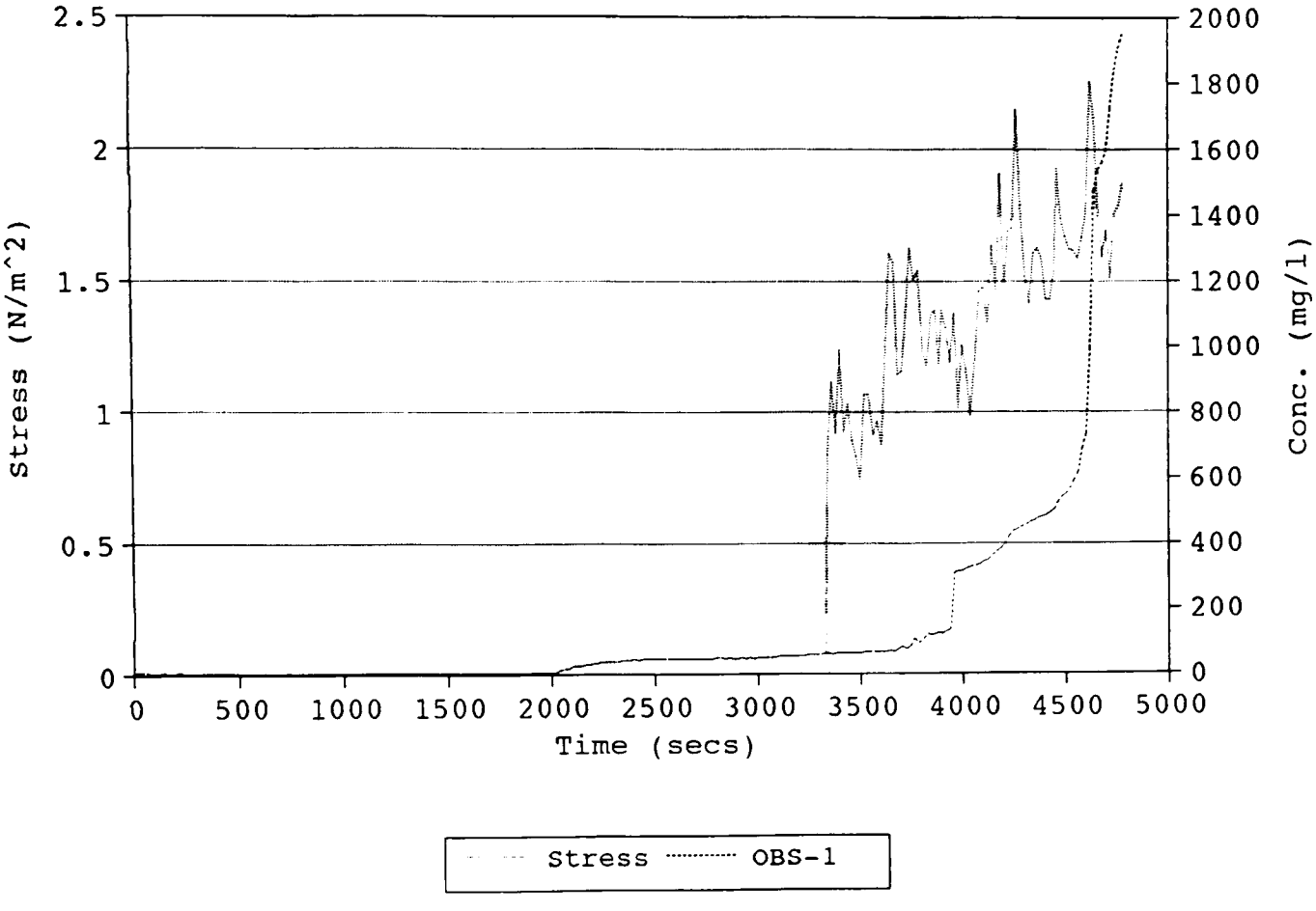

Fig (a.24b): Suspended Sediment Concentration and Rate of Erosion.

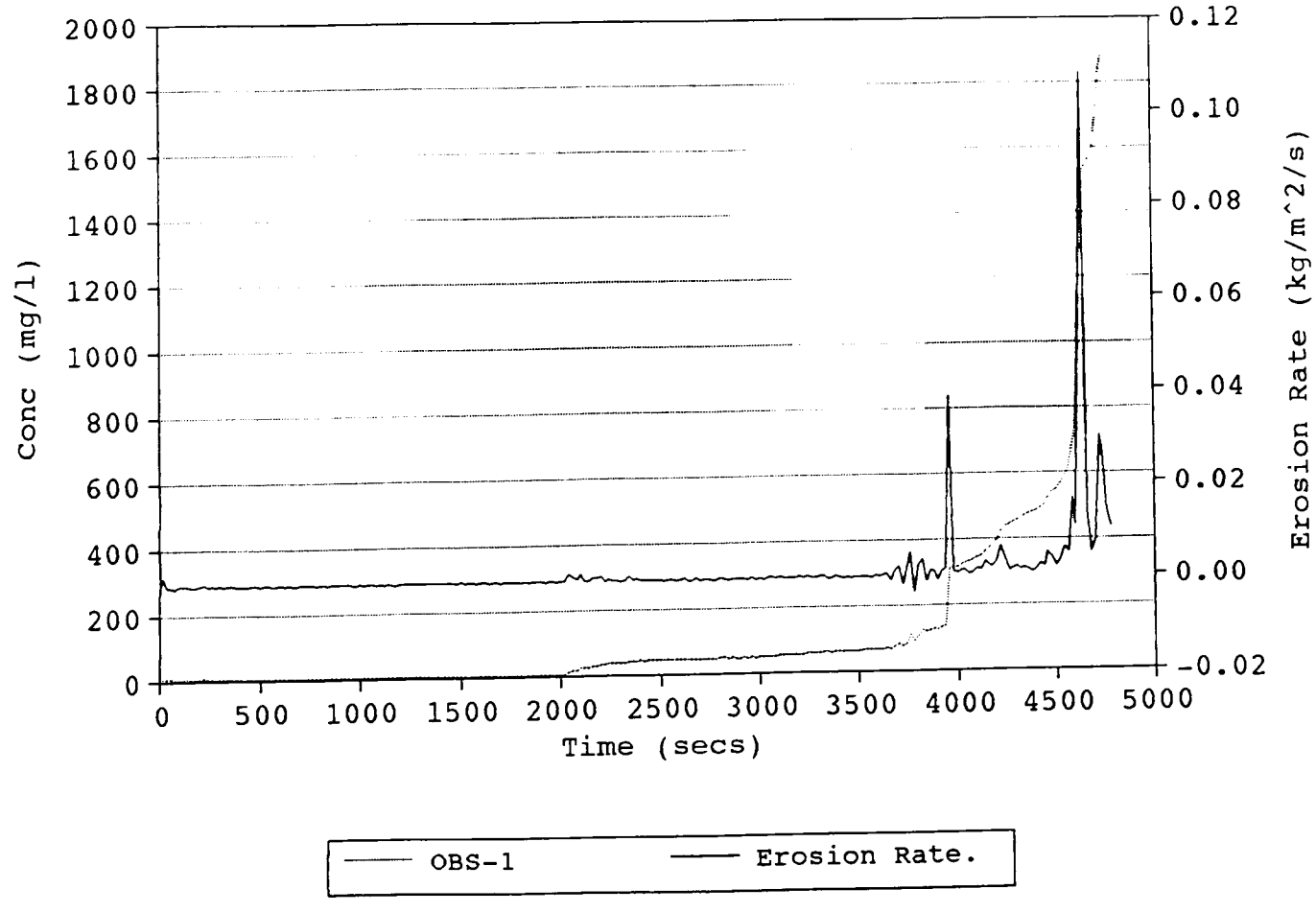

Fig (a.25a): Processed Data for Flume Run 25.

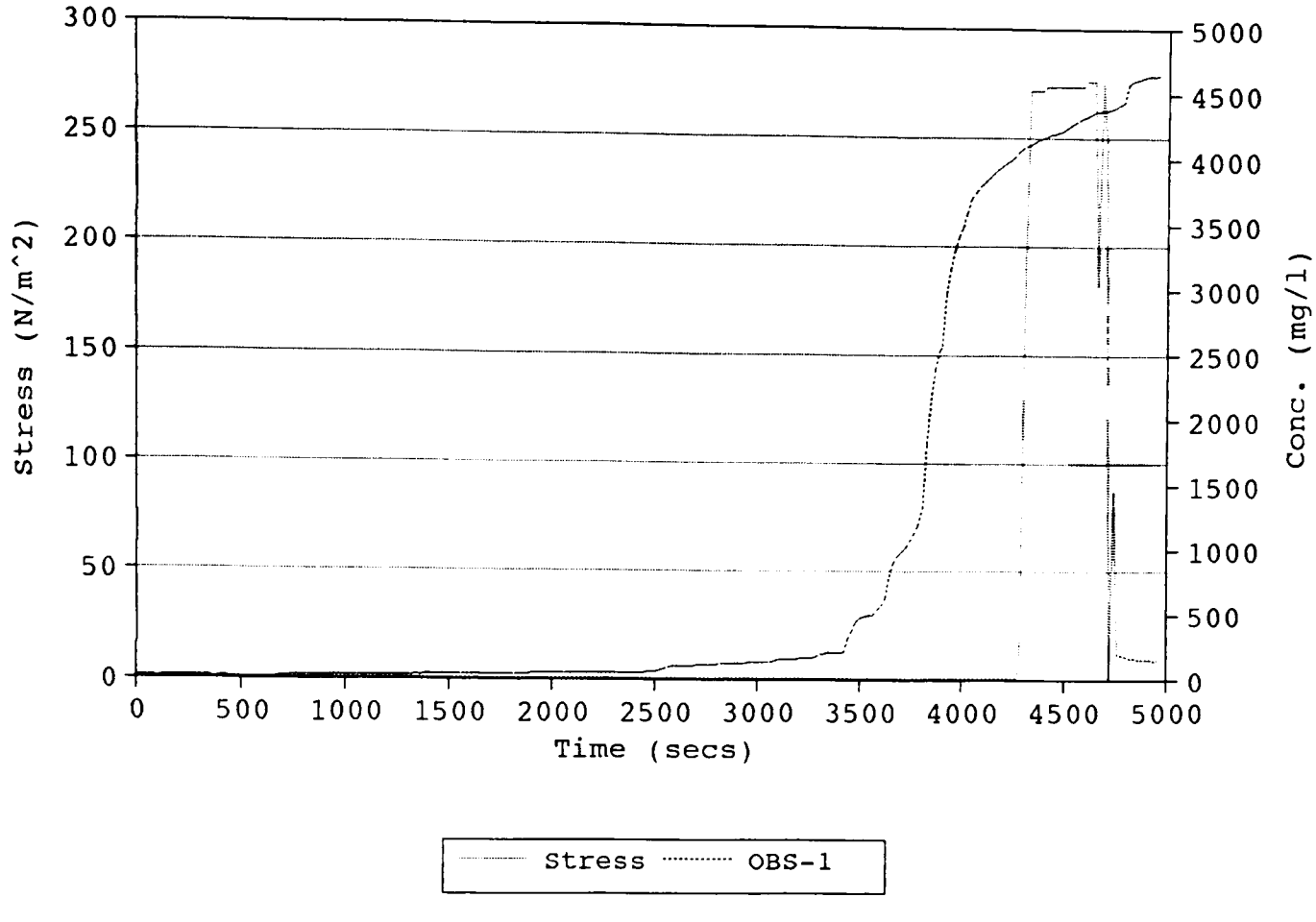

Fig (a.25b): Suspended Sediment Concentration and Rate of Erosion.

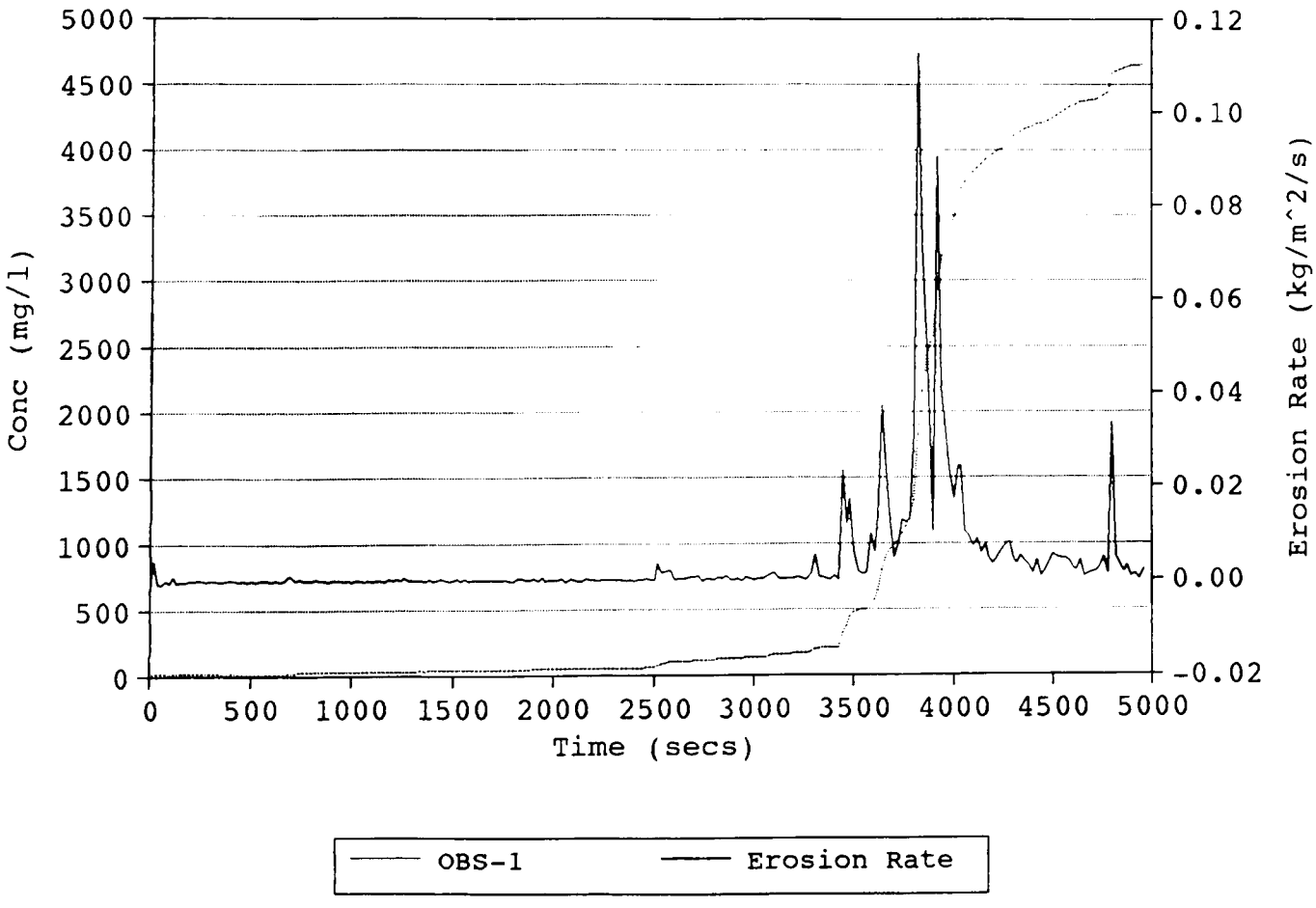

Fig (a.26a): Processed Data for Flume Run 26.

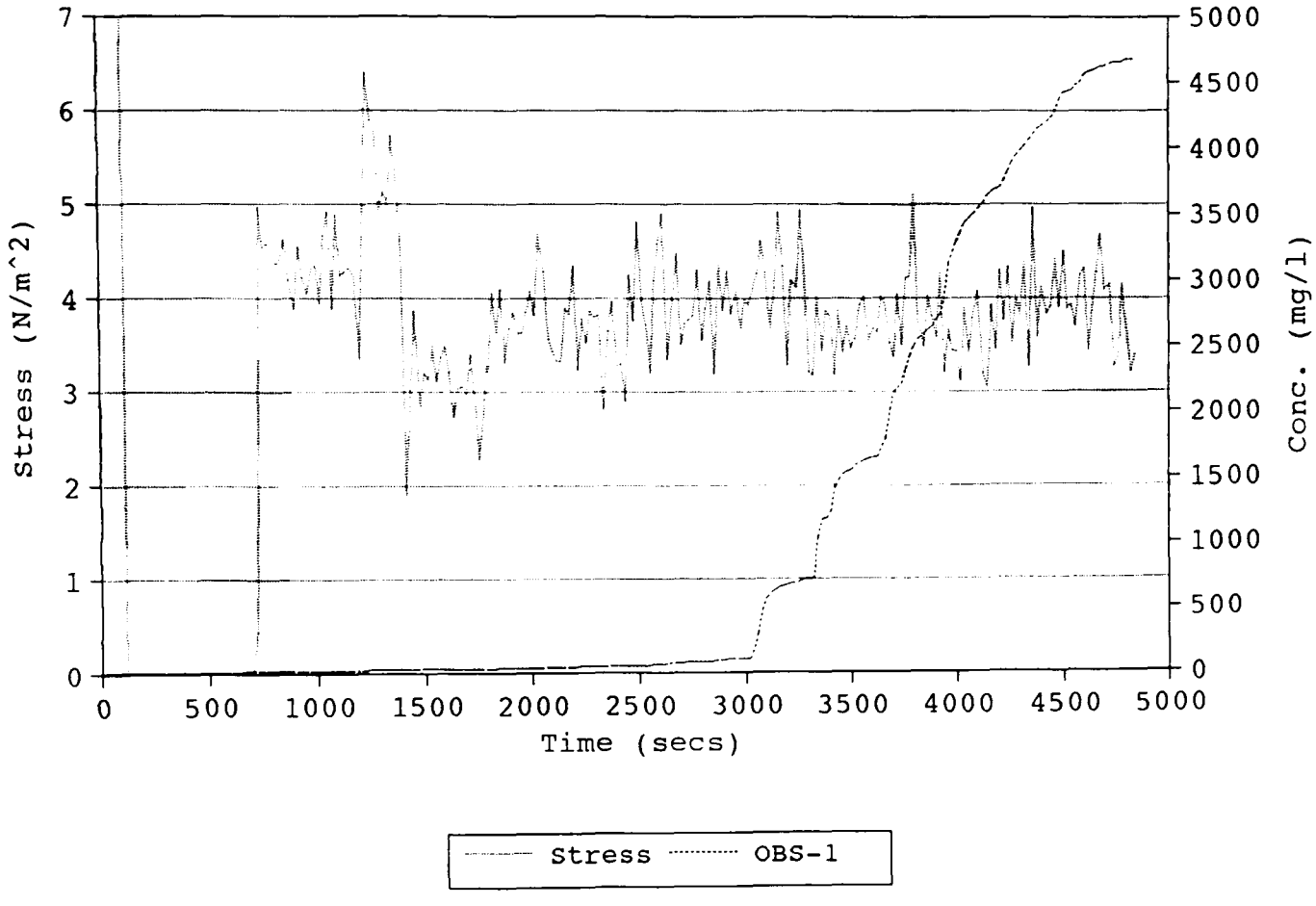

Fig (a.26b): Suspended Sediment Concentration and Rate of Erosion.

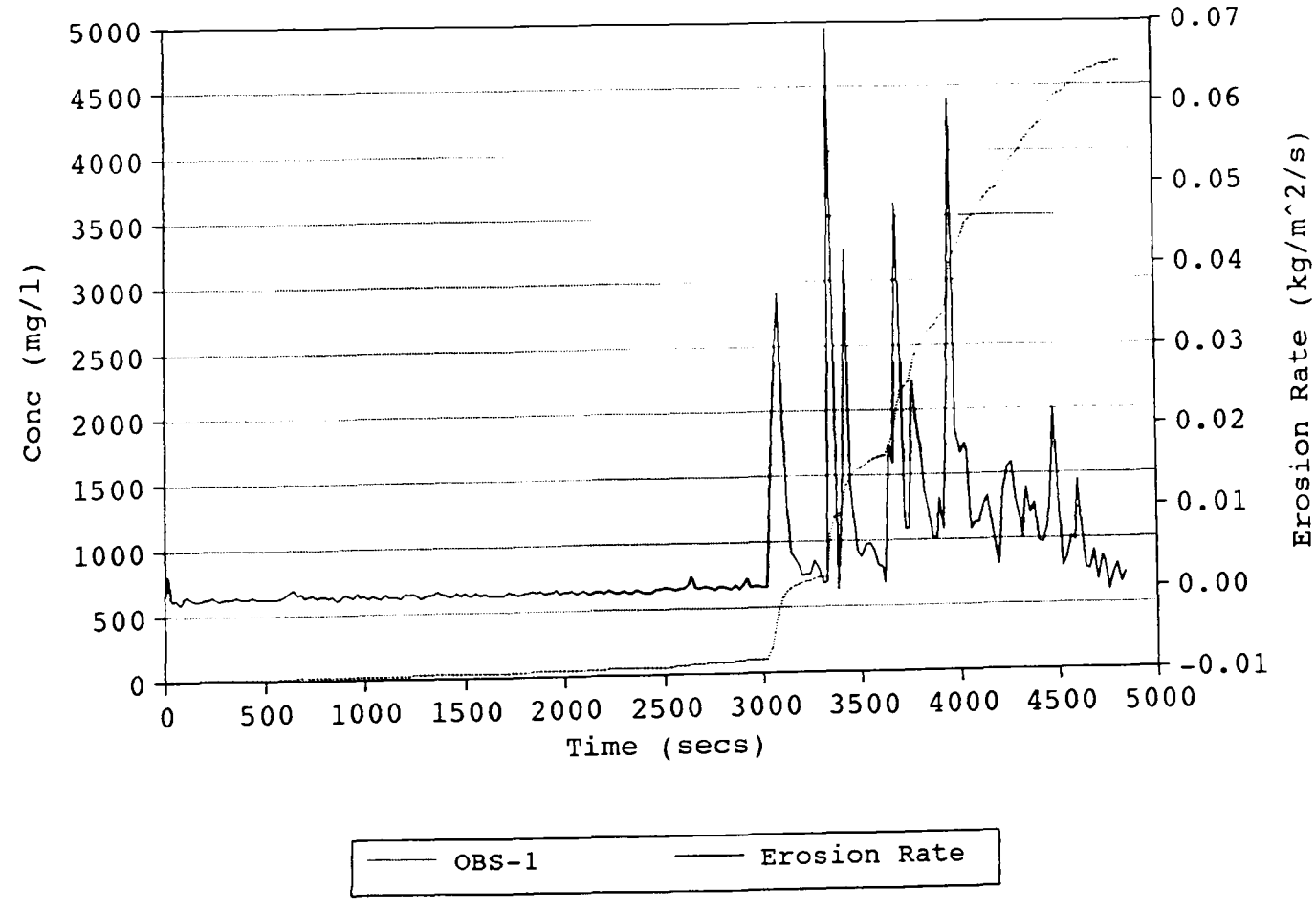

Fig (a.27a): Processed Data for Flume Run 27.

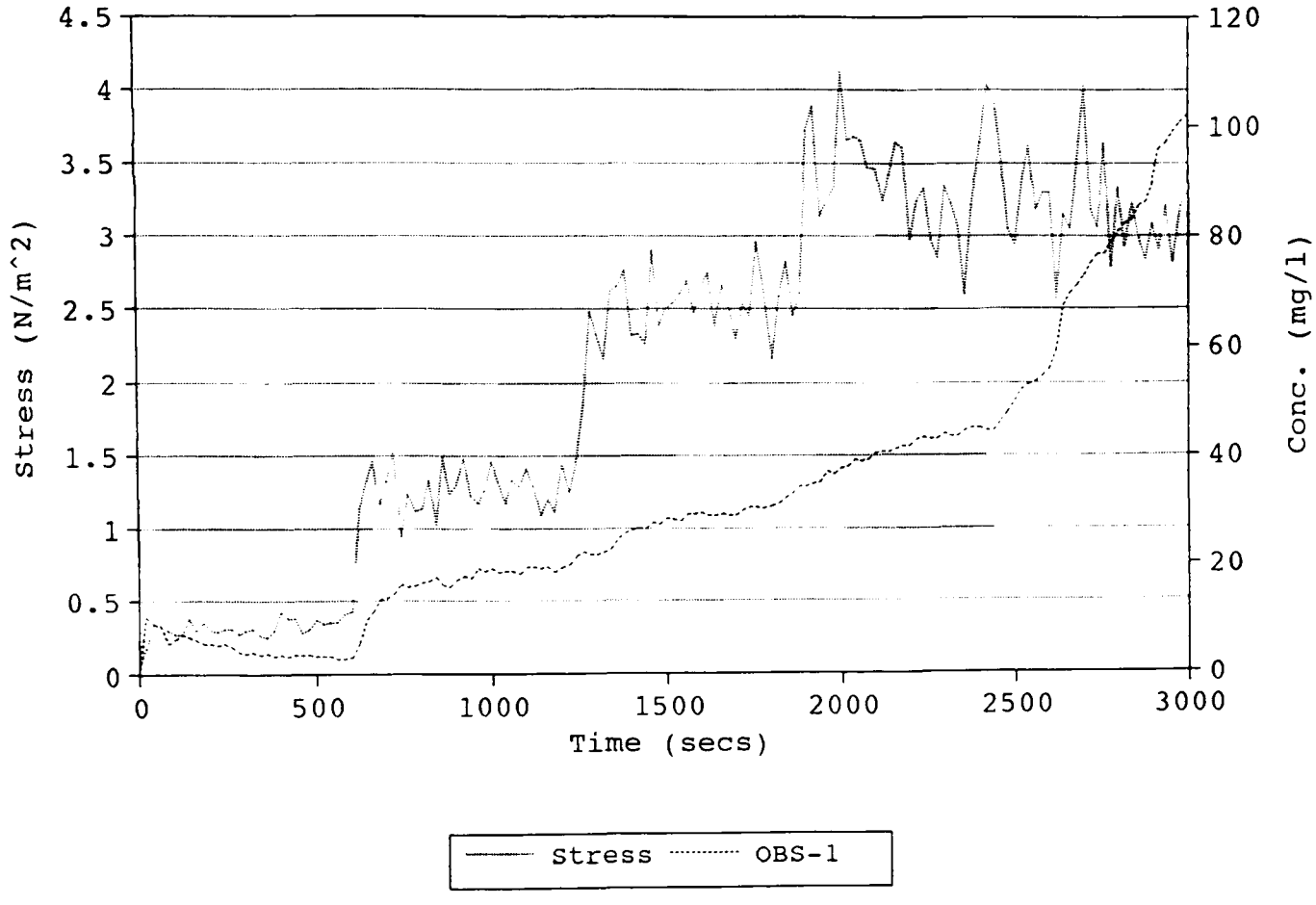

Fig (a.27b): Suspended Sediment Concentration and Rate of Erosion.

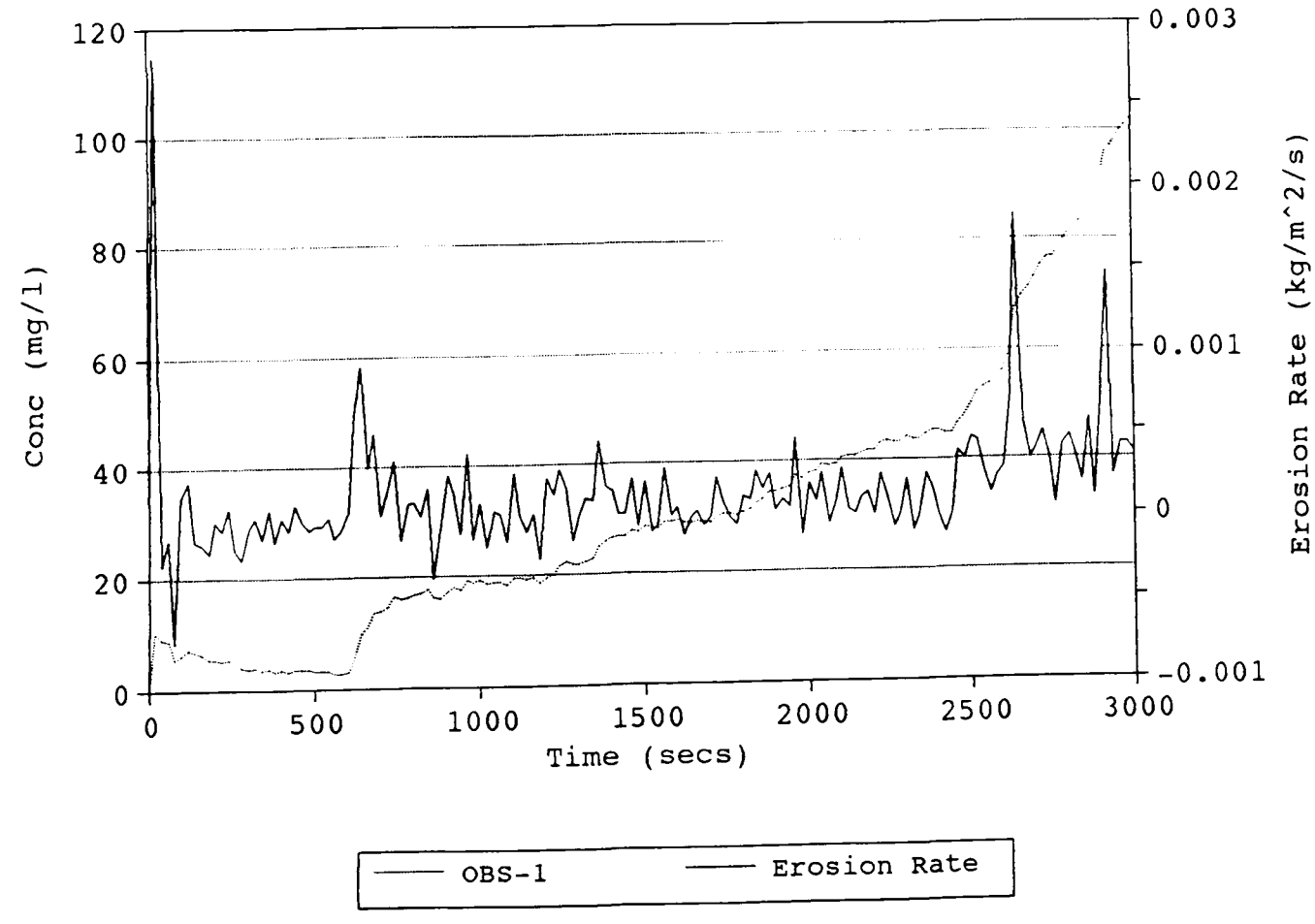

Fig (a.28a): Processed Data for Flume Run 28.

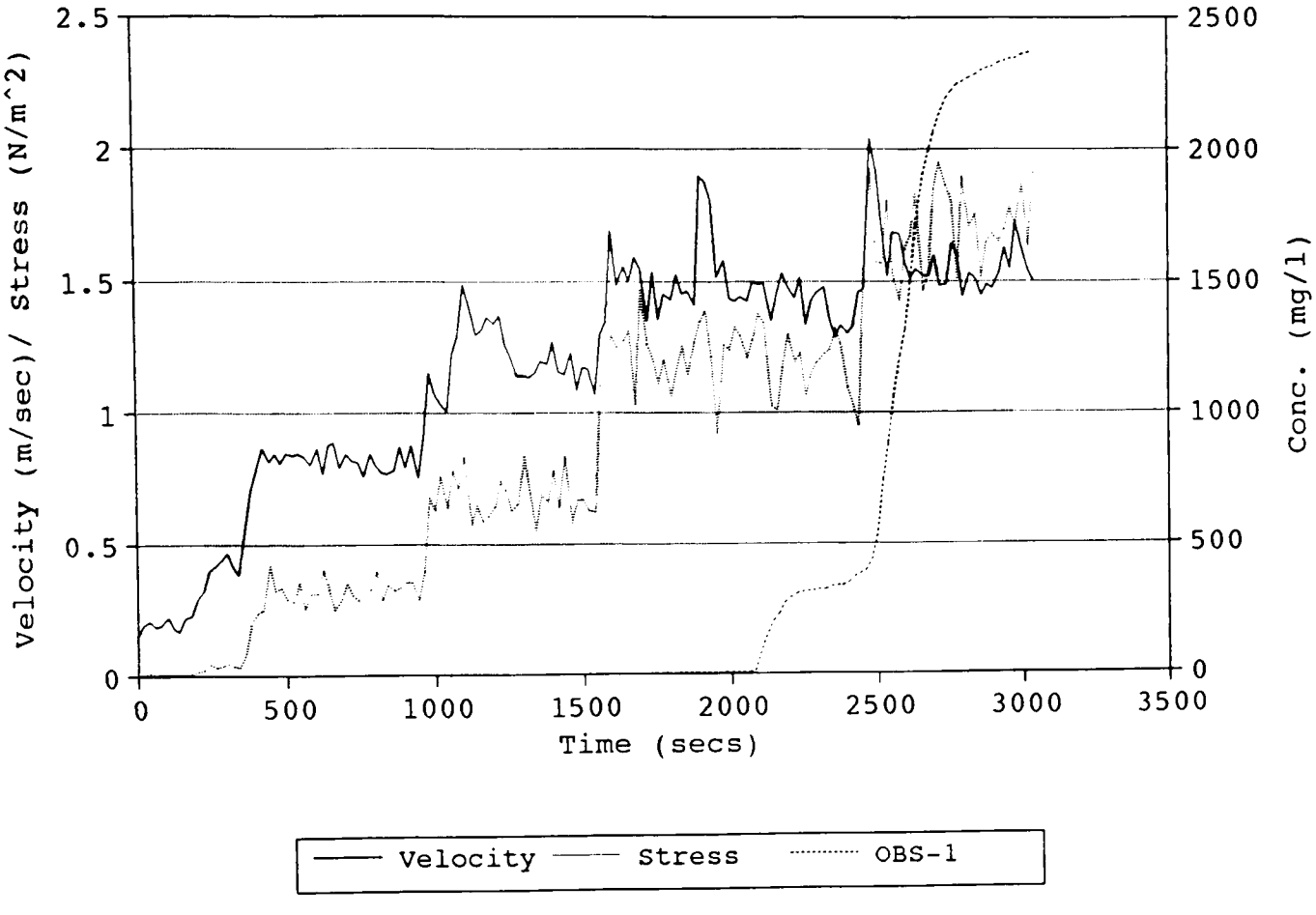

Fig (a.28b): Suspended Sediment Concentration and Rate of Erosion.

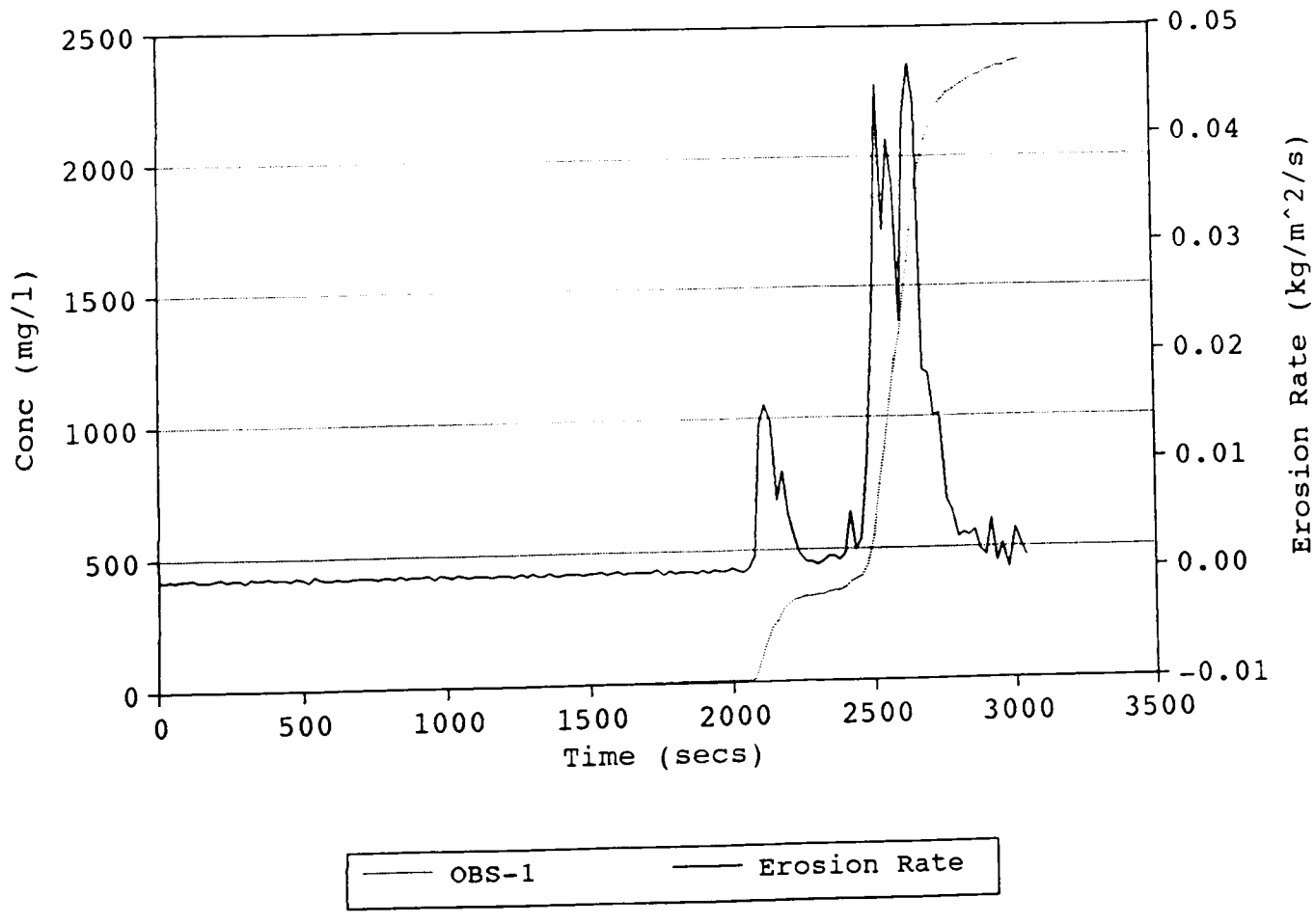

Fig (a.29a): Processed Data for Flume Run 29.

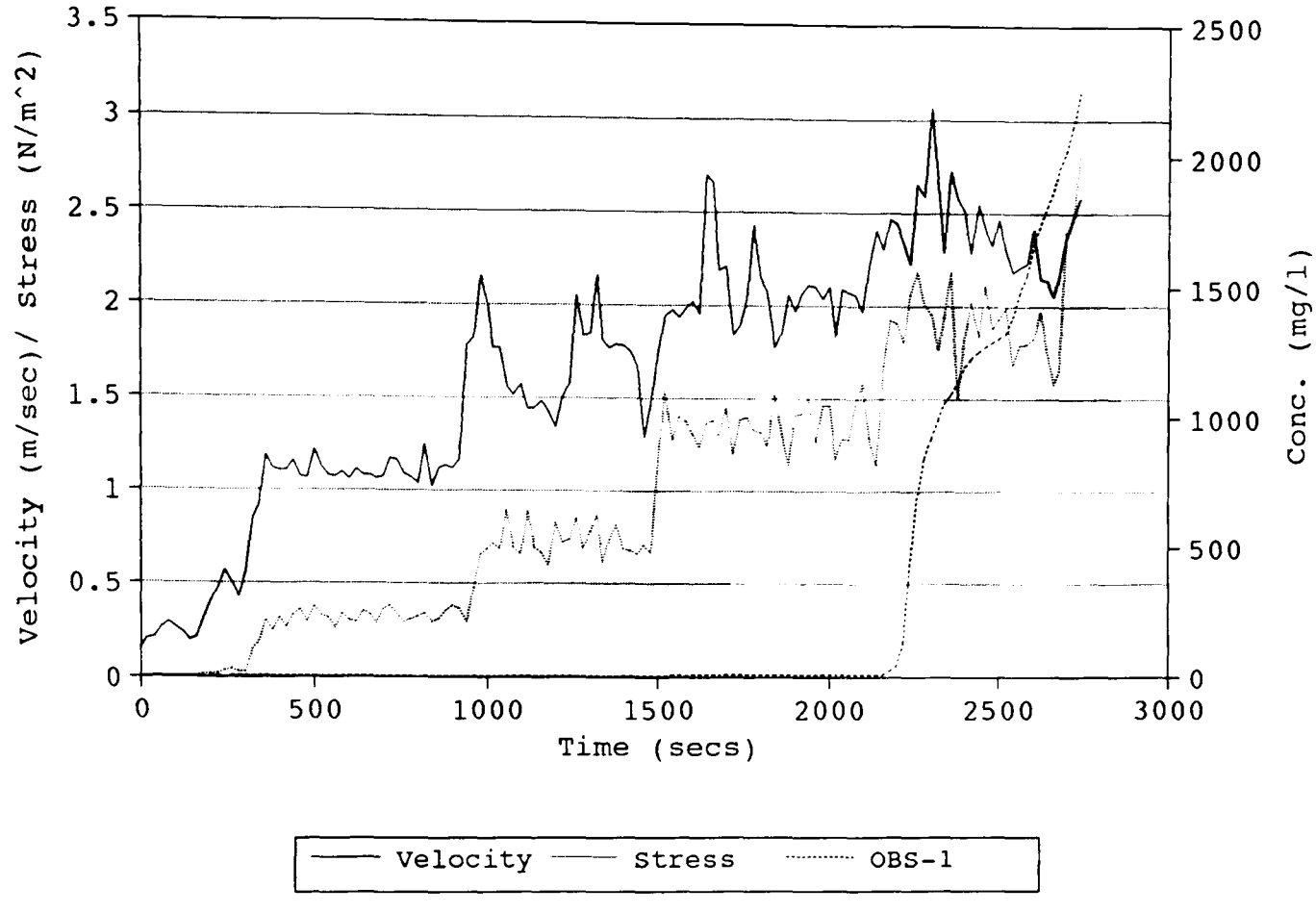

Fig (a.29b): Suspended Sediment Concentration and Rate of Erosion.

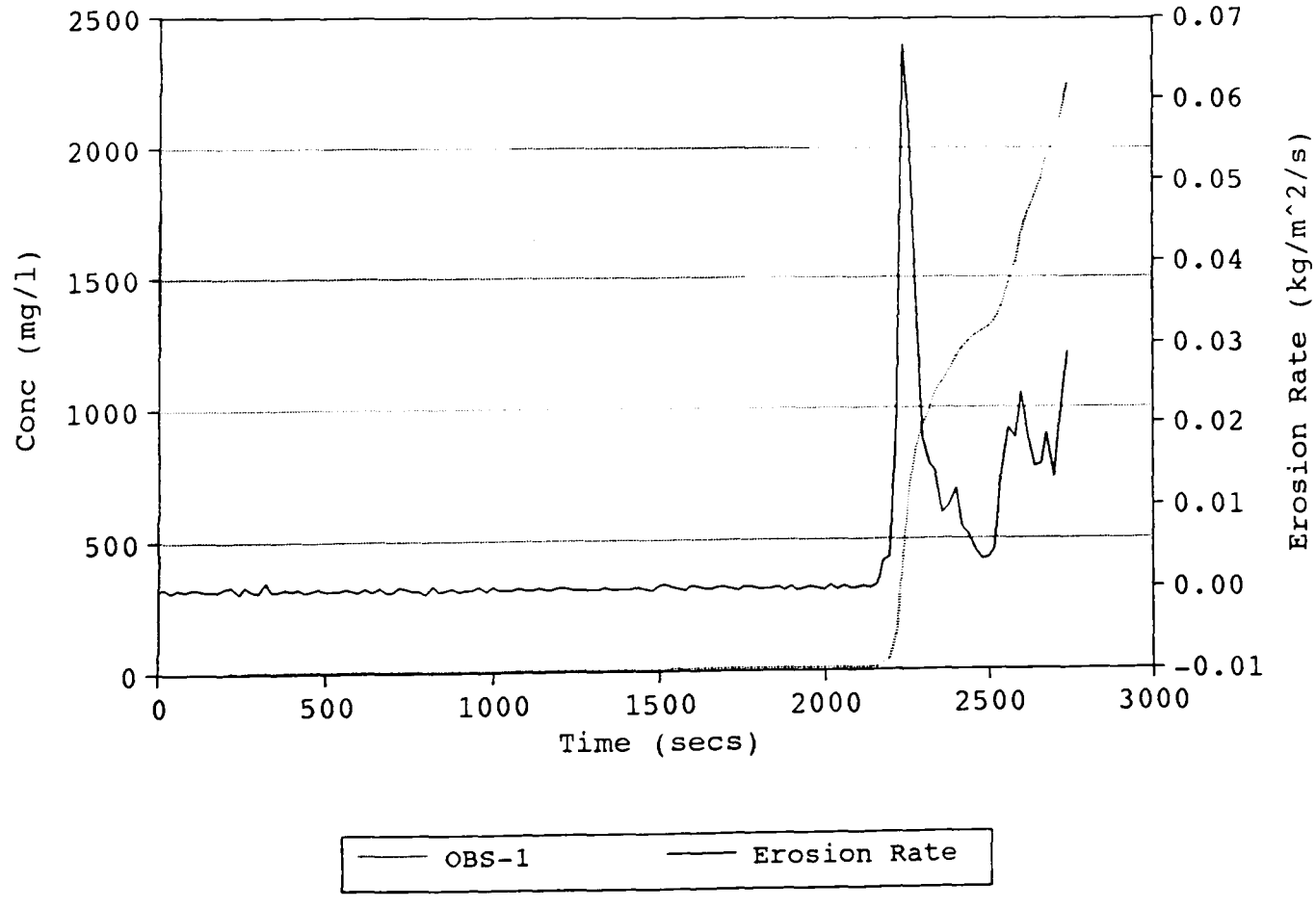

Fig (a.30a): Processed Data for Flume Run 30.

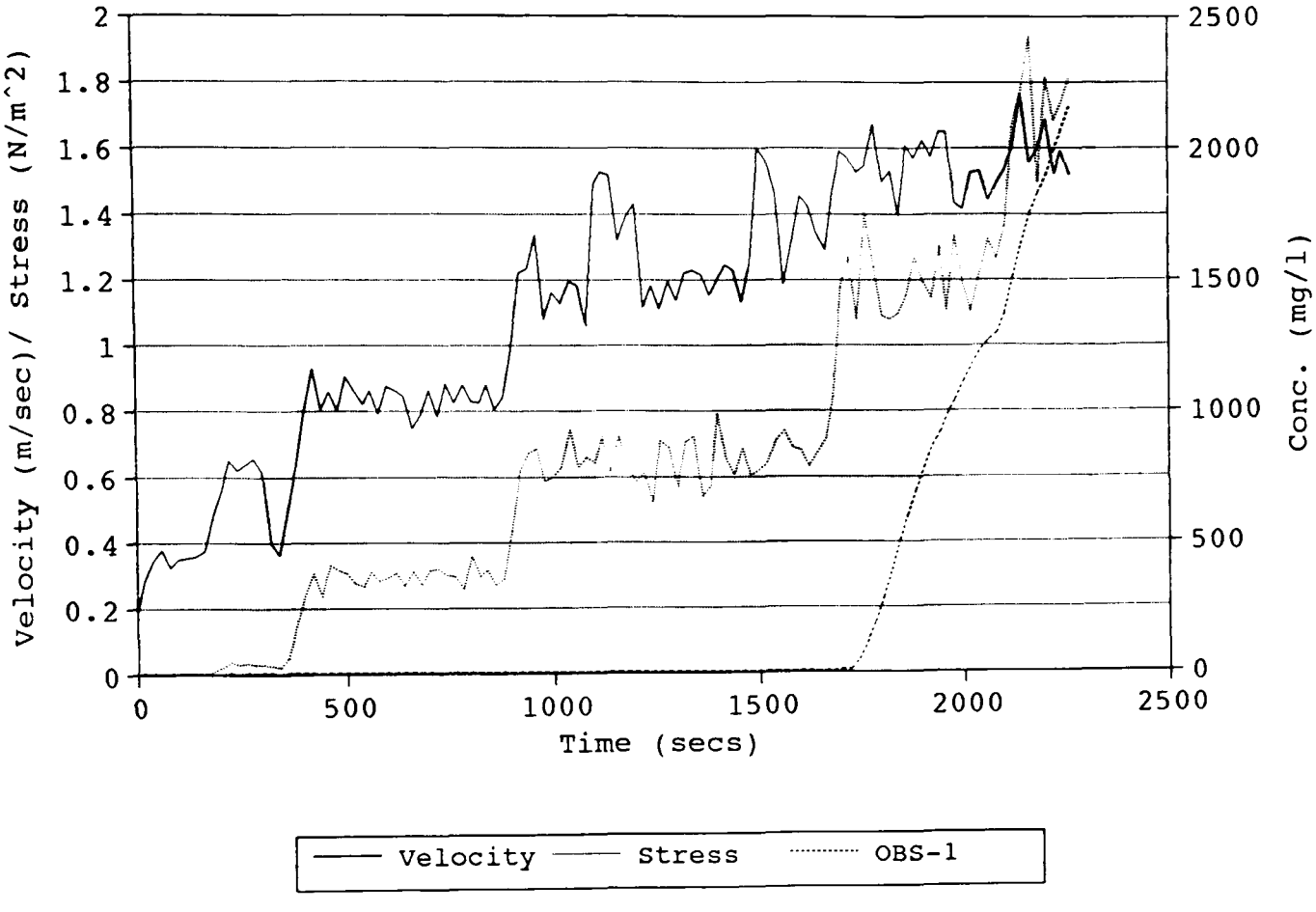

Fig (a.30b): Suspended Sediment Conc. and Rate of Erosion.

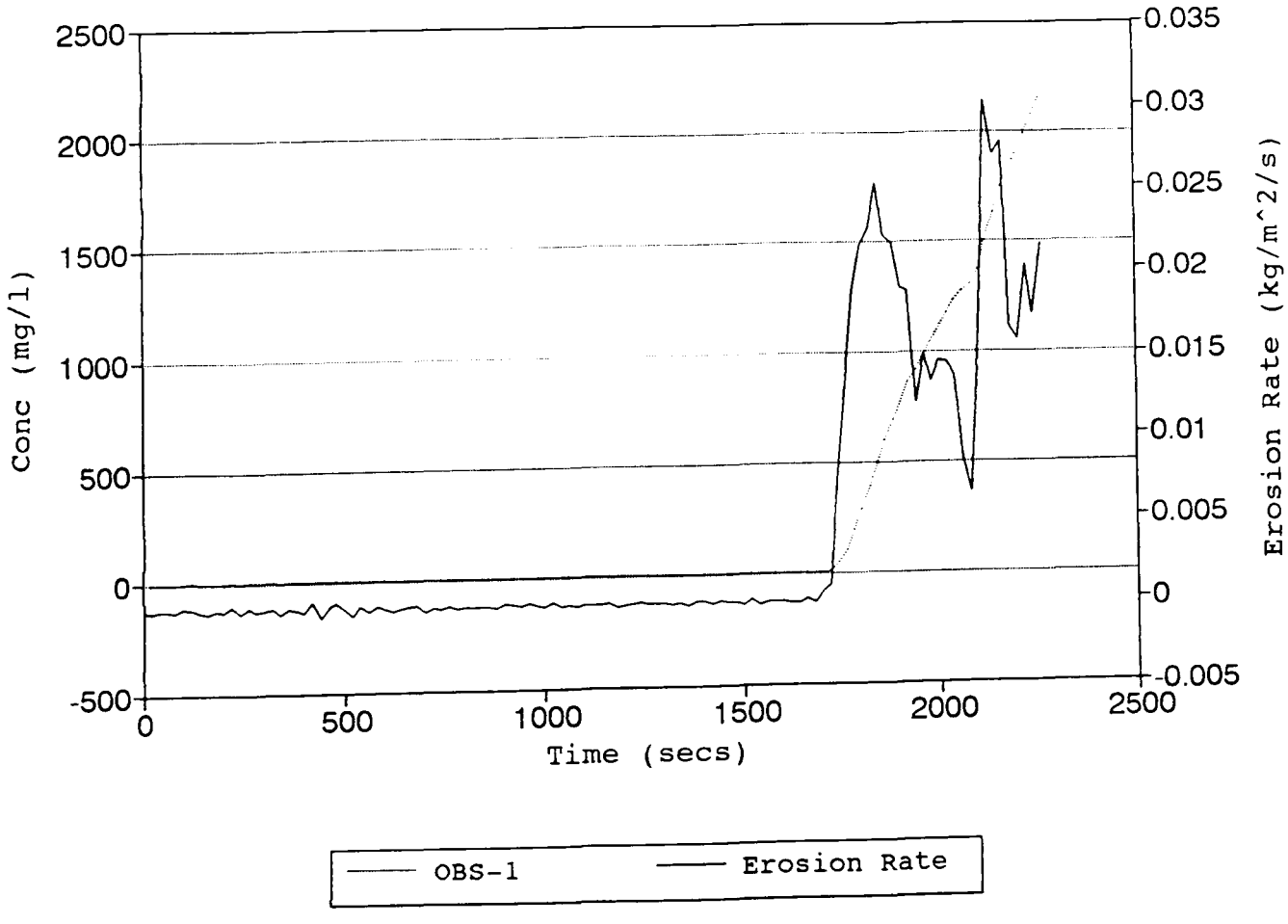

Fig (a.31a): Processed Data for Flume Run 31.

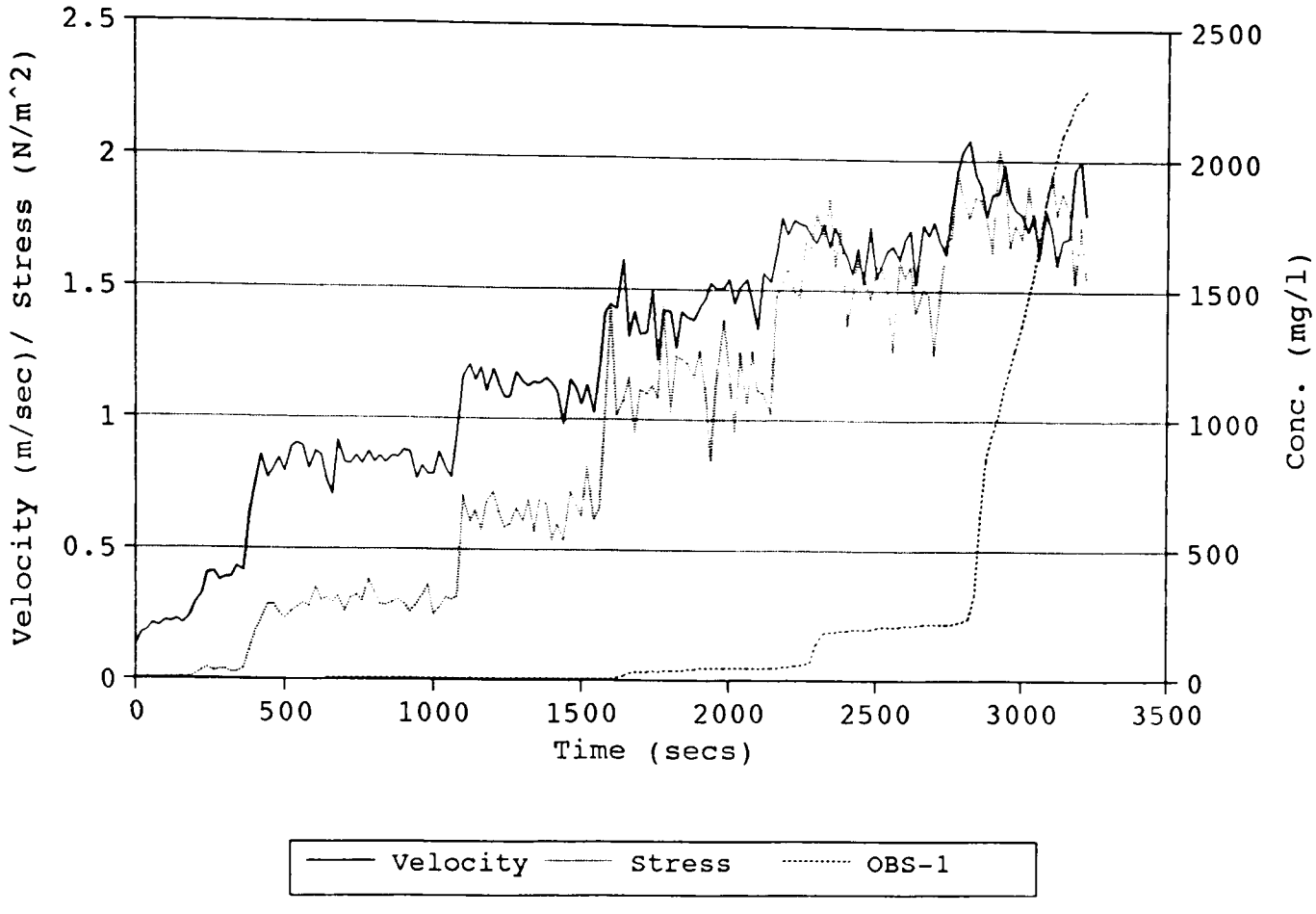

Fig (a.31b): Suspended Sediment Concentration and Rate of Erosion.

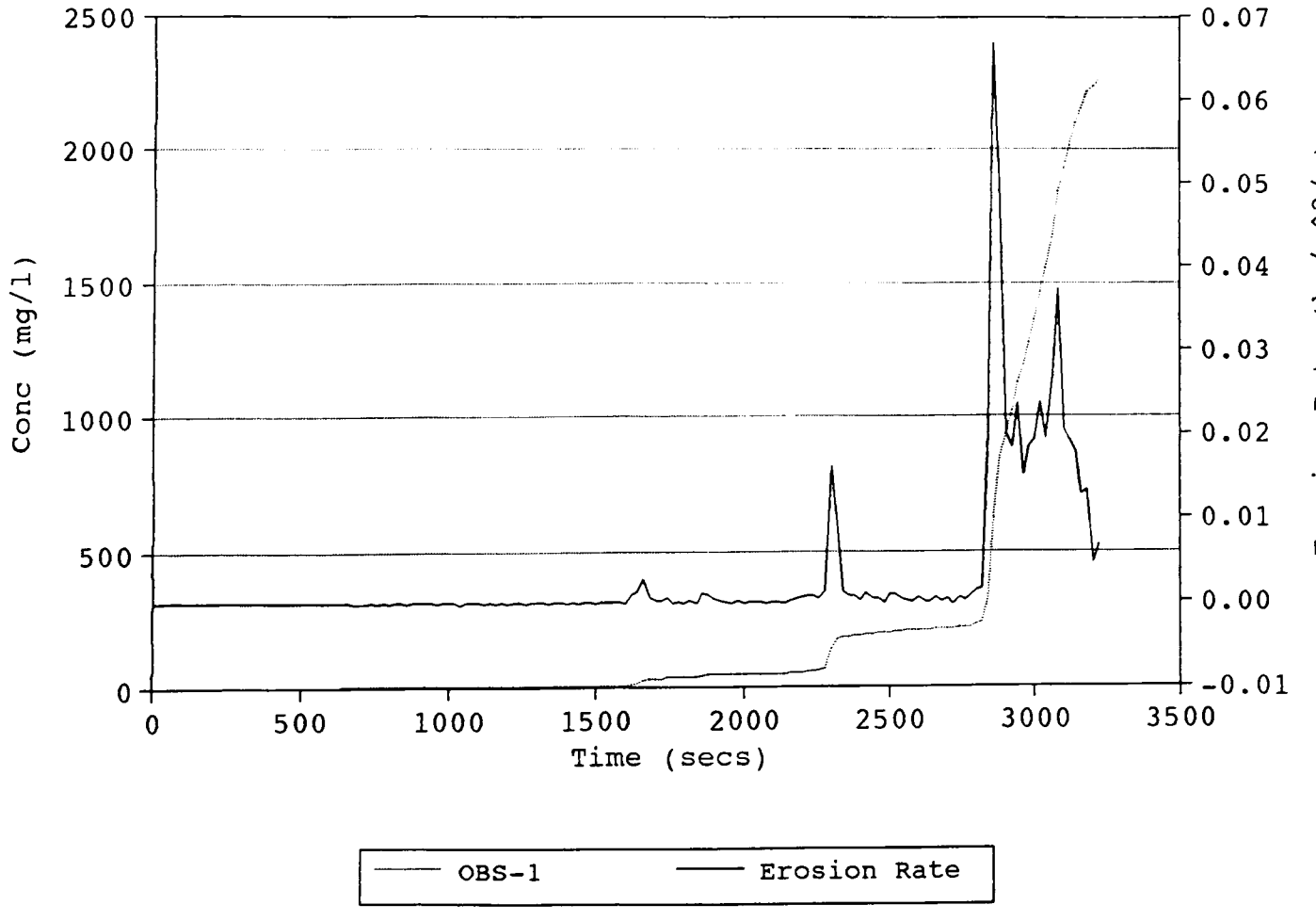

Fig (a.32a): Processed Data for Flume Run 32.

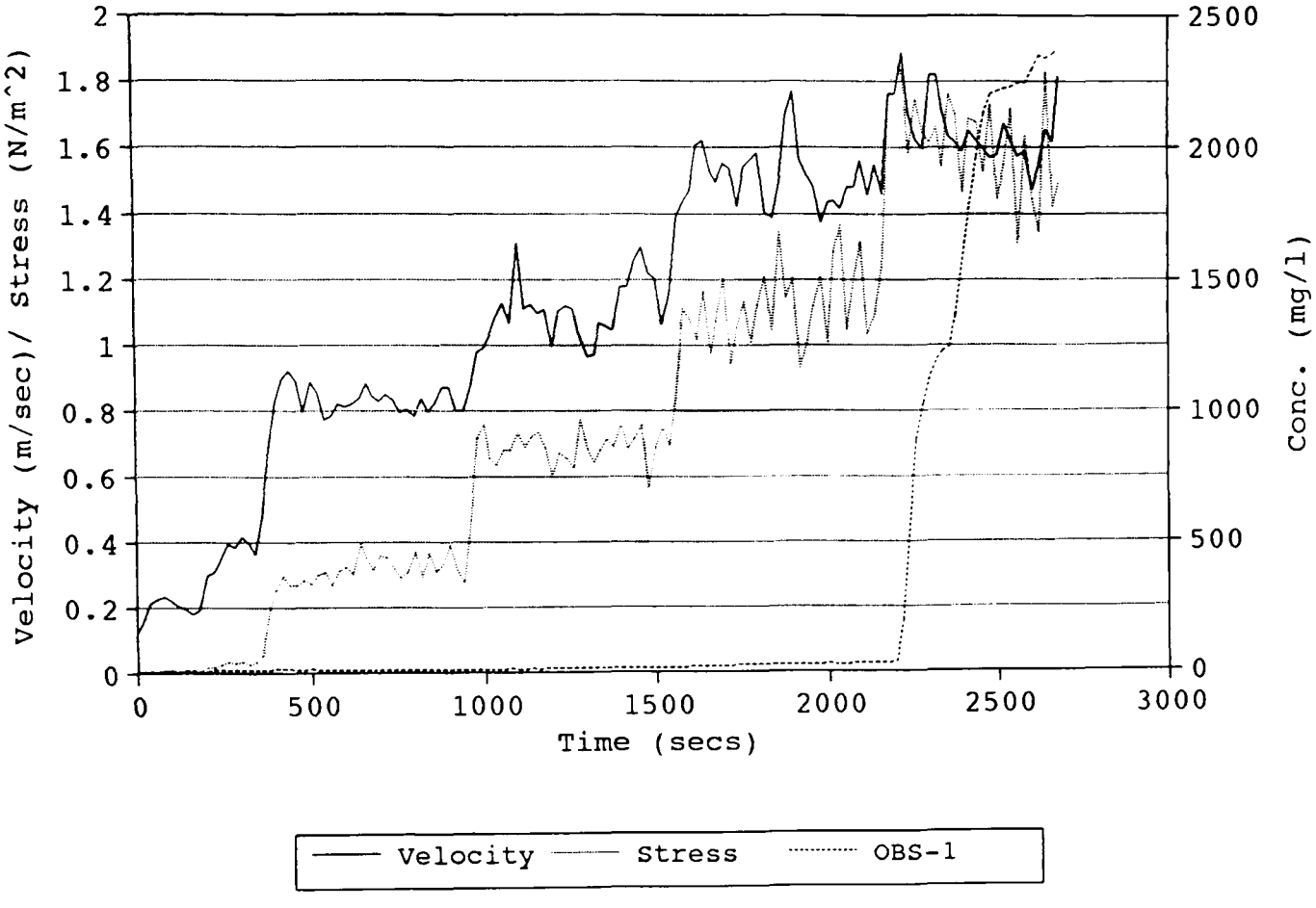

Fig (a.32b): Suspended Sediment Concentration and Rate of Erosion.

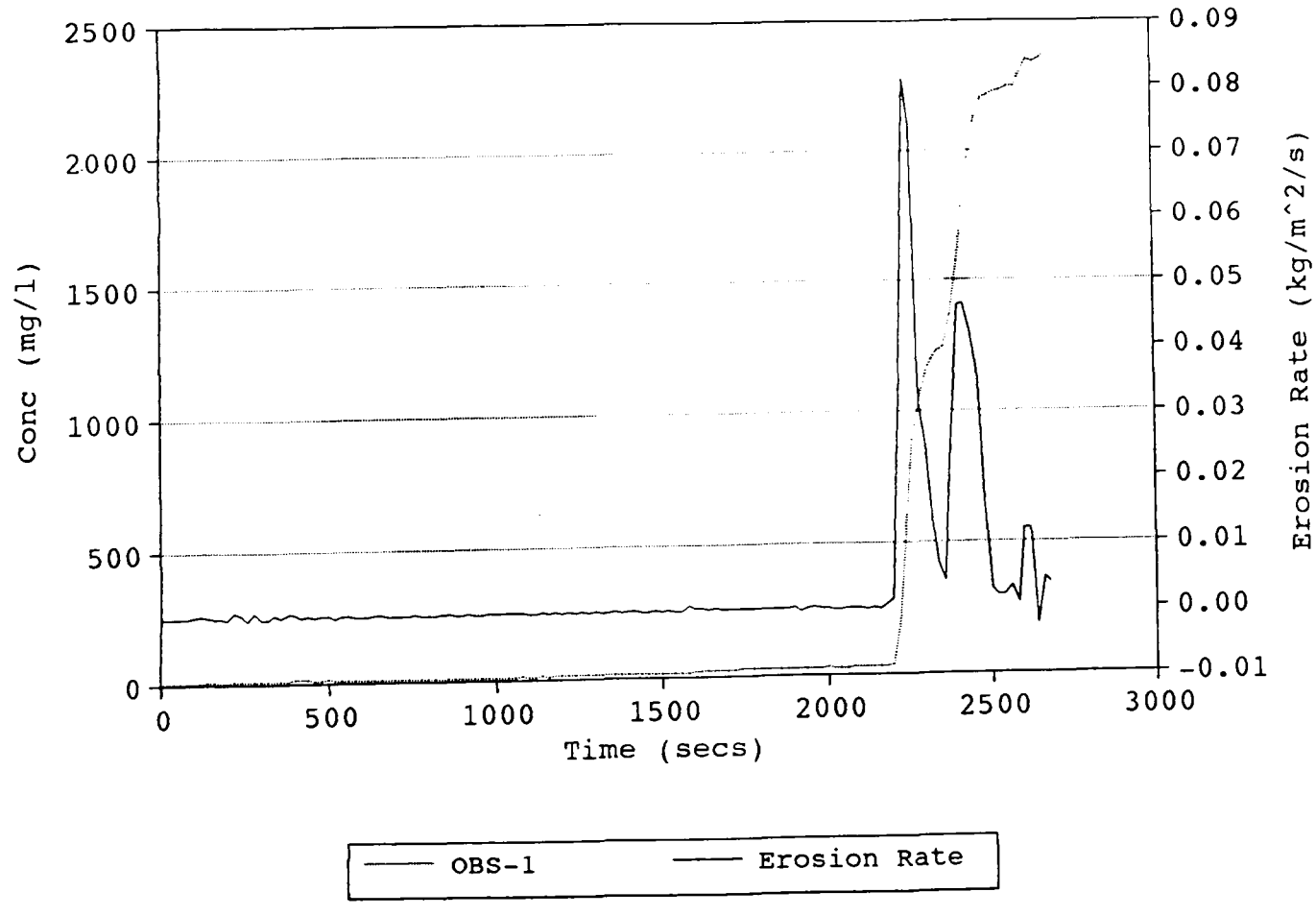

Fig (a.33a): Processed Data for Flume Run 33.

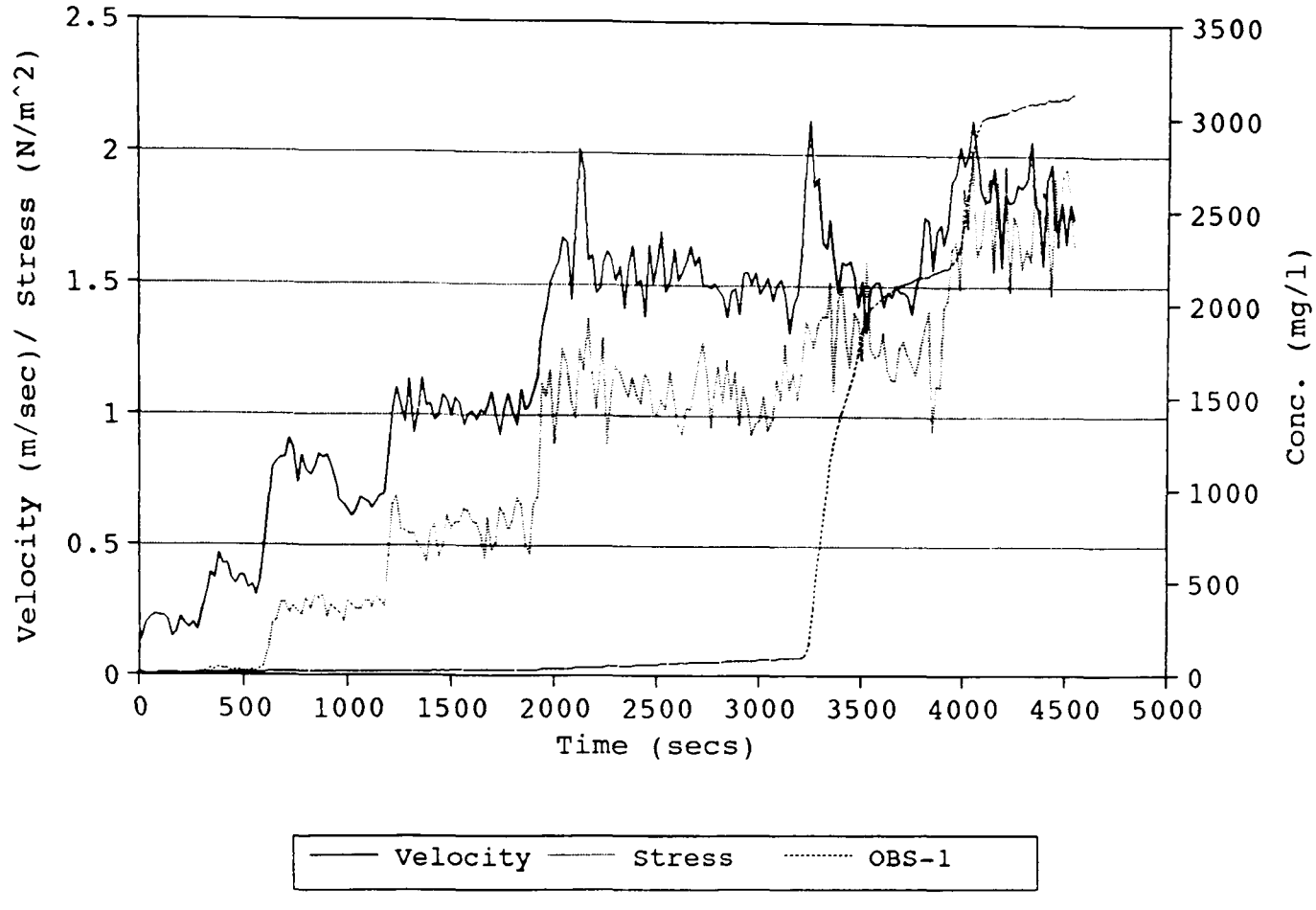

Fig (a.33b): Suspended Sediment Concentration and Rate of Erosion.

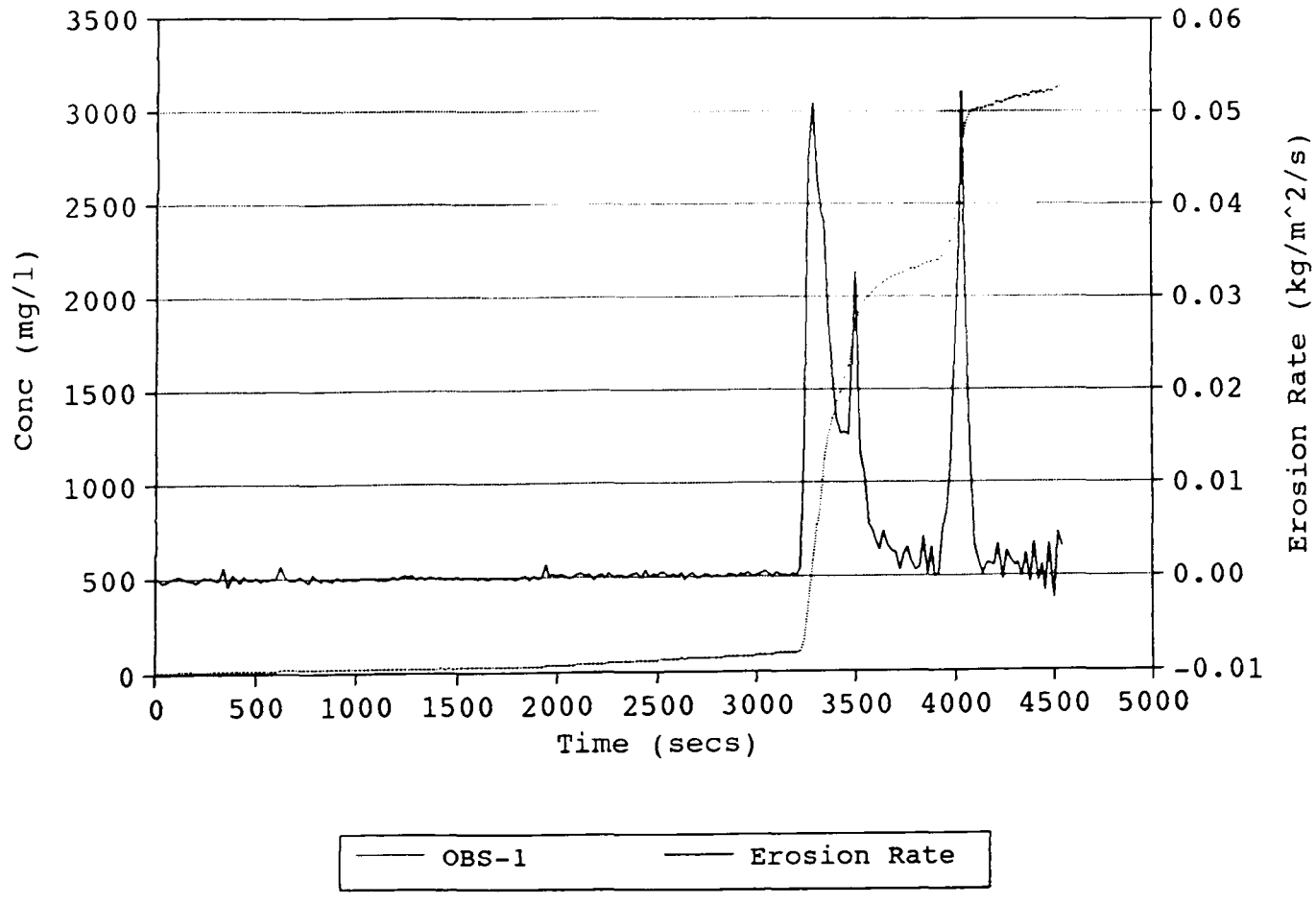

Fig (a.34a): Processed Data for Flume Run 34.

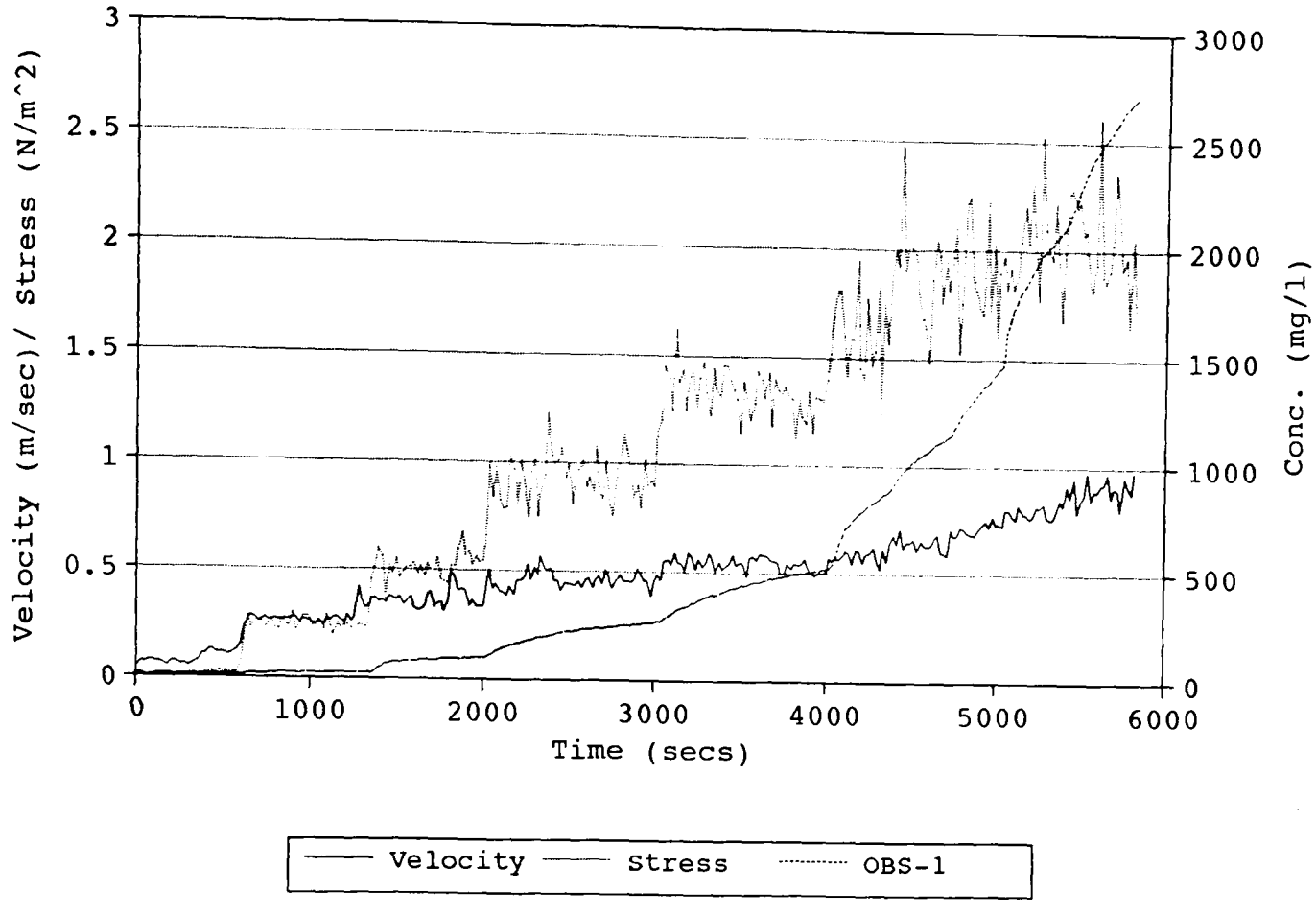

Fig (a.34b): Suspended Sediment Concentration and Rate of Erosion.

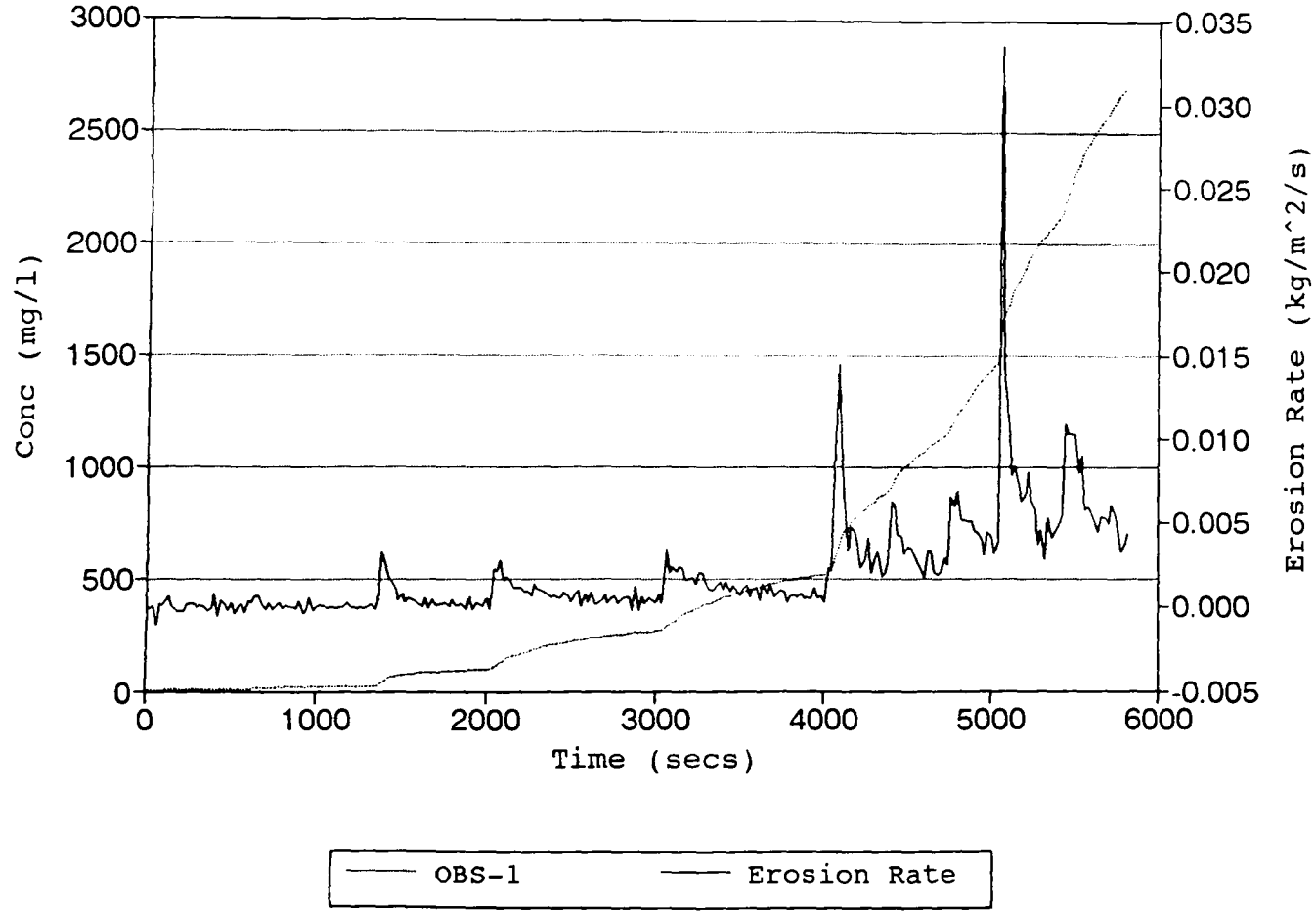

Fig (a.35a): Processed Data for Flume Run 35.

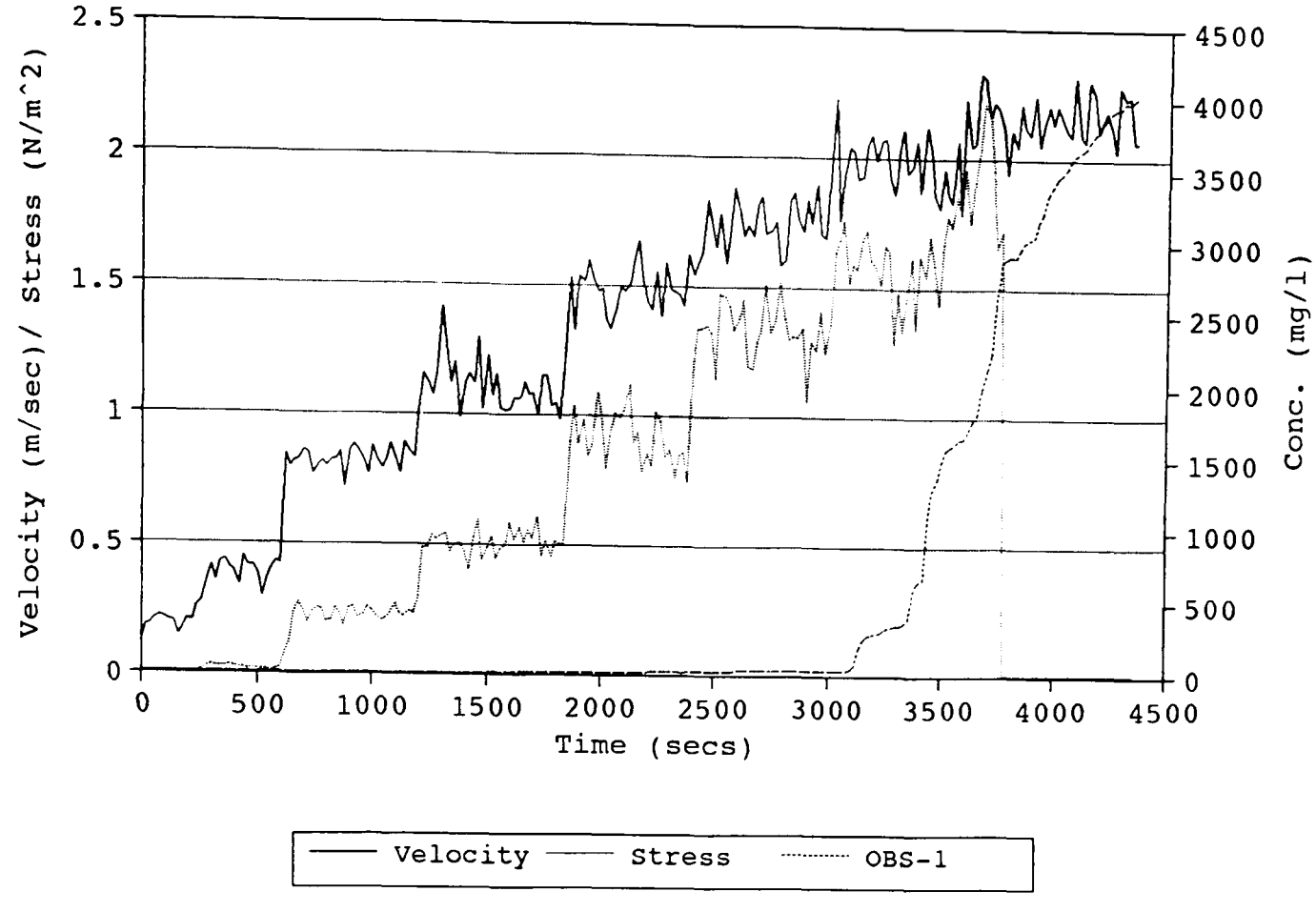

Fig (a.35b): Suspended Sediment Concentration and Rate of Erosion.

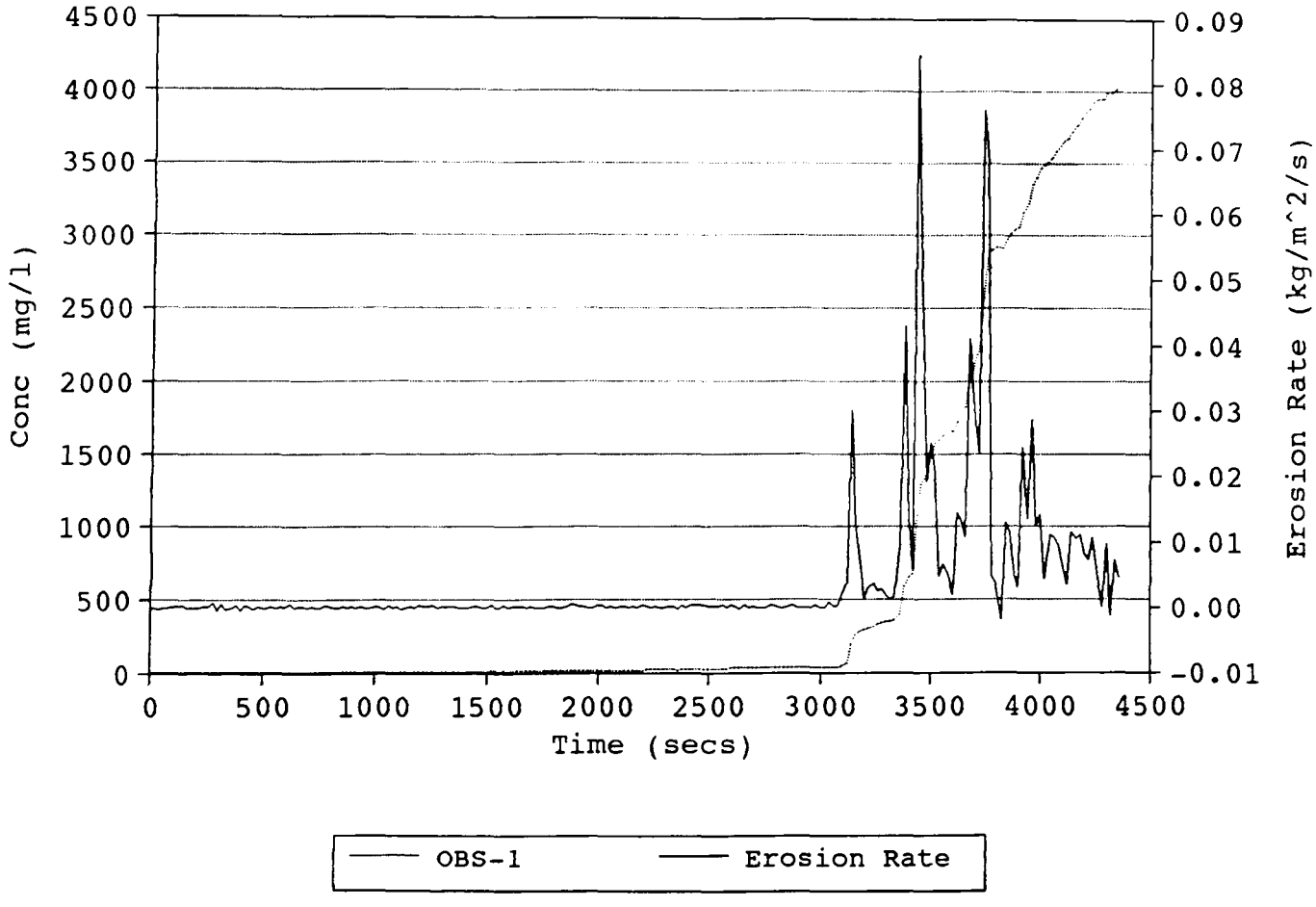

Fig (a.36a): Processed Data for Flume Run 36.

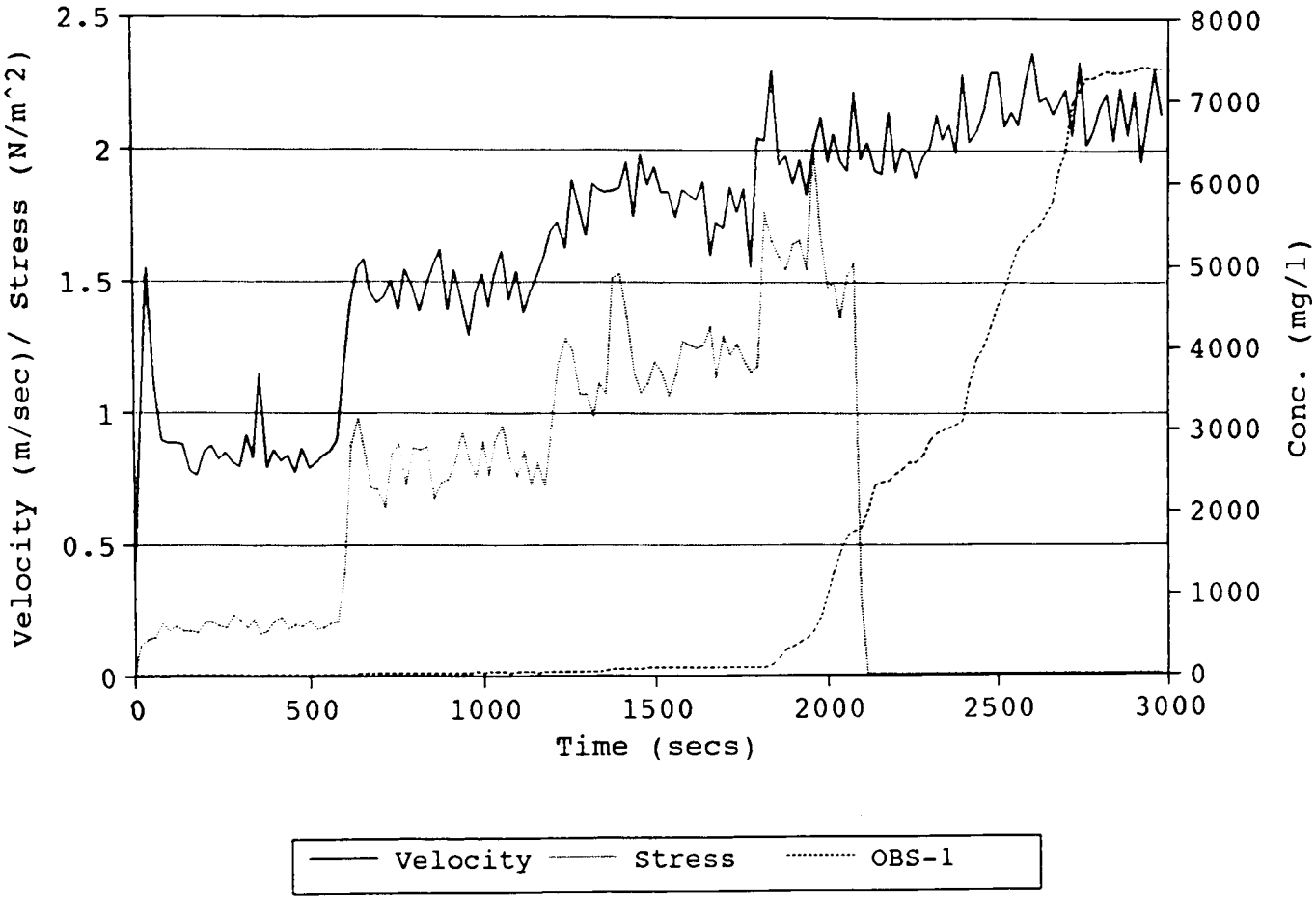

Fig (a.36b): Suspended Sediment Concentration and Rate of Erosion.

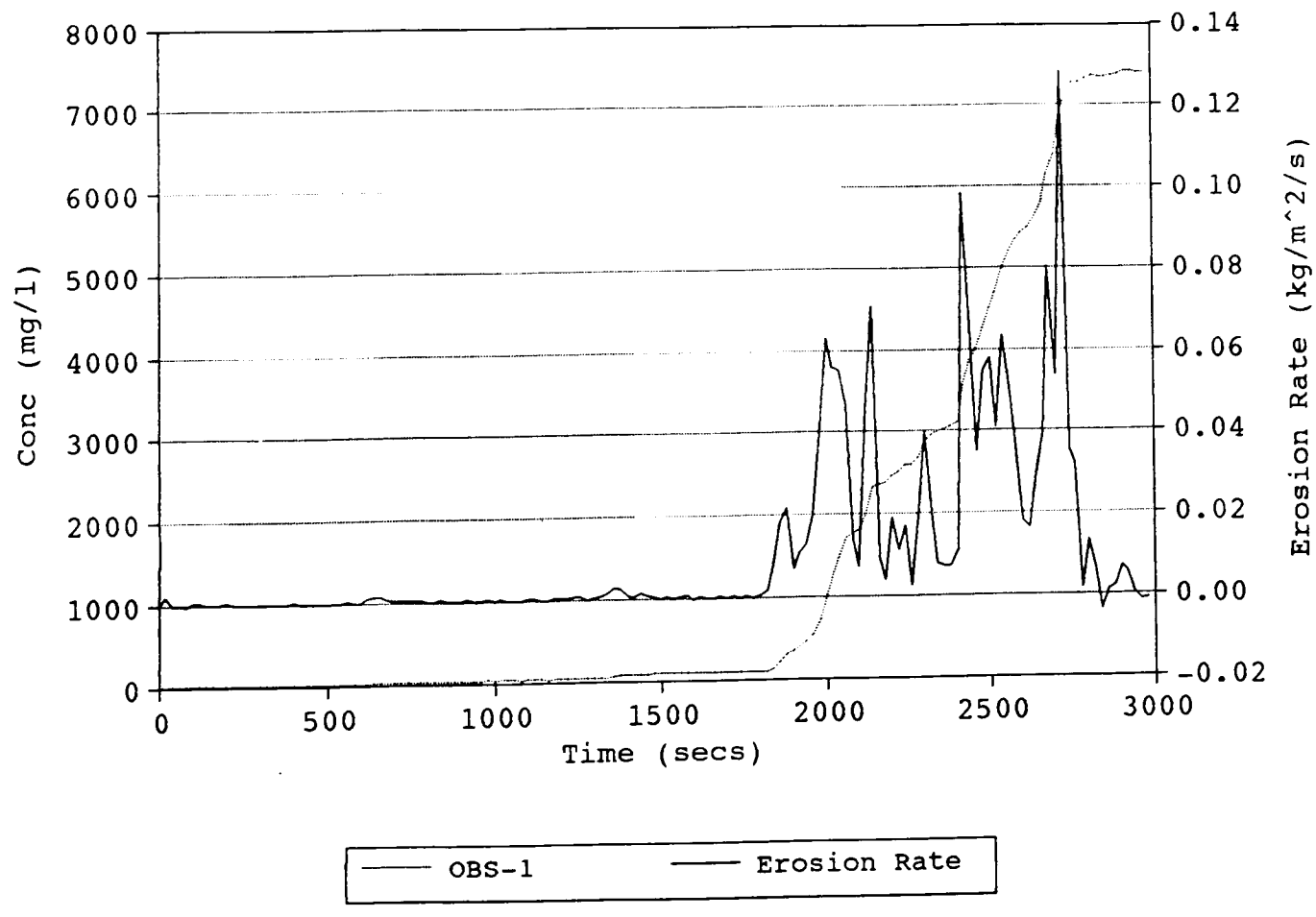

Fig (a.37a): Processed Data for Flume Flume Run37.

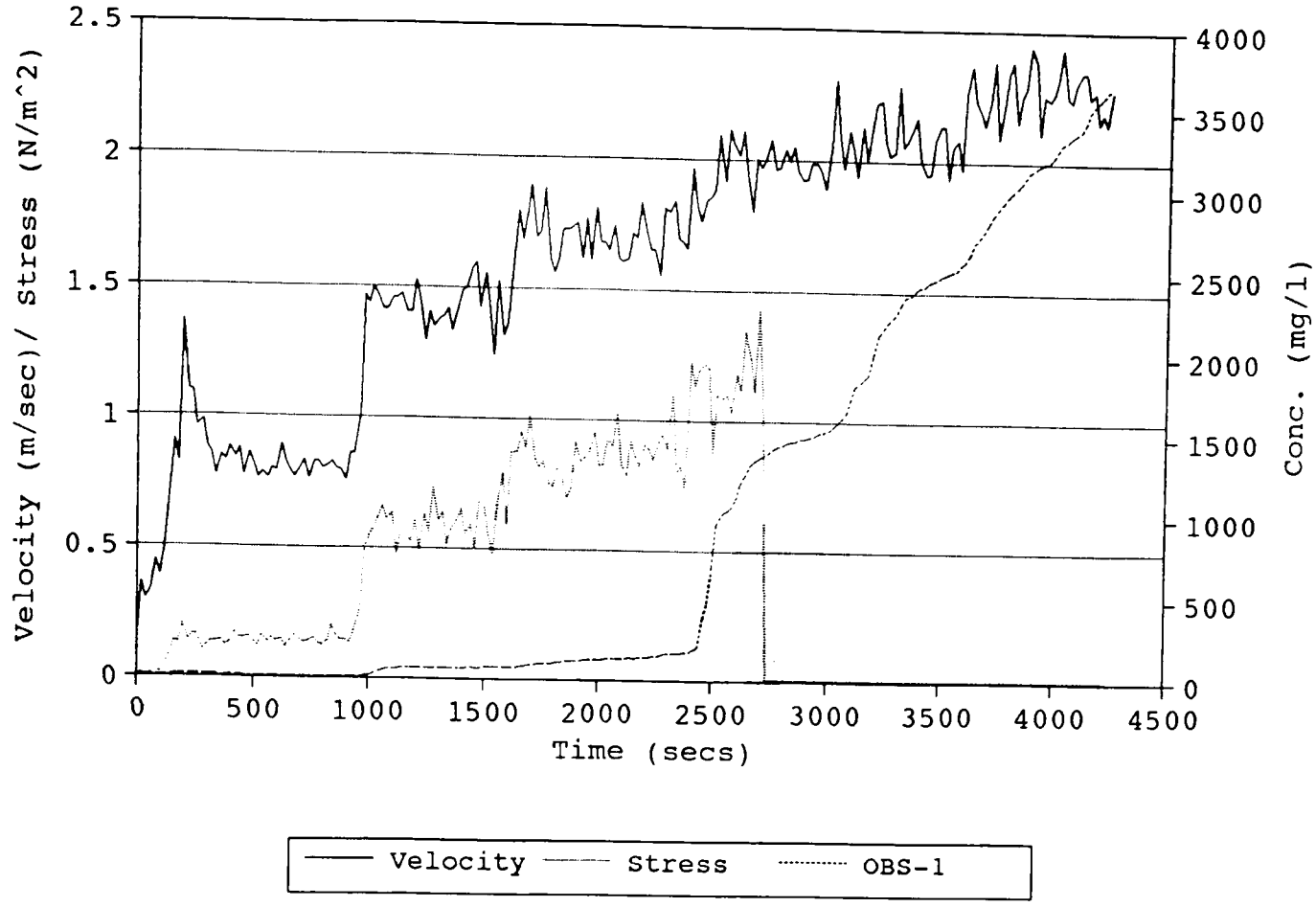

Fig (a.37b): Suspended Sediment Concentration and Rate of Erosion.

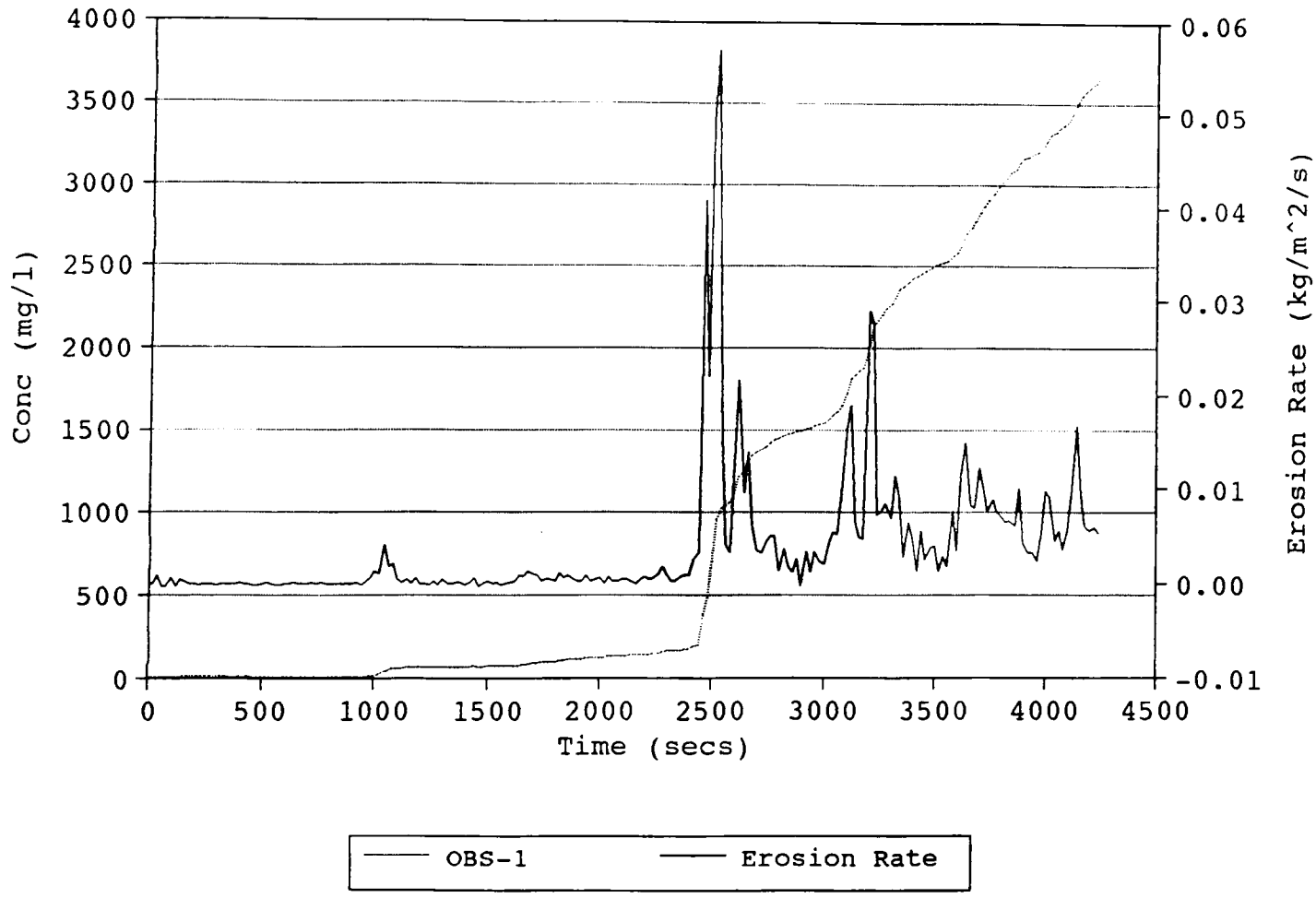

Fig (a.38a): Processed Data for Flume Run 38.

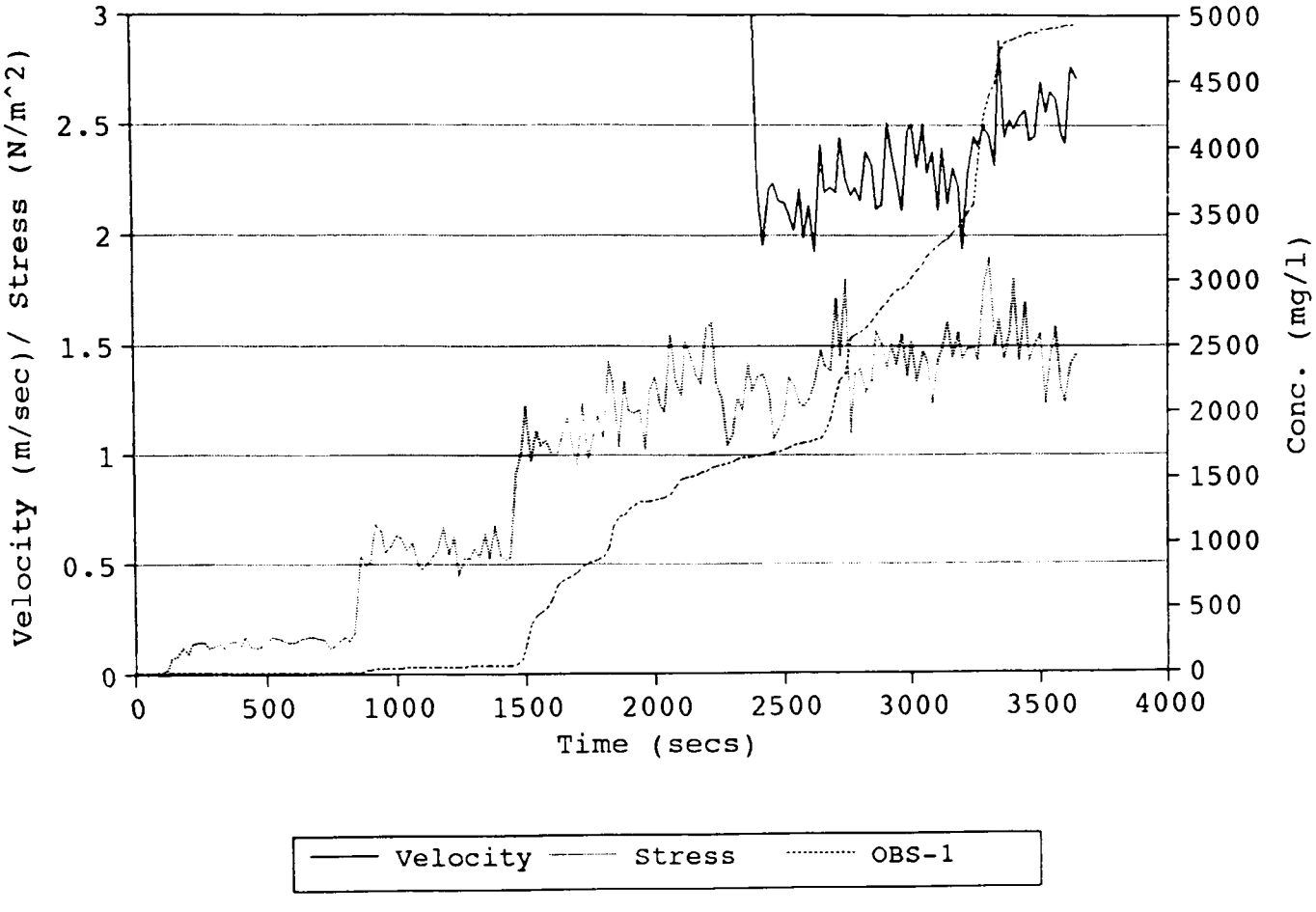

Fig (a.38b): Suspended Sediment Concentration and Rate of Erosion.

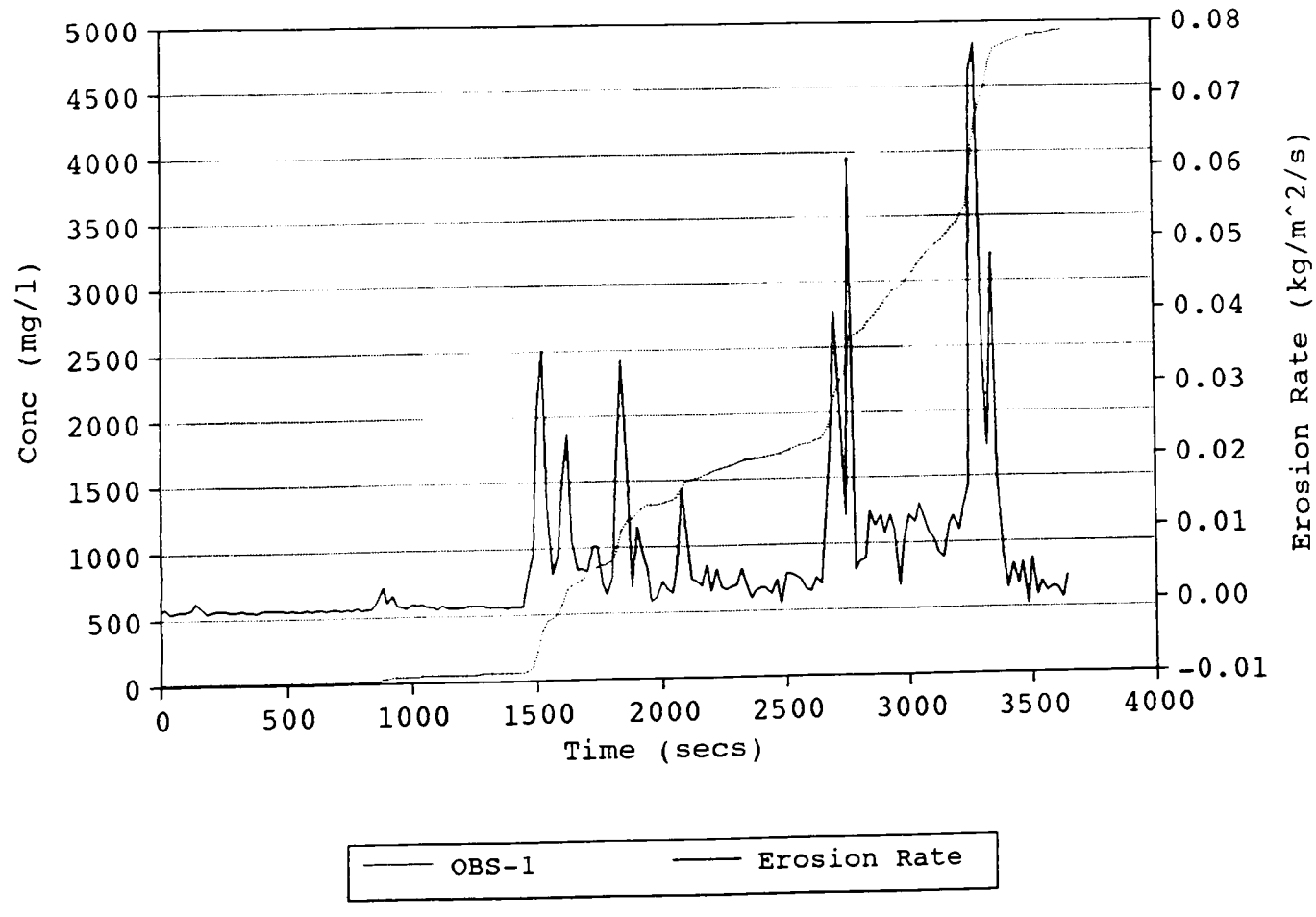

Fig (a.39a): Processed Data for Flume Run 39

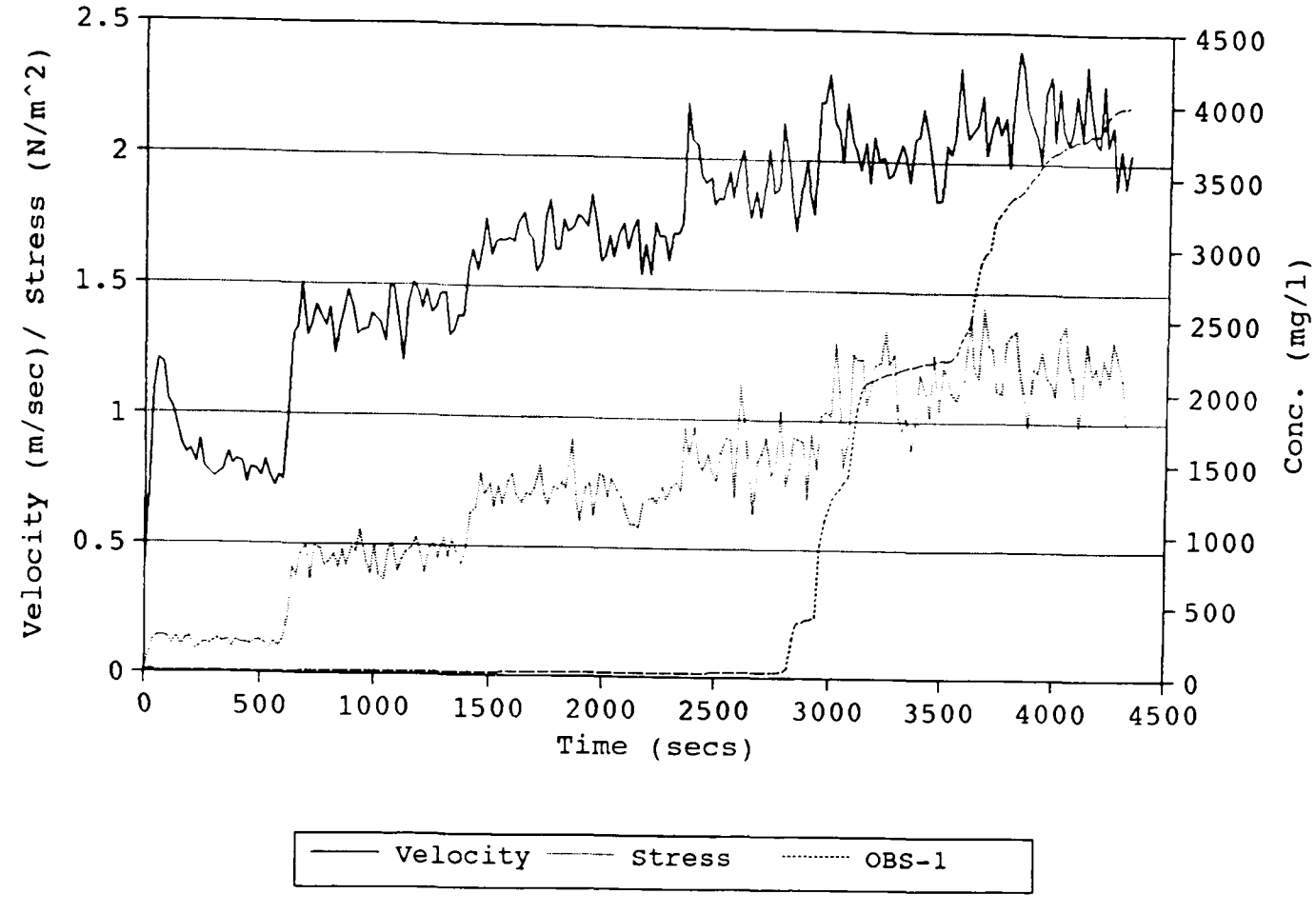

Fig (a.39b): Suspended Sediment Concentration and Rate of Erosion.

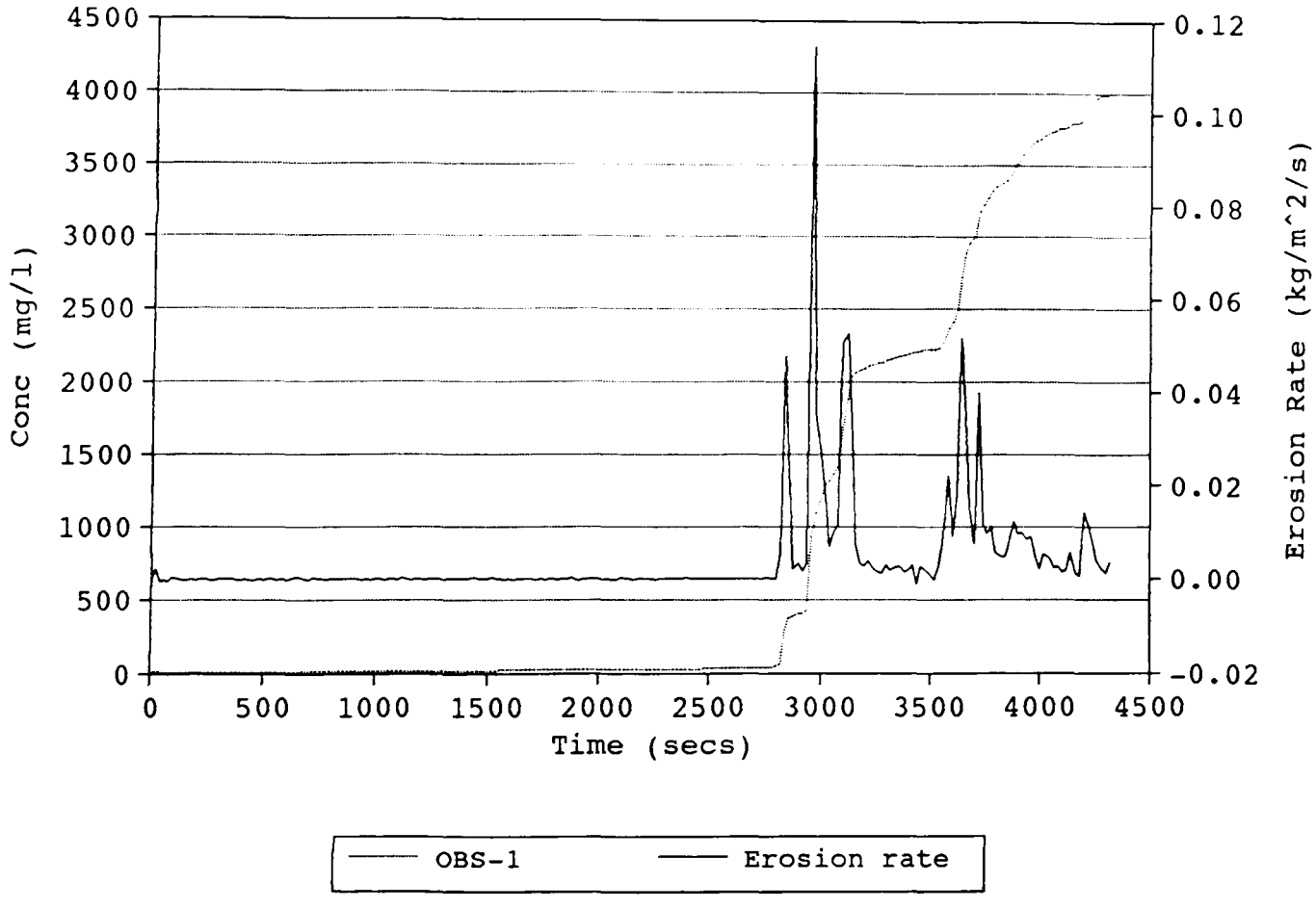

Fig (a.40a): Processed Data for Flume Run 40.

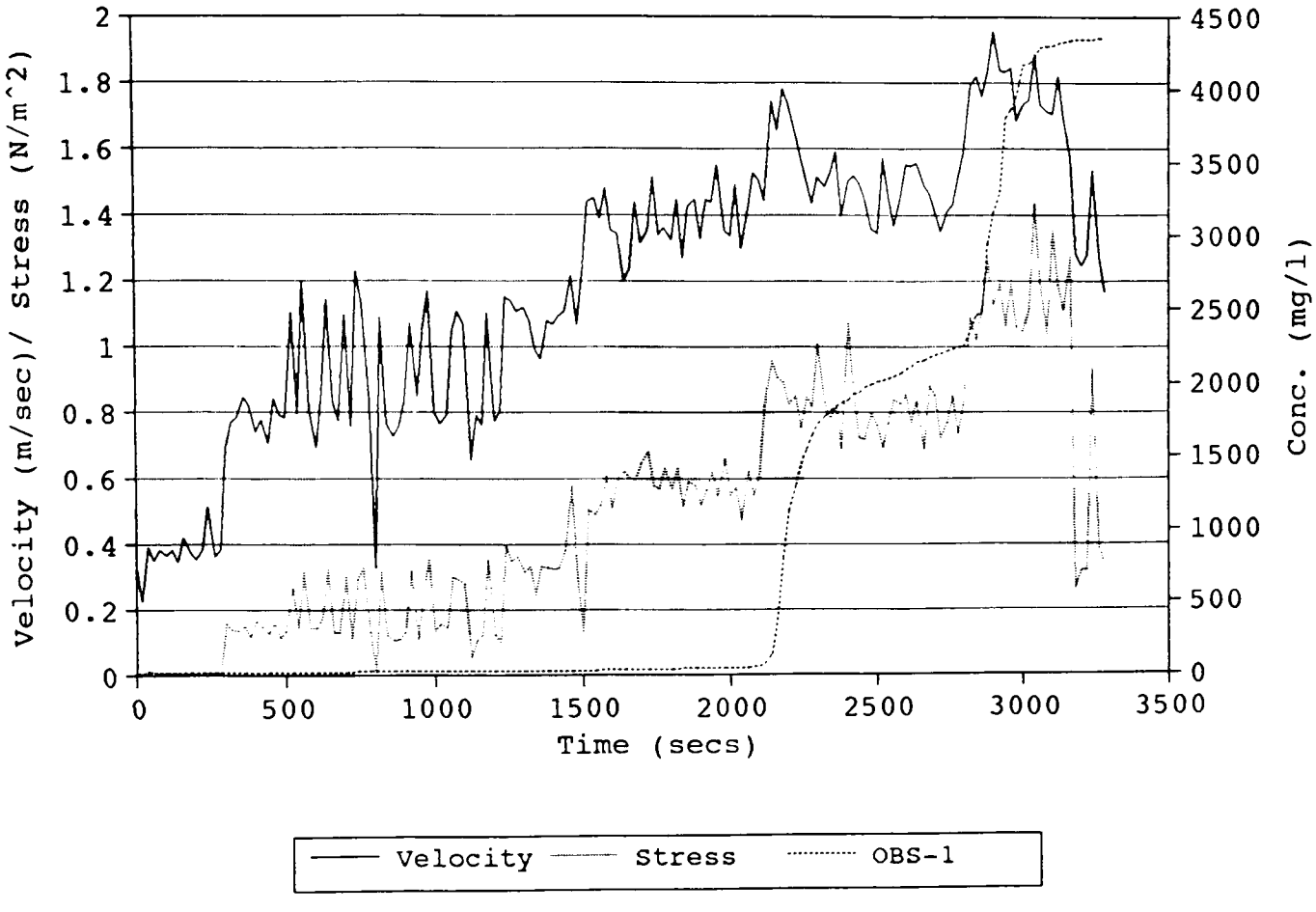

Fig (a.40b): Suspended Sediment Concentration and Rate of Erosion.